NBSIR 83-2742 (R)

Photonuclear Data - Abstract Sheets 1955 - 1982
Volume XII (Lanthanum - Lutetium)

U.S. DEPARTMENT OF COMMERCE
National Bureau of Standards
National Measurement Laboratory
Center for Radiation Research
Washington, DC 20234

U.S. DEPARTMENT OF COMMERCE
UREAU OF STANDARDS

NBSIR 83-2742

PHOTONUCLEAR DATA - ABSTRACT SHEETS 1955 - 1982 VOLUME XII (LANTHANUM - LUTETIUM)

E. G. Fuller, Henry Gerstenberg

U.S. DEPARTMENT OF COMMERCE
National Bureau of Standards
National Measurement Laboratory
Center for Radiation Research
Washington, DC 20234

U.S. DEPARTMENT OF COMMERCE, Malcolm Baldrige, *Secretary*
NATIONAL BUREAU OF STANDARDS, Ernest Ambler, *Director*

TABLE OF CONTENTS

Photonuclear Data-Abstract Sheets
1955-1982

I. Introduction

As used in connection with this collection of data-abstract sheets, the term photonuclear data is taken to mean any data leading to information on the electromagnetic matrix element between the ground state and excited states of a given nuclide. The most common types of reactions included in this compilation are: (e,e'), (γ,γ), (γ,γ'), (γ,n), (γ,p), etc. as well as ground-state particle capture reactions, e.g. (α,γ_0). Two reactions which fit the matrix element criterion are not included in the compilation because of their rather special nature. These are heavy particle Coulomb excitation and the thermal neutron capture reaction (n,γ_0). While the energy region of particular interest extends from 0 to 150 MeV, papers are indexed which report measurements in the region from 150 MeV to 4 GeV. Most of the experiments listed are concerned with the excitation energy range from 8 to 30 MeV, the region of the photonuclear giant resonance.

The hierarchical grouping of the photonuclear data-abstract sheets within the file is by: 1. Target Element, 2. Target Isotope, and 3. by the Bibliographic Reference Code assigned to the paper from which the data on the sheet were abstracted. In this file, colored pages are used to mark the beginning and end of the sheets for each chemical element. A brief historical sketch of the element is given on the divider sheet marking the start of each section; the information for this sketch was derived from references such as the Encyclopaedia Britannica. In those cases where the sheets for a given element make up a major part of a volume, colored pages are also used to delineate sections pertaining to the individual isotopes of the element. Each of the sections of the file, as delineated by two colored divider sheets, represents a 27 year history of the study of electromagnetic interactions in either a specific nuclide or a specifc element.

The data-abstract sheets are filed under the element and/or isotope in which the ground-state electromagnetic transition takes place. For example, the abstract sheet for a total neutron yield measurement for a naturally occurring copper sample would appear in the elemental section of the copper file. On the other hand, a measurement of the ^{62}Cu 9.73 minute positron activity produced in the same sample by photons with energies below the three-neutron separation energy for ^{65}Cu (28.68 MeV) would be filed with the sheets for ^{63}Cu. Similarly a measurement of the ground-state neutron capture cross section in ^{12}C would be filed under ^{13}C while the corresponding ground-state alpha-particle capture cross section would be filed under ^{16}O.

At the end of this volume there is a master list of the abbreviations that have been used in the index section of the abstract sheets. The listings are those used in the final published index, Photonuclear Data Index, 1973-1981, NBSIR 82-2543, issued in August 1982 by the U. S. Department of Commerce, National Bureau of Standards, Washington, DC 20234. In some cases two notations are entered for the same quantity. The second entry is the abbreviation that was used in one or more of the earlier published editions of the index.

# LANTHANUM
Z=57

Lanthanum is not a "true" earth. The rare earths are inner transition elements characterized by elections successively filling the incomplete 4f orbital shell. Geochemically, lanthanum is found in nature in close association with all the other rare earth elements. It was first separated by C. G. Mosander in 1839; he called it after the Greek word *lanthanein* meaning "to be concealed".

LA
A=139

LA
A=139

B.G. Chidley, L. Katz, S. Kowalski
Can. J. Phys. 36, 407 (1958)

ELEM. SYM.	A	Z
La	139	57

REF. NO.	
58 Ch 2	NVB

Betatron

REACTION	RESULT	EXCITATION ENERGY	SOURCE		DETECTOR		ANGLE
			TYPE	RANGE	TYPE	RANGE	
G,N	RLY	THR	C	THR	BF3-I		4PI

See 58 Ka 1 for cross sections

THRESHØLD

TABLE I

MEASURED PHOTONEUTRON THRESHOLDS

Reaction	Measured Q value, Mev.	Other Q values, Mev.	Method	Reference
$La^{139}(\gamma, n)La^{138}$	8.81±0.05			
		8.80 ±0.20	Threshold	Sher *et al.* (1951)
		8.73 ±0.20	Mass data	Johnson and Nier (1957)
		9.07 ±0.19	Mass data	Duckworth (unpublished)
			Q^- value	Glover and Walt (1957)

REF. E.G. Fuller, B. Petree, M.S. Weiss
Phys. Rev. 112, 554 (1958)

ELEM. SYM.	A	Z
La	139	57

METHOD Betatron; ion chamber

REF. NO.	
58 Fu 1	NVB

REACTION	RESULT	EXCITATION ENERGY	SOURCE TYPE	SOURCE RANGE	DETECTOR TYPE	DETECTOR RANGE	ANGLE
G,XN	ABY	7-40	C	7-40	BF3-I		4PI

TABLE I. Target properties and results.

Element	Form used	Weight grams	$\sigma^a(\gamma,n)$[a] barns	$\int\sigma dE$[b] / NZ/A Mev-b	"Γ"[a] Mev
Sn	Sn	4.81	0.30	0.064	5.0
I	I	8.55	0.36	0.085	6.0
La	La	10.43	0.34	0.063	5.2
Ce	Ce	4.99	0.45	0.080	4.5
Sm	Sm_2O_3	2.90	0.26	0.073	8.6
Tb	Tb_4O_7	3.04	0.39	0.087	8.7
Ho	Ho_2O_3	1.87	0.41	0.079	7.5
Er	Er_2O_3	5.41	0.50	0.100	8.5
Yb	Yb_2O_3	5.57	0.50	0.090	7.0
Ta	Ta	8.41	0.49	0.077	6.0
Au	Au	3.16	0.68	0.085	4.2
Pb	Pb	8.05	0.75	0.081	3.8

[a] $\sigma^a(\gamma,n)$ is the maximum value and "Γ" the full width at $\sigma^a(\gamma,n)/2$ of the neutron production cross section corrected for multiple neutron emission. Data were not fitted with resonance lines to determine these values.
[b] Integrated neutron production cross sections corrected for multiple neutrons above $(\gamma,2n)$ threshold.

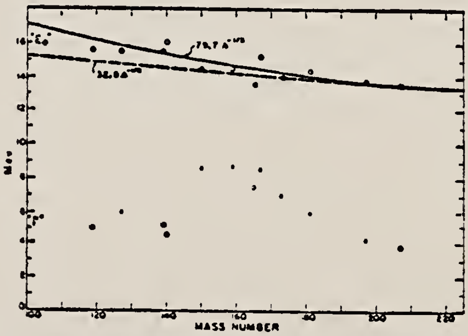

FIG. 6. Mean energy and width of giant resonances. "E_0" and "Γ" are the mean energy for photon absorption and the full width at half maximum of the giant resonance obtained from dashed histograms as in Fig. 5. No attempt was made to fit data with resonance curves to obtain these parameters.

L. Katz, G.B. Chidley Nuclear Reactions at Low and Medium Energies (Academy of Science, USSR: 1958) 371	ELEM. SYM.	A	Z
	La	139	57

METHOD		REF. NO.	
Betatron; neutron cross section; BF_3 counters; ion chamber monitor		58 Ka 1	NVB

REACTION	RESULT	EXCITATION ENERGY	SOURCE		DETECTOR		ANGLE
			TYPE	RANGE	TYPE	RANGE	
G,XN	ABX	9-22	C	9-22	BF3-I		4PI

Таблица 2

Пороги испускания фотонейтронов

Изотоп	B_n, Мэв	B_{nn}, Мэв	Изотоп	B_n, Мэв	B_{nn}, Мэв
V^{51}	11,16	20,5	L^{139}	8,81	16,1
Mn^{55}	10,14	19,2	Pr^{141}	9,46	17,6
Co^{59}	10,44	18,6	Tb^{159}	8,16	14,8
As^{75}	10,24	18,1	Ho^{165}	8,10	14,6
Y^{89}	11,82	20,7	[illegible]	8,00	14,7
Nb^{93}	8,86	17,1	[illegible]	7,77	14,2
Rh^{103}	9,46	16,8	Ta^{181}	7,66	13,8
J^{127}	9,14	16,2	Au^{197}	[illegible]	13,3
Cs^{133}	9,11	16,5	Bi^{209}	[illegible]	14,5

THRESHOLDS

не приведены, поскольку они превышают 22 *Мэв* во всех случаях, кроме золота, для которого $B_{3n}=21$ *Мэв*. Свойства сечений $\sigma_C(\gamma)$ сведены в табл. 3.

Таблица 1

Изотоп	$E_{макс}$, Мэв	$\sigma_n(E_\gamma)$, барн	Г, Мэв	Σ^m, Мэв · барн	Y(22), 10^4 нейтрон/100 р · моль
V^{51}	18,4	0,062	5,2	0,33	1,62
Mn^{55}	20,2	0.060	7,0	0,39	2.01
Co^{59}	18,3	0,068	6,3	0,44	2,30
As^{75}	16,6	0.090	9,5	0,74	4,25
Y^{89}	17,1	0,172	5.2	0,93	5,33
Nb^{93}	18,0	0,156	7,5	1,17	6,80
Rh^{103}	17,5	0.160	9,4	1,40	8,28
J^{127}	15.2	0,273	6,8	1,76	11,9
Cs^{133}	16,5	0,238	7,7	1,59	10,7
La^{139}	15,5	0,325	3,8	1,55	11,2
Pr^{141}	15,0	0,320	4,9	1,93	13,1
Tb^{159}	15,6	0,274	9,8	2,49	18,1
Ho^{165}	13,5	0,305	8,9	2,52	18,7
Tm^{169}	16,4	0,250	8,4	1,91	14,9
Lu^{175}	16,0	0,225	8,4	1,90	23,0
Ta^{181}	14,5	0,350	8,5	3,15	22,0
Au^{197}	13,8	0,475	4,7	3,04	22,6
Bi^{209}	13,2	0,455	5,9	2,89	23,2

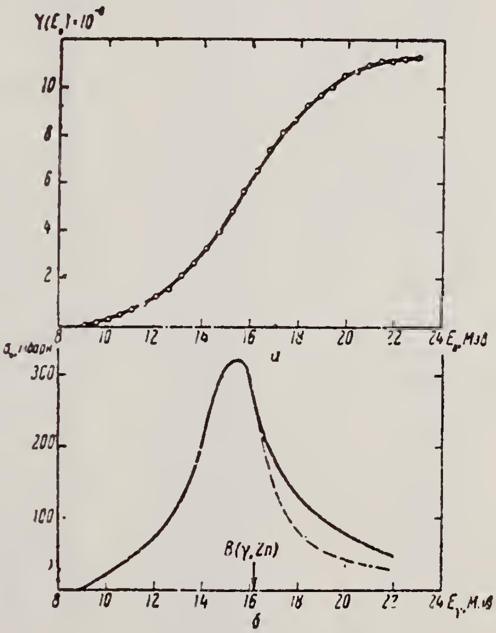

Рис. 10.

а — Выход фотонейтронов для La; б — $\sigma_n(E_\gamma)$ и $\sigma_C(\gamma)$ для La

Ref. B.M. Spicer, H.H. Thies, J.E. Baglin, F.R. Allum
Australian J. Phys. 11, 298 (1958)

Elem. Sym.	A	Z
La	139	57

Method 18 MeV electron synchrotron; neutron counters, 25 r Victoreen monitor

Ref. No.	
58 Sp 1	EH

Reaction	E or ΔE	E_o	Γ	$\int \sigma dE$	Jπ	Notes
La(γ,n)	Bremss. 8-18					

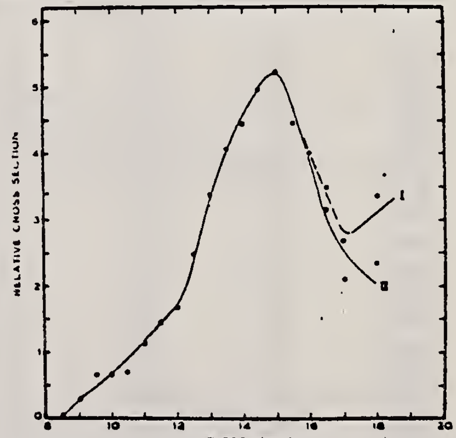

Fig. 6.—Cross section for nuclear absorption of γ-rays in lanthanum. Curve I is the cross section calculated from the neutron yield curve. Curve II is corrected for the effects of neutron multiplicity.

e.. J. Halpern, and E. J. Muirhead
.. 118, 1302-12 (1960)

	La	139	57
METHOD Betatron; neutron threshold; ion chamber	REF. NO. 60 Ge 3		NVB

REACTION	RESULT	EXCITATION ENERGY	SOURCE TYPE	SOURCE RANGE	DETECTOR TYPE	DETECTOR RANGE	ANGLE
G,N	NØX	THR	C	THR	BF3-I		4 PI

THRESHØLD

TABLE I. Summary and comparison of neutron separation energies inferred from present threshold measurements with values predicted from mass data and reaction energies. All energies are expressed in the center-of-mass system in Mev.

Reaction	No. runs	Present results	Other results	Method	Reference
$La^{139}(\gamma,n)La^{138}$	4	8.775±0.025	8.73 ±0.19	mass data	p
			8.81 ±0.05	threshold	f

[p] W. H. Johnson, Jr., and A. O. Nier, Phys. Rev. 105, 1014 (1957).

R.G. Baker, K.G. McNeill
Can. J. Phys. 39, 1158(1961)

ELEM. SYM.	A	Z
La	139	57

METHOD betatron; fast neutron yield; angular distribution; Al and Si threshold detectors; ion chamber

REF. NO.	
61 Ba 2	NVB

REACTION	RESULT	EXCITATION ENERGY	SOURCE TYPE	SOURCE RANGE	DETECTOR TYPE	DETECTOR RANGE *	ANGLE
G,XN	ABY	THR-22	C	22	THR-I	3-+	DST
G,XN	ABY	THR-22	C	22	THR-I	5-+	DST

In Tables 2 and 4:

$\bar{\sigma}$ = average cross section of detector weighted with neutron spectrum

Φ = neutrons/100 roentgen/mole

$$W(\theta) = a_o \sum_{n=1}^{\infty} [1 + A_n P_n (\cos \theta)]$$

* "3-+" is the detector range of Aluminum and "5-+" of Silicon.

TABLE II

Normalized yields for aluminum detectors

Element	Al(n,γ) reaction 30°	90°	150°	a_0	Al(n,p) reactions 30°	60°	90°	a_0	a_1	a_2	$(\bar{\sigma}\Phi)^* \times 10^6$
Bismuth	[illegible]	[illegible]±130	620	541±85	3632	5139±290	3168	4366±185	0.06±0.06	−0.35±0.1	17.76
	475	425±130	641	484±85	2562	5353±290	2955	4144±185	−0.05±0.06	−0.53±0.1	16.87
Lead	426	312±120	725	429±77	3123	5754±260	3154	4591±166	−0.004±0.05	−0.51±0.07	18.68
Tantalum	378	307±190	688	441±122	2757	3024±425	2088	2757±275	0.14±0.14	−0.19±0.17	11.22
Lanthanum	208	222±110	330	243±70	2139	3371±250	1891	2768±160	0.05±0.07	−0.43±0.10	11.27
Arsenic	77	100±50	108	97±32	788	937±115	764	865±74	0.02±0.11	−0.16±0.14	3.52
Copper	13	65±30	70	55±20	710	748±70	569	700±45	0.11±0.08	−0.14±0.11	2.85

*$(\bar{\sigma}\Phi)$ = 4.07 × [illegible] millibarn-neutron.

TABLE IV

I Element	II a_0	III a_1	IV a_2	V $(\bar{\sigma}\Phi) \times 10^{6*}$	VI Φ_{total} (22 Mev) × 10^9	VII Φ_{fast}/Φ_{total}
Vanadium	245 (1±0.06)	0.01±0.08	−0.00±0.10	6.05	0.21	0.12
Chromium	164 (1±0.03)	0.04±0.04	−0.05±0.05	4.05	0.17	0.10
Manganese	308 (1±0.02)	0.07±0.03	−0.09±0.04	7.61	0.25	0.12
Iron	200 (1±0.03)	0.05±0.04	−0.17±0.05	4.94	0.18	0.11
Cobalt	390 (1±0.02)	0.08±0.03	−0.22±0.04	9.63	0.26	0.15
Nickel	145 (1±0.05)	0.07±0.07	−0.23±0.09	3.58	0.12	0.12
Copper	347 (1±0.02)	0.05±0.03	−0.29±0.04	8.57	0.30	0.12
Arsenic	482 (1±0.03)	0.11±0.04	−0.24±0.05	11.91	0.33	0.15
Rubidium	638 (1±0.05)	0.13±0.06	−0.14±0.08	15.76		
Strontium	409 (1±0.05)	0.10±0.06	−0.17±0.08	10.10		
Yttrium	290 (1±0.10)	0.08±0.12	−0.12±0.15	7.16		
Silver	590 (1±0.04)	0.10±0.06	−0.22±0.08	14.57	0.87	0.07
Cadmium	905 (1±0.02)	0.02±0.02	−0.26±0.03	22.35		
Iodine	1133 (1±0.03)	0.04±0.04	−0.29±0.05	27.99	1.42	0.08
Barium	1048 (1±0.04)	0.10±0.06	−0.38±0.08	25.89		
Lanthanum	1595 (1±0.02)	0.02±0.03	−0.42±0.04	39.40	1.04	0.15
Cerium	1316 (1±0.05)	0.05±0.06	−0.39±0.08	32.50		
Dysprosium	1652 (1±0.08)	0.04±0.10	−0.34±0.13	40.80		
Tantalum	1558 (1±0.02)	0.04±0.03	−0.22±0.04	38.48	2.50	0.06
Tungsten	1365 (1±0.02)	−0.07±0.03	−0.24±0.04	33.71		
Mercury	1345 (1±0.02)	0.04±0.03	−0.31±0.04	33.22		
Lead	2274 (1±0.01)	0.02±0.02	−0.42±0.03	56.17	2.72	0.08
Bismuth	2162 (1±0.02)	0.06±0.03	−0.45±0.04	53.40	3.36	0.06
Thorium	3031 (1±0.04)	0.06±0.05	−0.32±0.07	74.87		
Uranium	4630 (1±0.02)	0.05±0.03	−0.17±0.04	114.36		

*$(\bar{\sigma}\Phi)$ = 2.47 × 10^9 a_0 millibarn-neutron. Errors are standard errors due to counting statistics only.

REF.
J. Miller, C. Schuhl, C. Tzara
J. Phys. Radium 22, 529 (1961)

ELEM. SYM.	A	Z
La	139	57

METHOD
Positron annihilation; neutron cross section; BF_3 counter; ion chamber

REF. NO.	
61 Mi 1	NVB

REACTION	RESULT	EXCITATION ENERGY	SOURCE TYPE	SOURCE RANGE	DETECTOR TYPE	DETECTOR RANGE	ANGLE
G,XN	ABX	10-22	D	10-22	BF3-I		4PI

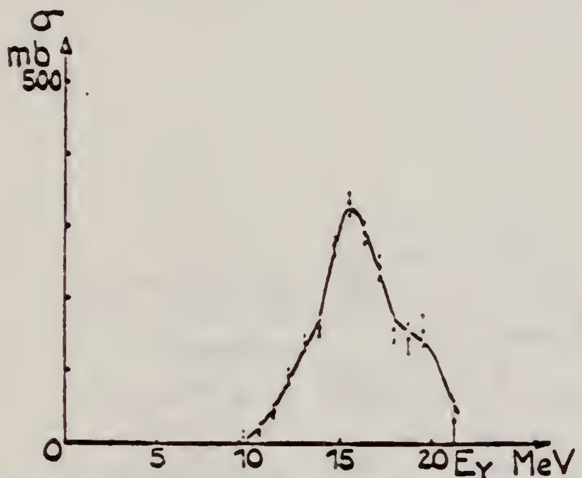

Fig. 6a. — Lanthane, $\sigma(\gamma,n) + 2\sigma(\gamma,2n) + \sigma(\gamma,np) + \ldots$

Ref. F. Tagliabue, J. Goldemberg Nuclear Phys. 23, 144 (1961)	Elem. Sym. La	A 139	Z 57
Method 22 MeV betatron; $Si^{28}(n,p)Al^{28}$ threshold detector.	Ref. No. 61 Ta 1		JHH

Reaction	E or ΔE	E_o	Γ	$\int \sigma dE$	Jπ	Notes
(γ, n)	Bremss. 22					$E_n > 6$ MeV. $W(\theta_n) = A + B \sin^2\theta$ where B/A = 0.67±0.48

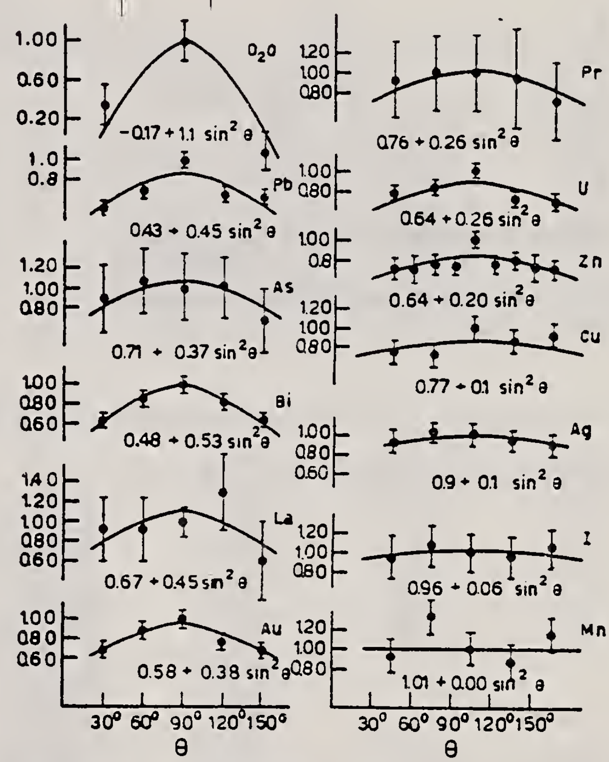

Fig. 4. Angular distributions of fast photoneutrons as observed with the $Si^{28}(n, p)Al^{28}$ detector. Data normalized at 90° in each case.

Figure 4: Angular distributions of fast photoneutrons as observed with the $Si^{28}(n,p)Al^{28}$ detector. Data normalized at 90° in each case.

Ref.	Elem. Sym.	A	Z
G.C. Reinhardt, W.D. Whitehead Nuclear Phys. 30, 201 (1962)	La	139	57

Method	Ref. No.	
55 MeV betatron; synchrotron; $Si^{28}(n,p)Al^{28}$ activity; $Cu^{63}(\gamma,n)Cu^{62}$ monitor.	62 Re 1	EGF

Reaction	E or ΔE	E_o	Γ	$\int \sigma dE$	Jπ	Notes
(γ,n)	Bremss. 55					Figure 10: Dotted curve is of form $a_o + a_1\cos\theta + a_2\cos^2\theta + a_2\cos^2\theta - a_1\cos^2\theta$; solid curve is of form $a_o + a_1\cos\theta + a_2\cos^2\theta$; errors on points are statistical error in counting only.

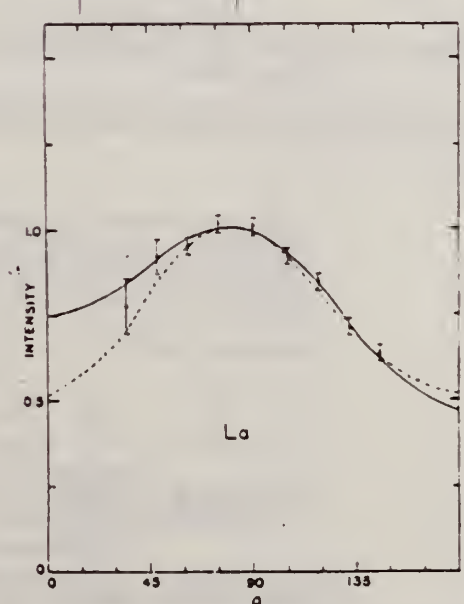

Fig. 10. Angular distribution of fast neutrons from lanthanum. See fig. 3

TABLE 2

Parameters of the fit 1 for the expressions $a_0 + a_1\cos\theta + a_2\cos^2\theta + \ldots$ and $1 + A_1P_1 + A_2P_2$

	Bi 1	Bi 2	Pr	Au	Y	Ho	La
	1.00 ± 0.02	1.00 ± 0.02	1.00 ± 0.02	1.00 ± 0.02	1.00 ± 0.03	1.00 ± 0.02	1.00 ± 0.01
	0.15 ± 0.04	0.18 ± 0.04	0.17 ± 0.04	0.14 ± 0.04	0.17 ± 0.06	0.12 ± 0.03	0.14 ± 0.03
	0.47 ± 0.06	0.40 ± 0.08	0.41 ± 0.09	0.21 ± 0.07	0.15 ± 0.11	0.34 ± 0.06	0.39 ± 0.06
	0.18 ± 0.04	0.21 ± 0.05	0.20 ± 0.05	0.15 ± 0.04	0.18 ± 0.06	0.14 ± 0.04	0.16 ± 0.03
	0.37 ± 0.06	0.31 ± 0.06	0.32 ± 0.07	0.15 ± 0.05	0.11 ± 0.08	0.26 ± 0.05	0.30 ± 0.04
	0.53 ± 0.06	0.60 ± 0.08	0.70 ± 0.01	0.71 ± 0.07	0.85 ± 0.11	0.66 ± 0.06	0.61 ± 0.06
	0.47 ± 0.06	0.40 ± 0.08	0.41 ± 0.09	0.21 ± 0.07	0.15 ± 0.11	0.34 ± 0.06	0.39 ± 0.06
	0.15 ± 0.03	0.18 ± 0.04	0.17 ± 0.04	0.14 ± 0.03	0.17 ± 0.06	0.12 ± 0.03	0.14 ± 0.03

normalized so that $A_0 = 1$

TABLE 4

Parameters of the fit 3 for the expressions $a_0 + a_1\cos\theta + a_2\cos^2\theta + a_3\cos^3\theta$, $1 + A_1P_1 + A_2P_2 + A_3P_3$

	Bi 1	Bi 2	Pr	Au	Y	Ho	La
	1.01 ± 0.02	1.00 ± 0.02	1.01 ± 0.03	0.98 ± 0.02	1.00 ± 0.03	1.00 ± 0.02	1.01 ± 0.02
	0.19 ± 0.05	0.17 ± 0.07	0.21 ± 0.07	0.07 ± 0.06	0.16 ± 0.09	0.12 ± 0.03	0.17 ± 0.05
	0.56 ± 0.11	0.37 ± 0.15	0.50 ± 0.16	0.05 ± 0.12	0.13 ± 0.20	0.33 ± 0.12	0.47 ± 0.11
	−0.17 ± 0.18	0.05 ± 0.24	−0.17 ± 0.25	0.31 ± 0.19	0.05 ± 0.32	0.03 ± 0.19	−0.17 ± 0.17
A_1*	0.11 ± 0.15	0.23 ± 0.18	0.13 ± 0.20	0.27 ± 0.13	0.20 ± 0.22	0.15 ± 0.14	0.09 ± 0.13
A_2*	0.17 ± 0.09	0.28 ± 0.11	0.30 ± 0.12	0.03 ± 0.08	0.09 ± 0.14	0.24 ± 0.09	0.37 ± 0.09
A_3*	−0.08 ± 0.09	0.02 ± 0.11	−0.08 ± 0.12	0.13 ± 0.08	0.02 ± 0.17	0.01 ± 0.08	−0.08 ± 0.08

* A normalized so that $A_0 = 1$

REF.	ELEM. SYM.	A	Z
L.B. Rice, L.N. Bolen, W.D. Whitehead Phys. Rev. 134, B557 (1964)	La	139	57

METHOD	REF. NO.	
Synchrotron, NBS chamber	64 Ri 1	NVB

REACTION	RESULT	EXCITATION ENERGY	SOURCE TYPE	SOURCE RANGE	DETECTOR TYPE	DETECTOR RANGE	ANGLE
G,XN	ABX	8-30	C	8-30	BF3-I		4PI

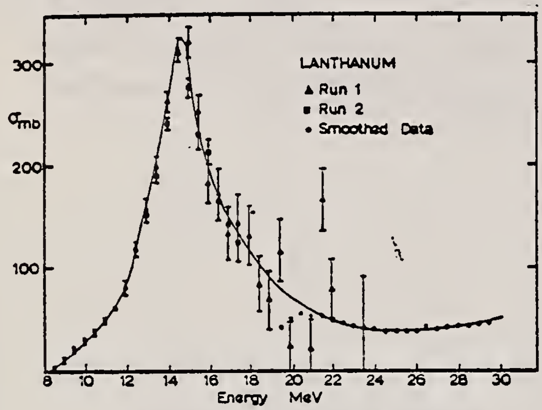

FIG. 1. Lanthanum (γ,n) cross section uncorrected for neutron multiplicity.

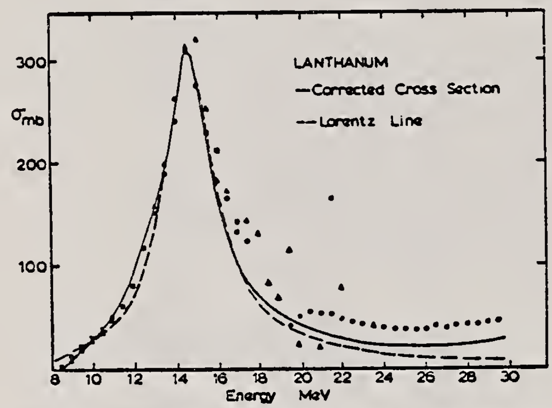

FIG. 3. Lanthanum (γ,n) cross section with neutron multiplicity correction (solid line); Lorentz line fitting to data points (dashed line).

TABLE I. Experimentally determined parameters for the neutron photoproduction cross sections σ_m, maximum value of cross sections; E_m, energy at which maximum occurs; DSR, classical dipole-sum rule limit; Γ_0 twice the energy from half-maximum on low-energy side of curve to E_m, Γ_{Lor} width used to fit the Lorentz curve

	σ_m mb	E_m MeV	$\int_{Thr}^{\infty} \sigma dE$ MeV-b	DSR MeV-b	Γ_0 MeV	Γ_{Lor} MeV
	Uncorrected for multiplicity					
La	315±15	14.8±0.4	1.76	2.02		
Pr	305±10	14.8±0.4	1.74	2.06		
	Corrected for (γ,2n)					
La	304	14.5	1.36	2.02	3.2±0.2	3.3
Pr	305	14.8	1.47	2.06	4.0±0.2	3.3

REF.	ELEM. SYM.	A	Z
G. Ben-David, B. Arad, J. Balderman, and Y. Schlesinger Phys. Rev. 146, B852 (1966)	La	139	57

METHOD	REF. NO.	
Nuclear Resonance Scattering using N,G reactions.	66 Be 3	JDM

REACTION	RESULT	EXCITATION ENERGY	SOURCE TYPE	SOURCE RANGE	DETECTOR TYPE	DETECTOR RANGE	ANGLE
G,G	RLX	5 - 10	D	5 - 10	NAI-D	5 - 10	135

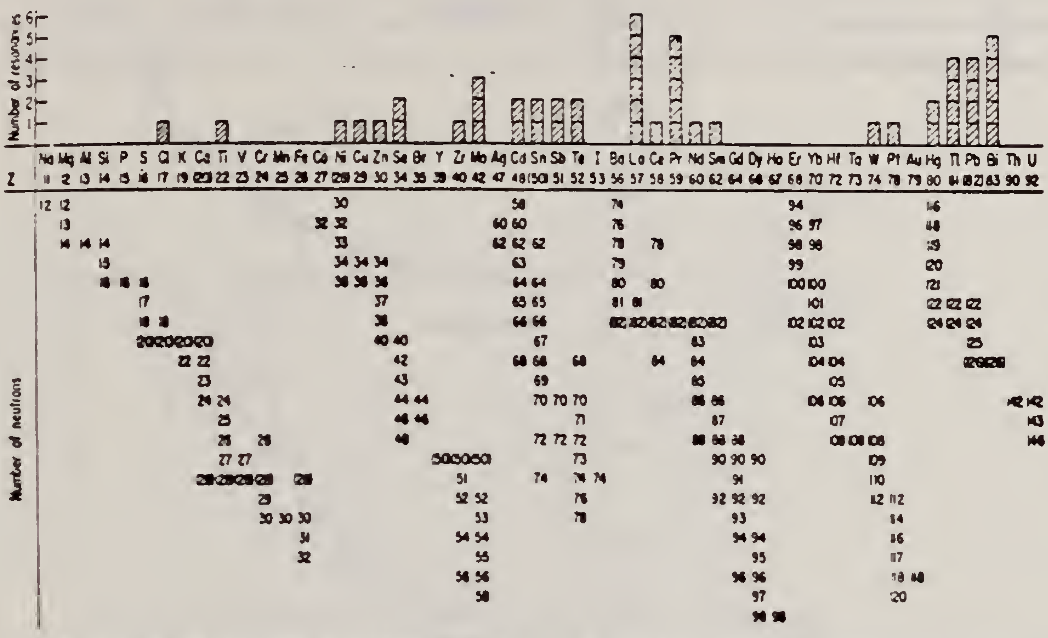

FIG. 3. Histogram of distribution of observed resonances among the different targets. The atomic number is given directly beneath the chemical symbol followed by the neutron numbers of the naturally occurring isotopes. Magic numbers are shown in brackets.

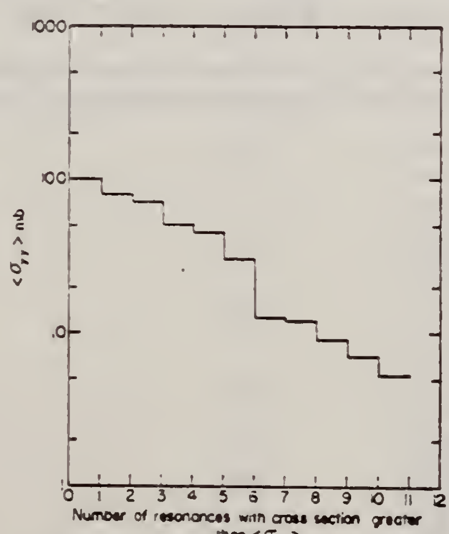

FIG. 5. Integral distribution of the effective cross sections for the 11 resonances in the mono-isotopic elements lanthanum and praseodymium.

TABLE III. List of effective cross sections.

Scatterer	Energy (MeV)	Gamma source	$\bar{\sigma}$ (mb)	Scatterer	Energy (MeV)	Gamma source	$\bar{\sigma}$ (mb)
Sm[illegible]	8.997	Ni	100	Sn	7.01	Cu	110
Pr^{141}	8.881	Cr	9	Nd	6.867	Co	30
La	8.532	Ni	6	Pr^{141}	6.867	Co	3
Te	8.532	Ni	3^{e}	Te	6.7	Ni	...
Cu	8.499	Cr	24	La	6.54	Ag	12
Zr	8.496	Se	3050	Cd	6.474	Co	110
Zn	8.119	Ni	13	Mo	6.44	Hg	25^{a}
Se	7.817	Ni	50	La	6.413	Ti	72
Se	7.76	K	90	Mo	6.413	Ti	10
Sb	7.67	V	...^{b}	Tl	6.413	Ti	25
Cd	7.64	Fe	40^{c}	W	~6.3	Ti	...^{b}
Ni	7.64	Fe	7^{c}	Sb	6.31	Hg	6^{a}
Pr^{141}	7.64	Fe	12^{c}	Ti	6.31	Hg	2^{a}
Tl	7.64	Fe	370^{c}	Sn	6.27	Ag	75
La	7.634	Cu	7	Pb^{208}	6.15	Gd	...^{g}
Mo	7.634	Cu	11	Te	5.8	Ni	...^{f}
Bi^{209}	7.634	Cu	4	La	6.12	Cl	35
Te	7.528	Ni	66^{d}	Pr^{141}	6.12	Cl	110
Bi^{209}	7.416	Se	100	Pt	5.99	Hg	$40^{a,g}$
Bi^{209}	7.300	As	80^{e}	Tl	5.99	Hg	5^{a}
Pb^{208}	7.285	Fe	4100	Pb^{208}	5.9	Sr	...^{h}
Cl	7.285	Fe	34	Ce	5.646	Co	17
Pr^{141}	7.185	Se	80	Bi^{209}	5.646	Co	55
Tl	7.16	Cu	120	Pb^{208}	5.53	Ag	70
La	7.15	Mn	50	Hg	5.44	Hg	75^{a}
Bi^{209}	7.149	Ti	2000	Hg	4.903	Co	385

[a] High-energy component of a complex spectrum.
[b] A broad scattered spectrum with no observable peak structure.
[c] There are actually two lines of energies 7.647 and 7.633 MeV having equal intensities in the iron capture gamma spectrum. The cross section has therefore been corrected, although there is no possibility at present of deciding which line is responsible for each resonance.
[d] Is probably an independent level in the complex spectrum of Ni γ rays on Te.
[e] Rough estimate.
[f] May be inelastic component from 7.528 level in Te.
[g] The relative line intensities in this case are due to Groshev and co-workers.
[h] No line is known for the source at this energy.
[i] Difficult to resolve among the many source lines present at this energy.

REF.	ELEM. SYM.	A	Z
R. R. Hurst and D. J. Donahue Nucl. Phys. A91, 365 (1967)	La	139	57

METHOD	REF. NO.	
Neutron capture gamma rays	67 Hu 1	EGF

REACTION	RESULT	EXCITATION ENERGY	SOURCE TYPE	SOURCE RANGE	DETECTOR TYPE	DETECTOR RANGE	ANGLE
G,N	ABX	9-11	D	9-11	BF3-I		4PI

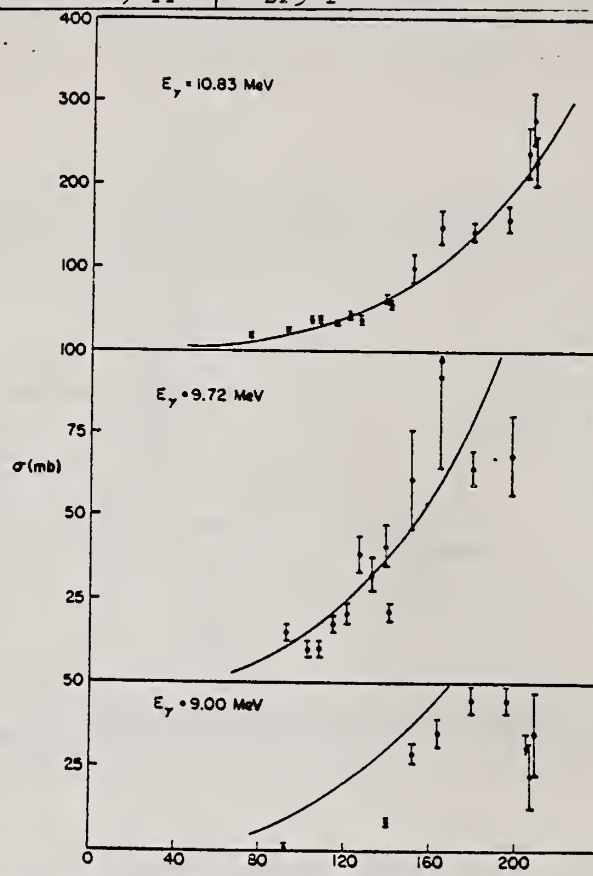

Fig. 1. Cross section (in mb) versus mass number of the target for gamma-ray energies of 9.00, 9.72 and 10.83 MeV. The solid lines are plots of eq. (1) in the text.

TABLE 1

Photoneutron cross sections (mb)

Target	7.72 MeV	9.00 MeV	9.72 MeV	10.83 MeV
^{59}Co				9.0 ± 0.8
^{75}As				20.4 ± 1.7
^{93}Nb		0.53 ± 0.10	14.6 ± 2.2	25.8 ± 2.1
^{103}Rh			10.6 ± 1.7	38.8 ± 3.1
^{107}Ag, ^{109}Ag			10.0 ± 1.5	37.6 ± 2.9
^{115}In			17.1 ± 2.6	33.3 ± 2.7
^{121}Sb, ^{123}Sb			20.7 ± 3.1	42.5 ± 3.6
^{127}I			38.7 ± 5.8	38.8 ± 3.1
^{133}Cs			31.7 ± 4.8	52.5 ± 3.8
^{139}La		8.61 ± 0.86	40.8 ± 6.5	63.0 ± 5.0
^{141}Pr			21.5 ± 3.2	58.3 ± 4.1
^{151}Eu, ^{153}Eu		28.9 ± 3.2	61.3 ± 14.7	102 ± 18
^{165}Ho		35.6 ± 4.3	92.2 ± 27.6	150 ± 20
^{181}Ta	4.14 ± 0.36	45.4 ± 3.7	65.0 ± 5.5	146 ± 12
^{197}Au		44.5 ± 3.6	68.4 ± 13.5	160 ± 15
^{206}Pb		<34.3		238 ± 29
^{208}Pb		22.6 ± 11.3		280 ± 31
^{209}Bi		36.1 ± 12.0		226 ± 27

U.S. DEPARTMENT OF COMMERCE
NATIONAL BUREAU OF STANDARDS

REF. R. Bergère, H. Beil and A. Veyssière
Nucl. Phys. A121, 463 (1968)

ELEM. SYM.	A	Z
La	139	57

METHOD

REF. NO.	
68 Be 5	egf

REACTION		RESULT	EXCITATION ENERGY	SOURCE TYPE	SOURCE RANGE	DETECTOR TYPE	DETECTOR RANGE	ANGLE
G,N	98	ABX	THR-30	D	7-30	MOD-I		4PI
G,2N	99	ABX	THR-30					
G,3N	iact	ABX	THR-30					

98+

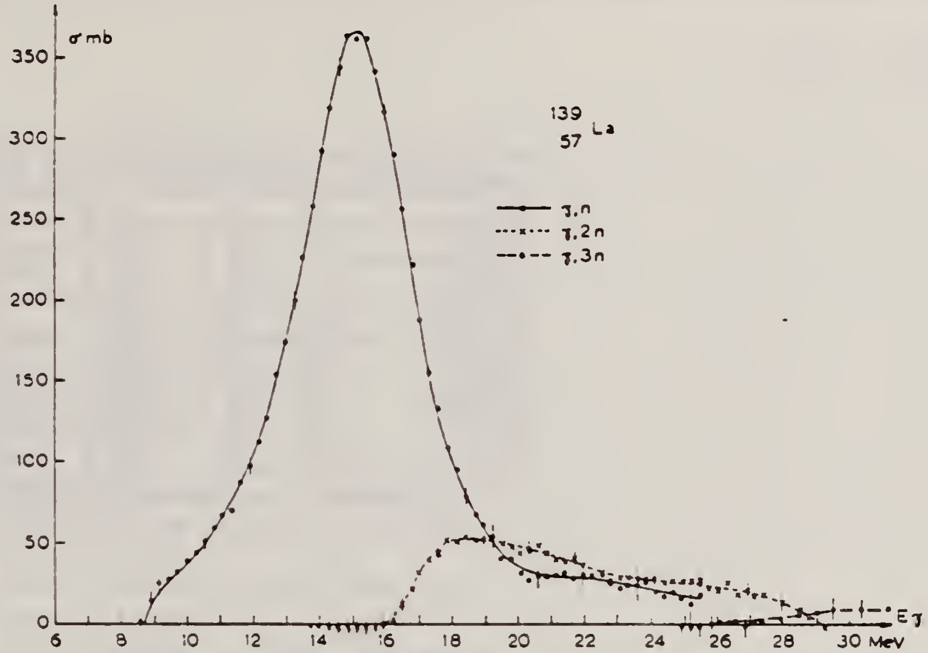

Fig. 9. Partial photonuclear cross sections $\sigma(\gamma, n)$, $\sigma(\gamma, 2n)$ and $\sigma(\gamma, 3n)$ of $^{139}_{57}$La.

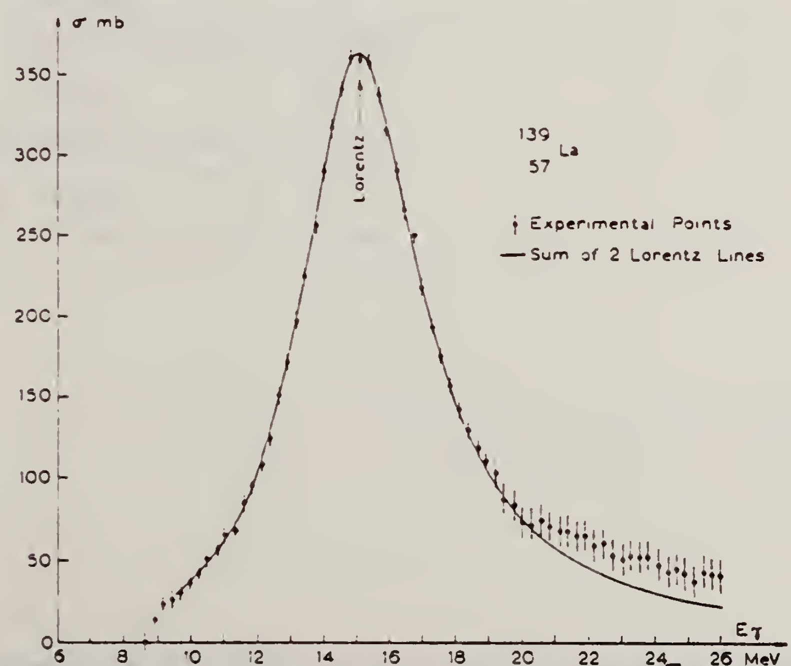

Fig. 10. Totalcross section data showing a one Lorentz line fit for a $^{139}_{57}$La target.

REF.	ELEM. SYM.	A	Z
J. W. Jury, J. S. Hewitt, and K. G. McNeill Can. J. Phys. 46, 1823 (1968)	La	139	57

METHOD	REF. NO.	
	68 Ju 1	EGF

REACTION	RESULT	EXCITATION ENERGY	SOURCE TYPE	SOURCE RANGE	DETECTOR TYPE	DETECTOR RANGE	ANGLE
G,N	NOX	THR-27	C	27	THR	5-	DST

$$W(\theta) = a_o + a_1 P_1 + a_2 P_2$$

TABLE I

Target element	Z	Energy	a_0*	a_1/a_0	a_2/a_0
Vanadium	23	32	640 ± 50	0.11 ± 0.10	−0.09 ± 0.11
Chromium	24	22	365 ± 39	0.02 ± 0.08	0.00 ± 0.10
Manganese	25	22	450 ± 33	0.07 ± 0.05	−0.11 ± 0.06
Bromine	35	27	874 ± 54	0.05 ± 0.06	−0.15 ± 0.08
Molybdenum	42	22	610 ± 60	0.09 ± 0.05	−0.35 ± 0.06
Ruthenium	44	27	1100 ± 25	0.12 ± 0.02	−0.29 ± 0.03
Rhodium	45	27	1270 ± 47	0.06 ± 0.03	−0.14 ± 0.03
Palladium	46	27	1350 ± 29	0.26 ± 0.02	−0.12 ± 0.02
Antimony	51	27	2140 ± 62	0.04 ± 0.08	−0.25 ± 0.11
Lanthanum	57	27	1940 ± 70	0.12 ± 0.10	−0.52 ± 0.14
Praseodymium	59	30	1800 ± 58	0.20 ± 0.08	−0.40 ± 0.09
Platinum	78	27	2600 ± 52	0.17 ± 0.02	−0.15 ± 0.03
Lead	82	22	2274 ± 59	0.08 ± 0.08	−0.46 ± 0.09

*The yield per mole per 100 r was normalized to a yield of 2274 for the lead sample at the same energy.

REF.	ELEM. SYM.	A	Z
R. B. Begzhanov and S. M. Akhrarov ZhETF Pis. Red. 10, 39 (1969) JETP Letters 10, 26 (1969)	La	139	57

METHOD	REF. NO.	
	69 Be 7	hmg

REACTION	RESULT	EXCITATION ENERGY	SOURCE TYPE	SOURCE RANGE	DETECTOR TYPE	DETECTOR RANGE	ANGLE
G,G	LFT	6.0	D	6.0	D		DST
		(6.413)		(6.413)			(90,135)

6.413 MEV

Self-Absorption.

Results of determination of the resonance-level parameters

Source-scatterer	E_γ, MeV	$\langle\sigma_{pp}\rangle$, mb	Γ_{γ_0}, eV	D, keV	Reference
Pb → Zn^{64}	7.38	33±4.5	0.58±0.12	53.70±10.13	This work
Ti → Mo^{96}	6.413	11.2 ±1.4	0.11±0.02	8.68± 1.57	"
Ti → La^{139}	6.413	16.04±2.10	0.28±0.05	8.03± 1.42	"
Ti → Bi^{209}	7.15	1200 ±230	0.32 ±0.07	1.84± 0.40	"
	6.996	1560	–	–	[1]
	7.15	2600 ±800	0.42±0.14	–	[5]
Ti → Cu^{65}	6.07	423 ±108	0.34±0.06	99.1±17.4	This work
	6.07	440 ±130	0.36 ±0.07		[5]
Ti → Cu^{63}	6.07	215 ± 71	0.18 ±0.04	57.14±12.70	This work
	6.07	200 ± 50	0.16± 0.03	–	[6]
Cr → Cu^{63}	8.50	22 ± 7	0.25±0.08	130 ±40	This work
	8.499	35	75	–	[1]
	8.50	19 ± 6	0.28±0.09	–	[6]
Cr → Cu^{65}	8.50	36 ± 9	0.47±0.10	21.36 ±4.54	This work
	8.499	80	10.5	–	[1]
	8.50	42 ±13	0.94±0.29	–	[6]
Cu → Sn^{117}	7.01	1150 ±240	0.15±0.04	0.44 ±0.12	This work
	7.01	1000	–	–	[1]
	7.01	1200 ±400	0.3 ±0.3	–	[5]
Hg → Mo^{96}	6.44	201 ±37	0.12 ±0.04	0.23 ±3.07	This work

REF.

K. Shoda, M. Sugawara, T. Saito & H. Miyase
PICNS-69 Proceedings of the Conference on Nuclear Isospin. Asilomar-Pacific Grove, California 1969 (Academic Press, New York & London 1969) p.137.

ELEM. SYM.	A	Z
La	139	57

METHOD

REF. NO.

69 Sh 8 egf

REACTION	RESULT	EXCITATION ENERGY	SOURCE TYPE	SOURCE RANGE	DETECTOR TYPE	DETECTOR RANGE	ANGLE
E,P	SPC	11-22	D	30	MAG-D		UKN

UKN=UKNOWN

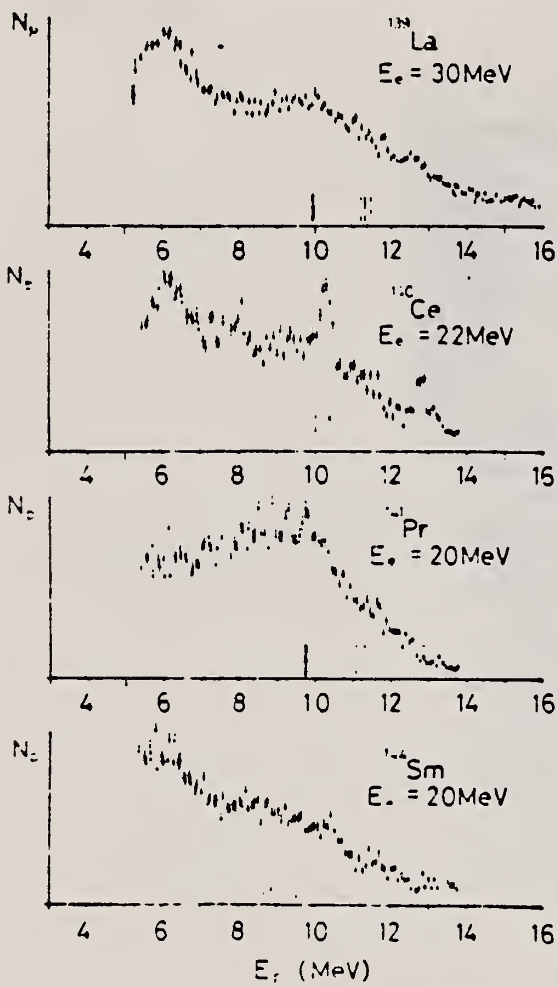

Fig. 1. Energy distributions of photoprotons. Vertical broken lines and solid lines indicate the position of p_0 corresponding to the ground IAS and electric dipole IAS (2).

REF. R. Moreh, S. Shlomo, and A. Wolf
Phys. Rev. C2, 1144 (1970)

ELEM. SYM.	A	Z
La	139	57

METHOD

REF. NO.	
70 Mo 2	hmg

REACTION	RESULT	EXCITATION ENERGY	SOURCE TYPE	SOURCE RANGE	DETECTOR TYPE	DETECTOR RANGE	ANGLE
G,G	ABX	6	D	6	SCD-D		DST
		(6.018)		(6.018)			

6 = 6.018, LFT

TABLE III. Summary of the results of spins, parities, and total widths of resonance levels excited by γ rays obtained from neutron capture in iron. Parities in parantheses are uncertain.

Isotope	Energy (MeV)	$\delta = \lvert E_\gamma - E_0 \rvert$ (eV)	$J^\pi{}_0$	$J^\pi{}_r$	Transition	Γ_0/Γ_γ (±8%)	Γ_γ (10^{-3} eV)
^{50}Cr	8.888	18 ± 1	0^+	1	···	0.90	750 ± 200
^{62}Ni	7.646	14 ± 1	0^+	1^-	$E1$	0.64	480 ± 50
^{74}Ge	6.018	4.5 ± 0.5	0^+	1^-	$E1$	0.19	120 ± 15
^{75}As	7.646	7.4 ± 0.3	$3/2^-$	$1/2^{(+)}$	···	0.11	360 ± 100
^{109}Ag	7.632	9 ± 1	$1/2^-$	3/2	···	0.7	2 ± 1
^{112}Cd	7.632	4.8 ± 0.4	0^+	1^-	$E1$	0.55	86 ± 15
^{139}La	6.018	8.2 ± 0.6	$7/2^+$	$7/2^-$	$E1$	0.50	51^{+14}_{-9}
^{141}Pr	7.632	$11.4^{+0.3}_{-0.9}$	$5/2^+$	$5/2^+$	$M1$	0.46	72^{+24}_{-9}
^{205}Tl	7.646	9.3 ± 0.3	$1/2^+$	$1/2^{(-)}$	···	0.58	980 ± 90
^{208}Pb	7.279	7.1 ± 0.3	0^+	1^+	$M1$	1.00	780 ± 60

TABLE IV. Effective elastic scattering cross section $\langle\sigma_r\rangle = \sigma_0^m(\Gamma_0/\Gamma_\gamma)\Psi(x_0,t_0)$, where δ, J, Γ_0, Γ_γ were taken from Table III. The temperature of the scatterer was 300°K, while that of the iron γ source was 640°K.

Target	Resonance energy (MeV)	$\langle\sigma_r\rangle$ (mb)
^{50}Cr	8.888	905
^{62}Ni	7.646	569
^{74}Ge	6.018	61
^{75}As	7.646	4.4
^{109}Ag	7.632	3.5
^{112}Cd	7.632	198
^{139}La	6.018	39
^{141}Pr	7.632	20
^{205}Tl	7.646	574
^{208}Pb	7.279	5560

REF.	ELEM. SYM.	A	Z
R. Moreh and A. Nof Phys. Rev. C2, 1938 (1970)	La	139	57

METHOD	REF. NO.	
[Page 1 of 2]	70 Mo 3	hmg

REACTION	RESULT	EXCITATION ENERGY	SOURCE		DETECTOR		ANGLE
			TYPE	RANGE	TYPE	RANGE	
G,G	LFT	6	D	6	NAI-D	0-8	DST
		(6.018,6.418)	(6.018,6.418)				

J-PI; 6.018, 6.418

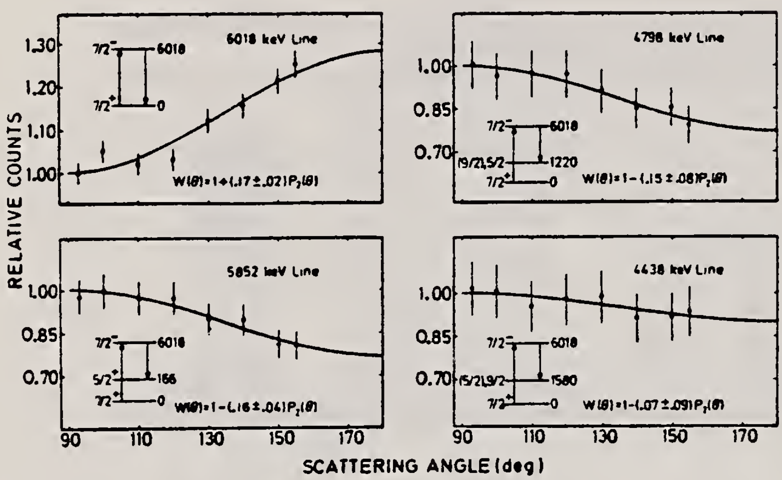

FIG. 4. Angular distribution of some intense γ lines scattered by ^{139}La using a γ source obtained from the Fe(n,γ) reaction; a 20-cc Ge(Li) detector was used. The solid lines have the form $W(\theta)=1+AP_2(\cos\theta)$ and are least-squares fits to the experimental distributions. In each case the corresponding γ-γ cascade is indicated.

The values of the parameters which best fitted all experiments were

6018 keV: $\Gamma_\gamma = 0.051^{+0.014}_{-0.006}$ eV, $\Gamma_0/\Gamma_\gamma = 0.5$,
$\langle\sigma_r\rangle = 39$ mb, $\delta = 8.2 \pm 0.6$ eV;

6418 keV: $\Gamma_\gamma = 0.081^{+0.013}_{-0.007}$ eV, $\Gamma_0/\Gamma_\gamma = 0.78$,
$\langle\sigma_r\rangle = 142$ mb, $\delta = 9.5 \pm 0.5$ eV.

The values of $\langle\sigma_r\rangle$ are at a γ-source temperature of 380°C and a target temperature of 25°C.

[over]

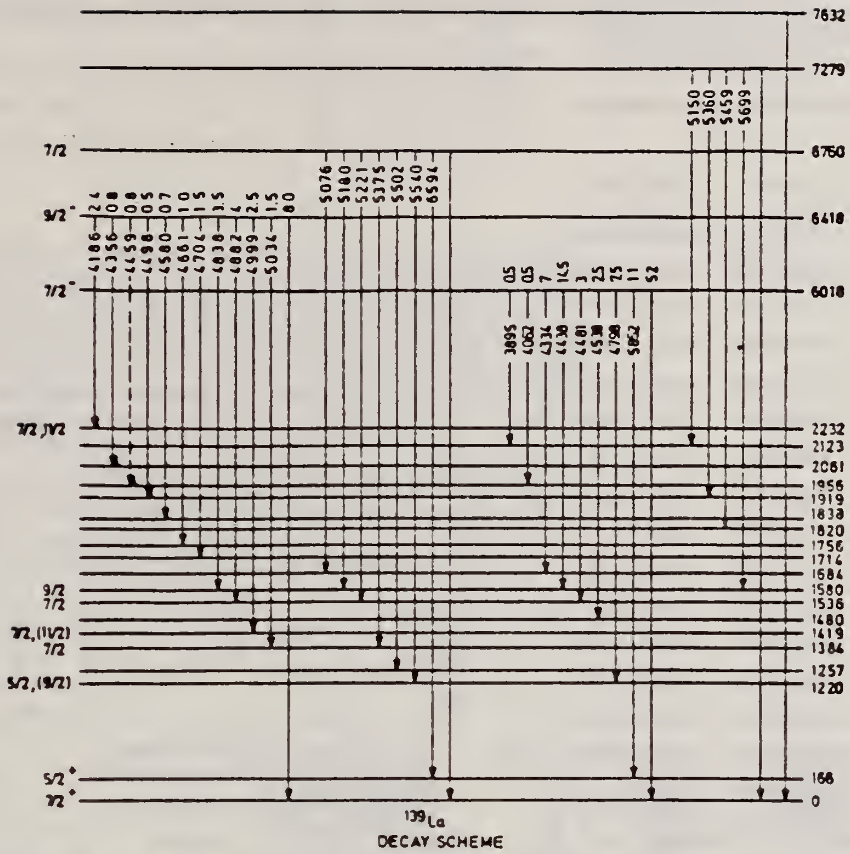

FIG. 3. Decay scheme of five resonance levels of ^{139}La showing branching ratios for only two strongly excited resonances where most of the inelastically scattered lines are believed to have been detected. Spin and parities for some levels assigned in the present work, are given. Parentheses and broken lines indicate uncertainties.

REF. R. Moreh and A. Nof
Phys. Rev. C2, 1938 (1970)

ELEM. SYM.	A	Z
La	139	57

METHOD

REF. NO.	
70 Mo 3	hmg

SOURCE		DETECTOR		ANGLE
TYPE	RANGE	TYPE	RANGE	

TABLE V. Most probable spins and parities of levels in ^{139}La as found in the present work. Also listed are the corresponding γ-line energies, the experimental angular-distribution coefficients A, and the $M2/E1$ mixing amplitudes x. The values of x are given for more than one possible spin value. The 1580-keV level was populated by more than one resonance. Parentheses indicate uncertainties.

Level energy (keV)	Spin and parity	γ-line energy (keV)	$A+\Delta A$	x $(M2/E1)$[a]
6760	$\frac{7}{2}^{(-)}$	6594	-0.15 ± 0.04	-0.013 ± 0.056
6418	$\frac{9}{2}^{-}$	6418	0.093 ± 0.004	-0.001 ± 0.004
6018	$\frac{7}{2}^{-}$	6018	0.17 ± 0.02	-0.01 ± 0.03
166	$\frac{5}{2}^{+}$	5852	-0.16 ± 0.04	-0.02 ± 0.06
1220	$\frac{5}{2}$	4798	-0.15 ± 0.08	-0.03 ± 0.08
1220	$(\frac{9}{2})$	4798	-0.15 ± 0.08	0.15 ± 0.10
1384	$\frac{7}{2}$	5034	0.04 ± 0.10	0.10 ± 0.18
1419	$\frac{7}{2}$	4999	0.06 ± 0.06	0.06 ± 0.12
1419	$(\frac{11}{2})$	4999	0.06 ± 0.06	0.02 ± 0.14
1536	$\frac{7}{2}$	4882	0.11 ± 0.04	-0.03 ± 0.08
1580	$\frac{9}{2}$	4838	-0.11 ± 0.04	$-0.09^{+0.29}_{-0.19}$
1580	$\frac{9}{2}$	4438	-0.07 ± 0.09	0.005 ± 0.115
1580	$\frac{9}{2}$	5180	-0.09 ± 0.11	0.03 ± 0.18
1580	$(\frac{5}{2})$	5180	-0.09 ± 0.11	0.07 ± 0.14
2232	$\frac{7}{2}$	4186	0.06 ± 0.10	0.07 ± 0.18
2232	$\frac{11}{2}$	4186	0.06 ± 0.10	0.01 ± 0.23

[a]Here it was tacitly assumed that all transitions are predominantly $E1$.

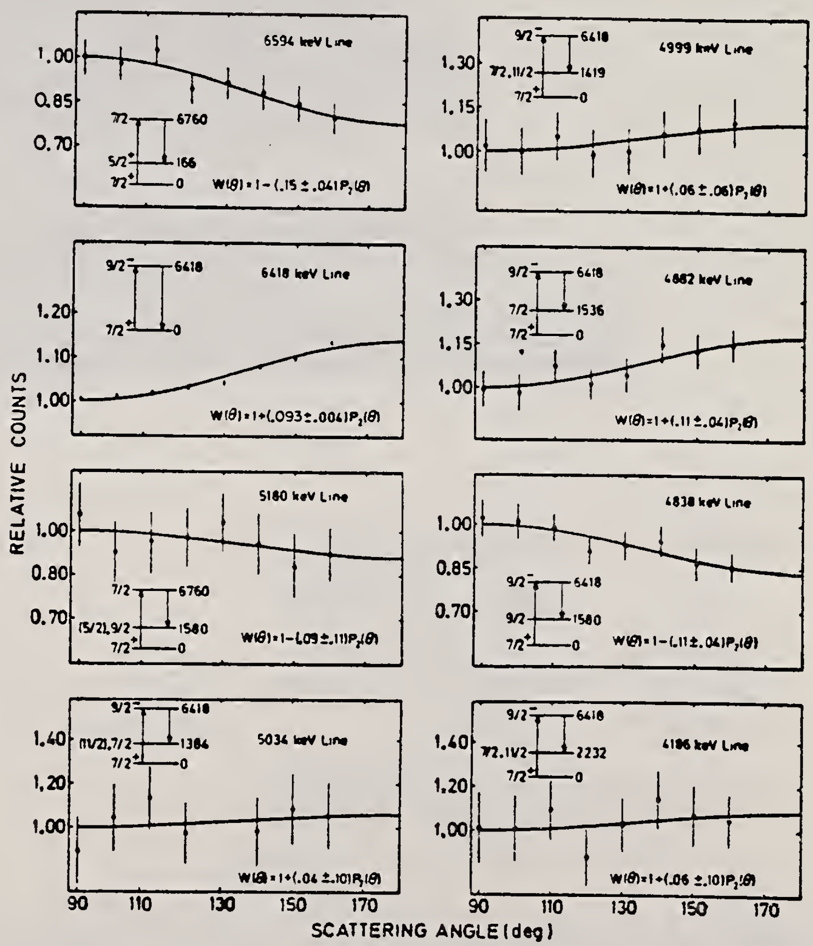

FIG. 5. Angular distributions of some intense γ lines scattered by ^{139}La using a γ source obtained from the Ti-(n,γ) reaction. See caption to Fig. 4.

REF.	H. Szichman, Y. Schlesinger, G. Ben-David, D. Pavel Nucl. Phys. A148, 369 (1970)	ELEM. SYM.	A	Z
		La	139	57
METHOD		REF. NO.		
		70 Sz 1		egf

REACTION	RESULT	EXCITATION ENERGY	SOURCE TYPE	SOURCE RANGE	DETECTOR TYPE	DETECTOR RANGE	ANGLE
G,G	LFT	6-9	D	6-9	SCD-D	4-9	DST

6 LEVELS

Abstract: Nuclear resonant scattering of photons from several (n, γ) reactions was used to study bound nuclear levels in the 6–9 MeV region in ^{139}La. The results obtained in the de-excitation of six resonant levels at energies 6115, 6418, 6760, 7637, 8527 and 8582 keV are presented. From the angular distribution of the elastically scattered photons, a spin of $\frac{5}{2}$ was deduced for the 6115 and 6418 keV levels. On the basis of the angular distribution of the inelastically scattered photons the following spin assignments were made for four of the low-lying levels: 1219($\frac{5}{2}$), 1421($\frac{7}{2}$ or $\frac{11}{2}$), 1687($\frac{3}{2}$) and 1770($\frac{5}{2}$). Hitherto unknown levels were found at 1894 and 2159 keV. Total radiation widths were measured and found to be 79 ± 17 meV for the 6115 keV resonant level, 45 ± 9 meV for the 6418 keV level and > 60 meV for the 6760 keV level.

E | NUCLEAR REACTIONS ^{139}La(γ,γ'), E = 6115, 6418, 6760, 7637, 8527 and 8582 keV; measured E_γ, E'_γ, $\sigma(E'_\gamma, \theta)$. ^{139}La deduced levels, J, total and partial radiation widths. Natural target, Ge(Li) detector.

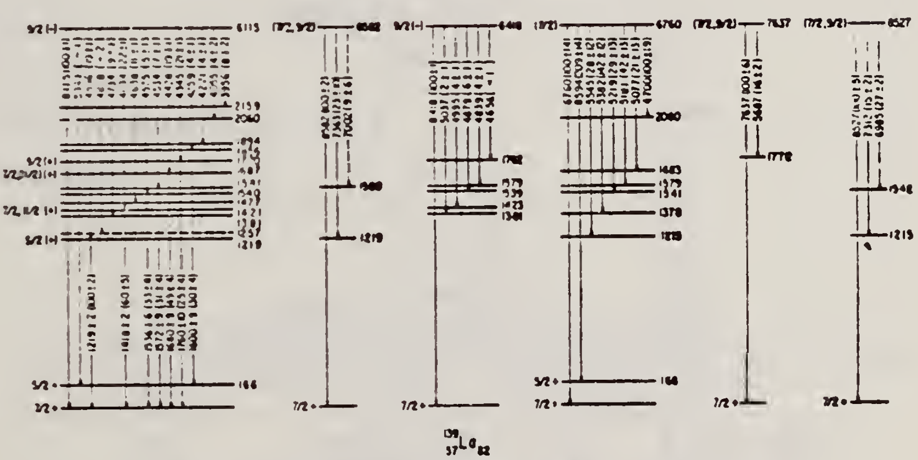

Fig. 3. Decay scheme for the observed resonant levels of ^{139}La.

REF.	ELEM. SYM.	A	Z
H. Beil, R. Bergere, P. Carlos, A. Lepretre, A. Veyssiere and A. Parlag Nucl. Phys. A172, 426 (1971)	La	139	57
METHOD	REF. NO. 71 Be 4		egf

REACTION	RESULT	EXCITATION ENERGY	SOURCE TYPE	SOURCE RANGE	DETECTOR TYPE	DETECTOR RANGE	ANGLE
G,SN 368+	ABX	8-18	D	8-18	MOD-I		4PI
							366+

TABLE 1

Lorentz line parameters corresponding to fits of total photoneutron cross sections presented in fig. 1

	$_{56}$Ba	$^{139}_{57}$La	$_{58}$Ce	$^{141}_{59}$Pr	$_{60}$Nd	$^{141}_{59}$Pr ^{a})
σ_1 (mb)	356 ±15	340 ±15	360 ±15	350 ±15	315 ±15	320 ±20
E_1 (MeV)	15.3 ± 0.1	15.2 ± 0.1	15.0 ± 0.10	15.1 ± 0.1	14.9 ± 0.1	15.16± 0.08
Γ_1 (MeV)	4.70± 0.15	4.45± 0.05	4.35± 0.05	4.26± 0.05	4.90± 0.05	4.49±0.05
$\frac{1}{2}\pi\sigma_1\Gamma_1$ (MeV · b)	2.6 ± 0.15	2.35± 0.13	2.42± 0.15	2.35± 0.13	2.43± 0.13	2.42± 0.17
$\dfrac{\frac{1}{2}\pi\sigma_1\Gamma_1}{0.06NZA^{-1}}$	1.30± 0.08	1.16± 0.08	1.19± 0.08	1.14± 0.08	1.15± 0.08	

^{a}) Lorentz line parameters given in ref. [10]) for ^{141}Pr.

[10] R. L. Bramblett, J.T. Caldwell, B.L. Berman, R. R. Harvey and S.C. Fultz, Phys. Rev. 148, 1198 (1966).

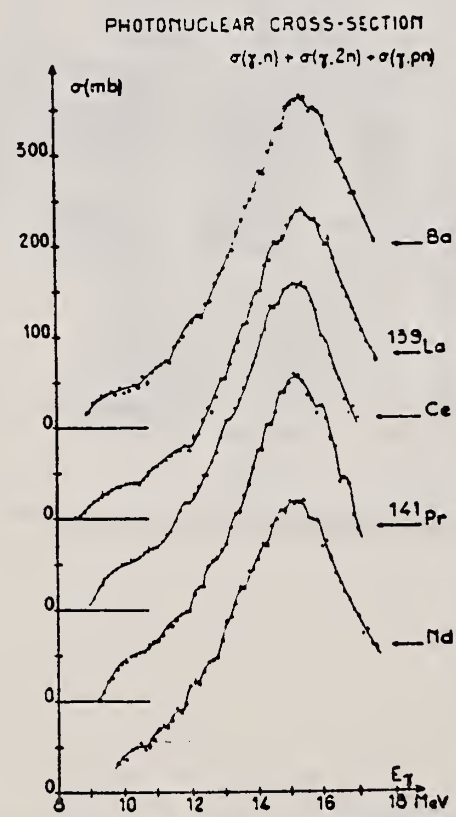

Fig. 1. Total photoneutron cross sections for Ba, ^{139}La, Ce, ^{141}Pr and Nd as a function of incident photon energy E.

REF.	T. Methasiri and S. A. E. Johansson Nucl. Phys. A167, 97 (1971)	ELEM. SYM.	A	Z
		La	139	57
METHOD		REF. NO.		
		71 Me 1		egf

REACTION	RESULT	EXCITATION ENERGY	SOURCE TYPE	SOURCE RANGE	DETECTOR TYPE	DETECTOR RANGE	ANGLE
G,F	ABY	THR-900	C	300-900	FRG-I		4PI

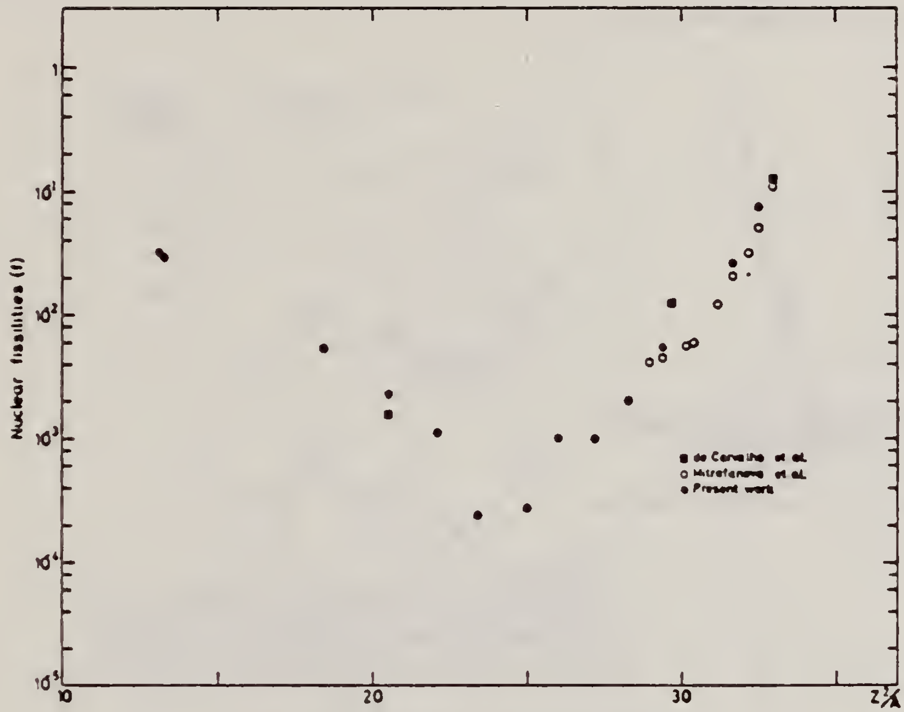

Fig. 2. Nuclear fissilities as a function of Z^2/A.

TABLE 1

The constant fission cross sections above the threshold

Element	σ_f (cm²)	Element	σ_f (cm²)
Pb	$(5.0\pm0.2)\times10^{-27}$	La	$(1.1\pm0.1)\times10^{-29}$
Au	$(1.7\pm0.1)\times10^{-27}$	Sn	$(4.3\pm1.1)\times10^{-29}$
Ta	$(3.3\pm0.2)\times10^{-28}$	Ag	$(8.4\pm2.0)\times10^{-29}$
Yb	$(1.2\pm0.2)\times10^{-28}$	Mo	$(1.7\pm0.4)\times10^{-28}$
Ho	$(5.5\pm0.3)\times10^{-29}$	Cu	$(6.6\pm1.2)\times10^{-28}$
Gd	$(5.3\pm0.8)\times10^{-29}$	Ni	$(5.8\pm0.1)\times10^{-28}$
Nd	$(1.3\pm0.2)\times10^{-29}$		

[over]

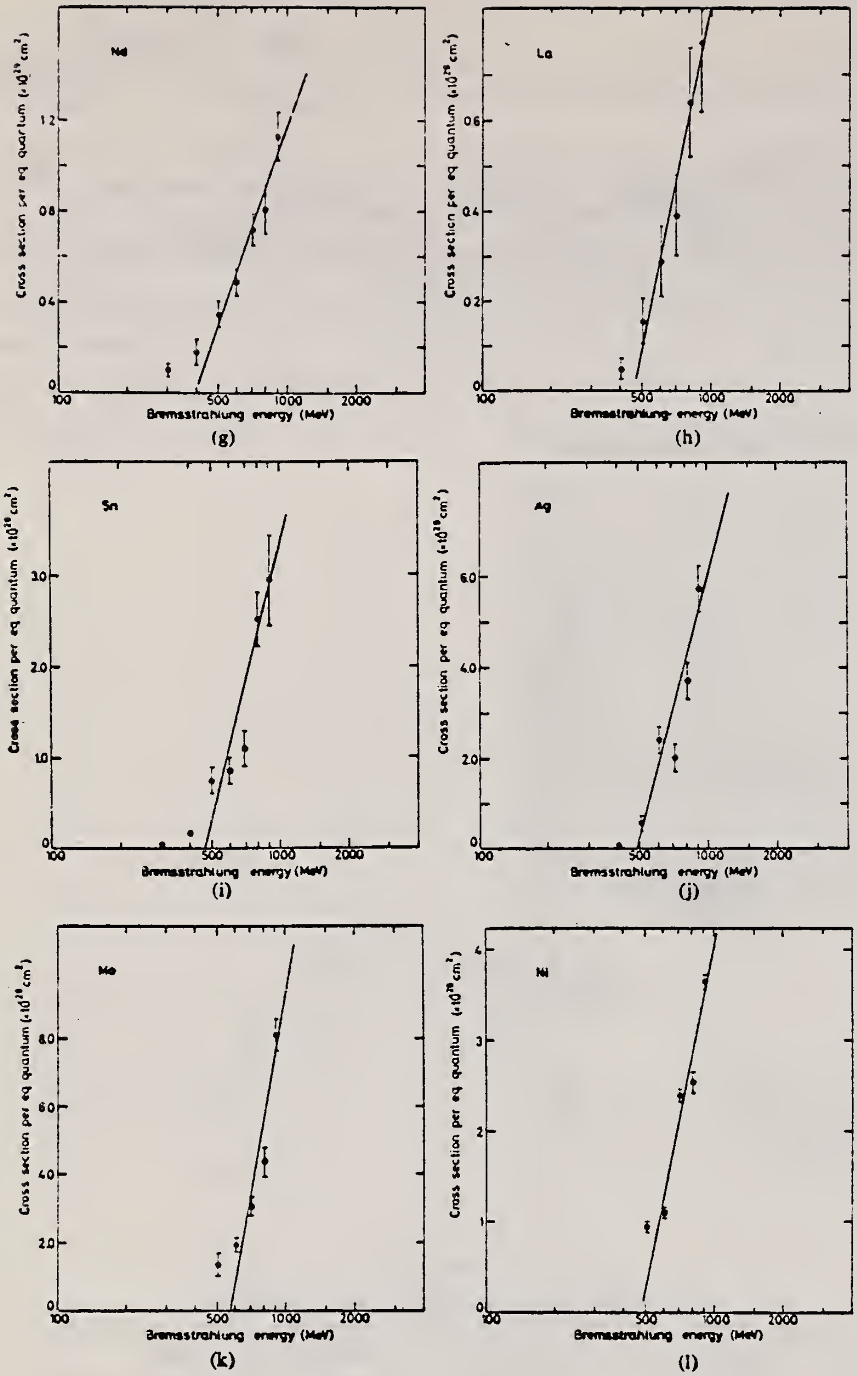

Fig. 1. Cross sections per equivalent quantum $\sigma_q(\overline{E})$ as a function of log $\overline{E}$.

REF.

R. Pitthan and Th. Walcher
Phys. Letters 36B, 563 (1971)

ELEM. SYM.	A	Z
La	139	57

METHOD

REF. NO.	
71 Pi 1	egf

REACTION	RESULT	EXCITATION ENERGY	SOURCE		DETECTOR		ANGLE
			TYPE	RANGE	TYPE	RANGE	
E,E/	SPC	4-18		50,65	MAG-D		DST

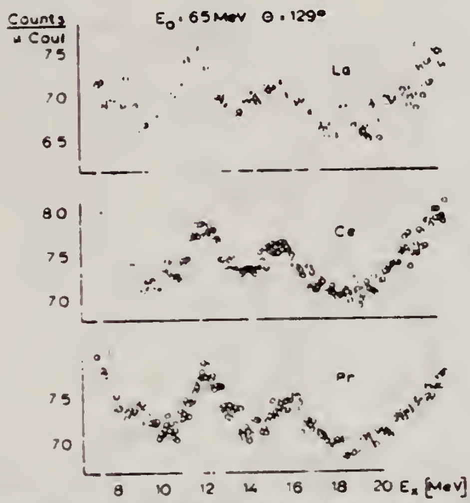

Fig. 2. Spectra of electrons scattered inelastically from La, Ce and Pr targets at the same primary energy and the same laboratory scattering angle. No background has been subtracted. Note the suppressed zeros of the ordinate scales.

REF.	ELEM. SYM.	A	Z
T.K. Deague and R.J.J. Stewart Nucl. Phys. A191, 305 (1972)	La	139	57

METHOD	REF. NO.	
	72 De 3	egf

REACTION	RESULT	EXCITATION ENERGY	SOURCE		DETECTOR		ANGLE
			TYPE	RANGE	TYPE	RANGE	
G,XN	ABX	9-24	C	8-24	BF3-I		4PI

559

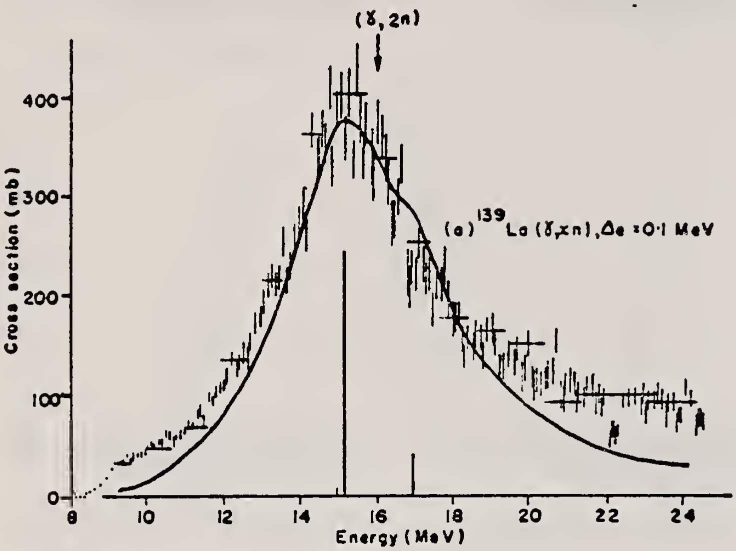

TABLE I

The integrated ^{139}La(γ, xn) and ^{141}Pr(γ, xn) cross sections and their minus-first and minus-second moments, compared with the appropriate sum rules

Nucleus	Ref.	σ_0 (b · MeV)	$0.06\ NZA^{-1}$	σ_{-1} (mb)	$0.16\ A^{\frac{4}{3}}$	σ_{-2} (mb · MeV^{-1})	$0.00225\ A^{\frac{5}{3}}$
^{139}La	present work	2.51 ± 0.5	2.02	158 ± 30	115	10.4 ± 2	8.4
	ref. [20]	2.20 ± 0.3		141 ± 12		9.4 ± 0.7	
^{141}Pr	present work	1.84 ± 0.3	2.06	121 ± 20	117	8.1 ± 1.3	8.6
	ref. [10]	1.83 ± 0.16					

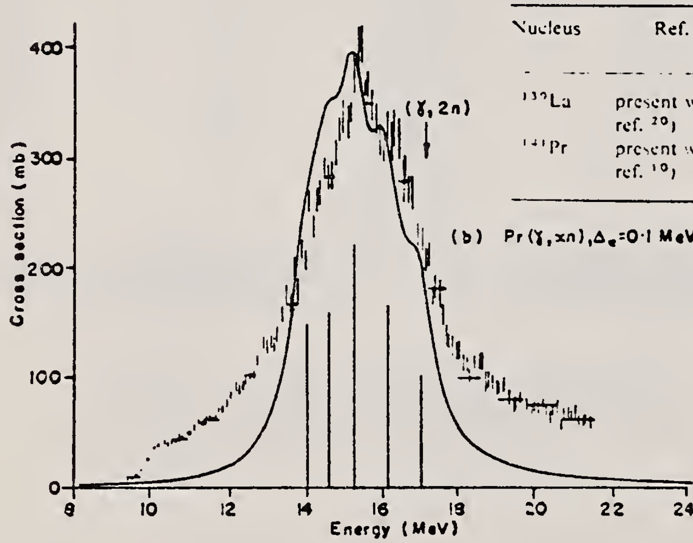

Fig. 1. (a) The ^{139}La(γ, xn) cross section, obtained by VBPL unfolding from yield data measured in 0.1 MeV steps. Also shown is the DCM dipole spectrum for ^{142}Nd, and a fit to it of Lorentz line shapes with widths 4.0 MeV (solid line). (b) The ^{141}Pr(γ, xn) cross section, obtained by VBPL unfolding from yield data measured in 0.1 MeV steps. Also shown is the DCM dipole spectrum for ^{146}Nd, and a fit to it of Lorentz line shapes with widths 1.0 MeV (solid line).

REF.	ELEM. SYM.	A	Z
B.W. Thomas, D.M. Crawford and H. H. Thies Nucl. Phys. A196, 89 (1972)	La	139	57

METHOD	REF. NO.	
	72 Th 2	egf

REACTION	RESULT	EXCITATION ENERGY	SOURCE		DETECTOR		ANGLE
			TYPE	RANGE	TYPE	RANGE	
G,XN	RLX	9-17	C	8-16	BF3-I		4PI

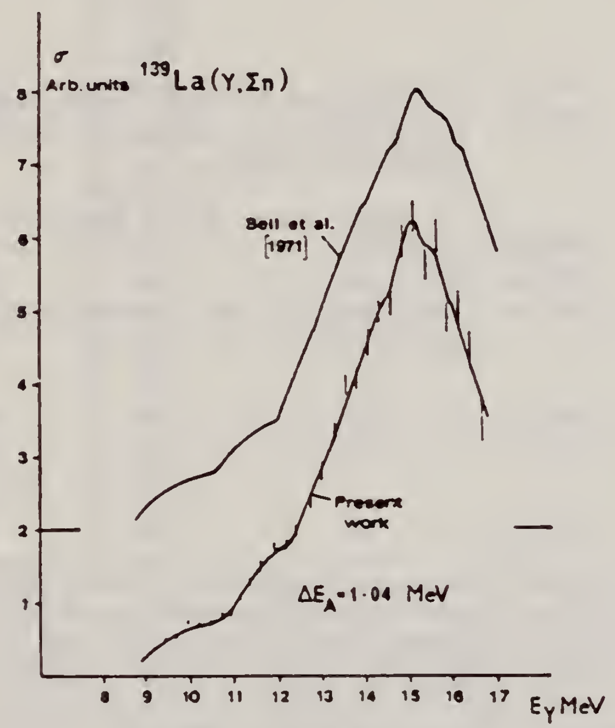

Fig. 7. Cross section for ^{139}La(γ, Σn).

REF.	ELEM. SYM.	A	Z
R.F. Barrett, J.R. Birkelund, B.J. Thomas, K.S. Lam, and H.H. Thies Nucl. Phys. A210, 355 (1973)	La	139	57

METHOD	REF. NO.	
	73 Ba 20	egf

REACTION	RESULT	EXCITATION ENERGY	SOURCE TYPE	SOURCE RANGE	DETECTOR TYPE	DETECTOR RANGE	ANGLE
G,N	NOX	THR- 27	C	10- 27	BF3-I		4PI

MEAN NEUT ENERGY

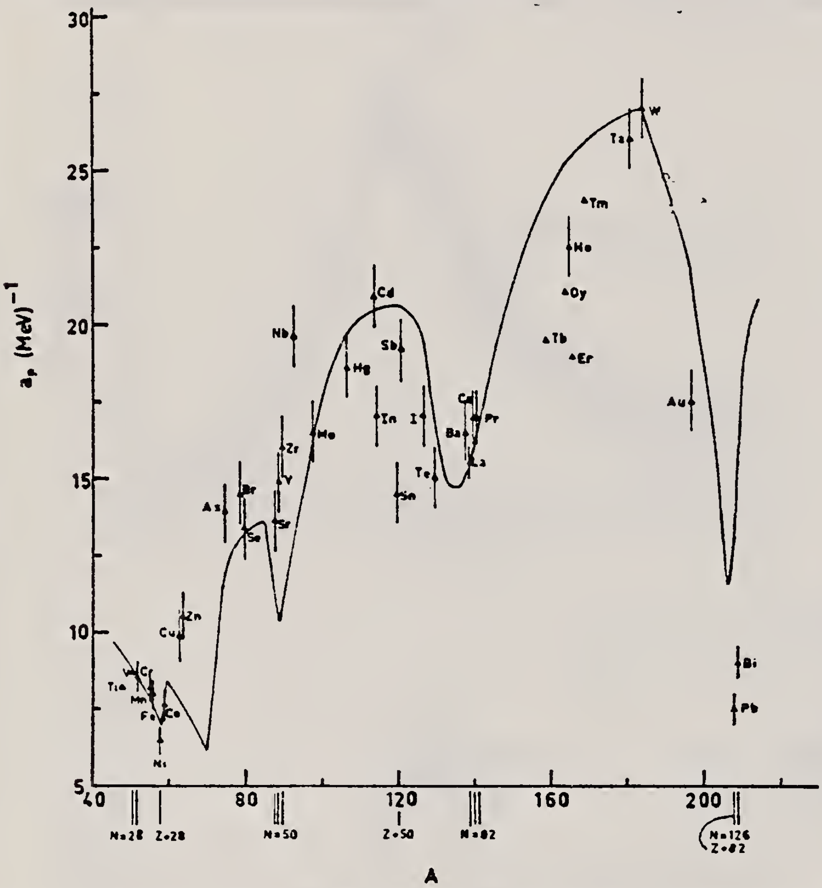

Fig. 12. Experimental values of the level density parameter a_p (Fermi gas formula plus pairing correction) versus atomic number A. The continuous curve is a least-squares fit to the data of a theoretical calculation from Newton [15]).

1
H. Baba and S. Baba, Japan Atomic Energy Research Institute report JAERI-1183 (1969).
2
H. Baba, Nucl. Phys. A159, 625 (1970).
15
T.D. Newton, Can. J. Phys. 34, 804 (1956).

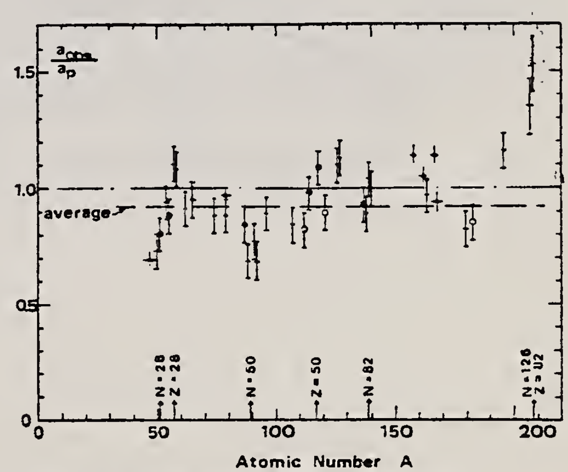

Fig. 15. Ratio a_{obs}/a_p versus atomic number A. Here a_{obs} is the level density parameter taken from the neutron resonance work of refs. [1,2]), and a_p is the level density parameter derived from the present (γ, n) work. Filled circles represent points where nuclei in the neutron resonance and in the (γ, n) experiment were the same. Open circles represent points where the respective nuclei were approximately matched. Triangles represent points which are based on measurement of neutron mean energies at two bremsstrahlung energies only.

(over)

Target	N (residual nucleus) [a]		Goodness of fit [b] no p.c.	with p.c.	$\hat{E}_n(24)$ (MeV) [c]	T (MeV) [d]	a_p (MeV^{-1}) [e]	a_{obs} (MeV^{-1}) [f]	a_{obs}/a_p
Ba	75	1%		F	1.16		16.5–^{136}Ba	15.39–^{136}Ba	0.93
	77	2%							
	78	7%							
	79	8%							
	80	11%							
	81	71%							
La	80	100%	F	F	1.25	0.72	15.5–^{138}La	13.76–^{139}La	0.89
Ce	81	89%	F	G	1.24	0.70	17.0–^{139}Ce	17.8 –^{141}Ce	1.04
	83	11%							
Pr	81	100%	G	G	1.17	0.65	17.0–^{140}Pr	17.05–^{142}Pr	1.00
Tb [g]	93	100%			1.15		19.3–^{158}Tb	21.85–^{160}Tb	1.14
Dy [g]	93	2%			1.06		20.9–$^{161.5}$Dy	21.9 –^{162}Dy	1.05
	94	19%							
	95	25%							
	96	25%							
	97	28%							
Ho	97	100%	P	G	1.06	0.56	21.4–^{164}Ho	20.66–^{166}Ho	0.97
Er [g]	95	2%			1.11		19.2–^{166}Er	21.9 –^{166}Er	1.14
	97	33%							
	98	23%							
	99	27%							
	101	15%							
Tm [g]	99	100%			1.03		24.0–^{168}Tm	22.58–^{170}Tm	0.94
Ta	107	100%		G	1.00	0.49	26.0–^{180}Ta	21.2 –^{181}Ta	0.82
W	107	26%	G	F	0.98	0.50	27.0–^{183}W	23.0 –^{183}W	0.85
	108	14%							
	109	31%							
	111	28%							
Au	117	100%		G	1.19		17.5–^{196}Au	20.24–^{198}Au	1.16
Pb ($Z = 82$)	123	24%		V.P.	1.87	1.20	7.5–^{206}Pb	10.1 –^{207}Pb	1.35
	124	23%							
	125	52%							
Bi	125	100%		F	1.65	1.03	9.0–^{208}Bi	13.8 –^{210}Bi	1.53

[a]) Neutron numbers and abundances of respective residual nuclei in (γ, n) experiments.
[b]) These give an assessment of the goodness of fit of a calculated $\hat{E}_n$ versus E_0 curve to the observed data, using the Fermi gas level density formula both without and with pairing corrections.
[c]) Bremsstrahlung photoneutron mean energies $\hat{E}_n$ for peak bremsstrahlung energy E_0 = 24 MeV.
[d]) Nuclear temperature from fit with constant-temperature formula.
[e]) Level density parameter a_p derived from the present (γ, n) experiment, using a Fermi gas formula plus pairing correction, and corresponding residual nucleus (the atomic weight shown is the weighted average of atomic weights of the respective isotopes present).
[f]) As column 7, but using data on n-resonance absorption from refs. [1,2]).
[g]) Measurements of $\hat{E}_n(E_0)$ for these nuclei were made only for E_0 = 21, 23 and 24 MeV.

REF.	F.R. Buskirk, H.D. Graf, R. Pitthan, H. Theissen, O. Titze, and Th. Walcher PICNS-73, Vol.I, p.703 Asilomar	ELEM. SYM.	A	Z
		La	139	57
METHOD		REF. NO.		
		73 Bu 14		hmg

REACTION	RESULT	EXCITATION ENERGY	SOURCE TYPE	SOURCE RANGE	DETECTOR TYPE	DETECTOR RANGE	ANGLE
E,E/	SPC	2- 20	C	50,65	MAG-D		DST

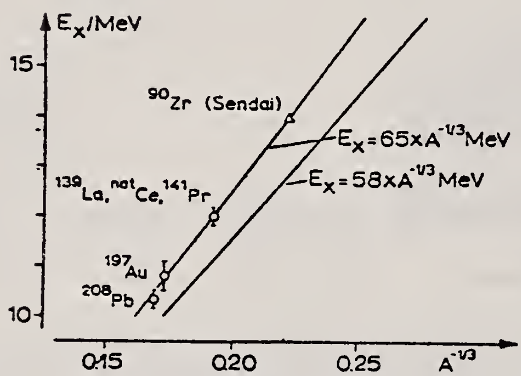

Fig. 2

The E2 resonance which is clearly visible at 10.8±0.2 MeV exhausts more than 50 % of the sum rule. Fig. 2 shows the excitation energy of this resonance as a function of $A^{-1/3}$ for the nuclei measured at Darmstadt and the Sendai result for ^{90}Zr [5]. Bohr and Mottelson [9] predicted a collective E2 resonance whose isoscalar part should depend on A through E_x=58 $A^{-1/3}$MeV. The data of Fig. 2 are consistent with E_x=65 $A^{-1/3}$MeV suggesting to identify the observed resonances with this type of E2 excitation.

REF.		ELEM. SYM.	A	Z
	Rainer Pitthan Z. Physik 260, 283 (1973)	La	139	57
METHOD		REF. NO.		
		73 Pi 3		egf

REACTION	RESULT	EXCITATION ENERGY	SOURCE		DETECTOR		ANGLE
			TYPE	RANGE	TYPE	RANGE	
E,E/	ABX	7- 21	D	50	MAG-D		165

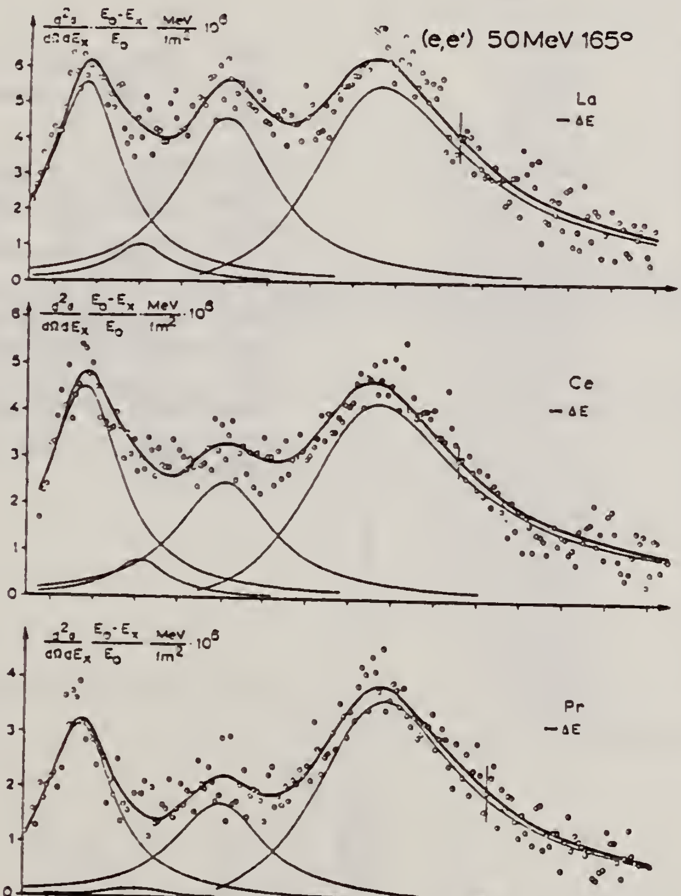

Fig. 7. Spektren von unelastisch an La, Ce und Pr gestreuten Elektronen, sonst wie Fig. 5, s. Text

REF.	ELEM. SYM.	A	Z
V. Emma, S. Lo Nigro, C. Milone Nucl. Phys. A257, 438 (1976)	La	139	57

METHOD	REF. NO.	
	76 Em 2	egf

REACTION	RESULT	EXCITATION ENERGY	SOURCE TYPE	SOURCE RANGE	DETECTOR TYPE	DETECTOR RANGE	ANGLE
G,F	ABY	THR-999	C	999	TRK-I		4PI

999 = 1 GEV

TABLE 1

Measured values of σ_q at $E = 1000$ MeV and deduced values of σ_k assumed constant from E_0 to 1000 MeV

Element	Z^2/A	σ_q (mb)	E_0 (MeV)	σ_k (mb)
Bi	32.96	12.3 ± 0.6	200	7.6 ± 0.6
Pb	32.45	5.4 ± 0.4	220	3.6 ± 0.3
Tl	32.10	4.1 ± 0.3	230	2.8 ± 0.3
Au	31.68	2.0 ± 0.15	240	1.4 ± 0.2
Pt	31.18	1.1 ± 0.08	255	$(8 \pm 0.7) \times 10^{-1}$
Re	30.21	$(3.7 \pm 0.3) \times 10^{-1}$	280	$(2.9 \pm 0.3) \times 10^{-1}$
W	29.78	$(3.5 \pm 0.3) \times 10^{-1}$	290	$(2.8 \pm 0.3) \times 10^{-1}$
Ta	29.45	$(3.3 \pm 0.3) \times 10^{-1}$	300	$(2.7 \pm 0.3) \times 10^{-1}$
Hf	29.04	$(1.7 \pm 0.2) \times 10^{-1}$	310	$(1.4 \pm 0.2) \times 10^{-1}$
Yb	28.31	$(1.3 \pm 0.1) \times 10^{-1}$	330	$(1.2 \pm 0.1) \times 10^{-1}$
Tm	28.18	$(7.5 \pm 0.8) \times 10^{-2}$	335	$(6.8 \pm 0.8) \times 10^{-2}$
Ho	27.21	$(3.6 \pm 0.4) \times 10^{-2}$	355	$(3.5 \pm 0.4) \times 10^{-2}$
Dy	26.80	$(2.6 \pm 0.3) \times 10^{-2}$	360	$(2.5 \pm 0.3) \times 10^{-2}$
Tb	26.58	$(2.5 \pm 0.3) \times 10^{-2}$	370	$(2.5 \pm 0.3) \times 10^{-2}$
Gd	26.04	$(1.6 \pm 0.2) \times 10^{-2}$	380	$(1.7 \pm 0.2) \times 10^{-2}$
Sm	25.56	$(1.3 \pm 0.2) \times 10^{-2}$	390	$(1.4 \pm 0.2) \times 10^{-2}$
Nd	24.96	$(9.2 \pm 0.9) \times 10^{-3}$	405	$(1 \pm 0.1) \times 10^{-2}$
Ce	24.00	$(8 \pm 0.9) \times 10^{-3}$	420	$(9 \pm 1) \times 10^{-3}$
La	23.39	$(8.4 \pm 0.9) \times 10^{-3}$	430	$(1 \pm 0.1) \times 10^{-3}$
Sb	21.36	$(1.2 \pm 0.2) \times 10^{-2}$	460	$(1.5 \pm 0.3) \times 10^{-2}$
Te	21.19	$(8.8 \pm 1) \times 10^{-3}$	465	$(1.2 \pm 0.2) \times 10^{-2}$
Sn	21.06	$(1.3 \pm 0.2) \times 10^{-2}$	465	$(1.7 \pm 0.3) \times 10^{-2}$
Cd	20.49	$(1.7 \pm 0.3) \times 10^{-2}$	470	$(2.2 \pm 0.4) \times 10^{-2}$
Ag	20.47	$(2 \pm 0.3) \times 10^{-2}$	470	$(2.6 \pm 0.4) \times 10^{-2}$
Zn	13.76	$(2 \pm 0.4) \times 10^{-1}$	515	$(3 \pm 0.6) \times 10^{-1}$
Cu	13.44	$(2.4 \pm 0.5) \times 10^{-1}$	515	$(3.6 \pm 0.8) \times 10^{-1}$
Ni	13.35	$(2.4 \pm 0.5) \times 10^{-1}$	510	$(3.6 \pm 0.8) \times 10^{-1}$
Fe	12.10	$(3 \pm 0.6) \times 10^{-1}$	510	$(4.4 \pm 0.9) \times 10^{-1}$

[4]A.V. Mitrofanova et al. Sov. J. Nucl. Phys. 6, 512 (1968).

[7]T. Methasiri et al., Nucl. Phys. A167, 97 (1971).

[12]J.R. Nix et al., Nucl. Phys. 81, 61 (1966).

[20]N.A. Perifilov et al., JETP (Sov. Phys.) 14, 623 (1962); Proc. Symp. on the physics & chemistry of fission, Salzburg 1965, vol. 2 (IAEA) Vienna, 1965, p.283.

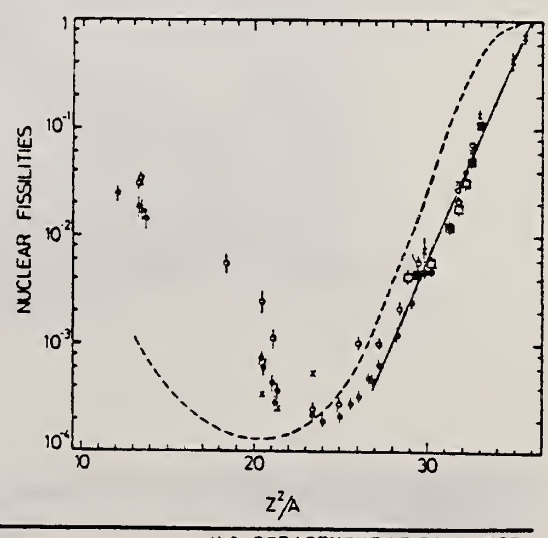

Fig. 2. Nuclear fissilities as a function of Z^2/A. Experimental points: solid circles represent our data; squares, the data from ref. [4]); open circles, the data from ref. [7]); and crosses, the data from (p,f) experiments[20]). The straight line is the best fit calculated from our data for $Z^2/A > 26$. The dashed curve is the curve VI calculated by Nix and Sassi[12]).

A. Järund and B. Forkman
Z. Physik A281, 39 (1977)

La	139	57
REF. NO. 77 Ja 2		egf

REACTION	RESULT	EXCITATION ENERGY	SOURCE TYPE	SOURCE RANGE	DETECTOR TYPE	DETECTOR RANGE	ANGLE
G,NA24	ABY	THR-999	C	400-999	ACT-I		4PI

999=1 GEV

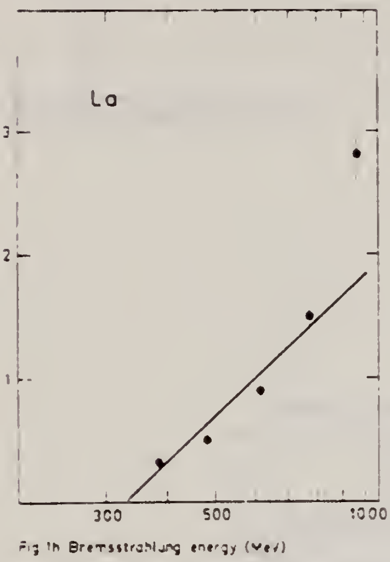

Fig. 1a–j. The measured yield as a function of bremsstrahlung end point energy. The error bars give the statistical errors in the numbers of γ-quanta detected. The solid lines are fitted to the yield points with the least-squares method. The yield from Cu (Fig. 1a) is measured in [1] and has been recalculated using the monitor curve of [5]

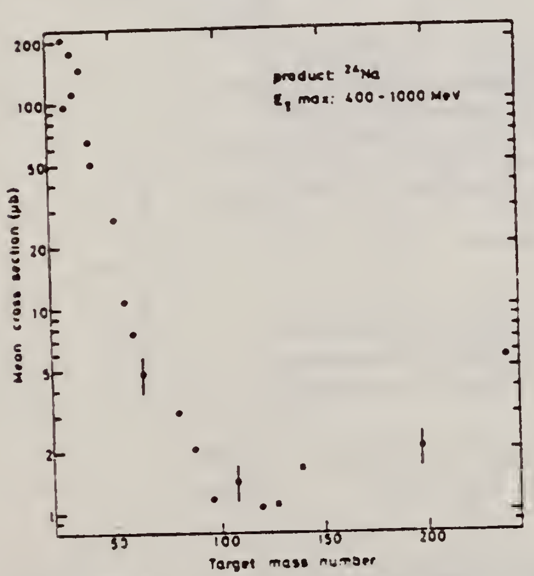

Fig. 2. The mean cross section in the energy range 400 to 1000 MeV calculated from the yields of Figure 1 in this work and of Figures 1 to [illegible]. The error is given by bars in some points

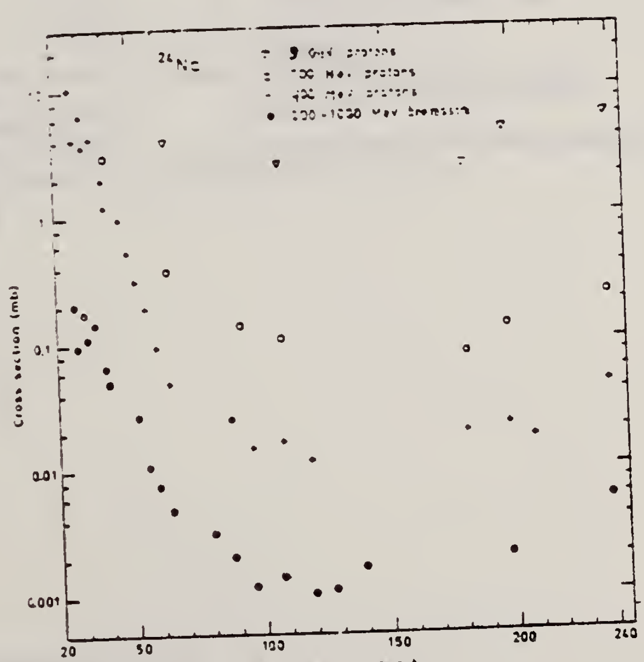

Fig. 4. Mean cross sections of the present work and of [1] (●) compared with the cross sections in proton irradiations: + 400 MeV from [4], ○ 700 MeV from [16] and an extrapolated value from [17]. ▽ 3 GeV from [18]

REF. I. Jacob, R. Moreh and A. Wolf
Nucl. Phys. A291, 1 (1977)

ELEM. SYM.	A	Z
La	139	57

METHOD

REF. NO.	
77 Ja 4	egf

REACTION	RESULT	EXCITATION ENERGY	SOURCE TYPE	SOURCE RANGE	DETECTOR TYPE	DETECTOR RANGE	ANGLE
G,MUT	LFT	7	D	7	NAI-D		0
		(7.29,7.632)		(7.29,7.632)			

7.28,7.63MeV,RES ABS

Abstract: A variable-energy γ-source is obtained by nuclear resonance scattering of neutron-capture γ-rays through various scattering angles. An energy resolution of less than 10^{-6} is obtained. Pb and Cd targets were employed to scatter the 7.279 and 7.632 MeV photons, respectively, of the neutron capture γ-rays of Fe. Variation of the angle of the resonantly scattered photons between 60°–150° permits an energy scan of ≈ 370 eV (for Pb) and ≈ 760 eV (for Cd) in any absorber. Thus nuclear energy levels in ^{139}La, Ce, Cd and ^{209}Bi absorbers were photoexcited and the corresponding values of $g\Gamma_0$ were extracted from the measured absorption curve.

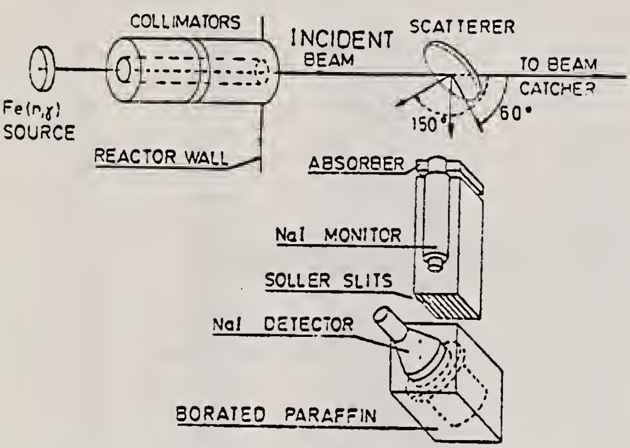

Fig. 1. Schematic diagram of the experimental arrangement.

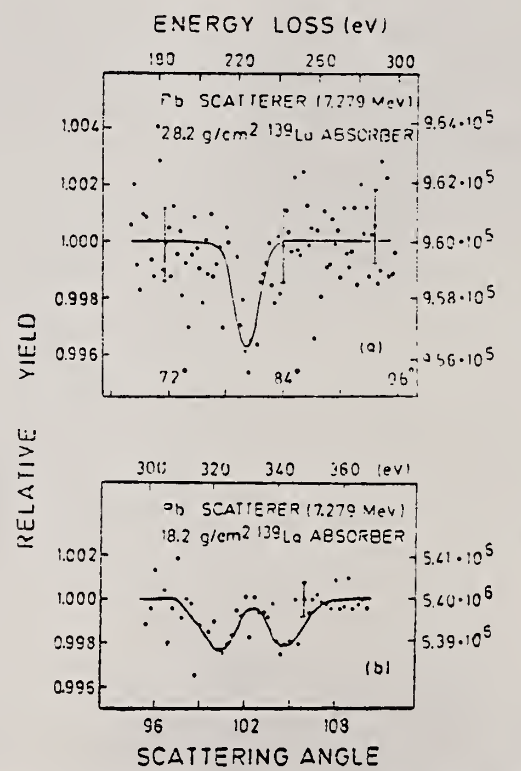

Fig. 3. (a) Portion of the normalized absorption spectrum obtained using a 28.2 g/cm² thick La absorber. (b) Another portion of the spectrum obtained with a 18.2 g/cm² thick absorber using higher statistics of ≈ 5 × 10⁶ counts/channel.

over

TABLE 2

Summary of experimental data and measured values of $g\Gamma_0$ obtained using the γ-monochromator

Isotope	Thickness (g/cm^2)	Angle of dip (deg)	ΔE [c]) (eV)	Effect (%)	$g\Gamma_0$ (meV)
^{112}Cd [a])	35	128.0	505	3.5	150 ± 20
^{139}La	28.2	80.0	225	0.40	8.0 ± 2.0
^{139}La	18.2	100.5	322	0.27	7.1 ± 1.9
^{139}La	18.2	104.8	345	0.22	5.5 ± 1.8
^{140}Ce [b])	26.5	90.0	273	1.3	25 ± 3
^{209}Bi	31.5	73.5	196	2.0	43 ± 8
^{209}Bi*	31.5	68.8	404	1.8	92 ± 12

The asterisk denotes a level at 7.632 MeV photoexcited by a Cd scatterer. All other levels are at 7.279 MeV and were photoexcited by a Pb scatterer.

[a]) The absorbing isotope was arbitrarily assumed to be ^{112}Cd.

[b]) The absorbing isotope was arbitrarily assumed to be ^{140}Ce.

[c]) Here ΔE is the energy difference between the incident γ-line and the resonance level (assuming no recoil correction in the absorbing nucleus).

REF.	J.I. Uegaki and K. Shoda Nucl. Phys. <u>A294</u>, 141 (1978)	ELEM. SYM.	A	Z
		La	139	57
METHOD		REF. NO.		
		78 Ue 1		rs

REACTION	RESULT	EXCITATION ENERGY	SOURCE TYPE	SOURCE RANGE	DETECTOR TYPE	DETECTOR RANGE	ANGLE
E,P	ABX	14- 17	D	15- 18	MAG-D		125

TABLE 1

Strength of the resonance in the (γ, p_0) and (γ, p) reactions on ^{139}La and ^{141}Pr, and the ratio of proton group 1 and proton group 2 emitted through the $f_{7/2}$ IAR

	$\int\sigma^{IAS}_{(\gamma,p_0)}dE$ (μb · MeV)	$\int\sigma^{IAS}_{(\gamma,p)}dE$ (μb · MeV)	Proton group 1 (%)	Proton group 2 (%)
^{141}Pr	44±9	240±30	40±10	60±10
^{139}La	<5	260±30	5± 5	95± 5

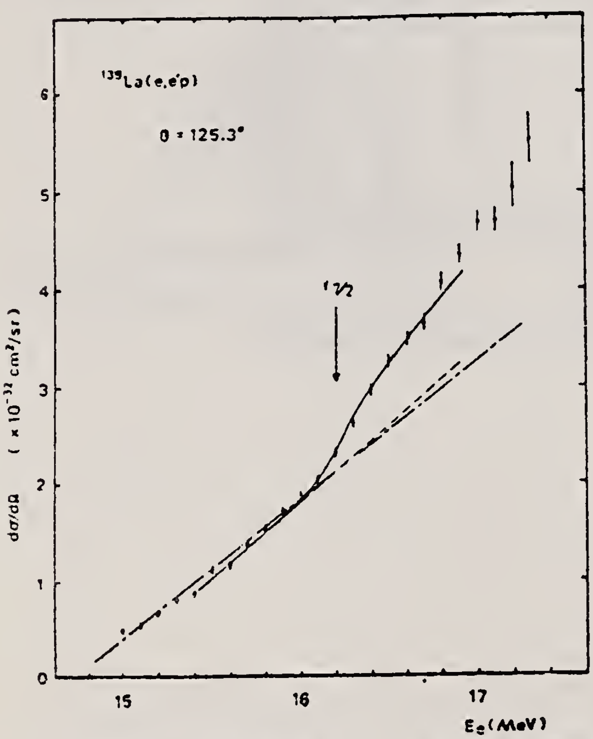

Fig. 2. The differential cross section of the ^{139}La(e, e'p) reaction for θ = 125.3°. The solid line shows the result of a least-square fitting with eq. (4). The dashed line shows the $T_<$ part. The dash-dot line is used in order to define the position of the sudden increase as shown in fig. 6.

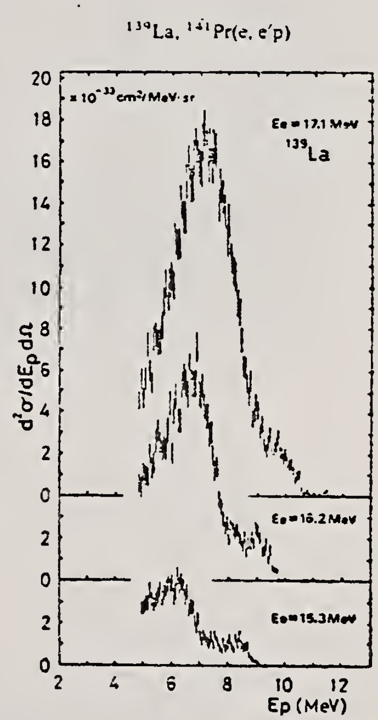

Fig. 5. The proton spectra of the ^{139}La(e, e'p) reactions for θ = 125.3°.

over

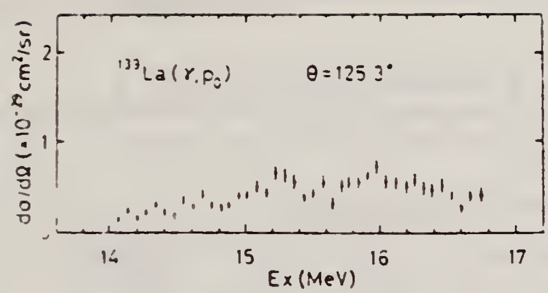

Fig. 7 The ^{139}La(γ,p) cross section

REF. J. Uegaki, K. Shoda
Nucl. Phys. A341, 125 (1980)

ELEM. SYM.	A	Z
La	139	57

METHOD

REF. NO.	
80 Ue 1	hg

REACTION	RESULT	EXCITATION ENERGY	SOURCE TYPE	SOURCE RANGE	DETECTOR TYPE	DETECTOR RANGE	ANGLE
E,P	ABX	11-25	D	15-25	MAG-D		125

VIRT PHOTON ANALYSIS

Abstract: The cross sections and the proton energy distributions of the (e, p) reactions on ^{139}La and ^{141}Pr have been measured around the $T_>$ GDR. The energies of the $T_>$ GDR have been given as $E_R = 21.0$ MeV in ^{139}La and $E_R = 20.4$ MeV in ^{141}Pr. The decay protons of the $T_>$ GDR have been studied. The proton groups which leave the residual nucleus in the neutron particle-hole states have been clearly seen in the same energy regions as the decay protons emitted through the low-lying IAR.

E NUCLEAR REACTIONS ^{139}La, ^{141}Pr(e, p), E = 15–25 MeV; measured $\sigma(E_e)$, $\sigma(E_p)$; deduced $\sigma(\gamma, p)$ vs. E_p. Natural target.

TABLE 1

Results of the energy-weighted integrated cross-section calculations

Element	$E_R^<$ (MeV)	$E_R^>$ (MeV)	$E_R^> - E_R^<$ (MeV) exp.	theor.	$\sigma_{-1}^<$ [a]) (mb)	$\sigma_{-1}^>$ [a]) (mb)	$\sigma_{-1}^>/\sigma_{-1}^<$ (%) exp.	theor.
^{139}La	15.2±0.1 [b])	21.0±0.2	5.8±0.3	5.83 [c])	136 [b])	1.01±0.07	0.74	2.3 [c])
^{141}Pr	15.1±0.1 [b])	20.4±0.2	5.3±0.3	5.32 [c])	125 [b])	1.27±0.24	1.0	3.0 [c])

[a]) The notation shows $\sigma_{-1}^< = \int(\sigma_</E)dE$, $\sigma_{-1}^> = \int(\sigma_>\ E)dE$.
[b]) Ref. [10]). Integrals were carried out up to 25.0 MeV by present authors.
[c]) Calculated by using eqs. (1) and (2) in the text. Refs. [3,4]).

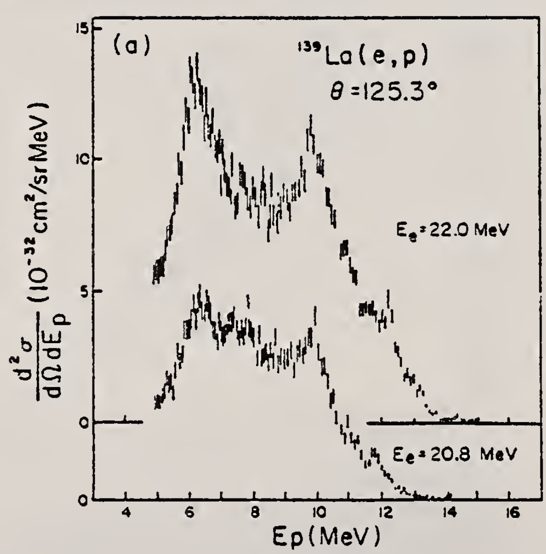

Fig. 1. The proton spectra of the (e, p) reaction at θ = 125.3° laboratory. (a) ^{139}La. Bombarding energies are E_e = 22.0 MeV and E_e = 20.8 MeV, respectively. (b) ^{141}Pr. Bombarding energies are E_e = 21.4 MeV and E_e = 20.2 MeV, respectively.

OVER

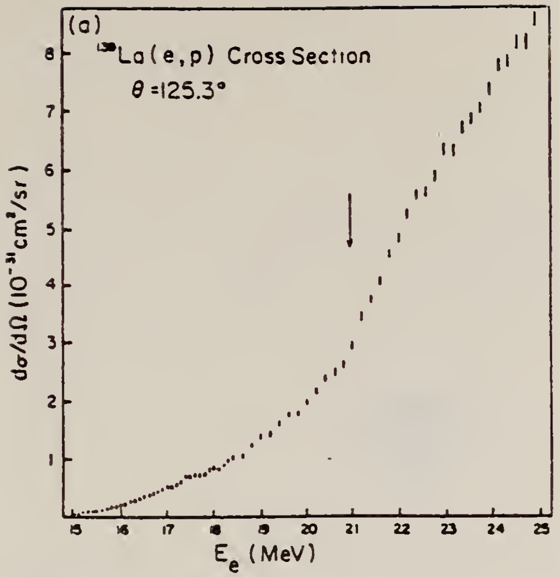

Fig. 2. The differential cross sections of the (e, p) reaction at θ = 125.3° lab. The arrows show the positions of inflection caused by $T_>$ GDR. (a) ^{139}La. (b) ^{141}Pr.

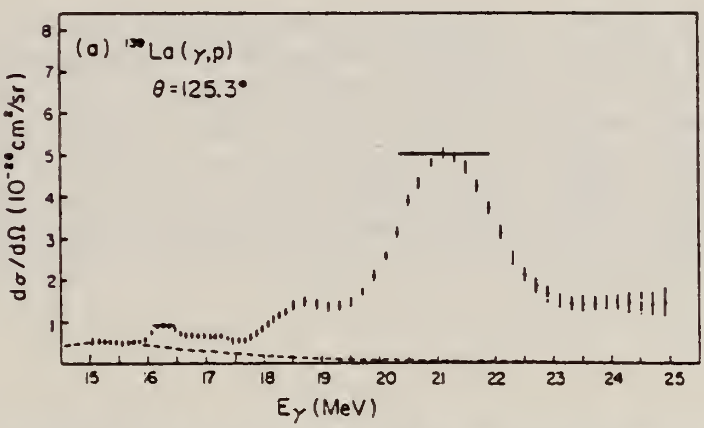

Fig. 3. The (γ, p) differential cross sections calculated from the present (e, p) differential cross section by the least structure method [ref. [11]]. The broken lines indicate assumed contribution of the $T_<$ GDR to the (γ, p) cross section. (a) ^{139}La. (b) ^{141}Pr.

CERIUM
Z=58

Cerium was discovered in 1803 by J. Berzelius and W. Hisinger working together as well as by M. Klaproth working separately. An interesting alloy of cerium is misch metal which contains 50% cerium, 25% lanthanum, and various other rare earths as well as iron. It is this material, used in lighter flints, that produces the shower of sparks. It is also used in making tracer bullets that ignite from the friction of the air and display the bullet's trajectory.

CE

E.G. Fuller, B. Petree, M.S. Weiss
Phys. Rev. 112, 554 (1958)

ELEM. SYM.	A	Z
Ce		58

METHOD: Betatron; ion chamber

REF. NO.: 58 Fu 1 — NVB

REACTION	RESULT	EXCITATION ENERGY	SOURCE TYPE	SOURCE RANGE	DETECTOR TYPE	DETECTOR RANGE	ANGLE
G,XN	ABY	7-40	C	7-40	BF3-I		4PI

TABLE I. Target properties and results.

Element	Form used	Weight grams	$\sigma^a(\gamma,n)$[a] barns	$\int\sigma dE$[b] / NZ/A Mev-b	"Γ"[a] Mev
Sn	Sn	4.81	0.30	0.064	5.0
I	I	8.55	0.36	0.085	6.0
La	La	10.43	0.34	0.063	5.2
Ce	Ce	4.99	0.45	0.080	4.5
Sm	Sm_2O_3	2.90	0.26	0.073	8.6
Tb	Tb_4O_7	3.04	0.39	0.087	8.7
Ho	Ho_2O_3	1.87	0.41	0.079	7.5
Er	Er_2O_3	5.41	0.50	0.100	8.5
Yb	Yb_2O_3	3.57	0.50	0.090	7.0
Ta	Ta	8.41	0.49	0.077	6.0
Au	Au	3.16	0.68	0.085	4.2
Pb	Pb	8.05	0.75	0.081	3.8

[a] $\sigma^a(\gamma,n)$ is the maximum value and "Γ" the full width at $\sigma^a(\gamma,n)/2$ of the neutron production cross section corrected for multiple neutron emission. Data were not fitted with resonance lines to determine these values.
[b] Integrated neutron production cross sections corrected for multiple neutrons above $(\gamma,2n)$ threshold.

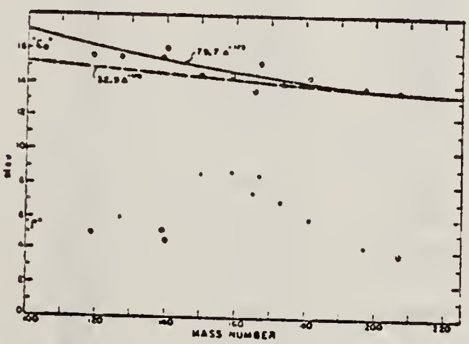

FIG. 6. Mean energy and width of giant resonances. "E_0" and "Γ" are the mean energy for photon absorption and the full width at half maximum of the giant resonance obtained from dashed histograms as in Fig. 5. No attempt was made to fit data with resonance curves to obtain these parameters.

REF.	ELEM. SYM.	A	Z
F. I. Havlicek Nuovo Cimento 13, 969-73 (1959)	Ce		58

METHOD	REF. NO.	
Betatron	59 Ha 2	NVB

REACTION	RESULT	EXCITATION ENERGY	SOURCE		DETECTOR		ANGLE
			TYPE	RANGE	TYPE	RANGE	
G,A	SPC	THR - 30	C	30	EMU-D	2 - 5	DST

R.G. Baker, K.G. McNeill
Can. J. Phys. 39, 1158 (1961)

ELEM. SYM.	A	Z
Ce		58

METHOD Betatron; fast neutron yield angular distribution; Si threshold detector; ion chamber

REF. NO.	
61 Ba 2	NVB

REACTION	RESULT	EXCITATION ENERGY	SOURCE		DETECTOR		ANGLE
			TYPE	RANGE	TYPE	RANGE	
G,XN	ABY	THR-22	C	22	THR-I	5-+	DST

In Table 4:

$\bar{\sigma}$ = average cross section of detector weighted with neutron spectrum

Φ = neutrons/100 roentgen/mole

$$W(\theta) = a_o \sum_{n=1}^{\infty} [1 + A_n P_n (\cos \theta)]$$

TABLE IV

I Element	II a_0	III a_1	IV a_2	V $(\bar{\sigma}\Phi)\times 10^{**}$	VI Φ_{total} (22 Mev)$\times 10^9$	VII Φ_{fast}/Φ_{total}
Vanadium	245 (1±0.06)	0.01±0.08	−0.00±0.10	6.05	0.21	0.12
Chromium	164 (1±0.03)	0.04±0.04	−0.05±0.05	4.05	0.17	0.10
Manganese	308 (1±0.02)	0.07±0.03	−0.09±0.04	7.61	0.25	0.12
Iron	200 (1±0.03)	0.05±0.04	−0.17±0.05	4.94	0.18	0.11
Cobalt	390 (1±0.02)	0.08±0.03	−0.22±0.04	9.63	0.26	0.15
Nickel	145 (1±0.05)	0.07±0.07	−0.23±0.09	3.58	0.12	0.12
Copper	347 (1±0.02)	0.05±0.03	−0.20±0.04	8.57	0.30	0.12
Arsenic	482 (1±0.03)	0.11±0.04	−0.24±0.05	11.91	0.33	0.15
Rubidium	638 (1±0.05)	0.13±0.06	−0.14±0.08	15.76		
Strontium	409 (1±0.05)	0.10±0.06	−0.17±0.08	10.10		
Yttrium	290 (1±0.10)	0.08±0.12	−0.12±0.15	7.16		
Silver	590 (1±0.04)	0.10±0.06	−0.22±0.08	14.57	0.87	0.07
Cadmium	905 (1±0.02)	0.02±0.02	−0.26±0.03	22.35		
Iodine	1133 (1±0.03)	0.04±0.04	−0.29±0.05	27.99	1.42	0.08
Barium	1048 (1±0.04)	0.10±0.06	−0.38±0.08	25.89		
Lanthanum	1595 (1±0.02)	0.02±0.03	−0.42±0.04	39.40	1.04	0.15
Cerium	1316 (1±0.05)	0.05±0.06	−0.39±0.08	32.50		
Dysprosium	1652 (1±0.08)	0.04±0.10	−0.34±0.13	40.80		
Tantalum	1558 (1±0.02)	0.04±0.03	−0.22±0.04	38.48	2.50	0.06
Tungsten	1365 (1±0.02)	−0.07±0.03	−0.24±0.04	33.71		
Mercury	1345 (1±0.02)	0.04±0.03	−0.31±0.04	33.22		
Lead	2274 (1±0.01)	0.02±0.02	−0.42±0.03	56.17	2.72	0.08
Bismuth	2162 (1±0.02)	0.05±0.03	−0.45±0.04	53.40	3.36	0.06
Thorium	3031 (1±0.04)	0.06±0.05	−0.32±0.07	74.87		
Uranium	4630 (1±0.02)	0.05±0.03	−0.17±0.04	114.38		

$^*(\bar{\sigma}\Phi) = 2.47\times 10^9$ as millibarn-neutron. Errors are standard errors due to counting statistics only.

REF.	ELEM. SYM.	A	Z
J. Miller, C. Schuhl, C. Tzara J. Phys. Radium 22, 529 (1961)	Ce		58

METHOD	REF. NO.	
Positron annihilation; neutron cross section; BF_3 counter; ion chamber	61 Mi 1	NVB

REACTION	RESULT	EXCITATION ENERGY	SOURCE		DETECTOR		ANGLE
			TYPE	RANGE	TYPE	RANGE	
G,XN	ABX	8-21	D	8-21	BF3-I		4PI

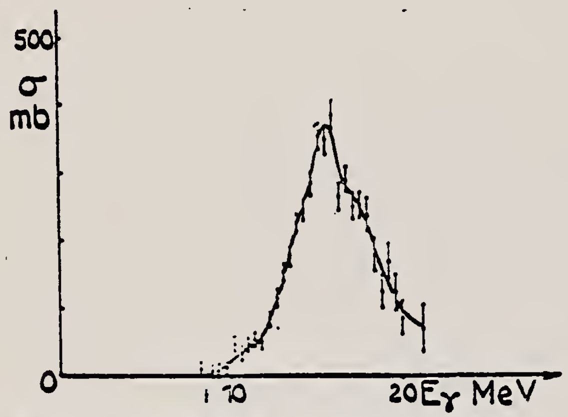

FIG. 4b. — Cérium, $\sigma(\gamma, n) + 2\sigma(\gamma, 2n) + \sigma(\gamma, np) + \dots$

Ref. J. Miller, C. Schuhl, C. Tzara
Nuclear Phys. 32, 236 (1962)

Elem. Sym.	A	Z
Ce		58

Method
Linac; monoergic photons by e^+ annihilation in flight; NaI monitor; BF_3 detector

Ref. No.	
62 Mi 3	JHH

Reaction	E or ΔE	E_0	Γ	$\int \sigma dE$	$J\pi$	Notes
Ce (γ,xn)	10-21.2	15.6±0.5		$\int_0^{21.2} = 1.88\pm0.03$ MeV-b		

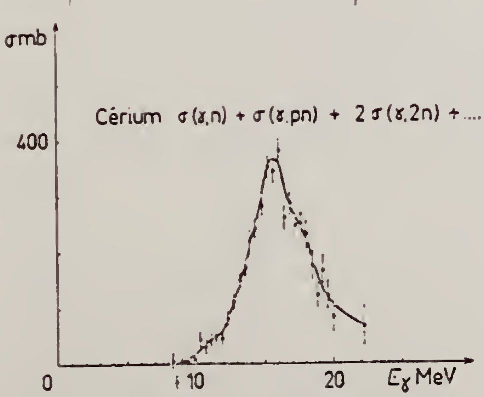

Fig. 8. Section efficace
$\sigma = \sigma(\gamma,n) + \sigma(\gamma,np) + 2\sigma(\gamma,2n) + \ldots$ pour le cérium.

TABLEAU 5
Résultats expérimentaux

Eléments	Fig. No	E_m (MeV)	σ_{int} (MeV · b) *)	σ_{int} / $0.06NZ/A$	Seuils γ, n	Seuils γ, p	Seuils γ, 2n	Seuils γ, np
Cu	6	17 ±0.5	0.45±0.013	0.47±0.015				
La	7	15.6±0.5	1.91±0.03	0.94±0.015	8.80 [13]		14.25 [13]	14.90 [13]
Ce 140	8	15.6±0.5	1.88±0.03	0.92±0.015	9.05 [14]	8.50 [14]	14.1 [14]	
Ce 142					7.15 [14]	9.50 [14]	14.3 [14]	
Ta 181	9	13 ±0.5 16.5±0.5	2.97±0.05	1.13±0.02	7.55 [13]		13.84 [13]	13.47 [13]
Au 197	10	14.2±0.5	3.00±0.05	1.06±0.02	7.90 [13]		13.71 [13]	12.94 [13]
Pb 206	11	13.8±0.5	4.10±0.06	1.38±0.02	10.6 [13]	7.1 [13]	14.3 [13]	14.5 [13]
Pb 207					7.2 [13]	8.2 [13]	14.3 [13]	17.9 [13]
Pb 208					6.9 [13]	8.4 [13]	15.0 [13]	14.2 [13]
Bi 209	12	14.0±0.5	3.73±0.06	1.24±0.02	7.44 [14]	3.78 [14]	10.4 [14]	

*) L'integrale $\int_0^x \sigma dE$ est prise jusqu'à x égal à 19.6 MeV pour Cu, à 21.2 MeV pour La et Ce et à 22 MeV pour Ta, Au, Pb et Bi. D'autre part, les erreurs indiquées sont les erreurs statistiques.

REF.	ELEM. SYM.	A	Z
R.B. Begzhanov and A.A. Islamov Zhur. Eksp. i Teoret. Fiz. 46, 1486-1488 (1964) Soviet Phys. JETP 19, 1005 (1964)	Ce		58
METHOD Radioactive source La^{140}; resonance scattering cross section, self-absorption	**REF. NO.** 64 Be 4		NVB

REACTION	RESULT	EXCITATION ENERGY	SOURCE		DETECTOR		ANGLE
			TYPE	RANGE	TYPE	RANGE	
G,G	LFT	2	D	2	NAI-D		120
		(1.597)		(1.597)			

Average resonance scattering cross section = $(3.7 \pm 0.4) \times 10^{-26}$ cm^2

Lifetime of 1.597 MeV state = $(2.15 \pm 0.080) \times 10^{-13}$ sec.

REF. G. Ben-David, B. Arad, J. Balderman, and Y. Schlesinger Phys. Rev. <u>146</u>, B852 (1966)			ELEM. SYM.	A	Z
			Ce		58

METHOD	REF. NO.	
Nuclear Resonance Scattering using N,G reactions.	66 Be 3	JDM

REACTION	RESULT	EXCITATION ENERGY	SOURCE TYPE	SOURCE RANGE	DETECTOR TYPE	DETECTOR RANGE	ANGLE
G,G	RLX	5 - 10	D	5 - 10	NAI-D	5 - 10	135

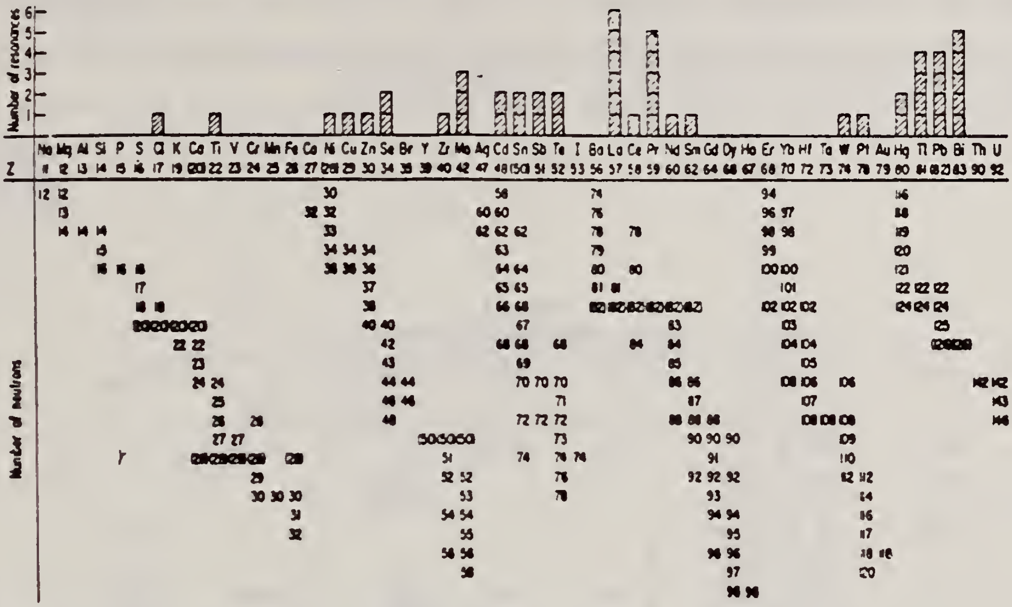

FIG. 3. Histogram of distribution of observed resonances among the different targets. The atomic number is given directly beneath the chemical symbol followed by the neutron numbers of the naturally occurring isotopes. Magic numbers are shown in brackets.

TABLE III. List of effective cross sections.

Scatterer	Energy (MeV)	Gamma source	δ (mb)	Scatterer	Energy (MeV)	Gamma source	δ (mb)
Sm^{144}	8.997	Ni	100	Sn	7.01	Cu	110
Pr^{141}	8.981	Cr	9	Nd	6.867	Co	30
La	8.532	Ni	6	Pr^{141}	6.867	Co	3
Te	8.532	Ni	3[a]	Te	6.7	Ni	...
Cu	8.499	Cr	24	La	6.54	Ag	12
Zr	8.496	Se	3050	Cd	6.474	Co	110
Zn	8.119	Ni	13	Mo	6.44	Hg	25[e]
Se	7.817	Ni	50	La	6.413	Ti	72
Se	7.76	K	90	Mo	6.413	Ti	10
Sb	7.67	V	...[b]	Tl	6.413	Ti	25
Cd	7.64	Fe	40[c]	W	~6.3	Ti	...[b]
Ni	7.64	Fe	7[c]	Sb	6.31	Hg	6[e]
Pr^{141}	7.64	Fe	12[c]	Ti	6.31	Hg	2[e]
Tl	7.64	Fe	370[c]	Sn	6.27	Ag	75
La	7.634	Cu	7	Pb^{208}	6.15	Gd	...[g]
Mo	7.634	Cu	11	Te	5.8	Ni	...[f]
Bi^{209}	7.634	Cu	4	La	6.12	Cl	35
Te	7.528	Ni	66[d]	Pr^{141}	6.12	Cl	110
Bi^{209}	7.416	Se	100	Pt	5.99	Hg	40[a,e]
Bi^{209}	7.300	As	80[c]	Tl	5.99	Hg	5[e]
Pb^{208}	7.285	Fe	4100	Pb^{208}	5.9	Sr	...[h]
Cl	7.285	Fe	34	Ce	5.646	Co	17
Pr^{141}	7.185	Se	80	Bi^{209}	5.646	Co	55
Tl	7.16	Cu	120	Pb^{208}	5.53	Ag	70
La	7.15	Mn	50	Hg	5.44	Hg	75[e]
Bi^{209}	7.149	Ti	2000	Hg	4.903	Co	385

[a] High-energy component of a complex spectrum.
[b] A broad scattered spectrum with no observable peak structure.
[c] There are actually two lines of energies 7.647 and 7.633 MeV having equal intensities in the iron capture gamma spectrum. The cross section has therefore been corrected, although there is no possibility at present of deciding which line is responsible for each resonance.
[d] Is probably an independent level in the complex spectrum of Ni γ rays on Te.
[e] Rough estimate.
[f] May be inelastic component from 7.528 level in Te.
[g] The relative line intensities in this case are due to Groshev and co-workers.
[h] No line is known for the source at this energy.
[i] Difficult to resolve among the many source lines present at this energy.

REF.	ELEM. SYM.	A	Z
R. Bergere, H. Beil, P. Carlos and A. Veyssiere Nucl. Phys. A133, 417 (1969)	Ce		58
METHOD	REF. NO. 69 Be 6		egf

REACTION	RESULT	EXCITATION ENERGY	SOURCE TYPE	SOURCE RANGE	DETECTOR TYPE	DETECTOR RANGE	ANGLE
G,N	ABX	8-23	D	8-30	MOD-I		4PI
G,2N	ABX	12-30	D	8-30	MOD-I		4PI
G,3N	ABX	24-30	D	8-30	MOD-I		4PI

x = fraction of total cross section resulting in a direct neutron

n_d = fraction of neutrons emitted by direct effect at an energy where all the evaporation neutrons go to (γ,2n) cross section

$n_d = x/(2-x)$

603+(G,N)
604 (G,2N)
477+(G,3N)

TABLEAU 3
Moments quadrupolaires intrinsèques

Cible	% isotopes	a/b ex	β_2 ex	$\beta_2[B(E_2)]$	Q_0 ex (b)	Q'_0
$_{53}$I	100 % ^{127}I	0.85	0.172		−2.3±0.4	
$_{58}$Ce	88.5 % ^{140}Ce			0.104		
	11.1 % ^{142}Ce			0.118		
$_{62}$Sm	15 % ^{147}Sm	1.23	0.219		4.5±0.4	0.158
	11.2 % ^{148}Sm					
	13.8 % ^{149}Sm					
	7.5 % ^{150}Sm			0.190		3.53
	26.6 % ^{152}Sm			0.304		5.93
	22.5 % ^{154}Sm			0.351		6.58
$_{68}$Er	33.4 % ^{166}Er	1.314	0.288	0.341	6.96±0.4	7.60
	22.9 % ^{167}Er					7.80
	27.1 % ^{168}Er			0.339		7.60
	14.9 % ^{170}Er			0.329		7.45
$_{71}$Lu	97.4 % ^{175}Lu	1.282	0.262		6.95±0.3	7.20

TABLEAU 5
Valeurs de la température nucléaire et du paramètre *a* de densité des niveaux

	x	n_d	Θ (MeV)	$E'_\gamma - E_n$ (MeV)	a (MeV^{-1})	a' (MeV^{-1})	a'' (MeV^{-1})
I	0.05±0.005	0.03±0.03	1.30±0.20	10	6±2.5	10±3	10±2
^{140}Ce	0.21±0.05	0.12±0.03	1.05±0.20	10	9±3.5		7±3
^{142}Ce			0.8 ±0.20	6	9±4		8±3
Sm	0.18±0.04	0.10±0.03					
Er	0.20±0.05	0.11±0.03					(12±4)
Lu	0.26±0.06	0.15±0.03	0.85±0.1	9	12.5±2.5		15±3

[over]

TABLEAU 4

Règles de somme

Noyau cible (éléments naturels)	σ_0 (MeV · b)	σ'_0 (MeV · b)	$0.06\,\frac{NZ}{A}$	$\frac{\sigma_0 A}{0.06\,NZ}$	$\frac{\sigma'_0 A}{0.06\,NZ}$	σ_{-1} (mb)	$\sigma_{-1}A^{-4/3}$	σ_{-2} (mb · MeV^{-1})	$\sigma_{-2}A^{-5/3}$
$_{53}$I	2.02 ±0.14	2.30±0.12	1.85	1.09±0.07	1.24±0.07	129±0.10	0.20 ±0.02	8.6±0.6	2.7 ±0.2
$_{58}$Ce	2.13 ±0.15	2.53±0.13	2.04	1.05±0.07	1.24±0.07	140±0.12	0.19 ±0.02	9.5±0.6	2.5 ±0.2
$_{62}$Sm	2.48 ±0.17	2.92±0.14	2.18	1.14±0.07	1.34±0.07	167±0.14	0.21 ±0.02	11.8±0.8	2.75±0.2
$_{68}$Er	2.70 ±0.19	3.04±0.16	2.42	1.12±0.07	1.26±0.07	186±0.15	0.20 ±0.02	13.6±1	2.7 ±0.2
$_{71}$Lu	2.65 ±0.18	2.96±0.16	2.53	1.05±0.07	1.17±0.07	182±0.15	0.185±0.02	12.9±1	2.35±0.2
valeur moyenne pour ces 5 corps				1.09±0.07	1.25±0.07		0.20±0.02		2.6 ±0.2

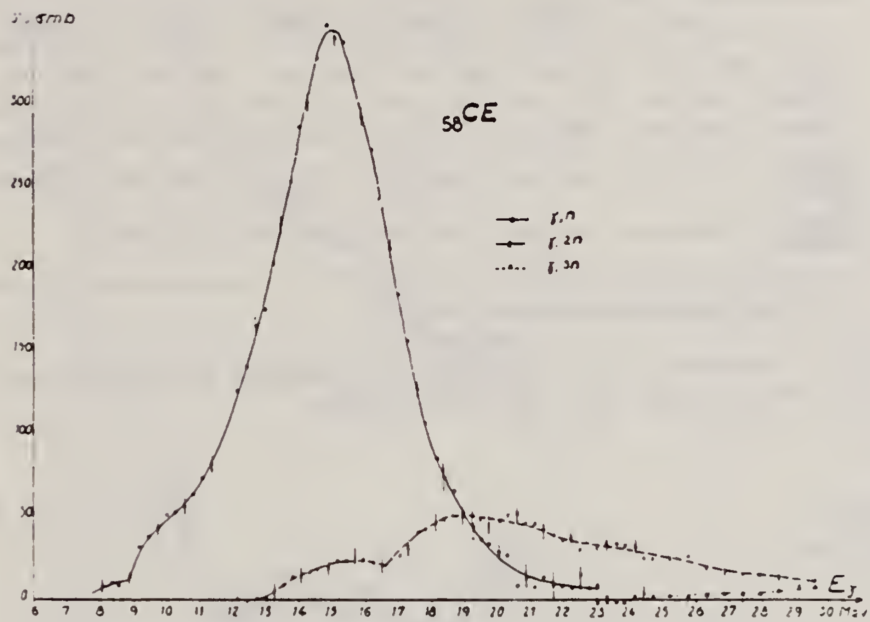

Fig. 3.

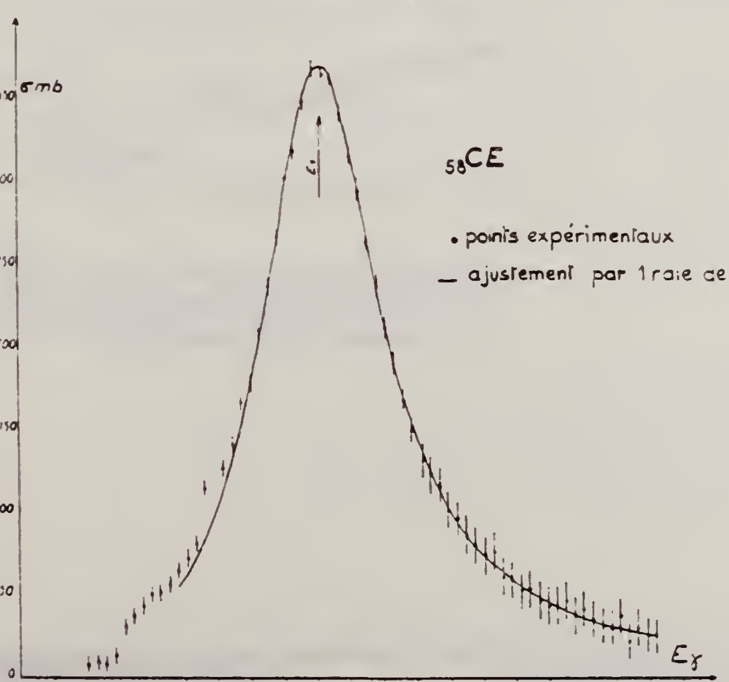

Fig. 4.

REF.	ELEM. SYM.	A	Z
H. Beil, R. Bergere, P. Carlos, A. Lepretre, A. Veyssiere and A. Parlag Nucl. Phys. A172, 426 (1971)	Ce		58
METHOD	REF. NO. 71 Be 4		egf

REACTION	RESULT	EXCITATION ENERGY	SOURCE		DETECTOR		ANGLE
			TYPE	RANGE	TYPE	RANGE	
G,SN	ABX	9-18	D	9-18	MOD-I		4PI

363+

TABLE 1

Lorentz line parameters corresponding to fits of total photoneutron cross sections presented in fig. 1

	$_{56}$Ba	$^{139}_{57}$La	$_{58}$Ce	$^{141}_{59}$Pr	$_{60}$Nd	$^{141}_{59}$Pr [a])
σ_1 (mb)	356 ±15	340 ±15	360 ±15	350 ±15	315 ±15	320 ±20
E_1 (MeV)	15.3 ± 0.1	15.2 ± 0.1	15.0 ± 0.10	15.1 ± 0.1	14.9 ± 0.1	15.16 ± 0.08
Γ_1 (MeV)	4.70 ± 0.15	4.45 ± 0.05	4.35 ± 0.05	4.26 ± 0.05	4.90 ± 0.05	4.49 ± 0.05
$\frac{1}{2}\pi\sigma_1\Gamma_1$ (MeV · b)	2.6 ± 0.15	2.35 ± 0.13	2.42 ± 0.15	2.35 ± 0.13	2.43 ± 0.13	2.42 ± 0.17
$\frac{\frac{1}{2}\pi\sigma_1\Gamma_1}{0.06NZA^{-1}}$	1.30 ± 0.08	1.16 ± 0.08	1.19 ± 0.08	1.14 ± 0.08	1.15 ± 0.08	

[a]) Lorentz line parameters given in ref. [10]) for ^{141}Pr.

[10] R.L. Bramblett, J.T. Caldwell, B.L. Berman, R.R. Harvey and S.C. Fultz, Phys. Rev. 148, 1198 (1966).

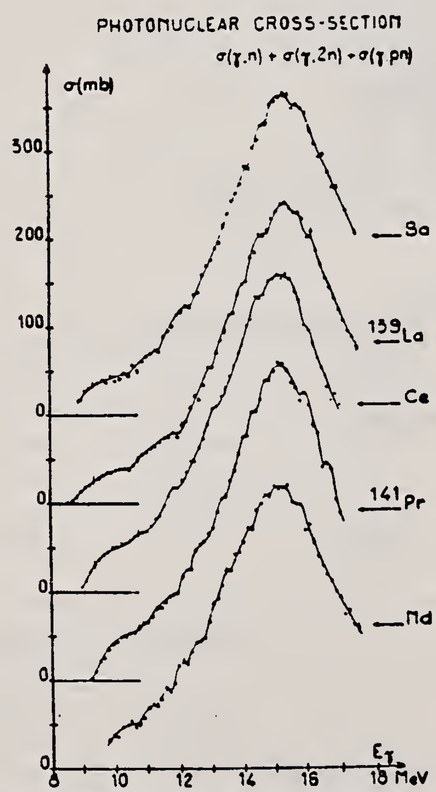

Fig. 1. Total photoneutron cross sections for Ba, ^{139}La, Ce, ^{141}Pr and Nd as a function of incident photon energy E.

REF.	ELEM. SYM.	A	Z
R. Pitthan and Th. Walcher Phys. Letters 36B, 563 (1971)	Ce		58
METHOD	REF. NO. 71 Pi 1		egf

REACTION	RESULT	EXCITATION ENERGY	SOURCE TYPE	SOURCE RANGE	DETECTOR TYPE	DETECTOR RANGE	ANGLE
E,E/	SPC	4 - 18		50,65	MAG-D		DST

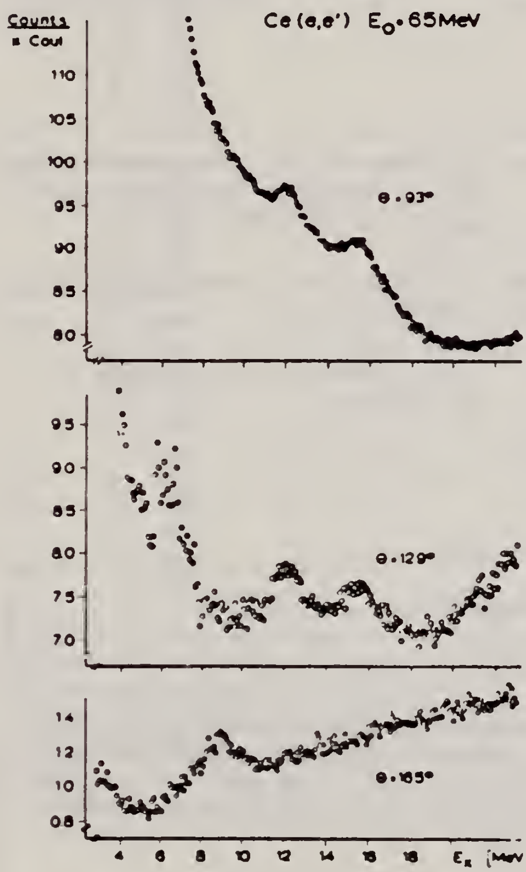

Fig. 1. Spectra of electrons scattered inelastically from cerium; parameters as indicated. No background has been subtracted. Note the suppressed zeros and the different scales of the ordinates.

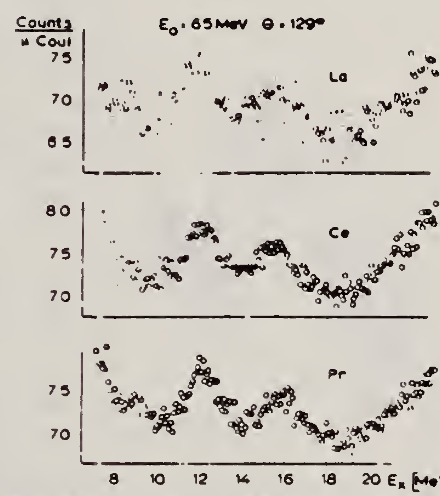

Fig. 2. Spectra of electrons scattered inelastically from La, Ce and Pr targets at the same primary energy and the same laboratory scattering angle. No background has been subtracted. Note the suppressed zeros of the ordinate scales.

REF.

R.F. Barrett, J.R. Birkelund, B.J. Thomas, K.S. Lam, and H.H. Thies
Nucl. Phys. A210, 355 (1973)

ELEM. SYM.	A	Z
Ce		58

METHOD

REF. NO.	
73 Ba 20	egf

REACTION	RESULT	EXCITATION ENERGY	SOURCE TYPE	SOURCE RANGE	DETECTOR TYPE	DETECTOR RANGE	ANGLE
G,N	NOX	THR- 27	C	10- 27	BF3-I		4PI

MEAN NEUT ENERGY

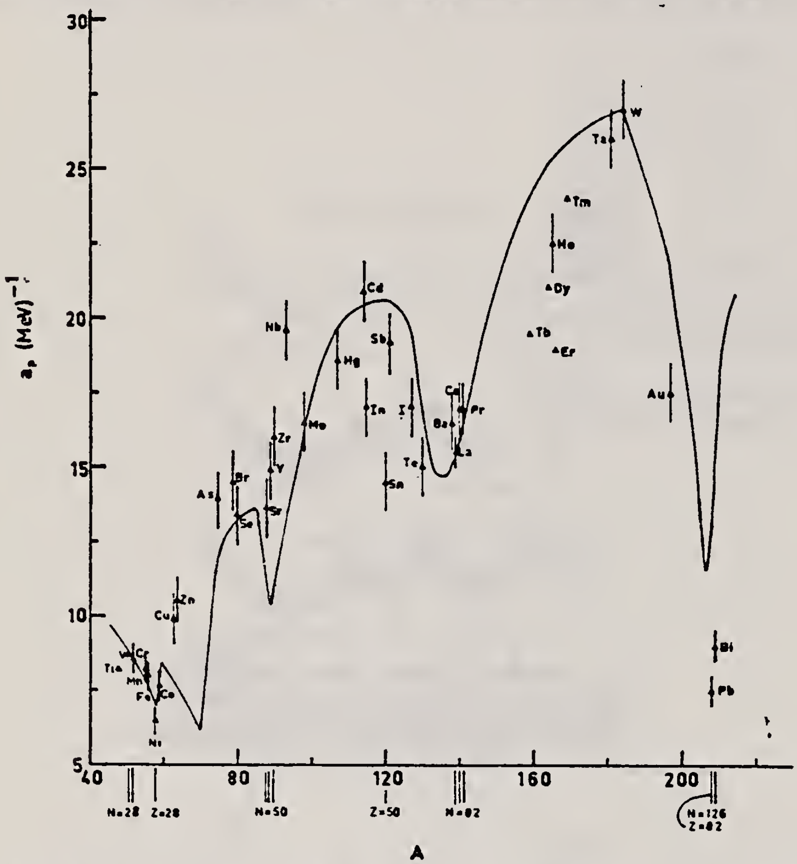

Fig. 12. Experimental values of the level density parameter a_p (Fermi gas formula plus pairing correction) versus atomic number A. The continuous curve is a least-squares fit to the data of a theoretical calculation from Newton [15]).

[1] H. Baba and S. Baba, Japan Atomic Energy Research Institute report JAERI-1183 (1969).

[2] H. Baba, Nucl. Phys. A159, 625 (1970).

[15] T.D. Newton, Can. J. Phys. 34, 804 (1956).

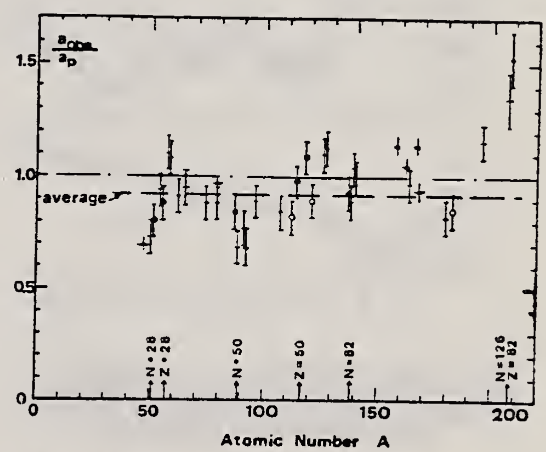

Fig. 15. Ratio a_{obs}/a_p versus atomic number A. Here a_{obs} is the level density parameter taken from the neutron resonance work of refs. [1,2]), and a_p is the level density parameter derived from the present (γ, n) work. Filled circles represent points where nuclei in the neutron resonance and in the (γ, n) experiment were the same. Open circles represent points where the respective nuclei were approximately matched. Triangles represent points which are based on measurement of neutron mean energies at two bremsstrahlung energies only.

(over)

Table 3 (continued)

Target	N (residual nucleus) [a]		Goodness of fit [b] no p.c.	Goodness of fit [b] with p.c.	$\hat{E}_n(24)$ (MeV) [c]	T (MeV) [d]	a_p (MeV^{-1}) [e]	a_{obs} (MeV^{-1}) [f]	a_{obs}/a_p
Ba	75	1%		F	1.16		16.5–^{136}Ba	15.39–^{136}Ba	0.93
	77	2%							
	78	7%							
	79	8%							
	80	11%							
	81	71%							
La	80	100%	F	F	1.25	0.72	15.5–^{138}La	13.76–^{139}La	0.89
Ce	81	89%	F	G	1.24	0.70	17.0–^{139}Ce	17.8 –^{141}Ce	1.04
	83	11%							
Pr	81	100%	G	G	1.17	0.65	17.0–^{140}Pr	17.05–^{142}Pr	1.00
Tb [g]	93	100%			1.15		19.3–^{158}Tb	21.85–^{160}Tb	1.14
Dy [g]	93	2%			1.06		20.9–$^{161.5}$Dy	21.9 –^{162}Dy	1.05
	94	19%							
	95	25%							
	96	25%							
	97	28%							
Ho	97	100%	P	G	1.06	0.56	21.4–^{164}Ho	20.66–^{166}Ho	0.97
Er [g]	95	2%			1.11		19.2–^{166}Er	21.9 –^{166}Er	1.14
	97	33%							
	98	23%							
	99	27%							
	101	15%							
Tm [g]	99	100%			1.03		24.0–^{168}Tm	22.58–^{170}Tm	0.94
Ta	107	100%		G	1.00	0.49	26.0–^{180}Ta	21.2 –^{181}Ta	0.82
W	107	26%	G	F	0.98	0.50	27.0–^{183}W	23.0 –^{183}W	0.85
	108	14%							
	109	31%							
	111	28%							
Au	117	100%		G	1.19		17.5–^{196}Au	20.24–^{198}Au	1.16
Pb ($Z = 82$)	123	24%		V.P.	1.87	1.20	7.5–^{206}Pb	10.1 –^{207}Pb	1.35
	124	23%							
	125	52%							
Bi	125	100%		F	1.65	1.03	9.0–^{208}Bi	13.8 –^{210}Bi	1.53

a) Neutron numbers and abundances of respective residual nuclei in (γ, n) experiments.
b) These give an assessment of the goodness of fit of a calculated $\hat{E}_n$ versus E_0 curve to the observed data, using the Fermi gas level density formula both without and with pairing corrections.
c) Bremsstrahlung photoneutron mean energies $\hat{E}_n$ for peak bremsstrahlung energy $E_0 = 24$ MeV.
d) Nuclear temperature from fit with constant-temperature formula.
e) Level density parameter a_p derived from the present (γ, n) experiment, using a Fermi gas formula plus pairing correction, and corresponding residual nucleus (the atomic weight shown is the weighted average of atomic weights of the respective isotopes present).
f) As column 7, but using data on n-resonance absorption from refs. [1,2]).
g) Measurements of $\hat{E}_n(E_0)$ for these nuclei were made only for $E_0 = 21$, 23 and 24 MeV.

REF.	F.R. Buskirk, H.D. Graf, R. Pitthan, H. Theissen, O. Titze, and Th. Walcher PICNS-73, Vol.I, p.703 Asilomar	ELEM. SYM.	A	Z
		Ce		58
METHOD		REF. NO.		
		73 Bu 14		hmg

REACTION	RESULT	EXCITATION ENERGY	SOURCE		DETECTOR		ANGLE
			TYPE	RANGE	TYPE	RANGE	
E,E/	SPC	2- 20	C	50, 65	MAG-D		DST

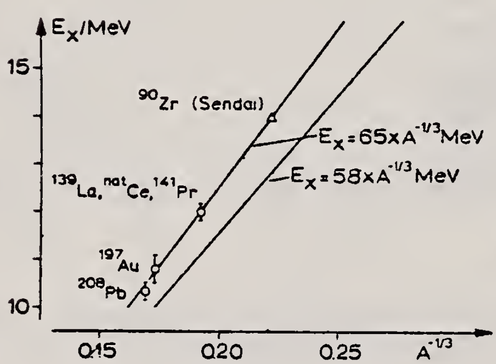

Fig. 2

The E2 resonance which is clearly visible at 10.8 ± 0.2 MeV exhausts more than 50 % of the sum rule. Fig. 2 shows the excitation energy of this resonance as a function of $A^{-1/3}$ for the nuclei measured at Darmstadt and the Sendai result for ^{90}Zr [5]. Bohr and Mottelson [9] predicted a collective E2 resonance whose isoscalar part should depend on A through $E_x = 58\ A^{-1/3}$MeV. The data of Fig. 2 are consistent with $E_x = 65\ A^{-1/3}$MeV suggesting to identify the observed resonances with this type of E2 excitation.

REF. Rainer Pitthan
Z. Physik 260, 283 (1973)

ELEM. SYM.	A	Z
Ce		58

METHOD

REF. NO.	
73 Pi 3	egf

REACTION	RESULT	EXCITATION ENERGY	SOURCE TYPE	SOURCE RANGE	DETECTOR TYPE	DETECTOR RANGE	ANGLE
E,E/	ABX	7- 21	D	50, 65	MAG-D		DST

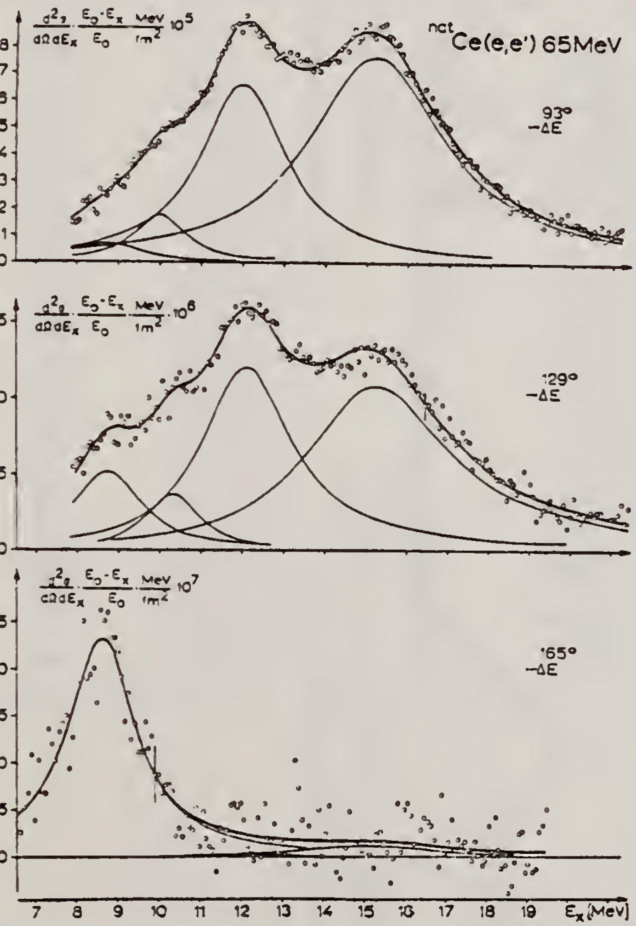

Fig. 5. Wie Fig. 2, aber nach Abzug des angepaßten Untergrundes. Die Zerlegung des Spektrums in die Einzelresonanzen (nach Gl. (2)) ist eingezeichnet, ΔE ist die Halbwertsbreite der elastischen Linie

(over)

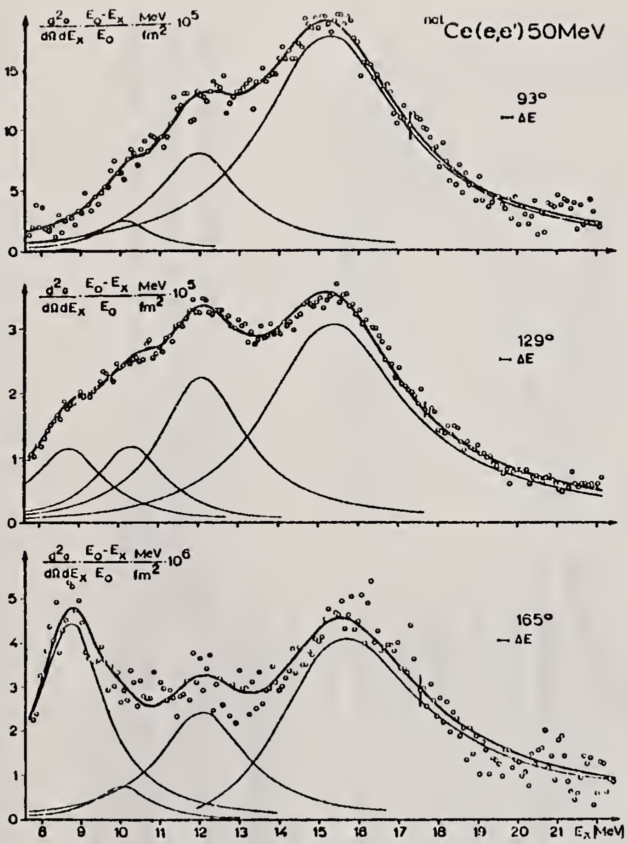

Fig. 6. Wie Fig. 5, aber für eine andere Primärenergie

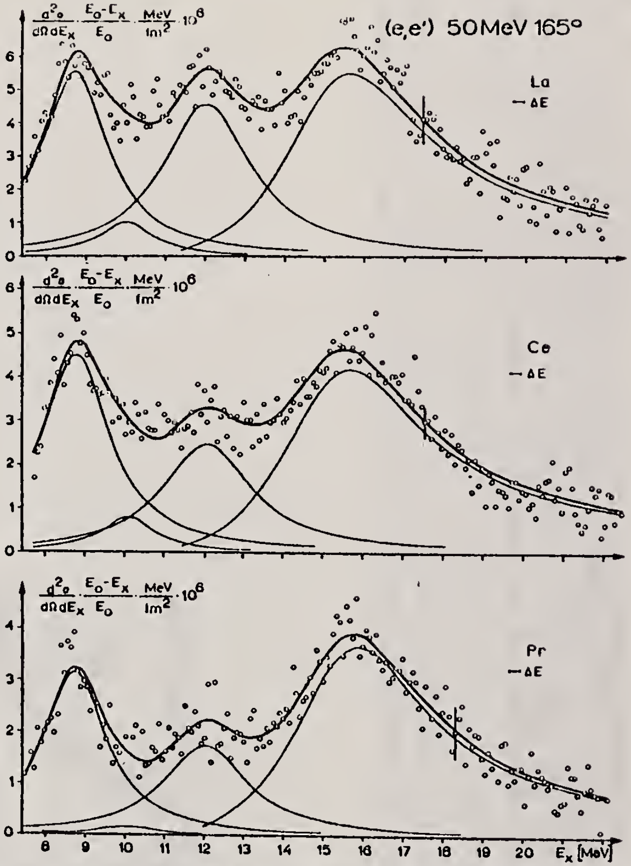

Fig. 7. Spektren von unelastisch an La, Ce und Pr gestreuten Elektronen, sonst wie Fig. 5, s. Text

REF.	ELEM. SYM.	A	Z
V. Emma, S. Lo Nigro, C. Milone Nucl. Phys. A257, 438 (1976)	Ce		58

METHOD	REF. NO.	
	76 Em 2	egf

REACTION	RESULT	EXCITATION ENERGY	SOURCE TYPE	SOURCE RANGE	DETECTOR TYPE	DETECTOR RANGE	ANGLE
G,F	ABY	THR-999	C	999	TRK-I		4PI

999 = 1 GEV

TABLE 1

Measured values of σ_q at $E = 1000$ MeV and deduced values of σ_k assumed constant from E_0 to 1000 MeV

Element	Z^2/A	σ_q (mb)	E_0 (MeV)	σ_k (mb)
Bi	32.96	12.3 ± 0.6	200	7.6 ± 0.6
Pb	32.45	5.4 ± 0.4	220	3.6 ± 0.3
Tl	32.10	4.1 ± 0.3	230	2.8 ± 0.3
Au	31.68	2.0 ± 0.15	240	1.4 ± 0.2
Pt	31.18	1.1 ± 0.08	255	$(8 \pm 0.7) \times 10^{-1}$
Re	30.21	$(3.7 \pm 0.3) \times 10^{-1}$	280	$(2.9 \pm 0.3) \times 10^{-1}$
W	29.78	$(3.5 \pm 0.3) \times 10^{-1}$	290	$(2.8 \pm 0.3) \times 10^{-1}$
Ta	29.45	$(3.3 \pm 0.3) \times 10^{-1}$	300	$(2.7 \pm 0.3) \times 10^{-1}$
Hf	29.04	$(1.7 \pm 0.2) \times 10^{-1}$	310	$(1.4 \pm 0.2) \times 10^{-1}$
Yb	28.31	$(1.3 \pm 0.1) \times 10^{-1}$	330	$(1.2 \pm 0.1) \times 10^{-1}$
Tm	28.18	$(7.5 \pm 0.8) \times 10^{-2}$	335	$(6.8 \pm 0.8) \times 10^{-2}$
Ho	27.21	$(3.6 \pm 0.4) \times 10^{-2}$	355	$(3.5 \pm 0.4) \times 10^{-}$
Dy	26.80	$(2.6 \pm 0.3) \times 10^{-2}$	360	$(2.5 \pm 0.3) \times 10^{-2}$
Tb	26.58	$(2.5 \pm 0.3) \times 10^{-2}$	370	$(2.5 \pm 0.3) \times 10^{-2}$
Gd	26.04	$(1.6 \pm 0.2) \times 10^{-2}$	380	$(1.7 \pm 0.2) \times 10^{-2}$
Sm	25.56	$(1.3 \pm 0.2) \times 10^{-2}$	390	$(1.4 \pm 0.2) \times 10^{-2}$
Nd	24.96	$(9.2 \pm 0.9) \times 10^{-3}$	405	$(1 \pm 0.1) \times 10^{-2}$
Ce	24.00	$(8 \pm 0.9) \times 10^{-3}$	420	$(9 \pm 1) \times 10^{-3}$
La	23.39	$(8.4 \pm 0.9) \times 10^{-3}$	430	$(1 \pm 0.1) \times 10^{-3}$
Sb	21.36	$(1.2 \pm 0.2) \times 10^{-2}$	460	$(1.5 \pm 0.3) \times 10^{-2}$
Te	21.19	$(8.8 \pm 1) \times 10^{-3}$	465	$(1.2 \pm 0.2) \times 10^{-2}$
Sn	21.06	$(1.3 \pm 0.2) \times 10^{-2}$	465	$(1.7 \pm 0.3) \times 10^{-2}$
Cd	20.49	$(1.7 \pm 0.3) \times 10^{-2}$	470	$(2.2 \pm 0.4) \times 10^{-2}$
Ag	20.47	$(2 \pm 0.3) \times 10^{-2}$	470	$(2.6 \pm 0.4) \times 10^{-2}$
Zn	13.76	$(2 \pm 0.4) \times 10^{-1}$	515	$(3 \pm 0.6) \times 10^{-1}$
Cu	13.44	$(2.4 \pm 0.5) \times 10^{-1}$	515	$(3.6 \pm 0.8) \times 10^{-1}$
Ni	13.35	$(2.4 \pm 0.5) \times 10^{-1}$	510	$(3.6 \pm 0.8) \times 10^{-1}$
Fe	12.10	$(3 \pm 0.6) \times 10^{-1}$	510	$(4.4 \pm 0.9) \times 10^{-1}$

[4] A.V. Mitrofanova et al. Sov. J. Nucl. Phys. 6, 512 (1968).

[7] T. Methasiri et al., Nucl. Phys. A167, 97 (1971).

[12] J.R. Nix et al., Nucl. Phys. 81, 61 (1966).

[20] N.A. Perifilov et al., JETP (Sov. Phys.) 14, 623 (1962); Proc. Symp. on the physics & chemistry of fission, Salzburg 1965, vol. 2 (IAEA) Vienna, 1965, p.283.

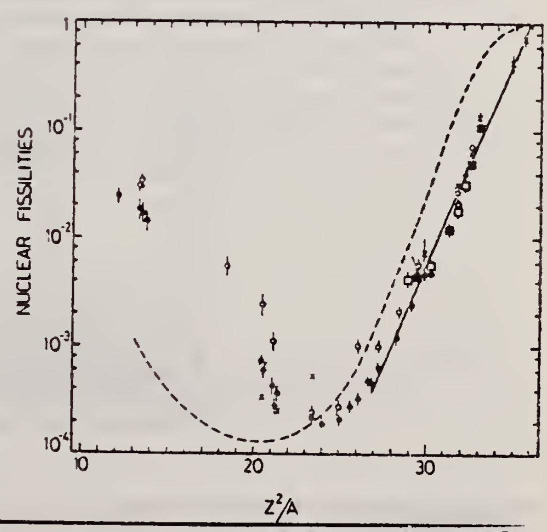

Fig. 2. Nuclear fissilities as a function of Z^2/A. Experimental points: solid circles represent our data; squares, the data from ref. [4]; open circles, the data from ref. [7]; and crosses, the data from (p,f) experiments[20]. The straight line is the best fit calculated from our data for $Z^2/A > 26$. The dashed curve is the curve VI calculated by Nix and Sassi[12].

REF.	I. Jacob, R. Moreh and A. Wolf Nucl. Phys. A291, 1 (1977)	ELEM. SYM.	A	Z
		Ce		58
METHOD		REF. NO.		
		77 Ja 4		egf

REACTION	RESULT	EXCITATION ENERGY	SOURCE TYPE	SOURCE RANGE	DETECTOR TYPE	DETECTOR RANGE	ANGLE
G,MUT	LFT	7	D	7	NAI-D		0
		(7.29,7.632)		(7.29,7.632)			

Abstract: A variable-energy γ-source is obtained by nuclear resonance scattering of neutron-capture γ-rays through various scattering angles. An energy resolution of less than 10^{-6} is obtained. Pb and Cd targets were employed to scatter the 7.279 and 7.632 MeV photons, respectively, of the neutron capture γ-rays of Fe. Variation of the angle of the resonantly scattered photons between 60°–150° permits an energy scan of ≈ 370 eV (for Pb) and ≈ 760 eV (for Cd) in any absorber. Thus nuclear energy levels in ^{139}La, Ce, Cd and ^{209}Bi absorbers were photoexcited and the corresponding values of $g\Gamma_0$ were extracted from the measured absorption curve.

7.28,7.63MeV,RES ABS

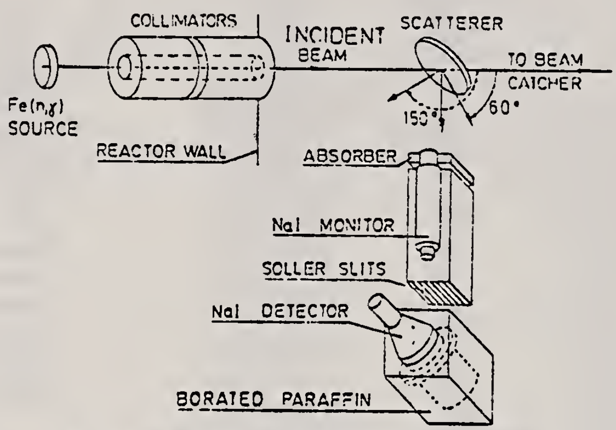

Fig. 1. Schematic diagram of the experimental arrangement.

TABLE 2

Summary of experimental data and measured values of $g\Gamma_0$ obtained using the γ-monochromator

Isotope	Thickness (g/cm^2)	Angle of dip (deg)	ΔE [c]) (eV)	Effect (%)	$g\Gamma_0$ (meV)
^{112}Cd [a])	35	128.0	505	3.5	150 ± 20
^{139}La	28.2	80.0	225	0.40	8.0 ± 2.0
^{139}La	18.2	100.5	322	0.27	7.1 ± 1.9
^{139}La	18.2	104.8	345	0.22	5.5 ± 1.8
^{140}Ce [b])	26.5	90.0	273	1.3	25 ± 3
^{209}Bi	31.5	73.5	196	2.0	43 ± 8
^{209}Bi*	31.5	68.8	404	1.8	92 ± 12

The asterisk denotes a level at 7.632 MeV photoexcited by a Cd scatterer. All other levels are at 7.279 MeV and were photoexcited by a Pb scatterer.

[a]) The absorbing isotope was arbitrarily assumed to be ^{112}Cd.

[b]) The absorbing isotope was arbitrarily assumed to be ^{140}Ce.

[c]) Here ΔE is the energy difference between the incident γ-line and the resonance level (assuming no recoil correction in the absorbing nucleus).

REF.	R. Pitthan, H. Hass, D.H. Meyer, J.N. Dyer and F.R. Buskirk Phys. Rev. Lett. 41, 1276 (1978)	ELEM. SYM.	A	Z
		Ce		58
METHOD		REF. NO.		
		78 Pi 2		rs

REACTION	RESULT	EXCITATION ENERGY	SOURCE TYPE	SOURCE RANGE	DETECTOR TYPE	DETECTOR RANGE	ANGLE
E,E/	FMF	5- 45	D	0* 1	MAG-D		DST

*Q=0.3-0.7FM-1

(e,e') from the giant dipole resonance (GDR) in ^{140}Ce verifies the macroscopic model by Myers *et al.*, while ruling out the Steinwedel-Jensen model and, to a lesser extent, the Goldhaber-Teller model. This result leads to discrepancies between (α,α') and (e,e') concerning the existence of a giant-monopole (breathing-mode) state, particularly if one considers the independent verification of the Meyers *et al.* model by the experimental $A^{-0.23}$ energy dependence of the GDR.

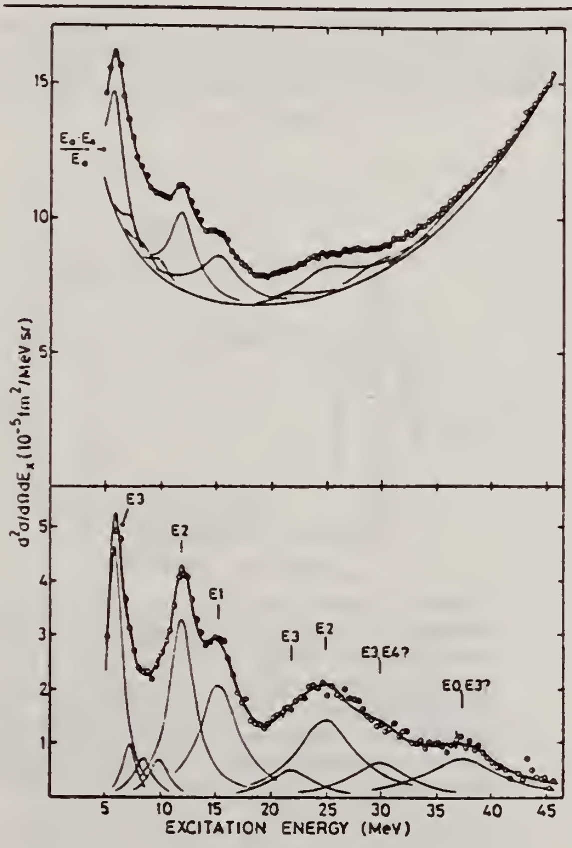

FIG. 1. Spectrum of 92.1-MeV electrons scattered inelastically from ^{140}Ce at 90°. The spectra with and without the background are shown together so that the difference between the two may be seen. The resonances which were used for fitting the spectrum and the background as described in the text are drawn. The "ghost peak" is subtracted from the lower graph. The spectrum was taken and fitted with 10 data points per MeV. For graphical purposes the number of points for the spectrum was reduced by a factor of 4. The fitting range was 4–46 MeV. The statistical error is shown on selected points. While the upper part has not been corrected for the constant dispersion of the magnetic spectrometer and thus shows the data points as measured, the subtracted spectrum has been corrected in order to show the cross sections of the resonances in their true relation. While lower states (ghost peak) and higher resonances (background sensitivity due to failure of the calculated radiation tail to account for the measured one above 20 MeV) have rather large uncertainties (up to 50%), the region between 10 and 20 MeV turned out to be very insensitive to the choice of the background function. Details of the principles of the analysis can be found in Ref. 9.

[9] R. Pitthan, F.R. Buskirk, E.B. Dally, J.O. Shannon, and W.H. Smith, Phys. Rev. C 16, 970 (1977).

Over

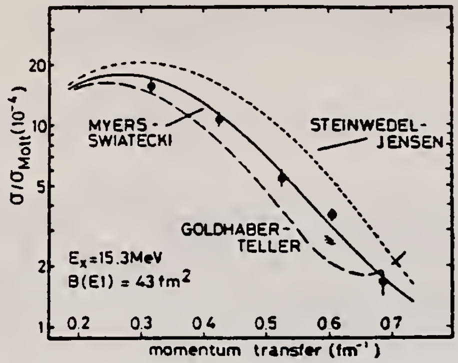

FIG. 2. Comparison between the experimental cross section divided by the Mott cross section [called form factor (squared) in the text] and DWBA calculations [S. T. Tuan *et al.*, Nucl. Instrum. Methods 60, 70 (1968)] as a function of momentum transfer. Since the data were taken at four different energies (150 MeV, 93°; 65 MeV, 93°; 80 MeV, 90°; 92 MeV, 90° and 105°), form factors were constructed from separate calculations at the correct momentum transfer for each energy and connected by a smooth curve. Other methods presenting (e,e') data in this case are possible, but ours has the advantage of not manipulating the experimental points.

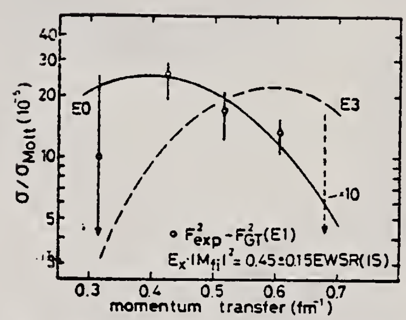

FIG. 3. The data points are identical to the *difference* between the cross section under the 15.3-MeV ($E1$) resonance and a DWBA calculation based on the GT model and normalized to (γ,n) results (lowest curve in Fig. 2). Comparison with a monopole DWBA calculation shows that this difference is compatible with the presence of 45% of the $E0$ EWSR. Reasons against such an interpretation are given in the text.

REF. R. Pitthan, H. Hass, D.H. Meyer, F.R. Buskirk, J.N. Dyer
Phys. Rev. C19, 1251 (1979)

ELEM. SYM.	A	Z
Ce		58

METHOD

REF. NO.	
79 Pi 4	hg

REACTION	RESULT	EXCITATION ENERGY	SOURCE TYPE	SOURCE RANGE	DETECTOR TYPE	DETECTOR RANGE	ANGLE
E,E/	ABX	6-38	D	50,92	MAG-D		DST
		-					

The cross section for electron scattering from natural cerium (89% ^{140}Ce) has been measured with electrons of 80 and 92 MeV at 90 and 105° between 4 and 48 MeV excitation energy. The nine resonances or resonance-like structures identified at E_x = 6 (31 $A^{-1/3}$), 7.4 (38 $A^{-1/3}$), 10 (52 $A^{-1/3}$), 12 (62 $A^{-1/3}$), 15.3 (79 $A^{-1/3}$), 22 (114 $A^{-1/3}$), 25 (130 $A^{-1/3}$), 31 (160 $A^{-1/3}$), and 37.5 (195 $A^{-1/3}$) MeV were classified on the basis of their momentum transfer dependence and discussed in the framework of the shell model. Since some of the arguments used are intricate we refer for quantitative particulars to the text. It is shown that the $E2$ sum rule strength not exhausted in the excitation range of this experiment may contribute up to 50% of the classical dipole sum rule to the photon cross section between 50 MeV and the pion threshold. The resonance at 10 MeV might be due to a separate oscillation of the excess neutrons against the rest of the nucleus.

NUCLEAR REACTIONS ^{140}Ce(e,e'), E_0 = 50 to 92 MeV, Measured $d^2\sigma/d\Omega dE_x$, bound and continuum states (giant resonances). Deduced multipolarity, reduced matrix element $B(E\lambda)$, radiative width Γ_γ^0, sum rule exhaustion of giant resonances, photon cross section to pion threshold, total width of continuum and clustered states.

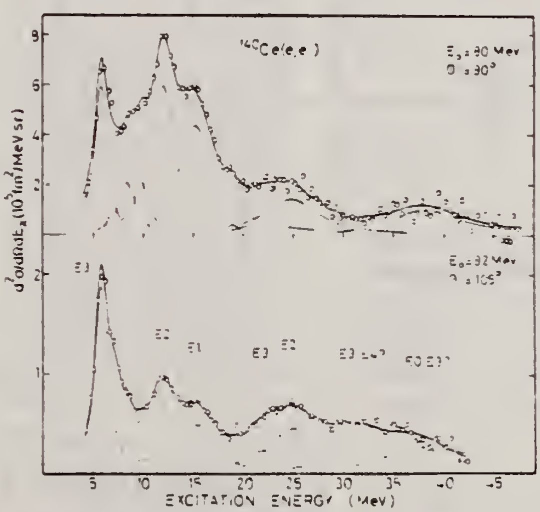

FIG. 3. Data of Fig. 2 after the fitted background (consisting of the radiation tail, the general room background, and experimental background) and the "ghost peak" as described in the text have beem subtracted. These two spectra are shown together so that the shrinkage of smaller multipolarity transitions versus the growth of higher multipolarity transitions may be seen. The relative change in peak heights of the single resonances indicate very clearly the various multipoles contributing. Note, e.g., that the $E2$ cross sections fall off more than a factor of 6 between the 80 MeV and the 92 MeV spectra.

ASSUMED TO BE 140-CE

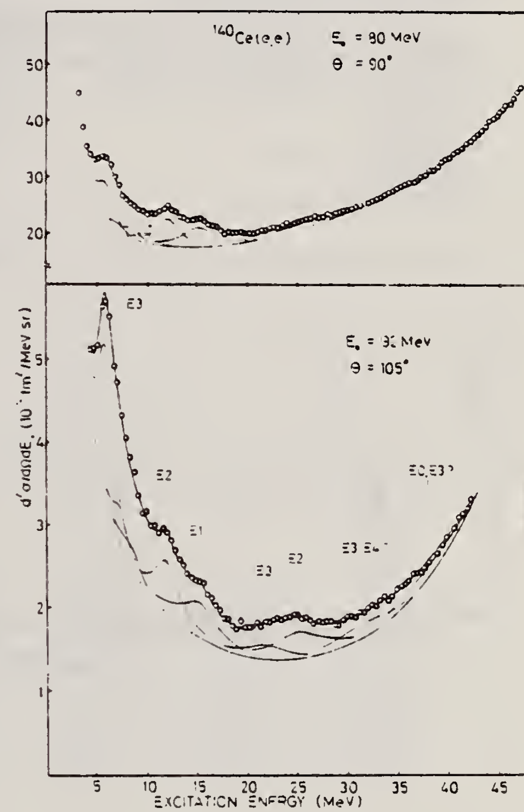

FIG. 2. Spectra of 80 and 92 MeV electrons scattered inelastically from ^{140}Ce. Resonances (or envelopes of discrete states) are indicated and discussed in more detail in the text. The bottom curved line in both parts is the fitted total background. Note that zero in the lower spectrum is *not* suppressed. The ghost peak has not been subtracted from the data, neither are the cross sections corrected for the constant dispersion of the magnetic spectrometer. The spectra were taken and fitted with 10 points per MeV, which were reduced for graphical purposes by a factor of 4. Resolution was 500 keV, approximately $\frac{1}{3}$ of the width of the smallest resonance found; the statistical error is shown on selected points in the lower spectrum; it was smaller than the circles in the upper one. The fitted range of the spectra shown was 4–48 MeV for the upper, and 4–42 MeV for the lower spectrum (see discussion in text in conjunction with the 37 MeV state).

(over)

TABLE X. Results in units of the reduced transition probabilities (B values), ground state radiation width (Γ_γ^0), and energy weighted sum rule exhaustion, for the major resonances found in this experiment. Some results for weaker states, and those inferred from differences between cross sections and DWBA calculation, are, together with the appropriate discussion, scattered in the text. The isospin assignments are not determined by this experiment, but were taken from comparison with other experiments and theory.

E_X (MeV)	$E_X A^{-1/3}$ (MeV)	Γ (MeV)	$E\lambda$	ΔT	B_{exp} (fm$^{2\lambda}$)[a]	Γ_γ^0 (eV)	R[b]	Std.[c] dev.	Total[d] error
6.0 ± 0.2	31	1.7 ± 0.2	3	0	1.3×10^5	2.0×10^{-3}	19	± 3	± 6
10.0 ± 0.2	52	1.8 ± 0.2	2	0	430	7.6	9	± 2	± 4
			0	0	770		13	± 2	± 6
12.0 ± 0.2	62	2.8 ± 0.2	2	0	2.5×10^3	10.0	63[e]	± 17	± 13
			2	0	2.0×10^3	8.7	50[f]	± 5	± 10
15.3 ± 0.2	79	4.4 ± 0.2	1	1	41	5.1×10^4	122[g]	± 12	± 20
			1	1	55	6.9×10^4	167[h]	± 40	± 27
22 ± 1	114	5 ± 1	3	0	3.7×10^4	4.9	19	± 2	± 10
25 ± 1	130	6.5 ± 1	2	1	1.3×10^3	2.1×10^3	50[i]	± 8	± 15
			2	1	2.1×10^3	3.3×10^3	77[h]	± 25	± 23
34 – 38	175	7 – 10	3	0	1.2×10^5	6.8×10^2	75	± 10	± 50/30
	195		0	1	2.8×10^3		130	± 20	± 30/45

[a] For the monopole the measured quantity is $|M_{if}|^2$ (fm^4).
[b] $R = E_X B(E\lambda)/\mathrm{EWSR}(E\lambda, \Delta T) \times 100$.
[c] The error given (in units of R) is the standard deviation of the average sum rule exhaustion and is, therefore, more a measure for the fit to a certain model than a measure for the total uncertainty.
[d] The total error (in units of R) is based on the maximum and minimum values found for the areas under the curves during the many attempts to fit the spectra.
[e] $c_{tr} = 1.0c$.
[f] $c_{tr} = 0.95c$.
[g] MS model with $\alpha = 0.76$.
[h] GT model.
[i] MS model with $\alpha = 1.0$.

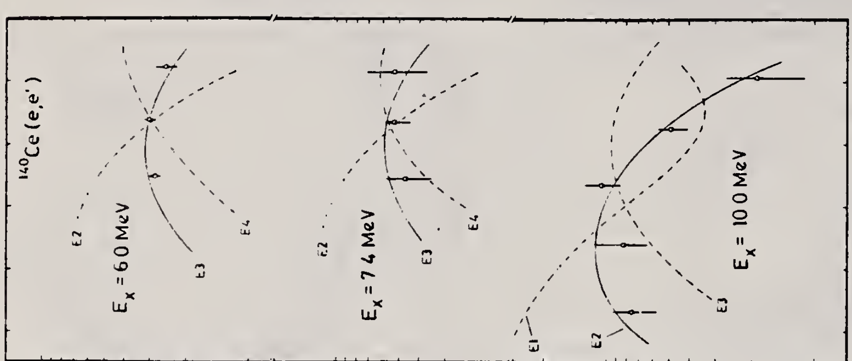

FIG. 12. Comparison of the DWBA and experimental form factors for the resonances found at 6.0, 7.4, and 10 MeV. The Goldhaber-Teller model for an $E3$ transition fits the experimental form factors of the 6.0 MeV resonance (Table X), while an $E2$ or $E4$ assignment of from factors can clearly be ruled out. The Goldhaber-Teller model for both an $E3$ and for an $E4$ transition fits the experimental form factors for the resonance found at 7.4MeV. An $E2$ assignment of the form factor, though, can be clearly ruled out. The Goldhaber-Teller model for an $E2$ ($E0$) transition fits the experimental form factors of the resonance found at 10 MeV, but the results depend on the interpretation of this mode (see Table V).

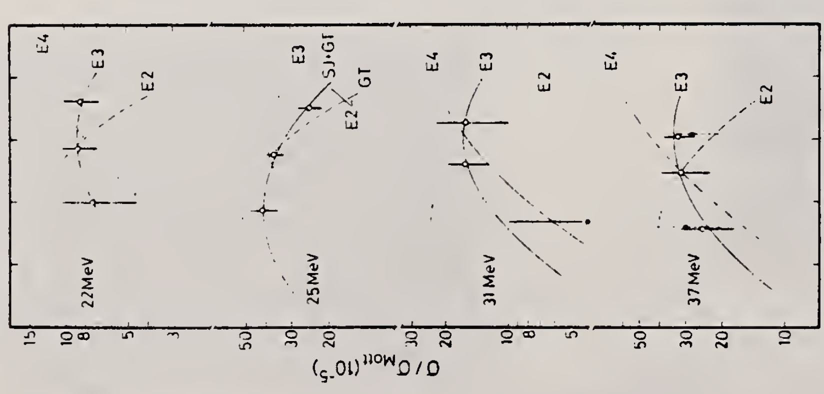

FIG. 10. Comparison of the DWBA and experimental form factors for the resonances found at 22, 25, 31, and 37 MeV. The Goldhaber-Teller model for an $E3$ transition fits the experimental form factors of the resonance found at 22 MeV. Both the Goldhaber-Teller and the Myers-Swiatecki $E2$ models were fit to the experimental form factors for the resonance found at 25 MeV (Table X). The Myers-Swiatecki model with a mixture ratio of 1.0 was found to fit the data better than the Goldhaber-Teller model as explained in the text. The assignment of an $E3$ transition can be clearly ruled out. The experimental form factor of the resonance found at 31 MeV fit the Goldhaber-Teller model for both $E3$ and $E4$ transition. An upper value could only be estimated for the form factor obtained from the 80 MeV/90° experiment, based on the statistical error of the measurement. The assignment of an $E2$ transition can be ruled out. The assignment of the resonance around 37 MeV is the most difficult. Because of the intricate arguments, we refer to the text.

REF.	ELEM. SYM.	A	Z
A. Leprêtre, H. Beil, R. Bergère, P. Carlos, J. Fagot, A. De Miniac, A. Veyssière Nucl. Phys. A367, 237 (1981)	Ce		58

METHOD	REF. NO.	
	81 Le 1	egf

REACTION	RESULT	EXCITATION ENERGY	SOURCE TYPE	SOURCE RANGE	DETECTOR TYPE	DETECTOR RANGE	ANGLE
G,SN	ABX	25-140	D	25-140	MOD-I		4PI
G,XN	ABX	25-140	D	25-140	MOD-I		4PI
		-					

(G,SN) NO G,1N IN G,SN
See 82LE3

Abstract: The total photonuclear absorption cross section for Sn, Ce, Ta, Pb and U has been studied from 25 to 140 MeV using a continuously variable monochromatic photon beam obtained from the annihilation in flight of monoenergetic positrons. The basic experimental results are a set of data giving sums of inclusive multiple photoneutron production cross sections of the form $\sigma^{(i)}(E_\gamma) = \sum_{i=j} \sigma(\gamma, in: E_\gamma)$ for neutron multiplicities ranging from $i = 1$ to 12. From these data the total photonuclear absorption cross section $\sigma(\text{tot}: E_\gamma)$ has been deduced. It is concluded that Levinger's modified quasideuteron model describes the total cross sections reasonably well. When these data are combined with lower energy data and integrated to 140 MeV they indicate the need for an enhancement factor K for the Thomas–Reiche–Kuhn sum rule of 0.76 ± 0.10. No evidence was found that would indicate an A-dependence for the enhancement factor.

$$\sigma^{(i)}(E_\gamma) = \sum_{i=i} \sigma(\gamma, in: E_\gamma).$$

E

PHOTONUCLEAR REACTIONS Sn, Ce, Ta, Pb, U(γ, xn), E_γ = 25–140↓ MeV; measured $a(E_\gamma)$ summed for x = 1–12; deduced $\sigma(E_\gamma$, total), integrated σ, interaction models. Monochromatic photons.

TABLE 3

Integrated cross sections

		Sn	Ce	Ta	Pb	U	U
$\sigma_0 = 0.06NZ/A$ (MeV · b)		1.74	2.04	2.61	2.97	3.40	3.40
$E_{\gamma 0}$(MeV)		29.7	25	25	25	18	18.30
$M = \int_{B_{1n}}^{E_{\gamma 0}} \sigma_{GDR}(E_\gamma)\,dE_\gamma$	(MeV · b)	2.0 ± 0.15 [a])	2.13 ± 0.15 [b])	2.90 ± 0.23 [b])	3.48 ± 0.23 [c])	2.98 ± 0.15 [d])	3.58 [e])
	(σ_0 unit)	1.15 ± 0.09	1.04 ± 0.07	1.11 ± 0.09	1.17 ± 0.08	0.88 ± 0.05	1.05
$N = \int_{E_{\gamma 0}}^{140\text{ MeV}} \sigma^{(2)}(E_\gamma)\,dE_\gamma$	(Mev · b)	0.96 ± 0.1	1.27 ± 0.1	1.73 ± 0.15	1.69 ± 0.15	2.59 ± 9.2	2.59 ± 0.2
	(σ_0 unit)	0.55 ± 0.06	0.63 ± 0.05	0.66 ± 0.06	0.57 ± 0.05	0.76 ± 0.06	0.76 ± 0.06
$M + N$	(MeV · b)	2.96 ± 0.2	3.40 ± 0.2	4.63 ± 0.3	5.17 ± 0.3	5.57 ± 0.3	6.17 ± 0.3
	(σ_0 unit)	1.70 ± 0.12	1.67 ± 0.10	1.77 ± 0.10	1.74 ± 0.10	1.64 ± 0.10	1.81 ± 0.10
$(M + N)$ + evaluation of the $\int_{E_{\gamma 0}}^{140\text{ MeV}} \lvert\sigma^{(1)} - \sigma^{(2)}\rvert\,dE_\gamma$ contribution $= (1 + K)$ (σ_0 unit)		1.74 ± 0.15	1.71 ± 0.15	1.81 ± 0.15	1.78 ± 0.15	1.68 ± 0.15	1.85 ± 0.15
$\int^{\infty} \sigma_L(E_\gamma)\,dE_\gamma$ (σ_0 unit)		1.28 [a])	1.24 [b])	1.30 [b])	1.35 [c])	1.18 [d])	1.43 [e])

[a]) Ref. [26]). [b]) Ref. [27]). [c]) Ref. [5]). [d]) Ref. [28]). [e]) Ref. [29]).

The symbols M and N are defined in the text. The last row gives the integrated cross sections for the Lorentz line fit, $\sigma_L(E_\gamma)$ to the GDR data, published in the above references.

(OVER)

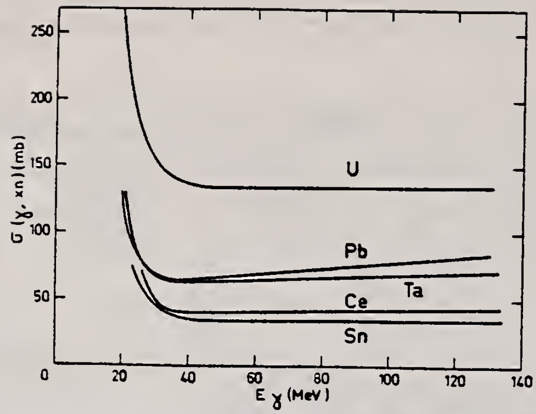

Fig. 11. The general behaviour of the "smoothed" average neutron yield cross sections $\sigma(\gamma, xn) = \sum_i i\sigma(\gamma, in: E_\gamma)$ for the Sn, Ce, Ta, Pb and U nuclei studied in the present paper (see text).

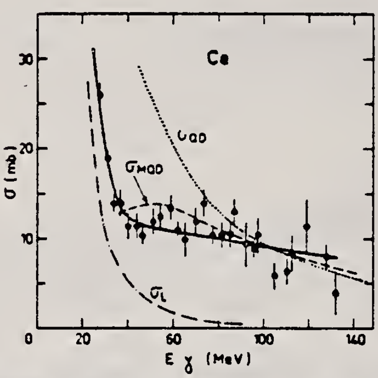

Fig. 15. Total photonuclear absorption cross sections $\sigma(\mathrm{tot}: E_\gamma) = \sigma^{(2)}(E_\gamma)$ from the present paper, represented by the experimental points and the corresponding full lines, are shown for Pb, Sn, Ce, Ta and U. These experimental results for photon energies E_γ between 20 and 140 MeV are compared with: (a) Lorentz line fits to the GDR data of the appropriate nucleus represented by the dot-dash $\sigma_L(E_\gamma)$ plots. (b) Quasideuteron cross sections, $\sigma_{QD}(E_\gamma) = (4.6NZ/A)\sigma_D(E_\gamma)$ for the appropriate nuclei, represented by the dotted $\sigma_{QD}(E_\gamma)$ plots. Here $\sigma_D(E_\gamma)$ is the photodisintegration cross section of deuterium. (c) Modified quasideuteron cross sections, $\sigma_{QDM}(E_\gamma) = (8NZ/A)\sigma_D(E_\gamma)\exp(-D/E_\gamma)$ with $D = 60$ MeV, represented by the dashed $\sigma_{MQD}(E_\gamma)$ plots. Pertinent GDR data for Pb, Sn, Ce, Ta and U were taken from refs. [5,26-28]).

REF. M. Schumacher, F. Smend, W. Mückenheim, P. Rullhusen, H.G. Börner
Z. Phys. A300, 193 (1981)

ELEM. SYM.	A	Z
Ce		58

METHOD

REF. NO.	
81 Sc 6	egf

REACTION	RESULT	EXCITATION ENERGY	SOURCE TYPE	SOURCE RANGE	DETECTOR TYPE	DETECTOR RANGE	ANGLE
G,G	ABX	2-7		2-7	SCD-D		90

2.60-6.76 MEV

Elastic scattering by nuclei in the range of mass numbers between 64 and 238 has been studied with monochromatic photons in the energy range between 2 and 8 MeV. These photons were provided either by a Ti(n,γ) source installed in the tangential through channel of the Grenoble high flux reactor, or by ^{24}Na and ^{56}Co sources produced by deuteron bombardment of Al or Fe at the Göttingen cyclotron. The photoexcitation of 23 nuclear levels has been observed and the decay properties and groundstate widths of the majority of these levels have been determined. For the lead scattering target the coherent elastic differential cross section has been studied in detail. There is evidence that below the photo-neutron threshold the elastic scattering via virtual photoexcitation of the nucleus can be approximated by extrapolating the real part of the Giant Dipole Resonance amplitude along a Lorentzian curve. Coulomb corrections to Delbrück scattering seem to play a small role at 6.5 MeV.

Table 4. Properties of levels observed by photoexcitation. $(d\sigma/d\Omega)^{NRF}$: experimental differential cross section per identified isotope or element for resonance scattering through $\Theta = 90°$. I^π: spin-parity of excited level; $W(\Theta)$: angular correlation function; $g = (2I_{ex}+1)/(2I_g+1)$; Γ_0: radiative groundstate transition width. Γ: total level width. Errors in the last digits are given in parentheses

Isotope	E_γ (MeV)	$(d\sigma/d\Omega)^{NRF}$ (μb/sr)	I^π	Γ_0/Γ [e]	$W(\Theta)g\Gamma_0^2/\Gamma$ (meV)	Γ_0 [f] (meV)	Γ_0 [g] (meV)
^{238}U	2.754	13 (4)	(1)	0.77	0.145	0.084	-
^{235}U	3.254	421 (5)	1^-	0.24	0.83	1.5	0.52(15) [d]
^{209}Bi	6.555	2.1 (4)·10^2	-	-	0.74	0.74 [b]	-
^{209}Bi	7.168	1.7 (3)·10^5	$9/2^-$ [e]	1.00	710	786	820 (40) [a]
^{203}Tl	6.418	8.75(30)·10^3	$1/2$ [e]	0.28	30	102	82 (15) [a]
Tl	6.759	7 (3)	-	-	-	-	-
Hg	6.555	68 (17)	-	-	-	-	-
^{186}W	6.418	5.2 (3)·10^2	1^- [e]	0.32	1.75	2.4	-
^{184}W	6.555	9.8 (10)·10^2	(1)	0.32	3.44	2.9	-
^{184}W	6.759	46 (10)	(1)	0.58	0.17	0.13	-
^{181}Ta	3.010	174 (17)	-	0.72	0.42	0.59	-
^{181}Ta	6.418	62 (4)	-	0.73	0.2	0.27 [c]	-
^{181}Ta	6.759	4.8 (12)	-	-	0.018	0.018 [b]	-
^{165}Ho	6.418	10.3 (30)	-	-	0.035	0.035 [b]	-
^{165}Ho	6.759	5.6 (14)	-	-	0.021	0.021 [b]	-
Nd	2.754	2.6 (5)	-	-	-	-	-
Nd	3.254	14.0 (10)	-	-	-	-	-
Ce	6.759	13.4 (10)	-	-	-	-	-
^{121}Sb	3.452	2.20 (5)·10^3	-	0.60	2.9	4.9 [b]	-
^{100}Mo	6.418	1.53 (4)·10^4	1^- [a]	0.88	52	26	25 (8) [a]
^{94}Mo	6.555	4.4 (4)·10^3	(1)	0.33	15	21	-
Mo	6.759	6.2 (15)	-	-	-	-	-
Mo	7.168	8.2 (26)·10^2	-	-	-	-	-

[a] [11] [b] $W(\Theta)g\Gamma_0/\Gamma = 1$ assumed [c] $W(\Theta)g = 1$ assumed
[d] [28] (a small correction has been applied to the data of [28])
[e] Upper limits in case not all the transitions to lower levels were observed
[f] Present work [g] Previous work

(OVER)

Table 1. Differential cross sections for elastic scattering $(d\sigma/d\Omega)^{exp}$ of photons from ^{56}Co and ^{24}Na sources by different scattering targets, in units of μb/sr. Errors in the last digits are given in parentheses.

Θ deg	Scattering targets	2.599[a] (MeV)	2.754[b] (MeV)	3.010[a] (MeV)	3.202[a] (MeV)	3.254[a] (MeV)	3.273[a] (MeV)	3.452[a] (MeV)
90	^{238}U	52.7(25)	57.5(25)[c]	56(16)	47(4)	456 (10)[c]	34(6)	49(14)
	^{209}Bi	33.1(30)	32 (2)	33(11)	32(4)	25.6(20)	29(6)	33(15)
	^{nat}Pb	31.5(23)	31.0(16)	35 (8)	27(3)	26.6(22)	25(4)	23 (8)
	^{nat}Tl	31.5(33)	-	27(12)	32(5)	24 (3)	22(7)	34(15)
	^{nat}Hg	30.0(27)	-	24(10)	28(5)	25.5(18)	26(8)	20 (8)
	^{nat}W	22.5(11)	-	17 (7)	19(3)	18.4(15)	18(5)	21 (6)
	^{181}Ta	20.0(15)	19.2 (6)	193(20)[c]	20(4)	17.3(21)	18(5)	21 (8)
	^{165}Ho	15.9(13)	-	17(10)	13(6)	15.6(20)	18(8)	-
	^{nat}Nd	11.4 (7)	14.2 (5)[d]	15 (7)	14(3)	24.2(12)[d]	13(3)	9 (6)
	^{nat}Ce	11.1 (9)	11.0 (5)	-	11(3)	9.5(13)	8(4)	-
	^{127}I	8.4(10)	8.6 (5)	-	9(2)	7 (1)	5(3)	-
	^{nat}Sb	8.0(11)	-	-	10(4)	6.8(19)	-	1,270(50)[c]
	^{nat}Sn	6.5 (7)	7.0 (5)	-	5(2)	7.6 (8)	6(3)	-
	^{nat}Cd	6.2 (5)	-	-	6(2)	6.6 (8)	7(3)	-
120	^{238}U	55.1(25)	64 (4)[c]	43(15)	55(5)	574 (10)[c]	48(5)	48(11)
	^{181}Ta	27.5(15)	25.0 (9)	227(20)[c]	22(5)	21 (2)	22(8)	-
	^{nat}Nd	17.9(30)	17.0 (9)[d]	-	-	29.8(47)[d]	-	-

[a] ^{56}Co source in Fe lattice [b] ^{24}Na source in Al lattice (part of data have been published elsewhere)
[c] Transitions to excited states observed in addition to the ground-state transition
[d] Photoexcitation of nuclear level identified from the size of the differential cross section

Table 2. Elastic differential cross sections $d\sigma/d\Omega(\Theta=90°)$ in μb/sr measured with the Ti(n,γ) source and compared with theoretical predictions. n: predicted number of levels in a $\Delta E = 25$ eV interval at 6.5 MeV. Errors in the last digits are given in parentheses

Scattering target	6.418 MeV		6.555 MeV		6.759 MeV		7.168 MeV		n
	exp.	th.	exp.	th.	exp.	th.	exp.	th.	
^{238}U	23 (12)	10.3	-	-	-	-	-	-	45
^{209}Bi	-	-	219(39)[b,c]	8.0	12 (4)	7.4	1.5(3)·10^{5}[b,c]	5.7	0.1
^{nat}Pb	7.0(15)	8.6	-	-	6.5(11)	7.4	-	-	0.05
^{nat}Tl	2,586 (92)[a,c]	7.5	-	-	13 (3)[b]	6.0	-	-	0.4
^{nat}Hg	12 (3)	7.8	74(17)[b]	6.5	6.7(15)	6.4	-	-	3.4
^{nat}W	159 (10)[a,c]	6.6	306(33)[a,c]	6.3	20 (2)[a,c]	5.6	-	-	13
^{181}Ta	68 (4)[a,c]	6.3	-	-	10.1(12)[b,c]	5.3	-	-	28
^{165}Ho	15 (3)[b]	4.7	-	-	9.5(14)[b]	3.9	-	-	18
^{nat}Ce	4.1(21)	4.1	-	-	17 (1)[b,c]	3.6	-	-	0.04
^{nat}Sn	4.2(13)	3.0	-	-	2.5 (5)	2.7	-	-	1.9
^{nat}Mo	1,474 (44)[a,c]	2.5	407(39)[a,c]	2.5	8.5(15)[b,c]	2.3	817(258)[b,c]	2.0	0.5
^{nat}Zn	2.4 (8)	1.6	-	-	1.8 (5)	1.5	-	-	0.3

[a] Transitions to excited states observed [b] Photoexcitation identified from size of differential cross section
[c] Photoexcitation reported in [11]

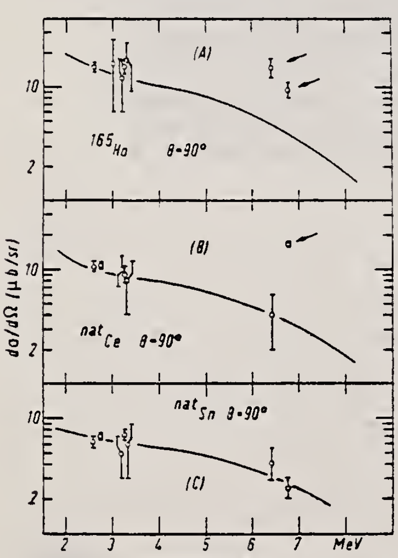

Fig. 11. Same as Fig. 9 but for (A) ^{165}Ho, (B) ^{nat}Ce and (C) ^{nat}Sn

REF.	A. Leprêtre, H. Beil, R. Bergère, P. Carlos, J. Fagot, A. Veyssière I. Halpern Nucl. Phys. A390, 221 (1982)	ELEM. SYM.	A	Z
		Ce		58
METHOD		REF. NO.		
		82 Le 3		EGF

REACTION	RESULT	EXCITATION ENERGY	SOURCE TYPE	SOURCE RANGE	DETECTOR TYPE	DETECTOR RANGE	ANGLE
G,XN	NOX	30-140	D	30-140	MOD-I		4PI

See also A. Lepretre et al. NP A390, 240 (1982) MULT ANAL 81LE1

Abstract: From event-by-event records of observed photoneutron multiplicities for photons from 30 to 140 MeV on several heavy targets (Sn, Ce, Ta and Pb), it was possible to determine the mean number of photoneutrons, $\bar{\nu}$, for each photon energy and the widths W of the multiplicity distributions. The mean neutron numbers increase smoothly from about three to six over the photon energy span for all four targets. The widths go from about one to two neutrons in the same interval. When these measurements are combined with other photonuclear information, it is possible to extract the average numbers of fast neutrons and fast protons and the average number of evaporation neutrons emitted per photoabsorption.

E | PHOTONUCLEAR REACTIONS Sn, Ce, Ta, Pb(γ, xn), E = 25–140 MeV; measured photoneutron mean numbers, width distributions; deduced fast evaporation neutron, fast proton average numbers. Monochromatic photons.

TABLE 2

Photonucleon emission features for four targets at 70 MeV

	Sn	Ce	Ta	Pb
$\bar{\nu}$	4.3 ± 0.2	4 ± 0.2	4.5 ± 0.2	4.8 ± 0.2
$\overline{\nu_f}$	0.50 ± 0.11	0.59 ± 0.13	0.71 ± 0.16	0.66 ± 0.15
$\overline{\pi_f}$	0.24 ± 0.05	0.26 ± 0.05	0.27 ± 0.05	0.23 ± 0.04
$\overline{\nu_s}$	3.8 ± 0.3	3.4 ± 0.3	3.8 ± 0.3	4.1 ± 0.3
$\overline{E_f}$ (MeV)	23.4 ± 5	26.3 ± 6	28.7 ± 6	26.6 ± 6
$\overline{E^*}$ (MeV)	46.6 ± 6	43.7 ± 5	41.3 ± 5	43.4 ± 5

(See caption under table 1.)

Experimental data are taken from ref. [1]) and fig. 2 of this paper. ν stands for neutrons and π for protons; f stands for fast particles and s for evaporated particles. $\bar{E}^*$ is the residual excitation energy after all fast particles have escaped – carrying with them energy $\bar{E}_f$. The coefficients α and β have to do with the ratio of fast neutrons to fast protons that are emitted. They are explained in the text. The uncertainties in this table are statistical only.

(OVER)

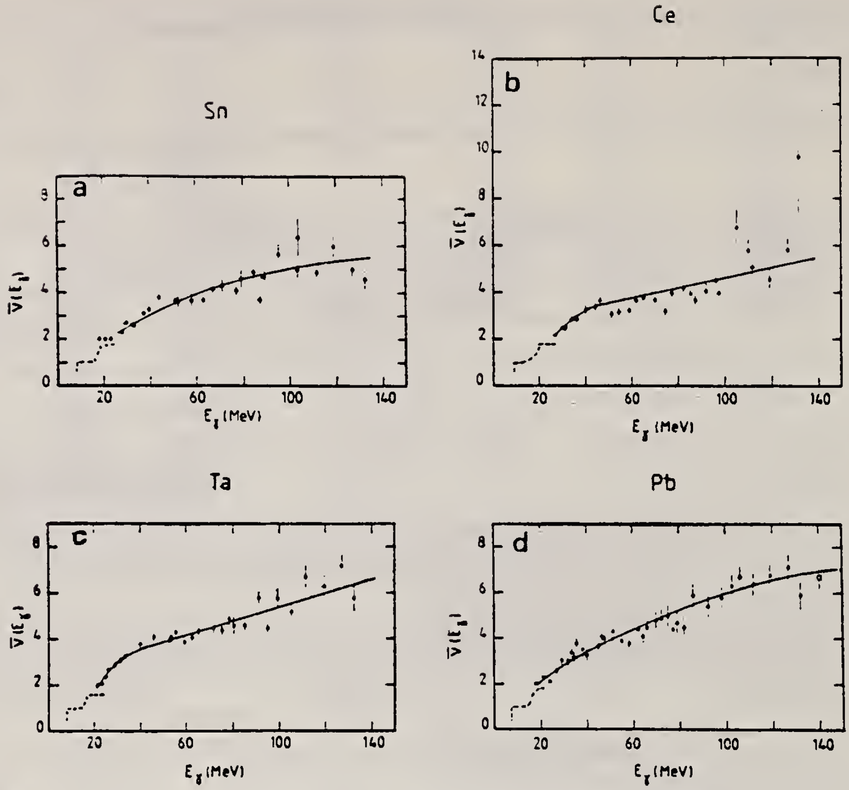

Fig. 2. Average experimental photoneutron multiplicities $\bar{\nu}(E_\gamma)$ plotted against photon energy E_γ, for 25 MeV $\leq E_\gamma \leq$ 140 MeV. Data points were evaluated using results from ref. [1]). The full line represents a smoothed average behaviour. The dashed line represents $\bar{\nu}(E_\gamma)$ values, measured in the giant dipole resonance (GDR) region, in previous Saclay experiments [7]). Fig. 2a: Sn; fig. 2b: Ce; fig. 2c: Ta; fig. 2d: Pb [where the □ point refers to the SIN [19]) measurement with stopped π^-].

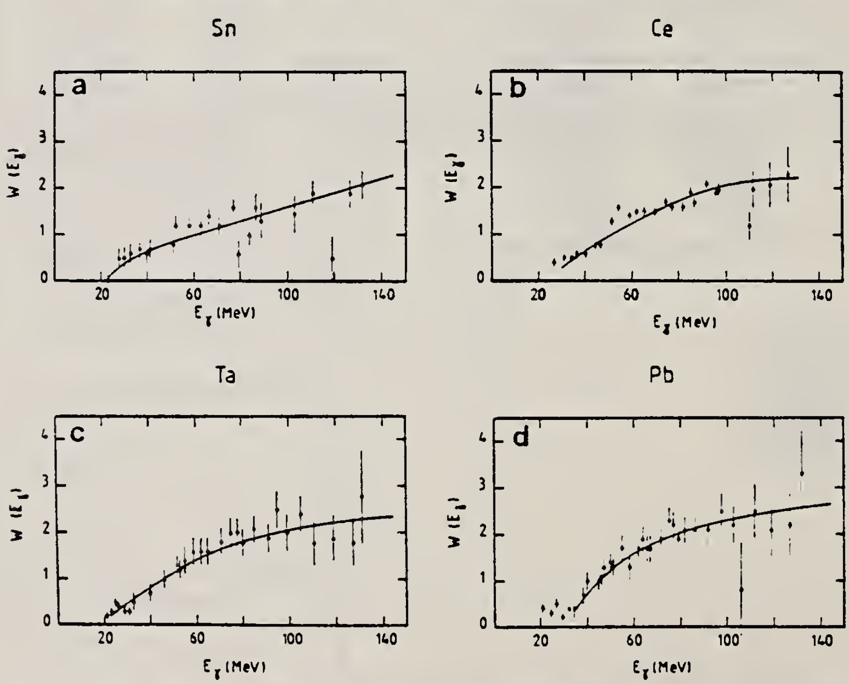

Fig. 3. Widths, $W(E_\gamma)$ of the experimental photoneutron multiplicity distributions as a function of the photon energy E_γ for 25 MeV $\leq E_\gamma \leq$ 140 MeV. Data points were evaluated using results from ref. [1]). The full line represents a smoothed average behaviour. Fig. 3a: Sn; fig. 3b: Ce; fig. 3c: Ta; fig. 3d: Pb.

Ce
A=138

Ce
A=138

REF.	ELEM. SYM.	A	Z
P. E. Haustein and A. F. Voigt J. inorg. nucl. Chem. <u>33</u>, 289 (1971)	Ce	138	58

METHOD	REF. NO.	
	71 Ha 2	egf

REACTION	RESULT	EXCITATION ENERGY	SOURCE TYPE	SOURCE RANGE	DETECTOR TYPE	DETECTOR RANGE	ANGLE
G,N	RLY	10-70	C	70	ACT-I		4PI

Isomer ratio = (yield to low spin state)/(yield to high spin state) <u>ISOMER RATIO</u>

Table 2. Isomer ratio measurements for ^{91}Mo, ^{137}Ce, and ^{141}Nd

Reaction	Isomer ratio	I^{π} Target	I^{π} Ground state	I^{π} Isomer	Threshold (MeV)	$41A^{-1/3}$ (MeV)
^{92}Mo(γ, n)^{91}Mo	$1{\cdot}92 \pm 0{\cdot}15$	0^+			13·13	16·60
			$9/2^+$	$1/2^-$		
^{94}Mo(γ, $3n$)^{91}Mo	$1{\cdot}59 \pm 0{\cdot}16$	0^+			30·72	16·52
^{138}Ce(γ, n)^{137}Ce	3·1	0^+			10·31	15·30
			$3/2^+$	$11/2^+$		
^{140}Ce(γ, $3n$)^{137}Ce	$1{\cdot}10 \pm 0{\cdot}12$	0^+			26·34	15·26
^{142}Nd(γ, n)^{141}Nd	$5{\cdot}2 \pm 0{\cdot}3$	0^+			9·79	15·22
			$3/2^+$	$11/2^+$		
^{144}Nd(γ, $3n$)^{141}Nd	$1{\cdot}80 \pm 0{\cdot}25$	0^+			23·67	15·17

Ce
A=140

Ce
A=140

Ce
A=140

J.H. Carver, G.E. Coote, T.R. Sherwood
Nuclear Phys. 37, 449 (1962)

Elem. Sym.	A	Z
Ce	140	58

Method: 30 MeV electron synchrotron; activation; NaI

Ref. No.: 62 Ca 1 — JHH

Reaction	E or ΔE	E_o	Γ	$\int \sigma dE$	Jπ	Notes
$Ce^{140}(\gamma,n)$	Bremss. 30					

TABLE 1

Isomeric ratios from (γ, n) reactions

Target nucleus	Ref.	J_0	Residual nucleus	Ground state Spin	Ground state Half-life	Metastable state Spin	Metastable state Half-life	Intermediate state Spin	Isomer ratio $Y_1/(Y_1+Y_2)$	σ
Co^{59}		$\frac{7}{2}^-$	Co^{58}	2^+	71.3 d	5^+	9.2 h		0.44 ± 0.02	3.2 ± 0.2
Ge^{76}		0^+	Ge^{75}	$\frac{1}{2}^-$	82 min	$\frac{7}{2}^+$	49 s		0.48 ± 0.07	2.8 ± 0.5
Br^{81}		$\frac{3}{2}^-$	Br^{80}	1^+	18 min	5^-	4.4 h	2^-	0.32 ± 0.02	6.5 ± 1.0
Sr^{86}		0^+	Sr^{85}	$\frac{9}{2}^+$	64 d	$\frac{1}{2}^-$	70 min	$\frac{7}{2}^+$	0.36 ± 0.07	2.2 ± 0.4
Zr^{90}		0^+	Zr^{89}	$\frac{9}{2}^+$	79 h	$\frac{1}{2}^-$	4.4 min		0.33 ± 0.10	2.8 ± 0.7
Mo^{92}		0	Mo^{91}	$\frac{9}{2}^+$	15.7 min	$\frac{1}{2}^-$	66 s		0.46 ± 0.04	6^{+4}_{-2}
Ag^{107}		$\frac{1}{2}^-$	Ag^{106}	1^+	24 min	6	8.3 d		0.04 ± 0.02	2.0 ± 0.3
In^{113}		$\frac{9}{2}^+$	In^{112}	1^+	14.5 min	4^+	20.7 min	7^-	0.8 ± 0.1	3.1 ± 0.7
Cd^{116}		0^+	Cd^{115}	$\frac{1}{2}^+$	53 h	$\frac{11}{2}^-$	43 d		$\leqq 0.2$	$\leqq 3$
Ce^{140}		0^+	Ce^{139}	$\frac{3}{2}^+$	140 d	$\frac{11}{2}^-$	55 s		0.08 ± 0.01	2.5 ± 0.2
Hg^{198}		0^+	Hg^{197}	$\frac{1}{2}^-$	65 h	$\frac{13}{2}^+$	24 h	$\frac{5}{2}^-$ $\frac{3}{2}^-$	0.05 ± 0.01	3.4 ± 0.5
Previous work										
Br^{81}	10)	$\frac{3}{2}^-$	Br^{80}	1^+	18 min	5^-	4.4 h	2^-	0.33	6.5
Se^{82}	12)	0^+	Se^{81}	$\frac{1}{2}^-$	18 min	$\frac{7}{2}^+$	57 min		0.5	3.0
Zr^{90}	11)	0^+	Zr^{89}	$\frac{9}{2}^+$	79 h	$\frac{1}{2}^-$	4.3 min		0.44 ± 0.06	4.5 ± 1
In^{115}	23)	$\frac{9}{2}^+$	In^{114}	1^+	72 s	5^+	50 d	8 ($T_{\frac{1}{2}} = 2.5$ s)	0.85	5.0

The yields Y_1 and Y_2 are for (γ, n) reactions ending in the isomeric- or ground-state. The yield Y_1 is for the higher-spin state.

References

1) J. R. Huizenga and R. Vandenbosch, Phys. Rev. 120 (1960) 1305
2) T. Ericson, Advances in Physics 9 (1960) 425
3) D. L. Allan, Nuclear Physics 24 (1961) 274
4) C. T. Hibdon, Phys. Rev. 114 (1959) 179
5) C. T. Hibdon, Phys. Rev. 122 (1961) 1235
6) T. Ericson, Nuclear Physics 11 (1959) 481
7) J. H. Carver, and G. A. Jones, Nuclear Physics 19 (1960) 184
8) A. C. Douglas and N. MacDonald, Nuclear Physics 13 (1959) 382
9) T. Ericson and V. M. Scrutinski, Nuclear Physics 8 (1958) 284
10) L. Katz, L. Pease and H. Moody, Can. J. Phys. 30 (1952) 476
11) L. Katz, R. G. Baker and R. Montalbetti, Can. J. Phys. 31 (1953) 250
12) E. Silva and J. Goldemberg, An Acad. Brasil Cience 28 (1956) 275
13) J. H. Carver and D. C. Peaslee, Phys. Rev. 120 (1960) 2155
14) J. M. Blatt and V. F. Weisskopf, Theoretical nuclear physics (John Wiley, New York, 1952)
15) S. H. Vegors, L. L. Marsden and R. L. Heath, U. S. Atomic Energy Commission Report IDO-16370 (1958)
16) Nuclear Data Sheets (National Research Council, Washington, 1960) sets 1-5 inclusive
17) R. Vandenbosch and J. R. Huizenga, Phys. Rev. 120 (1960) 1313
18) E. Weigold and R. N. Glover, Nuclear Physics 32 (1962) 106
19) K. J. Le Couteur and D. W. Lang, Nuclear Physics 13 (1959) 32
20) T. D. Newton, Can. J. Phys. 34 (1956) 804
21) D. W. Lang, Nuclear Physics 26 (1961) 434
22) M. E. Rose, Internal conversion coefficients (North Holland Publ. Co., Amsterdam, 1958)
23) J. Goldemberg and L. Katz, Phys. Rev. 90 (1953) 308

REF.	ELEM. SYM.	A	Z
H. Fuchs, R. Kosiek, U. Meyer-Berkhout Z. Physik 166, 590 (1962)	Ce	140	58

METHOD	REF. NO.	
Betatron; neutron yield; radioactivity	62 Fu 6	NVB

REACTION	RESULT	EXCITATION ENERGY	SOURCE		DETECTOR		ANGLE
			TYPE	RANGE	TYPE	RANGE	
G,N	RLY	5 - 31	C	31	ACT - I		4PI

$$\frac{Y(Ce^{139\ m+g})}{Y(Cu^{62})} = 3.2 \pm 0.35, \quad E_o = 31 \text{ MeV}$$

Tabelle 2. *Ausbeuteverhältnisse für die Reaktionen am Silber und Cer. E_0 ist die Maximalenergie der Bremsstrahlung, Y_1/Y_2 ist das Verhältnis der Ausbeute der in der ersten Spalte genannten Reaktion zu der Ausbeute der Reaktion in der zweiten Spalte*

Reaktion 1	Reaktion 2	E_0 (MeV)	Y_1/Y_2
$Ag^{107}(\gamma, n)Ag^{106m}$	$Ag^{107}(\gamma, n)Ag^{106g}$	34	0,08 ± 0,015
$Ag^{107}(\gamma, n)Ag^{106m}$	$Ag^{107}(\gamma, n)Ag^{106g}$	18	0,06 ± 0,010
$Ag^{107}(\gamma, n)Ag^{106m+g}$	$Ag^{107}(\gamma, n)Ag^{106g}$	34	1,08 ± 0,015
$Ag^{107}(\gamma, 2n)Ag^{105}$	$Ag^{107}(\gamma, n)Ag^{106g}$	34	0,12 ± 0,06
$Ag^{107}(\gamma, 2n)Ag^{105}$	$Ag^{107}(\gamma, n)Ag^{106g}$	18	0,06 ± 0,03
$Ag^{109}(\gamma, n)Ag^{108}$	$Ag^{107}(\gamma, n)Ag^{106g}$	34	0.92 ± 0.14
$Ce^{140}(\gamma, n)Ce^{139m}$	$Ce^{140}(\gamma, n)Ce^{139g}$	31	0,193 ± 0,014
$Ce^{140}(\gamma, n)Ce^{139m}$	$Ce^{140}(\gamma, n)Ce^{139g}$	23,8	0,182 ± 0,018

REF.	ELEM. SYM.	A	Z
Y. Oka, T. Kato and A. Yamadera Bull. Chem. Soc. Japan 41, 1606 (1968)	Ce	140	58

METHOD	REF. NO.	
	68 Ok 2	egf

REACTION	RESULT	EXCITATION ENERGY	SOURCE TYPE	SOURCE RANGE	DETECTOR TYPE	DETECTOR RANGE	ANGLE
G,N	ABY	THR-20	C	20	ACT-I		4PI

ISOMERIC YIELD

TABLE 1. THE PARTICULARS OF THE (γ,n) REACTION PRODUCTS AND THE DATA OBTAINED WITH 20 MeV BREMSSTRAHLUNG

Nuclide: Parent (Natural abundance, %)	Nuclide: Residual	Half-life of product (sec)	Gamma-ray determined: Energy (MeV)	Gamma-ray determined: Branching ratio (%)	Gamma-ray determined: Photopeak activity (cpm/mg)[a]	Limit of detection (μg)	Yield ($mol^{-1} \cdot R^{-1}$)
^{24}Mg(78.60)	^{23}Mg	9.9	0.511	200	2.04×10^{6}	0.49	8.1×10^{4}
^{74}Ge(7.67)	^{73m}Ge	48	0.139	100	6.37×10^{5}	1.6	1.1×10^{4}
^{78}Se(23.52)	^{77m}Se	17	0.162	100	1.82×10^{6}	0.55	1.2×10^{6}
^{92}Mo(15.86)	^{91m}Mo	65	0.650	57	2.22×10^{5}	4.5	2.7×10^{6}
^{140}Ce(88.48)	^{139m}Ce	58	0.745	100	1.06×10^{6}	0.95	1.3×10^{6}
^{142}Nd(27.13)	^{141m}Nd	64	0.760	100	3.19×10^{5}	3.1	1.4×10^{6}
^{159}Tb(100)	^{158m}Tb	11	0.111	100	2.56×10^{5}	3.8	2.2×10^{6}

a) The value corrected at the end of one-minute irradiation with the dose rate of 10^{7} R/min; Counting geometry is 20% with a 3"dia.×3"NaI(Tl) detector.

REF. K. Shoda, M. Sugawara, T. Saito, and H. Miyase
Phys. Letters 28B, 30 (1968)

ELEM. SYM.	A	Z
Ce	140	58

METHOD

REF. NO.	
68 Sh 4	egf

REACTION	RESULT	EXCITATION ENERGY	SOURCE		DETECTOR		ANGLE
			TYPE	RANGE	TYPE	RANGE	
E,P	SPC	13-30	D	30	MAG-D	5-15	90

ANALOGUE STATES

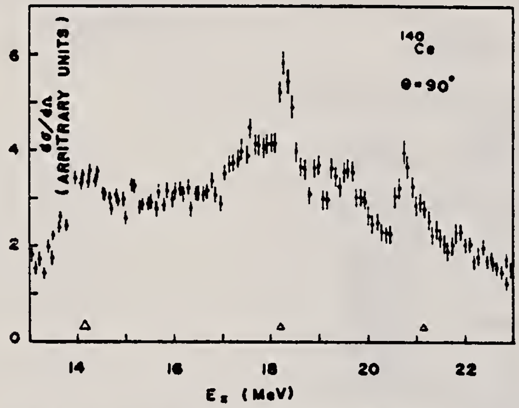

Fig. 2. Photoproton cross section for ^{140}Ce calculated from the energy distribution of the E_e = 30.0 MeV bombardment.

The scale was constructed under the assumption that observed protons correspond to ground-state transitions. The triangles show the energy resolution. The solid curve is the (γ,p_0) cross section calculated from the (p,γ_0)data.

REF.	ELEM. SYM.	A	Z
K. Shoda, M. Sugawara, T. Saito & H. Miyase PICNS-69 Proceedings of the Conference on Nuclear Isospin. Asilomar-Pacific Grove, California 1969 (Academic Press, New York & London 1969) p.137.	Ce	140	58
METHOD	REF. NO. 69 Sh 8		egf

REACTION	RESULT	EXCITATION ENERGY	SOURCE TYPE	SOURCE RANGE	DETECTOR TYPE	DETECTOR RANGE	ANGLE
E,P	SPC	13-22	D	20,22	MAG-D		DST

Table 1. Angular distributions of strong proton groups from ^{140}Ce and ^{141}Pr.

Nucleus	E_p(MeV)	W(θ)
^{140}Ce	10.3	$1+(0.4\pm0.1)P_1-(0.0\pm0.1)P_2$
	12.8	$1+(0.2\pm0.1)P_1-(0.4\pm0.2)P_2$
^{141}Pr	9.7	$1+(0.0\pm0.1)P_1+(0.1\pm0.2)P_2$

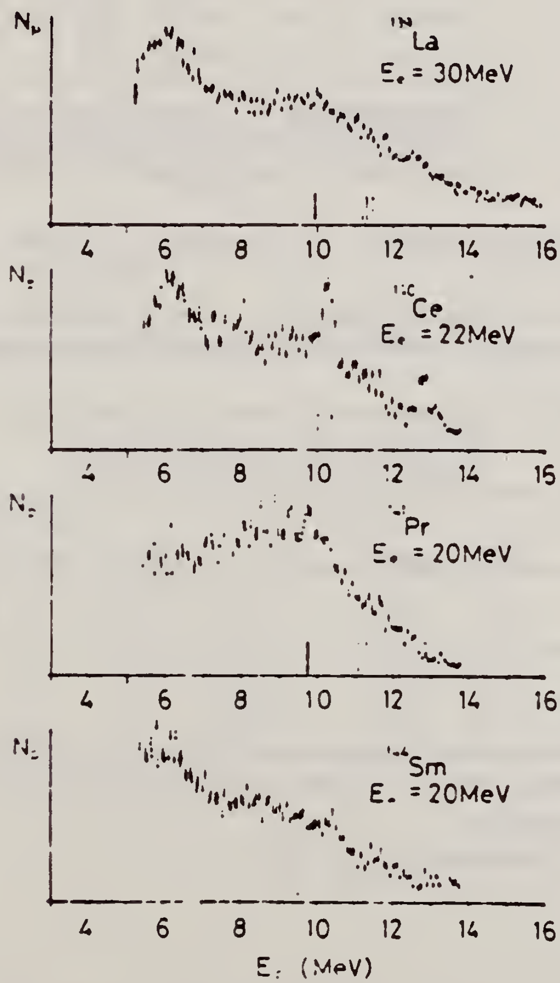

Fig. 1. Energy distributions of photoprotons. Vertical broken lines and solid lines indicate the position of p_0 corresponding to the ground IAS and electric dipole IAS (2).

(over)

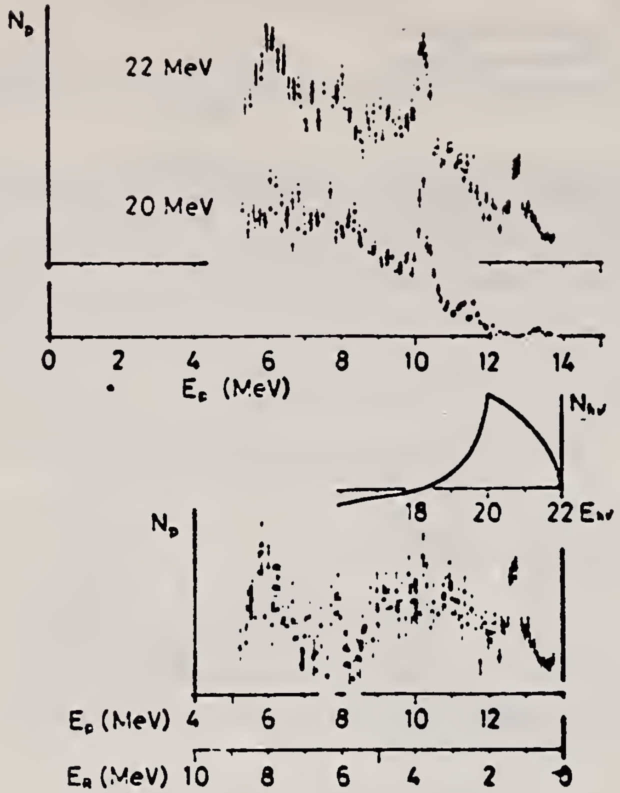

Fig. 2. Comparison of energy distributions on ^{140}Ce irradiated by 20.0 MeV and 22.0 MeV electron beam. The lowest spectrum is a difference of the two. Photon spectrum corresponding to this difference is also shown.

Table 2. The radiative widths of the main IAS. The results are compared with the single particle strength in W.u..

Nucleus	E_p (MeV)	E_x (MeV) (a)	Γ_{p_0}/Γ	Γ_{γ_0} (eV)	$2(T+1)\Gamma_{\gamma_0}$ (W.u.)
^{140}Ce	10.3	18.3	1 (b)	50	0.1
——	12.8	20.8	1 (b)	90	0.1
^{141}Pr	9.7	15.1	12/60(c)	40	0.2
^{144}Sm	10.6	16.6	1 (b)	20	0.05

(a) Ground state is assumed for the residual state.

(b) Assumption.

(c) P. VonBrentano *et al*. (2).

REF.	ELEM. SYM.	A	Z
R. Pitthan Z. Naturforsch. <u>25a</u>, 1358 (1970)	Ce	140	58

METHOD	REF. NO.	
	70 Pi 1	egf

REACTION	RESULT	EXCITATION ENERGY	SOURCE TYPE	SOURCE RANGE	DETECTOR TYPE	DETECTOR RANGE	ANGLE
E,E/	LFT	1-4	D	50,60	MAG-D		141

6 LEVELS, J-PI

E_x/MeV	I^π	Y_{Duke}	Y_{exp}	Γ_γ^0/eV	Γ_γ^0/Γ_W
1,60	2^+	0,65	0,67 ± 0,05	$6{,}7 \cdot 10^{-3}$	18 ± 2
2,08	4^+	2,20	2,27 ± 0,56	$1{,}5 \cdot 10^{-[illegible]}$	21 ± 4
2,46	3^-	1,28	1,31 ± 0,11	$6{,}2 \cdot 10^{-[illegible]}$	26 ± 3
2,90	1^+	0,29	–		
	2^+	0,65	0,58 ± 0,19	$9{,}5 \cdot 10^{-3}$	1,3 ± 0,5
3,12	1^+	0,29	–		
	2^+	0,65	0,58 ± 0,13	$26 \cdot 10^{-3}$	2,6 ± 0,5
3,32	1^+	0,29	–		
	2^+	0,65	0,73 ± 0,28	$19 \cdot 10^{-3}$	1,3 ± 0,6

Tab. 1. Vorläufige Ergebnisse. Y ist das Verhältnis der bei 60 MeV und 50 MeV Primärenergie gemessenen differentiellen Wirkungsquerschnitte ($\Theta = 141°$). Spins und Paritäten I^π nach Ref. [10]. Γ_W: Weisskopf-Einheit (WE) nach WILKINSON [13]

[10] H.W. Baer, J.J. Reidy u. M.L. Wiedenbeck, Nucl. Phys. <u>A113</u>, 33 (1968).

[13] D.H. Wilkinson, in F. Ajzenberg-Selove, Nucl. Spectroscopy, New York und London 1960.

REF.	ELEM. SYM.	A	Z
P. E. Haustein and A. F. Voigt J. inorg. nucl. Chem. 33, 289 (1971)	Ce	140	58

METHOD	REF. NO.	
	71 Ha 2	egf

REACTION	RESULT	EXCITATION ENERGY	SOURCE TYPE	SOURCE RANGE	DETECTOR TYPE	DETECTOR RANGE	ANGLE
G,3N	RLY	26-70	C	70	ACT-I		4PI

Isomer ratio = (yield to low spin state)/(yield to high spin state)

ISOMER RATIO

Table 2. Isomer ratio measurements for ^{91}Mo, ^{137}Ce, and ^{141}Nd

Reaction	Isomer ratio	I^{π} Target	I^{π} Ground state	I^{π} Isomer	Threshold (MeV)	$41A^{-1/3}$ (MeV)
^{92}Mo(γ, n)^{91}Mo	1·92 ± 0·15	0+	9/2+	1/2−	13·13	16·60
^{94}Mo(γ, 3n)^{91}Mo	1·59 ± 0·16	0+			30·72	16·52
^{138}Ce(γ, n)^{137}Ce	3·1	0+	3/2+	11/2+	10·31	15·30
^{140}Ce(γ, 3n)^{137}Ce	1·10 ± 0·12	0+			26·34	15·26
^{142}Nd(γ, n)^{141}Nd	5·2 ± 0·3	0+	3/2+	11/2+	9·79	15·22
^{144}Nd(γ, 3n)^{141}Nd	1·80 ± 0·25	0+			23·67	15·17

REF.	ELEM. SYM.	A	Z
K. Shoda, T. Saito, M. Sugawara, H. Miyase, S. Oikawa, A. Suzuki Phys. Rev. C4, 1842 (1971)	Ce	140	58

METHOD	REF. NO.	
	71 Sh 3	hmg

REACTION	RESULT	EXCITATION ENERGY	SOURCE TYPE	SOURCE RANGE	DETECTOR TYPE	DETECTOR RANGE	ANGLE
E,P	ABX	15-22	D	23	MAG-D		90

ISOBARIC ANALOGS

The energy distributions of protons from the $(e,e'p)$ reaction on $N=82$ nuclei with even Z have been measured. The cross sections of the (γ,p_0+p_1) reaction have been estimated. Two prominent isobaric analogs have been found in each nucleus. The results were used for the systematic discussion of the odd-odd parent nuclei ^{138}Cs, ^{140}La, ^{142}Pr, and ^{144}Pm. The 1^- states are estimated at 600 and ~2500 keV for ^{138}Cs, 500 and 3000 keV for ^{140}La, 1100 and 3700 keV for ^{142}Pr, and 1400 and 4300 keV for ^{144}Pm. The parameters of these states are discussed in terms of a quasiproton and single-neutron model.

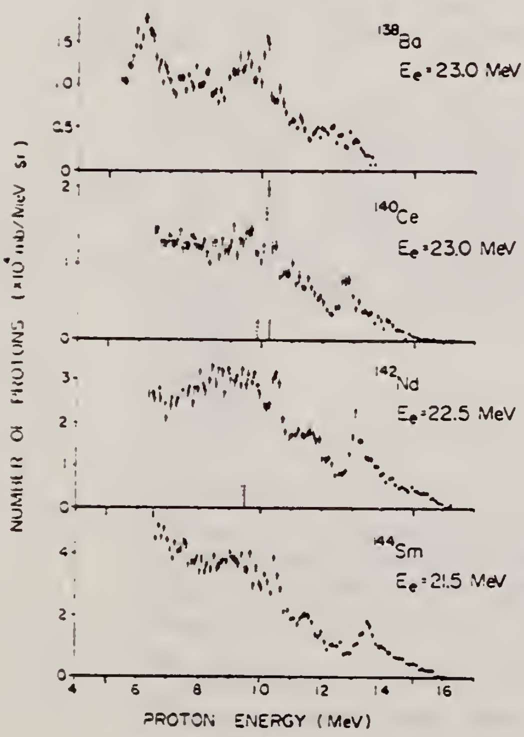

FIG. 1. Energy distributions of protons emitted from the $(e,e'p)$ reaction at $\theta = 90°$.

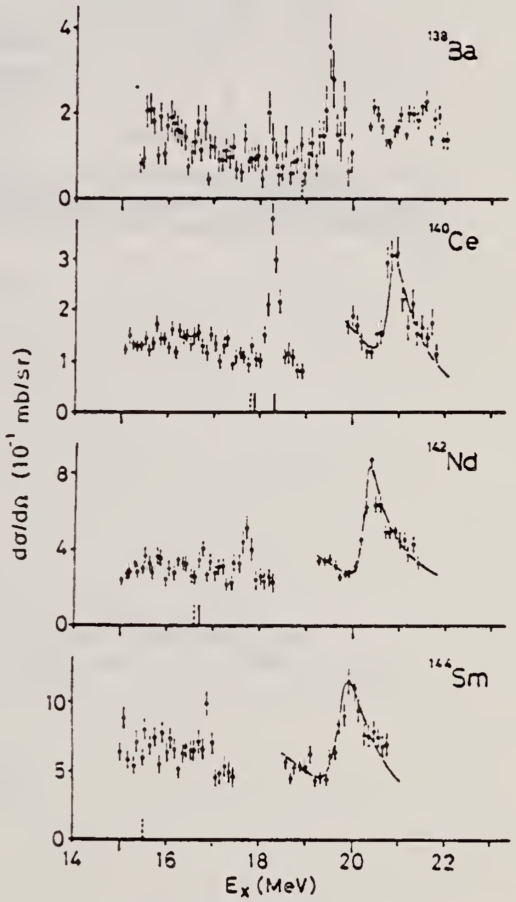

FIG. 2. The photoproton cross sections for p_0+p_1 at $\theta = 90°$ in the vicinity of the isobaric analog resonances. The curves for the broad resonances were obtained from the fitting of the interference formula.

(over)

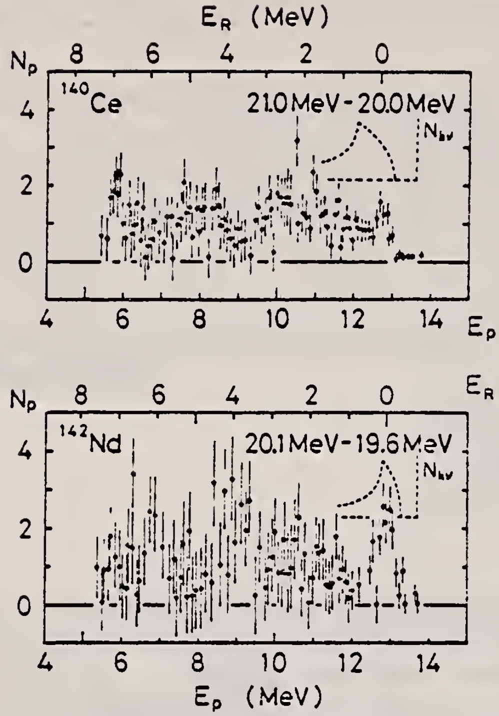

FIG. 5. The proton groups emitted through the isobaric analogs at 20.8 MeV in ^{140}Ce and at 20.3 MeV in ^{142}Nd. The energies of the residual states are also indicated by E_R.

REF.		ELEM. SYM.	A	Z
	Rainer Pitthan Z. Physik 260, 283 (1973)	Ce	140	58

METHOD	REF. NO.	
	73 Pi 3	egf

REACTION	RESULT	EXCITATION ENERGY	SOURCE TYPE	SOURCE RANGE	DETECTOR TYPE	DETECTOR RANGE	ANGLE
E,E/	LFT	1- 3	D	50, 65	MAG-D		DST

2+, 3-, 4+ LEVELS

Tabelle 2. Meßergebnisse der untersuchten Kernniveaus in Ce. Die B-Werte sind die $B(E\lambda, q=0, 0^+ \rightarrow \lambda^\pi)$, vgl. [1]. Weisskopfeinheiten Γ_W für die Ergebnisse dieser Arbeit nach Wilkinson, D. H. (in: Nuclear Spectroscopy, ed. F. Ajzenberg-Selove, New York und London 1960) mit $R=1,2$ fm; die zitierten Werte anderer Autoren weichen davon bis zu 3% ab

Isotop	λ_n^π	E_x MeV	$B(E\lambda, 0)$ $fm^{2\lambda}$	Γ_γ^0 eV	Γ_γ^0/Γ_W	Andere Autoren Γ_γ^0/Γ_W	Theoret. Werte Γ_γ^0/Γ_W
^{140}Ce	2_1^+	1,60	$2,7 \cdot 10^3$	$4,6 \cdot 10^{-3}$	$12,5 \pm {}^2_4$	$16,0 \pm 2,5^a$	$13,0^e$
						$12,5 \pm 1,8^b$	$12,5^f$
						$8,3 \pm 0,8^d$	$15,0^g$
	3_1^-	2,46	$2,0 \cdot 10^5$	$6,4 \cdot 10^{-6}$	$24 \pm {}^3_6$	$93 \pm (30-45)^c$	$6,7^g$
						$6,0 \pm 0,6^d$	
	4_1^+	2,08	$5,9 \cdot 10^6$	$5,4 \cdot 10^{-11}$	20 ± 4	$5,5 \pm 0,6^d$	
^{142}Ce	2_1^+	0,64	$6,5 \cdot 10^3$	$1,1 \cdot 10^{-5}$	30 ± 15	$19,5 \pm 0,5^b$	$35,0^f$
	3_1^-	1,65	$9,0 \cdot 10^5$	$1,8 \cdot 10^{-6}$	110 ± 40	135 ± 70^c	
	4_1^+	1,22	$1,3 \cdot 10^7$	$9,7 \cdot 10^{-13}$	45 ± 25		

[a] Ofer, S., Schwarzschild, A.: Phys. Rev. 116, 725 (1959).
[b] Eccleshall, D., Yates, M. J. L., Simpson, J. J.: Nucl. Phys. 78, 481 (1966).
[c] Ref. [21].
[d] Ref. [24].
[e] Ref. [27].
[f] Ref. [29].
[g] Ref. [28].

[21] Hansen, O., Nathan, N.: Nucl. Phys. 42, 197 (1963).

[24] Baker, F.T., Tickle, R.S.: Phys. Lett. 32B, 47 (1970). Die Übergänge sind zitiert nach: Baer, H.W., Griffin, H.C., Gray, W.S.: Phys. Rev. C3, 1398 (1971), denn die Autoren selbst geben keine Zahlen an.

[27] Rho, M.: Nucl. Phys. 65, 497 (1965).

[28] Waroquier, M., Heyde, K.: Nucl. Phys. A164, 113 (1971).

[29] Mustafa, S.M.: Nucl. Phys. A185, 309 (1972).

REF.	ELEM. SYM.	A	Z
J. Tenenbaum, R. Moreh, and A. Nof Nucl. Phys. A218, 95 (1974)	Ce	140	58

METHOD	REF. NO.	
	74 Te 1	egf

REACTION	RESULT	EXCITATION ENERGY	SOURCE TYPE	SOURCE RANGE	DETECTOR TYPE	DETECTOR RANGE	ANGLE
G,G	LFT	5	D	4- 8	SCD-D		DST

5=5.66

TABLE 2

Measured angular distribution coefficients A_2, the ratios $N_{||}/N_{\perp}$, the spins and parities of the ground and the resonance levels, J_0^π and J_r^π, and the character of the ground state transition

Scatterer	E_γ (keV)	A_2	$N_{\parallel}/N_{\perp}$	J_0^π	J_r^π	Transition
^{55}Mn	7491	0.01±0.02	1.00±0.02	$\frac{5}{2}^-$	$\frac{3}{2}$	
^{140}Ce	5660	0.51±0.02	1.14±0.04	0^+	1^-	E1
^{141}Pr	6877	0.11±0.02	0.95±0.03	$\frac{5}{2}^+$	$\frac{7}{2}^+$	M1
^{142}Nd	6877	0.51±0.03	1.10±0.04	0^+	1^-	E1
^{202}Hg	4922	0.51±0.02	1.18±0.03	0^+	1^-	E1
^{209}Bi	5603	0.06±0.02	0.97±0.02	$\frac{9}{2}^-$	$\frac{11}{2}^-$	M1

TABLE 4

Values of Γ, Γ_0 and the energy separation δ (between the incident γ-line and the resonance level) as obtained from the analysis of the various experiments

Scatterer	E_γ (keV)	Γ (meV)	Γ_0 (meV)	δ (eV)	D (eV)	K_{E1} (10^{-9} MeV^{-3})	K_{M1} (10^{-9} MeV^{-3})
^{55}Mn	7491	450±250	80± 40	17 ±1			
^{140}Ce [a]	5660	13± 3	12± 2	4.7±0.3	6800	0.33	
^{141}Pr [a]	6877	85± 35	17± 9	6.7±1.5	450		116
^{142}Nd [a]	6877	340± 40	270± 20	12.4±0.3	1200	26	
^{202}Hg	4922	300± 50	260± 20	4.2±0.5	19000	3.4	
^{209}Bi [a]	5603	950±200	950±200	13 ±1	34000		160

The radiative strengths K_{E1} and K_{M1} are also given. The level spacing D refers to the excitation energy of the resonance level E_γ.

[a]) These values are slightly different from those of ref. [8]) and were obtained from a renewed analysis of the experimental results.

8
A. Wolf, R. Moreh, A. Nof, O. Shahal, J. Tenenbaum,
Phys. Rev. C6, 2276 (1972).

REF.	R.M. Laszewski, R.J. Holt, and H.E. Jackson Phys. Rev. C13, 2257 (1976)	ELEM. SYM.	A	Z
		Ce	140	58
METHOD		REF. NO. 76 La 4		hmg

REACTION	RESULT	EXCITATION ENERGY	SOURCE		DETECTOR		ANGLE
			TYPE	RANGE	TYPE	RANGE	
G,N	RLX	9	C	9	TOF-D		DST
		(9.203)					

THRESHOLD MEAS

The $^{140}Ce(\gamma,n)\,^{139}Ce$ reaction has been studied near threshold with high energy resolution. The angular distribution of photoneutrons was measured at 90° and 135°, and the $M1$ and $E1$ strength functions at an excitation of approximately 9.1 MeV were determined. The measured integrated $M1$ strength was found to be consistent with the existence of a giant $M1$ resonance centered at 8.7 MeV as suggested both by calculation and previous electron scattering data. The integrated $E1$ strength was also found to be consistent with what is known of the $E1$ strength function in the threshold region.

TABLE II. $M1$ and $E1$ ground-state transition strengths integrated over the 40-keV interval centered at 9.08 MeV. Statistical uncertainties are estimated to be of the order 1%. Possible systematic uncertainties of the order 10% are estimated as discussed in the text.

Transitions	$\sum\Gamma_{\gamma 0}(M(E)1)$	$B(\uparrow, M(E)1)$	$\bar{k}_{M(E)1}$
$M1$	1.1 eV	$0.39\left(\frac{e\hbar}{2mc}\right)^2$	37×10^{-3}
$E1$	1.7 eV	$6.6\times10^{-3}\ e^2\,\mathrm{fm}^2$	2.2×10^{-3}

REF.		ELEM. SYM.	A	Z
	A. Lepretre, H. Beil, R. Bergere, P. Carlos, J. Fagot, A. De Miniac, A. Veyssiere, H. Miyase Nucl. Phys. A258, 350 (1976)	Ce	140	58
METHOD		REF. NO.		
		76 Le 2		egf

REACTION	RESULT	EXCITATION ENERGY	SOURCE TYPE	SOURCE RANGE	DETECTOR TYPE	DETECTOR RANGE	ANGLE
G,N	ABX	8- 26	D	8- 26	MOD-I		4PI
G,2N	ABX	16- 26	D	8- 26	MOD-I		4PI

1014+

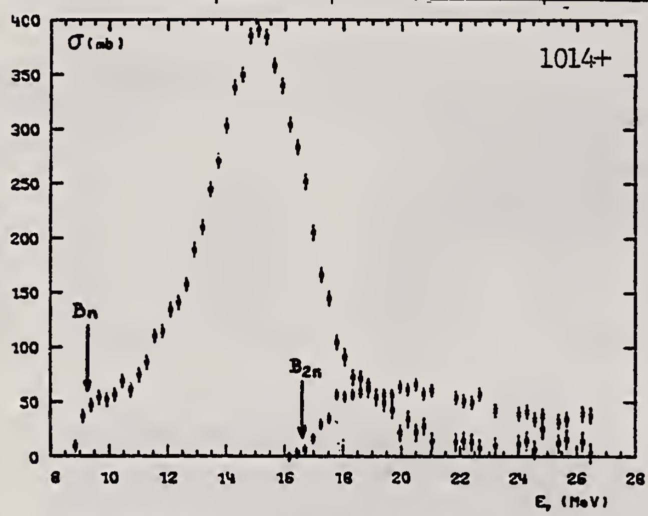

Fig. 5. Partial photoneutron cross sections [$\sigma(\gamma, n)+\sigma(\gamma, pn)$] and $\sigma(\gamma, 2n)$ for ^{140}Ce. Arrows B_n and B_{2n} indicate theoretical threshold values for (γ, n) and (γ, 2n) reactions respectively.

TABLE 3

Lorentz line parameters corresponding to best fits shown in figs. 9 and 10

Nucleus	^{124}Te	^{126}Te	^{128}Te	^{130}Te	^{140}Ce	^{142}Ce
σ_1 (mb)	281±15	294±15	304±15	318±16	384±20	332±17
Γ_1 (MeV)	5.5±0.2	5.6±0.2	5.4±0.2	5.1±0.2	4.4±0.1	5.2±0.2
E_1 (MeV)	15.2±0.1	15.1±0.1	15.1±0.1	15.1±0.1	15.0±0.1	14.9±0.1

TABLE 4

Integrated photoneutron cross sections and comparison with sum rules

Nucleus	^{124}Te	^{126}Te	^{128}Te	^{130}Te	^{140}Ce	^{142}Ce
E_M (MeV)	26.5	25.1	26.2	25.9	26.5	23.5
σ_0 (MeV · b)	2.04	2.04	2.11	2.19	2.40	2.21
$\frac{\sigma_0 A}{0.06\,NZ}$	1.12	1.11	1.14	1.17	1.18	1.07
σ'_0 (MeV · b)	2.44	2.56	2.58	2.55	2.65	2.69
$\frac{\sigma'_0 A}{0.06\,NZ}$	1.34	1.39	1.39	1.36	1.30	1.30
σ_{-1} (mb)	128	130	135	140	154	149
$\sigma_{-1}A^{-4/3}$ (mb)	0.21	0.20	0.21	0.21	0.21	0.20
σ_{-2} (mb · MeV^{-1})	8.4	8.6	9.1	9.4	10.3	10.6
$\sigma_{-2}A^{-5/3}$ (μb · MeV^{-1})	2.7	2.7	2.8	2.8	2.7	2.7

The notation used is defined in the text. The average experimental errors $\Delta\sigma_0/\sigma_0$, $\Delta\sigma_{-1}/\sigma_{-1}$ and $\Delta\sigma_{-2}/\sigma_{-2}$ are approximately 8 %.

REF. D. Meuer, G. Kühner, S. Müller, A. Richter, E. Spamer, O. Titze, W. Knüpfer
Phys. Lett. 106B, 289 (1981)

ELEM. SYM.	A	Z
Ce	140	58

METHOD

REF. NO.	
81 Me 2	hg

REACTION	RESULT	EXCITATION ENERGY	SOURCE		DETECTOR		ANGLE
			TYPE	RANGE	TYPE	RANGE	
E,E/	ABX	6-11	D	30-50	MAG-D		DST

A broad structure at $E_x \approx 9$ MeV in ^{140}Ce which hitherto had been interpreted as the M1 giant resonance is shown to consist of an accumulation of $J^\pi = 2^-$ states with a total strength of about $6 \times 10^3\ \mu_K^2 \mathrm{fm}^2$. There is no indication of an M1 giant resonance in the energy region $E_x \approx 7.5-10$ MeV, contrary to a recent theoretical prediction.

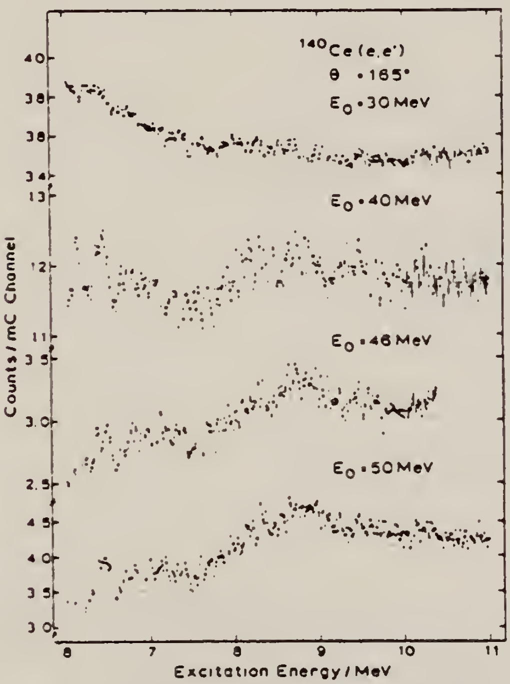

Fig. 1. Spectra of inelastically scattered electrons on ^{140}Ce without the background subtracted.

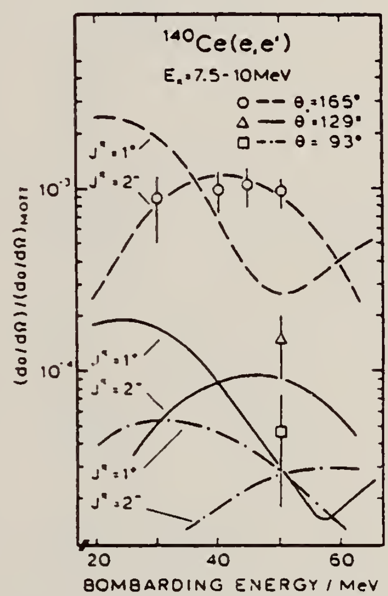

Fig. 2. Comparison of the experimental form factor for the broad structure between $E_x \approx 7.5-10$ MeV in fig. 1 (open symbols with error bars) and DWBA form factors in the frame of the RPA–MSI. The data definitely rule out an M1 form factor since its shape and relative magnitude between different angles disagrees with the data.

Ce
A=141

Ce
A=141

REF.	I. Bergqvist, B. Palsson, L. Nilsson, A. Lindholm, D.M. Drake E. Arthur, D.K. McDaniels and P. Varghese Nucl. Phys. A295, 256 (1978)	ELEM. SYM. Ce	A 141	Z 58
METHOD		REF. NO. 78 Be 1		rs

REACTION	RESULT	EXCITATION ENERGY	SOURCE TYPE	SOURCE RANGE	DETECTOR TYPE	DETECTOR RANGE	ANGLE
N,G	ABX	11- 21	D	6- 16	NAI-D		90

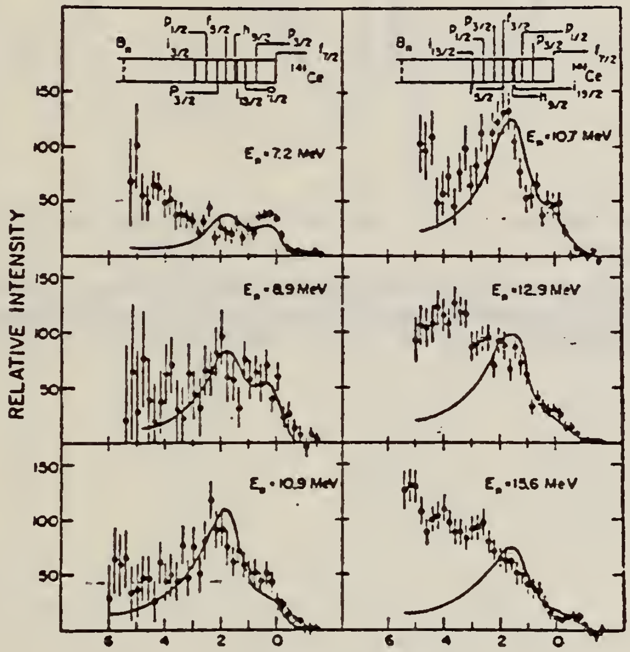

Fig. 2. Comparison of the measured spectra from neutron capture in cerium and those predicted from the DSD capture theory. The single-particle level scheme for ^{141}Ce is shown because ^{140}Ce is the dominant isotope (88.5 %). The binding energies of single-particle levels in ^{143}Ce are about the same except for the $2f_{7/2}$ state (see text and table 1). The observed and theoretical spectra were normalized to each other in the region corresponding to excitation energies below 2.6 MeV in ^{141}Ce. The interaction parameters chosen were v_1 = 75 MeV and w_1 = 115 MeV. (For further notation, see caption to fig. 1.)

over

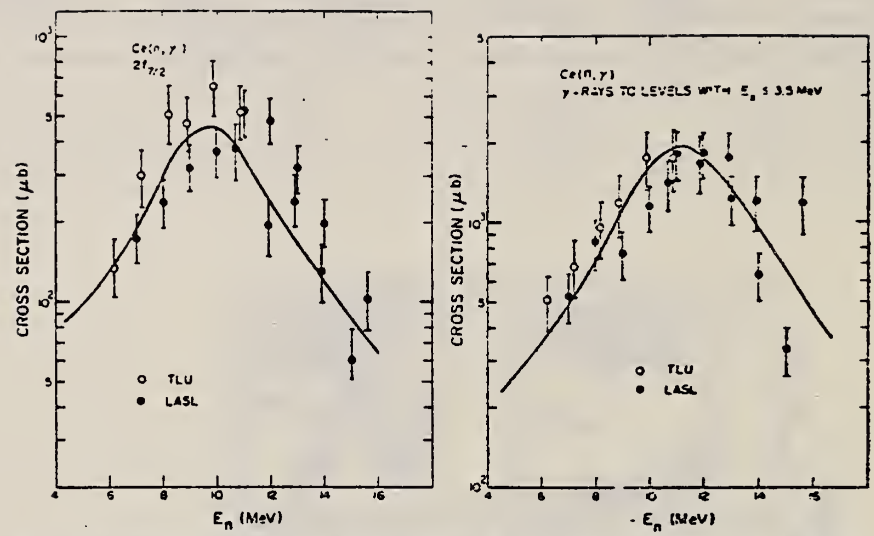

Fig. 4. Experimental (n, γ) cross sections for γ-ray transitions to the $2f_{7/2}$ states in ^{141}Ce (E_B = 5.44 MeV) and ^{143}Ce (E_B = 5.15 MeV), and the integrated cross section for γ-ray transitions to levels in the regions corresponding to excitation energies below 3.5 MeV in ^{141}Ce. (For further notation, see caption to fig. 3.)

Ce
A=142

Ce
A=142

Ce
A=142

K. N. Ge..er. J. Halpern, and E. G. Muirhead
Phys. Rev. 113, 1302-12 (1960)

ELEM. SYM.	A	Z
Ce	142	58

METHOD

Betatron; neutron threshold; ion chamber

REF. NO.	
60 Ge 3	NVB

REACTION	RESULT	EXCITATION ENERGY	SOURCE TYPE	SOURCE RANGE	DETECTOR TYPE	DETECTOR RANGE	ANGLE
G,N	NØX	THR	C THR		BF3-I		4 PI

THRESHØLD

TABLE I. Summary and comparison of neutron separation energies inferred from present threshold measurements with values predicted from mass data and reaction energies. All energies are expressed in the center-of-mass system in Mev.

Reaction	No. runs	Present results	Other results	Method	Reference
$Ce^{142}(\gamma,n)Ce^{141}$	1	$\leq$ 7.24 ±0.07	6.97 ±0.07	mass data	p

p W. H. Johnson, Jr., and A. O. Nier, Phys. Rev. 105, 1014 (1957).

TABLE II. Comparison of measured threshold energies with neutron binding energies predicted by mass data for transitions with $\Delta I \geq 7/2$. All energies in Mev.

Reaction	ΔI[a]	Observed threshold	Mass data Q value	$E_{th}-Q$	Excited state energy
$Cr^{52}(\gamma,n)Cr^{51}$	7/2	12.18±0.14	12.053±0.004[b]	0.13±0.14	...
$Y^{89}(\gamma,n)Y^{88}$	7/2	11.59±0.08	11.53 ±0.40[c]	0.06±0.41	0.387[d]
$In^{115}(\gamma,n)In^{114}$	7/2	9.22±0.03	9.35 ±0.43[c]	−0.13±0.43	0.191[a]
$Ce^{142}(\gamma,n)Ce^{141}$	(7/2)[e]	7.24±0.07	6.97 ±0.07[f]	0.27±0.10	...
$Nd^{145}(\gamma,n)Nd^{144}$	7/2	6.38±0.16	5.97 ±0.19[f]	0.41±0.25	0.690[a]
$Sm^{149}(\gamma,n)Sm^{148}$	7/2	6.45±0.16	5.87 ±0.28[f]	0.58±0.33	0.562[a]
$Er^{167}(\gamma,n)Er^{166}$	7/2	6.65±0.08	6.45 ±0.06[g]	0.20±0 10	0.081[a]
$Hf^{177}(\gamma,n)Hf^{176}$	7/2	6.69±0.03	6.28 ±0.06[g]	0.64±0.07	0.088[a]
$Hf^{179}(\gamma,n)Hf^{178}$	9/2	6.31±0.07	6.17 ±0.06[g]	0.14±0.09	0.093[a]
$Hf^{180}(\gamma,n)Hf^{179}$	9/2	7.85±0.11	7.32 ±0.06[g]	0.53±0.13	0.375[a]

a D. Strominger, J. M. Hollander, and G. T. Seaborg, Revs. Modern Phys. 30, 585 (1958).
b C. F. Giese and J. L. Benson, Phys. Rev. 110, 712 (1958).
c Henry E. Duckworth, *Mass Spectroscopy* (Cambridge University Press, New York, 1958), p. 177.
d S. Dzelepov and L. K. Peker, Atomic Energy of Canada Limited Report Tr. AECL-457 (unpublished).
e The discrepancy in the case of Ce^{142} predicts a ground-state spin for Ce^{142} of 0, since the spin of Ce^{141} is known to be 7/2.
f W. H. Johnson, Jr., and A. O. Nier, Phys. Rev. 105, 1014 (1957).
g W. H. Johnson, Jr., and V. B. Bhanot, Phys. Rev. 107, 6 (1957).

REF.		ELEM. SYM.	A	Z
Rainer Pitthan Z. Physik 260, 283 (1973)		Ce	142	58
METHOD		REF. NO. 73 Pi 3		egf

REACTION	RESULT	EXCITATION ENERGY	SOURCE TYPE	SOURCE RANGE	DETECTOR TYPE	DETECTOR RANGE	ANGLE
E,E/	LFT	0- 2	D	50, 65	MAG-D		DST

2+, 3-, 4+ LEVELS

Tabelle 2. Meßergebnisse der untersuchten Kernniveaus in Ce. Die B-Werte sind die $B(E\lambda, q=0, 0^+ \rightarrow \lambda^\pi)$, vgl. [1]. Weisskopfeinheiten Γ_W für die Ergebnisse dieser Arbeit nach Wilkinson, D. H. (in: Nuclear Spectroscopy, ed. F. Ajzenberg-Selove, New York und London 1960) mit $R=1,2$ fm; die zitierten Werte anderer Autoren weichen davon bis zu 3% ab

Isotop	λ_n^π	E_x MeV	$B(E\lambda, 0)$ $fm^{2\lambda}$	Γ_γ^0 eV	Γ_γ^0/Γ_W	Andere Autoren Γ_γ^0/Γ_W	Theoret. Werte Γ_γ^0/Γ_W
^{140}Ce	2_1^+	1,60	$2,7 \cdot 10^3$	$4,6 \cdot 10^{-3}$	$12,5 \pm {}^{2}_{4}$	$16,0 \pm 2,5^a$	$13,0^e$
						$12,5 \pm 1,8^b$	$12,5^f$
						$8,3 \pm 0,8^d$	$15,0^g$
	3_1^-	2,46	$2,0 \cdot 10^5$	$6,4 \cdot 10^{-6}$	$24 \pm {}^{3}_{6}$	$93 \pm (30-45)^c$	$6,7^g$
						$6,0 \pm 0,6^d$	
	4_1^+	2,08	$5,9 \cdot 10^6$	$5,4 \cdot 10^{-11}$	20 ± 4	$5,5 \pm 0,6^d$	
^{142}Ce	2_1^+	0,64	$6,5 \cdot 10^3$	$1,1 \cdot 10^{-5}$	30 ± 15	$19,5 \pm 0,5^b$	$35,0^f$
	3_1^-	1,65	$9,0 \cdot 10^5$	$1,8 \cdot 10^{-6}$	110 ± 40	135 ± 70^c	
	4_1^+	1,22	$1,3 \cdot 10^7$	$9,7 \cdot 10^{-13}$	45 ± 25		

[a] Ofer, S., Schwarzschild, A.: Phys. Rev. 116, 725 (1959).
[b] Eccleshall, D., Yates, M. J. L., Simpson, J. J.: Nucl. Phys. 78, 481 (1966).
[c] Ref. [21].
[d] Ref. [24].
[e] Ref. [27].
[f] Ref. [29].
[g] Ref. [28].

[21] Hansen, O., Nathan, N.: Nucl. Phys. 42, 197 (1963).

[24] Baker, F.T., Tickle, R.S.: Phys. Lett. 32B, 47 (1970). Die Übergänge sind zitiert nach: Baer, H.W., Griffin, H.C., Gray, W.S.: Phys. Rev. C3, 1398 (1971), denn die Autoren selbst geben keine Zahlen an.

[27] Rho, M.: Nucl. Phys. 65, 497 (1965).

[28] Waroquier, M., Heyde, K.: Nucl. Phys. A164, 113 (1971).

[29] Mustafa, S.M.: Nucl. Phys. A185, 309 (1972).

REF.	A. Lepretre, H. Beil, R. Bergere, P. Carlos, J. Fagot, A. De Miniac, A. Veyssiere, H. Miyase Nucl. Phys. A258, 350 (1976)	ELEM. SYM. Ce	A 142	Z 58
METHOD		REF. NO. 76 Le 2		egf

REACTION	RESULT	EXCITATION ENERGY	SOURCE TYPE	SOURCE RANGE	DETECTOR TYPE	DETECTOR RANGE	ANGLE
G,N	ABX	8- 20	D	8- 26	MOD-I		4PI
G,2N	ABX	12- 24	D	8- 26	MOD-I		4PI

1017+

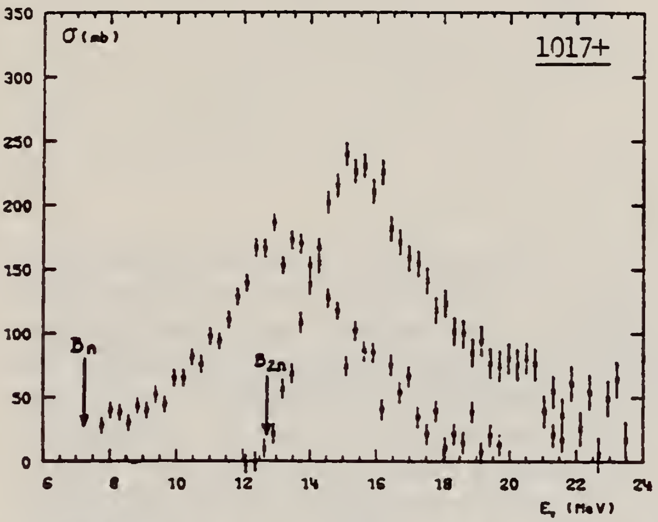

Fig. 6. Partial photoneutron cross sections $[\sigma(\gamma, n)+\sigma(\gamma, pn)]$ and $\sigma(\gamma, 2n)$ for ^{142}Ce. Arrows B_n and B_{2n} indicate theoretical threshold values for (γ, n) and $(\gamma, 2n)$ reactions respectively. Data are not corrected for impurities.

TABLE 3

Lorentz line parameters corresponding to best fits shown in figs. 9 and 10

Nucleus	^{124}Te	^{126}Te	^{128}Te	^{130}Te	^{140}Ce	^{142}Ce
σ_1 (mb)	281±15	294±15	304±15	318±16	384±20	332±17
Γ_1 (MeV)	5.5±0.2	5.6±0.2	5.4±0.2	5.1±0.2	4.4±0.1	5.2±0.2
E_1 (MeV)	15.2±0.1	15.1±0.1	15.1±0.1	15.1±0.1	15.0±0.1	14.9±0.1

TABLE 4

Integrated photoneutron cross sections and comparison with sum rules

Nucleus	^{124}Te	^{126}Te	^{128}Te	^{130}Te	^{140}Ce	^{142}Ce
E_M (MeV)	26.5	25.1	26.2	25.9	26.5	23.5
σ_0 (MeV · b)	2.04	2.04	2.11	2.19	2.40	2.21
$\frac{\sigma_0 A}{0.06\,NZ}$	1.12	1.11	1.14	1.17	1.18	1.07
σ'_0 (MeV · b)	2.44	2.56	2.58	2.55	2.65	2.69
$\frac{\sigma'_0 A}{0.06\,NZ}$	1.34	1.39	1.39	1.36	1.30	1.30
σ_{-1} (mb)	128	130	135	140	154	149
$\sigma_{-1}A^{-\frac{4}{3}}$ (mb)	0.21	0.20	0.21	0.21	0.21	0.20
σ_{-2} (mb · MeV^{-1})	8.4	8.6	9.1	9.4	10.3	10.6
$\sigma_{-2}A^{-\frac{5}{3}}$ (μb · MeV^{-1})	2.7	2.7	2.8	2.8	2.7	2.7

The notation used is defined in the text. The average experimental errors $\Delta\sigma_0/\sigma_0$, $\Delta\sigma_{-1}/\sigma_{-1}$ and $\Delta\sigma_{-2}/\sigma_{-2}$ are approximately 8 %.

PRASEODYMIUM
Z=59

Praseodymium was discovered by C. A. von Welsbach in 1885 by separating from a green salt(didymium) the fractions of praseodymium and neodymium. The name is a shortened variant of the word praeseodidymium meaning green didymium. Welsbach invented the automatic gas lighter based on a pyrophoric alloy of cerium and iron. He also invented the first lightbulb that used a metallic filament(osmium). Welsbach is best remembered for his invention of the incandescent gas mantel —— a truly great advance in the history of illumination.

Pr
A=141

Pr
A=141

B.G. Chidley, L. Katz, S. Kowalski
Can. J. Phys. 36, 407 (1958)

ELEM. SYM.	A	Z
Pr	141	59

METHOD: Betatron

REF. NO.: 58 Ch 2 — NVB

REACTION	RESULT	EXCITATION ENERGY	SOURCE TYPE	SOURCE RANGE	DETECTOR TYPE	DETECTOR RANGE	ANGLE
G,N	RLY	THR	C	THR	BF3-I		4PI

See 58 Ka 1 for cross sections

THRESHØLD

TABLE I

MEASURED PHOTONEUTRON THRESHOLDS

Reaction	Measured Q value, Mev.	Other Q values, Mev.	Method	Reference
$Pr^{141}(\gamma, n)Pr^{140}$	9.46±0.05			
		9.40 ±0.10	Threshold	Hanson *et al.* (1949)
		9.8 ±0.3	Threshold	Ogle *et al.* (1950)
		9.30 ±0.06	Mass data	Johnson and Nier (1957)

TABLE II

COMPARISON OF THRESHOLDS FROM MASS DATA AND FROM PHOTONEUTRON REACTIONS

Reaction	Photoneutron threshold, Mev.	Mass data threshold, Mev.	Difference, Mev.
$Na^{23}(\gamma, n)Na^{22}$	12.47±0.05	12.417±0.0[illegible]	−0.05±0.05
$Al^{27}(\gamma, n)Al^{26}$	12.96±0.06	13.03 ±0.06	+0.07±0.08
$P^{31}(\gamma, n)P^{30}$	12.48±0.05	12.39 ±0.03	−0.09±0.06
$Co^{59}(\gamma, n)Co^{58}$	10.44±0.05	10.49 ±0.01	+0.05±0.05
$Pr^{141}(\gamma, n)Pr^{140}$	9.46±0.05	9.30 ±0.06	−0.16±0.08

L. Katz, G.B. Chidley
Nuclear Reactions at Low and Medium Energies (Academy of Science, USSR: 1958) 371

ELEM. SYM.	A	Z
Pr	141	59

METHOD Betatron; neutron cross section; BF_3 counters; ion chamber monitor

REF. NO.	
58 Ka 1	NVB

REACTION	RESULT	EXCITATION ENERGY	SOURCE TYPE	SOURCE RANGE	DETECTOR TYPE	DETECTOR RANGE	ANGLE
G,XN	ABX	10-22	C	10-22	BF3-I		4PI

301

Таблица 2

Пороги испускания фотонейтронов

Изотоп	B_n, *Мэв*	B_{2n}, *Мэв*	Изотоп	B_n, *Мэв*	B_{2n}, *Мэв*
V^{51}	11,16	20,5	L^{139}	8,81	16,1
Mn^{55}	10,14	19,2	Pr^{141}	9,46	17,6
Co^{59}	10,44	18,6	Tb^{159}	8,16	14,8
As^{75}	10,24	18,1	Ho^{165}	8,10	14,6
Y^{89}	11,82	20,7	Tm^{169}	8,00	14,7
Nb^{93}	8,86	17,1	Lu^{175}	7,77	14,2
Rh^{103}	9,46	16,8	Ta^{181}	7,66	13,8
J^{127}	9,14	16,2	Au^{197}	7,96	13.3
Cs^{133}	9,11	16,5	Bi^{209}	7,43	14,5

THRESHOLDS

не приведены, поскольку они превышают 22 *Мэв* во всех случаях, кроме золота, для которого $B_{3n}=21$ *Мэв*. Свойства сечений $\sigma_C(\gamma)$ сведены в табл. 3.

Таблица 1

Изотоп	$E_{макс}$, *Мэв*	$\sigma_n(E_\gamma)$, *барн*	Г, *Мэв*	Σ^{22}, *Мэв·барн*	Y(22), 10^8 *нейтрон/100 р·моль*
V^{51}	18,4	0,062	5,2	0,33	1,62
Mn^{55}	20,2	0.060	7,0	0,39	2,01
Co^{59}	18,3	0,068	6,3	0,44	2,30
As^{75}	16,4	0,090	9,5	0,74	4,25
Y^{89}	17,1	0,172	5.2	0,93	5,33
Nb^{93}	18,0	0,156	7,5	1,17	6,80
Rh^{103}	17,5	0,160	9,4	1,40	8,28
J^{127}	15,2	0,273	6,8	1,76	11,9
Cs^{133}	16,5	0,238	7,7	1,59	10,7
La^{139}	15,5	0,325	3,8	1,55	11,2
Pr^{141}	15,0	0,320	4,9	1,93	13,1
Tb^{159}	15,6	0,274	9,8	2,49	18,1
Ho^{165}	13,5	0,305	8,9	2,52	18,7
Tm^{169}	16,4	0,250	8,4	1,91	14.9
Lu^{175}	16,0	0,225	8,4	1,90	23,0
Ta^{181}	14,5	0,380	8,5	3,15	22,0
Au^{197}	13,8	0,475	4,7	3,04	22,6
Bi^{209}	13,2	0,455	5,9	2,89	23,2

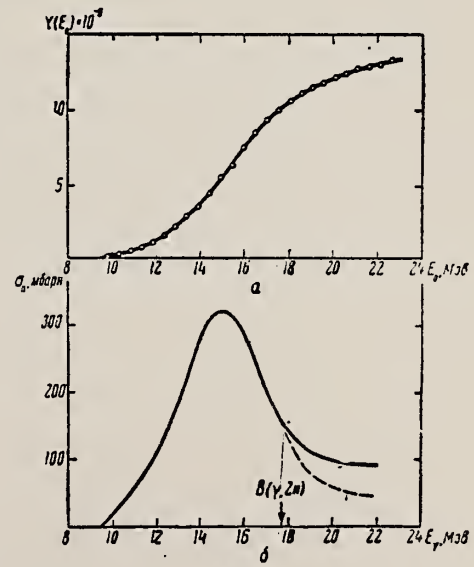

Рис. 11.

а — Выход фотонейтронов для Pr; б — $\sigma_n(E_\gamma)$ и $\sigma_C(\gamma)$ для Pr

Ref. J.H. Carver, W. Turchinetz
Proc. Phys. Soc. 73, 110 (1959)

Elem. Sym.	A	Z
Pr	141	59

Method: 33 MeV electron synchrotron; neutron yield; radioactivity

Ref. No.: 59 Ca 2 | EH

Reaction	E or ΔE	E_0	Γ	$\int \sigma dE$	$J\pi$	Notes 299 +
$Pr^{141}(\gamma,n)$	Bremss.			$\}\int^{31} = 2.6\pm0.4$ MeV-b		
$Pr^{141}(\gamma,2n)$	33 (300)					$E_{th}(\gamma,2n) = 18.3$ MeV.

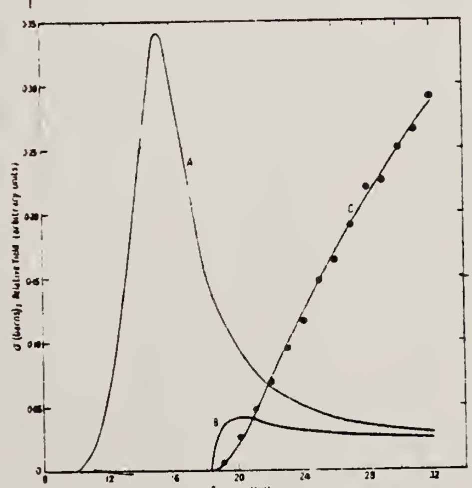

Cross sections for the reactions: A, $^{141}Pr(\gamma, n)$; B, $^{141}Pr(\gamma, 2n)$; C, the activation curve for $^{141}Pr(\gamma, 2n)$.

Ref. J.H. Carver, W. Turchinetz Proc. Phys. Soc. 73, 69 (1959)	Elem. Sym. Pr	A 141	Z 59
Method 33 MeV synchrotron; radioactivity; NaI spectrometer; r chamber	Ref. No. 59 Ca 3		EH

Reaction	E or ΔE	E_0	Γ	$\int \sigma dE$	$J\pi$	Notes 298
$Pr^{141}(\gamma,n)$	Bremss. 10-32	15.3	4.3 MeV	2.2±0.3 MeV-b		

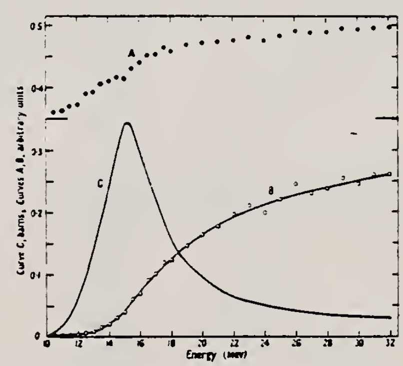

Figure 7. A, the ratio of activation curves $^{141}Pr(\gamma,n)/^{181}Ta(\gamma,n)$; B, activation curve for $^{141}Pr(\gamma,n)$; C, derived cross section: $^{141}Pr(\gamma,n)$.

Table 2

Activity	$T_{1/2}$ (min)	W_0 (MeV)	K/β^+	K-capture / Total capture	W_K
^{140}Pr	3·4	3·25	0·63	0·89	0·89
^{141}Nd	150	1·80	48	0·89	0·90
^{143}Sm	8·5	3·47	0·60	0·89	0·91

REF.	ELEM. SYM.	A	Z
G. Di Caporiacco, M. Mandò, and F. Ferrero Nuovo Cimento 13, 522 (1959)	Pr	141	59

METHOD	REF. NO.	
Betatron; ion chamber	59 Di 1	NVB

REACTION	RESULT	EXCITATION ENERGY	SOURCE		DETECTOR		ANGLE
			TYPE	RANGE	TYPE	RANGE	
G,N	RLY	9-30	C	30	ACT-I		4PI

REL TØ CU63 (G,N)

Yield ratio: $\dfrac{^{141}\text{Pr}(\gamma,n)}{^{63}\text{Cu}(\gamma,n)} = 3.79$

Ref. F. Ferrero, R. Malvano, E. Silva
Nuclear Phys. 10, 423 (1959)

Elem. Sym.	A	Z
Pr	141	59

Method
31 MeV Betatron; radioactivity

Ref. No.	
59 Fe 2	EH

Reaction	E or ΔE	E_0	Γ	$\int \sigma dE$	Jπ	Notes
(γ,n)	30					E_{th} = 9.5 MeV
(γ,2n)						E_{th} = 16.5 MeV

[Erratum in 61 Bo 2; see figures 1 and 2 below of 61 Bo 2]

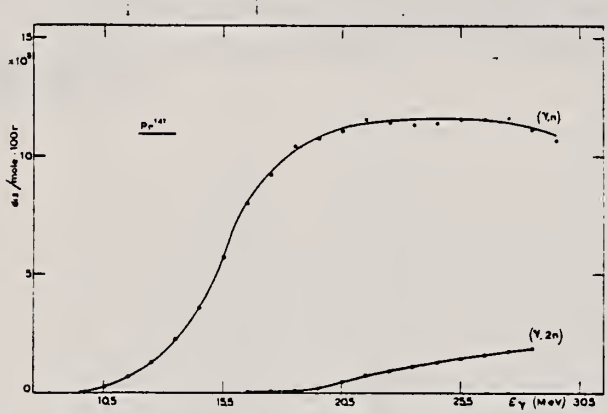

Fig. 1. Excitation functions for $Pr^{141}(\gamma, n)Pr^{140}$ and $Pr^{141}(\gamma, 2n)Pr^{139}$ reactions.

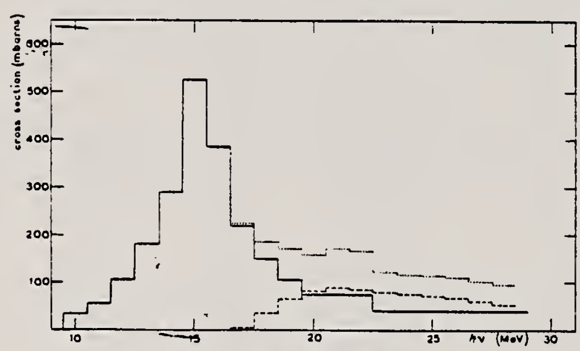

Fig. 2. Cross sections versus energy:
——— $Pr^{141}(\gamma, n)Pr^{140}$;
- - - - - - $Pr^{141}(\gamma, 2n)Pr^{140}$;
. . . . . . sum of the two above processes.

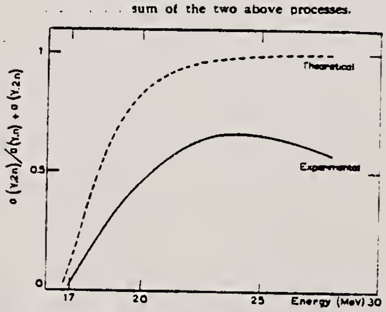

Fig. 3. Comparison between the statistical theory of nuclear reactions (theoretical) and the experimental ratio $\sigma(\gamma, n)/[\sigma(\gamma, n)+\sigma(\gamma, 2n)]$.

FIGURES FROM 61 Bo 2:

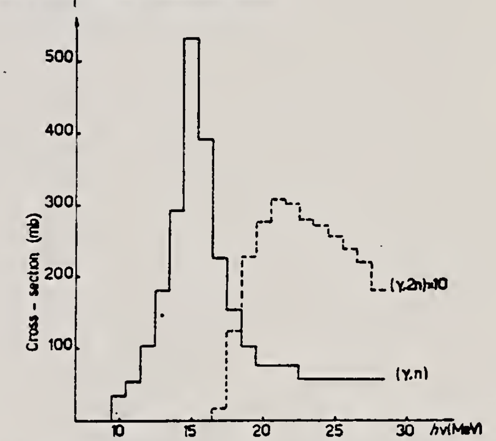

Fig. 1. The corrected (γ, n) and (γ, 2n) cross sections.

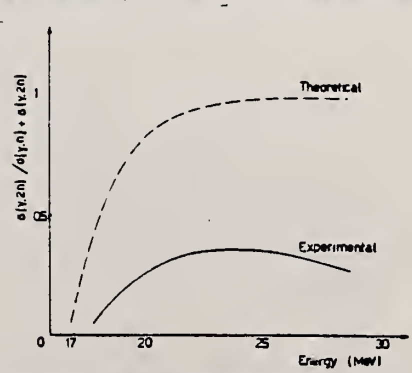

Fig. 2. Theoretical and experimental curves of the $(\gamma, 2n)/(\gamma, n)+(\gamma, 2n)$ ratio.

REF. K.N. Geller, J. Halpern, E.G. Muirhead
Phys. Rev. 118, 1302 (1960)

ELEM. SYM.	A	Z
Pr	141	59

METHOD

Betatron; neutron threshold; ion chamber

REF. NO.	
60 Ge 3	NVB

REACTION	RESULT	EXCITATION ENERGY	SOURCE TYPE	SOURCE RANGE	DETECTOR TYPE	DETECTOR RANGE	ANGLE
G,N	NØX	THR	C	THR	ACT-I		4PI

THRESHØLD

TABLE I. Summary and comparison of neutron separation energies inferred from present threshold measurements with values predicted from mass data and reaction energies. All energies are expressed in the center-of-mass system in Mev.

Reaction	No. runs	Present results	Other results	Method	Reference
$Pr^{141}(\gamma,n)Pr^{140}$	4	9.361±0.023	9.30 ±0.06	mass data	p
			9.46 ±0.05	threshold	f

p W. H. Johnson, Jr., and A. O. Nier, Phys. Rev. 105, 1014 (1957).

Ref. H.H. Thies, B.M. Spicer Australian J. Phys. 13, 505 (1960)	Elem. Sym. Pr	A 141	Z 59
Method: 18 MeV electron synchrotron; BF_3 counters; ion chamber	Ref. No. 60 Th 1		EH

Reaction	E or ΔE	E_0	Γ	$\int \sigma dE$	Jπ	Notes 302
$Pr^{141}(\gamma,xn)$	7-18	15.1				At E_n = 15.1 MeV, σ_{max} = 480 mb.

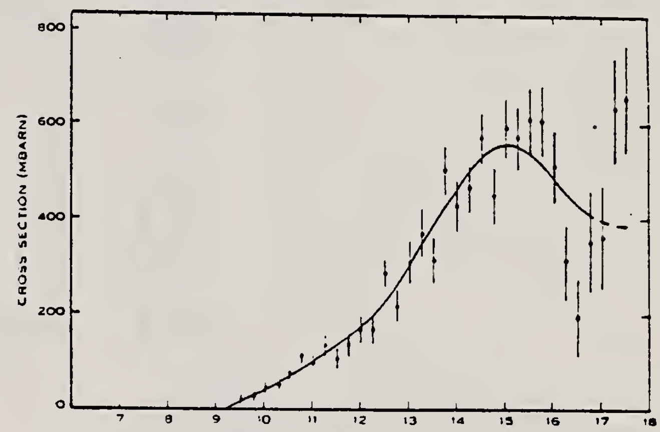

Fig. 5.—Total neutron production cross section for ¹⁴¹Pr. The points are obtained by analysis using the experimental points. The smooth curve is obtained by analysis of a smooth yield curve drawn through the experimental points.

TABLE 1

GIANT RESONANCE PARAMETERS FOR NON-DEFORMED NUCLEI

Nucleus . .	^{139}La	^{141}Pr	^{197}Au
Reference . .	Spicer *et al.* (1958)	Present Paper	Fullor and Weiss (1958)
E (MeV)	14·9	15·1	13·5
$(\sigma)_{max.}$ (mbarn)	460	480	590
$2\times\Gamma_{-\frac{1}{2}}$ (MeV)	4·2	4·4	4
$\Gamma_{G.R.}$ (MeV)	4·2	—	4·2

FORM NBS-418 (8-1-63) USCOMM-DC 18856-P63

U.S. DEPARTMENT OF COMMERCE NATIONAL BUREAU OF STANDARDS

Ref. O. Borello, S. Costa, F. Ferrero
Nuclear Phys. 27, 25 (1961)

Elem. Sym.	A	Z
Pr	141	59

Method 100 MeV synchrotron; Activation

Ref. No.	
61 Bo 1	JHH

Reaction	E or ΔE	E_o	Γ	$\int \sigma dE$	$J\pi$	Notes
(γ,n) $(\gamma,2n)$	10-29			3.0 MeV-mb $\Big\vert_0^{30}$		This paper is an erratum to results in Nuclear Phys. 10 423 (1959) [our file 59Fe2], incorporating a remeasured value of E.C./β^+ ratio in Pr^{139} = 4.8. This causes a correction factor to be applied to the old data: $\underset{[new]}{\sigma(\gamma,n)} = 1.02 \ \underset{[old]}{\sigma(\gamma,n)}$ $\underset{[new]}{\sigma(\gamma,2n)} = 0.35 \ \underset{[old]}{\sigma(\gamma,2n)}$

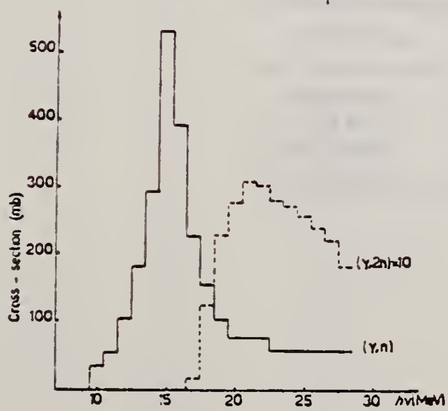

Fig. 1. The corrected (γ, n) and (γ, 2n) cross sections.

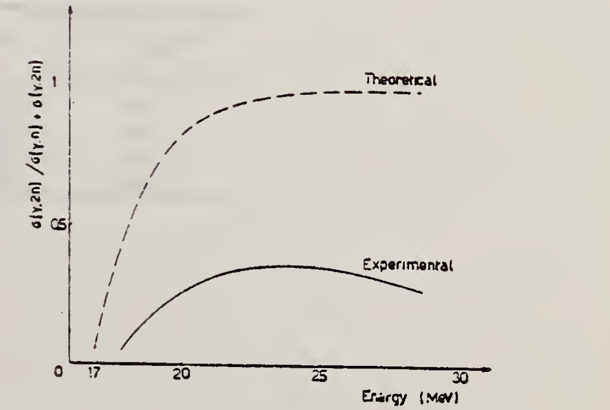

Fig. 2. Theoretical and experimental curves of the (γ, 2n)/(γ, n) + (γ, 2n) ratio.

REF.	ELEM. SYM.	A	Z
Ottavia Borello Rev. Un. Mat. Argent. As. Fis. Argent. 19, 251 (1961)	Pr	141	59

METHOD	REF. NO.	
	61 Bo 3	EGF

REACTION	RESULT	EXCITATION ENERGY	SOURCE TYPE	SOURCE RANGE	DETECTOR TYPE	DETECTOR RANGE	ANGLE
G,MU-T	ABX	11 - 20	C	11-20	ACT-I		

Used activity to measure total attenuation.

TABELA I

Reações	*Material*	*Meia vida* (Mev)	*Limiar* (Mev)	*Energia do Bétatron*		*Energia Média* (Mev)	
				P^{31} (Mev)	Pr^{141} (Mev)	P^{31}	Pr^{141}
(a) $Cu^{63}(\gamma, n) Cu^{62}$	Cobre	10,1	10,6	11,4	11,8	11,0	11,2
(b) $Fe^{54}(\gamma, n) Fe^{53}$	Ferro	9,0	11,9	--	16,0	—	14,6
(c) $O^{16}(\gamma, n) O^{15}$	Acido borico	2,1	15,6	17,4	17,6	16,5	16,[illegible]
(d) $C^{12}(\gamma, n) C^{11}$	Polic-tileno	20,5	18,7	20,3	20,1	19,5	19,6

TABELA II — P^{31}

Energia em Mev	μ (*cm* cm^2/g)	σ (*cm m barns*)
11,0	0,0237 ± 0,0003	1220 ± 15
16,5	0,0235 ± 0,0002	1210 ± 10
19,5	0,0250 ± 0,0003	1287 ± 15

TABELA III Pr^{141}

Energia em Mev	μ (*cm* cm^2/g)	σ (*cm barns*)
11,2	0,0435 ± 0,0009	10,19 ± 0,21
14,6	0,0481 ± 0,0008	11,26 ± 0,19
16,6	0,0505 ± 0,0008	11,83 ± 0,19
19,6	0,0550 ± 0,0005	13,00 ± 0,12

Ref. G.E. Coote, W.E. Turchinetz, I.F. Wright
Nuclear Phys. 23, 468 (1961)

Elem. Sym.	A	Z
Pr	141	59

Method
$Li^7(p,\gamma)$ source; activation; NaI

Ref. No.	
61 Co 2	JHH

Reaction	E or ΔE	E_o	Γ	$\int \sigma dE$	$J\pi$	Notes
(γ,n)						σ = 181±20 mb, relative to 59±6 mb for $Cu^{63}(\gamma,n)$, measured for 440 keV (E_p) resonance radiation from Li^7.

Ref. G. Moscati
Nuclear Phys. 26, 321 (1961)

Elem. Sym.	A	Z
Pr	141	59

Method
33 MeV bremss. (Saclay Linac); activity measured NaI crystals; annihilation radiation.

Ref. No.
61 Mo 1

EGF

Reaction	E or ΔE	E_o	Γ	$\int \sigma dE$	$J\pi$	Notes
$Pr^{141}(\gamma,3n)$	Bremss. 27-33			1 MeV-mb		E_{th} = 26.6±6 MeV [refer Johnson and Nier, Phys. Rev. 105, 1014 (1957)] assumed linear.

Ref.		Elem. Sym.	A	Z
V.G. Shevchenko, B.A. Yur'ev Zhur. Eksp. i Teoret. Fiz. 41, 1421 (1961) Soviet Phys. JETP 14, 1015 (1962)		Pr	141	59
Method: 35 MeV betatron; emulsions		Ref. No.: 61 Sh 2		JHH

Reaction	E or ΔE	E_o	Γ	$\int \sigma dE$	Jπ	Notes
(γ,p)	Bremss.:	*				
	22.5	6-7 9-10				$\sim 8 \times 10^4$ protons/mole-roentgen
	33.5	6-7 9-10				$\sim 1.3 \times 10^5$ protons/mole-roentgen

Angular distributions fitted to:

$$a + b \sin^2\theta \, (1 + p \cos\theta)^2$$

(see Table I parameters)

Conclusion: $\sigma(\gamma,p)$ is mostly due to $E_\gamma \gtrsim 22$ MeV, and is mainly quadrupole.

*Peaks in proton energy distribution at 6-7 and 9-10 MeV.

(For Figures see page 2)

Table I. Parameters of type (1) curves approximating the angular distributions of photoprotons from Pr^{141}, and values of $\sigma_{E2}/\sigma_{E1+E2}$ derived from the $\sigma_{E2}/\sigma_{E1} = p^2/5$

$E_{\gamma max}$, Mev	Proton energy, Mev	a	b	p	$\sigma_{E2}/\sigma_{E1+E2}$, %
22.5	4.5—7.25	31	15.7	0.42	~3
	7.25—11.25	44	68	0.32	~2
	≥11.25	12	27.5	0.44	~4
33.5	4.5—7.25	71	23.4	1.4	~30
	7.25—11.25	153	57	2.2	~50
	≥11.25	50	71.4	1.8	~40

Ref.	V.G. Shevchenko, B.A. Yur'ev Zhur. Eksp. i Teoret. Fiz. 41, 1421 (1961) Soviet Phys. JETP 14, 1015 (1962)	Elem. Sym. Pr	A 141	Z 59
Method		Ref. No. 61 Sh 2 (PAGE 2)		JHH

Reaction	E or ΔE	E_o	Γ	$\int \sigma dE$	Jπ	Notes

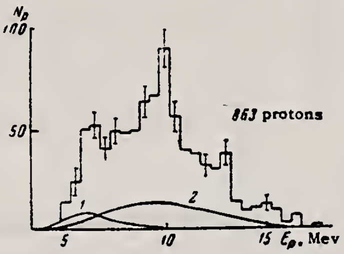

FIG. 2. Energy distribution of photoprotons from Pr^{141} produced by radiation having $E_{\gamma max}$ = 22.5 Mev. The continuous curve 1 is the computed spectrum of evaporation protons; curve 2 is the computed spectrum of direct-photoeffect protons.

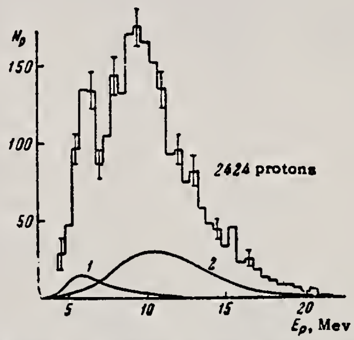

FIG. 3. Energy distribution of photoprotons from Pr^{141} produced by radiation having $E_{\gamma max}$ = 33.5 Mev. The notation is the same as in Fig. 2.

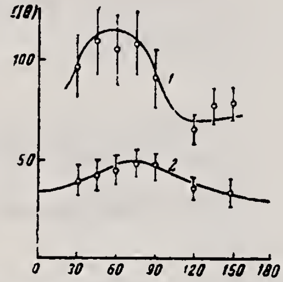

FIG. 4. Angular distribution of 4.5–7.25 Mev photoprotons (first group): 1 – for $E_{\gamma max}$ = 33.5 Mev; 2 – for $E_{\gamma max}$ = 22.5 Mev. The continuous approximating curves have the parameters given in Table I.

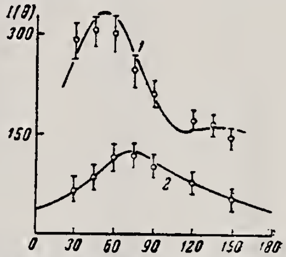

FIG. 5. Angular distribution of 7.25–11.25 Mev photoprotons (second group): 1 – for $E_{\gamma max}$ = 33.5 Mev; 2 – for $E_{\gamma max}$ = 22.5 Mev.

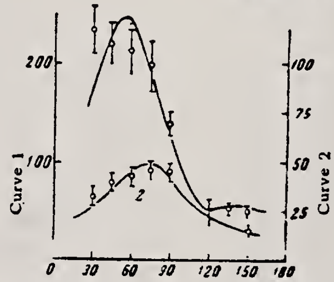

FIG. 6. Angular distribution of photoprotons of ⩾ 11.25 Mev (third group): 1 – for $E_{\gamma max}$ = 33.5 Mev; 2 – for $E_{\gamma max}$ = 22.5 Mev.

Ref. F. Tagliabue, J. Goldemberg
Nuclear Phys. 23, 144 (1961)

Elem. Sym.	A	Z
Pr	141	59

Method 22 MeV betatron; $Si^{28}(n,p)Al^{28}$ threshold detector.

Ref. No.	
61 Ta 1	JHH

Reaction	E or ΔE	E_0	Γ	$\int \sigma dE$	$J\pi$	Notes
(γ,n)	Bremss. 22					$E_n > 6$ MeV. $W(\theta_n) = A + B \sin^2\theta$ where $B/A = 0.34 \pm 0.16$

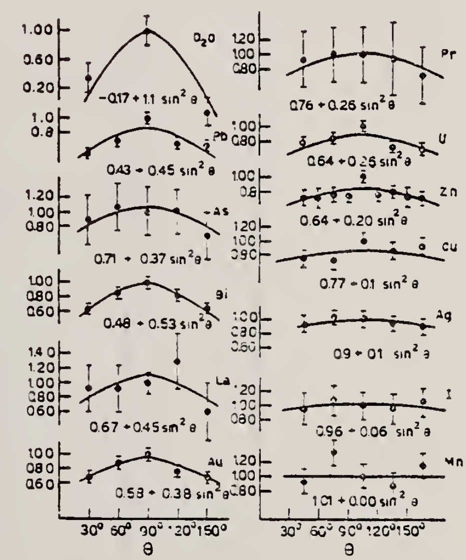

Figure 4: Angular distributions of fast photoneutrons as observed with the $Si^{28}(n,p)Al^{28}$ detector. Data normalized at 90° in each case.

Ref.		Elem. Sym.	A	Z
G. Ben-David (Davis); B. Huebschmann Phys. Letters 3, 87 (1962)		Pr	141	59
Method (n,γ) reaction - NaI(Tl)		Ref. No. 62Be2		BG

Reaction	E or ΔE	E_o	Γ	$\int \sigma dE$	Jπ	Notes
(γ,γ)	discrete energies in the range 5.44 - 8.997	6.12 7.64 8.881 8.997	-	-		σ_s(total)(mb) — γ source 230 — Cl 4.0 — Fe 1 — Cr 0.4 — Ni Detector at 135°.

Ref.	W.E. Del Bianco, W.E. Stephens Phys. Rev. 126, 709 (1962)	Elem. Sym.	A	Z
		Pr	141	59
Method	Electrostatic generator, $H^3(p,\gamma)He^4$ reaction; activation of positron emitter; 2 NaI in coincidence.	Ref. No. 62 De 1		JHH

Reaction	E or ΔE	E_o	Γ	$\int \sigma dE$	Jπ	Notes
(γ,n)	20.48					$\sigma(\gamma,n) = 51.7 \pm 5.4$ mb

Ref. G.C. Reinhardt, W.D. Whitehead
Nuclear Phys. 30, 201 (1962)

Elem. Sym.	A	Z
Pr	141	59

Method 55 MeV betatron; synchrotron; $Si^{28}(n,p)Al^{28}$ activity; $Cu^{63}(\gamma,n)Cu^{62}$ monitor.

Ref. No.	
62 Re 1	EGF

Reaction	E or ΔE	E_o	Γ	$\int \sigma dE$	$J\pi$	Notes
(γ,n)	Bremss. 55					Figure 9: Dotted curve is of form $a_o + a_1\cos\theta + a_2\cos^2\theta + a_2\cos^2\theta - a_1\cos^2\theta$; solid curve is of form $a_o + a_1\cos\theta + a_2\cos^2\theta$; errors on points are statistical errors in counting only.

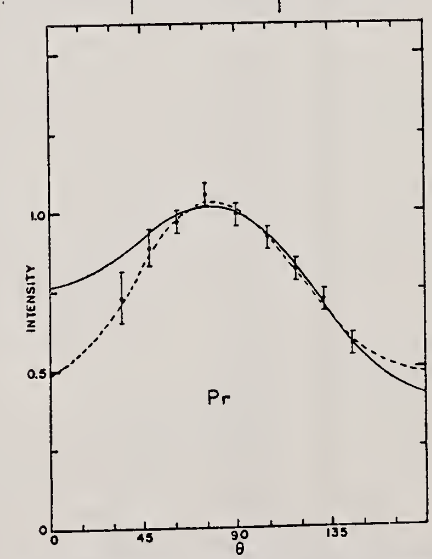

Fig. 9. Angular distribution of fast neutrons from praseodymium. See fig. 5.

TABLE 2

Parameters of the fit (1) for the expressions $a_0 - a_1\cos\theta + a_2\cos^2\theta$, $a + b\sin^2\theta - c\cos\theta$ and $A_0 - A_1P_1 - A_2P_2$

	Bi(1)	Bi(2)	Pr	Au	Y	Ho	La
a_0	1.00±0.02	1.00±0.02	1.00±0.02	1.00±0.02	1.00±0.03	1.00±0.02	1.00±0.01
a_1	0.15±0.03	0.18±0.04	0.17±0.04	0.14±0.03	0.17±0.06	0.12±0.03	0.14±0.03
$-a_2$	0.47±0.06	0.40±0.08	0.41±0.09	0.21±0.07	0.15±0.11	0.34±0.06	0.39±0.06
A_1*)	0.18±0.04	0.21±0.05	0.20±0.05	0.15±0.04	0.18±0.06	0.14±0.04	0.16±0.03
$-A_2$*)	0.37±0.05	0.31±0.06	0.32±0.07	0.15±0.05	0.11±0.08	0.26±0.05	0.30±0.04
a	0.53±0.06	0.60±0.08	0.59±0.09	0.79±0.07	0.85±0.11	0.66±0.06	0.61±0.06
b	0.47±0.06	0.40±0.08	0.41±0.09	0.21±0.07	0.15±0.11	0.34±0.06	0.39±0.06
c	0.15±0.03	0.18±0.04	0.17±0.04	0.14±0.03	0.17±0.06	0.12±0.03	0.14±0.03

*) Renormalized so that $A_0 = 1$

TABLE 4

Parameters of the fit (3) for the expressions $a_0 + a_1\cos\theta + a_2\cos^2\theta - a_3\cos^3\theta$, $1 + A_1P_1 - A_2P_2 + A_3P_3$

	Bi(1)	Bi(2)	Pr	Au	Y	Ho	La
a_0	1.01±0.02	1.00±0.02	1.01±0.03	0.98±0.02	1.00±0.03	1.00±0.02	1.01±0.02
a_1	0.19±0.05	0.17±0.07	0.21±0.07	0.07±0.06	0.16±0.09	0.12±0.05	0.17±0.05
$-a_2$	0.56±0.11	0.37±0.15	0.50±0.16	0.05±0.12	0.13±0.20	0.33±0.12	0.47±0.11
a_3	−0.17±0.18	0.05±0.24	−0.17±0.25	0.31±0.19	0.05±0.32	0.03±0.19	−0.17±0.17
A_1*)	0.11±0.15	0.23±0.18	0.13±0.20	0.27±0.13	0.20±0.22	0.15±0.14	0.09±0.13
$-A_2$*)	0.45±0.09	0.28±0.11	0.39±0.12	0.03±0.08	0.09±0.14	0.24±0.09	0.37±0.09
A_3*)	−0.08±0.09	0.02±0.11	−0.08±0.12	0.13±0.08	0.02±0.13	0.01±0.08	−0.08±0.08

*) Renormalized so that $A_0 = 1$

Ref.	V.G. Shevchenko, B.A. Yurev Nuclear Phys, 37, 495 (1962)	Elem. Sym. Pr	A 141	Z 59
Method	35 MeV betatron; emulsions	Ref. No. 62 Sh 4		JHH

Reaction	E or ΔE	E_0	Γ	$\int \sigma dE$	Jπ	Notes
$Pr^{141}(\gamma,p)$	Bremss. 22.5 33.5					Parameters a, b and p for $\omega(\theta_p) = a + b \sin^2\theta\,(1+ p\cos\theta)^2$ in Table I.

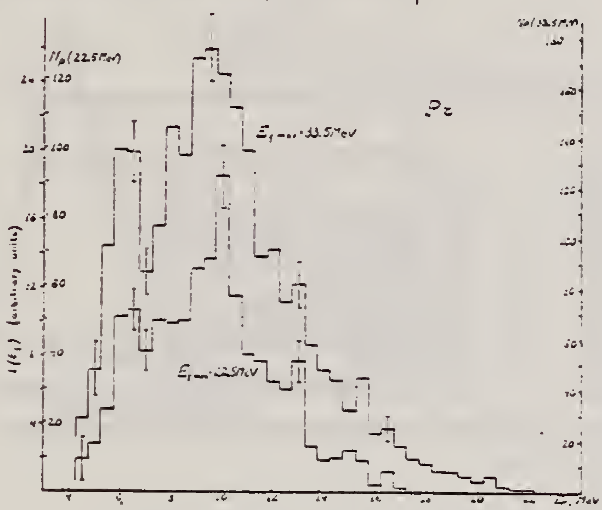

Fig. 3. Energy distributions of photoprotons from Pr^{141}.

Coefficients of expressions of type 1 [illegible] and estimates of the contribution [illegible]

Element	Z	$E_{\gamma max}$ (MeV)	E_p (MeV)	a	b	p	$\sigma_{E2}/(\sigma_{E1}-\sigma_{E2})$ (%)
Rh	45	22.5	3.25-9.25	1.9	0	0	0
			> 9.25	2.8	1.9	0.2	1
		33.5	3.25- 9.25	12.2	0	0	0
			> 9.25	4.5	3.7	1.2	≈ 20
Pr	59	22.5	4.5-7.25	1.4	0.7	0.42	3
			7.25-11.25	2.9	[illegible]	0.32	2
			> 11.25	1.5	[illegible]	0.44	4
		33.5	4.5-7.25	3.3	1.2	1.0	≈ 15
			7.25-11.25	4.2	1.55	2.2	≈ 50
			> 11.25	0.8	1.2	1.5	≈ 40
W	74	22.5	6.25-8.75	0.8	0	0	0
			8.75-12.75	2.8	1.6	1.6	≈ 35
			> 12.75	2.2	0.5	2.6	≈ 55
		33.5	6.25-8.75	1.2	0.95	0.44	4
			8.75-12.75	1.3	0.55	2.6	≈ 55
			> 12.75	0.55	0.5	3.4	≈ 70
Pt	78	22.5	6.25-8.75	0.6	1.0	0.4	3
			8.75-11.75	2.5	1.3	1.2	≈ 20
			> 11.75	1.4	0.56	2.6	≈ 55
		33.5	7.25-14.25	2.1	1.1	2.6	≈ 55
			> 14.25	0.5	0.5	3.4	≈ 70
Pb	82	22.5	5.25-10.25	1.05	0.75	0.8	≈ 10
			> 10.25	0.75	0.75	2.2	≈ 50
		33.5	5.25-10.25	1.9	1.2	1.2	≈ 20
			10.25-14.25	1.15	0.65	3.0	≈ 65
			> 14.25	1.5	1.0	3.3	≈ 70

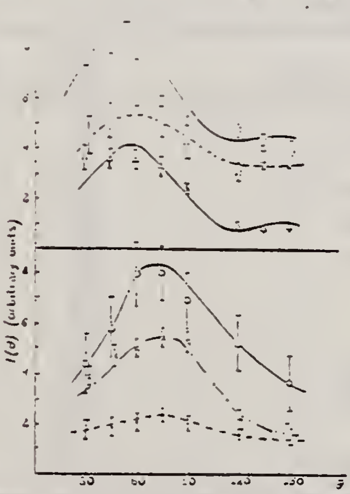

Fig. 8. Angular distributions of photoprotons from Pr^{141}. The experimental points for $E_{\gamma max}$ = 22.5 MeV are denoted by solid dots for E_p = 4.5-7.25 MeV, by centred circles for E_p = 7.25-11.25 MeV and by crosses for E_p > 11.25 MeV. For the case of $E_{\gamma max}$ = 33.5 MeV solid squares denote E_p = 4.5-7.25 MeV, centred squares E_p = 7.25-11.25 MeV and centred triangles E_p > 11.25 MeV.

TABLE 2

Measured photoproton yields and comparison with estimates by the models of evaporation and direct [illegible]

Element	$E_{\gamma max}$ (MeV)	Y_{exp} [a]	Y_{exp}/Y_{evap}	Y_{exp}/Y_{direct}
Rh^{103}	22.5	1.3 × [illegible]	≈ 3	≈ 3
	33.5	2.8 × [illegible]	≈ [illegible]	≈ 4.5
Pr^{141}	22.5	6.7 × [illegible]	≈ 16	≈ 4.5
	33.5	[illegible]	≈ 25	≈ [illegible]
W	22.5	[illegible]	≈ 1.3 × [illegible]	≈ 6
	33.5	[illegible]	≈ [illegible] × 10^2	≈ 11
Pt	22.5	[illegible]	≈ [illegible]	≈ [illegible]
	33.5	[illegible]	≈ 2 × 10^2	≈ 20
Pb	22.5	2.9 × 10^4	≈ 1.5 × 10^3	≈ 11
	33.5	[illegible]	≈ [illegible] × 10^3	≈ 25

[a]) The yield Y_{exp} is expressed in protons per mol per [illegible].

References

1) M. E. Toms and W. E. Stephens, Phys. Rev. 98 (1955) 626
2) M. M. Hoffman and A. G. W. Cameron, Phys. Rev. 92 (1953) 1184
3) W. C. Barber and V. J. Vanhuyse, Nuclear Physics 16 (1960) 381
4) M. E. Toms and W. E. Stephens, Phys. Rev. 92 (1953) 362
5) E. D. Makhnovsky, JETP 33 (1960) 95
6) R. B. Taylor, Nuclear Physics 19 (1960) 453
7) A. G. W. Cameron, W. Harms and L. Katz, Phys. Rev. 83 (1951) 1264
8) V. G. Neudachin, V. G. Shevchenko and N. P. Yudin, Report at the Second All-Union Conf. for Nuclear Reactions at Low and Medium Energies, Moscow, 1960
9) E. D. Courant, Phys. Rev. 82 (1951) 703
10) V. V. Balashov, V. G. Shevchenko and N. P. Yudin, JETP 41 (1961) 1929

REF.	ELEM. SYM.	A	Z
B. Arad (Huebschmann), G. Ben-David (Davis), I. Pelah, Y. Schlesinger Phys. Rev. 133, B684-700 (1964)	Pr	141	59

METHOD	REF. NO.	
Reactor, (n,γ) reactions source	64 Ar 1	NVB

REACTION	RESULT	EXCITATION ENERGY	SOURCE TYPE	SOURCE RANGE	DETECTOR TYPE	DETECTOR RANGE	ANGLE
G,G	ABX	6-9	D	6-9	NAI-D		135
		(See Table II)					

TABLE II. Capture gamma-ray sources and their properties.[a]

Source	Chemical composition	Mass kg	Principal γ rays (in MeV)
Al	Metal	1.640	7.73
Cl	polyvinyl Chloride	0.380	8.55, 7.78, 7.41, 6.96, 6.64, 6.12, 5.72
Co	CoO	0.230	7.49, 7.20, 6.98, 6.87, 6.68, 6.48, 5.97, 5.67
Cr	Metallic powder	0.480	9.72, 8.88, 8.49, 7.93, 7.09, 6.65, 5.60
Cu	Metal	1.860	7.91, 7.63, 7.29, 7.14, 7.00, 6.63
Fe	Metallic powder	0.440	9.30, 7.64, 7.28, 6.03
Hg	$Hg_2(NO_3)_2 \cdot 2H_2O$	0.310	6.44, 6.31, 5.99, 5.67, 5.44
Mn	MnO_2	0.240	7.26, 7.15, 7.04, 6.96, 6.79, 6.10, 5.76
Ni	Metal	0.900	9.00, 8.50, 8.10, 7.83, 7.58, 6.84, 6.64
Ti	TiO_2	0.210	6.75, 6.56, 6.42
V	V_2O_5	0.120	7.30, 7.16, 6.86, 6.51, 6.46, 5.87, 5.73
Y	Y_2O_3	0.200	6.07, 5.63

[a] For more detailed information, additional lines, intensities, etc., see Ref. 6.

TABLE III. Effective cross sections.

γ source	Energy (MeV)	Scatterer Element	Protons	Neutrons	$\langle\sigma_{\gamma\gamma}\rangle$ (mb)	Notes
Hg	5.44	Hg	80	116, 118, 119, 120, 121, 122, 124	128	
Cl	6.12	Pr^{141}	59	*82*	103	a
V	6.508	Sn	*50*	62, 64–70, 72	14	
Co	6.690	Pr^{141}	59	*82*	2.7	a
Co	6.867	Nd	60	82, 83, 84, 85, 86, 88	22	
Al	6.98	Pb^{208}	*82*	*126*	2900	b
Cl	6.98	Pb	*82*	124, 125, *126*	346	a
Ti	6.996	Bi^{209}	83	*126*	1560	b
Cu	7.01	Sn	*50*	62, 64–70, 72	1000	b
Ti	7.149	Pb^{208}	*82*	*126*	1000	b
Co	7.201	Pb^{208}	*82*	*126*	25	
Mn	7.261	Pb^{208}	*82*	*126*	25	a
Fe	7.285	Pb^{208}	*82*	*126*	4100	a
V	7.305	Pb^{208}	*82*	*126*	12.5	
Hg	7.32	Pb	*82*	124, 125, *126*	5500	c
Fe	7.639	Ni	*28*	30, 32, 34, 36	10.5	d
Fe	7.639	Pr^{141}	59	*82*	10	d
Cr	8.499	Cu	29	34, 36	24.4	
Cr	8.881	Pr^{141}	59	*82*	9.3	
Ni	8.997	Sm	62	*82*, 85–88, 90, 92	2.8	

[a] A large error could be introduced in the cross-section values because of large differences in line intensities quoted by Bartholomew and Higgs and by Groshev *et.al.* (Ref. 6).
[b] Because of the low counting rate, thick scatterers were used, which will introduce a systematic error in estimating $\langle\sigma_{\gamma\gamma}\rangle$ for resonances having a high nuclear cross section.
[c] The cross section was evaluated assuming the gamma intensity to be 0.02 photons per 100 captured neutrons (see text).
[d] Reference 6 gives the 7.639 line of iron capture gamma rays as a single line. However, a recent paper by Fiebiger, Kand, and Segel [Phys. Rev. 125, 2031 (1962)] reports two different lines of equal intensities having energies of 7.647 and 7.633 MeV. The present experiment cannot resolve an energy difference of 14 keV, therefore, there is no possibility of deciding which line is responsible for the scattering.

REF.	ELEM. SYM.	A	Z
L.B. Rice, L.N. Bolen, W.D. Whitehead Phys. Rev. 134, B557 (1964)	Pr	141	59

METHOD	REF. NO.	
Synchrotron, NBS chamber	64 Ri 1	NVB

REACTION	RESULT	EXCITATION ENERGY	SOURCE TYPE	SOURCE RANGE	DETECTOR TYPE	DETECTOR RANGE	ANGLE
G,XN	ABX	9-30	C	9-30	BF3-I		4PI

580

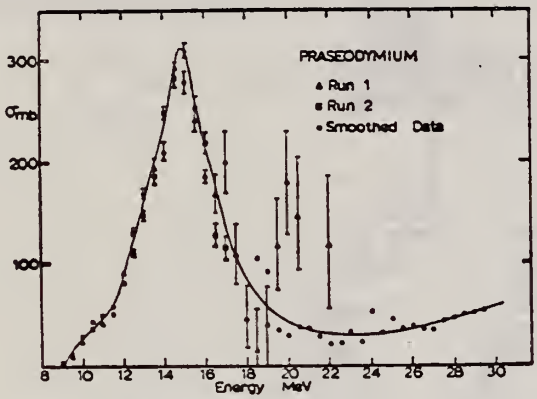

FIG. 2. Praseodymium (γ,n) cross section uncorrected for neutron multiplicity.

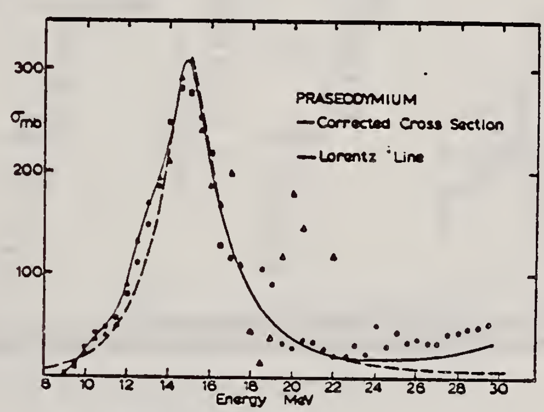

FIG. 4. Praseodymium (γ,n) cross section with neutron multiplicity correction (solid line); Lorentz line fitting to data points (dashed line).

TABLE I. Experimentally determined parameters for the neutron photoproduction cross sections σ_m, maximum value of cross sections; E_m, energy at which maximum occurs; DSR, classical dipole-sum rule limit; Γ_0 twice the energy from half-maximum on low-energy side of curve to E_m, Γ_{Lor} width used to fit the Lorentz curve

	σ_m mb	E_m MeV	$\int_{Thr}^{30} \sigma dE$ MeV-b	DSR MeV-b	Γ_0 MeV	Γ_{Lor} MeV
	Uncorrected for multiplicity					
La	315±15	14.8±0.4	1.76	2.02		
Pr	305±10	14.8±0.4	1.74	2.06		
	Corrected for $(\gamma,2n)$					
La	304	14.5	1.36	2.02	3.2±0.2	3.3
Pr	305	14.8	1.47	2.06	4.0±0.2	3.3

line in each figure is a result of a Lorentz curve fitting to the low-lying points on the low-energy side of the peak.

REF.	ELEM. SYM.	A	Z
G. Ben-David, B. Arad, J. Balderman, and Y. Schlesinger Phys. Rev. <u>146</u>, B852 (1966)	Pr	141	59

METHOD	REF. NO.	
Nuclear Resonance Scattering using N,G reactions.	66 Be 3	JDM

REACTION	RESULT	EXCITATION ENERGY	SOURCE TYPE	SOURCE RANGE	DETECTOR TYPE	DETECTOR RANGE	ANGLE
G,G	RLX	5 - 10	D	5 - 10	NAI-D	5 - 10	135

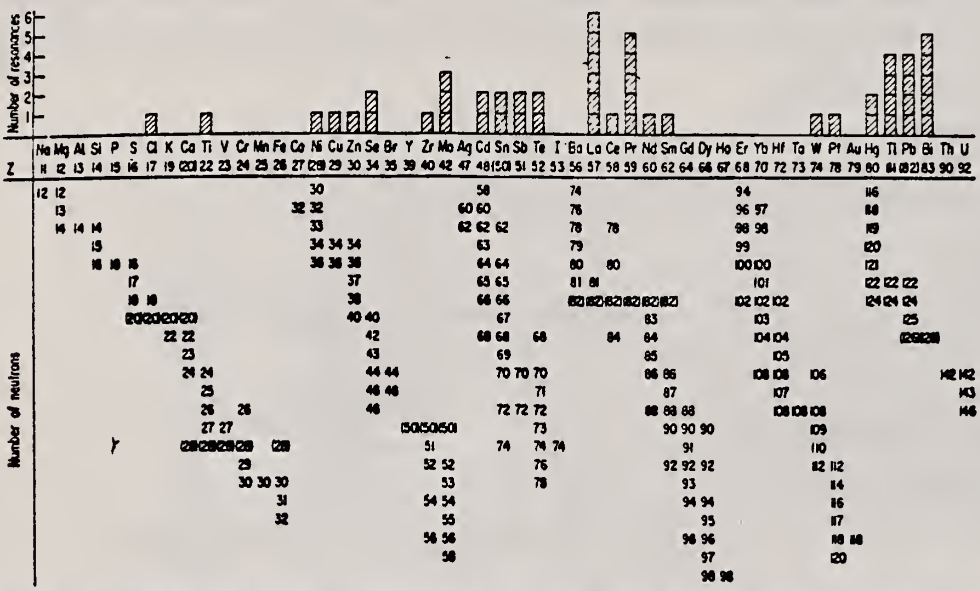

FIG. 3. Histogram of distribution of observed resonances among the different targets. The atomic number is given directly beneath the chemical symbol followed by the neutron numbers of the naturally occurring isotopes. Magic numbers are shown in brackets.

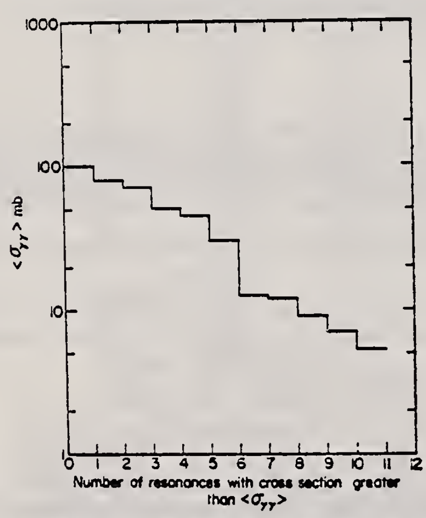

FIG. 5. Integral distribution of the effective cross sections for the 11 resonances in the mono-isotopic elements lanthanum and praseodymium.

TABLE III. List of effective cross sections.

Scatterer	Energy (MeV)	Gamma source	$\bar{\sigma}$ (mb)	Scatterer	Energy (MeV)	Gamma source	$\bar{\sigma}$ (mb)
Sm^{144}	8.997	Ni	100	Sn	7.01	Cu	110
Pr^{141}	8.881	Cr	9	Nd	6.867	Co	30
La	8.532	Ni	6	Pr^{141}	6.867	Co	3
Te	8.532	Ni	3[a]	Te	6.7	Ni	...
Cu	8.499	Cr	24	La	6.54	Ag	12
Zr	8.496	Se	3050	Cd	6.474	Co	110
Zn	8.119	Ni	13	Mo	6.44	Hg	25[g]
Se	7.817	Ni	50	La	6.413	Ti	72
Se	7.76	K	90	Mo	6.413	Ti	10
Sb	7.67	V	...[b]	Tl	6.413	Ti	25
Cd	7.64	Fe	40[c]	W	~6.3	Ti	...[b]
Ni	7.64	Fe	7[c]	Sb	6.31	Hg	6[e]
Pr^{141}	7.64	Fe	12[c]	Ti	6.31	Hg	2[e]
Tl	7.64	Fe	370[c]	Sn	6.27	Ag	75
La	7.634	Cu	7	Pb^{208}	6.15	Gd	...[g]
Mo	7.634	Cu	11	Te	5.8	Ni	...[f]
Bi^{209}	7.634	Cu	4	La	6.12	Cl	35
Te	7.528	Ni	66[d]	Pr^{141}	6.12	Cl	110
Bi^{209}	7.416	Se	100	Pt	5.99	Hg	40[a,e]
Bi^{209}	7.300	As	80[e]	Tl	5.99	Hg	5[g]
Pb^{208}	7.285	Fe	4100	Pb^{208}	5.9	Sr	...[h]
Cl	7.285	Fe	34	Ce	5.646	Co	17
Pr^{141}	7.185	Se	80	Bi^{209}	5.646	Co	55
Tl	7.16	Cu	120	Pb^{208}	5.53	Ag	70
La	7.15	Mn	50	Hg	5.44	Hg	75[g]
Bi^{209}	7.149	Ti	2000	Hg	4.903	Co	385

[a] High-energy component of a complex spectrum.
[b] A broad scattered spectrum with no observable peak structure.
[c] There are actually two lines of energies 7.647 and 7.633 MeV having equal intensities in the iron capture gamma spectrum. The cross section has therefore been corrected, although there is no possibility at present of deciding which line is responsible for each resonance.
[d] Is probably an independent level in the complex spectrum of Ni γ rays on Te.
[e] Rough estimate.
[f] May be inelastic component from 7.528 level in Te.
[g] The relative line intensities in this case are due to Groshev and co-workers.
[h] No line is known for the source at this energy.
[i] Difficult to resolve among the many source lines present at this energy.

REF.	R. L. Bramblett, J. T. Caldwell, B. L. Berman, R. R. Harvey and S. C. Fultz Phys. Rev. 148, B1198 (1966)	ELEM. SYM.	A	Z
		Pr	141	59

METHOD	REF. NO.	
	66 Br 1	JDM

REACTION	RESULT	EXCITATION ENERGY	SOURCE TYPE	SOURCE RANGE	DETECTOR TYPE	DETECTOR RANGE	ANGLE
G,N	ABX	THR- 33	D	8- 33	BF3		4PI
G,2N	ABX	THR- 30	D	8- 33	BF3		4PI
G,3N	ABX	THR- 30	D	8- 33	BF3		4PI
	-	-					

$$\int_{Thr}^{30} \sigma dE_{\gamma} = (2.3 \pm 0.2) \text{ MeV b}$$

(G,N) 304+
(G,2N) 305
(G,3N) 306+
(G,SN) 307

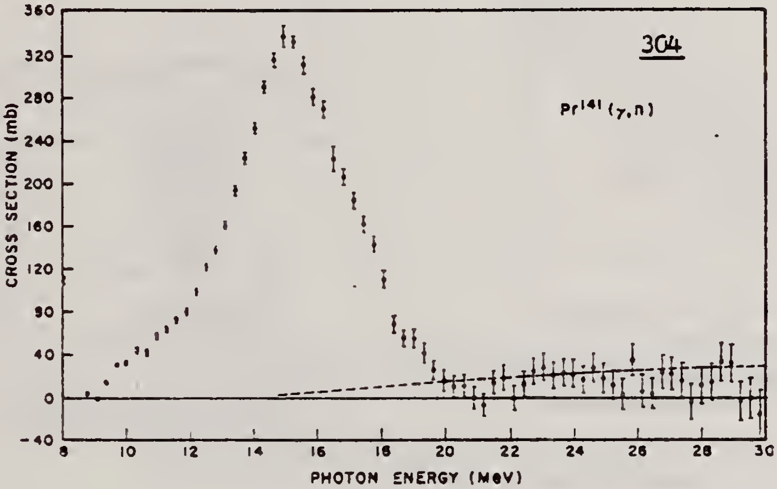

FIG. 1. The $Pr^{141}(\gamma,n)$ cross section obtained using annihilation photons and 4π neutron detector. A multiplicity-of-neutrons counting technique was used to separate the (γ,n) events from the $(\gamma,2n)$ and $(\gamma,3n)$ events. The error bars represent only statistical errors measured in standard deviations. The dashed line is an estimate of the systematic uncertainty due to normalization of position and electron runs.

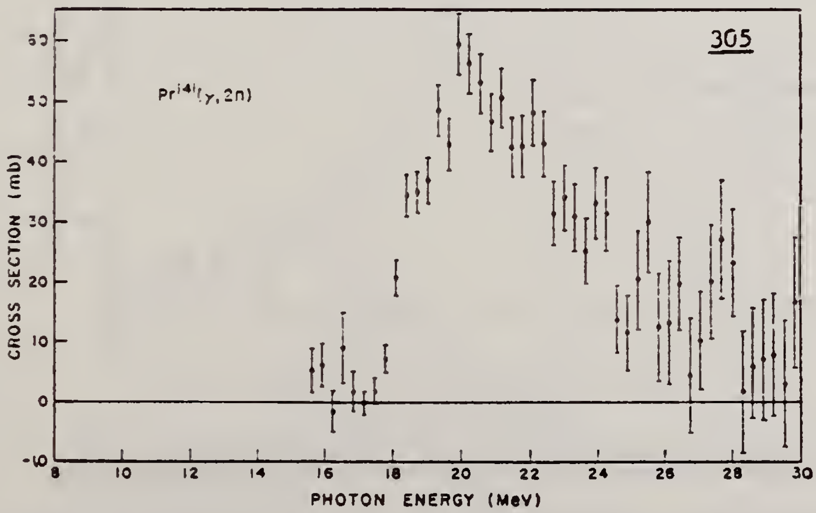

FIG. 2. The $Pr^{141}(\gamma,2n)$ cross section.

(over)

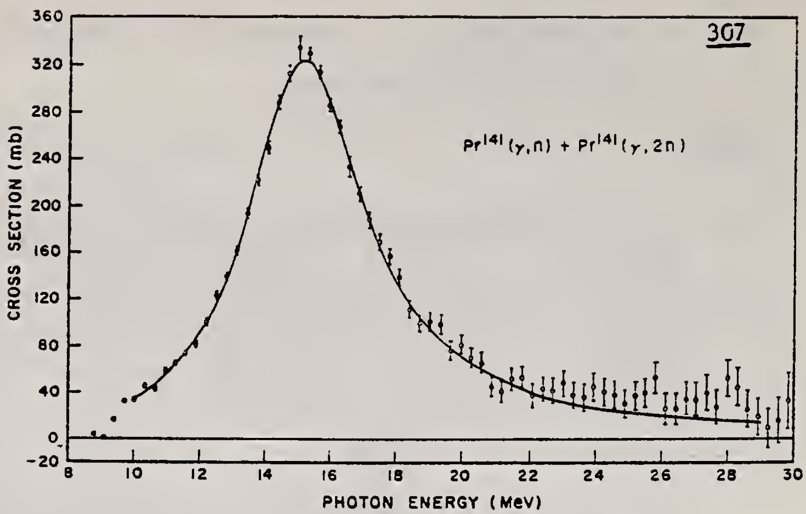

FIG. 4. The photon-absorption cross section of Pr^{141}. Charged particle emission has been neglected so the absorption cross section is the sum of the (γ,n), $(\gamma,2n)$ and $(\gamma,3n)$ cross sections. A Lorentz-shaped curve has been least-squares adjusted to fit the data from 10 to 25 MeV.

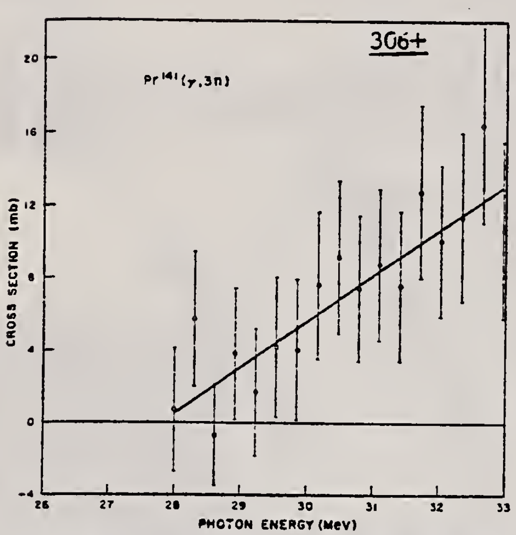

FIG. 3. The $Pr^{141}(\gamma,3n)$ cross section. The straight line has been adjusted to fit the data by a least-squares procedure.

TABLE II. Giant resonance parameters of Pr^{141} and I^{127}.

Parameter	Pr^{141}	I^{127}
E_a (MeV)	15.16±0.08	15.21±0.08
E_b (MeV)	···	1.04 E_a
Γ_a (MeV)	4.49±0.05	4.1 ±0.2
Γ_b (MeV)	···	7.9 ±1.5
σ_a (b)	0.32±0.02	0.18±0.02
σ_b (b)	···	0.05±0.01
$\int_{\text{threshold}}^{30} \sigma dE$ (MeV b)	2.10±0.15	1.79±0.13
$\pi\sigma_0\Gamma/2$ (MeV b)	2.27±0.14	1.8 ±0.2
$0.06NZ/A$ (MeV b)	2.06	1.85
$\int_{\text{threshold}}^{30} \sigma dE$+wings[a] (MeV b)	2.42±0.17	2.09±0.14

[a] The wing corrections were obtained from the areas of the Lorentz curves which were adjusted to fit the giant resonance.

REF.	ELEM. SYM.	A	Z
B.C. Cook, D.R. Hutchinson, R.C. Waring, J.N. Bradford, R.G. Johnson, and J.E. Griffin Phys. Rev. 143, B730 (1966)	Pr	141	59
METHOD 70 MeV synchrotron	REF. NO. 66 Co 3		JDM

REACTION	RESULT	EXCITATION ENERGY	SOURCE TYPE	SOURCE RANGE	DETECTOR TYPE	DETECTOR RANGE	ANGLE
G,N	ABX	THR - 65	C	THR - 70	ACT-I		4PI

114+

$$\int_0^{30} \sigma dE = 1790 \pm 100 \text{ MeV mb}$$

$$\int_{30}^{65} \sigma dE = 440 \text{ MeV mb}$$

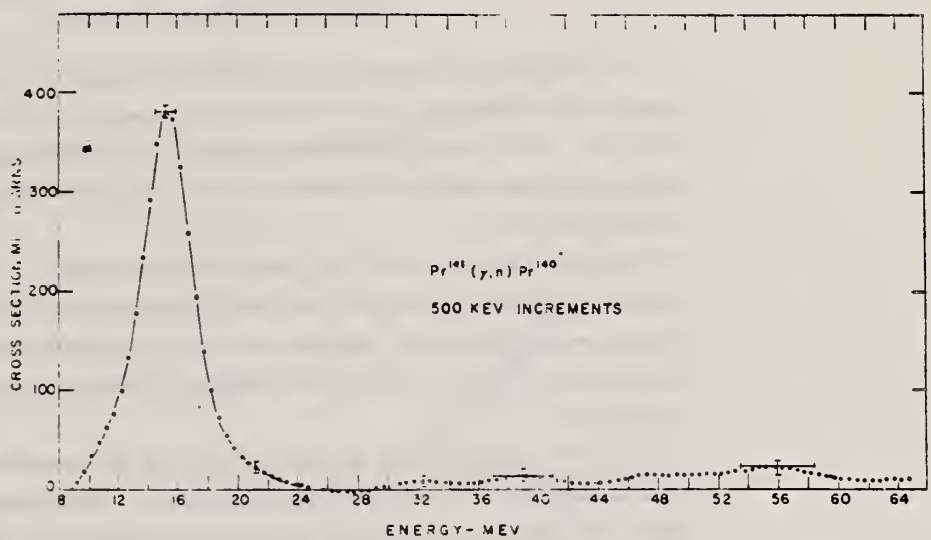

FIG. 1. Cross section for $Pr^{141}(\gamma,n)Pr^{140}$ from threshold energy to 65 MeV. The cross-section curve was calculated from yield data taken at 0.500-MeV increments. Horizontal error bars represent full width at half-maximum (FWHM) of experiment resolution and not uncertainty in energy.

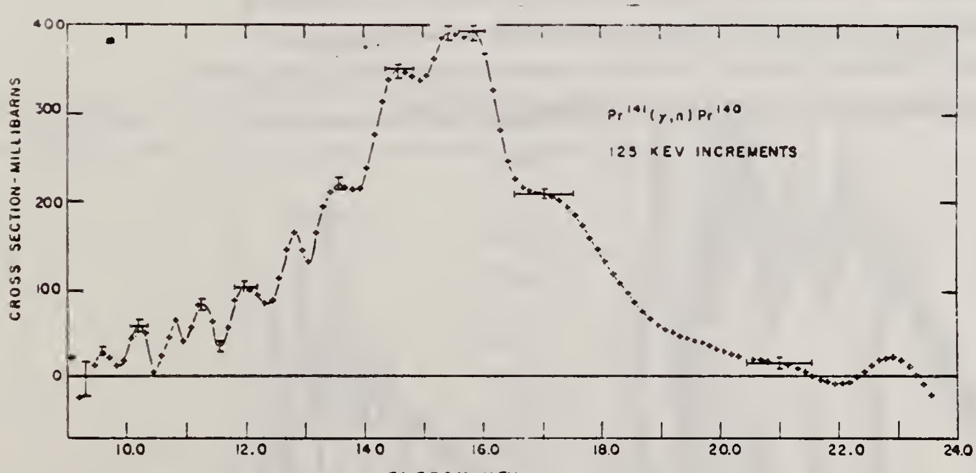

FIG. 2. Cross section for $Pr^{141}(\gamma,n)Pr^{140}$ from threshold energy to 24 MeV. The cross-section curve was calculated from yield data taken at 0.125-MeV increments. Horizontal error bars represent FWHM of experiment resolution and not uncertainty in energy.

REF. P.H. Cannington, D.G. Owen, R.J.J. Stewart, E.G. Muirhead, B.M. Spicer
PICNS-67 Contributions, International Conference on Nuclear Structure, Tokyo, Japan 1967 (Institute for Nuclear Study, University of Tokyo, Tanashi-shi, Tokyo, Japan) 10.15, p. 379

Pr	141	59
REF. NO. 67 Ca 1		EGF

METHOD

REACTION	RESULT	EXCITATION ENERGY	SOURCE		DETECTOR		ANGLE
			TYPE	RANGE	TYPE	RANGE	
G,N	RLX	9-17	C	9-17	ACT-I		4PI

576

Experimental Measurements of Vibrational Splitting of the Giant Dipole Resonance*

P. H. Cannington, D. G. Owen, R.J.J. Stewart, E. G. Muirhead and B. M. Spicer
University of Melbourne, Australia

The yield curve for the reaction $Zn^{64}(\gamma,n)$ has been measured in 0.1 MeV steps from threshold to 23 MeV, and that for $Pr^{141}(\gamma,n)$ has been measured in 0.05 MeV steps from threshold to 17.5 MeV. In both cases, the positron activity of the residual nucleus was detected by counting annihilation radiation. The cross sections were obtained from the yield curve by the Leiss-Penfold method.

The cross section for the $Zn^{64}(\gamma,n)$ reaction is shown in Fig. 1. Also shown are the predictions of Greiner[1], whose model considers the Goldhaber-Teller type dipole vibration, the low energy surface vibrations of spherical nuclei, and the coupling of these two vibrations. The predictions show only the energy, and integrated absorption cross section for the several transitions.

The $Pr^{141}(\gamma,n)$ cross section is shown in Fig. 2, and the calculations of Huber[2] are shown in blocked form; their detail is the same as above. In this case, the surface vibration phonon energy was not so easily fixed as in the case of even-A Zn^{64}. There were, in the case of Pr^{141}, two possible choices indicated by the low energy spectra of neighbouring nuclei. The more suitable one is indicated in Fig. 2.

In both cases, the amount of structure found experimentally exceeds that predicted by the dipole-surface vibration-interference model. However, by worsening the experimental resolution, the agreement can be readily improved. The surplus structure in both cross sections is presumably due to single particle effects which are neglected in the model.

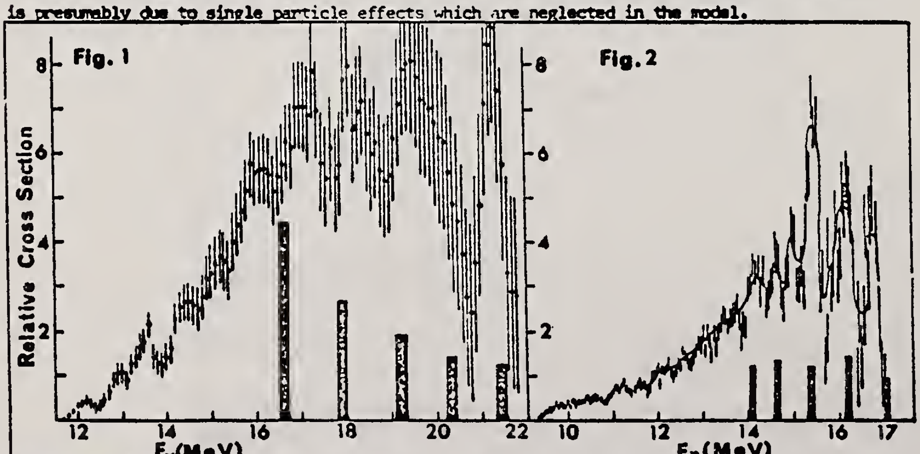

*Supported in part by the U.S. Army Research Office and the Australian Research Grants Committee.

References: 1) W. Greiner, private communication (1966).
2) M. Huber, private communication (1966).

REF.	ELEM. SYM.	A	Z
R. R. Hurst and D. J. Donahue Nucl. Phys. A91, 365 (1967)	Pr	141	59

METHOD	REF. NO.	
Neutron capture gamma rays	67 Hu 1	EGF

REACTION	RESULT	EXCITATION ENERGY	SOURCE TYPE	SOURCE RANGE	DETECTOR TYPE	DETECTOR RANGE	ANGLE
G,N	ABX	10,11	D	10,11	BF3-I		4PI

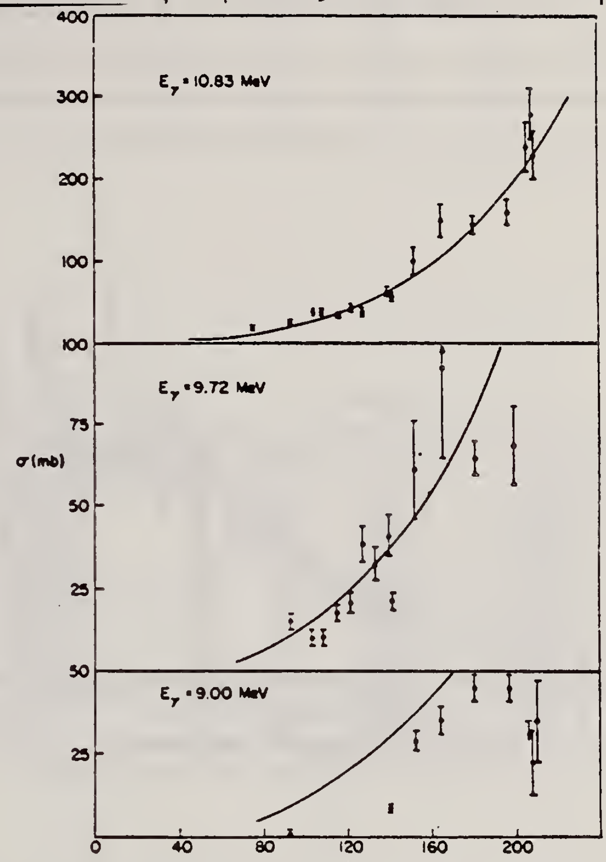

Fig. 1. Cross section (in mb) versus mass number of the target for gamma-ray energies of 9.00, 9.72 and 10.83 MeV. The solid lines are plots of eq. (1) in the text.

TABLE 1
Photoneutron cross sections (mb)

Target	7.72 MeV	9.00 MeV	9.72 MeV	10.83 MeV
^{59}Co				9.0 ± 0.8
^{75}As				20.4 ± 1.7
^{93}Nb		0.53 ± 0.10	14.6 ± 2.2	25.8 ± 2.1
^{103}Rh			10.6 ± 1.7	38.8 ± 3.1
^{107}Ag, ^{109}Ag			10.0 ± 1.5	37.6 ± 2.9
^{115}In			17.1 ± 2.6	33.3 ± 2.7
^{121}Sb, ^{123}Sb			20.7 ± 3.1	42.5 ± 3.6
^{127}I			38.7 ± 5.8	38.8 ± 3.1
^{133}Cs			31.7 ± 4.8	52.5 ± 3.8
^{139}La		8.61 ± 0.86	40.8 ± 6.5	63.0 ± 5.0
^{141}Pr			21.5 ± 3.2	58.3 ± 4.1
^{151}Eu, ^{153}Eu		28.9 ± 3.2	61.3 ± 14.7	102 ± 18
^{165}Ho		35.6 ± 4.3	92.2 ± 27.6	150 ± 20
^{181}Ta	4.14 ± 0.36	45.4 ± 3.7	65.0 ± 5.5	146 ± 12
^{197}Au		44.5 ± 3.6	68.4 ± 13.5	160 ± 15
^{206}Pb		<34.3		238 ± 29
^{208}Pb		22.6 ± 11.3		280 ± 31
^{209}Bi		36.1 ± 12.0		226 ± 27

REF. P. H. Cannington, R. J. J. Stewart, B. M. Spicer and M. G. Huber
Nucl. Phys. A109, 385 (1968)

ELEM. SYM.	A	Z
Pr	141	59

METHOD

REF. NO.	
68 Ca 1	EGF

REACTION	RESULT	EXCITATION ENERGY	SOURCE TYPE	SOURCE RANGE	DETECTOR TYPE	DETECTOR RANGE	ANGLE
G,N	ABX	9-17	C	9-17	ACT-I		4PI

69

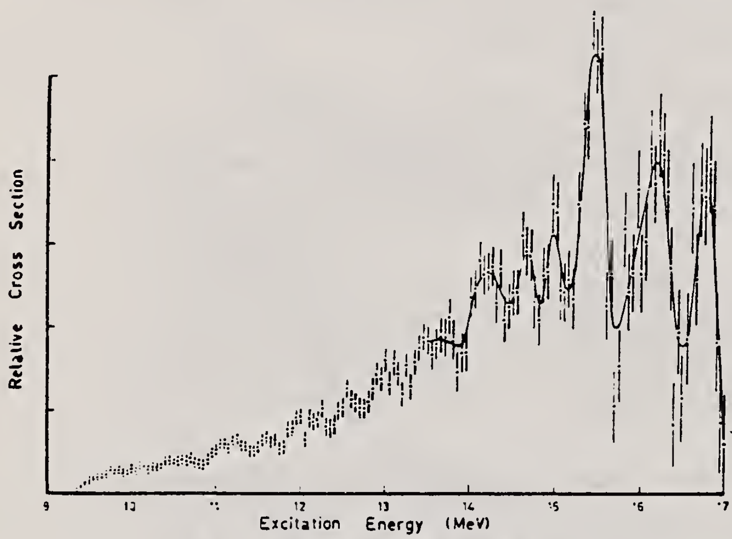

Fig. 1. The $^{141}Pr(\gamma, n)^{140}Pr$ cross section.

REF.	ELEM. SYM.	A	Z
J. W. Jury, J. S. Hewitt, and K. G. McNeill Can. J. Phys. 46, 1823 (1968)	Pr	141	59

METHOD	REF. NO.	
	68 Ju 1	EGF

REACTION	RESULT	EXCITATION ENERGY	SOURCE		DETECTOR		ANGLE
			TYPE	RANGE	TYPE	RANGE	
G,N	NOX	THR-30	C	30	THR	5-	DST

$W(\theta) = a_0 + a_1P_1 + a_2P_2$

TABLE I

Target element	Z	Energy	a_0*	a_1/a_0	a_2/a_0
Vanadium	23	32	640 ± 50	0.11 ± 0.10	-0.09 ± 0.11
Chromium	24	22	365 ± 39	0.02 ± 0.08	0.00 ± 0.10
Manganese	25	22	450 ± 33	0.07 ± 0.05	-0.11 ± 0.06
Bromine	35	27	874 ± 54	0.05 ± 0.06	-0.15 ± 0.08
Molybdenum	42	22	610 ± 60	0.09 ± 0.05	-0.35 ± 0.06
Ruthenium	44	27	1100 ± 25	0.12 ± 0.02	-0.29 ± 0.03
Rhodium	45	27	1270 ± 47	0.06 ± 0.03	-0.14 ± 0.03
Palladium	46	27	1350 ± 29	0.26 ± 0.02	-0.12 ± 0.02
Antimony	51	27	2140 ± 62	0.04 ± 0.08	-0.25 ± 0.11
Lanthanum	57	27	1940 ± 70	0.12 ± 0.10	-0.52 ± 0.14
Praseodymium	59	30	1800 ± 58	0.20 ± 0.08	-0.40 ± 0.09
Platinum	78	27	2600 ± 52	0.17 ± 0.02	-0.15 ± 0.03
Lead	82	22	2274 ± 59	0.08 ± 0.08	-0.46 ± 0.09

*The yield per mole per 100 r was normalized to a yield of 2274 for the lead sample at the same energy.

REF.	ELEM. SYM.	A	Z
R. Moreh and M. Friedman Phys. Letters 26B, 579 (1968)	Pr	141	59

METHOD	REF. NO.	
	68 Mo 1	EGF

REACTION	RESULT	EXCITATION ENERGY	SOURCE TYPE	SOURCE RANGE	DETECTOR TYPE	DETECTOR RANGE	ANGLE
G,G	NOX	7	D	7	NAI-D	5-8	90

Compton polarimeter.

Table 1

Properties of levels populated by resonance scattering of iron capture γ rays; J_0 and J denote the spins of the ground and resonance levels, respectively.

Scattering isotope	J_0	Resonance level (MeV)	Resonance spin	$N(90,90)/N(90,0)$ exp.	calc.	Transition character
^{208}Pb	0^+	7.279	1	1.18 ± 0.03	1.18	E1
^{112}Cd	0^+	7.632	1	0.87 ± 0.04	0.855	M1
^{141}Pr	$\frac{5}{2}^+$	7.632	$\frac{7}{2}$	1.03 ± 0.02	1.03	E1
^{62}Ni	0^+	7.646	1	0.88 ± 0.04	0.855	M1
^{203}Tl	$\frac{1}{2}^+$	7.646	$\frac{1}{2}$	1.00 ± 0.01	1.00	-

REF.		ELEM. SYM.	A	Z
H. Ejiri, P. Richard, S. Ferguson, R. Heffner and D. Perry Nucl. Phys. A128, 388 (1969)		Pr	141	59
METHOD		REF. NO.		
		69 Ej 1		egf

REACTION	RESULT	EXCITATION ENERGY	SOURCE TYPE	SOURCE RANGE	DETECTOR TYPE	DETECTOR RANGE	ANGLE
P,G	ABX	15	D	9-11	SCI-D	6-15	DST

15=14.95 MEV

$Y(90^{\circ})/Y(125^{\circ}) = 1.18$

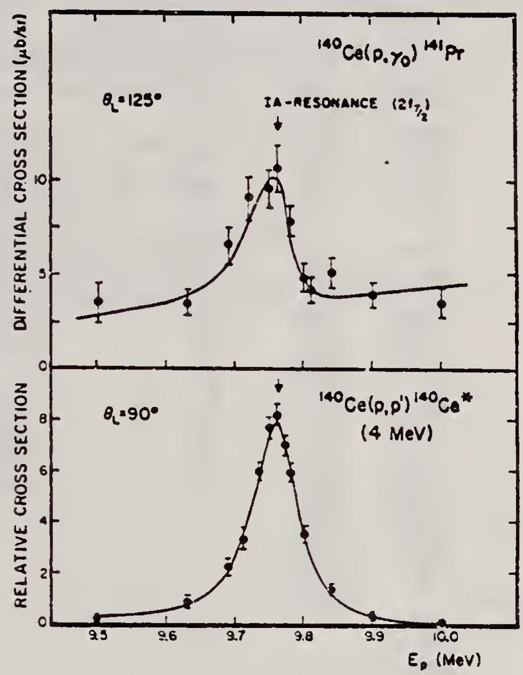

Fig. 4. Excitation function of the ^{140}Ce(p, γ)^{141}Pr reaction through the $2f_{\frac{7}{2}}$ IA resonance for the two-quanta escape peak of the ground state transition (upper part) and that of the ^{140}Ce(p, p')^{140*}Ce reaction leaving the 4$^-$ particle-hole state at 4 MeV (lower part). Solid lines are calculated ones. For the fit to the (p, p') excitation function, a slight interference effect $\sqrt{\Gamma_{p'}}\,(E-\bar{E})$ is also used.

REF.	ELEM. SYM.	A	Z
V. E. Michalk and J. A. McIntyre Nucl. Phys. A137, 115 (1969)	Pr	141	59

METHOD	REF. NO.	
	69 Mi 1	egf

REACTION	RESULT	EXCITATION ENERGY	SOURCE TYPE	SOURCE RANGE	DETECTOR TYPE	DETECTOR RANGE	ANGLE
G,G	SPC	6-8	D	6-8	SCD-D	4-8	DST

BRANCHING RATIOS

TABLE 1

Experimental results

Target (source)	Isotope		Levels excited (MeV)		Level spin		Partial branching ratio [h])	Branching ratio [k])	
	literature [a])	this work	literature [a])	this work	literature [a])	this work	this work	literature [a])	this work
Cd(Fe)	112 [b])	112	7.629 [d])	7.629	1 [b])	1			
	112		0	0	0		1.000	0.48±0.06 [b])	< 0.574±0.011
	112		0.62	0.62	2		0.212±0.011		< 0.122±0.086
	112		1.22	1.22	0(1)	0	0.159±0.013		< 0.092±0.009
	112		1.86	1.86	0(1)	0	0.371±0.019		< 0.213±0.011
Sn(Cu)	117 [m])	118	7.01 [d])	7.01	1 [e])	1			
	118		0	0	0		1.000		< 0.802±0.042
	118		1.23	1.23	2		0.247±0.038		< 0.198±0.030
Pr(Cl)	141		6.12 [d])	6.12					
	141		0	0	$\frac{5}{2}$		1.000(1.0)• •		< 0.600±0.032
	141		0.145	0.145	$\frac{7}{2}$		0.494±0.050(0.42±0.04)•		< 0.296±0.030
	141		1.451 [f])	1.46	$\frac{3}{2}$ [f])		0.173±0.045(0.13±0.04)•		< 0.104±0.025
Pr(Fe)	141		7.629 [d])	7.629	$\frac{5}{2}$ [f])				
	141		0	0	$\frac{5}{2}$		(1.0)•	0.48 [f])	
	141		0.145	0.145	$\frac{7}{2}$		(0.2±0.1)•	0.075 [f])	
	141		1.13	1.13	$\frac{3}{2}$ [f])		(0.17±0.1)•	0.085 [f])	
	141		1.451 [f])	1.46	$\frac{3}{2}$ [f])		(0.33±0.1)•	0.165 [f])	
	141		2.235 [f])	2.25	$\frac{3}{2}$ [f])		(0.2±0.1)•	0.08 [f])	
Cd(Co)		?	6.990 [e])	6.990					
		110	6.490 [d])	6.490		1			
	110		0.658	0.658	2				
	110		1.78	1.79					
		doubly even		6.278		(1)			
Pb(Fe)	208 [g])		7.277 [g])		1 [e])				
Bi(Ti)	209		7.149 [d])						
Zr(Se)	doubly even		8.496		1 [e])				

[a]) Unless otherwise noted, data are from Nuclear Data Sheets, National Academy of Sciences - National Research Council, 2101 Constitution Avenue, Washington 25, D.C.; or from C. M. Lederer, J. A. Hollander and I. Perlman, Table of Isotopes, Sixth Edition (John Wiley and Sons, Inc., New York, 1967). Energy values are from refs. [12-13]).

[b]) Ref. [3]). [d]) Ref. [10]). [e]) Ref. [5]). [f]) Ref. [9]). [g]) Ref. [20]). [h]) Γ(resonance level → excited level)/Γ(resonance level → ground level).
[k]) Γ(resonance level → excited level)/Γ(total width). [m]) Ref. [2]). • Ratios taken only at 150°.

[over]

References

1) M. Giannini, P. Oliva, D. Prosperi and S. Sciuti, Nucl. Phys. 65 (1965) 344
2) M. Giannini, P. Oliva, D. Prosperi and G. Toumbev, Nucl. Phys. A101 (1967) 145
3) K. Min, Phys. Rev. 152 (1966) 1062
4) G. P. Estes and K. Min, Phys. Rev. 154 (1967) 1104
5) S. Ramchandran and J. A. McIntyre, Phys. Rev. 179 (1969) 1153
6) Y. Schlesinger, B. Arad and G. Ben-David, Israel Atomic Energy Commission Report IA-1128 (1966) and later reports
7) J. A. McIntyre and V. E. Michalk, Bull. Am. Phys. Soc. 12 (1967) 1205
8) R. Moreh and A. Nof, Bull. Am. Phys. Soc. 13 (1968) 1451
9) R. Moreh and A. Nof, report of the Nuclear Research Centre - Negev, Beer Sheva, Israel; Use of the (γ,γ') reaction for studying ^{141}Pr levels
10) G. Ben-David, B. Arad, T. Balderman and Y. Schlesinger, Phys. Rev. 146 (1966) 852
11) N. V. DeCastro Faria and R. J. A. Levesque, Nucl. Instr. 46 (1967) 325
12) L. V. Groshev, V. N. Lutsenko, A. M. Demidov and V. I. Pelekov, Atlas of gamma spectra from radiative capture of thermal neutrons, translated from Russian by J. S. Sykes (Pergamon Press, 1959)
13) G. A. Bartholomew, A. Doveika, K. M. Eastwood, S. Monaro, L. V. Groshev, A. M. Demidov, V. I. Pelekhov and L. L. Sokolovskii, Nucl. Data A3 (1967) 367
14) C. M. Lederer, J. A. Hollander and I. Perlman, Table of isotopes, Sixth ed. (J. Wiley, New York, 1967)
15) Nuclear Data Sheets, National Academy of Sciences - National Research Council, 2101 Constitution Avenue, Washington 25, D.C.
16) H. Ferentz and N. Rosenzweig, Argonne Nat. Lab. Rep. ANL-5324
17) R. Moreh and M. Friedman, Phys. Lett. 26B (1968) 579
18) D. B. Beery, W. H. Kelly and W. C. McHarris, Phys. Rev. 171 (1968) 1283
19) H. W. Bear and J. Bardwick, Bull. Am. Phys. Soc. 13 (1968) 1430;
B. H. Wildenthal, R. L. Auble, E. Newman and J. A. Nolen, Bull. Am. Phys. Soc. 13 (1968) 1430
20) C. S. Young and D. T. Donahue, Phys. Rev. 132 (1963) 1724

REF.	ELEM. SYM.	A	Z
K. Shoda, M. Sugawara, T. Saito & H. Miyase PICNS-69 Proceedings of the Conference on Nuclear Isospin. Asilomar-Pacific Grove, California 1969 (Academic Press, New York & London 1969) p.137.	Pr	141	59
METHOD	REF. NO. 69 Sh 8		egf

REACTION	RESULT	EXCITATION ENERGY	SOURCE TYPE	SOURCE RANGE	DETECTOR TYPE	DETECTOR RANGE	ANGLE
E,P	SPC	10-19	D	20	MAG-D		DST

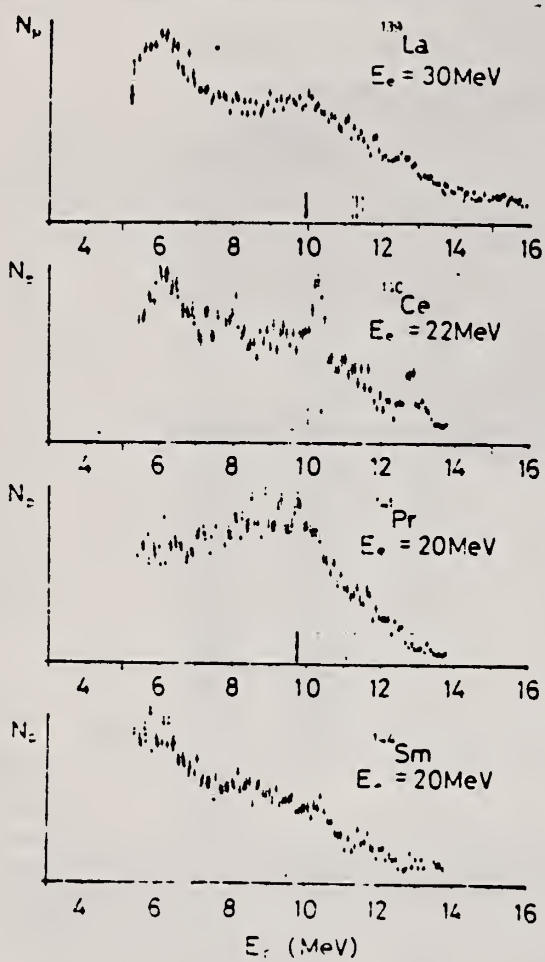

Fig. 1. Energy distributions of photoprotons. Vertical broken lines and solid lines indicate the position of p_0 corresponding to the ground IAS and electric dipole IAS (2).

Table 1. Angular distributions of strong proton groups from ^{140}Ce and ^{141}Pr.

Nucleus	E_p(MeV)	W(θ)
^{140}Ce	10.3	$1+(0.4\pm0.1)P_1-(0.0\pm0.1)P_2$
	12.8	$1+(0.2\pm0.1)P_1-(0.4\pm0.2)P_2$
^{141}Pr	9.7	$1+(0.0\pm0.1)P_1+(0.1\pm0.2)P_2$

Table 2. The radiative widths of the main IAS. The results are compared with the single particle strength in W.u..

Nucleus	E_p (MeV)	E_x (a) (MeV)	Γ_{p_0}/Γ	Γ_γ (eV)	$2(T+1)\Gamma_{\gamma_0}$ (W.u.)
^{140}Ce	10.3	18.3	1 (b)	50	0.1
	12.8	20.8	1 (b)	90	0.1
^{141}Pr	9.7	15.1	12/60(c)	40	0.2
^{144}Sm	10.6	16.6	1 (b)	20	0.05

(a) Ground state is assumed for the residual state.

(b) Assumption.

(c) P. VonBrentano et al. (2).

REF.	K. G. McNeill, J. W. Jury, and J. S. Hewitt Can. J. Phys. 48, 950 (1970)	ELEM. SYM.	A	Z
		Pr	141	59
METHOD		REF. NO.		
		70 Mc 1		egf

REACTION	RESULT	EXCITATION ENERGY	SOURCE TYPE	SOURCE RANGE	DETECTOR TYPE	DETECTOR RANGE	ANGLE
G,XN	SPC	11-28	C	28	TOF-D	2-8	98

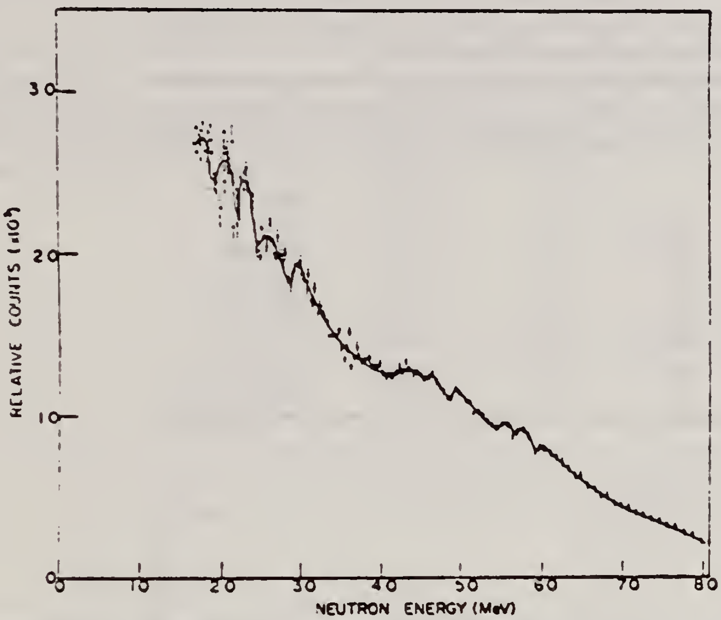

FIG. 1. The photoneutron spectrum obtained by the irradiation of praseodymium by bremsstrahlung of maximum energy 27.5 MeV, the flight path direction being at 98° to the bremsstrahlung beam. The line is merely to guide the eye.

TABLE I

Correlation between peaks in the cross section and the neutron spectrum for the reaction $^{141}Pr(\gamma,n)^{140}Pr$*

Neutron energy E_n (MeV)	Excitation energy $E_n + E_{threshold}$ (9.3 MeV)	Peaks in $\sigma(\gamma,n)$ Cannington *et al.* (1968) (MeV)†
2.2	11.5	11.6?
2.4	11.7	
2.7	12.0	12.0
3.0	12.3	12.2?
		12.6?
3.9	13.2	13.1
4.4	13.7	13.7
4.7	14.0	
5.0	14.3	14.25
5.5	14.8	14.7
5.75	15.05	15.0

*The error on the experimentally determined neutron energy is in all cases between 70 and 100 kV.

†The question marks indicate doubts expressed in the text of Cannington *et al.*

REF. R. Moreh, S. Shlomo, and A. Wolf
Phys. Rev. C2, 1144 (1970)

ELEM. SYM.	A	Z
Pr	141	59

METHOD

REF. NO.	
70 Mo 2	hmg

REACTION	RESULT	EXCITATION ENERGY	SOURCE TYPE	SOURCE RANGE	DETECTOR TYPE	DETECTOR RANGE	ANGLE
G,G	ABX	8	D	8	SCD-D		DST
		(7.632)		(7.632)			

8 = 7.632, LFT

TABLE III. Summary of the results of spins, parities, and total widths of resonance levels excited by γ rays obtained from neutron capture in iron. Parities in parantheses are uncertain.

Isotope	Energy (MeV)	$\delta=\lvert E_\gamma-E_e\rvert$ (eV)	J^π_0	J^π_r	Transition	Γ_0/Γ_γ (±8%)	Γ_γ (10^{-3} eV)
^{50}Cr	8.888	18 ±1	0^+	1	...	0.90	750±200
^{62}Ni	7.646	14 ±1	0^+	1^-	$E1$	0.64	480± 50
^{74}Ge	6.018	4.5±0.5	0^+	1^-	$E1$	0.19	120± 15
^{75}As	7.646	7.4±0.3	$3/2^-$	$1/2^{(+)}$	...	0.11	360±100
^{103}Ag	7.632	9 ±1	$1/2^-$	3/2	...	0.7	2± 1
^{112}Cd	7.632	4.8±0.4	0^+	1^-	$E1$	0.55	86± 15
^{139}La	6.018	8.2±0.6	$7/2^+$	$7/2^-$	$E1$	0.50	51^{+14}_{-6}
^{141}Pr	7.632	$11.4^{+0.3}_{-0.9}$	$5/2^+$	$5/2^+$	$M1$	0.46	72^{+24}_{-4}
^{205}Tl	7.646	9.3±0.3	$1/2^+$	$1/2^{(-)}$	...	0.58	980± 90
^{208}Pb	7.279	7.1±0.3	0^+	1^+	$M1$	1.00	780± 60

TABLE IV. Effective elastic scattering cross section $\langle\sigma_r\rangle=\sigma_0^m(\Gamma_0/\Gamma_\gamma)\Psi(x_0,t_0)$, where δ, J, Γ_0, Γ_γ were taken from Table III. The temperature of the scatterer was 300°K, while that of the iron γ source was 640°K.

Target	Resonance energy (MeV)	$\langle\sigma_r\rangle$ (mb)
^{50}Cr	8.388	905
^{62}Ni	7.646	569
^{74}Ge	6.018	61
^{75}As	7.646	4.4
^{109}Ag	7.632	3.5
^{112}Cd	7.632	198
^{139}La	6.018	39
^{141}Pr	7.632	20
^{205}Tl	7.646	574
^{208}Pb	7.279	5560

REF.					ELEM. SYM.	A	Z
R. E. Sund, V. V. Verbinski, H. Weber, and L. A. Kull Phys. Rev. C2, 1129 (1970)					Pr	141	59
METHOD					REF. NO.		
					70 Su 1		hmg

REACTION	RESULT	EXCITATION ENERGY	SOURCE TYPE	SOURCE RANGE	DETECTOR TYPE	DETECTOR RANGE	ANGLE
G,N	ABX	9-24	D	9-24	ACT-I		4PI

277

The $^{141}Pr(\gamma, n)$ cross section was measured from threshold to 24 MeV with a photon beam produced by the in-flight annihilation of positrons. The photon beam resolution was determined to be 1.2% (full width at half maximum) by elastically scattering the γ rays from the 15.1-MeV level in ^{12}C. The (γ, n) cross section was found to have a maximum value of $\sim$348 mb and an integrated value up to 24 MeV of 1.72 ± 0.16 MeV b. Within the statistics and the photon resolution of the measurement, the results indicate that there is no structure in the cross section, with the possible exception of a weak bump at approximately 17.5 MeV. The results are compared with previous measurements and with theory; the latter comparison indicates that the widths of states in the dynamic collective theory should be considerably broader than those which have been typically used.

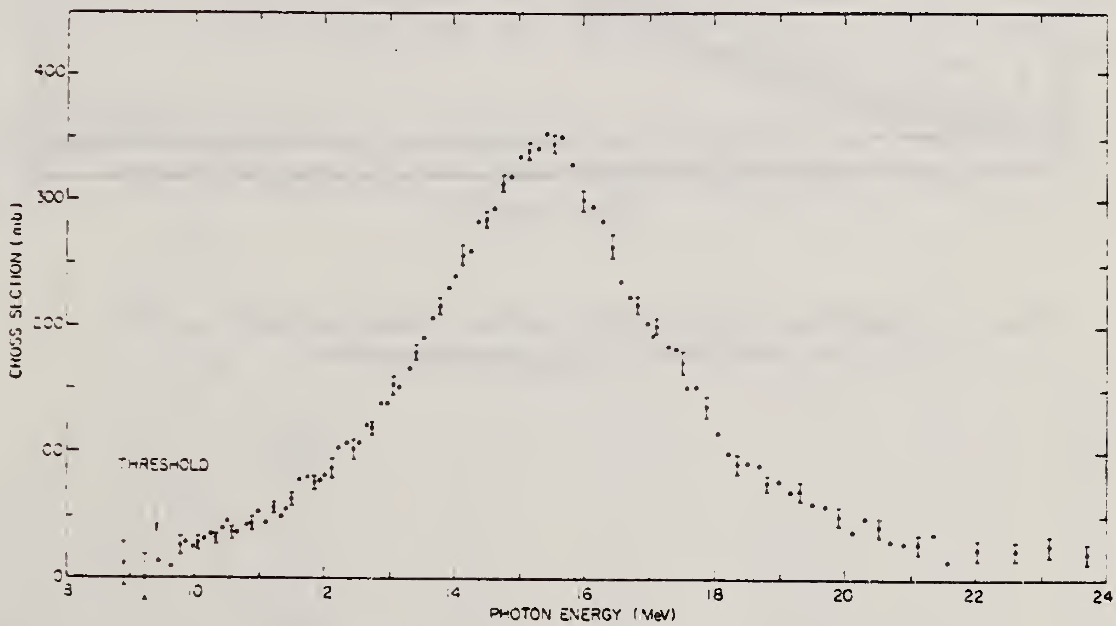

FIG. 4. $^{141}Pr(\gamma, n)$ cross section.

REF.	ELEM. SYM.	A	Z
J. Ahrens, H. Borchert, H.B. Eppler, H. Gimm, H. Gundrum, P. Riehn, G. Sita Ram, A. Zieger, and B. Ziegler Elba-71, Tagungsbericht Elektronen Beschleuniger Arbeits Gruppen (Sept. 1971) Justus Liebig-Universitat Giessen.	Pr	141	59

METHOD	REF. NO.	
	71 Ah 1	hmg

REACTION	RESULT	EXCITATION ENERGY	SOURCE TYPE	SOURCE RANGE	DETECTOR TYPE	DETECTOR RANGE	ANGLE
G,MU-T	ABX	THR-150	C	10-150	MGC-D		4PI

579

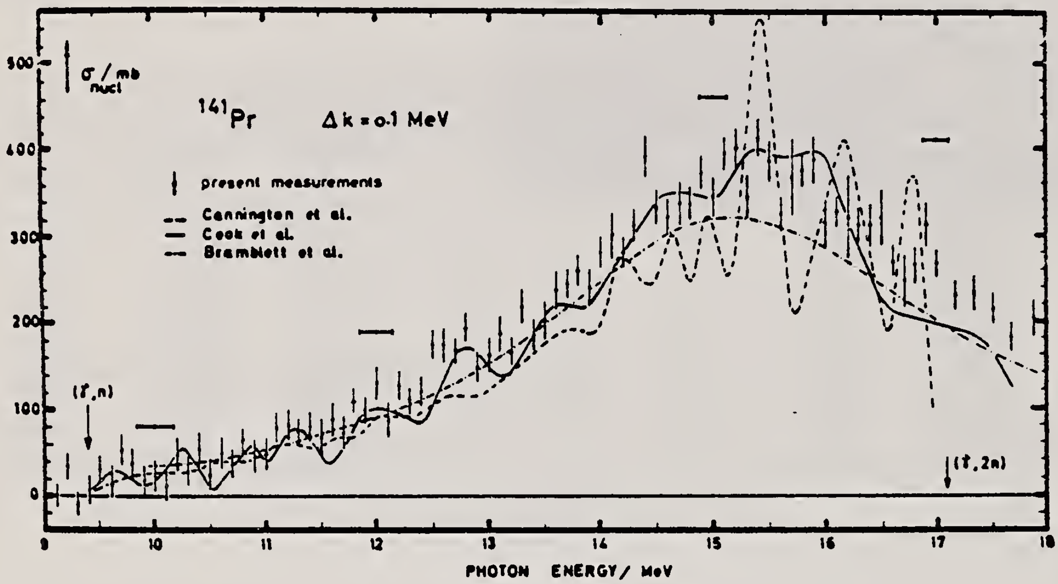

fig. 9: comparison of the total nuclear cross-section in ^{141}Pr with the results of (γ,n)-measurements

REF.	ELEM. SYM.	A	Z
H. Beil, R. Bergere, P. Carlos, A. Lepretre, A. Veyssiere and A. Parlag Nucl. Phys. A172, 426 (1971)	Pr	141	59

METHOD	REF. NO.	
	71 Be 4	egf

REACTION	RESULT	EXCITATION ENERGY	SOURCE TYPE	SOURCE RANGE	DETECTOR TYPE	DETECTOR RANGE	ANGLE
G, N	ABX	9-17	D	9-17	MOD-I		4PI
							390

TABLE I

Lorentz line parameters corresponding to fits of total photoneutron cross sections presented in fig. 1

	$_{56}$Ba	$^{139}_{57}$La	$_{58}$Ce	$^{141}_{59}$Pr	$_{60}$Nd	$^{141}_{59}$Pr ^{a})
σ_1 (mb)	356 $\pm$15	340 $\pm$15	360 $\pm$15	350 $\pm$15	315 $\pm$15	320 $\pm$20
E_1 (MeV)	15.3 $\pm$ 0.1	15.2 $\pm$ 0.1	15.0 $\pm$ 0.10	15.1 $\pm$ 0.1	14.9 $\pm$ 0.1	15.16$\pm$ 0.08
Γ_1 (MeV)	4.70$\pm$ 0.15	4.45$\pm$ 0.05	4.35$\pm$ 0.05	4.26$\pm$ 0.05	4.90$\pm$ 0.05	4.49$\pm$0.05
$\frac{1}{2}\pi\sigma_1\Gamma_1$ (MeV · b)	2.6 $\pm$ 0.15	2.35$\pm$ 0.13	2.42$\pm$ 0.15	2.35$\pm$ 0.13	2.43$\pm$ 0.13	2.42$\pm$ 0.17
$\frac{\frac{1}{2}\pi\sigma_1\Gamma_1}{0.06NZA^{-1}}$	1.30$\pm$ 0.08	1.16$\pm$ 0.08	1.19$\pm$ 0.08	1.14$\pm$ 0.08	1.15$\pm$ 0.08	

^{a}) Lorentz line parameters given in ref. [10]) for ^{141}Pr.

[10] R. L. Bramblett, J. T. Caldwell, B. L. Berman, R. R. Harvey and S. C. Fultz, Phys. Rev. 148, 1198 (1966).

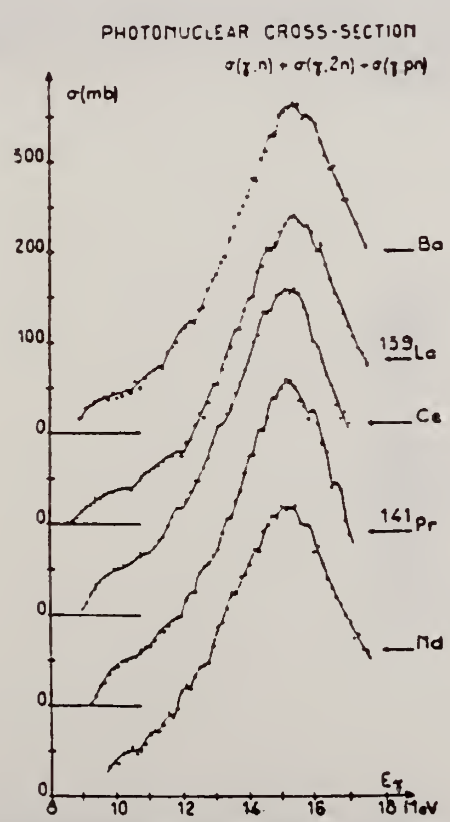

Fig. 1. Total photoneutron cross sections for Ba, ^{139}La, Ce, ^{141}Pr and Nd as a function of incident photon energy E.

U.S. DEPARTMENT OF COMMERCE
NATIONAL BUREAU OF STANDARDS

REF.	ELEM. SYM.	A	Z
D. Pavel, G. Ben-David, Y. Schlesinger, H. Szichman Nucl. Phys. A160, 409 (1971)	Pr	141	59

METHOD	REF. NO.	
	71 Pa 2	egf

REACTION	RESULT	EXCITATION ENERGY	SOURCE TYPE	SOURCE RANGE	DETECTOR TYPE	DETECTOR RANGE	ANGLE
G,G	LFT	6-9	D	6-9	SCD-D	3-9	DST
		-	-				

5 LEVELS

TABLE 1

Experimental A_{22} coefficients compared with theory assuming pure dipole transitions

Energy of transitions (keV)	Energy of final state (keV)	A_{22} coefficients for various assumed spin sequences					
		$\frac{5}{2}\rightarrow\frac{3}{2}\rightarrow\frac{5}{2}$ + 0.01000 [a])	$\frac{5}{2}\rightarrow\frac{5}{2}\rightarrow\frac{5}{2}$ + 0.1828 [a])	$\frac{5}{2}\rightarrow\frac{5}{2}\rightarrow\frac{7}{2}$ − 0.05713 [a])	$\frac{5}{2}\rightarrow\frac{7}{2}\rightarrow\frac{5}{2}$ + 0.1071 [a])	$\frac{5}{2}\rightarrow\frac{7}{2}\rightarrow\frac{7}{2}$ − 0.1428 [a])	$\frac{5}{2}\rightarrow\frac{7}{2}\rightarrow\frac{9}{2}$ + 0.05001 [a])
6115	0				+ 0.090±0.037		
5970	145.4					− 0.161±0.068	
4657	1457.9				+ 0.082±0.078		+ 0.082±0.078
7188	0		+ 0.225±0.069				

[a]) Theoretical value [5]).

[5]M. Ferentz and N. Rosenzweig, Table of angular correlations coefficients, in Alpha-, beta- and gamma-ray spectroscopy, vol. 2, ed. K. Siegbahn, (North-Holland, Amsterdam, 1965) App.8.

TABLE 2

Partial radiation reduced widths of the 6115 keV resonance level

Energy of transitions (keV)	Energy of final state (keV)	Branching ratio Γ_i/Γ	Reduced widths k(E1) (eV·MeV^{-4})	k(M1) × 10^3	Most likely character
6115	0	0.557±0.010	27±5	725±139	E1
5970	145.4	0.264±0.006	14±3	370± 71	E1
4822	1292.8	0.013±0.004	1.3±0.4	35± 11	E1 or M1
4657	1457.9	0.087±0.011	9.5±2.6	256± 55	E1
4511	1603.7	0.013±0.004	1.6±0.5	42± 13	E1 or M1
4109	2006	0.011±0.006	1.7±0.8	47± 22	E1 or M1
3806	2309.3	0.014±0.003	2.7±0.7	76± 19	E1
3775	2340	0.015±0.004	3.1±0.9	83± 23	E1
3490	2625	0.025±0.003	6.5±1.0	174± 37	E1

[over]

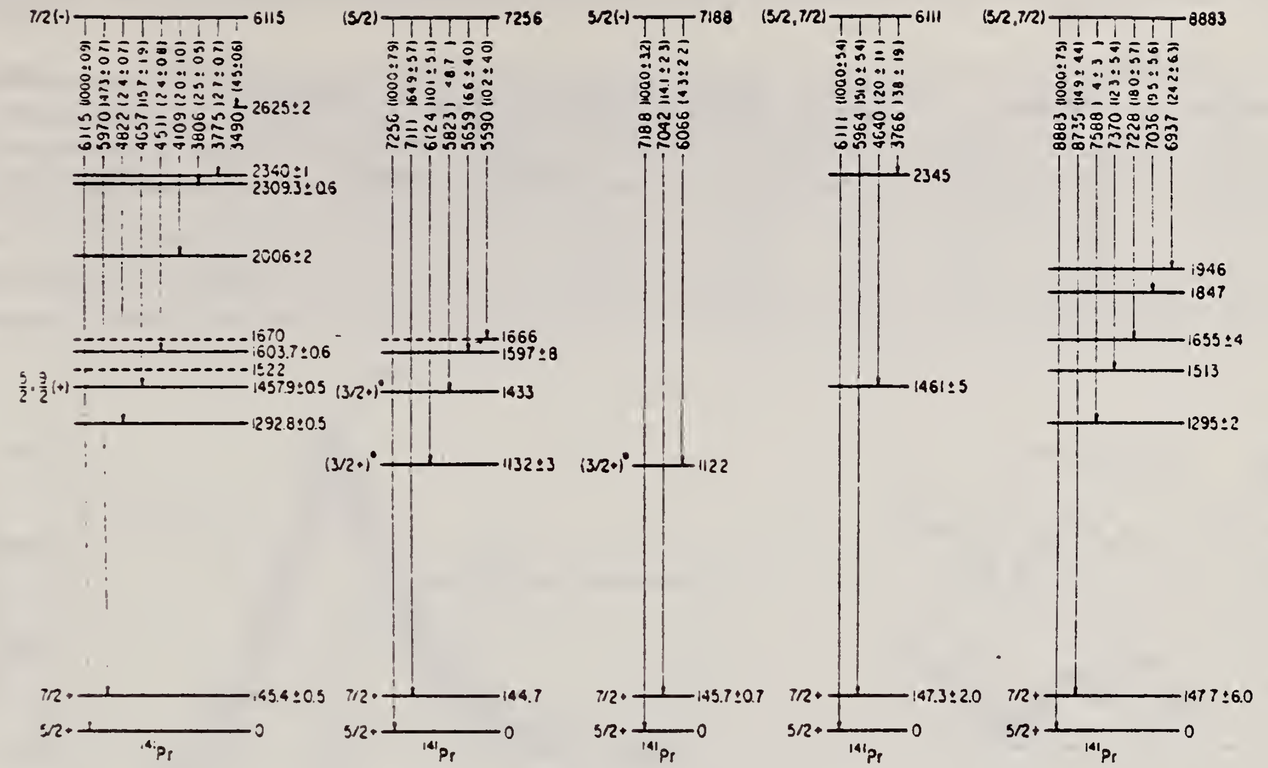

Fig. 2. Decay schemes of the observed resonant levels of ^{141}Pr. The uncertainties in the energy of the levels are estimated as ± 6 keV unless indicated explicitly.

REF.

R. Pitthan and Th. Walcher
Phys. Letters 36B, 563 (1971)

ELEM. SYM.	A	Z
Pr	141	59

METHOD

REF. NO.

71 Pi 1 egf

REACTION	RESULT	EXCITATION ENERGY	SOURCE TYPE	SOURCE RANGE	DETECTOR TYPE	DETECTOR RANGE	ANGLE
E,E/	SPC	4-18		50,65	MAG-D		DST

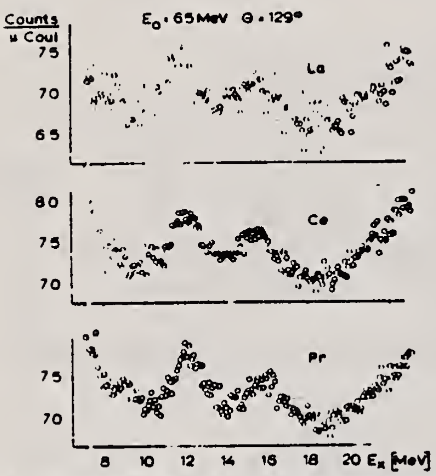

Fig. 2. Spectra of electrons scattered inelastically from La, Ce and Pr targets at the same primary energy and the same laboratory scattering angle. No background has been subtracted. Note the suppressed zeros of the ordinate scales.

REF.	ELEM. SYM.	A	Z
T.K. Deague and R.J.J. Stewart Nucl. Phys. A191, 305 (1972)	Pr	141	59
METHOD	REF. NO.		
	72 De 3		egf

REACTION	RESULT	EXCITATION ENERGY	SOURCE		DETECTOR		ANGLE
			TYPE	RANGE	TYPE	RANGE	
G,XN	ABX	9-22	C	9-22	BF3-I		4PI

560+

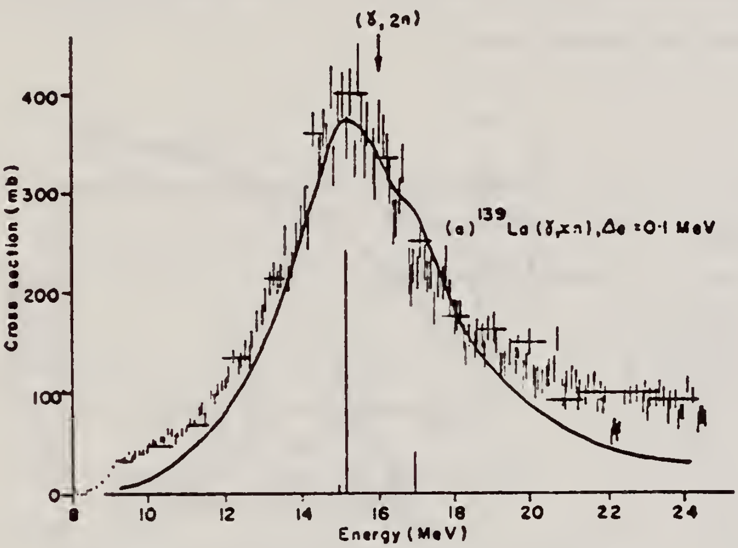

TABLE 1

The integrated ^{139}La(γ, xn) and ^{141}Pr(γ, xn) cross sections and their minus-first and minus-second moments, compared with the appropriate sum rules

Nucleus	Ref.	σ_0 (b · MeV)	$0.06\ NZA^{-1}$	σ_{-1} (mb)	$0.16\ A^{\frac{4}{3}}$	σ_{-2} (mb · MeV^{-1})	$0.00225\ A^{\frac{5}{3}}$
^{139}La	present work	2.51 ± 0.5	2.02	158 ± 30	115	10.4 ± 2	8.4
	ref. [20])	2.20 ± 0.3		141 ± 12		9.4 ± 0.7	
^{141}Pr	present work	1.84 ± 0.3	2.06	121 ± 20	117	8.1 ± 1.3	8.6
	ref. [10])	1.83 ± 0.16					

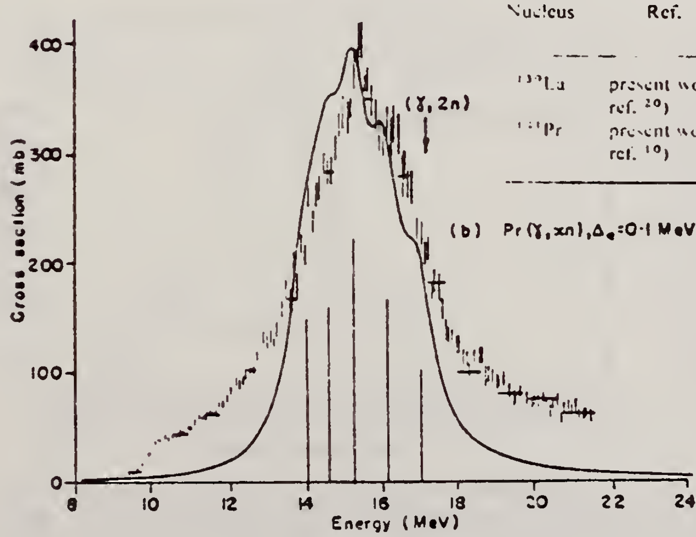

Fig. 1. (a) The ^{139}La(γ, xn) cross section, obtained by VBPL unfolding from yield data measured in 0.1 MeV steps. Also shown is the DCM dipole spectrum for ^{142}Nd, and a fit to it of Lorentz line shapes with widths 4.0 MeV (solid line). (b) The ^{141}Pr(γ, xn) cross section, obtained by VBPL unfolding from yield data measured in 0.1 MeV steps. Also shown is the DCM dipole spectrum for ^{146}Nd, and a fit to it of Lorentz line shapes with widths 1.0 MeV (solid line).

El-Hussieny M. Diefallah

REF. Int. J. Appl. Rad. & Isotopes 23, 153 (1972)

ELEM. SYM.	A	Z
Pr	141	59

METHOD

REF. NO.	
72 Di 7	egf

REACTION	RESULT	EXCITATION ENERGY	SOURCE TYPE	SOURCE RANGE	DETECTOR TYPE	DETECTOR RANGE	ANGLE
G,P	ABY	THR-300	C	106-300	ACT-I		4PI

One monitor unit = 0.735 x 10^7 ergs in beam.
Pr-140 yield is of the order of 10^8 reactions per monitor unit.

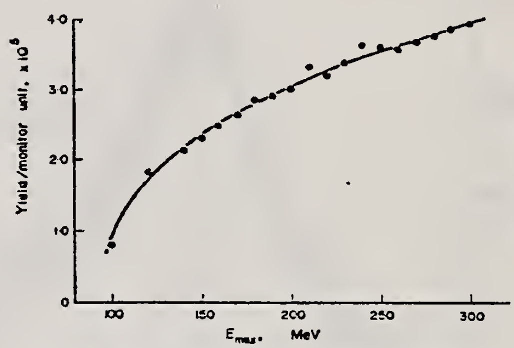

FIG. 2. Yield data from the production of ^{140}Nd in Pr_6O_{11} targets.

REF.	ELEM. SYM.	A	Z
F. Dreyer, H. Dahmen, J. Staude & H. H. Thies Nucl. Phys. A181, 477 (1972)	Pr	141	59

METHOD	REF. NO.	
	72 Dr 2	egf

REACTION	RESULT	EXCITATION ENERGY	SOURCE TYPE	SOURCE RANGE	DETECTOR TYPE	DETECTOR RANGE	ANGLE
G,N	ABX	9-20	C	9-20	ACT-I		4PI

447

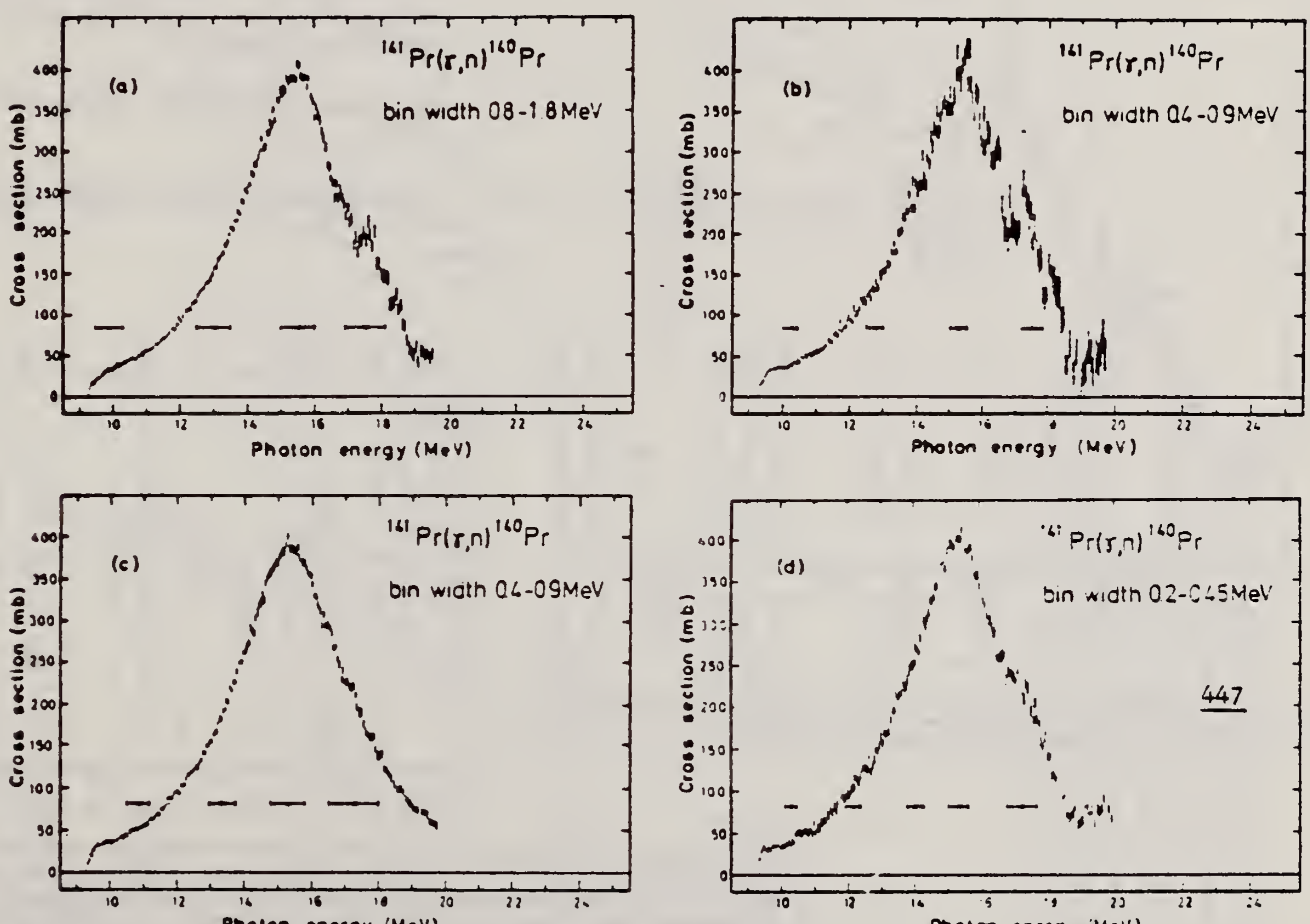

Fig. 3. Cross section for ^{141}Pr(γ, n)^{140}Pr from threshold energy to 19.5 MeV. (a) and (b) show the cross-section curve obtained with two different analysis bin widths using the LP method. The horizontal bars represent the bin width ΔE_0 increasing with the bremsstrahlung endpoint energy E_0. (c) and (d) show the same cross section calculated with bin width from 0.4 to 0.9 MeV respectively 0.2 to 0.45 MeV using the CLS method. The horizontal bars represent the FWHM of experimental resolution and not the uncertainty in energy

REF.	ELEM. SYM.	A	Z
R.F. Barrett, J.R. Birkelund, B.J. Thomas, K.S. Lam, and H.H. Thies Nucl. Phys. A210, 355 (1973)	Pr	141	59

METHOD	REF. NO.	
	73 Ba 20	egf

REACTION	RESULT	EXCITATION ENERGY	SOURCE TYPE	SOURCE RANGE	DETECTOR TYPE	DETECTOR RANGE	ANGLE
G,N	NOX	THR- 27	C	10- 27	BF3-I		4PI

MEAN NEUT ENERGY

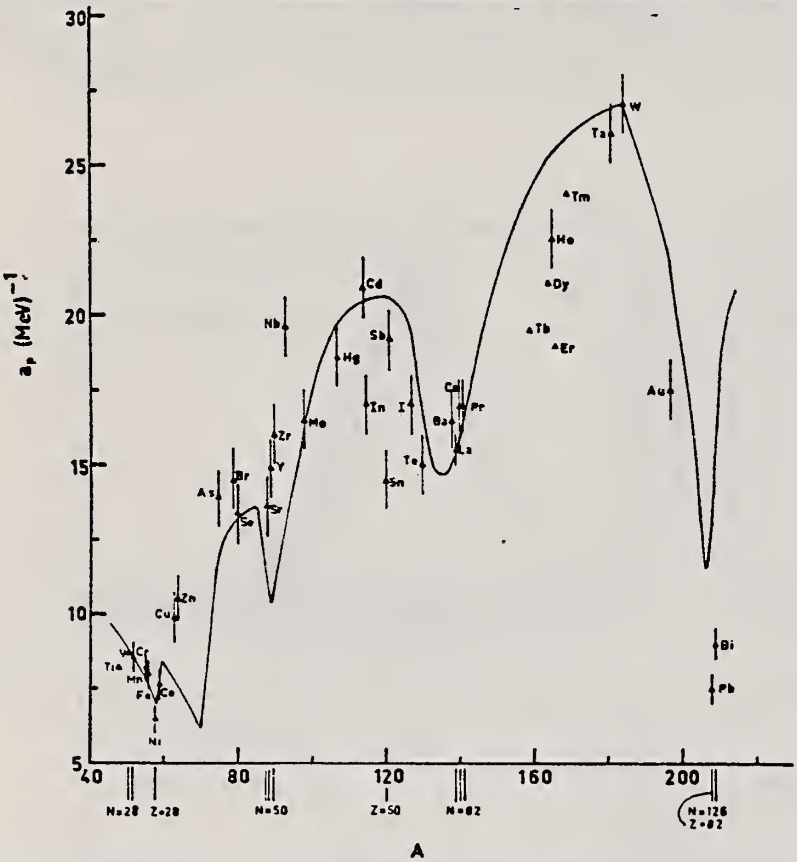

Fig. 12. Experimental values of the level density parameter a_p (Fermi gas formula plus pairing correction) versus atomic number A. The continuous curve is a least-squares fit to the data of a theoretical calculation from Newton [15]).

1
H. Baba and S. Baba, Japan Atomic Energy Research Institute report JAERI-1183 (1969).
2
H. Baba, Nucl. Phys. A159, 625 (1970).
15
T.D. Newton, Can. J. Phys. 34, 804 (1956).

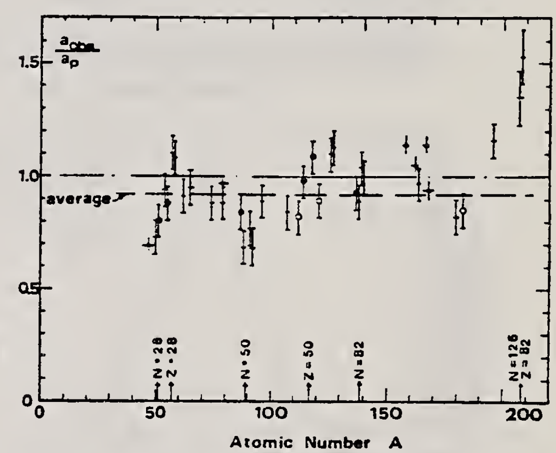

Fig. 15. Ratio a_{obs}/a_p versus atomic number A. Here a_{obs} is the level density parameter taken from the neutron resonance work of refs. [1,2]), and a_p is the level density parameter derived from the present (γ, n) work. Filled circles represent points where nuclei in the neutron resonance and in the (γ, n) experiment were the same. Open circles represent points where the respective nuclei were approximately matched. Triangles represent points which are based on measurement of neutron mean energies at two bremsstrahlung energies only.

(over)

TABLE 3 (continued)

Target	N (residual nucleus) [a]		Goodness of fit [b] no p.c.	with p.c.	$\hat{E}_n(24)$ (MeV) [c]	T (MeV) [d]	a_p (MeV^{-1}) [e]	a_{obs} (MeV^{-1}) [f]	a_{obs}/a_p
Ba	75	1%		F	1.16		16.5–^{136}Ba	15.39–^{136}Ba	0.93
	77	2%							
	78	7%							
	79	8%							
	80	11%							
	81	71%							
La	80	100%	F	F	1.25	0.72	15.5–^{138}La	13.76–^{139}La	0.89
Ce	81	89%	F	G	1.24	0.70	17.0–^{139}Ce	17.8 –^{141}Ce	1.04
	83	11%							
Pr	81	100%	G	G	1.17	0.65	17.0–^{140}Pr	17.05–^{142}Pr	1.00
Tb [g]	93	100%			1.15		19.3–^{158}Tb	21.85–^{160}Tb	1.14
Dy [g]	93	2%			1.06		20.9–$^{161.5}$Dy	21.9 –^{162}Dy	1.05
	94	19%							
	95	25%							
	96	25%							
	97	28%							
Ho	97	100%	P	G	1.06	0.56	21.4–^{164}Ho	20.66–^{166}Ho	0.97
Er [g]	95	2%			1.11		19.2–^{166}Er	21.9 –^{166}Er	1.14
	97	33%							
	98	23%							
	99	27%							
	101	15%							
Tm [g]	99	100%			1.03		24.0–^{168}Tm	22.58–^{170}Tm	0.94
Ta	107	100%		G	1.00	0.49	26.0–^{180}Ta	21.2 –^{181}Ta	0.82
W	107	26%	G	F	0.98	0.50	27.0–^{183}W	23.0 –^{183}W	0.85
	108	14%							
	109	31%							
	111	28%							
Au	117	100%		G	1.19		17.5–^{196}Au	20.24–^{198}Au	1.16
Pb (Z = 82)	123	24%		V.P.	1.87	1.20	7.5–^{206}Pb	10.1 –^{207}Pb	1.35
	124	23%							
	125	52%							
Bi	125	100%		F	1.65	1.03	9.0–^{208}Bi	13.8 –^{210}Bi	1.53

[a]) Neutron numbers and abundances of respective residual nuclei in (γ, n) experiments.

[b]) These give an assessment of the goodness of fit of a calculated $\hat{E}_n$ versus E_0 curve to the observed data, using the Fermi gas level density formula both without and with pairing corrections.

[c]) Bremsstrahlung photoneutron mean energies $\hat{E}_n$ for peak bremsstrahlung energy E_0 = 24 MeV.

[d]) Nuclear temperature from fit with constant-temperature formula.

[e]) Level density parameter a_p derived from the present (γ, n) experiment, using a Fermi gas formula plus pairing correction, and corresponding residual nucleus (the atomic weight shown is the weighted average of atomic weights of the respective isotopes present).

[f]) As column 7, but using data on n-resonance absorption from refs. [1,2]).

[g]) Measurements of $\hat{E}_n(E_0)$ for these nuclei were made only for E_0 = 21, 23 and 24 MeV.

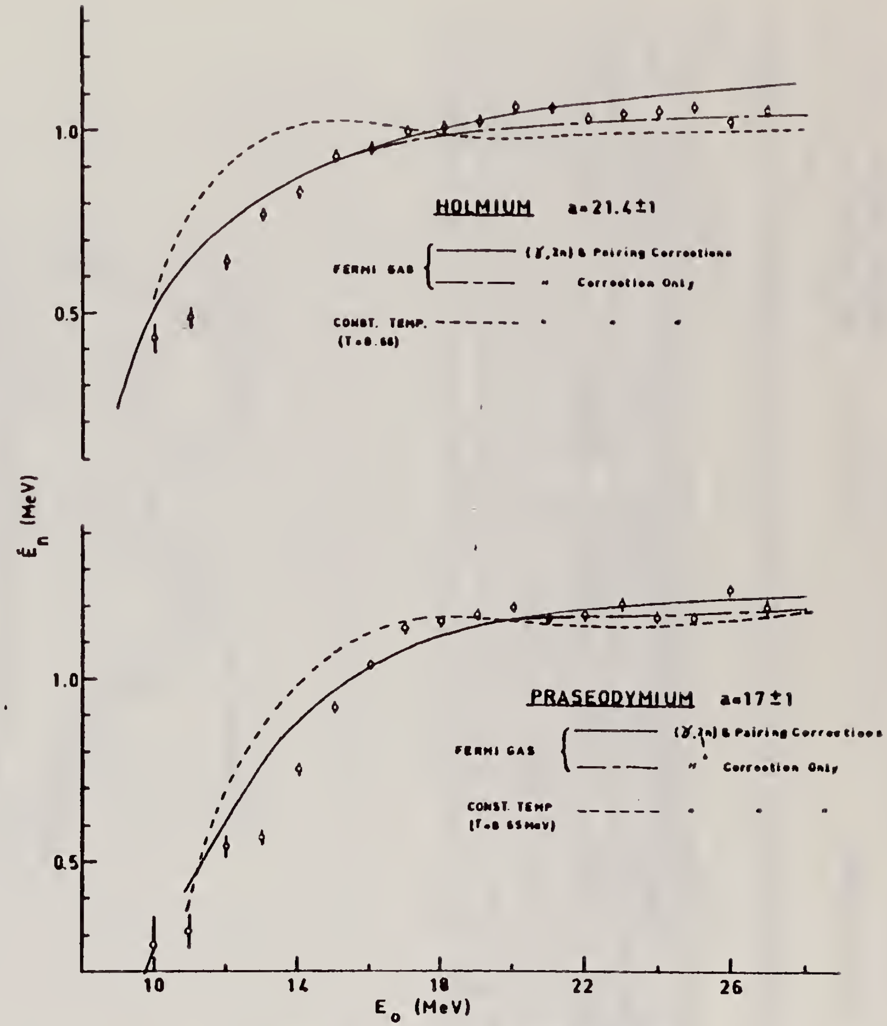

Fig. 10. Same as fig. 5, for praseodymium and holmium.

REF.	F.R. Buskirk, H.D. Graf, R. Pitthan, H. Theissen, O. Titze, and Th. Walcher PICNS-73, Vol.I, p.703 Asilomar	ELEM. SYM.	A	Z
		Pr	141	59
METHOD		REF. NO.		
		73 Bu 14		hmg

REACTION	RESULT	EXCITATION ENERGY	SOURCE		DETECTOR		ANGLE
			TYPE	RANGE	TYPE	RANGE	
E,E/	SPC	2- 20	C	50, 65	MAG-D		DST

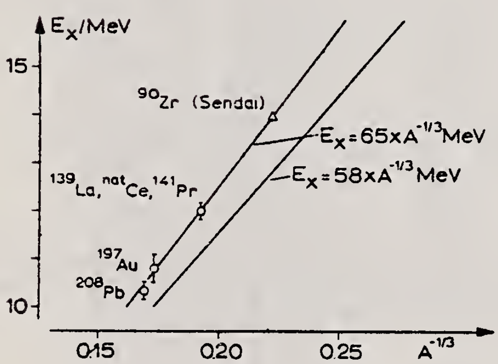

Fig. 2

The E2 resonance which is clearly visible at 1o.8±o.2 MeV exhausts more than 5o % of the sum rule. Fig. 2 shows the excitation energy of this resonance as a function of $A^{-1/3}$ for the nuclei measured at Darmstadt and the Sendai result for ^{90}Zr [5]. Bohr and Mottelson [9] predicted a collective E2 resonance whose isoscalar part should depend on A through E_x=58 $A^{-1/3}$MeV. The data of Fig. 2 are consistent with E_x=65 $A^{-1/3}$MeV suggesting to identify the observed resonances with this type of E2 excitation.

REF. Rainer Pitthan
Z. Physik 260, 283 (1973)

ELEM. SYM.	A	Z
Pr	141	59

METHOD

REF. NO.	
73 Pi 3	egf

REACTION	RESULT	EXCITATION ENERGY	SOURCE TYPE	SOURCE RANGE	DETECTOR TYPE	DETECTOR RANGE	ANGLE
E,E/	ABX	7- 21	D	50	MAG-D		165

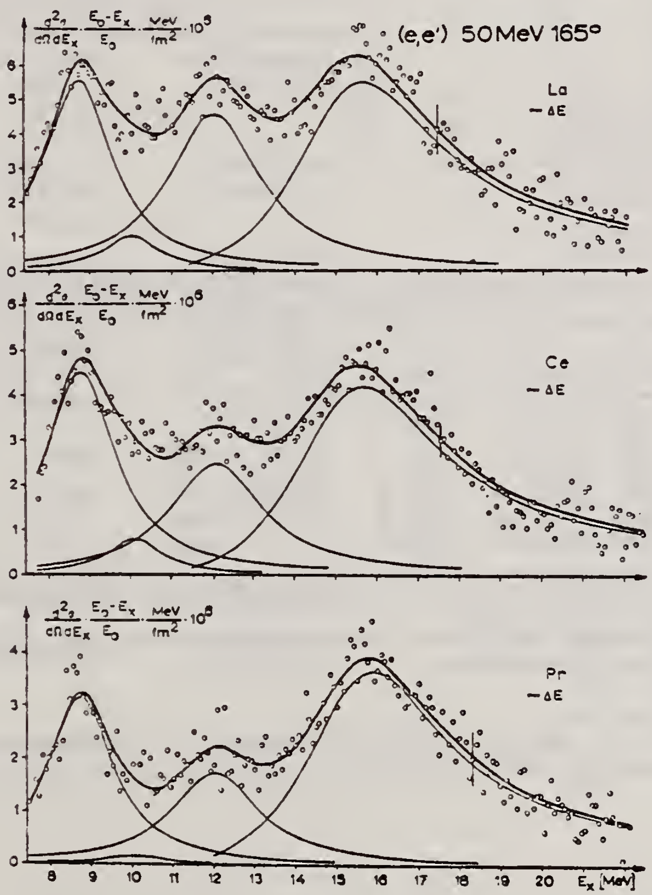

Fig. 7. Spektren von unelastisch an La, Ce und Pr gestreuten Elektronen, sonst wie Fig. 5, s. Text

REF.	ELEM. SYM.	A	Z
J. Tenenbaum, R. Moreh, and A. Nof Nucl. Phys. A218, 95 (1974)	Pr	141	59

METHOD	REF. NO.	
	74 Te 1	egf

REACTION	RESULT	EXCITATION ENERGY	SOURCE TYPE	SOURCE RANGE	DETECTOR TYPE	DETECTOR RANGE	ANGLE
G,G	LFT	6	D	4- 8	SCD-D		DST

6=6.877

TABLE 2

Measured angular distribution coefficients A_2, the ratios $N_{\|}/N_{\perp}$, the spins and parities of the ground and the resonance levels, J_0^{π} and J_r^{π}, and the character of the ground state transition

Scatterer	E_γ (keV)	A_2	$N_{\|}/N_{\perp}$	J_0^{π}	J_r^{π}	Transition
^{55}Mn	7491	0.01±0.02	1.00±0.02	$\frac{5}{2}^-$	$\frac{3}{2}$	
^{140}Ce	5660	0.51±0.02	1.14±0.04	0^+	1^-	E1
^{141}Pr	6877	0.11±0.02	0.95±0.03	$\frac{5}{2}^+$	$\frac{7}{2}^+$	M1
^{142}Nd	6877	0.51±0.03	1.10±0.04	0^+	1^-	E1
^{202}Hg	4922	0.51±0.02	1.18±0.03	0^+	1^-	E1
^{209}Bi	5603	0.06±0.02	0.97±0.02	$\frac{9}{2}^-$	$\frac{11}{2}^-$	M1

TABLE 4

Values of Γ, Γ_0 and the energy separation δ (between the incident γ-line and the resonance level) as obtained from the analysis of the various experiments

Scatterer	E_γ (keV)	Γ (meV)	Γ_0 (meV)	δ (eV)	D (eV)	K_{E1} (10^{-9} MeV^{-3})	K_{M1} (10^{-9} MeV^{-3})
^{55}Mn	7491	450±250	80± 40	17 ±1			
^{140}Ce ^{a})	5660	13± 3	12± 2	4.7±0.3	6800	0.33	
^{141}Pr ^{a})	6877	85± 35	17± 9	6.7±1.5	450		116
^{142}Nd ^{a})	6877	340± 40	270± 20	12.4±0.3	1200	26	
^{202}Hg	4922	300± 50	260± 20	4.2±0.5	19000	3.4	
^{209}Bi ^{a})	5603	950±200	950±200	13 ±1	34000		160

The radiative strengths K_{E1} and K_{M1} are also given. The level spacing D refers to the excitation energy of the resonance level E_γ.

^{a}) These values are slightly different from those of ref. [8]) and were obtained from a renewed analysis of the experimental results.

[8] A. Wolf, R. Moreh, A. Nof, O. Shahal, J. Tenenbaum, Phys. Rev. C6, 2276 (1972).

REF.	H. E. Jackson, G. E. Thomas, K. J. Wetzel Phys. Rev. C11, 1664 (1975)	ELEM. SYM.	A	Z
		Pr	141	59
METHOD		REF. NO.		
		75 Ja 1		hmg

REACTION	RESULT	EXCITATION ENERGY	SOURCE TYPE	SOURCE RANGE	DETECTOR TYPE	DETECTOR RANGE	ANGLE
G,G	ABX	11	D	11	SCD-D		150
		(11.387)		(11.387)			
		-					

RATIO RAMAN/ELASTIC

TABLE I. Differential cross sections measured for elastic and inelastic scattering of 11.39-MeV photons. State or states populated by inelastic scattering are indicated in parentheses beside the target. The errors given result from the statistical error in the measurement of the cross section relative to the calibration value, the 90° uranium elastic cross section.

θ (deg)	$d\sigma/d\omega$ (elastic) (mb/sr)	$d\sigma/d\omega$ (inelastic) (mb/sr)
	^{238}U (2^+, 45 keV)	
90	0.169 ± 0.011	0.173 ± 0.016
150	0.355 ± 0.041	0.236 ± 0.24
	^{232}Th (2^+, 45 keV)	
150	0.331 ± 0.035	0.210 ± 0.022
	^{181}Ta ($\frac{9}{2}^+$, 136 keV) ($\frac{11}{2}^+$, 301 keV)	
90	0.073 ± 0.008	0.020 ± 0.004 0.009 ± 0.004
150	0.145 ± 0.015	0.017 ± 0.004 0.017 ± 0.004
	^{165}Ho ($\frac{9}{2}^+$, 95 keV) ($\frac{11}{2}^+$, 210 keV)	
150	0.141 ± 0.014	0.022 ± 0.004 0.013 ± 0.004
	^{159}Tb ($\frac{5}{2}^+$, 58 keV) ($\frac{7}{2}^+$, 138 keV)	
90	0.062 ± 0.006	0.024 ± 0.003 0.013 ± 0.003
150	0.134 ± 0.012	0.042 ± 0.004 0.019 ± 0.004
	^{141}Pr	
150	0.030 ± 0.008	...

TABLE III. Comparison of calculated and observed values of the cross sections for elastic scattering and of the ratio of Raman to elastic scattering by various nuclei for 11.387-MeV photons at 90 and 150°. The parameters used in the calculations for column 5 are given in Table II. Column 4 describes results obtained by perturbing those parameter to meet the constraint of Eq. (3) (see text).

Target	$d\sigma(\theta)d\Omega$ (mb/sr) Calc.	Exp.	$d\sigma_{\mathrm{Raman}}(\theta)/d\sigma_{\mathrm{elastic}}(\theta)$		
		$\theta = 150°$			
Pr	0.025	0.030 ± 0.008		0.0	0.0
Tb	0.094	0.134 ± 0.012	0.53	0.57	0.46 ± 0.04
Ho	0.170	0.141 ± 0.014	0.28	0.28	0.25 ± 0.04
Ta	0.160	0.145 ± 0.015	0.23	0.22	0.23 ± 0.04
Th	0.253	0.331 ± 0.035	0.59	0.63	0.64 ± 0.08
U	0.289	0.355 ± 0.041	0.78	0.73	0.67 ± 0.07
		$\theta = 90°$			
Tb	0.062	0.062 ± 0.006	0.76	0.82	0.60 ± 0.07
Ta	0.109	0.074 ± 0.008	0.32	0.30	0.33 ± 0.07
U	0.172	0.169 ± 0.008	1.29	1.15	1.03 ± 0.10

REF.		ELEM. SYM.	A	Z
	J.I. Uegaki and K. Shoda Nucl. Phys. A294, 141 (1978)	Pr	141	59
METHOD		REF. NO. 78 Ue 1		rs

REACTION	RESULT	EXCITATION ENERGY	SOURCE TYPE	SOURCE RANGE	DETECTOR TYPE	DETECTOR RANGE	ANGLE
E,P	ABX	12- 15	D	14- 17	MAG-D		125

TABLE I

Strength of the resonance in the (γ, p_0) and (γ, p) reactions on ^{139}La and ^{141}Pr, and the ratio of proton group 1 and proton group 2 emitted through the $f_{7/2}$ IAR

	$\int \sigma^{IAS}_{(\gamma, p_0)} dE$ (μb · MeV)	$\int \sigma^{IAS}_{(\gamma, p)} dE$ (μb · MeV)	Proton group 1 (%)	Proton group 2 (%)
^{141}Pr	44±9	240±30	40±10	60±10
^{139}La	<5	260±30	5± 5	95± 5

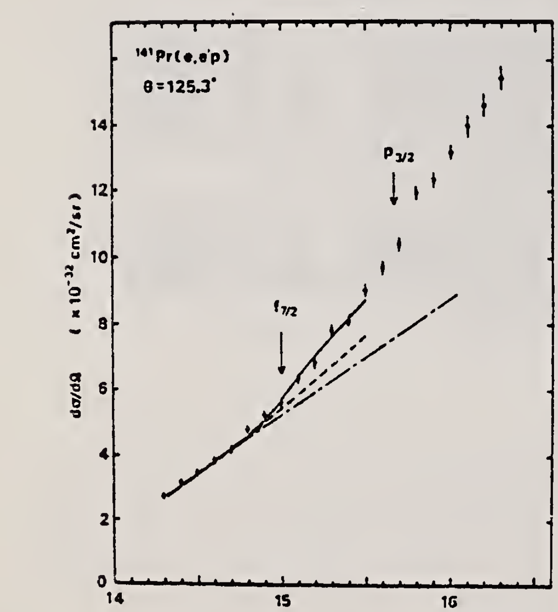

Fig. 3. The differential cross section of the ^{141}Pr(e, e'p) reaction for θ = 125.3° (see caption to fig. 2).

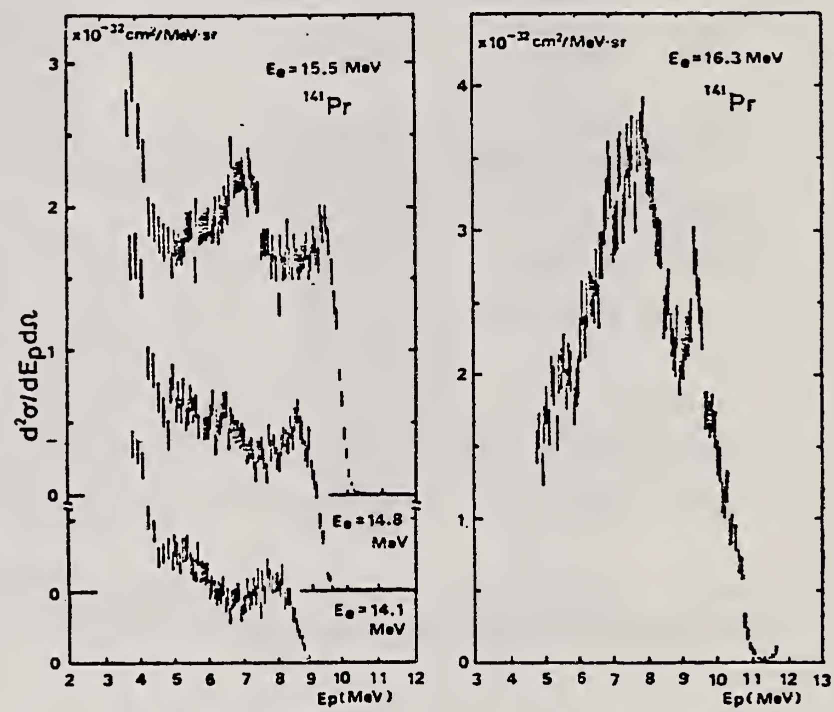

Fig. 4. The proton spectra of the ^{141}Pr(e, e'p) reactions for θ = 125.3°.

over

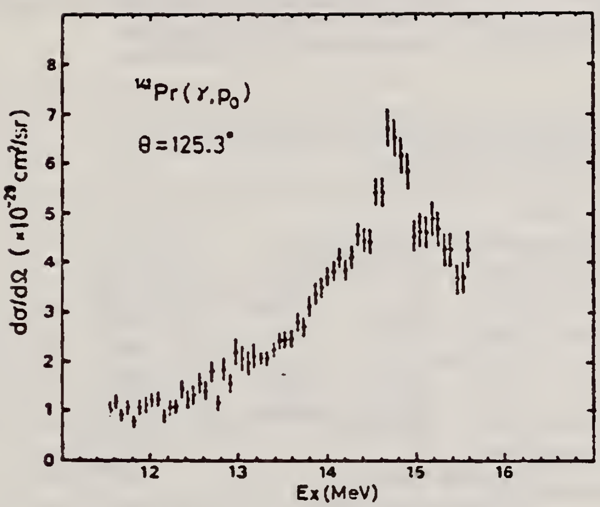

Fig. 8. The $^{141}Pr(\gamma, p_0)$ cross section.

REF. J. Uegaki, K. Shoda
Nucl. Phys. A341, 125 (1980)

ELEM. SYM.	A	Z
Pr	141	59

METHOD

REF. NO.	
80 Ue 1	hg

REACTION	RESULT	EXCITATION ENERGY	SOURCE TYPE	SOURCE RANGE	DETECTOR TYPE	DETECTOR RANGE	ANGLE
E,P	ABX	10-25	D	14-25	MAG-D		125

VIRT PHOTON ANALYSIS

Abstract: The cross sections and the proton energy distributions of the (e, p) reactions on ^{139}La and ^{141}Pr have been measured around the $T_>$ GDR. The energies of the $T_>$ GDR have been given as $E_R = 21.0$ MeV in ^{139}La and $E_R = 20.4$ MeV in ^{141}Pr. The decay protons of the $T_>$ GDR have been studied. The proton groups which leave the residual nucleus in the neutron particle-hole states have been clearly seen in the same energy regions as the decay protons emitted through the low-lying IAR.

E | NUCLEAR REACTIONS ^{139}La, ^{141}Pr(e, p), $E = 15$–25 MeV; measured $\sigma(E_e)$, $\sigma(E_p)$; deduced $\sigma(\gamma, p)$ vs. E_p. Natural target.

TABLE I

Results of the energy-weighted integrated cross-section calculations

Element	$E_R^<$ (MeV)	$E_R^>$ (MeV)	$E_R^> - E_R^<$ (MeV) exp.	theor.	$\sigma_{-1}^<$ [a] (mb)	$\sigma_{-1}^>$ [a] (mb)	$\sigma_{-1}^>/\sigma_{-1}^<$ (%) exp.	theor.
^{139}La	15.2±0.1 [b]	21.0±0.2	5.8±0.3	5.83 [c]	136 [b]	1.01±0.07	0.74	2.3 [c]
^{141}Pr	15.1±0.1 [b]	20.4±0.2	5.3±0.3	5.32 [c]	125 [b]	1.27±0.24	1.0	3.0 [c]

[a]) The notation shows $\sigma_{-1}^< = \int(\sigma_</E)dE$, $\sigma_{-1}^> = \int(\sigma_>/E)dE$.
[b]) Ref. [10]). Integrals were carried out up to 25.0 MeV by present authors.
[c]) Calculated by using eqs. (1) and (2) in the text. Refs. [3,4]).

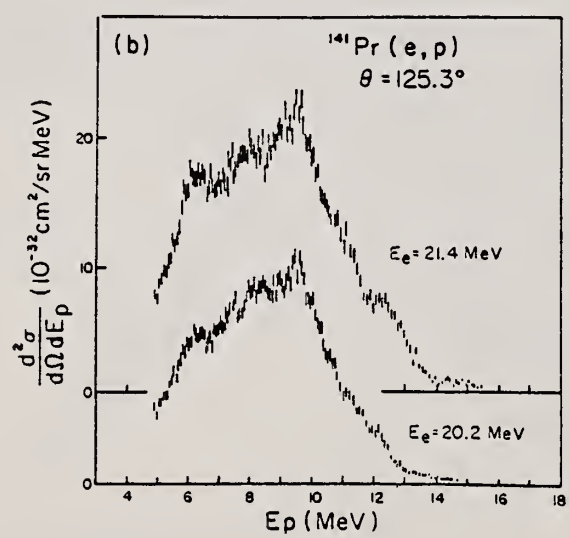

Fig. 1. The proton spectra of the (e, p) reaction at $\theta = 125.3°$ laboratory. (a) ^{139}La. Bombarding energies are $E_e = 22.0$ MeV and $E_e = 20.8$ MeV, respectively. (b) ^{141}Pr. Bombarding energies are $E_e = 21.4$ MeV and $E_e = 20.2$ MeV, respectively.

OVER

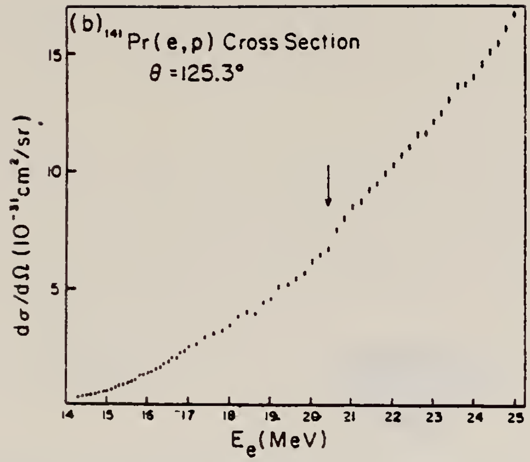

Fig. 2. The differential cross sections of the (e, p) reaction at θ = 125.3° lab. The arrows show the positions of inflection caused by $T_>$ GDR. (a) ^{139}La. (b) ^{141}Pr.

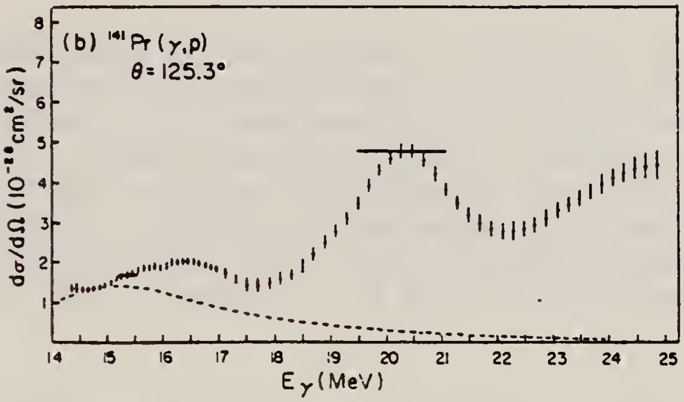

Fig. 3. The (γ, p) differential cross sections calculated from the present (e, p) differential cross sections by the least structure method [ref. [11])]. The broken lines indicate assumed contribution of the $T_<$ GDR to the (γ, p) cross section. (a) ^{139}La. (b) ^{141}Pr.

NEODYMIUM
Z=60

Neodymium was discovered in 1885 by C. A. Welsbach when he separated didymium salts, a metal he thought was a simple element, into two chemically distinct fractions, neodymium (*neo*, "new") and prasesdymium. The crude oxide of neodymium is used for clearing the color, due to iron, in glass. A mixture of neodymium and praesedymium absorbs light in the region of the harmful sodium D lines and thus is used in welder's and glass blower's goggles.

REF.	ELEM. SYM.	A	Z
F. I. Havlicek Nuovo Cimento 13, 969-73 (1959)	Nd		60

METHOD	REF. NO.	
Betatron	59 Ha 2	NVB

REACTION	RESULT	EXCITATION ENERGY	SOURCE		DETECTOR		ANGLE
			TYPE	RANGE	TYPE	RANGE	
G,A	SPC	THR - 30	C	30	EMU-D	2-5	DST

REF.	ELEM. SYM.	A	Z
B. Arad (Huebschmann), G. Ben-David (Davis), I. Pelah, Y. Schlesinger Phys. Rev. 133, B684-700 (1964)	Nd		60

METHOD	REF. NO.	
Reactor, (n,γ) reactions source	64 Ar 1	NVB

REACTION	RESULT	EXCITATION ENERGY	SOURCE TYPE	SOURCE RANGE	DETECTOR TYPE	DETECTOR RANGE	ANGLE
G,G	ABX	7	D	7	NAI-D		135
		(6.867)		(6.867)			

TABLE II. Capture gamma-ray sources and their properties.[a]

Source	Chemical composition	Mass kg	Principal γ rays (in MeV)
Al	Metal	1.640	7.73
Cl	polyvinyl Chloride	0.380	8.55, 7.78, 7.41, 6.96, 6.64, 6.12, 5.72
Co	CoO	0.230	7.49, 7.20, 6.98, 6.87, 6.68, 6.48, 5.97, 5.67
Cr	Metallic powder	0.480	9.72, 8.88, 8.49, 7.93, 7.09, 6.65, 5.60
Cu	Metal	1.860	7.91, 7.63, 7.29, 7.14, 7.00, 6.63
Fe	Metallic powder	0.440	9.30, 7.64, 7.28, 6.03
Hg	$Hg_2(NO_3)_2 \cdot 2H_2O$	0.310	6.44, 6.31, 5.99, 5.67, 5.44
Mn	MnO_2	0.240	7.26, 7.15, 7.04, 6.96, 6.79, 6.10, 5.76
Ni	Metal	0.900	9.00, 8.50, 8.10, 7.83, 7.58, 6.84, 6.64
Ti	TiO_2	0.210	6.75, 6.56, 6.42
V	V_2O_5	0.120	7.30, 7.16, 6.86, 6.51, 6.46, 5.87, 5.73
Y	Y_2O_3	0.200	6.07, 5.63

[a] For more detailed information, additional lines, intensities, etc., see Ref. 6.

TABLE III. Effective cross sections.

γ source	Energy (MeV)	Scatterer Element	Protons	Neutrons	$\langle\sigma_{\gamma\gamma}\rangle$ (mb)	Notes
Hg	5.44	Hg	80	116, 118, 119, 120, 121, 122, 124	128	
Cl	6.12	Pr^{141}	59	*82*	103	a
V	6.508	Sn	*50*	62, 64–70, 72	14	
Co	6.690	Pr^{141}	59	*82*	2.7	a
Co	6.867	Nd	60	82, 83, 84, 85, 86, 88	22	
Al	6.98	Pb^{208}	*82*	*126*	2900	b
Cl	6.98	Pb	*82*	124, 125, *126*	346	a
Ti	6.996	Bi^{209}	83	*126*	1560	b
Cu	7.01	Sn	*50*	62, 64–70, 72	1000	b
Ti	7.149	Pb^{208}	*82*	*126*	1000	b
Co	7.201	Pb^{208}	*82*	*126*	25	
Mn	7.261	Pb^{208}	*82*	*126*	25	a
Fe	7.285	Pb^{208}	*82*	*126*	4100	a
V	7.305	Pb^{208}	*82*	*126*	12.5	
Hg	7.32	Pb	*82*	124, 125, *126*	5500	c
Fe	7.639	Ni	*28*	30, 32, 34, 36	10.5	d
Fe	7.639	Pr^{141}	59	*82*	10	d
Cr	8.499	Cu	29	34, 36	24.4	
Cr	8.881	Pr^{141}	59	*82*	9.3	
Ni	8.997	Sm	62	*82*, 85–88, 90, 92	2.8	

[a] A large error could be introduced in the cross-section values because of large differences in line intensities quoted by Bartholomew and Higgs and by Groshev *et.al.* (Ref. 6).
[b] Because of the low counting rate, thick scatterers were used, which will introduce a systematic error in estimating $\langle\sigma_{\gamma\gamma}\rangle$ for resonances having a high nuclear cross section.
[c] The cross section was evaluated assuming the gamma intensity to be 0.02 photons per 100 captured neutrons (see text).
[d] Reference 6 gives the 7.639 line of iron capture gamma rays as a single line. However, a recent paper by Fiebiger, Kand, and Segel [Phys. Rev. 125, 2031 (1962)] reports two different lines of equal intensities having energies of 7.647 and 7.633 MeV. The present experiment cannot resolve an energy difference of 14 keV, therefore, there is no possibility of deciding which line is responsible for the scattering.

REF. G. Ben-David, B. Arad, J. Balderman, and Y. Schlesinger
Phys. Rev. 146, B852 (1966)

ELEM. SYM.	A	Z
Nd		60

METHOD

Nuclear Resonance Scattering using N,G reactions.

REF. NO.	
66 Be 3	JDM

REACTION	RESULT	EXCITATION ENERGY	SOURCE TYPE	SOURCE RANGE	DETECTOR TYPE	DETECTOR RANGE	ANGLE
G,G	RLX	5 - 10	D	5 - 10	NAI-D	5 - 10	135

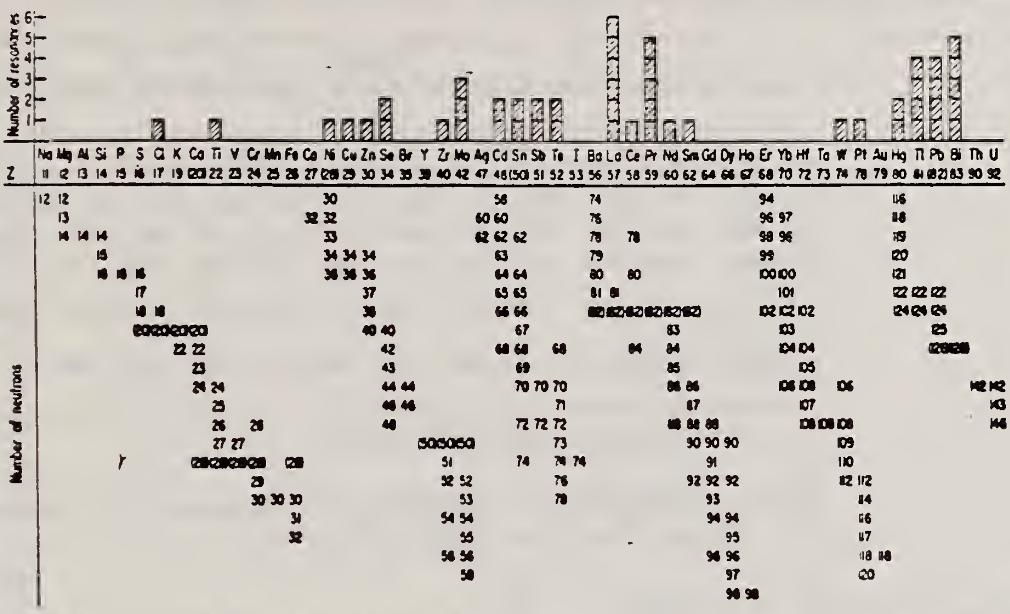

Fig. 3. Histogram of distribution of observed resonances among the different targets. The atomic number is given directly beneath the chemical symbol followed by the neutron numbers of the naturally occurring isotopes. Magic numbers are shown in brackets.

Table III. List of effective cross sections.

Scatterer	Energy (MeV)	Gamma source	σ (mb)	Scatterer	Energy (MeV)	Gamma source	σ (mb)
Sm^{144}	8.997	Ni	100	Sn	7.01	Cu	110
Pr^{141}	8.881	Cr	9	Nd	6.867	Co	30
La	8.532	Ni	6	Pr^{141}	6.867	Co	3
Te	8.532	Ni	3[a]	Te	6.7	Ni	...
Cu	8.499	Cr	24	La	6.54	Ag	12
Zr	8.496	Se	3050	Cd	6.474	Co	110
Zn	8.119	Ni	13	Mo	6.44	Hg	25[e]
Se	7.817	Ni	50	La	6.413	Ti	72
Se	7.76	K	90	Mo	6.413	Ti	10
Sb	7.67	V	...[b]	Tl	6.413	Ti	25
Cd	7.64	Fe	40[c]	W	~6.3	Ti	...[i]
Ni	7.64	Fe	7[c]	Sb	6.31	Hg	6[e]
Pr^{141}	7.64	Fe	12[c]	Tl	6.31	Hg	2[e]
Tl	7.64	Fe	370[c]	Sn	6.27	Ag	75
La	7.634	Cu	7	Pb^{208}	6.15	Gd	...[e]
Mo	7.634	Cu	11	Te	5.8	Ni	...[f]
Bi^{209}	7.634	Cu	4	La	6.12	Cl	35
Te	7.528	Ni	66[d]	Pr^{142}	6.12	Cl	110
Bi^{209}	7.416	Se	100	Pt	5.99	Hg	40[e,g]
Bi^{209}	7.300	As	80[e]	Tl	5.99	Hg	5[g]
Pb^{208}	7.285	Fe	4100	Pb^{208}	5.9	Sr	...[h]
Cl	7.285	Fe	34	Ce	5.646	Co	17
Pr^{141}	7.185	Se	80	Bi^{209}	5.646	Co	55
Tl	7.16	Cu	120	Pb^{208}	5.53	Ag	70
La	7.15	Mn	50	Hg	5.44	Hg	75[e]
Bi^{209}	7.149	Tl	2000	Hg	4.903	Co	385

[a] High-energy component of a complex spectrum.
[b] A broad scattered spectrum with no observable peak structure.
[c] There are actually two lines of energies 7.647 and 7.633 MeV having equal intensities in the iron capture gamma spectrum. The cross section has therefore been corrected, although there is no possibility at present of deciding which line is responsible for each resonance.
[d] Is probably an independent level in the complex spectrum of Ni γ rays on Te.
[e] Rough estimate.
[f] May be inelastic component from 7.528 level in Te.
[g] The relative line intensities in this case are due to Groshev and co-workers.
[h] No line is known for the source at this energy.
[i] Difficult to resolve among the many source lines present at this energy.

REF.	ELEM. SYM.	A	Z
H. Beil, R. Bergere, P. Carlos, A. Lepretre, A. Veyssiere and A. Parlag Nucl. Phys. A172, 426 (1971)	Nd		60
METHOD	REF. NO. 71 Be 4		egf

REACTION	RESULT	EXCITATION ENERGY	SOURCE TYPE	SOURCE RANGE	DETECTOR TYPE	DETECTOR RANGE	ANGLE
G,SN	ABX	10-18	D	10-18	MOD-I		4PI
							382+

TABLE 1

Lorentz line parameters corresponding to fits of total photoneutron cross sections presented in fig. 1

	$_{56}$Ba	$^{139}_{57}$La	$_{58}$Ce	$^{141}_{59}$Pr	$_{60}$Nd	$^{141}_{59}$Pr [a])
σ_1 (mb)	356 ±15	340 ±15	360 ±15	350 ±15	315 ±15	320 ±20
E_1 (MeV)	15.3 ± 0.1	15.2 ± 0.1	15.0 ± 0.10	15.1 ± 0.1	14.9 ± 0.1	15.16 ± 0.08
Γ_1 (MeV)	4.70 ± 0.15	4.45 ± 0.05	4.35 ± 0.05	4.26 ± 0.05	4.90 ± 0.05	4.49 ± 0.05
$\frac{1}{2}\pi\sigma_1\Gamma_1$ (MeV · b)	2.6 ± 0.15	2.35 ± 0.13	2.42 ± 0.15	2.35 ± 0.13	2.43 ± 0.13	2.42 ± 0.17
$\frac{\frac{1}{2}\pi\sigma_1\Gamma_1}{0.06NZA^{-1}}$	1.30 ± 0.08	1.16 ± 0.08	1.19 ± 0.08	1.14 ± 0.08	1.15 ± 0.08	

[a]) Lorentz line parameters given in ref. [10]) for ^{141}Pr.

[10] R. L. Bramblett, J.T. Caldwell, B.L. Berman, R. R. Harvey and S.C. Fultz, Phys. Rev. 148, 1198 (1966).

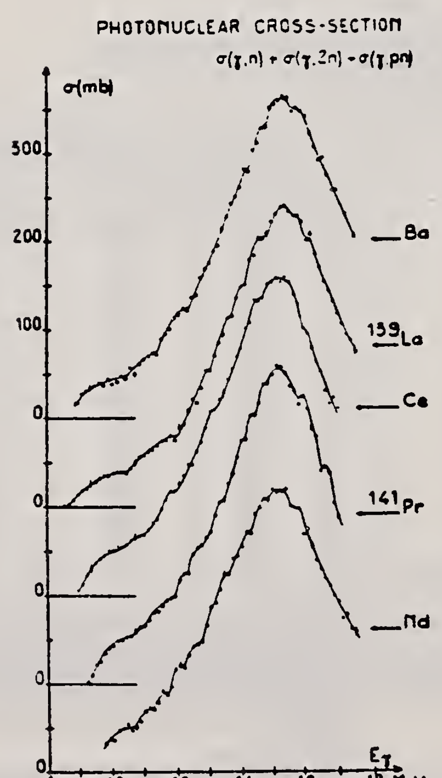

Fig. 1. Total photoneutron cross sections for Ba, ^{139}La, Ce, ^{141}Pr and Nd as a function of incident photon energy E.

REF. T. Methasiri and S. A. E. Johansson
Nucl. Phys. A167, 97 (1971)

ELEM. SYM.	A	Z
Nd		60

METHOD

REF. NO.	
71 Me 1	egf

REACTION	RESULT	EXCITATION ENERGY	SOURCE TYPE	SOURCE RANGE	DETECTOR TYPE	DETECTOR RANGE	ANGLE
G,F	ABY	THR-900	C	300-900	FRG-I		4PI

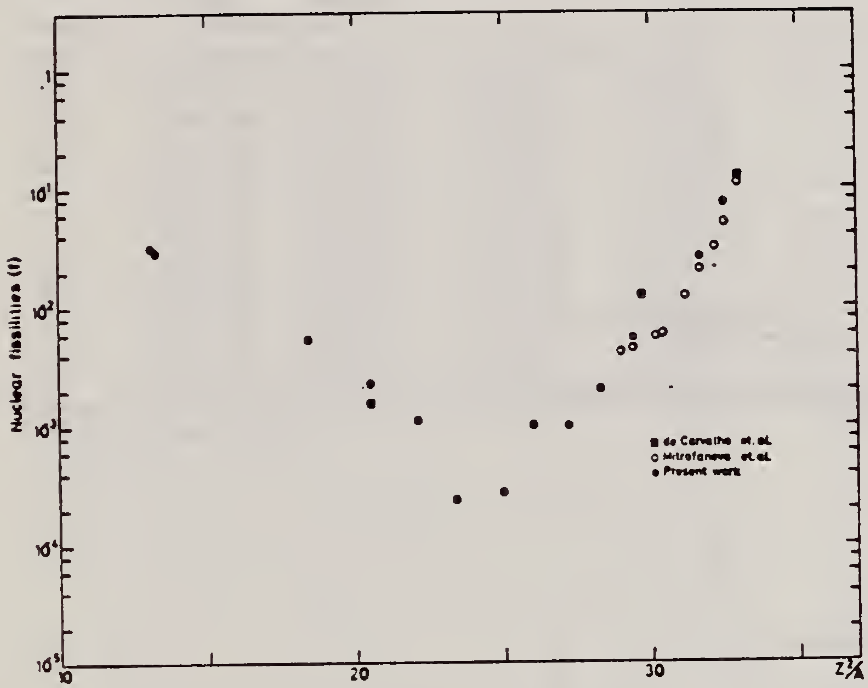

Fig. 2. Nuclear fissilities as a function of Z^2/A.

TABLE 1

The constant fission cross sections above the threshold

Element	σ_f (cm^2)	Element	σ_f (cm^2)
Pb	$(5.0\pm0.2)\times10^{-27}$	La	$(1.1\pm0.1)\times10^{-29}$
Au	$(1.7\pm0.1)\times10^{-27}$	Sn	$(4.3\pm1.1)\times10^{-29}$
Ta	$(3.3\pm0.2)\times10^{-28}$	Ag	$(8.4\pm2.0)\times10^{-29}$
Yb	$(1.2\pm0.2)\times10^{-28}$	Mo	$(1.7\pm0.4)\times10^{-28}$
Ho	$(5.5\pm0.3)\times10^{-29}$	Cu	$(6.6\pm1.2)\times10^{-28}$
Gd	$(5.3\pm0.8)\times10^{-29}$	Ni	$(5.8\pm0.1)\times10^{-28}$
Nd	$(1.3\pm0.2)\times10^{-29}$		

[over]

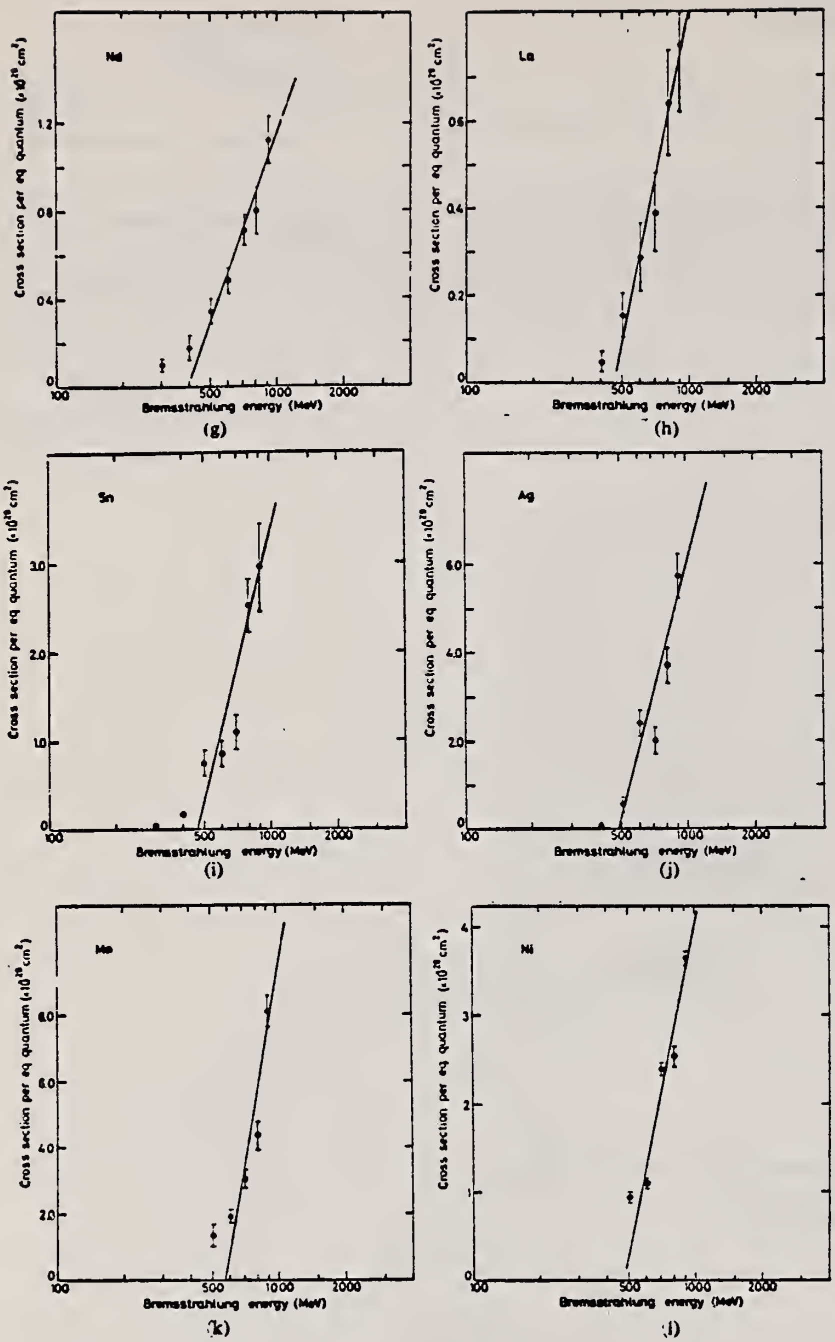

Fig. 1. Cross sections per equivalent quantum $\sigma_q(\bar{E})$ as a function of log $\bar{E}$.

REF.	ELEM. SYM.	A	Z
E. Hayward, W. C. Barber, and J.J. McCarthy Phys. Rev. C10, 2652 (1974)	Nd		60

METHOD	REF. NO.	
	74 Ha 4	hmg

REACTION	RESULT	EXCITATION ENERGY	SOURCE TYPE	SOURCE RANGE	DETECTOR TYPE	DETECTOR RANGE	ANGLE
$ G,G	ABX	15	D	15	NAI-D		90
		(15.1)		(15.1)			

POL PHOTONS

TABLE I. Results.

Target	$d\sigma^{\parallel}/d\Omega_F$ (Arbitrary units)	$d\sigma^{\perp}/d\Omega_F$	η_F	η	η (DCM)
Cd	0.042 ± 0.028	0.39 ± 0.05	0.11 ± 0.07	0.09 ± 0.07	-0.19
In [a]	0.026 ± 0.020	0.54 ± 0.04	0.05 ± 0.04	0.03 ± 0.04	0.19
Sn	0.084 ± 0.036	0.65 ± 0.06	0.13 ± 0.06	0.11 ± 0.06	0.07
Sb [a]	0.14 ± 0.030	0.77 ± 0.05	0.18 ± 0.05	0.16 ± 0.05	
Nd [a]	0.14 ± 0.07	1.03 ± 0.10	0.14 ± 0.07	0.12 ± 0.07	
Ta	0.24 ± 0.10	1.47 ± 0.14	0.16 ± 0.07	0.14 ± 0.07	0.20
W	0.52 ± 0.10	1.66 ± 0.12	0.31 ± 0.07	0.29 ± 0.07	0.20
Pt	0.23 ± 0.08	1.94 ± 0.13	0.12 ± 0.04	0.10 ± 0.04	0.08
Au	0.39 ± 0.11	2.08 ± 0.15	0.19 ± 0.06	0.17 ± 0.06	0.07
Hg [a]	0.33 ± 0.09	2.16 ± 0.15	0.15 ± 0.04	0.13 ± 0.04	0.03
Pb [a]	0.19 ± 0.14	2.42 ± 0.19	0.08 ± 0.06	0.06 ± 0.06	0
Bi	0.10 ± 0.15	2.65 ± 0.26	0.04 ± 0.06	0.02 ± 0.06	0
Th [a]	0.31 ± 0.12	2.26 ± 0.19	0.14 ± 0.05	0.12 ± 0.05	0.07
U [a]	0.21 ± 0.11	2.38 ± 0.19	0.09 ± 0.05	0.07 ± 0.05	0.08

[a] Data not previously reported.

TABLE II. Comparison with Saclay data.

Target	$\lvert A_0\rvert^2$ This experiment (Arbitrary units)	$\lvert A_0\rvert^2$ Saclay (mb)	Ratio
Cd	0.337 ± 0.058	0.508	0.663 ± 0.114
In [a]	0.507 ± 0.046	0.591	0.859 ± 0.078
Sn	0.550 ± 0.072	0.822	0.669 ± 0.096
Sb [a]	0.590 ± 0.061	0.794	0.743 ± 0.077
Nd [a]	0.837 ± 0.100	1.170	0.715 ± 0.086
Ta	1.19 ± 0.18	1.88	0.633 ± 0.096
W	1.05 ± 0.17	2.05	0.512 ± 0.083
Pt	1.67 ± 0.16	2.70	0.619 ± 0.059
Au	1.62 ± 0.20	2.92	0.555 ± 0.068
Hg [a]	2.16 ± 0.20	3.29	0.540 ± 0.060
Pb [a]	2.20 ± 0.27	3.43	0.641 ± 0.078
Bi	2.53 ± 0.31	3.43	0.737 ± 0.090
Th [a]	1.89 ± 0.22	2.73	0.692 ± 0.080
U [a]	2.13 ± 0.22	2.83	0.754 ± 0.077
			0.656 ± 0.021

[a] Data not previously reported.

REF.	ELEM. SYM.	A	Z
V. Emma, S. Lo Nigro, C. Milone Nucl. Phys. A257, 438 (1976)	Nd		60

METHOD	REF. NO.	
	76 Em 2	egf

REACTION	RESULT	EXCITATION ENERGY	SOURCE TYPE	SOURCE RANGE	DETECTOR TYPE	DETECTOR RANGE	ANGLE
G,F	ABY	THR-999	C	999	TRK-I		4PI

999 = 1 GEV

TABLE 1

Measured values of σ_q at $E = 1000$ MeV and deduced values of σ_k assumed constant from E_0 to 1000 MeV

Element	Z^2/A	σ_q (mb)	E_0 (MeV)	σ_k (mb)
Bi	32.96	12.3 ± 0.6	200	7.6 ± 0.6
Pb	32.45	5.4 ± 0.4	220	3.6 ± 0.3
Tl	32.10	4.1 ± 0.3	230	2.8 ± 0.3
Au	31.68	2.0 ± 0.15	240	1.4 ± 0.2
Pt	31.18	1.1 ± 0.08	255	$(8 \pm 0.7) \times 10^{-1}$
Re	30.21	$(3.7 \pm 0.3) \times 10^{-1}$	280	$(2.9 \pm 0.3) \times 10^{-1}$
W	29.78	$(3.5 \pm 0.3) \times 10^{-1}$	290	$(2.8 \pm 0.3) \times 10^{-1}$
Ta	29.45	$(3.3 \pm 0.3) \times 10^{-1}$	300	$(2.7 \pm 0.3) \times 10^{-1}$
Hf	29.04	$(1.7 \pm 0.2) \times 10^{-1}$	310	$(1.4 \pm 0.2) \times 10^{-1}$
Yb	28.31	$(1.3 \pm 0.1) \times 10^{-1}$	330	$(1.2 \pm 0.1) \times 10^{-1}$
Tm	28.18	$(7.5 \pm 0.8) \times 10^{-2}$	335	$(6.8 \pm 0.8) \times 10^{-2}$
Ho	27.21	$(3.6 \pm 0.4) \times 10^{-2}$	355	$(3.5 \pm 0.4) \times 10^{-2}$
Dy	26.80	$(2.6 \pm 0.3) \times 10^{-2}$	360	$(2.5 \pm 0.3) \times 10^{-2}$
Tb	26.58	$(2.5 \pm 0.3) \times 10^{-2}$	370	$(2.5 \pm 0.3) \times 10^{-2}$
Gd	26.04	$(1.6 \pm 0.2) \times 10^{-2}$	380	$(1.7 \pm 0.2) \times 10^{-2}$
Sm	25.56	$(1.3 \pm 0.2) \times 10^{-2}$	390	$(1.4 \pm 0.2) \times 10^{-2}$
Nd	24.96	$(9.2 \pm 0.9) \times 10^{-3}$	405	$(1 \pm 0.1) \times 10^{-2}$
Ce	24.00	$(8 \pm 0.9) \times 10^{-3}$	420	$(9 \pm 1) \times 10^{-3}$
La	23.39	$(8.4 \pm 0.9) \times 10^{-3}$	430	$(1 \pm 0.1) \times 10^{-3}$
Sb	21.36	$(1.2 \pm 0.2) \times 10^{-2}$	460	$(1.5 \pm 0.3) \times 10^{-2}$
Te	21.19	$(8.8 \pm 1) \times 10^{-3}$	465	$(1.2 \pm 0.2) \times 10^{-2}$
Sn	21.06	$(1.3 \pm 0.2) \times 10^{-2}$	465	$(1.7 \pm 0.3) \times 10^{-2}$
Cd	20.49	$(1.7 \pm 0.3) \times 10^{-2}$	470	$(2.2 \pm 0.4) \times 10^{-2}$
Ag	20.47	$(2 \pm 0.3) \times 10^{-2}$	470	$(2.6 \pm 0.4) \times 10^{-2}$
Zn	13.76	$(2 \pm 0.4) \times 10^{-1}$	515	$(3 \pm 0.6) \times 10^{-1}$
Cu	13.44	$(2.4 \pm 0.5) \times 10^{-1}$	515	$(3.6 \pm 0.8) \times 10^{-1}$
Ni	13.35	$(2.4 \pm 0.5) \times 10^{-1}$	510	$(3.6 \pm 0.8) \times 10^{-1}$
Fe	12.10	$(3 \pm 0.6) \times 10^{-1}$	510	$(4.4 \pm 0.9) \times 10^{-1}$

[4] A.V. Mitrofanova et al. Sov. J. Nucl. Phys. 6, 512 (1968).

[7] T. Methasiri et al., Nucl. Phys. A167, 97 (1971).

[12] J.R. Nix et al., Nucl. Phys. 81, 61 (1966).

[20] N.A. Perifilov et al., JETP (Sov. Phys.) 14, 623 (1962); Proc. Symp. on the physics & chemistry of fission, Salzburg 1965, vol. 2 (IAEA) Vienna, 1965, p.283.

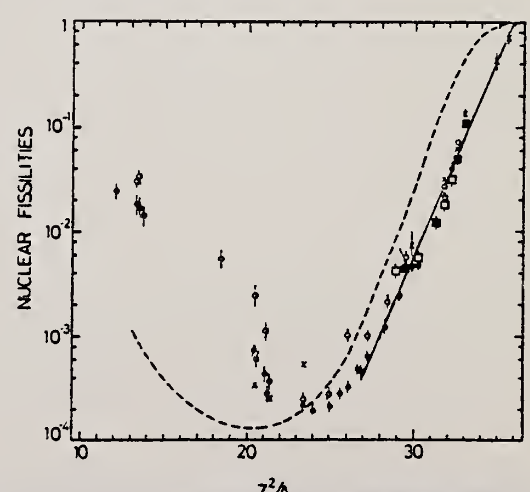

REF.	W. Mückenheim, P. Rullhusen, F. Smend, M. Schumacher Phys. Lett. 92B, 71 (1980)	ELEM. SYM.	A	Z
		Nd		60
METHOD		REF. NO.		
		80 Mu 4		hg

REACTION	RESULT	EXCITATION ENERGY	SOURCE TYPE	SOURCE RANGE	DETECTOR TYPE	DETECTOR RANGE	ANGLE
G,G	ABX	2-4	D	2-4	UKN-D		DST
		(2.754-3.254)	D	(2.5-3.5)			

LEV., 2.754, 3.205, 3.254

Elastic photon scattering investigated at energies of 2.5–3.5 MeV using radioactive sources has revealed a large probability for observing photoexcitation of nuclear levels. This finding removes inconsistencies in previously investigated properties of Delbrück scattering and provides a new access to nuclear resonance fluorescence.

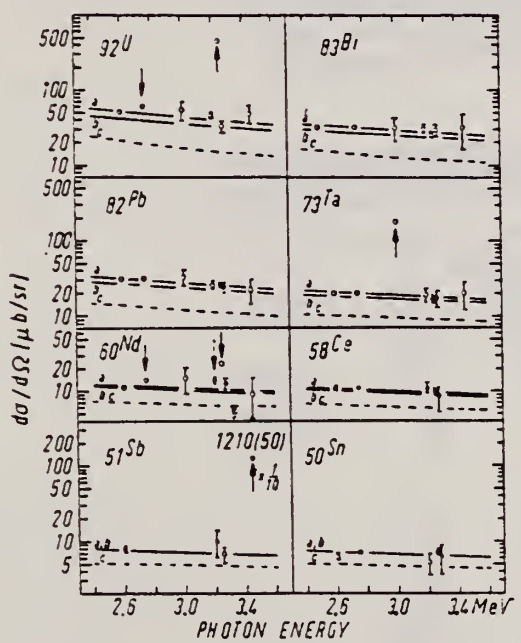

Fig. 1. Elastic differential cross sections versus photon energy. Unless error bars are given, the error intervals are at most equal to the diameter of the circles. Predicted differential cross sections: (a) including Coulomb corrections in addition to lowest-order D-, T-, R- and N-amplitudes, (b) including lowest-order D-, T-, R- and N-amplitudes, (c) including T-, R- and N-amplitudes.

Table 1
Levels observed via photoexcitation. ΔE: width of exciting photon line. D: predicted level spacing at 3 MeV. J^π: spin–parity. $(d\sigma/d\Omega)_{res}$: elastic differential cross section for resonance fluorescence by the identified isotope or element measured for $\theta = 90°$. Γ_0: partial width of the level for γ-transition to the ground state. Γ: total level width. $g = (2J_{ex}+1)/(2J_g+1)$. $W(\theta)$: angular correlation function.

Isotope	Level (MeV)	ΔE (eV)	D (eV)	J^π	$(d\sigma/d\Omega)_{res}$ (μb/sr)	$W(\theta) g \Gamma_0^2/\Gamma$ (meV)	Γ_0/Γ	Γ_0 (meV)
^{238}U	2.754	451	10^3	(1, 2)	13 ± 4	0.145	≤ 0.77	≥ 0.084 a)
	3.254	57		1^-	399 ± 5	0.79	0.24	1.5
^{181}Ta	3.010	81	5×10^2	–	165 ± 17	0.40	≤ 0.72	≥ 0.56 b)
natNd	2.754	451	2×10^3	–	2.6 ± 0.5	–	–	
	3.202	63		–	3.3 ± 1.5	–	–	
	3.254	57		–	12.8 ± 1.0	–	–	
^{121}Sb	3.452	35	10^3	$(3/2, 5/2)^+$	2100 ± 50	2.8	0.60	4.7 b)

a) $J = 1$ assumed. b) $gW(\theta) = 1$ assumed.

REF.	M. Schumacher, F. Smend, W. Mückenheim, P. Rullhusen, H.G. Börner Z. Phys. A300, 193 (1981)	ELEM. SYM. Nd	A	Z 60
METHOD		REF. NO. 81 Sc 6		egf

REACTION	RESULT	EXCITATION ENERGY	SOURCE TYPE	SOURCE RANGE	DETECTOR TYPE	DETECTOR RANGE	ANGLE
G,G	ABX	2,3		2,3	SCD-D		90

2.75,3.25 MEV

Elastic scattering by nuclei in the range of mass numbers between 64 and 238 has been studied with monochromatic photons in the energy range between 2 and 8 MeV. These photons were provided either by a Ti(n,γ) source installed in the tangential through channel of the Grenoble high flux reactor, or by ^{24}Na and ^{56}Co sources produced by deuteron bombardment of Al or Fe at the Göttingen cyclotron. The photoexcitation of 23 nuclear levels has been observed and the decay properties and groundstate widths of the majority of these levels have been determined. For the lead scattering target the coherent elastic differential cross section has been studied in detail. There is evidence that below the photo-neutron threshold the elastic scattering via virtual photoexcitation of the nucleus can be approximated by extrapolating the real part of the Giant Dipole Resonance amplitude along a Lorentzian curve. Coulomb corrections to Delbrück scattering seem to play a small role at 6.5 MeV.

Table 4. Properties of levels observed by photoexcitation. $(d\sigma/d\Omega)^{NRF}$: experimental differential cross section per identified isotope or element for resonance scattering through $\Theta=90°$. I^π: spin-parity of excited level; $W(\Theta)$: angular correlation function; $g=(2I_{ex}+1)/(2I_g+1)$; Γ_0: radiative groundstate transition width, Γ: total level width. Errors in the last digits are given in parentheses

Isotope	E_γ (MeV)	$(d\sigma/d\Omega)^{NRF}$ (μb/sr)	I^π	Γ_0/Γ^e	$W(\Theta)g\Gamma_0^2/\Gamma$ (meV)	Γ_0^f (meV)	Γ_0^g (meV)
^{238}U	2.754	13 (4)	(1)	0.77	0.145	0.084	-
^{238}U	3.254	421 (5)	1^-	0.24	0.83	1.5	0.52(15)^d
^{209}Bi	6.555	2.1 (4)·10^2	-	-	0.74	0.74^b	-
^{209}Bi	7.168	1.7 (3)·10^5	$9/2^{+a}$	1.00	710	786	820 (40)^a
^{203}Tl	6.418	8.75(30)·10^3	$1/2^a$	0.28	30	102	82 (15)^a
Tl	6.759	7 (3)	-	-	-	-	-
Hg	6.555	68 (17)	-	-	-	-	-
^{186}W	6.418	5.2 (3)·10^2	1^{-a}	0.32	1.75	2.4	-
^{184}W	6.555	9.8 (10)·10^2	(1)	0.52	3.44	2.9	-
^{184}W	6.759	46 (10)	(1)	0.58	0.17	0.13	-
^{191}Ta	3.010	174 (17)	-	0.72	0.42	0.59	-
^{181}Ta	6.418	62 (4)	-	0.73	0.2	0.27^c	-
^{181}Ta	6.759	4.8 (12)	-	-	0.018	0.018^b	-
^{165}Ho	6.418	10.3 (30)	-	-	0.035	0.035^b	-
^{165}Ho	6.759	5.6 (14)	-	-	0.021	0.021^b	-
Nd	2.754	2.6 (5)	-	-	-	-	-
Nd	3.254	14.0 (10)	-	-	-	-	-
Ce	6.759	13.4 (10)	-	-	-	-	-
^{121}Sb	3.452	2.20 (5)·10^3	-	0.60	2.9	4.9^b	-
^{100}Mo	6.418	1.53 (4)·10^4	1^{-a}	0.88	52	26	25 (8)^a
^{94}Mo	6.555	4.4 (4)·10^3	(1)	0.33	15	21	-
Mo	6.759	6.2 (15)	-	-	-	-	-
Mo	7.168	8.2 (26)·10^2	-	-	-	-	-

^{a} [11] ^{b} $W(\Theta)g\Gamma_0/\Gamma=1$ assumed ^{c} $W(\Theta)g=1$ assumed
^{d} [28] (a small correction has been applied to the data of [28])
^{e} Upper limits in case not all the transitions to lower levels were observed
^{f} Present work ^{g} Previous work

(OVER)

Table 1. Differential cross sections for elastic scattering $(d\sigma/d\Omega)^{exp}$ of photons from ^{56}Co and ^{24}Na sources by different scattering targets, in units of μb/sr. Errors in the last digits are given in parentheses.

θ deg	Scattering targets	2.599[a] (MeV)	2.754[b] (MeV)	3.010[a] (MeV)	3.202[a] (MeV)	3.254[a] (MeV)	3.273[a] (MeV)	3.452[a] (MeV)
90	^{238}U	52.7(25)	57.5(25)[c]	56(16)	47(4)	456 (10)[c]	34(6)	49(14)
	^{209}Bi	33.1(30)	32 (2)	33(11)	32(4)	25.6(20)	29(6)	33(15)
	^{nat}Pb	31.5(23)	31.0(16)	35 (8)	27(3)	26.6(22)	25(4)	23 (8)
	^{nat}Tl	31.5(33)	-	27(12)	32(5)	24 (3)	22(7)	34(15)
	^{nat}Hg	30.0(27)	-	24(10)	28(5)	25.5(18)	26(8)	20 (8)
	^{nat}W	22.5(11)	-	17 (7)	19(3)	18.4(15)	18(5)	21 (6)
	^{181}Ta	20.0(15)	19.2 (6)	193(20)[c]	20(4)	17.3(21)	18(5)	21 (8)
	^{165}Ho	15.9(13)	-	17(10)	13(6)	15.6(20)	18(8)	-
	^{nat}Nd	11.4 (7)	14.2 (5)[d]	15 (7)	14(3)	24.2(12)[d]	13(3)	9 (6)
	^{nat}Ce	11.1 (9)	11.0 (5)	-	11(3)	9.5(13)	8(4)	-
	^{127}J	8.4(10)	8.6 (5)	-	9(2)	7 (1)	5(3)	-
	^{nat}Sb	8.0(11)	-	-	10(4)	6.8(19)	-	1,270(50)[c]
	^{nat}Sn	6.5 (7)	7.0 (5)	-	5(2)	7.6 (8)	6(3)	-
	^{nat}Cd	6.2 (5)	-	-	6(2)	6.6 (8)	7(3)	-
120	^{238}U	55.1(25)	64 (4)[c]	43(15)	55(5)	574 (10)[c]	48(5)	48(11)
	^{181}Ta	27.5(15)	25.0 (9)	227(20)[c]	22(5)	21 (2)	22(8)	-
	^{nat}Nd	17.9(30)	17.0 (9)[d]	-	-	29.8(47)[d]	-	-

[a] ^{56}Co source in Fe lattice [b] ^{24}Na source in Al lattice (part of data have been published elsewhere)

[c] Transitions to excited states observed in addition to the ground-state transition

[d] Photoexcitation of nuclear level identified from the size of the differential cross section

Ref. J.H. Carver, W. Turchinetz Proc. Phys. Soc. 73, 69 (1959)	Elem. Sym. Nd	A	Z 60
Method 33 MeV synchrotron; radioactivity; NaI spectrometer; r chamber	Ref. No. 59 Ca 3		EH

Reaction	E or ΔE	E_0	Γ	$\int \sigma dE$	Jπ	Notes
$Nd^{142}(\gamma,n)$	Bremss.					
	10-32	14.8	< 5.0 MeV	< 2.3±0.3 MeV-b		

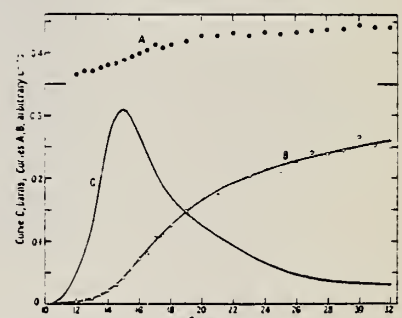

Figure 8. A, the ratio of activation curves $^{142}Nd(\gamma,n)/^{181}Ta(\gamma,n)$; B, activation curve for $^{142}Nd(\gamma,n)$; C, derived cross section: $^{142}Nd(\gamma,n)$.

Table 1

Isotope	% abundance	N	ε	B(n) (Mev)	B(2n) (Mev)	(γ,n) product nucleus Half-life	Principal γ-rays
^{141}Pr	100	82	~0	9·99	18·28	3·4 min	K x-ray, γ^+
^{142}Nd	27·13	82	0·04	10·47	19·3	2·5 hr	K x-ray, γ^+
^{144}Sm	3·16	82	—	10·2†	19·7†	8·5 min	K x-ray, γ^+
^{150}Nd	5·60	90	0·24	7·87	12·97	1·8 hr	2 groups: at 118 & 212 kev
^{154}Sm	22·53	92	0·32	8·2	14·77	47 hr	K x-ray, 102 kev
^{160}Gd	21·90	96	0·44	7·6†	12·70	18 hr	K x-ray, 362 kev
^{181}Ta	99·988	108	0·22	7·72	13·8†	8·15 hr	K x-ray

† Threshold determined from semi-empirical mass tables (Cameron 1957). The other thresholds are based on measured values (Johnson and Nier 1957, Wapstra 1955).

Table 2

Activity	$T_{1/2}$ (min)	W_0 (Mev)	K/β^+	K-capture / Total capture	W_K
^{140}Pr	3·4	3·25	0·63	0·89	0·89
^{141}Nd	150	1·80	48	0·89	0·90
^{143}Sm	8·5	3·47	0·60	0·89	0·91

Nd
A=142

Nd
A=142

Nd
A=142

REF.	ELEM. SYM.	A	Z
Y. Oka, T. Kato and A. Yamadera Bull. Chem. Soc. Japan 41, 1606 (1968)	Nd	142	60

METHOD	REF. NO.	
	68 Ok 2	egf

REACTION	RESULT	EXCITATION ENERGY	SOURCE TYPE	SOURCE RANGE	DETECTOR TYPE	DETECTOR RANGE	ANGLE
G,N	ABY	THR-20	C	20	ACT-I		4PI

ISOMERIC YIELD

TABLE 1. THE PARTICULARS OF THE (γ,n) REACTION PRODUCTS AND THE DATA OBTAINED WITH 20 MeV BREMSSTRAHLUNG

Nuclide: Parent (Natural abundance, %)	Nuclide: Residual	Half-life of product (sec)	Gamma-ray determined: Energy (MeV)	Gamma-ray determined: Branching ratio (%)	Gamma-ray determined: Photopeak activity (cpm/mg)[a]	Limit of detection (μg)	Yield ($mol^{-1} \cdot R^{-1}$)
^{24}Mg(78.60)	^{23}Mg	9.9	0.511	200	2.04×10^{6}	0.49	8.1×10^{4}
^{74}Ge(7.67)	^{73m}Ge	48	0.139	100	6.37×10^{5}	1.6	1.1×10^{4}
^{78}Se(23.52)	^{77m}Se	17	0.162	100	1.82×10^{6}	0.55	1.2×10^{6}
^{92}Mo(15.86)	^{91m}Mo	65	0.650	57	2.22×10^{5}	4.5	2.7×10^{6}
^{140}Ce(88.48)	^{139m}Ce	58	0.745	100	1.06×10^{6}	0.95	1.3×10^{6}
^{142}Nd(27.13)	^{141m}Nd	64	0.760	100	3.19×10^{5}	3.1	1.4×10^{6}
^{159}Tb(100)	^{158m}Tb	11	0.111	100	2.56×10^{5}	3.8	2.2×10^{6}

a) The value corrected at the end of one-minute irradiation with the dose rate of 10^7 R/min; Counting geometry is 20% with a 3"dia.×3"NaI(Tl) detector.

REF.	ELEM. SYM.	A	Z
P. Carlos, H. Beil, R. Bergere, A. Lepretre, A. Veyssiere Nucl. Phys. A172, 437 (1971)	Nd	142	60
METHOD	REF. NO. 71 Ca 1		egf

REACTION		RESULT	EXCITATION ENERGY	SOURCE TYPE	SOURCE RANGE	DETECTOR TYPE	DETECTOR RANGE	ANGLE
G,N	391	ABX	10-20	D	8-20	MOD-I		4PI
G,2N	392+	ABX	10-20	D	8-20	MOD-I		4PI

391+

Table 2

Parameters of the one- or two-Lorentz line fits to the σ_T curves for neodymium isotopes: parameters for Ce and Er extracted from earlier results [13]) are also shown

	Ce	^{142}Nd	^{143}Nd	^{144}Nd	^{145}Nd	^{146}Nd	^{148}Nd	^{150}Nd	Er
σ_1 (mb)	360 ±15	359 ±15	360 ±15	317 ±15	297 ±20	308 ±16	263 ±15	174 ±20	225 ±15
Γ_1 (MeV)	4.35±0.05	4.43± 0.20	4.5 ±0.2	5.3 ± 0.25	6.5±0.4	6 ± 0.3	7.2± 0.3	3.3 ± 0.1	2.9 ±0.05
E_1 (MeV)	15.0 ± 0.10	14.95± 0.1	15 ± 0.1	15.05± 0.1	15 ± 0.15	14.8 ± 0.1	14.7± 0.15	12.3 ± 0.15	12.00± 0.1
σ_2 (mb)								223 ±20	260 ±15
Γ_2 (MeV)								5.2 ± 0.15	5.0 ± 0.05
E_2 (MeV)								16 ± 0.15	15.45± 0.1
$\frac{1}{2}\pi\sigma\Gamma$ MeV · b		2.5 ± 0.2	2.54± 0.2	2.6 ± 0.2	3.0± 0.3	2.9 ± 0.2	3.0± 0.2	2.7 ± 0.3	
$\frac{\frac{1}{2}\pi\sigma\Gamma}{0.06\, NZA^{-1}}$		1.20± 0.10	1.22± 0.10	1.25± 0.10	1.4± 0.15	1.35± 0.10	1.4± 0.1	1.27± 0.15	

[13] R. Bergere, H. Beil, P. Carlos et A. Veyssiere, Nucl. Phys. A133, 417 (1969).

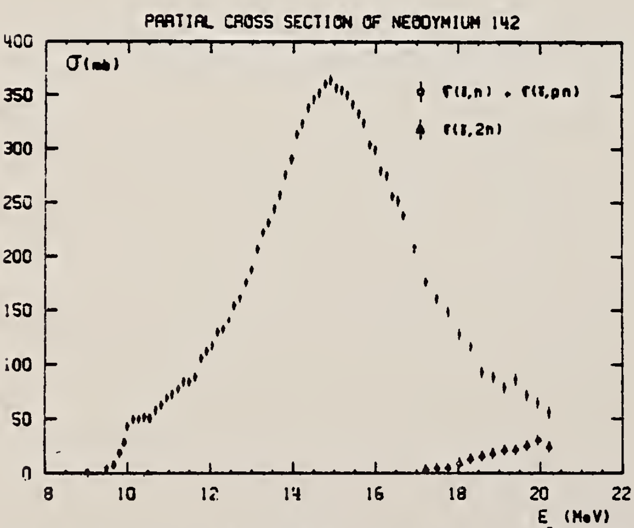

Fig. 2. Partial photoneutron cross sections $\sigma(\gamma, n)$ and $\sigma(\gamma, 2n)$ of ^{142}Nd.

(over)

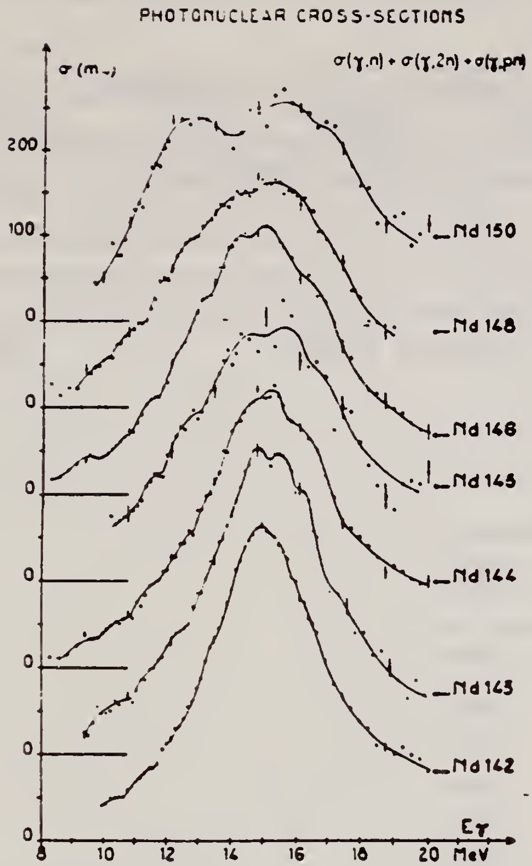

Fig. 9. Total photonuclear cross-section σ_T of neodymium isotopes. The full line drawn through the experimental points is merely meant to facilitate the identification of structure.

REF.	ELEM. SYM.	A	Z
P. E. Haustein and A. F. Voigt J. inorg. nucl. Chem. 33, 289 (1971)	Nd	142	60
METHOD	REF. NO. 71 Ha 2		egf

REACTION	RESULT	EXCITATION ENERGY	SOURCE TYPE	SOURCE RANGE	DETECTOR TYPE	DETECTOR RANGE	ANGLE
G,N	RLY	10-70	C	70	ACT-I		4PI

Isomer ratio = (yield to low spin state)/(yield to high spin state)

ISOMER RATIO

Table 2. Isomer ratio measurements for ^{91}Mo, ^{137}Ce, and ^{141}Nd

Reaction	Isomer ratio	I^π Target	I^π Ground state	I^π Isomer	Threshold (MeV)	$41A^{-1/3}$ (MeV)
^{92}Mo(γ, n)^{91}Mo	$1 \cdot 92 \pm 0 \cdot 15$	0^+	$9/2^+$	$1/2^-$	13·13	16·60
^{94}Mo(γ, 3n)^{91}Mo	$1 \cdot 59 \pm 0 \cdot 16$	0^+			30·72	16·52
^{138}Ce(γ, n)^{137}Ce	3·1	0^+	$3/2^+$	$11/2^+$	10·31	15·30
^{140}Ce(γ, 3n)^{137}Ce	$1 \cdot 10 \pm 0 \cdot 12$	0^+			26·34	15·26
^{142}Nd(γ, n)^{141}Nd	$5 \cdot 2 \pm 0 \cdot 3$	0^+	$3/2^+$	$11/2^+$	9·79	15·22
^{144}Nd(γ, 3n)^{141}Nd	$1 \cdot 80 \pm 0 \cdot 25$	0^+			23·67	15·17

REF.	ELEM. SYM.	A	Z
D. W. Madsen, L. S. Cardman, J. R. Legg, C. K. Bockelman Nucl. Phys. A168, 97 (1971)	Nd	142	60
METHOD	REF. NO. 71 Ma 1		egf

REACTION	RESULT	EXCITATION ENERGY	SOURCE TYPE	SOURCE RANGE	DETECTOR TYPE	DETECTOR RANGE	ANGLE
E,E/	FMF	1,2	D	60	MAG-D		DST

1=1.57, 2=2.09

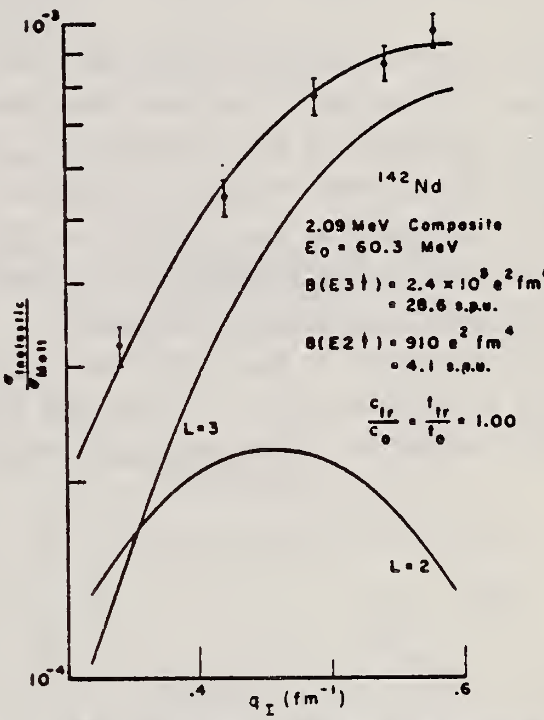

Fig. 15. Inelastic form factors for the excitation at approximately 2.09 MeV in ^{142}Nd. The experimental points are the findings of this experiment while the solid line through them represents the best fit obtained by an addition of the $L = 2$ and $L = 3$ curves shown. (L is the transition multipolarity.) The individual $B(EL\uparrow)$ values are given in the figure. See text.

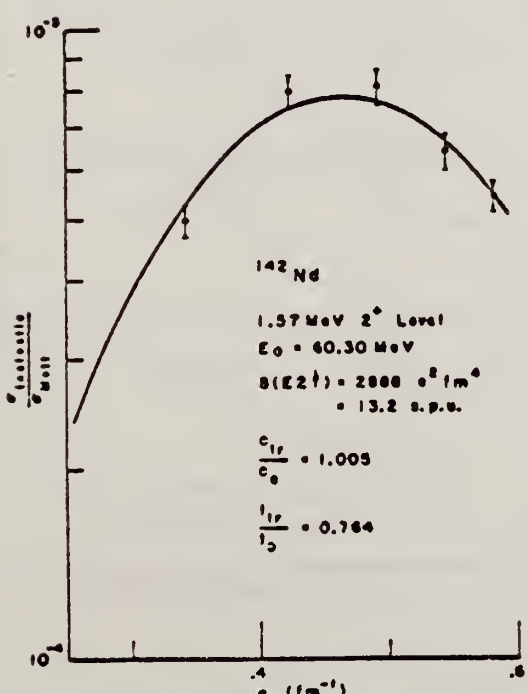

Fig. 14. Inelastic form factors for the 2^+ level at 1.57 MeV in ^{142}Nd as a function of inelastic momentum transfer. The experimental points are the findings of this experiment and the solid line is the best fit obtained with the parameters shown.

[over]

U.S. DEPARTMENT OF COMMERCE
NATIONAL BUREAU OF STANDARDS

Table 11

A comparison of this experiment's $B(EL\uparrow)$ values with those of other experiments and theory

Nucleus	State (MeV)	This work	Pulsed beam	Heavy particle Coulomb excitation	Theory
			2+ states		
^{142}Nd	1.57	13.1 ± 1.7		25.0 ± 7.3 a) 19.1 ± 2.3 b) 15.5 ± 7.8 c)	16.4 d) 16.3 e)
^{142}Nd	2.09	4.1 ± 1.1			
^{146}Nd	0.45	30.9 ± 4.6		28.5 ± 0.4 b) 28.1 ± 6.6 a)	92.1 d)
^{150}Nd	0.13	62.9 ± 10.5	113.9 ± 1.8 f) 116.8 ± 3.2 g) 112.4 ± 5.1 h)	112.7 ± 4.2 i)	
			3− state		
^{142}Nd	2.09	28.6 ± 5.0		52 ± 21 j)	

a) Ref. [39]. b) Ref. [40]. c) Ref. [41]. d) Ref. [37]. e) Ref. [42]. f) Ref. [43]. g) Ref. [44]. h) Ref. [45]. i) Ref. [38]. j) Ref. [33].

[33] O. Hansen et al., Nucl. Phys. 42 (1963) 197.

[37] L. S. Kisslinger et al., Rev. Mod. Phys. 35 (1963) 853.

[38] J. Bjerregard et al., Nucl. Phys. 44 (1963) 280.

[39] G. A. Burginyon, Thesis, Yale University (1967) unpub.

[40] D. Eccleshall et al., Nucl. Phys. 78 (1966) 481.

[41] O. Nathan et al., Nucl. Phys. 21 (1960) 631.

[42] M. Rho, Nucl. Phys. 65 (1965) 497.

[43] J. D. Kurfess et al., Phys. Rev. 161 (1967) 1185.

[44] F. W. Richter et al., Z. Phys. 213 (1968) 202.

[45] M. Birk et al., Phys. Rev. 116 (1959) 730.

REF.	ELEM. SYM.	A	Z
K. Shoda, T. Saito, M. Sugawara, H. Miyase, S. Oikawa, A. Suzuki Phys. Rev. C4, 1842 (1971)	Nd	142	60

METHOD	REF. NO.	
	71 Sh 3	hmg

REACTION	RESULT	EXCITATION ENERGY	SOURCE TYPE	SOURCE RANGE	DETECTOR TYPE	DETECTOR RANGE	ANGLE
E,P	ABX	15-22	D	23	MAG-D		90

ISOBARIC ANALOGS

The energy distributions of protons from the $(e,e'p)$ reaction on $N=82$ nuclei with even Z have been measured. The cross sections of the (γ,p_0+p_1) reaction have been estimated. Two prominent isobaric analogs have been found in each nucleus. The results were used for the systematic discussion of the odd-odd parent nuclei ^{138}Cs, ^{140}La, ^{142}Pr, and ^{144}Pm. The 1^- states are estimated at 600 and ~2500 keV for ^{138}Cs, 500 and 3000 keV for ^{140}La, 1100 and 3700 keV for ^{142}Pr, and 1400 and 4300 keV for ^{144}Pm. The parameters of these states are discussed in terms of a quasiproton and single-neutron model.

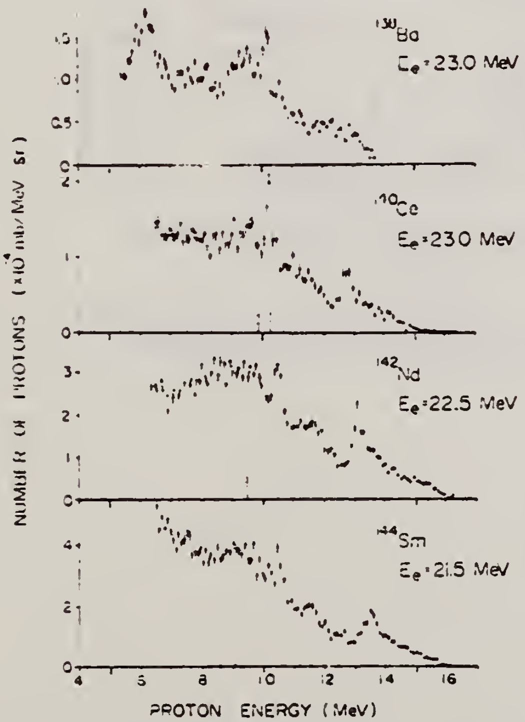

FIG. 1. Energy distributions of protons emitted from the $(e,e'p)$ reaction at $\theta=90°$.

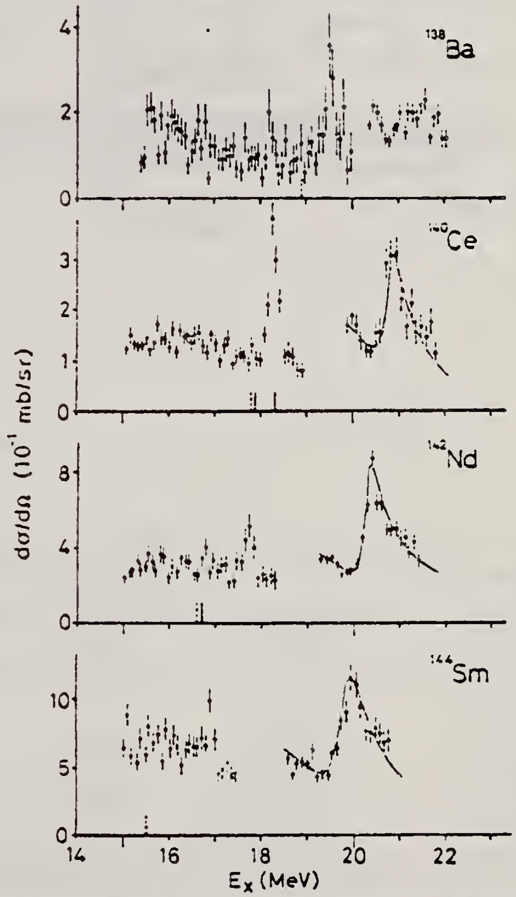

FIG. 2. The photoproton cross sections for p_0+p_1 at $\theta=90°$ in the vicinity of the isobaric analog resonances. The curves for the broad resonances were obtained from the fitting of the interference formula.

(over)

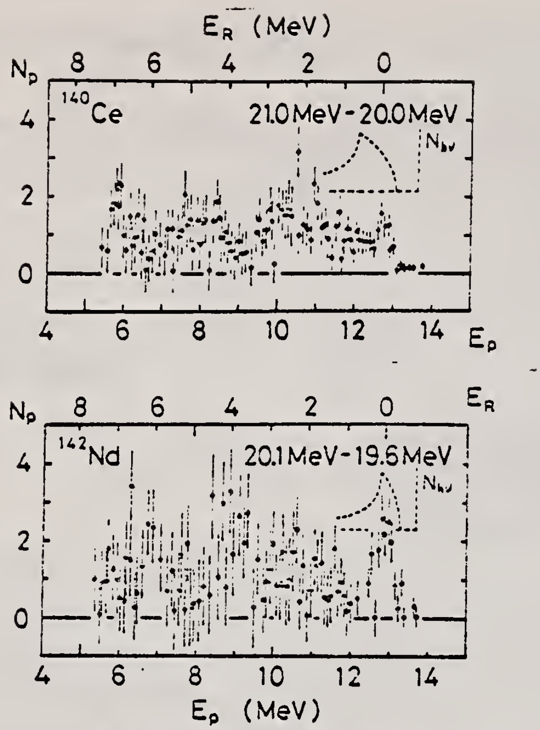

FIG. 5. The proton groups emitted through the isobaric analogs at 20.8 MeV in ^{140}Ce and at 20.3 MeV in ^{142}Nd. The energies of the residual states are also indicated by E_R.

REF. M. Hasinoff, G.A. Fisher, P. Kurjan and S. S. Hanna
Nucl. Phys. A195, 78 (1972)

ELEM. SYM.	A	Z
Nd	142	60

METHOD

REF. NO. 72 Ha 3 egf

REACTION	RESULT	EXCITATION ENERGY	SOURCE TYPE	SOURCE RANGE	DETECTOR TYPE	DETECTOR RANGE	ANGLE
P,G	ABX	14-24	D	6-17	NAI-D		DST

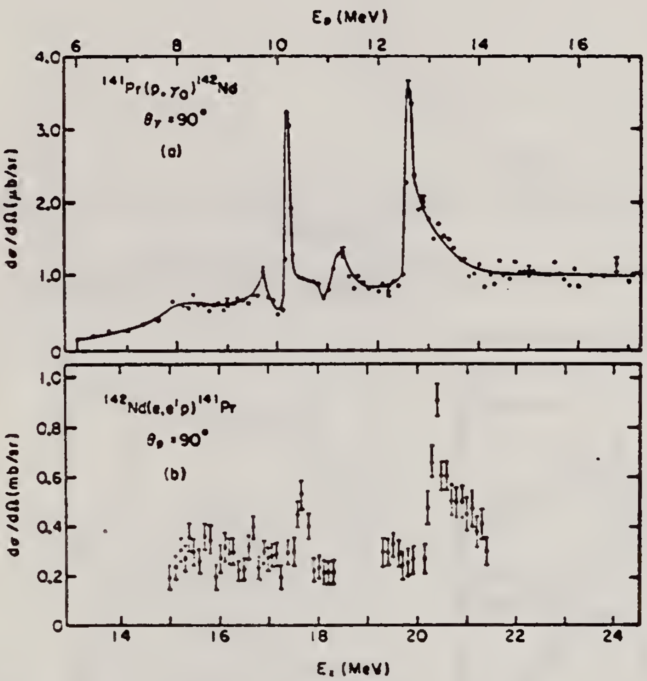

Fig. 3. (a) Differential yield curve of $^{141}Pr(p,\gamma_0)^{142}Nd$ at $\theta_\gamma = 90°$. The line drawn is merely to guide the eye. (b) The $^{142}Nd(e,e'p_0+p_1)^{141}Pr$ data of ref. [15]).

[15] K. Shoda et al., Phys. Rev. C4 (1971) 1842.
[19] P. A. Moore et al., Phys. Rev. 180 (1969) 1213.
[20] G. Clausnitzer et al., Nucl. Phys. A106 (1968) 99.
[21] P. Von Brentano et al. Phys. Lett. 17 (1965) 124.
[22] H. Ejiri et al. Nucl. Phys. A128 (1969) 388.

TABLE 2

Resonance parameters obtained for three of the 1^-, $T_>$ analogue resonances observed in $^{141}Pr(p,\gamma_0)^{142}Nd$

E_p (MeV)	E_x (MeV)	Γ (keV)	$\Gamma_{p_0}\Gamma_{\gamma_0}$ (keV^2)	$\phi_A-\phi_{GR}$ (deg.)
10.18	17.30	79± 4	1.1 ±0.3	− 20±10
			5.9 ±1.9	−120±15
11.20	18.30	220±30	0.55±0.28	− 25±10
			35 ±18	−120±15
12.59	19.73	180±20	6.5 ±2.0	− 20±10
			42 ±13	−115±15

For each resonance the first solution is given on the first line and the alternative solution on the second line.

The errors for $\Gamma_{p_0}\Gamma_{\gamma_0}$ include both the fitting errors and the estimated error in the determination of the absolute cross section (≈ 30 %).

(over)

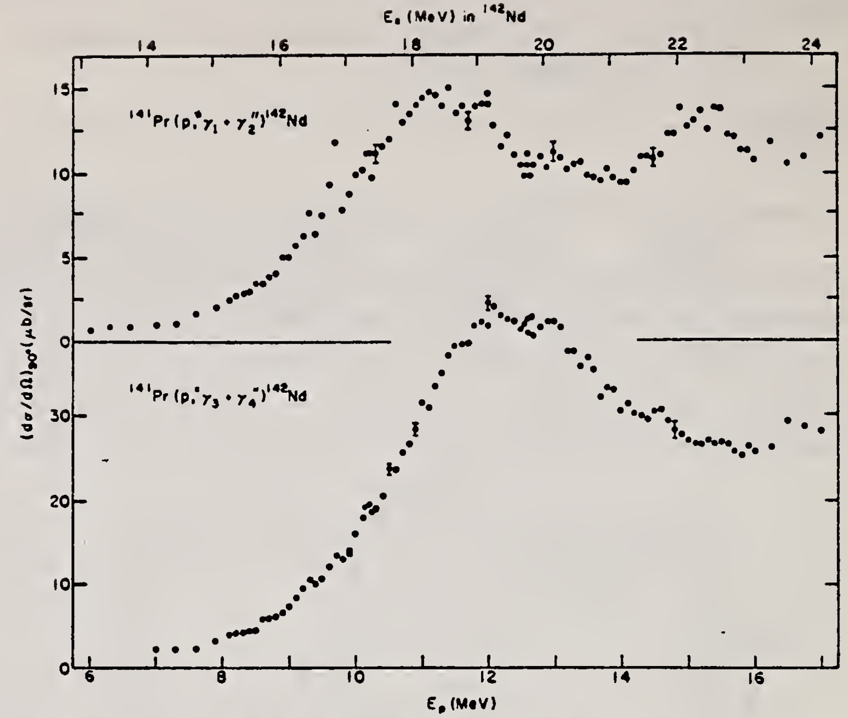

Fig. 4. Differential yield curves of ^{141}Pr(p, "$\gamma_1+\gamma_2$")^{142}Nd and ^{141}Pr(p, "$\gamma_3+\gamma_4$")^{142}Nd at $\theta_\gamma = 90°$.

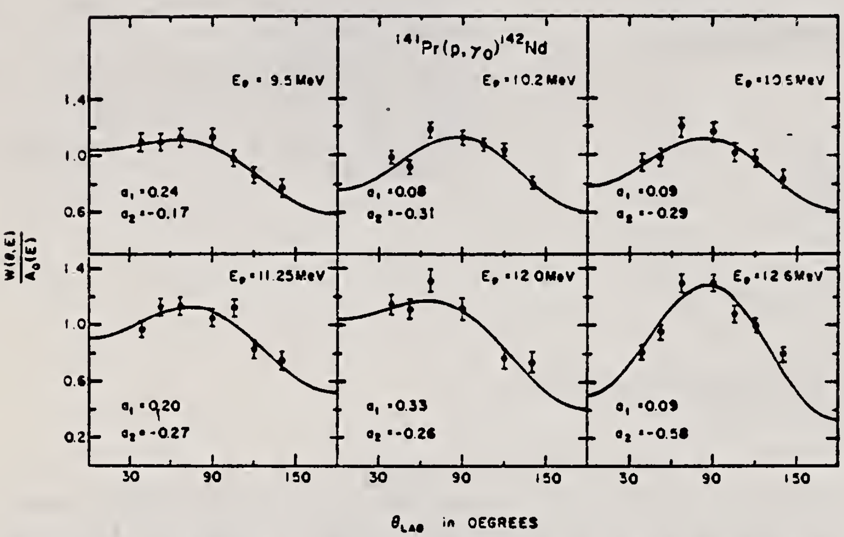

Fig. 5. Angular distributions in ^{141}Pr(p,γ_0)^{142}Nd measured on and off the three upper resonances. The on-resonance measurements are at E_p = 10.2, 11.25 and 12.6 MeV. The curves are fits obtained with the series $1+a_1P_1+a_2P_2$. The values of a_1 and a_2 are listed in each case.

Table 3

Comparison of radiative strengths for the two strong 1^-, $T_>$ levels in ^{142}Nd

E_p (MeV)	$\Gamma_{\gamma_0}\Gamma_{p_0}/\Gamma$ a) (eV)	$\Gamma_{\gamma_0}(\Gamma_{p_0}+\Gamma_{p_1})/\Gamma$ b) (eV)	Γ_{γ_0} a) (eV)	Γ_{γ_0} b) (eV)	Γ_{γ_0} c) (eV)	$\Gamma_\gamma^W/2(T_0+1)$ (eV)
10.18	13.8 ± 4.1	6 ± 1	69 ± 22 d)	20 ± 3 d)	13 ± 5	680
	75 ± 25		375 ± 130 d)		62 ± 26	
12.59	37 ± 11	58 ± 2	530 ± 160 e)	580 ± 20 e)		1000
	230 ± 71		3300 ± 1000 e)			

a) Present work. The second line in each case corresponds to the alternative solution.
b) Ref. [15]).
c) The E1 strength of the $2f_{\frac{7}{2}} \to 2d_{\frac{5}{2}}$ transition in ^{140}Ce(p,γ_0)^{141}Pr [ref. [22])].
d) If $\Gamma_{p_0}/\Gamma \approx 0.2$ as obtained from refs. [19-21]). An estimate for Γ_{p_1}/Γ of 0.5 Γ_{p_0}/Γ is used.
e) If $(\Gamma_{p_0}+\Gamma_{p_1})/\Gamma \approx 0.10$ as given in ref. [15]). An estimate for Γ_{p_1}/Γ of 0.5 Γ_{p_0}/Γ is used.

REF.	ELEM. SYM.	A	Z
K. Shoda, M. Sugawara, T. Saito, H. Miyase, A. Suzuki, S. Oikawa, and J. Uegaki PICNS-72, 321 Sendai	Nd	142	60

METHOD	REF. NO.	
	72 Sh 10	hvm

REACTION	RESULT	EXCITATION ENERGY	SOURCE		DETECTOR		ANGLE
			TYPE	RANGE	TYPE	RANGE	
G,P	ABX	15- 22	C	15- 22	MAG-D		UKN

I A STATES

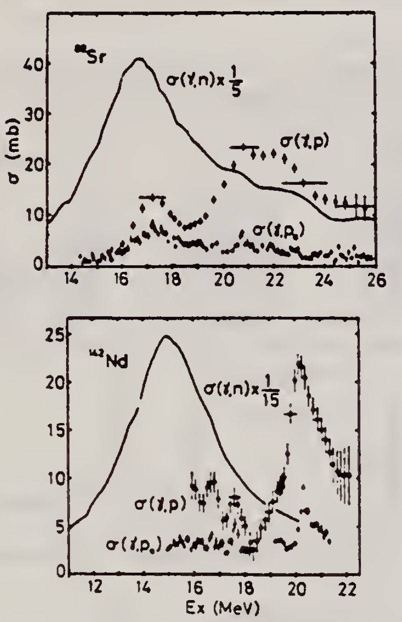

Fig. 11 The (γ,p) cross sections of ^{88}Sr and ^{142}Nd. The (γ,p_0) and (γ,n) cross sections are also shown.

REF.	T. Saito, S. Oikawa, K. Shoda, M. Sugawara, H. Miyase, A. Suzuki, and J. Uegaki PICNS-73, Vol.I, p.199 Asilomar	ELEM. SYM. Nd	A 142	Z 60
METHOD		REF. NO. 73 Sa 7		hmg

REACTION	RESULT	EXCITATION ENERGY	SOURCE TYPE	SOURCE RANGE	DETECTOR TYPE	DETECTOR RANGE	ANGLE
E,P	ABX	13- 26	C	15- 26	MAG-D		UKN

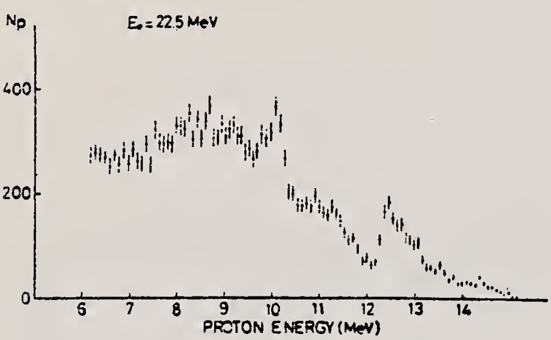

Fig. 1

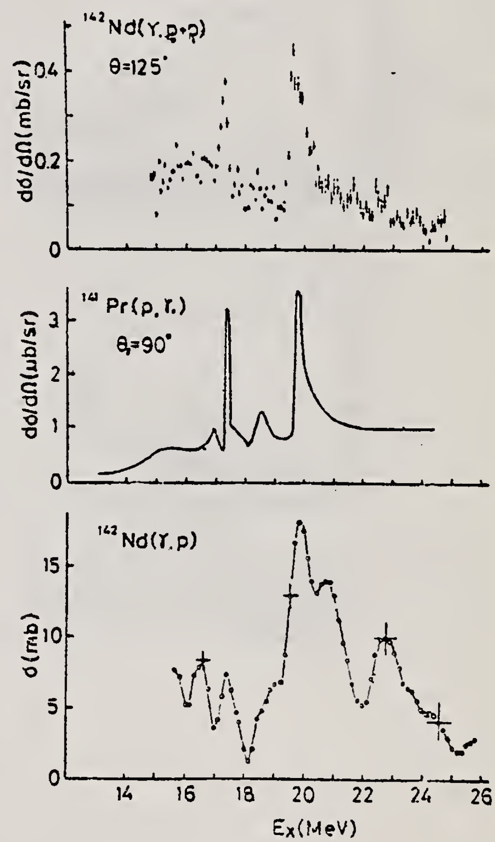

Fig. 3

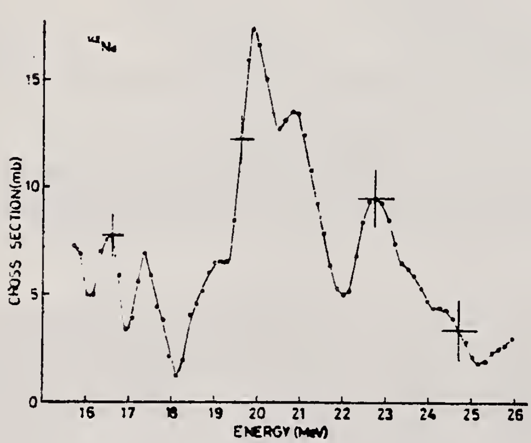

Fig. 2
Total σ(γ,p) from yield curve.

REF.

J. Tenenbaum, R. Moreh, and A. Nof
Nucl. Phys. A218, 95 (1974)

ELEM. SYM.	A	Z
Nd	142	60

METHOD

REF. NO.	
74 Te 1	egf

REACTION	RESULT	EXCITATION ENERGY	SOURCE TYPE	SOURCE RANGE	DETECTOR TYPE	DETECTOR RANGE	ANGLE
G,G	LFT	6	D	4- 8	SCD-D		DST

6=6.877

TABLE 2

Measured angular distribution coefficients A_2, the ratios $N_{||}/N_{\perp}$, the spins and parities of the ground and the resonance levels, J_0^{π} and J_r^{π}, and the character of the ground state transition

Scatterer	E_γ (keV)	A_2	$N_{\|\|}/N_{\perp}$	J_0^{π}	J_r^{π}	Transition
^{55}Mn	7491	0.01 ± 0.02	1.00 ± 0.02	$\frac{5}{2}^-$	$\frac{3}{2}$	
^{140}Ce	5660	0.51 ± 0.02	1.14 ± 0.04	0^+	1^-	E1
^{141}Pr	6877	0.11 ± 0.02	0.95 ± 0.03	$\frac{5}{2}^+$	$\frac{7}{2}^+$	M1
^{142}Nd	6877	0.51 ± 0.03	1.10 ± 0.04	0^+	1^-	E1
^{202}Hg	4922	0.51 ± 0.02	1.18 ± 0.03	0^+	1^-	E1
^{209}Bi	5603	0.06 ± 0.02	0.97 ± 0.02	$\frac{9}{2}^-$	$\frac{11}{2}^-$	M1

TABLE 4

Values of Γ, Γ_0 and the energy separation δ (between the incident γ-line and the resonance level) as obtained from the analysis of the various experiments

Scatterer	E_γ (keV)	Γ (meV)	Γ_0 (meV)	δ (eV)	D (eV)	K_{E1} (10^{-9} MeV^{-3})	K_{M1} (10^{-9} MeV^{-3})
^{55}Mn	7491	450 ± 250	80 ± 40	17 ± 1			
^{140}Ce ^{a})	5660	13 ± 3	12 ± 2	4.7 ± 0.3	6800	0.33	
^{141}Pr ^{a})	6877	85 ± 35	17 ± 9	6.7 ± 1.5	450		116
^{142}Nd ^{a})	6877	340 ± 40	270 ± 20	12.4 ± 0.3	1200	26	
^{202}Hg	4922	300 ± 50	260 ± 20	4.2 ± 0.5	19000	3.4	
^{209}Bi ^{a})	5603	950 ± 200	950 ± 200	13 ± 1	34000		160

The radiative strengths K_{E1} and K_{M1} are also given. The level spacing D refers to the excitation energy of the resonance level E_γ.

^{a}) These values are slightly different from those of ref. [8]) and were obtained from a renewed analysis of the experimental results.

[8] A. Wolf, R. Moreh, A. Nof, O. Shahal, J. Tenenbaum, Phys. Rev. C6, 2276 (1972).

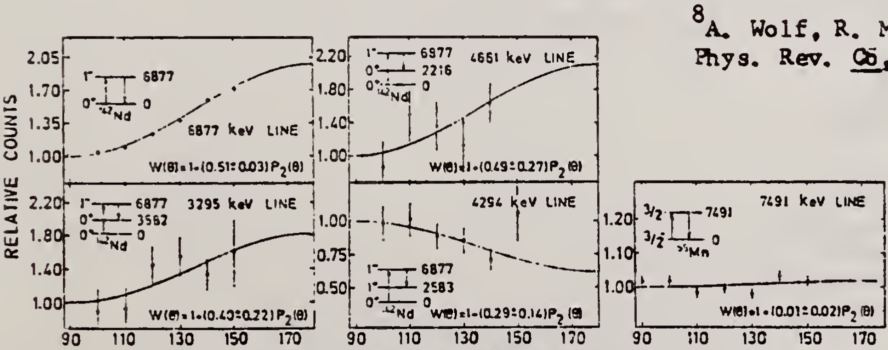

Fig. 5. Angular distributions of elastically scattered γ-lines from ^{55}Mn and ^{142}Nd. The distributions of three inelastic γ-lines from ^{142}Nd are also shown. The solid lines have the form $W(\theta) = 1+A_2P_2(\cos\theta)$ and are least squares fits to the experimental distribution. In each case the corresponding γ-γ cascade is indicated.

REF.	A. Schwierczinski, R. Frey, E. Spamer, H. Theissen, and Th. Walcher Phys. Lett. 55B, 171 (1975)	ELEM. SYM.	A	Z
		Nd	142	60
METHOD		REF. NO.		
		75 Sc 2		egf

REACTION	RESULT	EXCITATION ENERGY	SOURCE TYPE	SOURCE RANGE	DETECTOR TYPE	DETECTOR RANGE	ANGLE
E,E/	NOX	5- 28	D	50, 64	MAG-D		93

E,E/SPECTRUM (E2)

Inelastic electron scattering has been used to study the isoscalar E2 giant resonances in ^{142}Nd and ^{150}Nd, which were found at excitation energies of 12.0 and 11.2 MeV with total widths of 2.8 and 5.0 MeV, respectively. The energy shift and the larger width in ^{150}Nd indicate a splitting due to the deformation of ^{150}Nd.

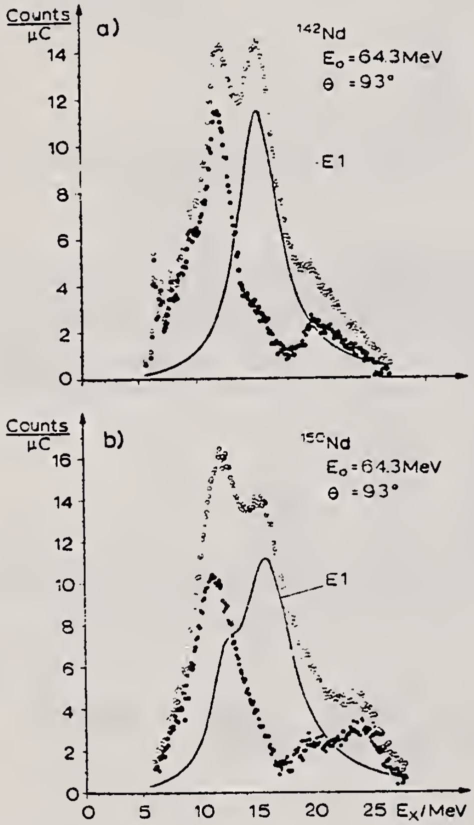

Fig. 1. Spectrum of inelastically scattered electrons after subtraction of radiation tail and background, a) ^{142}Nd, b) ^{150}Nd (open circles). Solid line: E1 cross section. Full circles: E1 cross section subtracted. The total number of counts/μC in the region of the giant resonances is about 100.

REF.	ELEM. SYM.	A	Z
H. Bartsch, K. Huber, U. Kneissl, H. Krieger Nucl. Phys. A256, 243 (1976)	Nd	142	60

METHOD	REF. NO.	
	76 Ba 1	egf

REACTION	RESULT	EXCITATION ENERGY	SOURCE TYPE	SOURCE RANGE	DETECTOR TYPE	DETECTOR RANGE	ANGLE
G,N	RLY	THR-UKN	C	UKN	SCD-D		4PI

ISOMER RATIO

TABLE 1

Experimental and theoretical results

Process	Target-spin	E_γ (keV)	$T_{\frac{1}{2}}$	Spin high	Spin low	$R_{exp} = \frac{\sigma_{high}}{\sigma_{low}}$	SCOP ($\hbar$)
$^{181}Ta(\gamma, 3n)$	$\frac{7}{2}^+$	93	2.2 h	7^-	1^+	0.51 ±0.09	3.6 ±0.2
			9.31 min				
			8.15 h				
$^{142}Nd(\gamma, n)$	0^+	755	63 s	$\frac{11}{2}^-$	$\frac{3}{2}^+$	0.055±0.006	2.20±0.06
		1100–1300,	2.5 h			0.19 ±0.01 [a])	
		145					
$^{92}Mo(\gamma, n)$	0^+	652.9	66 s	$\frac{9}{2}^+$	$\frac{1}{2}^-$	1.03 ±0.21	5.03±0.75
		1208, 1508,	15.49 min			0.85 ±0.07 [b])	4^{+6}_{-2}
		1581, 1637				1.92 ±0.15 [a])	
$^{100}Mo(\gamma, n)$	0^+	97.3	16.8 μs	$\frac{5}{2}^+$	$\frac{1}{2}^+$	0.85 ±0.24	1.72±0.25
		140.5	66.02 h				
$^{108}Pd(\gamma, n)$	0^+	214.5	22 s	$\frac{11}{2}^-$	$\frac{5}{2}^+$	0.5 ±0.2	3.4 ±0.5
		115	850 ns				
$^{110}Pd(\gamma, n)$	0^+	188	4.7 min	$\frac{11}{2}^-$	$\frac{5}{2}^+$	0.11 ±0.02	3.14±0.15
		113	390 ns	$\frac{11}{2}^-$	$\frac{1}{2}^+$	0.41 ±0.09	3.0 ±0.25
		87.7	13.47 h	$\frac{5}{2}^+$	$\frac{1}{2}^+$	3.2 ±0.7	3.3 ±0.4
$^{89}Y(\gamma, n)$	$\frac{1}{2}^-$	231.7	14.2 ms	8^+	1^+	0.056±0.008	
		442.3					
		392.5	300 μs				

[a]) Ref. [14]). [b]) Ref. [15]).

[14] P.E. Haustein et al., J. Inorg. Nucl. Chem. 33, 289 (1971)

[15] J. H. Carver et al., Nucl. Phys. 37, 449 (1962)

REF. T. Saito, S. Oikawa, K. Shoda, M. Sugawara, H. Miyase, and A. Suzuki Phys. Rev. C 16, 958 (1977)	ELEM. SYM.	A	Z
	Nd	142	60

METHOD	REF. NO.	
	77 Sa 5	hmg

REACTION	RESULT	EXCITATION ENERGY	SOURCE		DETECTOR		ANGLE
			TYPE	RANGE	TYPE	RANGE	
E,P	ABX	15-26	D	15-26	MAG-D		DST

The reaction ^{142}Nd$(e,e'p)^{141}$Pr has been used to study the $T_>$ giant resonance in ^{142}Nd. Cross sections for the ^{142}Nd$(\gamma,p)^{141}$Pr and ^{142}Nd$(\gamma,p_0+p_1)^{141}$Pr reactions were measured for excitation energies from 15.9 to 26.0 MeV. These cross sections are compared with previous ^{141}Pr$(p,\gamma_0)^{142}$Nd data. The angular distributions for the larger resonances at 17.3, 19.7, and 22.9 MeV were measured. Analysis indicates that the 22.9-MeV state has about a 13% $E2$ component. The decay proton spectra from the 19.7- and 22.9-MeV resonances were analyzed with a schematic shell model and indicates that the core excitation process is dominant in these isobaric analog resonances. The measured (γ,p) cross section together with the (γ,n) cross section is found to be fairly consistent with the predictions of isospin splitting theory.

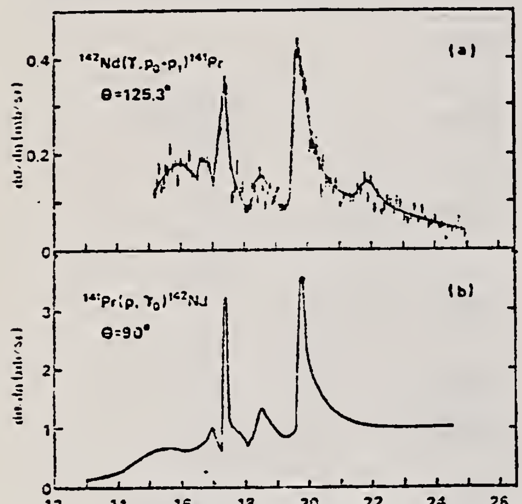

FIG. 2. (a) Differential cross section for the ^{142}Nd$(\gamma,p_0+p_1)^{141}$Pr reaction at $\theta_p = 125.3°$. The line drawn is merely to guide the eye. (b) Differential cross section for the ^{141}Pr$(p,\gamma_0)^{142}$Nd reaction at $\theta_\gamma = 90°$ from Ref. 7.

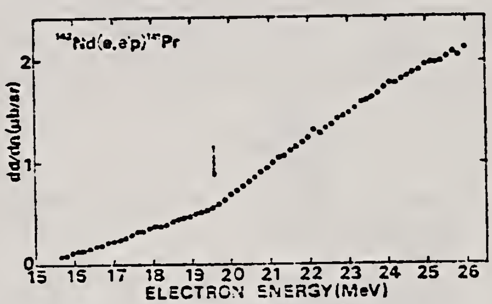

FIG. 3. Differential cross section for the ^{142}Nd$(e,e'p)^{141}$Pr reaction at $\theta = 125.3°$. The statistical errors of the cross section are smaller than the size of the circles. The arrow indicates the position of a big break.

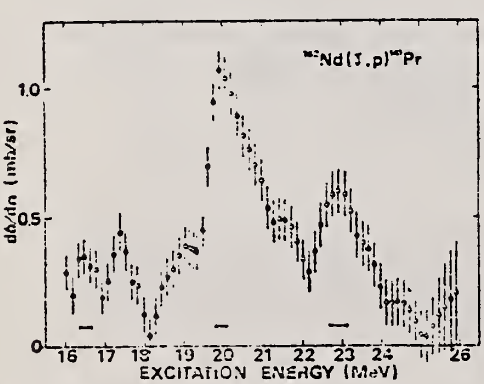

FIG. 4. Differential cross section for the ^{142}Nd$(\gamma,p)^{141}$Pr reaction at $\theta = 125.3°$. The vertical error bars indicate cross section error estimates, while the horizontal bars indicate the minimum full width at half-maximum allowed in the analysis.

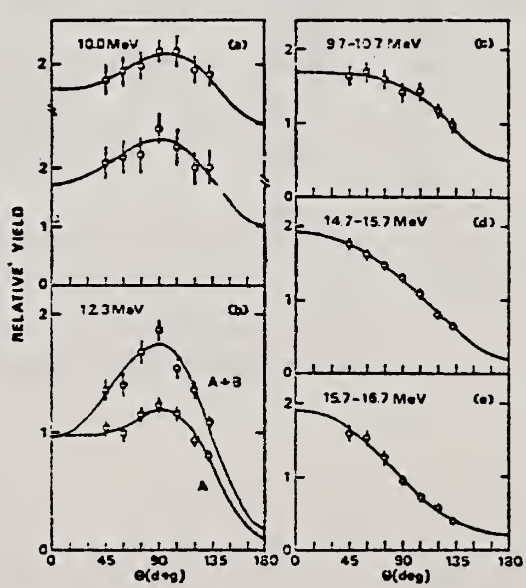

FIG. 6. Angular distributions for the ground-state transitions from the resonances and the continuum are shown on the left and right hand side, respectively. In the figure the energies of the proton group are shown. For the 10.0-MeV proton group the results for different bombarding energies are shown. In (b) the angular distributions of A and $A+B$ correspond to those of the proton groups indicated in Fig. 5. The solid curves show the Legendre polynomial fits.

[2]B. Goulard and S. Fallieros, Can. J. Phys. 45, 3221 (1967); R. Ö. Akyüz and S. Fallieros, Phys. Rev. Lett. 27, 1016 (1971).
[3]K. Shoda, T. Saito, M. Sugawara, H. Miyase, S. Oikawa, and A. Suzuki, Phys. Rev. C 4, 1842 (1971).
[7]M. Hasinoff, G. A. Fisher, P. Kurjan, and S. S. Hanna, Nucl. Phys. A195, 78 (1972).
[18]P. Carlos, H. Beil, R. Bergere, A. Lepretre, and A. Veyssiere, Nucl. Phys. A172, 437 (1971).
[19]M. Harchol, A. A. Jaffe, J. Zioni, and Ch. Drory, Nucl. Phys. A90, 473 (1967).

(over)

. DEPARTMENT OF COMMERCE
ONAL BUREAU OF STANDARDS

TABLE I. Excitation energies, integrated cross sections, radiative strengths, and branching ratios for the 1^- states in ^{142}Nd.

E_x (MeV) (γ,p)[a]	(γ,p_0+p_1)[a]	(p,γ_0)[b]	(p,n)[a]	$\int\sigma^R(\gamma,p)dE$[a] (mb MeV)	Γ_γ^R[a] (eV)	Γ_γ^{IAS}[b] (eV)	$\int\sigma^R(\gamma,p_0+p_1)dE$[a] (mb MeV)	$\int\sigma^R(\gamma,p_0+p_1)dE$[d] (mb MeV)	$\frac{\Gamma_{p_0}+\Gamma_{p_1}}{\Gamma}$[a]
16.5				3.2±1.0	76±23				
		16.85	16.9						
17.4	17.3	17.33	17.4	4.1±1.2	110±30	69±22	0.80±0.15	0.79±0.14	0.20±0.07
18.9	18.5	18.43		3.8±1.1	120±40		0.34±0.08		0.09±0.03
19.9	19.6	19.71		22 ±7	760±230	530±160	2.9 ±0.4	3.1 ±0.4	0.13±0.04
21.7	21.9			1.2±0.6	49±25		0.29±0.09		0.24±0.11
22.9				23 ±7	1100±300				

[a]Present data.
[b]Reference 7.
[c]Reference 19.
[d]Reference 3. $\int\sigma^R(\gamma,p_0+p_1)dE$ is corrected for the measured angular distribution.

TABLE II. Coefficients obtained from weighted least squares fits of the angular distributions for the ground-state transition to Legendre polynomials.

E_p (MeV)	E_x (MeV)	Present work a_1	a_2	a_3	Hashinoff *et al.* (Ref. 7) a_1	a_2
10.0	17.3	0.10±0.15	−0.34±0.13	0.07±0.23	0.05	−0.31
10.0	17.3	0.03±0.06	−0.32±0.05	0.12±0.10		
12.3[a]	19.6	0.25±0.09	−0.44±0.08	0.20±0.14	0.09	−0.58
12.3[b]	19.6	0.19±0.11	−0.57±0.10	0.10±0.15		
$9.7\le E_p\le 10.7$	$17.0\le E_x\le 18.0$	0.35±0.09	−0.20±0.09	0.05±0.13		
$14.7\le E_p\le 15.7$	$22.0\le E_x\le 23.0$	0.63±0.03	−0.13±0.02	0.02±0.04		
$15.7\le E_p\le 16.7$	$23.0\le E_x\le 24.0$	0.39±0.07	0.06±0.06	−0.04±0.10		

[a]$11.9\le E_p\le 12.5$.   [b]$11.9\le E_p\le 13.2$.

TABLE III. Coefficients obtained from weighted least squares fits of the angular distributions for the 17.3-, 19.7-, and 22.9-MeV resonances.

E_R (MeV)		a_1	a_2	a_3
17.3	$9.7\le E_p\le 10.8$	0.29±0.05	−0.22±0.05	0.10±0.08
	$4.7\le E_p\le 10.8$	0.13±0.01	−0.16±0.01	−0.01±0.02
19.7		0.15±0.11	−0.29±0.10	0.22±0.16
22.9		0.62±0.18	−0.27±0.17	−0.42±0.28

TABLE IV. Comparison of the experimental energy separation and relative strengths for $T_<$ and $T_>$ giant resonances with the theoretical predictions.

	(γ,p)[a]	(γ,n)[b]	Theory[c]
E_R (MeV)	19.7±0.2[d]	14.95±0.1	
	21.1±0.3[e]		
$\int\sigma dE$ (MeV mb)	33±10[f]	1950±150[f]	
	59±13[g]	2050±170[g]	
σ_{-1} (mb)	1.7±0.5[f]	130±10[f]	
	2.8±0.8[g]	135±11[g]	
$E_>-E_<$ (MeV)		4.8±0.2[d]	5.1
		6.2±0.3[e]	
$\frac{\sigma_{-1}(T_>)}{\sigma_{-1}(T_<)}$		0.013±0.004[f]	0.035
		0.021±0.007[g]	

[a]Present work.
[b]Reference 18.
[c]Reference 2.
[d]$E_>$ is evaluated by $\int_{17.5}^{22.0}\sigma(\gamma,p)dE/\int_{17.0}^{22.0}[\sigma(\gamma,p)/E]dE$.
[e]$E_>$ is evaluated by $\int_{17.0}^{26.0}\sigma(\gamma,p)dE/\int_{17.0}^{26.0}[\sigma(\gamma,p)/E]dE$.
[f]Integrated energy regions are 17.0–22.0 MeV and 9.5–22.0 MeV for (γ,p) and (γ,n) reactions, respectively.
[g]Integrated energy regions are 17.0–26.0 MeV and 9.5–26.0 MeV for (γ,p) and (γ,n) reactions, respectively.

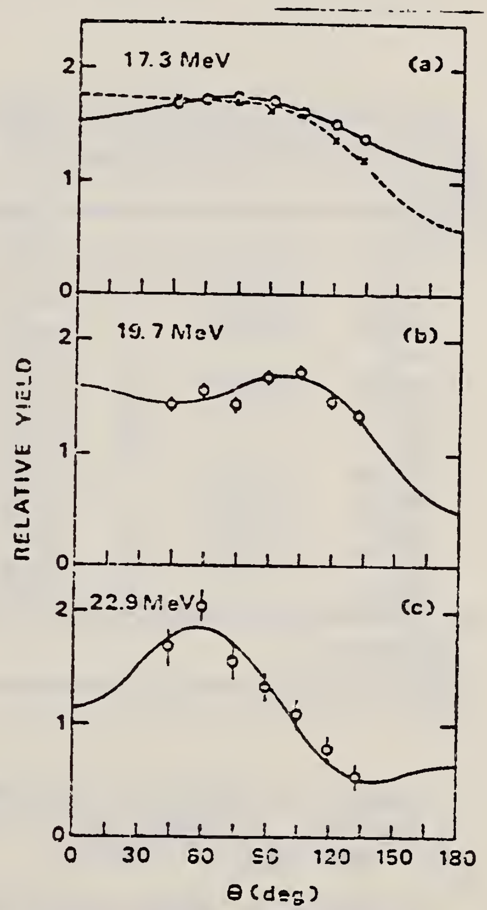

FIG. 9. Angular distributions for (a) 17.3-, (b) 19.7-, and (c) 22.9-MeV resonances. In (a) crosses and circles show the angular distribution for the p_0+p_1 groups and those for total protons, respectively, observed in bombardment of $E_p=18.0$ MeV. The solid curves show the Legendre polynomial fits.

REF.	ELEM. SYM.	A	Z
F.R. Metzger Phys. Rev. C 18, 1603 (1978)	Nd	142	60

METHOD	REF. NO.	
	78 Me 8	hg

REACTION	RESULT	EXCITATION ENERGY	SOURCE TYPE	SOURCE RANGE	DETECTOR TYPE	DETECTOR RANGE	ANGLE
$ G,G	LFT	1- 5	C	1- 5	SCD-D		DST

POL SCD GAMMA

The resonant scattering of electron bremsstrahlung by an enriched sample of ^{142}Nd has been studied for photon energies of up to 5 MeV. It provides estimates of the radiative widths for 13 levels. Based on the relative yields at scattering angles of 96° and 126°, unambiguous spin assignments were made to 6 of these levels. Where feasible, the yield measurements were supplemented by self-absorption data and by linear polarization studies. For the strongest excitation, at 3.425 MeV, the resonance fluorescence experiments led to its identification as a 1^- state with a radiative width $\Gamma_0 = 370 \pm 45$ MeV. The corresponding $E1$ strength is comparable to the $E1$ strengths measured in other even-even $N = 82$ nuclei for the 1^- member of the quintuplet arising from the coupling of the lowest octupole vibration to the 2_1^+ level. The sum of the excitation energies of the 2_1^+ state and the 3_1^- state in ^{142}Nd is consistent with such an interpretation of the 3.425-MeV level.

TABLE I. Spins and widths of ^{142}Nd levels, deduced from the yields of the reaction ^{142}Nd(γ,γ) at scattering angles of 96° and 126°. Standard deviations are listed throughout.

E_{level} (MeV)	$N(126°)/N(96°)$	Spin	Γ_0^2/Γ (meV)
1.576 (2)	0.45 ± 0.05	2	4.0 ± 0.3
2.385 (2)	0.52 ± 0.10	2	2.4 ± 0.4
2.583	...	1[a]	0.6 ± 0.7
2.846 (2)	0.40 ± 0.06	2	11.5 ± 1.0
3.046 (2)	0.34 ± 0.36	(2)	1.4 ± 0.6
3.128	...	1,2[b]	0.6 ± 0.9[c]
3.358	...	1,2[b]	0.1 ± 1.0[c]
3.425 (2)	1.19 ± 0.07	1	330 ± 40
4.095 (2)	1.20 ± 0.11	1	110 ± 20
4.145 (2)	1.09 ± 0.13	1	85 ± 15
4.255 (4)	1.5 ± 0.8	1,2	20 ± 7[c]
4.625 (3)	1.10 ± 0.24	(1)	100 ± 20
4.901 (3)	...	1,2	80 ± 30[c]

[a]See Ref. 15.
[b]According to Ref. 6.
[c]A spin of 1 ($g=3$) was assumed in calculating this width.

TABLE II. Self absorption by 11.87 g/cm^2 of Nd metal (natural composition), i.e., by 1.35×10^{22} ^{142}Nd nuclei/cm^2.

E_{level}	$\frac{N(\text{res. absorber})}{N(\text{comparison abs.})}$	Γ_0 (meV)[a]
3.425	0.52 ± 0.02	355 ± 30
4.095	0.82 ± 0.09	150 ± 100
4.145	0.87 ± 0.13	110 ± 130

[a]Assuming $\Gamma_0/\Gamma = 1$.

TABLE III. ^{142}Nd: Results of the experiments using the Ge(Li) polarimeter.

E (MeV)	$100 \times \frac{N_\parallel - N_\perp}{N_\parallel + N_\perp}$	Multipole character	J^π_{exc}
3.425	+1.9 ± 1.6	$E1$	1^-
4.095	−2.1 ± 4.2	$M1$ slightly favored	1^+
4.145	+8.9 ± 4.8	($E1$)	$1^{(-)}$

6
S. Raman, J.L. Foster, Jr., O. Dietzsch, D. Spalding, L. Bimbot, and B.H. Wildenthal, Nucl. Phys. A201, 21 (1973)
15
J. Tenenbaum, R. Moreh, and A. Nof, Nucl. Phys. A218, 95 (1974)

ND
A=143

ND
A=143

REF.	ELEM. SYM.	A	Z
P. Carlos, H. Beil, R Bergere, A. Lepretre, A. Veyssiere Nucl. Phys. A172, 437 (1971)	Nd	143	60
METHOD	REF. NO. 71 Ca 1		egf

REACTION		RESULT	EXCITATION ENERGY	SOURCE TYPE	SOURCE RANGE	DETECTOR TYPE	DETECTOR RANGE	ANGLE
G,N	394	ABX	9-20	D	8-20	MOD-I		4PI
G,2N	395+	ABX	9-20	D	8-20	MOD-I		4PI

394+

TABLE 2

Parameters of the one- or two-Lorentz line fits to the σ_T curves for neodymium isotopes: parameters for Ce and Er extracted from earlier results [13]) are also shown

	Ce	^{142}Nd	^{143}Nd	^{144}Nd	^{145}Nd	^{146}Nd	^{148}Nd	^{150}Nd	Er
σ_1 (mb)	360 ±15	359 ±15	360 ±15	317 ±15	297 ±20	308 ±16	263 ±15	174 ±20	225 ±15
Γ_1 (MeV)	4.35±0.05	4.43± 0.20	4.5 ±0.2	5.3 ± 0.25	6.5±0.4	6 ± 0.3	7.2± 0.3	3.3 ± 0.1	2.9 ±0.05
E_1 (MeV)	15.0 ± 0.10	14.95± 0.1	15 ± 0.1	15.05± 0.1	15 ± 0.15	14.8 ± 0.1	14.7± 0.15	12.3 ± 0.15	12.00± 0.1
σ_2 (mb)								223 ±20	260 ±15
Γ_2 (MeV)								5.2 ± 0.15	5.0 ± 0.05
E_2 (MeV)								16 ± 0.15	15.45± 0.1
$\frac{1}{2}\pi\sigma\Gamma$ MeV · b		2.5 ± 0.2	2.54± 0.2	2.6 ± 0.2	3.0± 0.3	2.9 ± 0.2	3.0± 0.2	2.7 ± 0.3	
$\frac{\frac{1}{2}\pi\sigma\Gamma}{0.06\, NZA^{-1}}$		1.20± 0.10	1.22± 0.10	1.25± 0.10	1.4± 0.15	1.35± 0.10	1.4± 0.1	1.27± 0.15	

13 R. Bergere, H. Beil, P. Carlos et A. Veyssiere, Nucl. Phys. A133, 417 (1969).

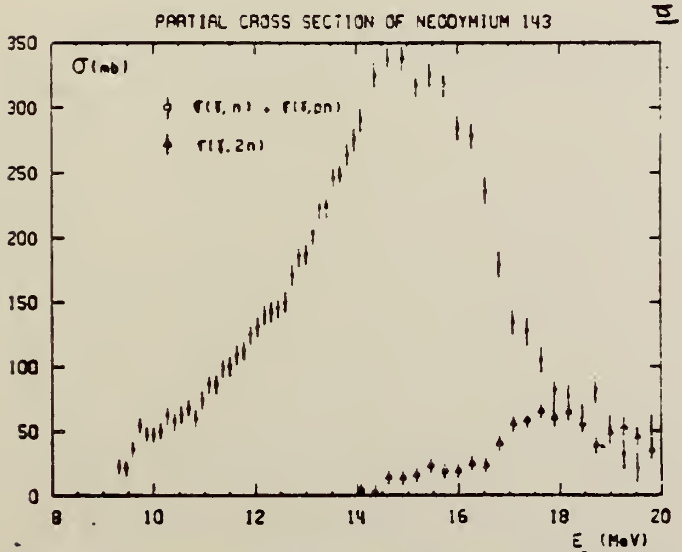

Fig. 3. Partial photoneutron cross sections $\sigma(\gamma, n)$ and $\sigma(\gamma, 2n)$ of ^{143}Nd.

(over)

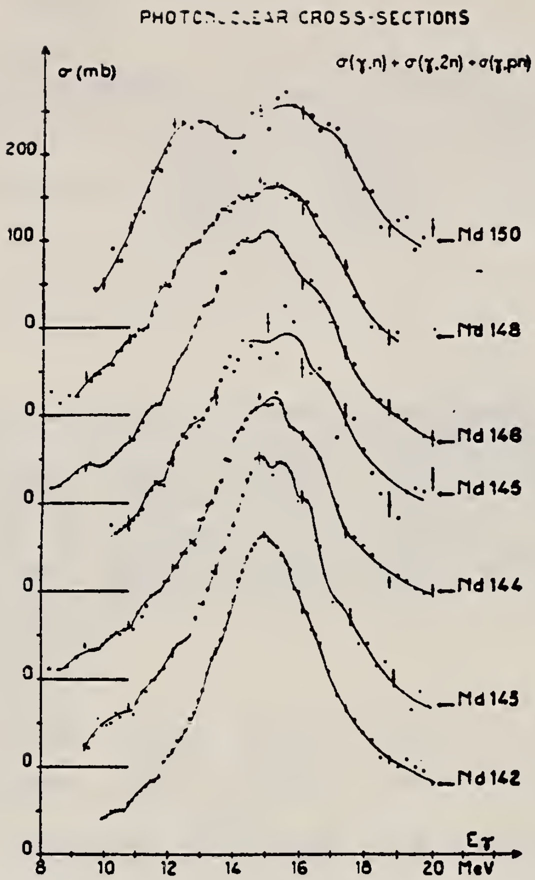

Fig. 9. Total photonuclear cross-section σ_T of neodymium isotopes. The full line drawn through the experimental points is merely meant to facilitate the identification of structure.

A=144

A=144

A=144

REF.	ELEM. SYM.	A	Z
J.P. Blanc, M. Lambert, C.F. Perdrisat Helva. Phys. Acta 36, 820 (1963)	Nd	144	60

METHOD	REF. NO.	
Radioactive source; photon scattering	63 Bl 2	NVB

REACTION	RESULT	EXCITATION ENERGY	SOURCE TYPE	SOURCE RANGE	DETECTOR TYPE	DETECTOR RANGE	ANGLE
G,G	ABX	2	D	2			
				(2.18)			

$\sigma = (0.26 \pm 0.18)\ 10^{-27}\ cm^2/atom$

$1.4 \times 10^{-14} \leq \tau \geq 3.4 \times 10^{-4}$ sec.

REF.	ELEM. SYM.	A	Z
P. Rice-Evans Proc. Phys. Soc. 82, 914 (1963)	Nd	144	60

METHOD	REF. NO.	
radioactive source; photon scattering; NaI spectrometer	63 Ri 2	NVB

REACTION	RESULT	EXCITATION ENERGY	SOURCE TYPE	SOURCE RANGE	DETECTOR TYPE	DETECTOR RANGE	ANGLE
G,G	LFT	2	D	2	NAI-D		90
		(2.18)		(2.18)			

SEP ISØTPS, G-WDTH

$\sigma = 1.93 \times 10^{-28} cm^2$

$\Gamma = 0.033$ eV

Lifetime $\tau \geq (2.0 \pm 0.4)\ 10^{-14}$ sec.

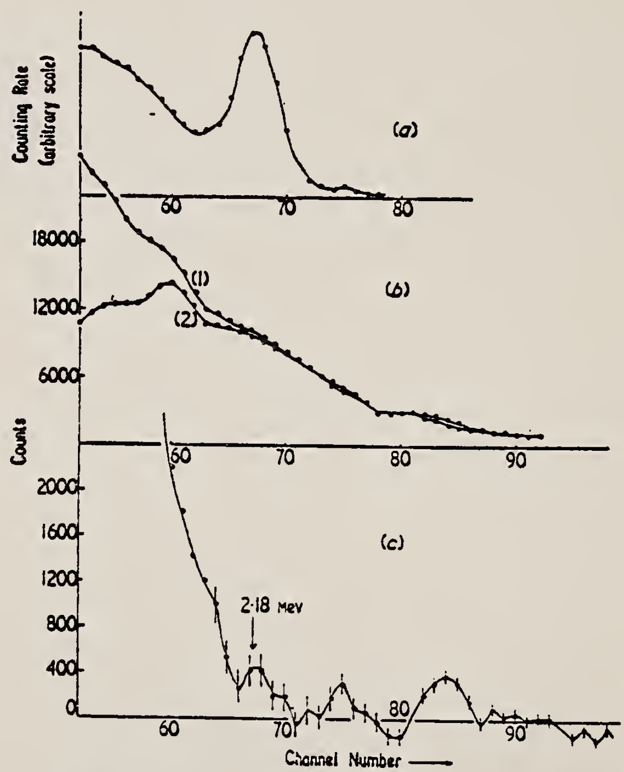

Figure 3. (*a*) Scintillation counter calibration; the 2·18 MeV γ ray as observed with the source in the position of the scatterer. (*b*) Actual pulse height distributions: (1) with source and scatterer present, (2) with only scatterer present (for 10 000 minute counting time). (*c*) Excess counts due to presence of ^{144}Nd source (for counting time of 10 000 minutes).

REF.	ELEM. SYM.	A	Z
F. R. Metzger Phys. Rev. 187, 1700 (1969)	Nd	144	60
METHOD	REF. NO. 69 Me 3		hmg

REACTION	RESULT	EXCITATION ENERGY	SOURCE TYPE	SOURCE RANGE	DETECTOR TYPE	DETECTOR RANGE	ANGLE
G,G	LFT	2,2	C	2,2	SCD-D		DST
		(2.074,2.186)		(2.174, 2.186)			(98,127)

B(EL), 2.074, 2.186

The resonant scattering of γ rays has been observed for the 2.186-MeV 1^- state in Nd^{144}. The electron bremsstrahlung from a Van de Graaff accelerator served as the exciting γ radiation. The scattered radiation was observed with a 40-cm^3 Ge(Li) detector. If the value $\Gamma_0/\Gamma=0.71$ is used for the branching ratio, the measured scattering yield corresponds to a partial width $\Gamma_0=(3.1\pm0.4)\times10^{-2}$ eV for the ground-state transition. The reduced $E1$ transition probability for the ground-state transition is intermediate between the $B(E1)$'s for the "spherical" nucleus Sm^{148} and the deformed nucleus Sm^{152}. A level with spin 2 and with an excitation energy of 2.074 MeV has also been excited in Nd^{144}. From the observed scattering, $\Gamma_0^2/\Gamma=(1.2\pm0.3)\times10^{-2}$ eV is obtained for this level.

REF.			ELEM. SYM.	A	Z
P. Carlos, H. Beil, R. Bergere, A. Lepretre, A. Veyssiere Nucl. Phys. A172, 437 (1971)			Nd	144	60
METHOD			REF. NO.		
			71 Ca 1		egf

REACTION		RESULT	EXCITATION ENERGY	SOURCE TYPE	SOURCE RANGE	DETECTOR TYPE	DETECTOR RANGE	ANGLE
G,N	397	ABX	8-20	D	8-20	MOD-I		4PI
G,2N	398+	ABX	8-20	D	8-20	MOD-I		4PI

397+

Table 2

Parameters of the one- or two-Lorentz line fits to the σ_T curves for neodymium isotopes: parameters for Ce and Er extracted from earlier results [13]) are also shown

	Ce	^{142}Nd	^{143}Nd	^{144}Nd	^{145}Nd	^{146}Nd	^{148}Nd	^{150}Nd	Er
σ_1 (mb)	360 ±15	359 ±15	360 ±15	317 ±15	297 ±20	308 ±16	263 ±15	174 ±20	225 ±15
Γ_1 (MeV)	4.35±0.05	4.43± 0.20	4.5 ±0.2	5.3 ± 0.25	6.5±0.4	6 ± 0.3	7.2± 0.3	3.3 ± 0.1	2.9 ±0.05
E_1 (MeV)	15.0 ± 0.10	14.95± 0.1	15 ± 0.1	15.05± 0.1	15 ± 0.15	14.8 ± 0.1	14.7± 0.15	12.3 ± 0.15	12.00± 0.1
σ_2 (mb)								223 ±20	260 ±15
Γ_2 (MeV)								5.2 ± 0.15	5.0 ± 0.05
E_2 (MeV)								16 ± 0.15	15.45± 0.1
$\frac{1}{2}\pi\sigma\Gamma$ MeV · b		2.5 ± 0.2	2.54± 0.2	2.6 ± 0.2	3.0± 0.3	2.9 ± 0.2	3.0± 0.2	2.7 ± 0.3	
$\frac{\frac{1}{2}\pi\sigma\Gamma}{0.06\, NZA^{-1}}$		1.20± 0.10	1.22± 0.10	1.25± 0.10	1.4± 0.15	1.35± 0.10	1.4± 0.1	1.27± 0.15	

[13] R. Bergere, H. Beil, P. Carlos et A. Veyssiere, Nucl. Phys. A133, 417 (1969).

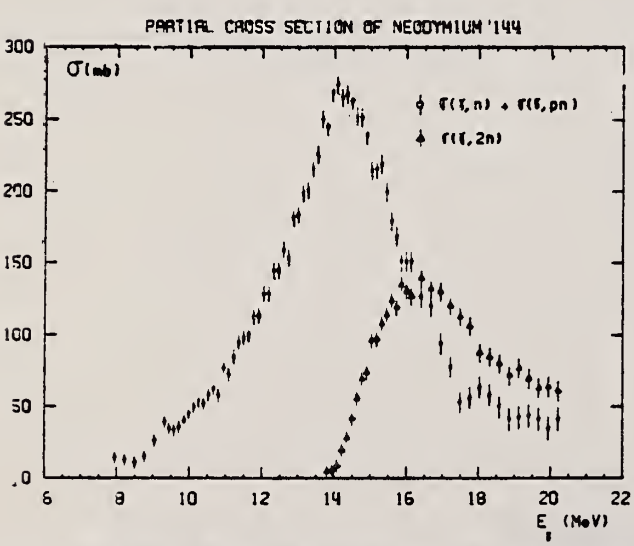

Fig. 4. Partial photoneutron cross sections $\sigma(\gamma, n)$ and $\sigma(\gamma, 2n)$ of ^{144}Nd.

(over)

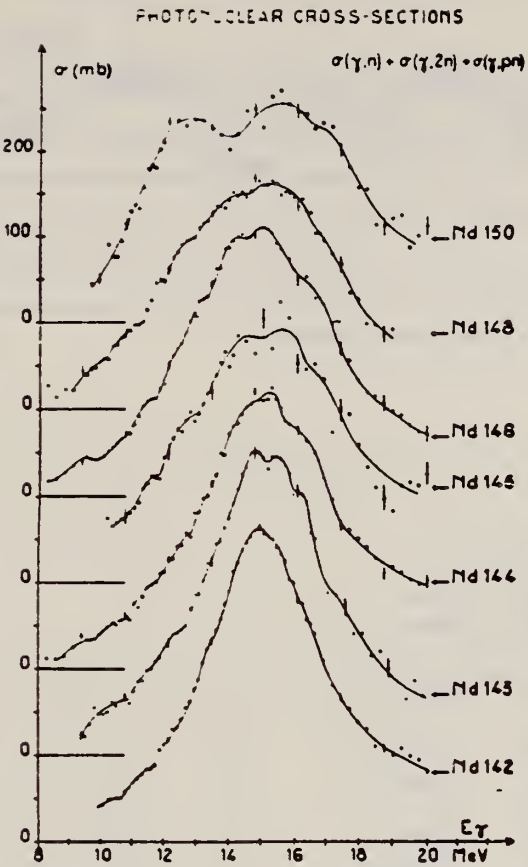

Fig. 9. Total photonuclear cross-section σ_T of neodymium isotopes. The full line drawn through the experimental points is merely meant to facilitate the identification of structure.

REF.	ELEM. SYM.	A	Z
P. E. Haustein and A. F. Voigt J. inorg. nucl. Chem. 33, 289 (1971)	Nd	144	60
METHOD	REF. NO. 71 Ha 2		egf

REACTION	RESULT	EXCITATION ENERGY	SOURCE TYPE	SOURCE RANGE	DETECTOR TYPE	DETECTOR RANGE	ANGLE
G,3N	RLY	24-70	C	70	ACT-I		4PI

Isomer ratio = (yield to low spin state)/(yield to high spin state) ISOMER RATIO

Table 2. Isomer ratio measurements for ^{91}Mo, ^{137}Ce, and ^{141}Nd

Reaction	Isomer ratio	I^π Target	I^π Ground state	I^π Isomer	Threshold (MeV)	$41A^{-1/3}$ (MeV)
^{92}Mo(γ, n)^{91}Mo	1·92 ± 0·15	0^+	9/2$^+$	1/2$^-$	13·13	16·60
^{94}Mo(γ, 3n)^{91}Mo	1·59 ± 0·16	0^+			30·72	16·52
^{138}Ce(γ, n)^{137}Ce	3·1	0^+	3/2$^+$	11/2$^+$	10·31	15·30
^{140}Ce(γ, 3n)^{137}Ce	1·10 ± 0·12	0^+			26·34	15·26
^{142}Nd(γ, n)^{141}Nd	5·2 ± 0·3	0^+	3/2$^+$	11/2$^-$	9·79	15·22
^{144}Nd(γ, 3n)^{141}Nd	1·80 ± 0·25	0^+			23·67	15·17

Nd
A=145

Nd
A=145

Nd
A=145

.er. J. Haipern, and E. G. Muirhead

..... .e. 118, 1302-12 (1960)

ELEM. SYM.	A	Z
Nd	145	60

THOD

Betatron; neutron threshold; ion chamber

REF. NO.	
60 Ge 3	NVB

REACTION	RESULT	EXCITATION ENERGY	SOURCE		DETECTOR		ANGLE
			TYPE	RANGE	TYPE	RANGE	
G,N	NØX	THR	C	THR	BF3-I		4 PI

THRESHØLD

TABLE I. Summary and comparison of neutron separation energies inferred from present threshold measurements with values predicted from mass data and reaction energies. All energies are expressed in the center-of-mass system in Mev.

Reaction	No. runs	Present results	Other results	Method	Reference
$Nd^{145}(\gamma,n)Nd^{144}$	1	$\leqslant$ 6.38 ±0.16	5.97 ±0.19	mass data	p

[p] W. H. Johnson, Jr., and A. O. Nier, Phys. Rev. 105, 1014 (1957).

TABLE II. Comparison of measured threshold energies with neutron binding energies predicted by mass data for transitions with $\Delta I \geq 7/2$. All energies in Mev.

Reaction	ΔI[a]	Observed threshold	Mass data Q value	$E_{th}-Q$	Excited state energy
$Cr^{53}(\gamma,n)Cr^{52}$	7/2	12.18±0.14	12.053±0.004[b]	0.13±0.14	...
$Y^{89}(\gamma,n)Y^{88}$	7/2	11.59±0.08	11.53 ±0.40[c]	0.06±0.41	0.387[d]
$In^{115}(\gamma,n)In^{114}$	7/2	9.22±0.03	9.35 ±0.43[c]	−0.13±0.43	0.191[a]
$Ce^{142}(\gamma,n)Ce^{141}$	(7/2)[e]	7.24±0.07	6.97 ±0.07[f]	0.27±0.10	...
$Nd^{145}(\gamma,n)Nd^{144}$	7/2	6.38±0.16	5.97 ±0.19[f]	0.41±0.25	0.690[a]
$Sm^{149}(\gamma,n)Sm^{148}$	7/2	6.45±0.16	5.87 ±0.28[f]	0.58±0.33	0.562[a]
$Er^{167}(\gamma,n)Er^{166}$	7/2	6.65±0.08	6.45 ±0.06[g]	0.20±0.10	0.081[a]
$Hf^{177}(\gamma,n)Hf^{176}$	7/2	6.69±0.03	6.28 ±0.06[g]	0.64±0.07	0.088[a]
$Hf^{179}(\gamma,n)Hf^{178}$	9/2	6.31±0.07	6.17 ±0.06[g]	0.14±0.09	0.093[a]
$Hf^{180}(\gamma,n)Hf^{179}$	9/2	7.85±0.11	7.32 ±0.06[g]	0.53±0.13	0.375[a]

[a] D. Strominger, J. M. Hollander, and G. T. Seaborg, Revs. Modern Phys. 30, 585 (1958).
[b] C. F. Giese and J. L. Benson, Phys. Rev. 110, 712 (1958).
[c] Henry E. Duckworth, *Mass Spectroscopy* (Cambridge University Press, New York, 1958), p. 177.
[d] S. Dzelepov and L. K. Peker, Atomic Energy of Canada Limited Report Tr. AECL-457 (unpublished).
[e] The discrepancy in the case of Ce^{142} predicts a ground-state spin for Ce^{142} of 0, since the spin of Ce^{141} is known to be 7/2.
[f] W. H. Johnson, Jr., and A. O. Nier, Phys. Rev. 105, 1014 (1957).
[g] W. H. Johnson, Jr., and V. B. Bhanot, Phys. Rev. 107, 6 (1957).

REF.	ELEM. SYM.	A	Z
P. Carlos, H. Beil, R. Bergere, A. Lepretre, A. Veyssiere Nucl. Phys. A172, 437 (1971)	Nd	145	60
METHOD	REF. NO. 71 Ca 1		egf

REACTION	RESULT	EXCITATION ENERGY	SOURCE TYPE	SOURCE RANGE	DETECTOR TYPE	DETECTOR RANGE	ANGLE
G,N 400	ABX	10-20	D	8-20	MOD-I		4PI
G,2N 401+	ABX	10-20	D	8-20	MOD-I		4PI

400+

TABLE 2

Parameters of the one- or two-Lorentz line fits to the σ_T curves for neodymium isotopes: parameters for Ce and Er extracted from earlier results [13]) are also shown

	Ce	^{142}Nd	^{143}Nd	^{144}Nd	^{145}Nd	^{146}Nd	^{148}Nd	^{150}Nd	Er
σ_1 (mb)	360 ±15	359 ±15	360 ±15	317 ±15	297 ±20	308 ±16	263 ±15	174 ±20	225 ±15
Γ_1 (MeV)	4.35 ±0.05	4.43 ± 0.20	4.5 ±0.2	5.3 ± 0.25	6.5 ±0.4	6 ± 0.3	7.2 ± 0.3	3.3 ± 0.1	2.9 ±0.05
E_1 (MeV)	15.0 ± 0.10	14.95 ± 0.1	15 ± 0.1	15.05 ± 0.1	15 ± 0.15	14.8 ± 0.1	14.7 ± 0.15	12.3 ± 0.15	12.00 ± 0.1
σ_2 (mb)								223 ±20	260 ±15
Γ_2 (MeV)								5.2 ± 0.15	5.0 ± 0.05
E_2 (MeV)								16 ± 0.15	15.45 ± 0.1
$\frac{1}{2}\pi\sigma\Gamma$ MeV · b		2.5 ± 0.2	2.54 ± 0.2	2.6 ± 0.2	3.0 ± 0.3	2.9 ± 0.2	3.0 ± 0.2	2.7 ± 0.3	
$\frac{\frac{1}{2}\pi\sigma\Gamma}{0.06\,NZA^{-1}}$		1.20 ± 0.10	1.22 ± 0.10	1.25 ± 0.10	1.4 ± 0.15	1.35 ± 0.10	1.4 ± 0.1	1.27 ± 0.15	

[13] R. Bergere, H. Beil, P. Carlos et A. Veyssiere, Nucl. Phys. A133, 417 (1969).

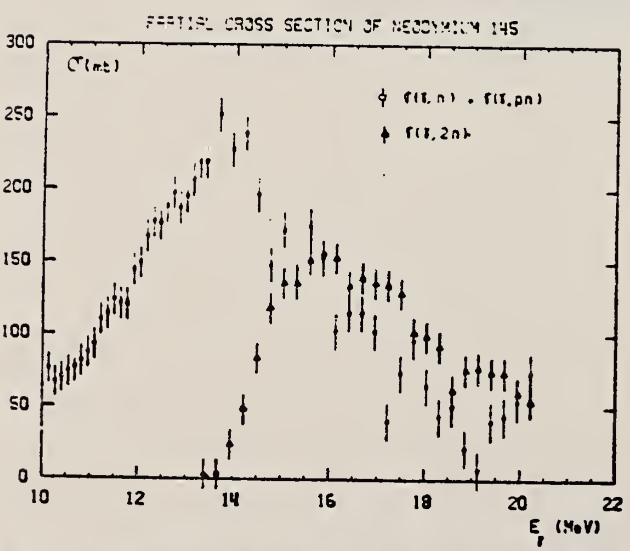

Fig. 5. Partial photoneutron cross sections $\sigma(\gamma, n)$ and $\sigma(\gamma, 2n)$ of ^{145}Nd.

(over)

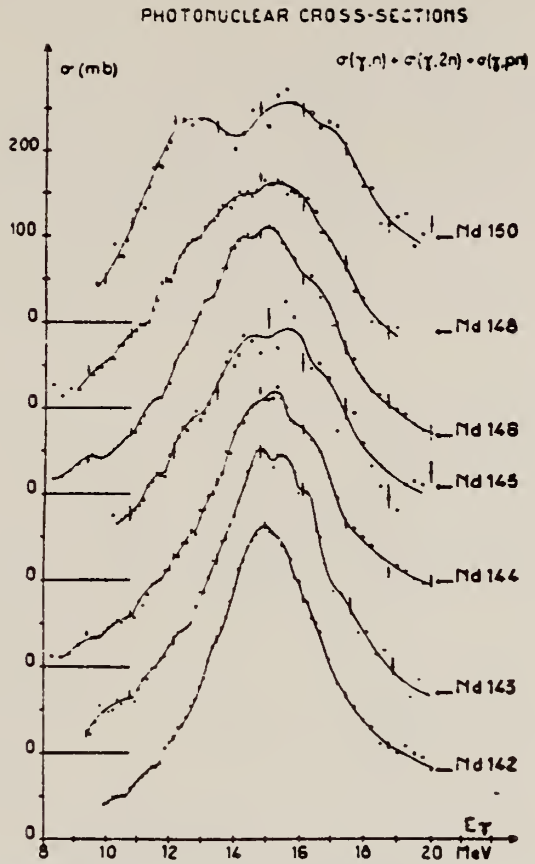

Fig. 9. Total photonuclear cross-section σ_T of neodymium isotopes. The full line drawn through the experimental points is merely meant to facilitate the identification of structure.

IID
A=146

IID
A=146

IID
A=146

REF.	EL EM. SYM.	A	Z
P. Carlos, H. Beil, R. Bergere, A. Lepretre, A. Veyssiere Nucl. Phys. A172, 437 (1971)	Nd	146	60
METHOD	REF. NO. 71 Ca 1		egf

REACTION		RESULT	EXCITATION ENERGY	SOURCE TYPE	SOURCE RANGE	DETECTOR TYPE	DETECTOR RANGE	ANGLE
G,N	403	ABX	8-20	D	8-20	MOD-I		4PI
G,2N	404+	ABX	8-20	D	8-20	MOD-I		4PI
								403+

Table 2

Parameters of the one- or two-Lorentz line fits to the σ_T curves for neodymium isotopes: parameters for Ce and Er extracted from earlier results [13]) are also shown

	Ce	^{142}Nd	^{143}Nd	^{144}Nd	^{145}Nd	^{146}Nd	^{148}Nd	^{150}Nd	Er
σ_1 (mb)	360 ±15	359 ±15	360 ±15	317 ±15	297 ±20	308 ±16	263 ±15	174 ±20	225 ±15
Γ_1 (MeV)	4.35±0.05	4.43± 0.20	4.5 ±0.2	5.3 ± 0.25	6.5±0.4	6 ± 0.3	7.2± 0.3	3.3 ± 0.1	2.9 ±0.05
E_1 (MeV)	15.0 ± 0.10	14.95± 0.1	15 ± 0.1	15.05± 0.1	15 ± 0.15	14.8 ± 0.1	14.7± 0.15	12.3 ± 0.15	12.00± 0.1
σ_2 (mb)								223 ±20	260 ±15
Γ_2 (MeV)								5.2 ± 0.15	5.0 ± 0.05
E_2 (MeV)								16 ± 0.15	15.45± 0.1
$\frac{1}{2}\pi\sigma\Gamma$ MeV · b		2.5 ± 0.2	2.54± 0.2	2.6 ± 0.2	3.0± 0.3	2.9 ± 0.2	3.0± 0.2	2.7 ± 0.3	
$\frac{\frac{1}{2}\pi\sigma\Gamma}{0.06\, NZA^{-1}}$		1.20± 0.10	1.22± 0.10	1.25± 0.10	1.4± 0.15	1.35± 0.10	1.4± 0.1	1.27± 0.15	

[13] R. Bergere, H. Beil, P. Carlos et A. Veyssiere, Nucl. Phys. A133, 417 (1969).

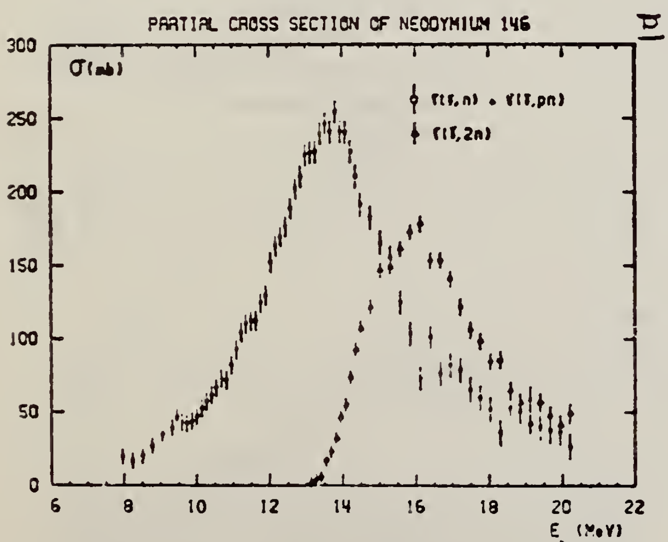

Fig. 6. Partial photoneutron cross sections $\sigma(\gamma, n)$ and $\sigma(\gamma, 2n)$ of ^{146}Nd.

(over)

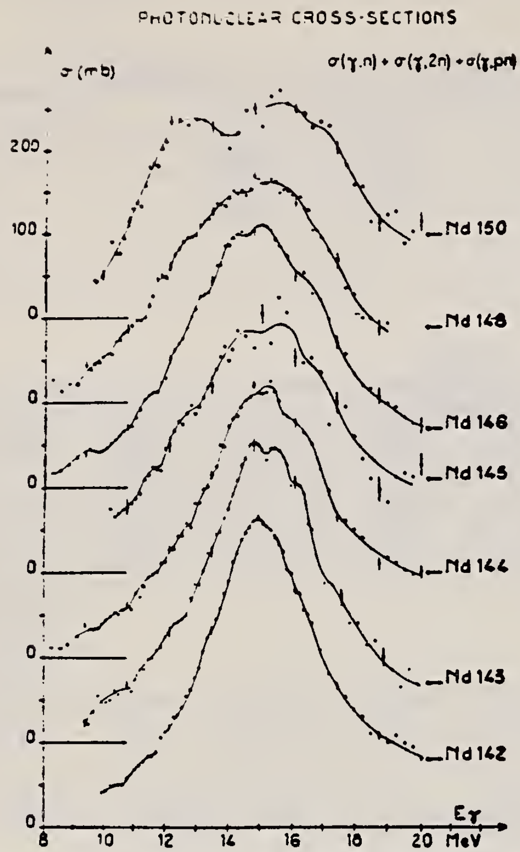

Fig. 9. Total photonuclear cross-section σ_T of neodymium isotopes. The full line drawn through the experimental points is merely meant to facilitate the identification of structure.

REF.	D. W. Madsen, L. S. Cardman, J. R. Legg, C. K. Bockelman Nucl. Phys. A168, 97 (1971)	ELEM. SYM.	A	Z
		Nd	146	60
METHOD		REF. NO.		
		71 Ma 1		egf

REACTION	RESULT	EXCITATION ENERGY	SOURCE		DETECTOR		ANGLE
			TYPE	RANGE	TYPE	RANGE	
E,E/	FMF	0	D	41	MAG-D		DST

0 = 0.45

Table 11

A comparison of this experiment's $B(EL\uparrow)$ values with those of other experiments and theory

Nucleus	State (MeV)	This work	Pulsed beam	Heavy particle Coulomb excitation	Theory
			2^+ states		
^{142}Nd	1.57	13.1 ± 1.7		25.0 ± 7.3 [a] 19.1 ± 2.3 [b] 15.5 ± 7.8 [c]	16.4 [d] 16.3 [e]
^{142}Nd	2.09	4.1 ± 1.1			
^{146}Nd	0.45	30.9 ± 4.6		28.5 ± 0.4 [b] 28.1 ± 6.6 [a]	92.1 [d]
^{150}Nd	0.13	62.9 ± 10.5	113.9 ± 1.8 [f] 116.8 ± 3.2 [g] 112.4 ± 5.1 [h]	112.7 ± 4.2 [i]	
			3^- state		
^{142}Nd	2.09	28.6 ± 5.0		52 ± 21 [j]	

[a]) Ref. [39]). [b]) Ref. [40]). [c]) Ref. [41]). [d]) Ref. [37]). [e]) Ref. [42]). [f]) Ref. [43]). [g]) Ref. [44]). [h]) Ref. [45]). [i]) Ref. [38]). [j]) Ref. [33]).

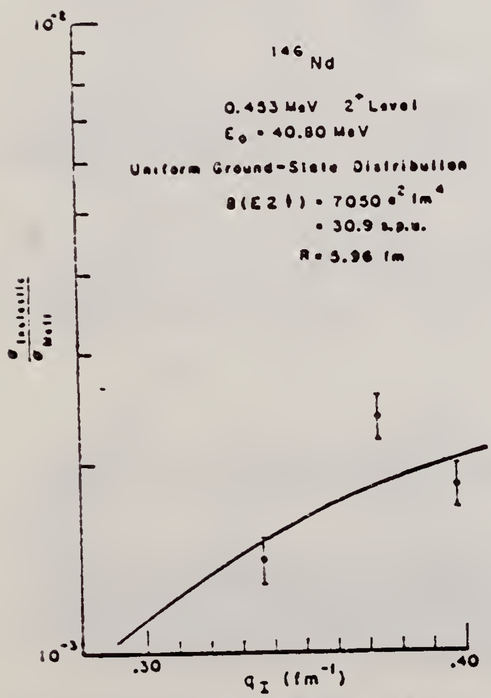

Fig. 16. Inelastic form factors for the 2$^+$ level at 453 keV in ^{146}Nd as a function of inelastic momentum transfer. The experimental points are the findings of this experiment and the solid line is the best fit assuming a uniform ground state charge distribution with $R = 4.96$ fm and creating a pseudo delta function for $\rho_{tr}^{(3)}$ in eq. (17).

33 O. Hansen et al., Nucl. Phys. 42 (1963) 197.
37 L. S. Kisslinger et al., Rev. Mod. Phys. 35 (1963) 853.
38 J. Bjerregard et al., Nucl. Phys. 44 (1963) 280.
39 G. A. Burginyon, Thesis, Yale University (1967) unpub.
40 D. Eccleshall et al., Nucl. Phys. 78 (1966) 481.
41 O. Nathan et al., Nucl. Phys. 21 (1960) 631.
42 M. Rho, Nucl. Phys. 65 (1965) 497.
43 J. D. Kurfess et al., Phys. Rev. 161 (1967) 1185.
44 F. W. Richter et al., Z. Phys. 213 (1968) 202.
45 M. Birk et al., Phys. Rev. 116 (1959) 730.

REF.	O. V. Vasil'ev, V. A. Semenov, and S. F. Semenko Yad. Fiz. <u>13</u>, 463 (1971) Sov. J. Nucl. Phys. <u>13</u>, 259 (1971)	ELEM. SYM. Nd	A 146	Z 60
METHOD		REF. NO. 71 Va 2		hmg

REACTION	RESULT	EXCITATION ENERGY	SOURCE TYPE	SOURCE RANGE	DETECTOR TYPE	DETECTOR RANGE	ANGLE
G,XN	ABX	7-24	C	7-24	BF3-I		4PI
		(7.6-23.25)		(7.6-23.25)			

Table II. Parameters of giant dipole resonance

Isotope	σ_1, mb	E_1, MeV	Γ_1, MeV	$\sigma_{int\,1}$, MeV·b	σ_2, mb	E_2, MeV	Γ_2, MeV	$\sigma_{int\,2}$, MeV·b	σ_{int}	$\frac{\sigma_{int}}{0.06\,NZ/A}$	$\frac{\sigma_{int\,2}}{\sigma_{int\,1}}$	$\frac{E_2}{E_1}$	β_{eff}
Nd^{146}	332	13,8	4,1						2,12	1,00			
Sm^{148}	335	14,1	4,0						2,08	0,96			
Gd^{152}	147	12,0	3,0	0,693	259	15,0	3,2	1,29	1,99	0,90	1,87	1,25	0,28
Gd^{154}	161	11,9	2,4	0,612	250	15,0	3,5	1,39	2,00	0,89	2,27	1,26	0,29
Gd^{156}	180	11,9	2,6	0,739	243	15,2	3,6	1,37	2,11	0,94	1,86	1,27	0,31
Gd^{158}	165	11,7	2,6	0,662	249	14,9	3,8	1,49	2,16	0,94	2,25	1,28	0,32
Eu^{151}	285	14,0	4,5						2,02	0,92			
Eu^{153}	159	11,9	2,3	0,563	237	15,1	3,0	1,34	1,90	0,86	2,39	1,27	0,31

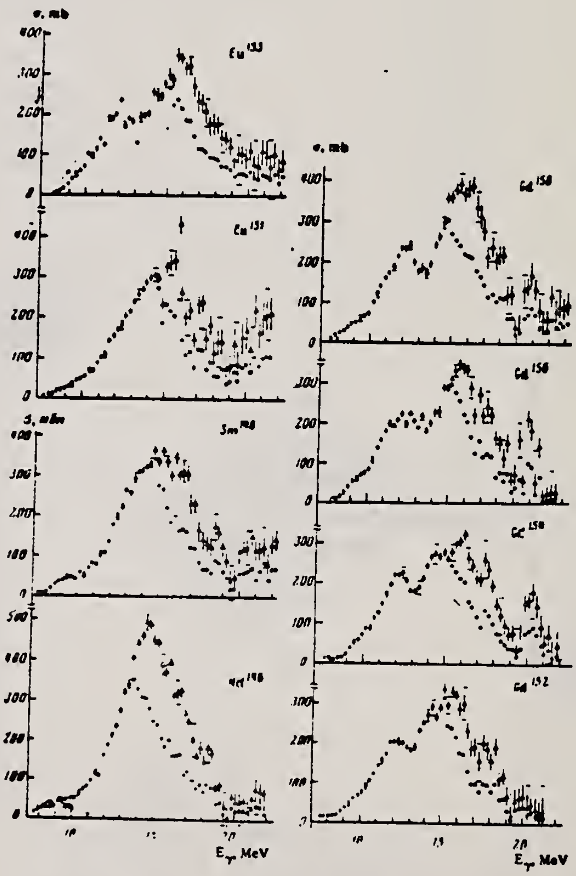

FIG. 1. Photoneutron cross sections and photoabsorption cross sections of Nd^{146}, Sm^{148}, Eu^{151}, Eu^{153}, Gd^{152}, Gd^{154}, Gd^{156} and Gd^{158}. Statistical and rms experimental errors are shown (the latter horizontal bars at 9.42 MeV, 10.42 MeV etc.) At photon energies above the (γ, 2n) threshold the photoabsorption cross section errors are not shown.

REF.	ELEM. SYM.	A	Z
Z. Berant, J. Tenenbaum and R. Moreh Nucl. Phys. A276, 221 (1977)	Nd	146	60
METHOD	REF. NO. 77 Be 7		egf

REACTION	RESULT	EXCITATION ENERGY	SOURCE TYPE	SOURCE RANGE	DETECTOR TYPE	DETECTOR RANGE	ANGLE
G,G	LFT	7	D	7	SCD-D		DST
	-	-					

7=7.163 MeV

TABLE 2

The γ-line energies E_γ of the scattered radiation from $^{144-146}$Nd together with level energies E_x and angular distribution coefficients A

Isotope	E_γ ($\pm$3 keV)	Intensity	A	E_x ($\pm$3 keV)	J^π	E_x ^{a})
^{146}Nd	6709	13$\pm$1	0.03$\pm$0.04	454	2	453.8
	5475	3$\pm$1		1688	0, 1, 2	1687
	5383	5$\pm$1	0.03$\pm$0.13	1778	2	1777.3
	4807	3$\pm$1		2349	0, 1, 2	2350
	4701	3$\pm$1		2460	0, 1, 2	2462
	4583	2$\pm$1		2578	0, 1, 2	2575
	3891	1$\pm$1		3280	0, 1, 2	3279
	7163	100	0.46$\pm$0.09	7163	1$^-$-	
^{145}Nd	7096	< 1		67		67.0
	6107	< 3		1056		1052
	5569	2$\pm$1		1594		1593.5
	5408	< 1		1755		1760
	7163	< 3		7163		
^{144}Nd	5820	< 1		695		696.49
	6515	< 1		6515		

The spins J^π are based either on the values of A or on the assumption that the resonance level is deexcited by dipole transitions.

^{a}) Only those levels of refs. [1,9,10]) are listed which were also observed in the present work.

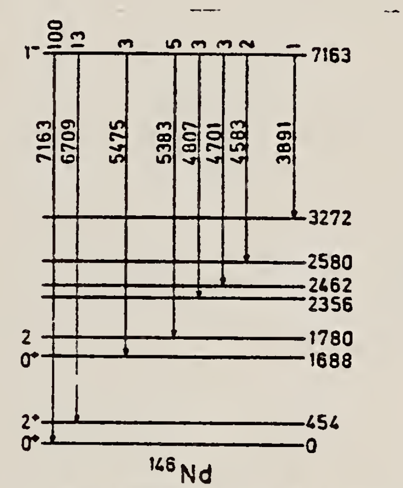

Fig. 3. Decay scheme of the 7163 keV level of ^{146}Nd showing level energies and relative intensities. The level spins are those obtained from the results of the present work (table 2).

[1] T.W. Burrows, Nucl. Data 14, no. 4 413 (1975)
[9] T.W. Burrows, Nucl. Data 12, 203 (1975)
[10] T.W. Burrows and R.L. Auble, Nucl. Data 16, 231 (1975)

TABLE 4

Values of Γ, Γ_0, and the energy separation δ (between the incident γ-line and the resonance level)

Scatterer	E_γ (keV)	Γ (meV)	Γ_0 (meV)	δ (eV)
^{146}Nd	7163	125$\pm$50	41$\pm$13	13.7$\pm$0.6
^{154}Sm	6465	105$\pm$50	25$\pm$13	3.6$\pm$2.0

Nd
A=148

Nd
A=148

Nd
A=148

REF.

O. V. Vasilijev, G. N. Zalesny, S. F. Semenko, V. A. Semenov
Phys. Letters 30B, 97 (1969)

ELEM. SYM.	A	Z
Nd	148	60

METHOD

REF. NO.	
69 Va 2	egf

REACTION	RESULT	EXCITATION ENERGY	SOURCE TYPE	SOURCE RANGE	DETECTOR TYPE	DETECTOR RANGE	ANGLE
G,XN	ABX	8-23	C	8-23	BF3-I		4PI

208

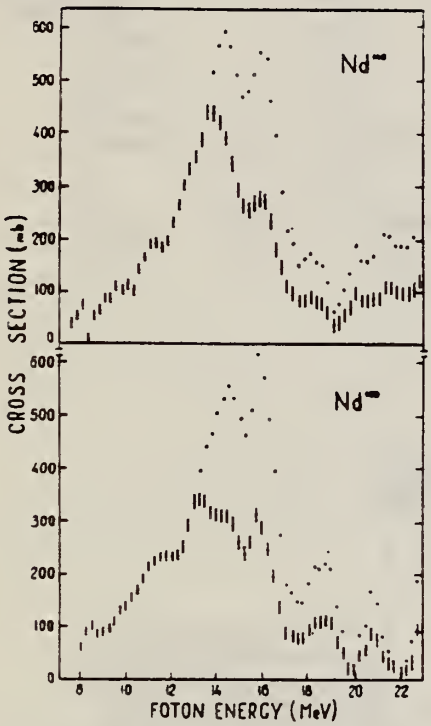

Fig. 2. The photoneutron cross section $\sigma(\gamma, n)$ and the photoabsorption cross sections σ_{tot} for ^{148}Nd and ^{150}Nd . The σ_{tot} are represented by dots. At the energies where σ_{tot} and $\sigma(\gamma, n)$ differ, the latter is represented by circles. Only statistical errors of σ_{tot} are plotted.

REF.	ELEM. SYM.	A	Z
O. V. Vasil'ev, G. N. Zalesnyi, S. F. Semenko, and V. A. Semenov Yad. Fiz. 10, 460 (1969) Sov. J. Nucl. Phys. 10, 263 (1970)	Nd	148	60

METHOD	REF. NO.	
	69 Va 3	egf

REACTION	RESULT	EXCITATION ENERGY	SOURCE TYPE	SOURCE RANGE	DETECTOR TYPE	DETECTOR RANGE	ANGLE
G,XN	ABX	8-22	C	8-22	BF3-I		4PI

SEE 69VA2 238

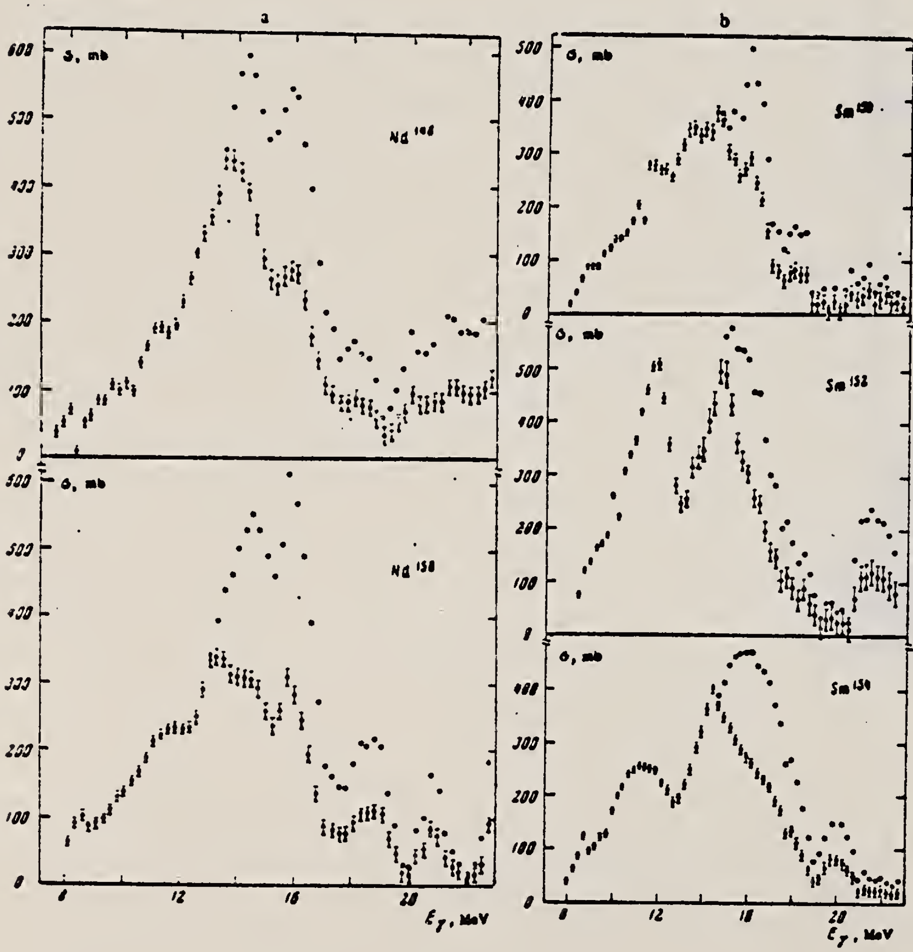

FIG. 2. Photoabsorption cross sections (black points) and photoneutron cross sections (light points): a — for Nd[148] and Nd[150] and b — for Sm[150], Sm[152], and Sm[154]. The indicated errors are statistical.

[over]

Table I. Giant resonance parameters of $Nd^{148,150}$ and $Sm^{150,152,154}$

Parameters	Nucleus				
	Nd^{148}	Nd^{150}	Sm^{150}	Sm^{152}	Sm^{154}
σ_a, mb		160.0		400.0	204.0
$\hbar\omega_a$, MeV		11.25		11.55	11.00
$\hbar\Gamma_a$, MeV		3.0		2.4	3.0
σ_a^{int}, MeV-b		0.750		1.319	0.962
σ_b, mb		270.0		420.0	320.0
$\hbar\omega_b$, MeV		14.50		14.65	15.25
$\hbar\Gamma_b$, MeV		4.0		3.4	4.0
σ_b^{int}, MeV-b		1.695		2.242	2.01
$\sigma_b^{int}/\sigma_a^{int}$		2.26		1.7	2.09
σ^{int}, MeV-b	2.406	2.213	2.213	3.079	2.478
0.06 NZ/A	2.140	2.160	2.182	2.203	2.222
β_0		0.32		0.30	0.41
β_0^{γ}		0.28		0.30	0.35
σ_d, mb	420		380		
$\hbar\omega_d$, MeV	13.65		13.6		
$\hbar\Gamma_d$, MeV	5.0		5.5		

REF.	ELEM. SYM.	A	Z
P. Carlos, H. Beil, R. Bergere, A. Lepretre, A. Veyssiere Nucl. Phys. A172, 437 (1971)	Nd	148	60

METHOD	REF. NO.	
	71 Ca 1	egf

REACTION		RESULT	EXCITATION ENERGY	SOURCE TYPE	SOURCE RANGE	DETECTOR TYPE	DETECTOR RANGE	ANGLE
G,N	406	ABX	8-20	D	8-20	MOD-I		4PI
G,2N	407+	ABX	8-20	D	8-20	MOD-I		4PI
								406+

Table 2

Parameters of the one- or two-Lorentz line fits to the σ_T curves for neodymium isotopes: parameters for Ce and Er extracted from earlier results [13]) are also shown

	Ce	^{142}Nd	^{143}Nd	^{144}Nd	^{145}Nd	^{146}Nd	^{148}Nd	^{150}Nd	Er
σ_1 (mb)	360 ±15	359 ±15	360 ±15	317 ±15	297 ±20	308 ±16	263 ±15	174 ±20	225 ±15
Γ_1 (MeV)	4.35±0.05	4.43± 0.20	4.5 ±0.2	5.3 ± 0.25	6.5±0.4	6 ± 0.3	7.2± 0.3	3.3 ± 0.1	2.9 ±0.05
E_1 (MeV)	15.0 ± 0.10	14.95± 0.1	15 ± 0.1	15.05± 0.1	15 ± 0.15	14.8 ± 0.1	14.7± 0.15	12.3 ± 0.15	12.00± 0.1
σ_2 (mb)								223 ±20	260 ±15
Γ_2 (MeV)								5.2 ± 0.15	5.0 ± 0.05
E_2 (MeV)								16 ± 0.15	15.45± 0.1
$\frac{1}{2}\pi\sigma\Gamma$ MeV · b		2.5 ± 0.2	2.54± 0.2	2.6 ± 0.2	3.0± 0.3	2.9 ± 0.2	3.0± 0.2	2.7 ± 0.3	
$\frac{\frac{1}{2}\pi\sigma\Gamma}{0.06\, NZA^{-1}}$		1.20± 0.10	1.22± 0.10	1.25± 0.10	1.4± 0.15	1.35± 0.10	1.4± 0.1	1.27± 0.15	

[13] R. Bergere, H. Beil, P. Carlos et A. Veyssiere, Nucl. Phys. A133, 417 (1969).

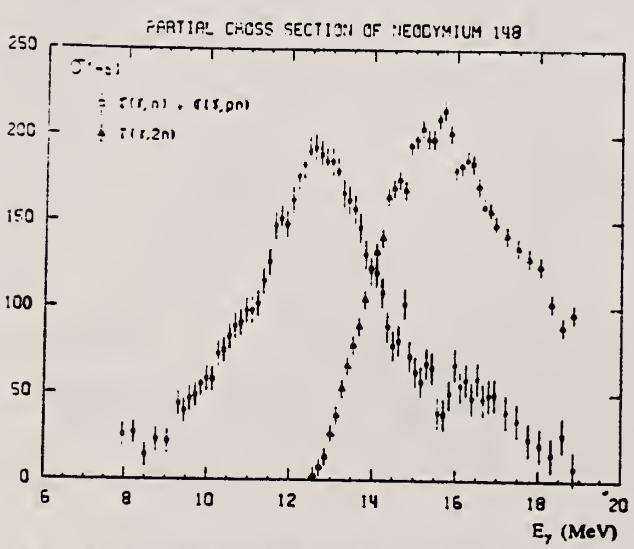

Fig. 7. Partial photoneutron cross sections $\sigma(\gamma, n)$ and $\sigma(\gamma, 2n)$ of ^{148}Nd.

(over)

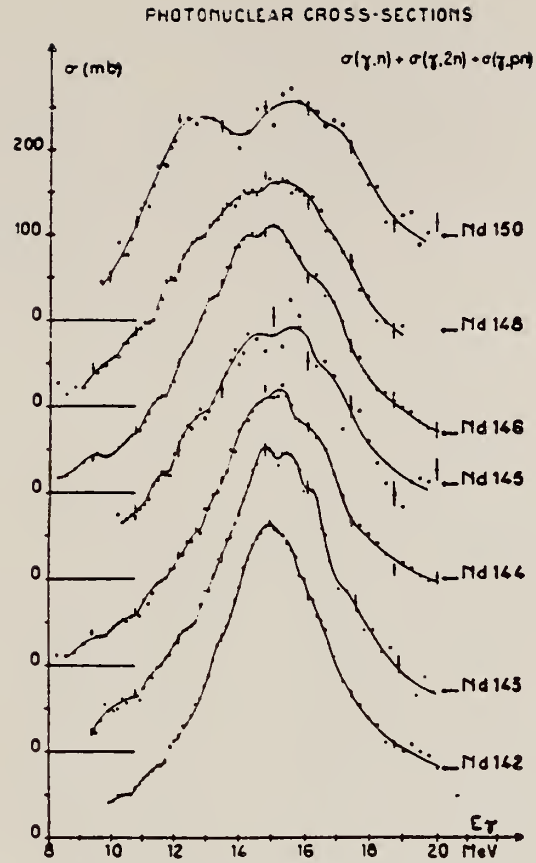

Fig. 9. Total photonuclear cross-section σ_T of neodymium isotopes. The full line drawn through the experimental points is merely meant to facilitate the identification of structure.

Ref. J.H. Carver, W. Turchinetz
Proc. Phys. Soc. 73, 69 (1959)

Elem. Sym.	A	Z
Nd	150	60

Method 33 MeV Synchrotron; radioactivity; NaI spectrometer; ionization chamber

Ref. No.	
59 Ca 3	EH

Reaction	E or ΔE	E_o	Γ	$\int \sigma dE$	$J\pi$	Notes
$Nd^{150}(\gamma,n)$	Bremss. ~ 8-32	13.2	5.7 MeV			

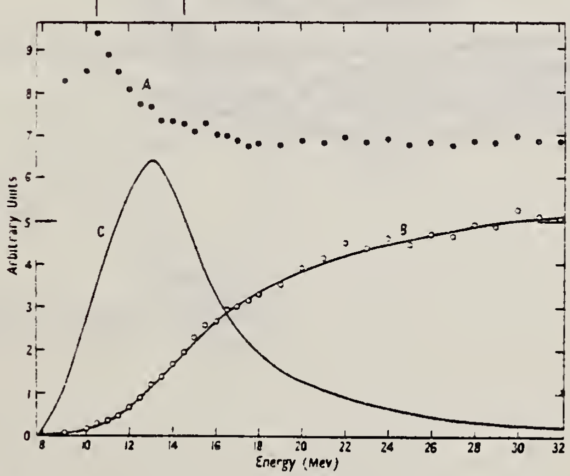

Figure 4. A, the ratio of activation curves $^{150}Nd(\gamma,n)/^{181}Ta(\gamma,n)$; B, activation curve for $^{150}Nd(\gamma,n)$; C, derived cross section: $^{150}Nd(\gamma,n)$.

REF.	ELEM. SYM.	A	Z
O. V. Vasilijev, G. N. Zalesny, S. F. Semenko, V. A. Semenov Phys. Letters 30B, 97 (1969)	Nd	150	60

METHOD	REF. NO.	
	69 Va 2	egf

REACTION	RESULT	EXCITATION ENERGY	SOURCE		DETECTOR		ANGLE
			TYPE	RANGE	TYPE	RANGE	
G,XN	ABX	8-23	C	8-23	BF3-I		4PI

209+

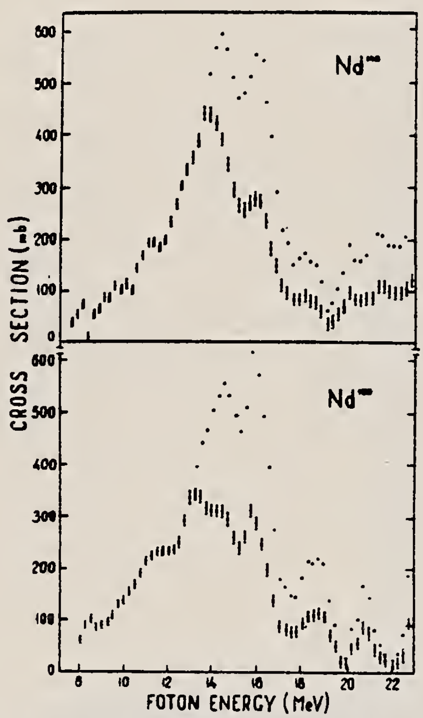

Fig. 2. The photoneutron cross section $\sigma(\gamma, n)$ and the photoabsorption cross sections σ_{tot} for ^{148}Nd and ^{150}Nd . The σ_{tot} are represented by dots. At the energies where σ_{tot} and $\sigma(\gamma, n)$ differ, the latter is represented by circles. Only statistical errors of σ_{tot} are plotted.

REF.	O. V. Vasil'ev, G. N. Zalesnyi, S. F. Semenko, and V. A. Semenov Yad. Fiz. 10, 460 (1969) Sov. J. Nucl. Phys. 10, 263 (1970)	ELEM. SYM.	A	Z
		Nd	150	60

METHOD	REF. NO.	
	69 Va 3	egf

REACTION	RESULT	EXCITATION ENERGY	SOURCE		DETECTOR		ANGLE
			TYPE	RANGE	TYPE	RANGE	
G,XN	ABX	8-22	C	8-22	BF3-I		4PI

239+ SEE 69VA2

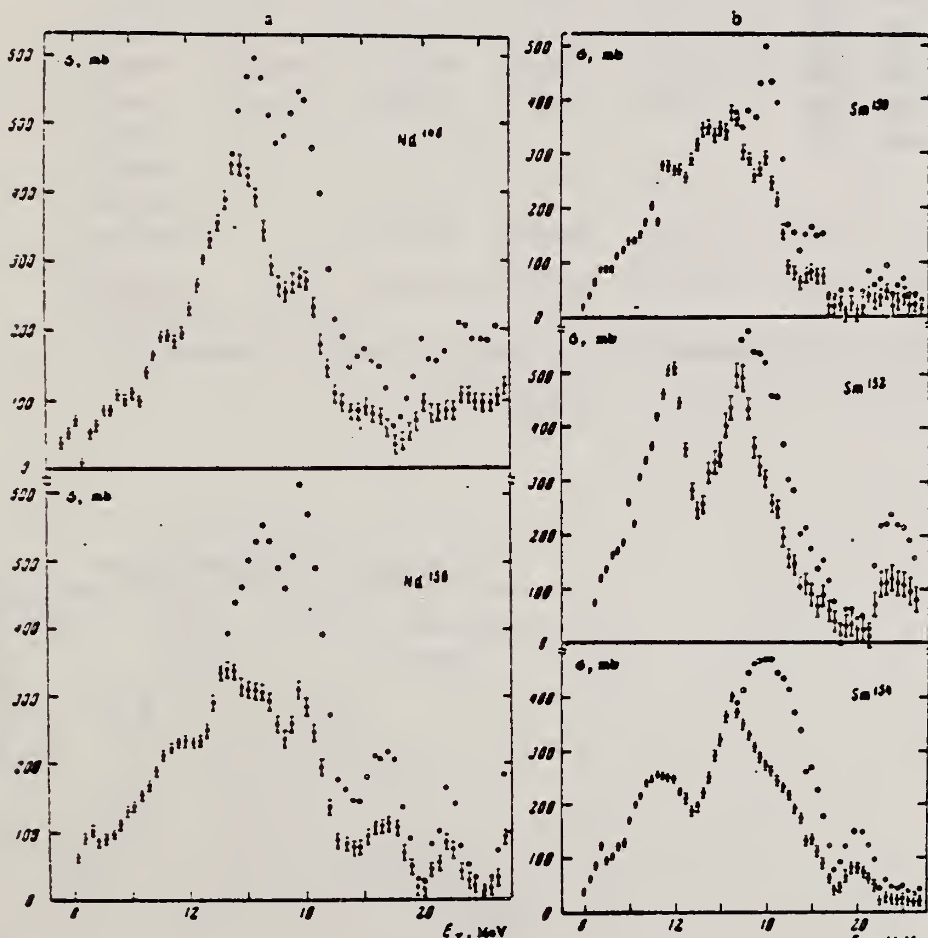

FIG. 2. Photoabsorption cross sections (black points) and photoneutron cross sections (light points): a — for Nd^{148} and Nd^{150} and b — for Sm^{150}, Sm^{152}, and Sm^{154}. The indicated errors are statistical.

[over]

Table I. Giant resonance parameters of $Nd^{148,150}$ and $Sm^{150,152,154}$

Parameters	Nucleus				
	Nd^{148}	Nd^{150}	Sm^{150}	Sm^{152}	Sm^{154}
σ_a, mb		160.0		400.0	204.0
$\hbar\omega_a$, MeV		11.25		11.55	11.00
$\hbar\Gamma_a$, MeV		3.0		2.4	3.0
σ_a^{int}, MeV-b		0.750		1.319	0.962
σ_b, mb		270.0		420.0	220.0
$\hbar\omega_b$, MeV		14.50		14.65	15.25
$\hbar\Gamma_b$, MeV		4.0		3.4	4.0
σ_b^{int}, MeV-b		1.695		2.242	2.01
$\sigma_b^{int}/\sigma_a^{int}$		2.26		1.7	2.09
σ^{int}, MeV-b	2.406	2.243	2.213	3.079	2.478
$0.06\ NZ/A$	2.140	2.160	2.182	2.203	2.222
β_0		0.32		0.30	0.41
β_0^C		0.28		0.30	0.25
σ_c, mb	420		360		
$\hbar\omega_c$, MeV	13.65		13.6		
$\hbar\Gamma_c$, MeV	5.0		5.5		

REF.

P. Carlos, H. Beil, R. Bergere, A. Lepretre, A. Veyssiere
Nucl. Phys. A172, 437 (1971)

ELEM. SYM.	A	Z
Nd	150	60

METHOD

REF. NO.	
71 Ca 1	egf

REACTION	RESULT	EXCITATION ENERGY	SOURCE		DETECTOR		ANGLE
			TYPE	RANGE	TYPE	RANGE	
G,N 409	ABX	10-20	D	8-20	MOD-I		4PI
G,2N 410 +	ABX	10-20	D	8-20	MOD-I		4PI

409+

TABLE 2

Parameters of the one- or two-Lorentz line fits to the σ_T curves for neodymium isotopes: parameters for Ce and Er extracted from earlier results [13]) are also shown

	Ce	^{142}Nd	^{143}Nd	^{144}Nd	^{145}Nd	^{146}Nd	^{148}Nd	^{150}Nd	Er
σ_1 (mb)	360 ±15	359 ±15	360 ±15	317 ±15	297 ±20	308 ±16	263 ±15	174 ±20	225 ±15
Γ_1 (MeV)	4.35±0.05	4.43± 0.20	4.5 ±0.2	5.3 ± 0.25	6.5±0.4	6 ± 0.3	7.2± 0.3	3.3 ± 0.1	2.9 ±0.05
E_1 (MeV)	15.0 ± 0.10	14.95± 0.1	15 ± 0.1	15.05± 0.1	15 ± 0.15	14.8 ± 0.1	14.7± 0.15	12.3 ± 0.15	12.00± 0.1
σ_2 (mb)								223 ±20	260 ±15
Γ_2 (MeV)								5.2 ± 0.15	5.0 ± 0.05
E_2 (MeV)								16 ± 0.15	15.45± 0.1
$\frac{1}{2}\pi\sigma\Gamma$ MeV · b		2.5 ± 0.2	2.54± 0.2	2.6 ± 0.2	3.0± 0.3	2.9 ± 0.2	3.0± 0.2	2.7 ± 0.3	
$\frac{\frac{1}{2}\pi\sigma\Gamma}{0.06\,NZA^{-1}}$		1.20± 0.10	1.22± 0.10	1.25± 0.10	1.4± 0.15	1.35± 0.10	1.4± 0.1	1.27± 0.15	

13 R. Bergere, H. Beil, P. Carlos et A. Veyssiere, Nucl. Phys. A133, 417 (1969).

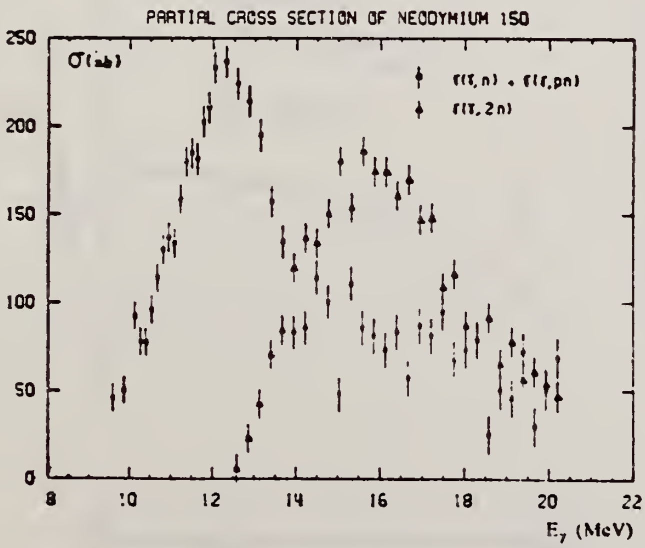

Fig. 8. Partial photoneutron cross sections $\sigma(\gamma, n)$ and $\sigma(\gamma, 2n)$ of ^{150}Nd.

(over)

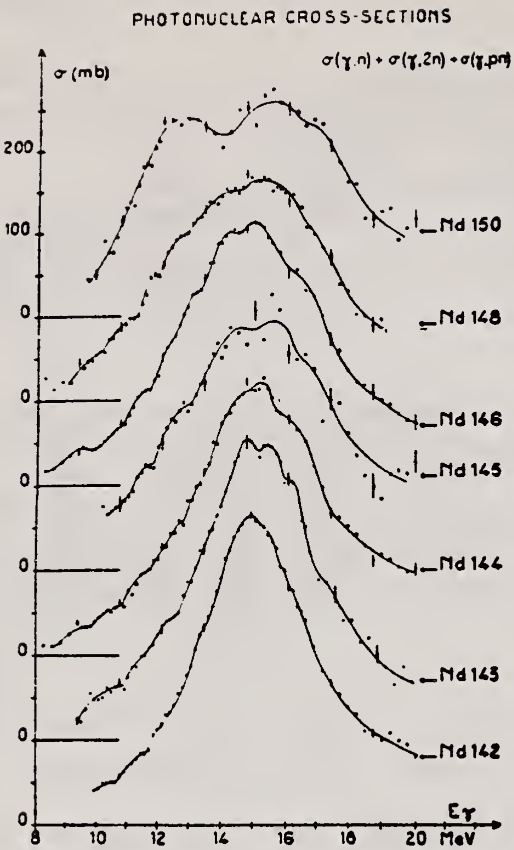

Fig. 9. Total photonuclear cross-section σ_T of neodymium isotopes. The full line drawn through the experimental points is merely meant to facilitate the identification of structure.

REF.		ELEM. SYM.	A	Z
	D. W. Madsen, L. S. Cardman, J. R. Legg, C. K. Bockelman Nucl. Phys. A168, 97 (1971)	Nd	150	60
METHOD		REF. NO. 71 Ma 1		egf

REACTION	RESULT	EXCITATION ENERGY	SOURCE TYPE	SOURCE RANGE	DETECTOR TYPE	DETECTOR RANGE	ANGLE
E,E/	FMF	0	D	60	MAG-D		DST

0 = 0.13

TABLE 11

A comparison of this experiment's $B(EL\uparrow)$ values with those of other experiments and theory

Nucleus	State (MeV)	This work	Pulsed beam	Heavy particle Coulomb excitation	Theory
			2^+ states		
^{142}Nd	1.57	13.1 ± 1.7		25.0 ± 7.3 [a] 19.1 ± 2.3 [b] 15.5 ± 7.8 [c]	16.4 [d] 16.3 [e]
^{142}Nd	2.09	4.1 ± 1.1			
^{146}Nd	0.45	30.9 ± 4.6		28.5 ± 0.4 [b] 28.1 ± 6.6 [c]	92.1 [d]
^{150}Nd	0.13	62.9 ± 10.5	113.9 ± 1.8 [f] 116.8 ± 3.2 [g] 112.4 ± 5.1 [h]	112.7 ± 4.2 [i]	
			3^- state		
^{142}Nd	2.09	28.6 ± 5.0		52 ± 21 [j]	

a) Ref. [39]. b) Ref. [40]. c) Ref. [41]. d) Ref. [37]. e) Ref. [42]. f) Ref. [43]. g) Ref. [44]. h) Ref. [45]. i) Ref. [38]. j) Ref. [33].

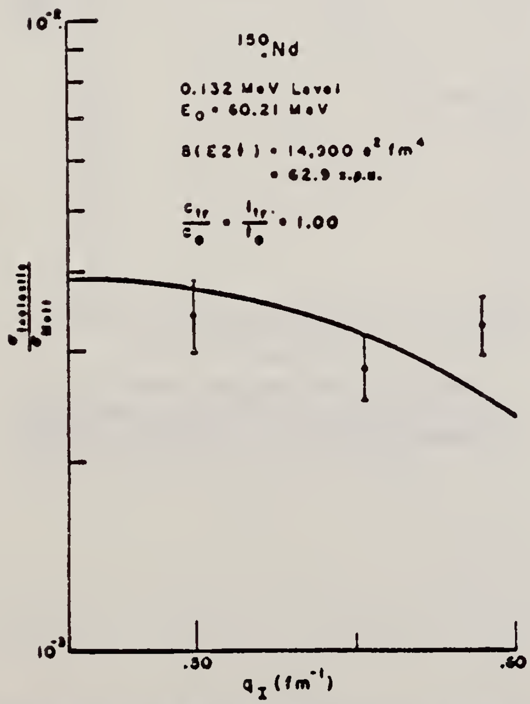

Fig. 17. Inelastic form factors for the 132 keV, 2^+ level in ^{150}Nd as a function of inelastic momentum transfer. The experimental points are the results of this experiment while the solid line traces out the best fit provided by parameters shown.

[33] O. Hansen et al.,Nucl. Phys. 42 (1963) 197.
[37] L. S. Kisslinger et al.,Rev. Mod. Phys. 35 (1963) 853.
[38] J. Bjerregard et al., Nucl. Phys. 44 (1963) 280.
[39] G. A. Burginyon, Thesis, Yale University (1967) unpub.
[40] D. Eccleshall et al., Nucl. Phys. 78 (1966) 481.
[41] O. Nathan et al., Nucl. Phys. 21 (1960) 631.
[42] M. Rho, Nucl. Phys. 65 (1965) 497.
[43] J. D. Kurfess et al., Phys. Rev. 161 (1967) 1185.
[44] F. W. Richter et al., Z. Phys. 213 (1968) 202.
[45] M. Birk et al., Phys. Rev. 116 (1959) 730.

REF.		ELEM. SYM.	A	Z
	A. Schwierczinski, R. Frey, E. Spamer, H. Theissen, and Th. Walcher Phys. Lett. 55B, 171 (1975)	Nd	150	60
METHOD		REF. NO.		
		75 Sc 2		egf

REACTION	RESULT	EXCITATION ENERGY	SOURCE TYPE	SOURCE RANGE	DETECTOR TYPE	DETECTOR RANGE	ANGLE
E,E/	NOX	5- 28	D	50, 64	MAG-D		93

E.E/SPECTRUM (E2)

Inelastic electron scattering has been used to study the isoscalar E2 giant resonances in ^{142}Nd and ^{150}Nd, which were found at excitation energies of 12.0 and 11.2 MeV with total widths of 2.8 and 5.0 MeV, respectively. The energy shift and the larger width in ^{150}Nd indicate a splitting due to the deformation of ^{150}Nd.

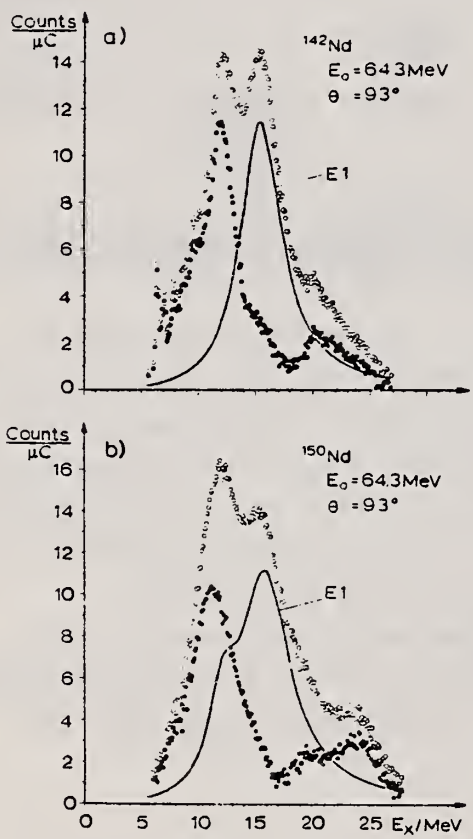

Fig. 1. Spectrum of inelastically scattered electrons after subtraction of radiation tail and background, a) ^{142}Nd, b) ^{150}Nd (open circles). Solid line: E1 cross section. Full circles: E1 cross section subtracted. The total number of counts/μC in the region of the giant resonances is about 100.

REF. C. Creswell, A. Hirsch, W. Bertozzi, J. Heisenberg, S. Kowalski, C.P. Sargent, W. Turchinetz & A. Dieperink
Phys. Rev. C18, 2432 (1978)

ELEM. SYM.	A	Z
Nd	150	60

METHOD

REF. NO.	
78 Cr 1	hg

REACTION	RESULT	EXCITATION ENERGY	SOURCE TYPE	SOURCE RANGE	DETECTOR TYPE	DETECTOR RANGE	ANGLE
E,E/	ABX	850*931	D	1*2	MAG-D		UKN

Recent electron scattering results on the 0.850 MeV level of ^{150}Nd, when analyzed in terms of the interacting boson model, are inconsistent with the interpretation of this level as a pure $J^{\pi}(K) = 2^{+}(0)$ state. Very recent $(n,n'\gamma)$ work has shown this level to be a 1^{-}, 2^{+} doublet. Assuming this level to be the band-head of a "$K^{\pi} = 0^{-}$" octupole band, a simple model is used to predict electron scattering form factors for the 0.850 MeV state and a 3^{-} octupole level observed at 0.931 MeV. Comparison is made between these predicted form factors and recent electron scattering data.

*E KEV; Q .8-2. FM-1

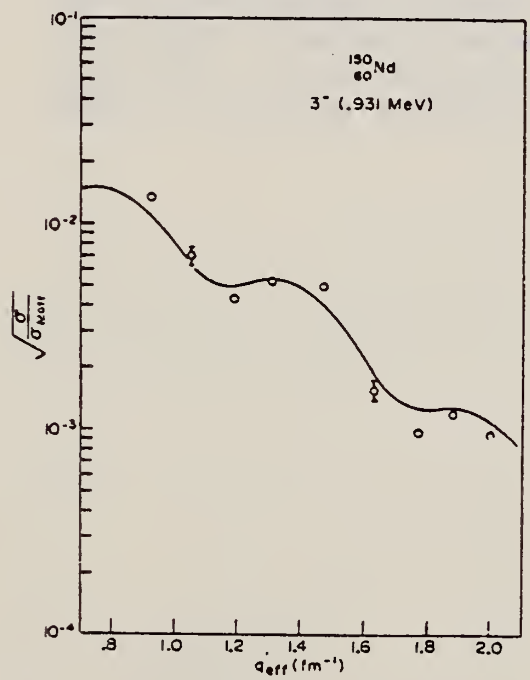

Fig. 2. Electron scattering form factor for the 3^- (0.931 MeV) state in ^{150}Nd. The curve represents a calculation in which the 3^- excitation is modeled as a small amplitude collective surface oscillation.

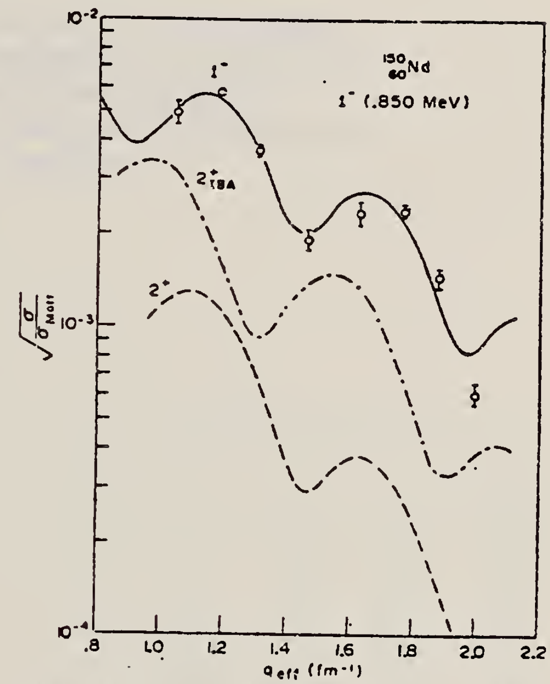

Fig. 3. Electron scattering form factor for the 0.850 MeV state in ^{150}Nd. The solid curve results from a calculation in which the state is represented as a $J^{\pi}(K) = 1^{-}(0)$ octupole surface oscillation belonging to the same band as the 3^- (0.931 MeV). The dashed curve is due to a calculation in which the state is represented as a $J^{\pi}(K) = 2^{+}(0)$ surface oscillation and the dot-dash curve represents the IBA 2^+ prediction.

SAMARIUM
Z=62

Samarium's discovery is generally credited to Boisbaudran who in 1879 isolated "samaria" from "didymia", a mixture of rare earths from which cerium and lanthanum had been extracted. It was identified by its spectrum and named in honor of a Russian engineer, Col. M. Samarski.

E.G. Fuller, B. Petree, M.S. Weiss
Phys. Rev. 112, 554 (1958)

ELEM. SYM.	A	Z
Sm		62

METHOD: Betatron; ion chamber

REF. NO.: 58 Fu 1 | NVB

REACTION	RESULT	EXCITATION ENERGY	SOURCE TYPE	SOURCE RANGE	DETECTOR TYPE	DETECTOR RANGE	ANGLE
G,XN	ABX	7-40	C	7-40	BF3-I		4PI

CF DANØS THEØRY

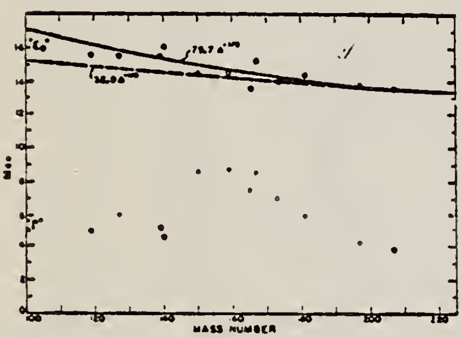

FIG. 6. Mean energy and width of giant resonances. "E_0" and "Γ" are the mean energy for photon absorption and the full width at half maximum of the giant resonance obtained from dashed histograms as in Fig. 5. No attempt was made to fit data with resonance curves to obtain these parameters.

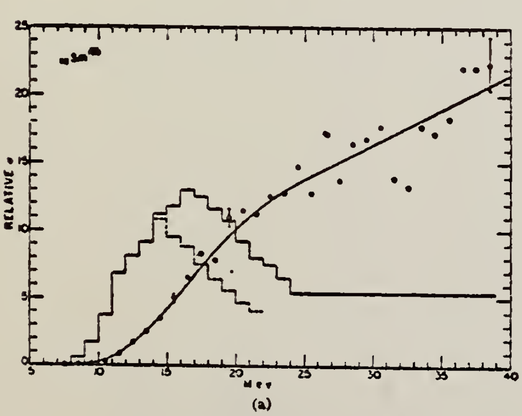

(a)

TABLE I. Target properties and results.

Element	Form used	Weight grams	$\sigma^a(\gamma,n)$[a] barns	$\frac{S\sigma dE}{NZ/A}$[b] Mev-b	"Γ"[a] Mev
Sn	Sn	4.81	0.30	0.064	5.0
I	I	8.55	0.36	0.085	6.0
La	La	10.43	0.34	0.063	5.2
Ce	Ce	4.99	0.45	0.080	4.5
Sm	Sm_2O_3	2.90	0.26	0.073	8.6
Tb	Tb_4O_7	3.04	0.39	0.087	8.7
Ho	Ho_2O_3	1.87	0.41	0.079	7.5
Er	Er_2O_3	5.41	0.50	0.100	8.5
Yb	Yb_2O_3	5.57	0.50	0.090	7.0
Ta	Ta	8.41	0.49	0.077	6.0
Au	Au	3.16	0.68	0.085	4.2
Pb	Pb	8.05	0.75	0.081	3.8

[a] $\sigma^a(\gamma,n)$ is the maximum value and "Γ" the full width at $\sigma^a(\gamma,n)/2$ of the neutron production cross section corrected for multiple neutron emission. Data were not fitted with resonance lines to determine these values.
[b] Integrated neutron production cross sections corrected for multiple neutrons above $(\gamma,2n)$ threshold.

FIG. 5. Relative photoneutron production cross sections for tin, iodine, samarium, holmium, erbium, and lead. The points and smooth curves represent the integral neutron-production cross section defined by $\int_0^E \sigma_{T_n}(E)dE$, where $\sigma_{T_n}(E) = \sigma(\gamma,n) + 2\sigma(\gamma,2n) + \sigma(\gamma,pn) + 3\sigma(\gamma,3n) + \ldots$. The scales are normalized to give approximately the same total neutron yield at 40 Mev. The errors indicated were obtained by propagating the statistical uncertainties, $(\sqrt{n})$, in the original activation curve data through the integral cross section matrix. Solid histograms represent first differences of integral cross section curves. Dashed histograms show result of correcting for neutron multiplicity above the $(\gamma,2n)$ threshold.

REF.	ELEM. SYM.	A	Z
F. I. Havlicek Nuovo Cimento 13, 969-73 (1959)	Sm		62
METHOD	**REF. NO.**		
Betatron	59 Ha 2		NVB

REACTION	RESULT	EXCITATION ENERGY	SOURCE		DETECTOR		ANGLE
			TYPE	RANGE	TYPE	RANGE	
G,A	SPC	THR - 30	C	30	EMU-D	1-5	DST

Ref.		Elem. Sym.	A	Z
K. Reibel; A.K. Mann Phys. Rev. 118, 701 (1960)		Sm		62

Method	Ref. No.	
γ's from $F^{19}(p,\alpha\gamma)$ reaction; protons from Vande Graaff; NaI.	60 Re 1	JHH

Reaction	E or ΔE	E_o	Γ	$\int \sigma dE$	Jπ	Notes
(γ,γ)	= ~7					$\langle\bar{\sigma}\rangle$ (E_p = 2.05 MeV) = < 0.67 mb

Ref. G. Ben-David (Davis); B. Huebschmann Phys. Letters 3, 87 (1962)	Elem. Sym. Sm	A	Z 62
Method (n,γ) reaction; NaI(Tℓ)	Ref. No. 62 Be 2		BG

Reaction	E or ΔE	E_o	Γ	$\int \sigma dE$	Jπ	Notes
Sm(γ,γ)	5.44 - 8.997	8.997				σ_t: 1 mb; γ source: Ni Detector at 135°.

REF.	ELEM. SYM.	A	Z
B. Arad (Huebschmann), G. Ben-David (Davis) I. Pelah, Y. Schlesinger Phys. Rev. 133, B684-700 (1964)	Sm		62

METHOD	REF. NO.	
Reactor, (n,γ) reactions source	64 Ar 1	NVB

REACTION	RESULT	EXCITATION ENERGY	SOURCE TYPE	SOURCE RANGE	DETECTOR TYPE	DETECTOR RANGE	ANGLE
G,G	ABX	9	D	9	NAI-D		135
		(8.997)		(8.997)			

TABLE II. Capture gamma-ray sources and their properties.[a]

Source	Chemical composition	Mass kg	Principal γ rays (in MeV)
Al	Metal	1.640	7.73
Cl	polyvinyl Chloride	0.380	8.55, 7.78, 7.41, 6.96, 6.64, 6.12, 5.72
Co	CoO	0.230	7.49, 7.20, 6.98, 6.87, 6.68, 6.48, 5.97, 5.67
Cr	Metallic powder	0.480	9.72, 8.88, 8.49, 7.93, 7.09, 6.65, 5.60
Cu	Metal	1.860	7.91, 7.63, 7.29, 7.14, 7.00, 6.63
Fe	Metallic powder	0.440	9.30, 7.64, 7.28, 6.03
Hg	$Hg_2(NO_3)_2 \cdot 2H_2O$	0.310	6.44, 6.31, 5.99, 5.67, 5.44
Mn	MnO_2	0.240	7.26, 7.15, 7.04, 6.96, 6.79, 6.10, 5.76
Ni	Metal	0.900	9.00, 8.50, 8.10, 7.83, 7.58, 6.84, 6.64
Ti	TiO_2	0.210	6.75, 6.56, 6.42
V	V_2O_5	0.120	7.30, 7.16, 6.86, 6.51, 6.46, 5.87, 5.73
Y	Y_2O_3	0.200	6.07, 5.63

[a] For more detailed information, additional lines, intensities, etc., see Ref. 6.

TABLE III. Effective cross sections.

γ source	Energy (MeV)	Scatterer Element	Protons	Neutrons	$\langle\sigma_{\gamma\gamma}\rangle$ (mb)	Notes
Hg	5.44	Hg	80	116, 118, 119, 120, 121, 122, 124	128	
Cl	6.12	Pr^{141}	59	*82*	103	a
V	6.508	Sn	*50*	62, 64–70, 72	14	
Co	6.690	Pr^{141}	59	*82*	2.7	a
Co	6.867	Nd	60	82, 83, 84, 85, 86, 88	22	
Al	6.98	Pb^{208}	*82*	*126*	2900	b
Cl	6.98	Pb	*82*	124, 125, *126*	346	a
Ti	6.996	Bi^{209}	83	*126*	1560	b
Cu	7.01	Sn	*50*	62, 64–70, 72	1000	b
Ti	7.149	Pb^{208}	*82*	*126*	1000	b
Co	7.201	Pb^{208}	*82*	*126*	23	
Mn	7.261	Pb^{208}	*82*	*126*	25	a
Fe	7.285	Pb^{208}	*82*	*126*	4100	a
V	7.305	Pb^{208}	*82*	*126*	12.5	
Hg	7.32	Pb	*82*	124, 125, *126*	5500	c
Fe	7.639	Ni	*28*	30, 32, 34, 36	10.5	d
Fe	7.639	Pr^{141}	59	*82*	10	d
Cr	8.499	Cu	29	34, 36	24.4	
Cr	8.881	Pr^{141}	59	*82*	9.3	
Ni	8.997	Sm	62	*82*, 85–88, 90, 92	2.8	

[a] A large error could be introduced in the cross-section values because of large differences in line intensities quoted by Bartholomew and Higgs and by Groshev et al. (Ref. 6).
[b] Because of the low counting rate, thick scatterers were used, which will introduce a systematic error in estimating $\langle\sigma_{\gamma\gamma}\rangle$ for resonances having a high nuclear cross section.
[c] The cross section was evaluated assuming the gamma intensity to be 0.02 photons per 100 captured neutrons (see text).
[d] Reference 6 gives the 7.639 line of iron capture gamma rays as a single line. However, a recent paper by Fiebiger, Kane, and Segel [Phys. Rev. 125, 2031 (1962)] reports two different lines of equal intensities having energies of 7.647 and 7.633 MeV. The present experiment cannot resolve an energy difference of 14 keV, therefore, there is no possibility of deciding which line is responsible for the scattering.

REF.

R. Bergere, H. Beil, P. Carlos and A. Veyssiere
Nucl. Phys. A133, 417 (1969)

ELEM. SYM.	A	Z
Sm		62

METHOD

REF. NO.	
69 Be 6	egf

REACTION		RESULT	EXCITATION ENERGY	SOURCE TYPE	SOURCE RANGE	DETECTOR TYPE	DETECTOR RANGE	ANGLE
G,N	478+	ABX	7-21	D	7-27	MOD-I		4PI
G,2N	479	ABX	13-25	D	7-27	MOD-I		4PI
G,3N	480	ABX	23-27	D	7-27	MOD-I		4PI

478+

x = fraction of total cross section resulting in a direct neutron

n_d = fraction of neutrons emitted by direct effect at an energy where all the evaporation neutrons go to (γ,2n) cross section

$n_d = x/(2-x)$

Tableau 3
Moments quadrupolaires intrinsèques

Cible	% isotopes	a/b ex	β_2 ex	$\beta_2[B(E_2)]$	Q_0 ex (b)	Q'_0
$_{53}$I	100 % ^{127}I	0.85	0.172		−2.3±0.4	
$_{58}$Ce	88.5 % ^{140}Ce			0.104		
	11.1 % ^{142}Ce			0.118		
$_{62}$Sm	15 % ^{147}Sm					0.158
	11.2 % ^{148}Sm					
	13.8 % ^{149}Sm	1.23	0.219		4.5±0.4	
	7.5 % ^{150}Sm			0.190		3.53
	26.6 % ^{152}Sm			0.304		5.93
	22.5 % ^{154}Sm			0.351		6.58
$_{68}$Er	33.4 % ^{166}Er			0.341		7.60
	22.9 % ^{167}Er	1.314	0.288		6.96±0.4	7.80
	27.1 % ^{168}Er			0.339		7.60
	14.9 % ^{170}Er			0.329		7.45
$_{71}$Lu	97.4 % ^{175}Lu	1.282	0.262		6.95±0.3	7.20

Tableau 5
Valeurs de la température nucléaire et du paramètre a de densité des niveaux

	x	n_d	Θ (MeV)	$E'_\gamma - E_n$ (MeV)	a (MeV^{-1})	a' (MeV^{-1})	a'' (MeV^{-1})
I	0.05±0.005	0.03±0.03	1.30±0.20	10	6±2.5	10±3	10±2
^{140}Ce	0.21±0.05	0.12±0.03	1.05±0.20	10	9±3.5		7±3
^{142}Ce			0.8 ±0.20	6	9±4		8±3
Sm	0.18±0.04	0.10±0.03					
Er	0.20±0.05	0.11±0.03					(12±4)
Lu	0.26±0.06	0.15±0.03	0.85±0.1	9	12.5±2.5		15±3

[over]

Tableau 4

Règles de somme

Noyau cible (éléments naturels)	σ_0 (MeV · b)	σ'_0 (MeV · b)	$0.06 \frac{NZ}{A}$	$\frac{\sigma_0 A}{0.06\, NZ}$	$\frac{\sigma'_0 A}{0.06\, NZ}$	σ_{-1} (mb)	$\sigma_{-1} A^{-4/3}$	σ_{-2} (mb · MeV^{-1})	$\sigma_{-2} A^{-5/3}$
$_{53}$I	2.02 ±0.14	2.30±0.12	1.85	1.09±0.07	1.24±0.07	129±0.10	0.20 ±0.02	8.6±0.6	2.7 ±0.2
$_{58}$Ce	2.13 ±0.15	2.53±0.13	2.04	1.05±0.07	1.24±0.07	140±0.12	0.19 ±0.02	9.5±0.6	2.5 ±0.2
$_{62}$Sm	2.48 ±0.17	2.92±0.14	2.18	1.14±0.07	1.34±0.07	167±0.14	0.21 ±0.02	11.8±0.8	2.75±0.2
$_{68}$Er	2.70 ±0.19	3.04±0.16	2.42	1.12±0.07	1.26±0.07	186±0.15	0.20 ±0.02	13.6±1	2.7 ±0.2
$_{71}$Lu	2.65 ±0.18	2.96±0.16	2.53	1.05±0.07	1.17±0.07	182±0.15	0.185±0.02	12.9±1	2.35±0.2
valeur moyenne pour ces 5 corps				1.09±0.07	1.25±0.07		0.20±0.02		2.6 ±0.2

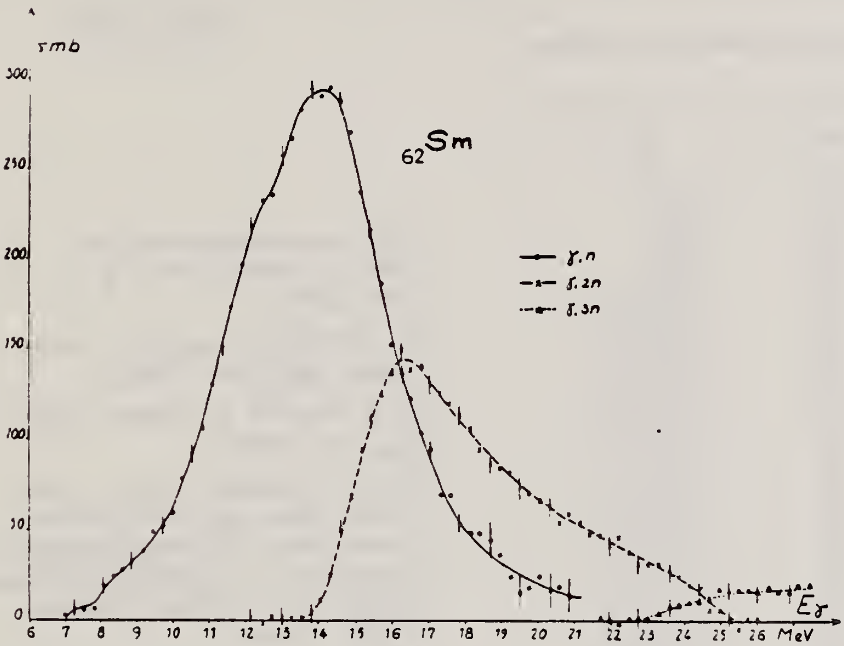

Fig. 5.

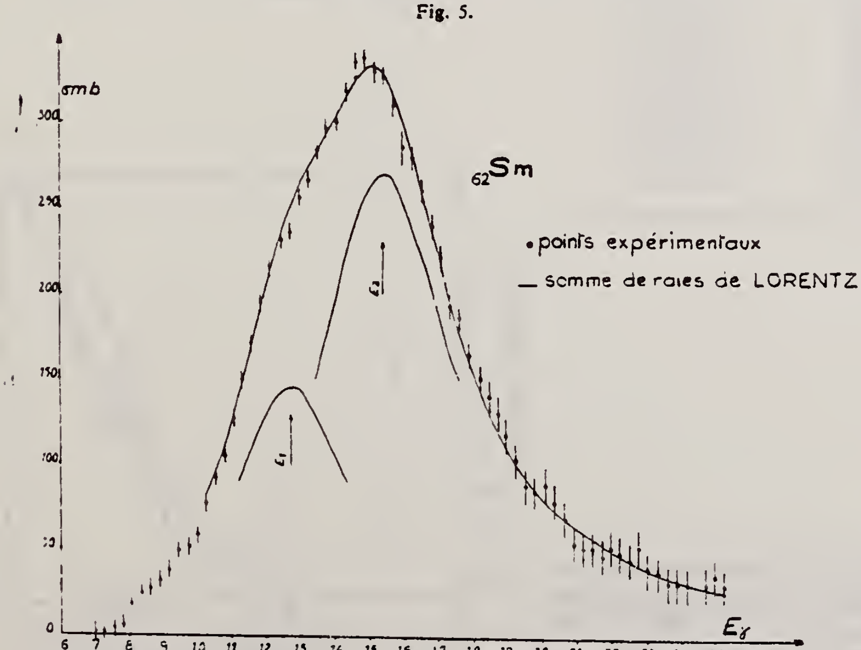

Fig. 6.

REF.

V. Emma, S. Lo Nigro, C. Milone
Nucl. Phys. A257, 438 (1976)

ELEM. SYM.	A	Z
Sm		62

METHOD

REF. NO.	
76 Em 2	egf

REACTION	RESULT	EXCITATION ENERGY	SOURCE TYPE	SOURCE RANGE	DETECTOR TYPE	DETECTOR RANGE	ANGLE
G,F	ABY	THR-999	C	999	TRK-I		4PI

999 = 1 GEV

TABLE 1

Measured values of σ_q at $E = 1000$ MeV and deduced values of σ_k assumed constant from E_0 to 1000 MeV

Element	Z^2/A	σ_q (mb)	E_0 (MeV)	σ_k (mb)
Bi	32.96	12.3 ± 0.6	200	7.6 ± 0.6
Pb	32.45	5.4 ± 0.4	220	3.6 ± 0.3
Tl	32.10	4.1 ± 0.3	230	2.8 ± 0.3
Au	31.68	2.0 ± 0.15	240	1.4 ± 0.2
Pt	31.18	1.1 ± 0.08	255	$(8 \pm 0.7) \times 10^{-1}$
Re	30.21	$(3.7 \pm 0.3) \times 10^{-1}$	280	$(2.9 \pm 0.3) \times 10^{-1}$
W	29.78	$(3.5 \pm 0.3) \times 10^{-1}$	290	$(2.8 \pm 0.3) \times 10^{-1}$
Ta	29.45	$(3.3 \pm 0.3) \times 10^{-1}$	300	$(2.7 \pm 0.3) \times 10^{-1}$
Hf	29.04	$(1.7 \pm 0.2) \times 10^{-1}$	310	$(1.4 \pm 0.2) \times 10^{-1}$
Yb	28.31	$(1.3 \pm 0.1) \times 10^{-1}$	330	$(1.2 \pm 0.1) \times 10^{-1}$
Tm	28.18	$(7.5 \pm 0.8) \times 10^{-2}$	335	$(6.8 \pm 0.8) \times 10^{-2}$
Ho	27.21	$(3.6 \pm 0.4) \times 10^{-2}$	355	$(3.5 \pm 0.4) \times 10^{-2}$
Dy	26.80	$(2.6 \pm 0.3) \times 10^{-2}$	360	$(2.5 \pm 0.3) \times 10^{-2}$
Tb	26.58	$(2.5 \pm 0.3) \times 10^{-2}$	370	$(2.5 \pm 0.3) \times 10^{-2}$
Gd	26.04	$(1.6 \pm 0.2) \times 10^{-2}$	380	$(1.7 \pm 0.2) \times 10^{-2}$
Sm	25.56	$(1.3 \pm 0.2) \times 10^{-2}$	390	$(1.4 \pm 0.2) \times 10^{-2}$
Nd	24.96	$(9.2 \pm 0.9) \times 10^{-3}$	405	$(1 \pm 0.1) \times 10^{-2}$
Ce	24.00	$(8 \pm 0.9) \times 10^{-3}$	420	$(9 \pm 1) \times 10^{-3}$
La	23.39	$(8.4 \pm 0.9) \times 10^{-3}$	430	$(1 \pm 0.1) \times 10^{-3}$
Sb	21.36	$(1.2 \pm 0.2) \times 10^{-2}$	460	$(1.5 \pm 0.3) \times 10^{-2}$
Te	21.19	$(8.8 \pm 1) \times 10^{-3}$	465	$(1.2 \pm 0.2) \times 10^{-2}$
Sn	21.06	$(1.3 \pm 0.2) \times 10^{-2}$	465	$(1.7 \pm 0.3) \times 10^{-2}$
Cd	20.49	$(1.7 \pm 0.3) \times 10^{-2}$	470	$(2.2 \pm 0.4) \times 10^{-2}$
Ag	20.47	$(2 \pm 0.3) \times 10^{-2}$	470	$(2.6 \pm 0.4) \times 10^{-2}$
Zn	13.76	$(2 \pm 0.4) \times 10^{-1}$	515	$(3 \pm 0.6) \times 10^{-1}$
Cu	13.44	$(2.4 \pm 0.5) \times 10^{-1}$	515	$(3.6 \pm 0.8) \times 10^{-1}$
Ni	13.35	$(2.4 \pm 0.5) \times 10^{-1}$	510	$(3.6 \pm 0.8) \times 10^{-1}$
Fe	12.10	$(3 \pm 0.6) \times 10^{-1}$	510	$(4.4 \pm 0.9) \times 10^{-1}$

[4] A.V. Mitrofanova et al. Sov. J. Nucl. Phys. 6, 512 (1968).

[7] T. Methasiri et al., Nucl. Phys. A167, 97 (1971).

[12] J.R. Nix et al., Nucl. Phys. 81, 61 (1966).

[20] N.A. Perifilov et al., JETP (Sov. Phys.) 14, 623 (1962); Proc. Symp. on the physics & chemistry of fission, Salzburg 1965, vol. 2 (IAEA) Vienna, 1965, p.283.

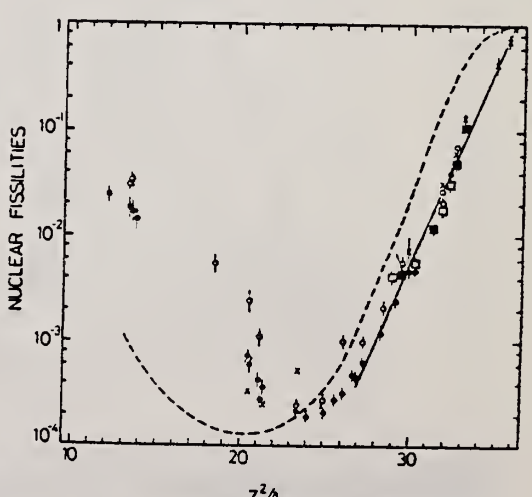

Fig. 2. Nuclear fissilities as a function of Z^2/A. Experimental points: solid circles represent our data; squares, the data from ref. [4]; open circles, the data from ref. [7]; and crosses, the data from (p,f) experiments[20]. The straight line is the best fit calculated from our data for $Z^2/A > 26$. The dashed curve is the curve VI calculated by Nix and Sassi[12].

Sm
A=144

Sm
A=144

M.D. DeSouza Santos, J. Goldemberg, R.R. Pieroni, E. Silva, O.A. Borello, S.S. Villaca, J.L. Lopes
Int. Conf. Peaceful Uses of Atomic Energy II (UN, NY), 169 (1955)

ELEM. SYM.	A	Z
Sm	144	62

METHOD Betatron; neutron yield; radioactivity; r-chamber

REF. NO.	
55 De 1	EGF

REACTION	RESULT	EXCITATION ENERGY	SOURCE		DETECTOR		ANGLE
			TYPE	RANGE	TYPE	RANGE	
G,N	ABX	9-23	C	9-23	ACT-I		4PI

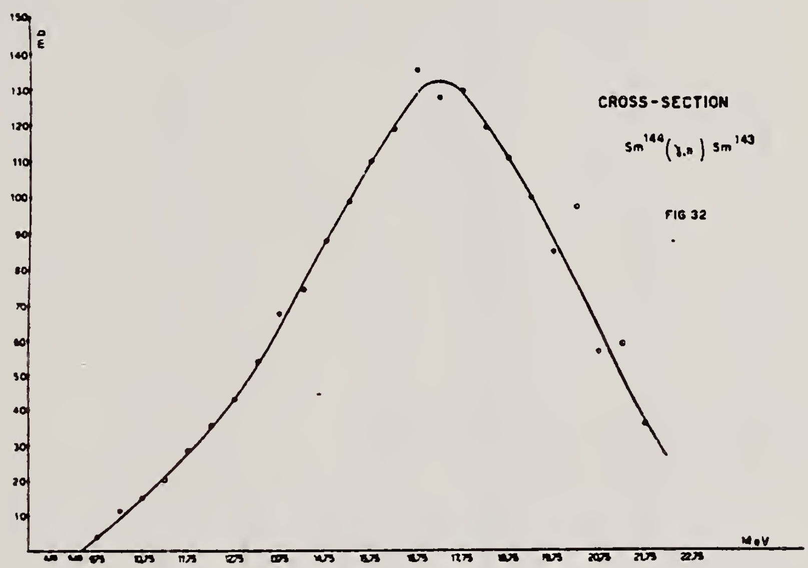

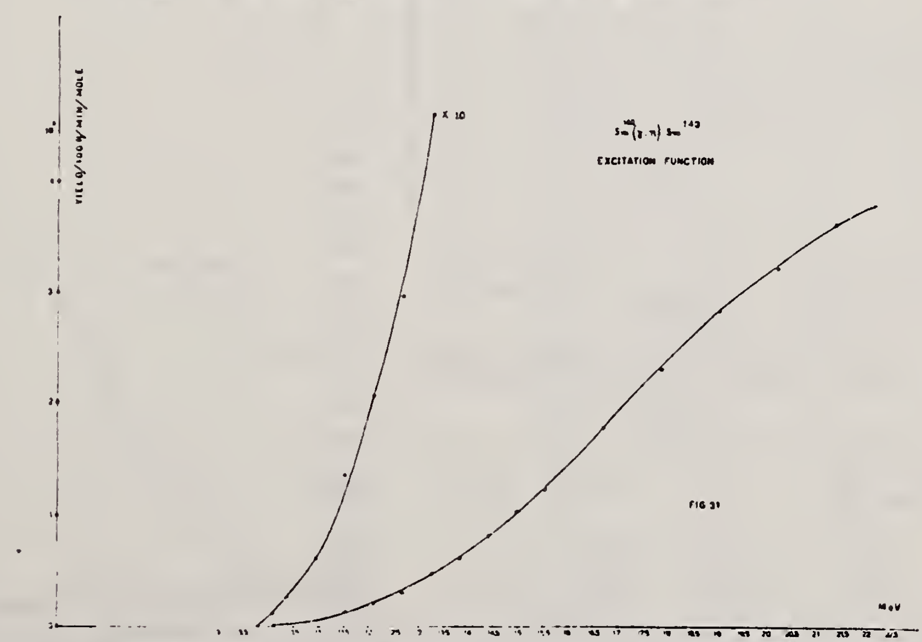

Ref. E. Silva, J. Goldemberg
Nuovo Cimento 3, 13 (1956)

Elem. Sym.	A	Z
Sm	144*	62
Ref. No. 56 Si 1		EGF

Method: Betatron; radioactivity

Reaction	E or ΔE	E_o	Γ	$\int \sigma dE$	$J\pi$	Notes
$Sm^{144}(\gamma,n)$	22	17.25	6.8	$\int_{8.7}^{22} = 0.91$ MeV-b		$E_{th} = 9.6$ MeV; $\sigma = 135$ mb. * Some question as to isotope.

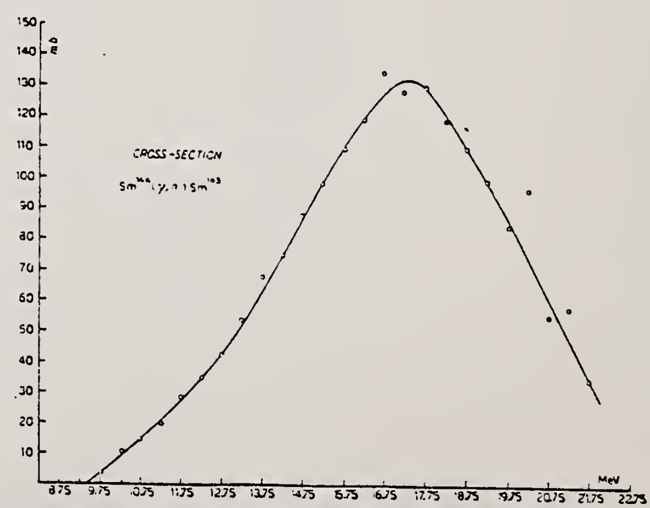

Fig. 3. – Cross section for the reaction $^{144}Sm(\gamma, n)^{143}Sm$.

Ref. J.H. Carver, W. Turchinetz
Proc. Phys. Soc. 73, 69 (1959)

Elem. Sym.	A	Z
Sm	144	62

Method 33 MeV Synchrotron; radioactivity; NaI spectrometer; r chamber

Ref. No.	
59 Ca 3	EH

Reaction	E or ΔE	E_0	Γ	∫σdE	Jπ	Notes
$Sm^{144}(\gamma,n)$	Bremss. 10-32	15.3	4.0 MeV	2.5±0.4 MeV-b		

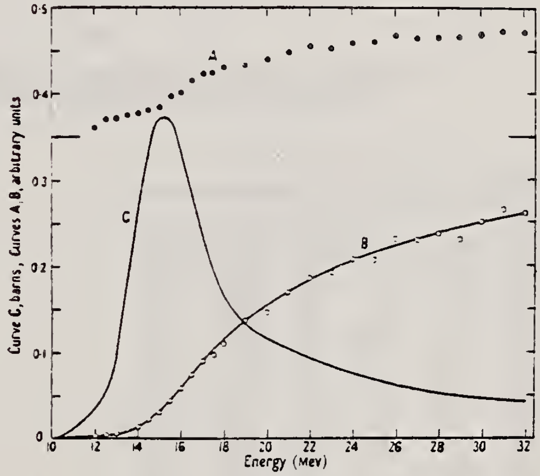

Figure 9. A, the ratio of activation curves $^{144}Sm(\gamma,n)/^{181}Ta(\gamma,n)$; B, activation curve for $^{144}Sm(\gamma,n)$; C, derived cross section: $^{144}Sm(\gamma,n)$.

Table 2

Activity	$T_{\frac{1}{2}}$ (min)	W_0 (Mev)	K/β^+	K-capture / Total capture	W_K
^{140}Pr	3·4	3·25	0·63	0·89	0·89
^{141}Nd	150	1·80	48	0·89	0·90
^{143}Sm	8·5	3·47	0·60	0·89	0·91

REF.	ELEM. SYM.	A	Z
G. Di Caporiacco, M. Mandò, and F. Ferrero Nuovo Cimento 13, 522 (1959)	Sm	144	62

METHOD	REF. NO.	
Betatron; ion chamber	59 Di 1	NVB

REACTION	RESULT	EXCITATION ENERGY	SOURCE TYPE	SOURCE RANGE	DETECTOR TYPE	DETECTOR RANGE	ANGLE
G,N	RLY	11-30	C	22,30	ACT-I		4PI

REL TØ CU63 (G,N)

Yield ratios: $\frac{^{144}Sm(\gamma,n)}{^{141}Pr(\gamma,n)} = 1.088$

$\frac{^{141}Pr(\gamma,n)}{^{63}Cu(\gamma,n)} = 3.79$

REF.	ELEM. SYM.	A	Z
G. Ben-David, B. Arad, J. Balderman, and Y. Schlesinger Phys. Rev. 146, B852 (1966)	Sm	144	62

METHOD	REF. NO.	
Nuclear Resonance Scattering using N,G reactions.	66 Be 3	JDM

REACTION	RESULT	EXCITATION ENERGY	SOURCE TYPE	SOURCE RANGE	DETECTOR TYPE	DETECTOR RANGE	ANGLE
G,G	RLX	5 - 10	D	5 - 10	NAI-D	5 - 10	135

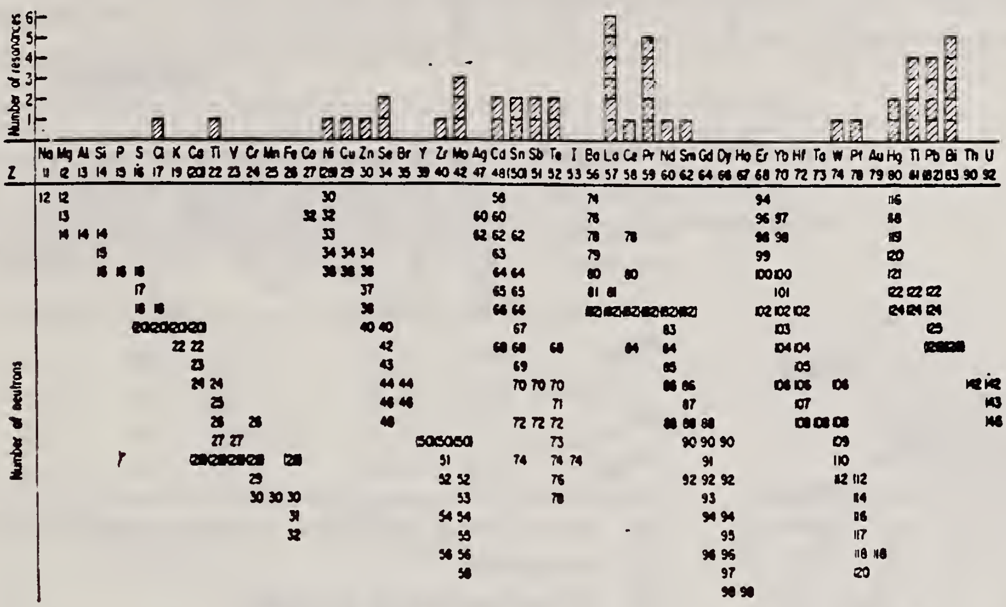

FIG. 3. Histogram of distribution of observed resonances among the different targets. The atomic number is given directly beneath the chemical symbol followed by the neutron numbers of the naturally occurring isotopes. Magic numbers are shown in brackets.

TABLE III. List of effective cross sections.

Scatterer	Energy (MeV)	Gamma source	δ (mb)	Scatterer	Energy (MeV)	Gamma source	δ (mb)
Sm^{144}	8.997	Ni	100	Sn	7.01	Cu	110
Pr^{141}	8.881	Cr	9	Nd	6.867	Co	30
La	8.532	Ni	6	Pr^{141}	6.867	Co	3
Te	8.532	Ni	3^a	Te	6.7	Ni	...
Cu	8.499	Cr	24	La	6.54	Ag	12
Zr	8.496	Se	3050	Cd	6.474	Co	110
Zn	8.119	Ni	13	Mo	6.44	Hg	25^e
Se	7.817	Ni	50	La	6.413	Ti	72
Se	7.76	K	90	Mo	6.413	Ti	10
Sb	7.67	V	$...^b$	Tl	6.413	Ti	25
Cd	7.64	Fe	40^c	W	~6.3	Ti	$...^b$
Ni	7.64	Fe	7^c	Sb	6.31	Hg	6^e
Pr^{141}	7.64	Fe	12^c	Ti	6.31	Hg	2^e
Tl	7.64	Fe	370^c	Sn	6.27	Ag	75
La	7.634	Cu	7	Pb^{208}	6.15	Gd	$...^g$
Mo	7.634	Cu	11	Te	5.8	Ni	$...^f$
Bi^{209}	7.634	Cu	4	La	6.12	Cl	35
Te	7.528	Ni	66^d	Pr^{141}	6.12	Cl	110
Bi^{209}	7.416	Se	100	Pt	5.99	Hg	$40^{a,e}$
Bi^{209}	7.300	As	80^e	Tl	5.99	Hg	5^e
Pb^{208}	7.285	Fe	4100	Pb^{208}	5.9	Sr	$...^h$
Cl	7.285	Fe	34	Ce	5.646	Co	17
Pr^{141}	7.185	Se	80	Bi^{209}	5.646	Co	55
Tl	7.16	Cu	120	Pb^{208}	5.53	Ag	70
La	7.15	Mn	50	Hg	5.44	Hg	75^e
Bi^{209}	7.149	Ti	2000	Hg	4.903	Co	385

[a] High-energy component of a complex spectrum.
[b] A broad scattered spectrum with no observable peak structure.
[c] There are actually two lines of energies 7.647 and 7.633 MeV having equal intensities in the iron capture gamma spectrum. The cross section has therefore been corrected, although there is no possibility at present of deciding which line is responsible for each resonance.
[d] Is probably an independent level in the complex spectrum of Ni γ rays on Te.
[e] Rough estimate.
[f] May be inelastic component from 7.528 level in Te.
[g] The relative line intensities in this case are due to Groshev and co-workers.
[h] No line is known for the source at this energy.
[i] Difficult to resolve among the many source lines present at this energy.

REF.	ELEM. SYM.	A	Z
K. Shoda, M. Sugawara, T. Saito & H. Miyase PICNS-69 Proceedings of the Conference on Nuclear Isospin, Asilomar-Pacific Grove, California 1969 (Academic Press, New York & London 1969) p.137.	Sm	144	62
METHOD	REF. NO. 69 Sh 8		egf

REACTION	RESULT	EXCITATION ENERGY	SOURCE		DETECTOR		ANGLE
			TYPE	RANGE	TYPE	RANGE	
E,P	SPC	11-20	D	20	MAG-D		UKN

UKN=UKNOWN

Table 2. The radiative widths of the main IAS. The results are compared with the single particle strength in W.u..

Nucleus	E_p (MeV)	E_x (MeV) (a)	Γ_{p_0}/Γ	Γ_γ (eV)	$2(T+1)\Gamma_{\gamma_0}$ (W.u.)
^{140}Ce	10.3	18.3	1 (b)	50	0.1
——	12.8	20.8	1 (b)	90	0.1
^{141}Pr	9.7	15.1	12/60(c)	40	0.2
^{144}Sm	10.6	16.6	1 (b)	20	0.05

(a) Ground state is assumed for the residual state.

(b) Assumption.

(c) P. VonBrentano *et al.* (2).

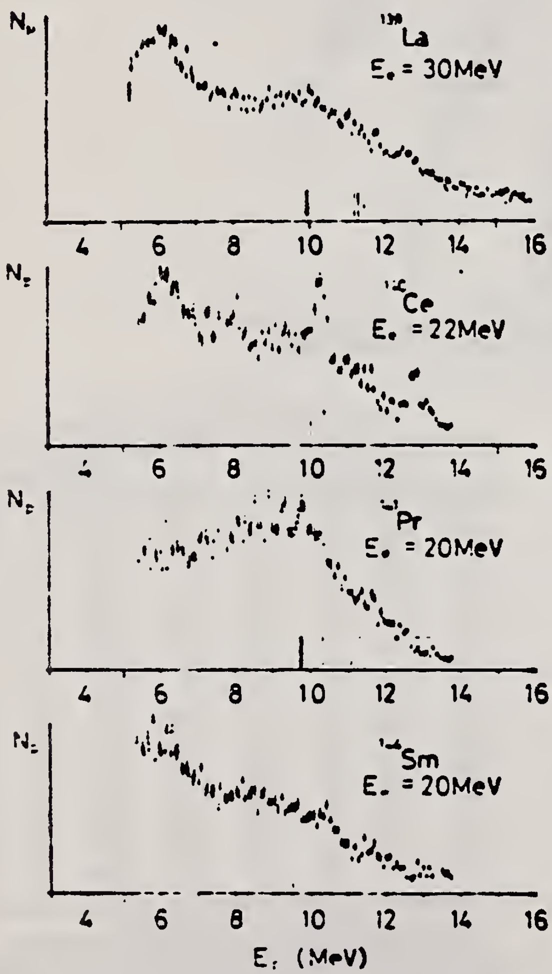

Fig. 1. Energy distributions of photoprotons. Vertical broken lines and solid lines indicate the position of p_0 corresponding to the ground IAS and electric dipole IAS (2).

U.S. DEPARTMENT OF COMMERCE
NATIONAL BUREAU OF STANDARDS

REF.	K. Shoda, T. Saito, M. Sugawara, H. Miyase, S. Oikawa, A. Suzuki Phys. Rev. C4, 1842 (1971)	ELEM. SYM. Sm	A 144	Z 62
METHOD		REF. NO. 71 Sh 3		hmg

REACTION	RESULT	EXCITATION ENERGY	SOURCE TYPE	SOURCE RANGE	DETECTOR TYPE	DETECTOR RANGE	ANGLE
E,P	ABX	15-22	D	22	MAG-D		90

ISOBARIC ANALOGS

The energy distributions of protons from the $(e,e'p)$ reaction on $N=82$ nuclei with even Z have been measured. The cross sections of the (γ,p_0+p_1) reaction have been estimated. Two prominent isobaric analogs have been found in each nucleus. The results were used for the systematic discussion of the odd-odd parent nuclei ^{138}Cs, ^{140}La, ^{142}Pr, and ^{144}Pm. The 1$^-$ states are estimated at 600 and ~2500 keV for ^{138}Cs, 500 and 3000 keV for ^{140}La, 1100 and 3700 keV for ^{142}Pr, and 1400 and 4300 keV for ^{144}Pm. The parameters of these states are discussed in terms of a quasiproton and single-neutron model.

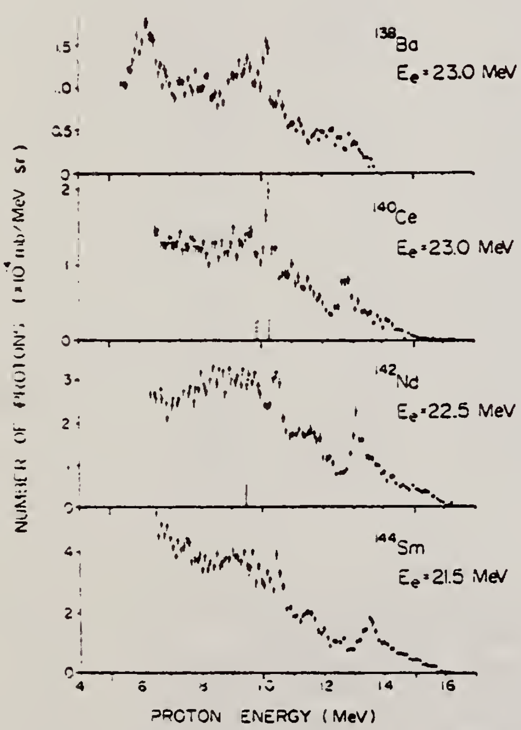

FIG. 1. Energy distributions of protons emitted from the $(e,e'p)$ reaction at $\theta=90°$.

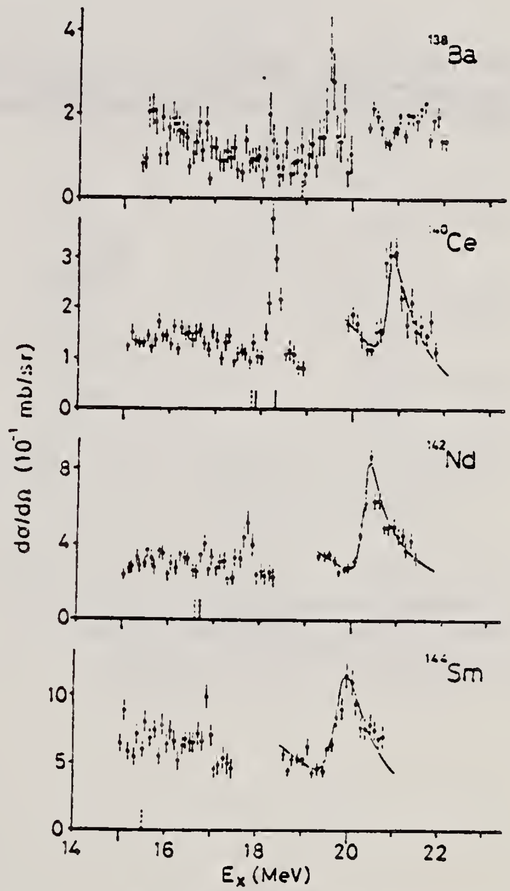

FIG. 2. The photoproton cross sections for p_0+p_1 at $\theta=90°$ in the vicinity of the isobaric analog resonances. The curves for the broad resonances were obtained from the fitting of the interference formula.

REF.	ELEM. SYM.	A	Z
B. Arad, G. Ben-David, Y. Schlesinger, M. Hass Phys. Rev. C6, 670 (1972)	Sm	144	62
METHOD	REF. NO. 72 Ar 1		hmg

REACTION	RESULT	EXCITATION ENERGY	SOURCE		DETECTOR		ANGLE
			TYPE	RANGE	TYPE	RANGE	
G,G	LFT	9	D	9	SCD-D		135

No new data; re-evaluation of old data gives the following:

SEE 66BE3, 9 = 8.998

Γ = .27±.08 eV

Γ_o = .063 ± .013 eV

D = 110 eV

The 8.998-MeV resonance level excited by the (γ,γ') reaction, which was previously assigned to ^{150}Sm, is shown to belong to ^{144}Sm. The level scheme of ^{144}Sm is given and the re-evaluated level parameters of the 8.998-MeV resonance are presented.

REF.		ELEM. SYM.	A	Z
R. Bergere, H. Beil, P. Carlos, A. Lepretre, A. Veyssiere PICNS-73, Vol.I, p.525 Asilomar		Sm	144	62
METHOD		REF. NO. 73 Be 10		hmg

REACTION	RESULT	EXCITATION ENERGY	SOURCE TYPE	SOURCE RANGE	DETECTOR TYPE	DETECTOR RANGE	ANGLE
G,SN	ABX	10-21	D	10- 21	BF3-I		4PI

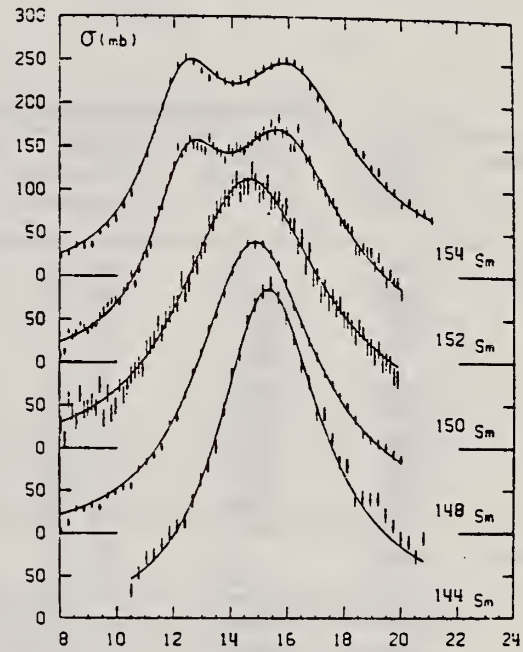

Fig. 19 Total photoneutron cross section $\sigma(\gamma,n)+\sigma(\gamma,2n)$ of Sm isotopes. The solid lines show the best 1 Lorentz line fit (^{144}Sm ^{148}Sm ^{150}Sm) or 2 Lorentz lines fit (^{152}Sm and ^{154}Sm).

Table III

	E_1 (MeV)	Γ_1 (MeV)	σ_1 (mb)
^{144}Sm	15.30±0.1	4.37±0.15	384±20
^{148}Sm	14.82±0.1	5.10±0.20	340±12
^{150}Sm	14.60±0.1	6.00±0.20	312±20

REF.	ELEM. SYM.	A	Z
H. Szichman Z. Physik 259, 217 (1973)	Sm	144	62

METHOD	REF. NO.	
	73 Sz 2	egf

REACTION	RESULT	EXCITATION ENERGY	SOURCE TYPE	SOURCE RANGE	DETECTOR TYPE	DETECTOR RANGE	ANGLE
G,G	LFT	9	D	9	SCD-D		DST

9 = 8.995

Table 1. Reduced partial radiation widths of resonance levels in ^{66}Zn, ^{144}Sm and ^{120}Sn

Nucleus	Energy of transition (keV)	Energy of final state	Relative intensity Γ_i/Γ_0 (in percent)	Reduced widths (eV · meV^{-4} × 10^3) $K(E1)$	$K(M1)$	Most likely characters	Derived spin and parity values $J\pi$
^{66}Zn	7693	0	100 ±1	6 ± 1	105± 21	$E1$	0+
	6654	1039.2	42 ±1	4 ± 1	68± 14	$E1$	2+
	5819	1874	<2	<0.3	<5	$E1$ or $M1$	0, 1, 2
	5321	2372	<3	<0.6	<9	$E1$ or $M1$	0, 1, 2
	4930	2763	<2	<0.5	<8	$E1$ or $M1$	0, 1, 2
	4755	2938.1	24 ±2	7 ± 2	106± 23	$E1$	0+
	4587	3105.8	8 ±1	2.4± 0.6	39± 9	$E1$ or $M1$	0, 1, 2
	4480	3212.6	21 ±2	7 ± 2	111± 25	$E1$	0+
	4452	3240.6	7 ±2	2.3± 0.8	38± 13	$E1$ or $M1$	0, 1, 2
	4361	3331.7	13 ±2	5 ± 1	75± 19	$E1$	0, 2+
	4263	3430.0	25 ±3	9 ± 2	154± 36	$E1$	0, 2+
	4187	3506.3	8 ±2	3 ± 1	52± 17	$E1$ or $M1$	0, 1, 2
^{144}Sm	8995	0	100 ±1	15 ± 3	412± 82	$E1$	0+
	7333	1662.0	33 ±1	9 ± 2	251± 50	$E1$	2+
	6828	2167	3 ±1	10 ± 4	28± 11	$E1$ or $M1$	0, 1, 2
	6568	2426.5	21 ±1	8 ± 2	222± 44	$E1$	2+
	6514	2480.7	46 ±1	18 ± 4	499±100	$E1$	0+
	6191	2804.1	12 ±1	6 ± 1	164± 33	$E1$	2+
^{120}Sn	7693	0	100 ±1.0	38 ±11	932±266	$E1$	0+
	6522	1171.4	7.3±0.5	5 ± 1	112± 32	$E1$	2+
	5520	2172.9	1.4±0.3	1.4± 0.4	35± 10	$E1$ or $M1$	0, 1, 2
	5337	2356.0	12.3±0.8	14 ± 4	343± 98	$E1$	2+

REF.	ELEM. SYM.	A	Z
P. Carlos, H. Beil, R. Bergere, A. Lepretre, A. De Miniac, and A. Veyssiere Nucl. Phys. A225, 171 (1974)	Sm	144	62

METHOD	REF. NO.	
	74 Ca 5	egf

REACTION	RESULT	EXCITATION ENERGY	SOURCE TYPE	SOURCE RANGE	DETECTOR TYPE	DETECTOR RANGE	ANGLE
G,N *	ABX	10- 21	D	10- 21	BF3-I		4PI
G,2N **	ABX	18- 21	D	18- 21	BF3-I		4PI

* 678 ✝
** 679

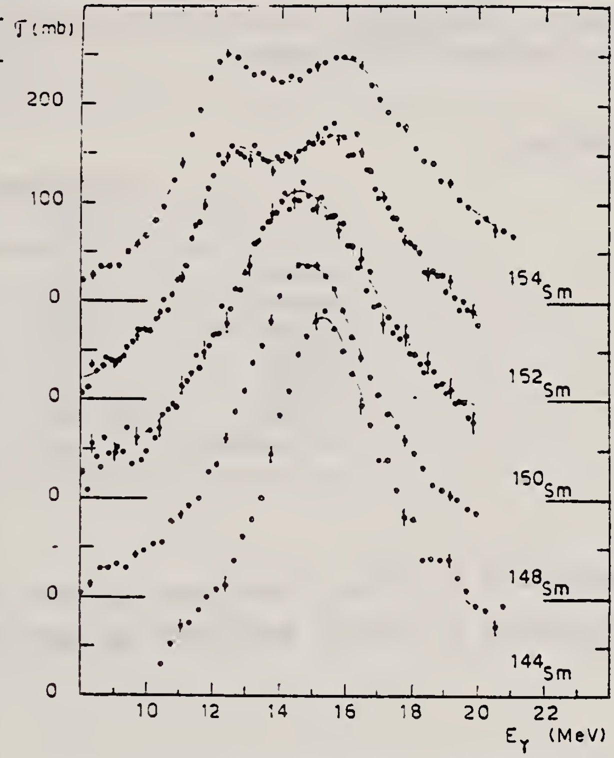

Fig. 7. Total photoneutron cross sections $\sigma_T(E)$ of the doubly even samarium isotopes. Best single Lorentz line fits are shown for ^{144}Sm, ^{148}Sm and ^{150}Sm. For ^{152}Sm and ^{154}Sm the best two Lorentz line fits are presented. Corresponding Lorentz line parameters are given in table 2.

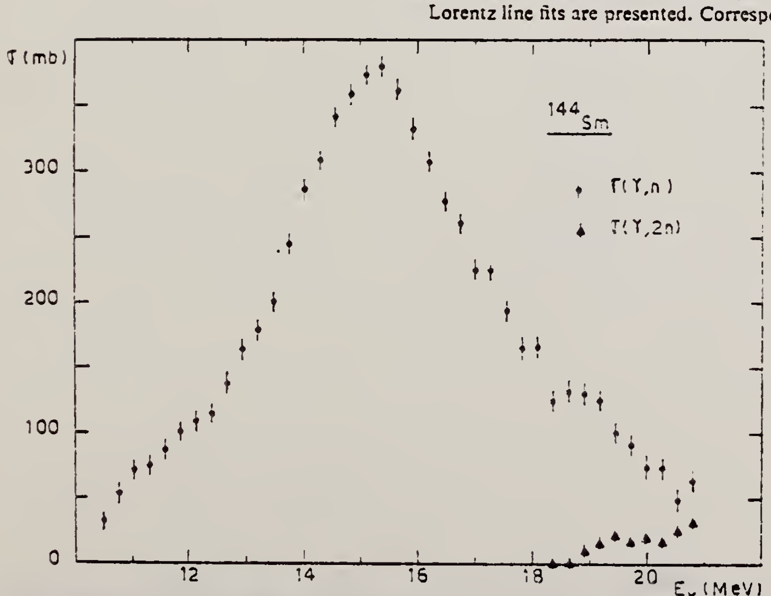

Fig. 2. Partial photoneutron cross sections $[\sigma(\gamma, n)+\sigma(\gamma, np)]$ and $\sigma(\gamma, 2n)$ of ^{144}Sm.

(over)

Table 2

Lorentz line parameters

	E_1 (MeV)	σ_1 (mb)	Γ_1 (MeV)	E_2 (MeV)	σ_2 (mb)	Γ_2 (MeV)
^{144}Sm*	15.3 ±0.1	384±20	4.37±0.15			
^{148}Sm*	14.8 ±0.1	339±12	5.1 ±0.2			
^{148}Sm**	14.1	335	4			
^{150}Sm*	14.6 ±0.1	312±20	6.0 ±0.2			
^{150}Sm**	13.6	360	5.5			
^{152}Sm*	12.45±0.10	183±10	3.2 ±0.15	15.85±0.10	226±10	5.1 ±0.2
^{152}Sm**	11.55	400	2.4	14.65	420	3.4
^{154}Sm*	12.35±0.10	192±10	3.35±0.15	16.1 ±0.1	204±10	5.25±0.[illegible]
^{154}Sm**	11	204	3	15.25	320	4

* Corresponding to best fits shown in fig. 7.

** Values taken from Vassilijev [23,24]) for comparison.

Table 3

Different integrated cross sections as defined in the text

	^{144}Sm	^{148}Sm	^{150}Sm	^{152}Sm	^{154}Sm
E_M (MeV)	21	20	20	20	21
σ_0 (MeV · b)	2 ±0.14	1.94±0.1	2 ±0.14	2.05±0.1	2.07±0.1
σ'_0 (MeV · b)	2.63	2.71	2.94	2.75	2.69
$\dfrac{\sigma'_0 A}{0.06\,NZ}$	1.24	1.25	1.35	1.24	1.2
σ_{-1} (mb)	131 ±15	134 ±10	141 ±15	144 ±10	145 [illegible]
σ_{-2} (mb · MeV^{-1})	8.7±0.8	9.5 ±0.7	10.3±0.9	10.6 ±0.7	10.[illegible] ±0.7

23. O. Vasilijev et al., Sov. J.Nucl.Phys. 10, 263 (1970)
24. O. Vasilijev et al., Sov.J. Nucl.Phys. 13, 463 (1971)

REF.	ELEM. SYM.	A	Z
F. R. Metzger Phys. Rev. C14, 543 (1976)	Sm	144	62

METHOD	REF. NO.	
	76 Me 6	hmg

REACTION	RESULT	EXCITATION ENERGY	SOURCE		DETECTOR		ANGLE
			TYPE	RANGE	TYPE	RANGE	
$ G,G	LFT	3	C	1- 4	SCD-D		DST
		(3.225)					

POLARIMETER EXPER

$$\frac{N_{\parallel} - N_{\perp}}{N_{\parallel} + N_{\perp}} = (+3.6 \pm 2.7)\%.$$

TABLE I. Properties of the low-lying 1^- levels in the stable even Sm isotopes.

Isotope	$E_{exc}(1^-)$	Γ_0 (meV)	$10^3 \times \frac{B(E1; 1^- \to 0^+)}{B(E1)_{s.p.}}$	N
^{144}Sm	3.225	220±30	3.5±0.5	82
^{148}Sm	1.465	3.1±0.4	0.5±0.1	86
^{150}Sm	1.166	5.4±0.5	1.8±0.2	88
^{152}Sm	0.963	7.3±0.6	4.2±0.4	90
^{154}Sm	0.921	7.4±1.0	4.8±0.7	92

REF.		ELEM. SYM.	A	Z
F.R. Metzger Phys. Rev. C 17, 939 (1978)		Sm	144	62
METHOD		REF. NO. 78 Me 2		egf

REACTION	RESULT	EXCITATION ENERGY	SOURCE TYPE	SOURCE RANGE	DETECTOR TYPE	DETECTOR RANGE	ANGLE
G,G	LFT	1- 5	C	5	SCD-D		DST

12 LEVELS SELF-ABS

Using electron bremsstrahlung with up to 5.2-MeV end-point energy, the resonant scattering of γ rays by an enriched sample of ^{144}Sm has been studied. Ground-state transitions were observed from a dozen levels, and the scattering yields, measured at 96° and 126°, were evaluated in terms of radiative widths and level spins. For the strongest excitations, these measurements were supplemented by self-absorption and linear-polarization studies. Some of the observed $E1$ transitions originate from 1^- states which, according to isobaric-analog-resonance studies, contain large neutron-particle-hole components. On the other hand, the 3.225— and 3.891-MeV levels, which exhibit the strongest $E1$ ground-state transitions, occur at energies which suggest that they arise from the coupling of the lowest octupole vibration to the 2_1^+ and 2_2^+ levels.

TABLE [illegible]. Spins and widths derived from the yields of the reaction ^{144}Sm(γ,γ) at scattering angles of 96° and 126°. Standard deviations are listed throughout.

E_{level} (MeV)	$N(126°)/N(96°)$	Spin	Γ_0^2/Γ (meV)
1.660(1)	0.42 ± 0.06	2	5.1 ± 1.2
2.423(1)	0.47 ± 0.08	2	14 ± 2
2.799(2)	0.58 ± 0.20	(2)	4.7 ± 0.9
3.225(1)	1.15 ± 0.09	1	220 ± 20
3.318(3)	0.8 ± 0.3	1,2	11 ± 3
3.891(2)	1.22 ± 0.17	1	210 ± 30
3.905(3)	2.0 ± 0.8	(1)	25 ± 8
3.966(2)	1.27 ± 0.17	1	70 ± 10
4.262(2)	1.20 ± 0.19	1	170 ± 30
5.015(5)	1.10 ± 0.40	(1)	140 ± 40
5.103(3)	0.9 ± 0.3	1,2	140 ± 40
5.151(3)	1.3 ± 0.3	(1)	290 ± 60

Sm
A=148

Sm
A=148

Sm
A=148

REF.	ELEM. SYM.	A	Z
F. R. Metzger Phys. Rev. 137, B1415-20 (1965)	Sm	148	62

METHOD	REF. NO.	
Radioactive source.	65 Me 1	NVB

REACTION	RESULT	EXCITATION ENERGY	SOURCE TYPE	SOURCE RANGE	DETECTOR TYPE	DETECTOR RANGE	ANGLE
G,G	LFT	1	D	1	NAI-D		DST
		(1.46)		(1.46)			

$$\tau = (1.4 \begin{smallmatrix} +0.6 \\ -0.3 \end{smallmatrix}) \times 10^{-13} \text{ sec.}$$

TABLE II. Summary of the transition probabilities determined in this work, and comparison with the predictions of the single-particle model (Ref. 16).

Nucleus	E_γ (MeV)	Transition	Transition probability (sec^{-1})	$B(E1)_d$ ($10^{-30}e^2$ cm^2)	$\frac{B(E1)_d}{B(E1)_{sp}}$
Sm^{144}	1.46	$1^- \rightarrow 0^+$	$(4.3 \pm 1.2) \times 10^{12}$	0.9	5×10^{-4}
	0.91	$1^- \rightarrow 2^+$	$(2.7 \pm 0.8) \times 10^{12}$	2.3	12×10^{-4}
Sm^{148}	0.96	$1^- \rightarrow 0^+$	$(11 \pm 1) \times 10^{12}$	7.9	4×10^{-3}
	0.84	$1^- \rightarrow 2^+$	$(14 \pm 2) \times 10^{12}$	15.4	8×10^{-3}

REF.	O. V. Vasil'ev, V. A. Semenov, and S. F. Semenko Yad. Fiz. 13, 463 (1971) Sov. J. Nucl. Phys. 13, 259 (1971)	ELEM. SYM.	A	Z
		Sm	148	62
METHOD		REF. NO.		
		71 Va 2		hmg

REACTION	RESULT	EXCITATION ENERGY	SOURCE TYPE	SOURCE RANGE	DETECTOR TYPE	DETECTOR RANGE	ANGLE
G,XN	ABX	8-24	C	8-24	BF3-I		4PI
		(8.1-23.25)		(8.1-23.25)			

Table II. Parameters of giant dipole resonance

Isotope	σ_1, mb	E_1, MeV	Γ_1, MeV	$\sigma_{int\,1}$, MeV·b	σ_2, mb	E_2, MeV	Γ_2, MeV	$\sigma_{int\,2}$, MeV·b	σ_{int}	$\frac{\sigma_{int}}{0.06\,NZ/A}$	$\frac{\sigma_{int\,2}}{\sigma_{int\,1}}$	$\frac{E_2}{E_1}$	β_{eff}
Nd^{146}	332	13,8	4,1						2,12	1,00			
Sm^{148}	335	14,1	4,0						2,08	0,96			
Gd^{152}	147	12,0	3,0	0,693	259	15,0	3,2	1,29	1,99	0,90	1,87	1,25	0,28
Gd^{154}	161	11,9	2,4	0,612	250	15,0	3,5	1,39	2,00	0,89	2,27	1,26	0,29
Gd^{156}	180	11,9	2,6	0,738	243	15,2	3,6	1,37	2,11	0,94	1,86	1,27	0,31
Gd^{158}	165	11,7	2,8	0,662	249	14,9	3,8	1,49	2,16	0,94	2,25	1,28	0,32
Eu^{151}	285	14,0	4,5						2,02	0,92			
Eu^{153}	159	11,9	2,3	0,562	237	15,1	3,6	1,34	1,90	0,86	2,39	1,27	0,31

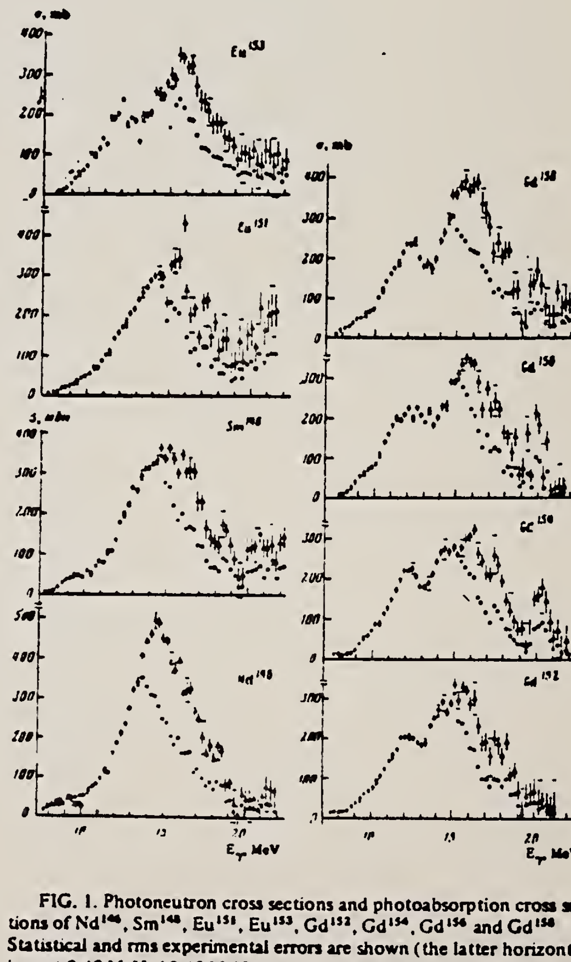

FIG. 1. Photoneutron cross sections and photoabsorption cross sections of Nd^{146}, Sm^{148}, Eu^{151}, Eu^{153}, Gd^{152}, Gd^{154}, Gd^{156} and Gd^{158} Statistical and rms experimental errors are shown (the latter horizontal bars at 9.42 MeV, 10.42 MeV etc.) At photon energies above the (γ, 2n) threshold the photoabsorption cross section errors are not shown.

REF. R. Bergere, H. Beil, P. Carlos, A. Lepretre, A. Veyssiere
PICNS-73, Vol. I, p. 525 Asilomar

ELEM. SYM.	A	Z
Sm	148	62

METHOD

REF. NO.	
73 Be 10	hmg

REACTION	RESULT	EXCITATION ENERGY	SOURCE TYPE	SOURCE RANGE	DETECTOR TYPE	DETECTOR RANGE	ANGLE
G,SN	ABX	8- 20	D	8- 20	BF3-I		4PI

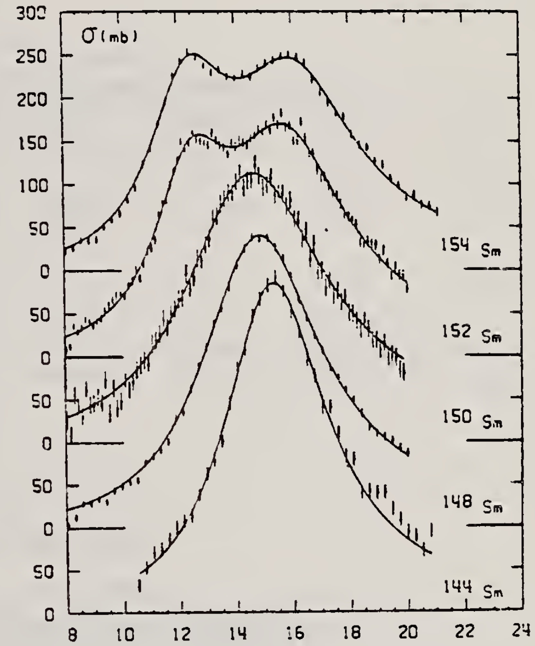

Fig. 19 Total photoneutron cross section $\sigma(\gamma,n)+\sigma(\gamma,2n)$ of Sm isotopes. The solid lines show the best 1 Lorentz line fit (^{144}Sm ^{148}Sm ^{150}Sm) or 2 Lorentz lines fit (^{152}Sm and ^{154}Sm).

Table III

	E_1 (MeV)	Γ_1 (MeV)	σ_1 (mb)
^{144}Sm	15.30±0.1	4.37±0.15	384±20
^{148}Sm	14.82±0.1	5.10±0.20	340±12
^{150}Sm	14.60±0.1	6.00±0.20	312±20

REF.	ELEM. SYM.	A	Z
P. Carlos, H. Beil, R. Bergere, A. Lepretre, A. De Miniac, and A. Veyssiere Nucl. Phys. A225, 171 (1974)	Sm	148	62
METHOD	REF. NO. 74 Ca 5		egf

REACTION	RESULT	EXCITATION ENERGY	SOURCE TYPE	SOURCE RANGE	DETECTOR TYPE	DETECTOR RANGE	ANGLE
G,N *	ABX	8- 20	D	8- 20	BF3-I		4PI
G,2N **	ABX	13- 20	D	13- 20	BF3-I		4PI

* 681 +
** 682+

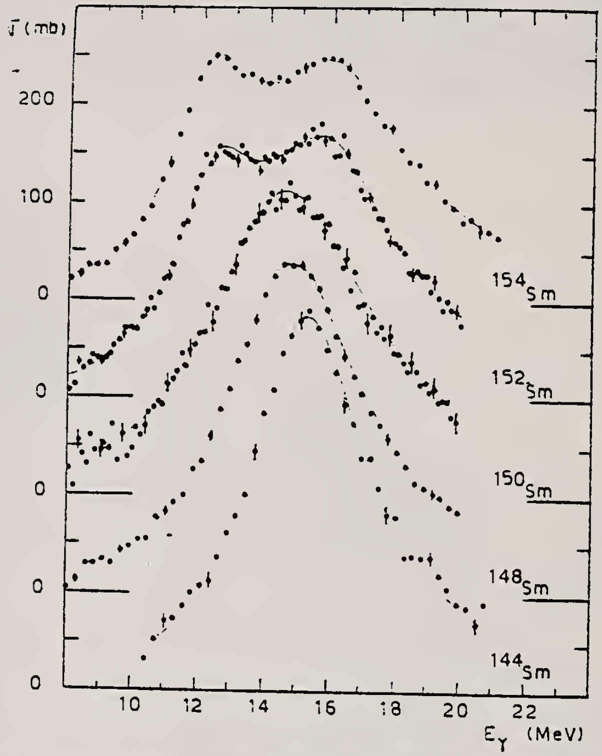

Fig. 7. Total photoneutron cross sections $\sigma_T(E)$ of the doubly even samarium isotopes. Best single Lorentz line fits are shown for ^{144}Sm, ^{148}Sm and ^{150}Sm. For ^{152}Sm and ^{154}Sm the best two Lorentz line fits are presented. Corresponding Lorentz line parameters are given in table 2.

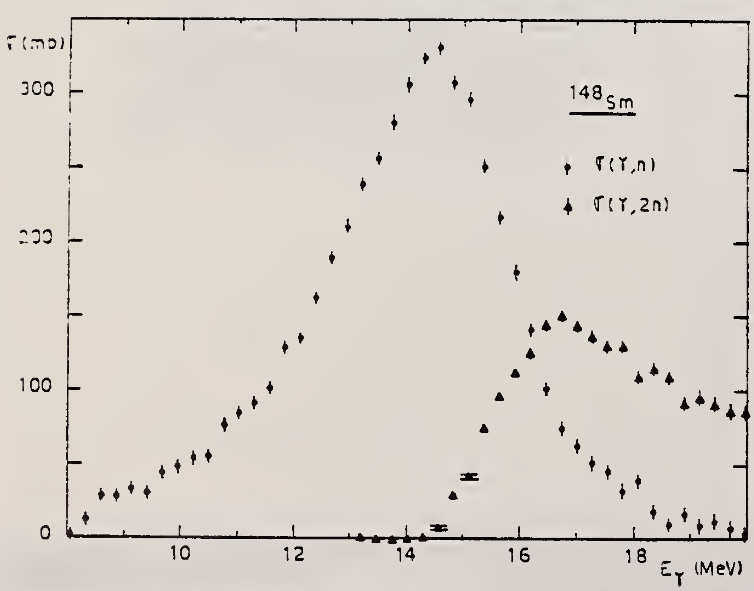

Fig. 3. Partial photoneutron cross sections $[\sigma(\gamma, n)+\sigma(\gamma, np)]$ and $\sigma(\gamma, 2n)$ of ^{148}Sm.

:T 276

(over)

Table 2

Lorentz line parameters

	E_1 (MeV)	σ_1 (mb)	Γ_1 (MeV)	E_2 (MeV)	σ_2 (mb)	Γ_2 (M[illegible]
^{144}Sm*	15.3 ±0.1	384±20	4.37±0.15			
^{148}Sm*	14.8 ±0.1	339±12	5.1 ±0.2			
^{148}Sm**	14.1	335	4			
^{150}Sm*	14.6 ±0.1	312±20	6.0 ±0.2			
^{150}Sm**	13.6	360	5.5			
^{152}Sm*	12.45±0.10	183±10	3.2 ±0.15	15.85±0.10	226±10	5.1 ±[illegible]
^{152}Sm**	11.55	400	2.4	14.65	420	[illegible]4
^{154}Sm*	12.35±0.10	192±10	3.35±0.15	16.1 ±0.1	204±10	5.25±[illegible]
^{154}Sm**	11	204	3	15.25	320	4

* Corresponding to best fits shown in fig. 7.

** Values taken from Vassilijev [23,24]) for comparison.

Table 3

Different integrated cross sections as defined in the text

	^{144}Sm	^{148}Sm	^{150}Sm	^{152}Sm	^{154}S[illegible]
E_M (MeV)	21	20	20	20	2[illegible]
σ_0 (MeV · b)	2 ±0.14	1.94±0.1	2 ±0.14	2.05±0.1	2.0[illegible]±[illegible]
σ'_0 (MeV · b)	2.63	2.71	2.94	2.75	2.6[illegible]
$\frac{\sigma'_0 A}{0.06\, NZ}$	1.24	1.25	1.35	1.24	1.2[illegible]
σ_{-1} (mb)	131 ±15	134 ±10	141 ±15	144 ±10	145 [illegible]
σ_{-2} (mb · MeV^{-1})	8.7±0.8	9.5 ±0.7	10.3±0.9	10.6 ±0.7	10.[illegible] ±[illegible]7

[23] O. Vasilijev et al., Sov.J.Nucl.Phys. 10, 263 (1970)

[24] O. Vasilijev et al., Sov.J.Nucl.Phys. 13, 463 (1971)

REF.	F. R. Metzger Phys. Rev. C14, 543 (1976)	ELEM. SYM.	A	Z
		Sm	148	62
METHOD		REF. NO.		
		76 Me 6		hmg

REACTION	RESULT	EXCITATION ENERGY	SOURCE		DETECTOR		ANGLE
			TYPE	RANGE	TYPE	RANGE	
G,G	LFT	2	C	1- 4	SCD-D		DST
		(1.465)					

$$\frac{N_{\parallel} - N_{\perp}}{N_{\parallel} + N_{\perp}} = (+3.6 \pm 2.7)\,\%.$$

TABLE I. Properties of the low-lying 1^- levels in the stable even Sm isotopes.

Isotope	$E_{exc}(1^-)$	Γ_0 (meV)	$10^3 \times \frac{B(E1;1^- \rightarrow 0^+)}{B(E1)_{s.p.}}$	N
^{144}Sm	3.225	220±30	3.5±0.5	82
^{148}Sm	1.465	3.1±0.4	0.5±0.1	86
^{150}Sm	1.166	5.4±0.5	1.8±0.2	88
^{152}Sm	0.963	7.3±0.6	4.2±0.4	90
^{154}Sm	0.921	7.4±1.0	4.8±0.7	92

REF. B.S. Dolbilkin, S. Ohsawa, Y. Torizuka, T. Saito, Y. Mizuno, K. Saito
Phys. Rev. C25, 2255 (1982)

ELEM. SYM.	A	Z
Sm	148	62

METHOD

REF. NO.	
82 Do 6	egf

REACTION	RESULT	EXCITATION ENERGY	SOURCE TYPE	SOURCE RANGE	DETECTOR TYPE	DETECTOR RANGE	ANGLE
E,E/		5-33	D	150-215	MAG-D		DST

Q .38-.64 FM-1

The electron scattering cross sections from the enriched ^{148}Sm (96.5%) and ^{152}Sm (99.2%) isotopes have been measured between 5 and 33 MeV excitation energies for incident energies in the range of between 150 and 215 MeV and scattering angles of 30°, 35°, and 40°. The giant resonances at $E_x = 14.8$ ($78A^{-1/3}$), 11.6 ($61A^{-1/3}$), 15.5 ($82A^{-1/3}$), and 24 ($129A^{-1/3}$) MeV for ^{148}Sm were classified according to their momentum transfer dependence. The K splittings of the giant $E1$ ($T=1$) and $E2$ ($T=0,1$) resonances for deformed ^{152}Sm were observed in agreement with a vibrating potential model. The splittings between the $K=0^+$ and 2^+ components for the isoscalar and isovector quadrupole resonances are ~2 MeV and ~5 MeV, respectively. The fitted parameters classified as the giant monopole resonance are the same for spherical ^{148}Sm and for deformed ^{152}Sm. The difference between the isoscalar giant resonance parameters for resonance energies and width found from hadron scattering and those for electron scattering is discussed for the rare-earth region.

[NUCLEAR REACTIONS ^{148,152}Sm(e,e'), enriched targets, $E_0 = 150$ to 215 MeV, $\theta = 30°, 35°, 40°$, $q = 0.38-0.64$ fm^{-1}. Measured $d^2\sigma/d\Omega dE_x$ up to 33 MeV in excitation energy; deduced multipolarity, excitation energy, width, sum rule exhaustion of giant resonances.]

TABLE IV. Comparison between (e,e') results and theoretical results for the giant multipole resonance energy (MeV).

Type	Nucleus	Isoscalar Present work	Isoscalar Ref. 10	Isoscalar Theory Ref. 9	Isoscalar Ref. 24	Isovector Present work	Isovector Theory Ref. 10	Isovector Theory Ref. 9
GMR	^{148}Sm	15.5±0.3			15.1			
	^{152}Sm	15.7±0.3		10.7	10.5			
				18.3	15.9			
GDR	^{148}Sm					14.8	14.8	
	^{152}Sm					12.45	12.3	12.0
						15.85	16.3	15.0
	^{148}Sm	11.6±0.2	10.9		11.9	24.3±0.4	26.4	
		10.6±0.2	9.9	11.0	10.5	21.0±0.9	24.1	19.5
GQR	^{152}Sm	11.4±0.4	10.4	12.0		23.2±1.0	25.2	22.5
		12.7±0.4	11.8	13.0	13.1	26.0±0.5	28.8	25.5

(OVER)

TABLE V. Parameters of the isoscalar GQR in the Sm isotopes.

Nucleus	E_x (MeV)	Γ (MeV)	EWSR (%)	Reaction	Reference
^{144}Sm	13.0±0.3	3.9±0.2	91±25	(α,α')	25
^{144}Sm	12.4±0.4	2.6±0.4	85±15	(α,α')	6
^{144}Sm	12.1±0.2	2.4±0.2	45±15	(α,α')	8
^{144}Sm	12.5	3.4	60	(α,α')	26
^{144}Sm	11.9±0.2	2.9±0.2		(e,e')	27
^{148}Sm	12.5±0.2	4.3±0.2	104±25	(α,α')	25
^{148}Sm	11.6±0.2	3.1±0.2	100±10	(e,e')	Present work
^{150}Sm	11.8±0.2	3.3±0.2		(e,e')	27
	10.6±0.2	2.4±0.2	20±5		
^{152}Sm	11.4±0.4	2.7±0.2	45±9	(e,e')	Present work
	12.7±0.4	3.0±0.2	35±7		
^{154}Sm	12.4±0.3	4.7±0.3	102±25	(α,α')	25
^{154}Sm	12.2	4.5		(α,α')	7
^{154}Sm	11.8±0.3	3.7±0.3		(α,α')	8
^{154}Sm	10.9±0.2	4.5±0.2		(e,e')	27

TABLE VI. Comparison of the GMR parameters in the Sm isotopes obtained from various reactions.

Nucleus	E_x (MeV)	Γ (MeV)	EWSR (%)	Reaction	Reference
^{144}Sm	15.1±0.5	2.9±0.5	100±50	(α,α')	6
^{144}Sm	14.6±0.2	3.0±0.3	140±40	(α,α')	8
^{144}Sm	15.2	2.5		(α,α')	26
^{144}Sm	15.5±0.5	2.5±0.5	100±25	(p,p')	31
^{144}Sm	14.7±0.2	2.9±0.2	67±13	(^{3}He,^{3}He')	32
^{144}Sm	14.8±0.2	2.4±0.15	20±10	(e,e')	30
^{148}Sm	15.5±0.3	3.0±0.2	100±10	(e,e')	Present work
^{150}Sm	15.1±0.25	3.0±0.25	60±19	(^{3}He,^{3}He')	32
^{152}Sm	14.8±0.25	3.1±0.25	54±9	(^{3}He,^{3}He')	32
^{152}Sm	15.7±0.3	3.1±0.4	100±20	(e,e')	Present work
^{154}Sm	15.5±0.5	2.5±0.5	100±25	(p,p')	31
^{154}Sm	14.9±0.3	2.6±0.4	55±15	(α,α')	8

Sm
A=149

Sm
A=149

Sm
A=149

REF.	ELEM. SYM.	A	Z
[illegible] Geller, J. Halpern, and E. G. Muirhead Phys. Rev. 118, 1302-12 (1960)	Sm	149	62

METHOD	REF. NO.	
Betatron; neutron threshold; ion chamber	60 Ge 3	NVB

REACTION	RESULT	EXCITATION ENERGY	SOURCE TYPE	SOURCE RANGE	DETECTOR TYPE	DETECTOR RANGE	ANGLE
G,N	NØX	THR	C THR		BF3-I		4 PI

THRESHØLD

TABLE I. Summary and comparison of neutron separation energies inferred from present threshold measurements with values predicted from mass data and reaction energies. All energies are expressed in the center-of-mass system in Mev.

Reaction	No. runs	Present results	Other results	Method	Reference
$Sm^{149}(\gamma,n)Sm^{148}$	1	6.45 ±0.16(5.89)	5.87 ±0.28	mass data	p

p W. H. Johnson, Jr., and A. O. Nier, Phys. Rev. 105, 1014 (1957).

TABLE II. Comparison of measured threshold energies with neutron binding energies predicted by mass data for transitions with $\Delta I \geq 7/2$. All energies in Mev.

Reaction	ΔI[a]	Observed threshold	Mass data Q value	$E_{th}-Q$	Excited state energy
$Cr^{52}(\gamma,n)Cr^{51}$	7/2	12.18±0.14	12.053±0.004[b]	0.13±0.14	...
$Y^{89}(\gamma,n)Y^{88}$	7/2	11.59±0.08	11.53 ±0.40[c]	0.06±0.41	0.387[d]
$In^{115}(\gamma,n)In^{114}$	7/2	9.22±0.03	9.35 ±0.43[c]	−0.13±0.43	0.191[a]
$Ce^{142}(\gamma,n)Ce^{141}$	(7/2)[e]	7.24±0.07	6.97 ±0.07[f]	0.27±0.10	...
$Nd^{145}(\gamma,n)Nd^{144}$	7/2	6.38±0.16	5.97 ±0.19[f]	0.41±0.25	0.690[a]
$Sm^{149}(\gamma,n)Sm^{148}$	7/2	6.45±0.16	5.87 ±0.28[f]	0.58±0.33	0.562[a]
$Er^{167}(\gamma,n)Er^{166}$	7/2	6.65±0.08	6.45 ±0.06[g]	0.20±0.10	0.081[a]
$Hf^{177}(\gamma,n)Hf^{176}$	7/2	6.69±0.03	6.28 ±0.06[g]	0.64±0.07	0.088[a]
$Hf^{179}(\gamma,n)Hf^{178}$	9/2	6.31±0.07	6.17 ±0.06[g]	0.14±0.09	0.093[a]
$Hf^{180}(\gamma,n)Hf^{179}$	9/2	7.85±0.11	7.32 ±0.06[g]	0.53±0.13	0.375[a]

[a] Strominger, J. M. Hollander, and G. T. Seaborg, Revs. Modern Phys. 30, 585 (1958).
[b] F. Giese and J. L. Benson, Phys. Rev. 110, 712 (1958).
[c] ... E. Duckworth, *Mass Spectroscopy* (Cambridge University Press, New York, 1958), p. 177.
[d] Dzelepov and L. K. Peker, Atomic Energy of Canada Limited Report Tr. AECL-457 (unpublished).
[e] ... discrepancy in the case of Ce^{142} predicts a ground-state spin for Ce^{142} of 0, since the spin of Ce^{141} is known to be 7/2.
[f] W. H. Johnson, Jr., and A. O. Nier, Phys. Rev. 105, 1014 (1957).
[g] W. H. Johnson, Jr., and V. B. Bhanot, Phys. Rev. 107, 6 (1957).

Sm
A=150

Sm
A=150

Sm
A=150

O. V. Vasilijev, G. N. Zalesny, S. F. Semenko, V. A. Semenov
Phys. Letters 30B, 97 (1969)

ELEM. SYM.	A	Z
Sm	150	62

METHOD

REF. NO.	
69 Va 2	egf

REACTION	RESULT	EXCITATION ENERGY	SOURCE TYPE	SOURCE RANGE	DETECTOR TYPE	DETECTOR RANGE	ANGLE
G,XN	ABX	8-23	C	8-23	BF3-I		4PI

210

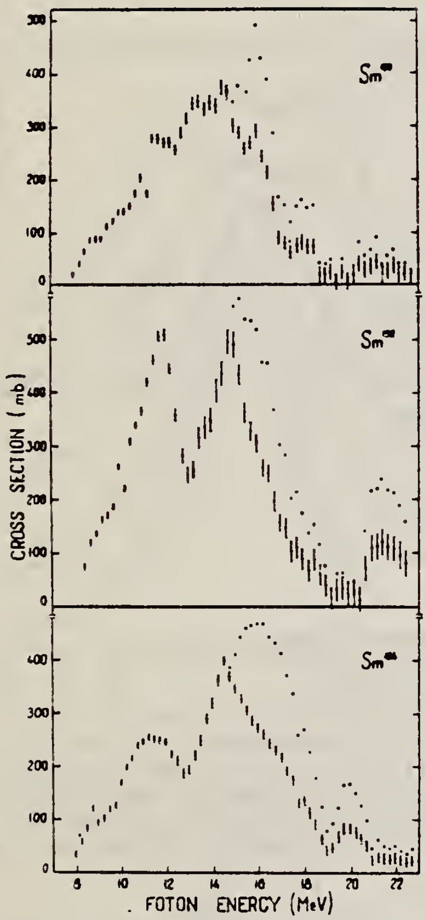

Fig. 3. The photoneutron and photoabsorption cross sections of ^{150}Sm, ^{152}Sm and ^{154}Sm. The symbols are the same as in fig. 2.

REF.	R. Bergere, H. Beil, P. Carlos, A. Lepretre, A. Veyssiere PICNS-73, Vol.I, p.525 Asilomar	ELEM. SYM. Sm	A 150	Z 62
METHOD		REF. NO. 73 Be 10		hmg

REACTION	RESULT	EXCITATION ENERGY	SOURCE TYPE	SOURCE RANGE	DETECTOR TYPE	DETECTOR RANGE	ANGLE
G,SN	ABX	8- 20	D	8- 20	BF3-I		4PI

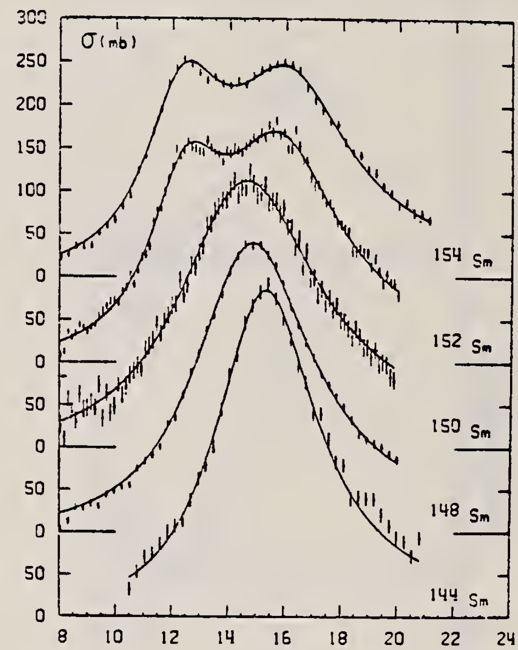

Fig. 19 Total photoneutron cross section $\sigma(\gamma,n)+\sigma(\gamma,2n)$ of Sm isotopes. The solid lines show the best 1 Lorentz line fit (^{144}Sm ^{148}Sm ^{150}Sm) or 2 Lorentz lines fit (^{152}Sm and ^{154}Sm).

Table III

	E_1 (MeV)	Γ_1 (MeV)	σ_1 (mb)
^{144}Sm	15.30±0.1	4.37±0.15	384±20
^{148}Sm	14.82±0.1	5.10±0.20	340±12
^{150}Sm	14.60±0.1	6.00±0.20	312±20

REF.	ELEM. SYM.	A	Z
P. Carlos, H. Beil, R. Bergere, A. Lepretre, A. De Miniac, and A. Veyssiere Nucl. Phys. A225, 171 (1974)	Sm	150	62

METHOD	REF. NO.	
	74 Ca 5	egf

REACTION	RESULT	EXCITATION ENERGY	SOURCE TYPE	SOURCE RANGE	DETECTOR TYPE	DETECTOR RANGE	ANGLE
G,N *	ABX	8- 20	D	8- 20	BF3-I		4PI
G,2N **	ABX	13- 20	D	13- 20	BF3-I		4PI

* 684 +
**685+

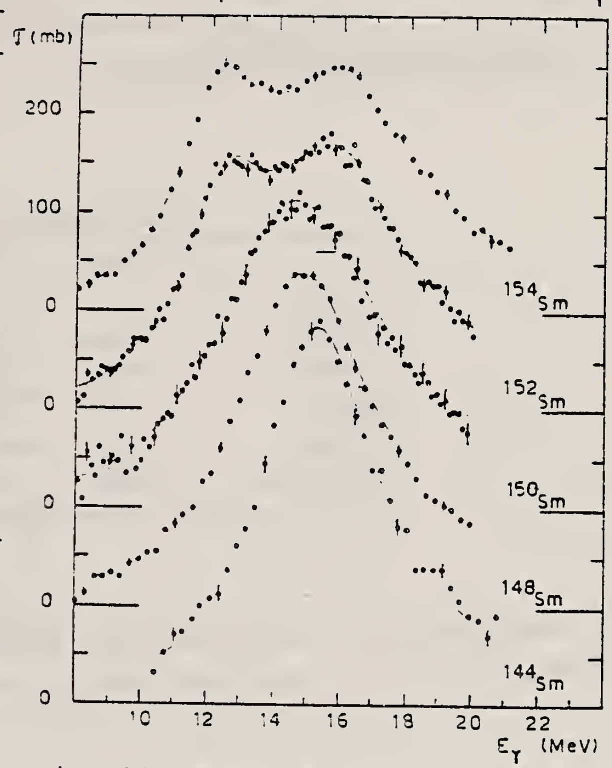

Fig. 7. Total photoneutron cross sections $\sigma_T(E)$ of the doubly even samarium isotopes. Best single Lorentz line fits are shown for ^{144}Sm, ^{148}Sm and ^{150}Sm. For ^{152}Sm and ^{154}Sm the best two Lorentz line fits are presented. Corresponding Lorentz line parameters are given in table 2.

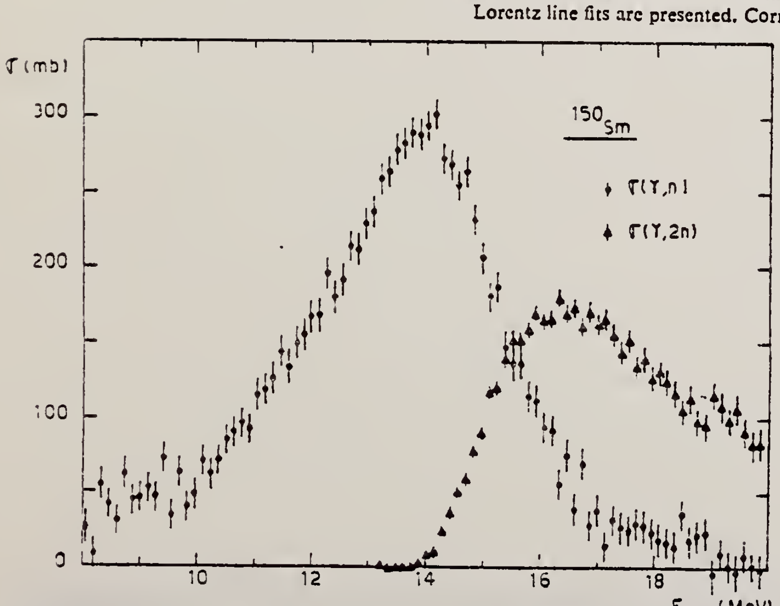

Fig. 4. Partial photoneutron cross sections $[\sigma(\gamma, n)+\sigma(\gamma, np)]$ and $\sigma(\gamma, 2n)$ of ^{150}Sm.

(over)

TABLE 2

Lorentz line parameters

	E_1 (MeV)	σ_1 (mb)	Γ_1 (MeV)	E_2 (MeV)	σ_2 (mb)	Γ_2 (MeV)
^{144}Sm*	15.3 ±0.1	384±20	4.37±0.15			
^{148}Sm*	14.8 ±0.1	339±12	5.1 ±0.2			
^{148}Sm**	14.1	335	4			
^{150}Sm*	14.6 ±0.1	312±20	6.0 ±0.2			
^{150}Sm**	13.6	360	5.5			
^{152}Sm*	12.45±0.10	183±10	3.2 ±0.15	15.85±0.10	226±10	5.1 ±[illegible]
^{152}Sm**	11.55	400	2.4	14.65	420	3.4
^{154}Sm*	12.35±0.10	192±10	3.35±0.15	16.1 ±0.1	204±10	5.25±[illegible]
^{154}Sm**	11	204	3	15.25	320	4

* Corresponding to best fits shown in fig. 7.

** Values taken from Vassilijev [23,24]) for comparison.

TABLE 3

Different integrated cross sections as defined in the text

	^{144}Sm	^{148}Sm	^{150}Sm	^{152}Sm	^{154}Sm
E_M (MeV)	21	20	20	20	21
σ_0 (MeV · b)	2 ±0.14	1.94±0.1	2 ±0.14	2.05±0.1	2.07±0.1
σ'_0 (MeV · b)	2.63	2.71	2.94	2.75	2.69
$\dfrac{\sigma'_0 A}{0.06\,NZ}$	1.24	1.25	1.35	1.24	1.21
σ_{-1} (mb)	131 ±15	134 ±10	141 ±15	144 ±10	145 ±10
σ_{-2} (mb · MeV^{-1})	8.7±0.8	9.5 ±0.7	10.3±0.9	10.6 ±0.7	10.6 ±0.7

[23] O. Vasilijev et al., Sov.J.Nucl.Phys. 10, 263 (1970)

[24] O. Vasilijev et al., Sov.J.Nucl.Phys. 13, 463 (1971)

REF.	F. R. Metzger Phys. Rev. C14, 543 (1976)	ELEM. SYM.	A	Z
		Sm	150	62
METHOD		REF. NO. 76 Me 6		hmg

REACTION	RESULT	EXCITATION ENERGY	SOURCE TYPE	SOURCE RANGE	DETECTOR TYPE	DETECTOR RANGE	ANGLE
G,G	LFT	2	C	1- 4	SCD-D		DST
		(1.166)					

$$\frac{N_{\parallel} - N_{\perp}}{N_{\parallel} + N_{\perp}} = (+3.6\pm2.7)\%$$

TABLE I. Properties of the low-lying 1^- levels in the stable even Sm isotopes.

Isotope	$E_{exc}(1^-)$	Γ_0 (meV)	$10^3\times\frac{B(E1;1^-\to0^+)}{B(E1)_{s.p.}}$	N
^{144}Sm	3.225	220±30	3.5±0.5	82
^{148}Sm	1.465	3.1±0.4	0.5±0.1	86
^{150}Sm	1.166	5.4±0.5	1.8±0.2	88
^{152}Sm	0.963	7.3±0.6	4.2±0.4	90
^{154}Sm	0.921	7.4±1.0	4.8±0.7	92

Sm
A=152

Sm
A=152

Sm
A=152

REF.	ELEM. SYM.	A	Z
F. R. Metzger Phys. Rev. 137, B1415-20 (1965)	Sm	152	62

METHOD	REF. NO.	
Radioactive source.	65 Me 1	NVB

REACTION	RESULT	EXCITATION ENERGY	SOURCE TYPE	SOURCE RANGE	DETECTOR TYPE	DETECTOR RANGE	ANGLE
G,G	LFT	1	D	1	NAI-D		105
		(0.96)		(0.96)			

$\tau = (3.9 \pm 0.4) \times 10^{-14}$ sec.

TABLE II. Summary of the transition probabilities determined in this work, and comparison with the predictions of the single-particle model (Ref. 16).

Nucleus	E_γ (MeV)	Transition	Transition probability (sec^{-1})	$B(E1)_d$ ($10^{[illegible]} e^2$ cm^2)	$B(E1)_d / B(E1)_{[illegible]}$
Sm[illegible]	1.46	$1^- \rightarrow 0^+$	$(4.3 \pm 1.2) \times 10^{12}$	0.9	$5 \times 10^{[illegible]}$
	0.91	$1^- \rightarrow 2^+$	$(2.7 \pm 0.8) \times 10^{12}$	2.3	$12 \times 10^{[illegible]}$
Sm[illegible]	0.96	$1^- \rightarrow 0^+$	$(11 \pm 1) \times 10^{12}$	7.9	$4 \times 10^{[illegible]}$
	0.84	$1^- \rightarrow 2^+$	$(14 \pm 2) \times 10^{12}$	15.4	$8 \times 10^{[illegible]}$

REF.	ELEM. SYM.	A	Z
R. B. Begzhanov, A. A. Islamov, and S. V. Starodubtsev J. Nucl. Phys. (USSR) 5, 250 (1967) Sov. J. Nucl. Phys. 5, 176 (1967)	Sm	152	62

METHOD	REF. NO.	
	67 Be 4	HMG

REACTION	RESULT	EXCITATION ENERGY	SOURCE TYPE	SOURCE RANGE	DETECTOR TYPE	DETECTOR RANGE	ANGLE
G,G	LFT	1.0	D	1.0	NAI-D		120
		(963 keV)					

$\tau = 5.15 \pm 0.50 \times 10^{-14}$ sec

Table I

E_{exc}, keV	Solid source		Liquid source		$N(E_p)_{sol}/N(E_p)_{liq}$	Γ_γ (963)*, 10^{-3} eV	$\bar{\tau}$, 10^{-14} sec
	$\bar{\sigma}$, 10^{-28} cm^2	$N(E_p)_{sol}$, eV^{-1}	σ, 10^{-28} cm^2	$N(E_p)_{liq}$, eV^{-1}			
963	6.0±0.2	0.0171	7.1±0.4	0.0202	0.85±0.02	3.8±0.4	7.6±0.8

*We used the values of $\bar{\sigma}_{liq}$ and the calculated value $N(E_p)_{das} = 0.0149$.

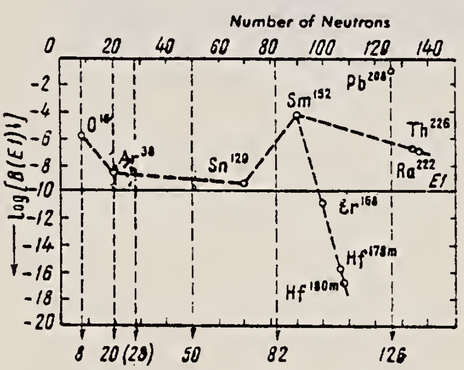

Fig. 2. Dependence of the logarithm of the reduced probability of the $E1$ transition on the number of neutrons for certain even-even nuclei.

REF.		ELEM. SYM.	A	Z
	G. K. Tandon and J. A. McIntyre Nucl. Instr. and Meth. 59, 181 (1968)	Sm	152	62
METHOD		REF. NO. 68 Ta 2		egf

REACTION	RESULT	EXCITATION ENERGY	SOURCE TYPE	SOURCE RANGE	DETECTOR TYPE	DETECTOR RANGE	ANGLE
G,G	LFT	1	D	1	NAI-D	1	90
		(963 keV)		(963 keV)			

COMPTON SCTD SOURCE

TABLE I
Lifetime measurements.

Line	Mean life (10^{-14} sec)	Investigator
	963-keV level in ^{63}Cu	
1	91 ± 6	Avg. of ref. [18–20]
2	110 ± 16	This measurement
	963-keV level in ^{152}Sm	
3	4.3 ± 0.3	Avg. of ref. [23,24]
4	7.1 ± 2.1	This measurement
	Ratio τ(Cu)/τ(Sm)	
5	21 ± 2	From 1 and 3
6	16 ± 5	This measurement

[18] J. B. Cumming, A. Schwarzschild, A. W. Sunyar and N. T Porile, Phys. Rev. 120 (1960) 2128.
[19] T. Rothem, F. R. Metzger and C. P. Swann, Nucl. Physics 22 (1961) 505.
[20] M. A. Eswaran, H. E. Gove, A. E. Litherland and C. Broude, Phys. Letters 8 (1964) 52.
[21] I. Marklund, Nucl. Physics 9 (1958) 83.
[22] L. Grodzins, Phys. Rev. 109 (1958) 1014.
[23] G. G. Shute and B. S. Sood, Proc. Roy. Soc. (London) A25 (1960) 52.
[24] F. R. Metzger, Phys. Rev. 137 (1965) B1415.

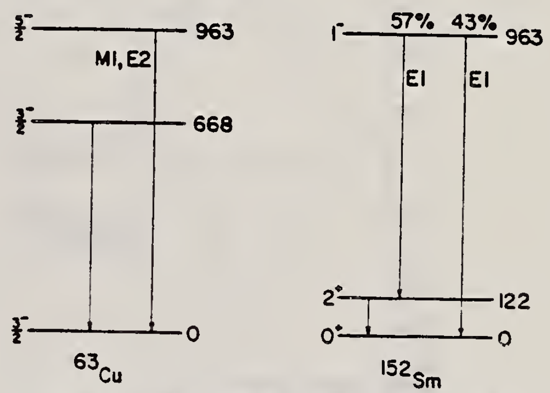

Fig. 11. Level schemes of ^{63}Cu and ^{152}Sm below 1000 keV. All energies are in keV.

REF.	ELEM. SYM.	A	Z
O. V. Vasilijev, G. N. Zalesny, S. F. Semenko, V. A. Semenov Phys. Letters 30B, 97 (1969)	Sm	152	62

METHOD	REF. NO.	
	69 Va 2	egf

REACTION	RESULT	EXCITATION ENERGY	SOURCE TYPE	SOURCE RANGE	DETECTOR TYPE	DETECTOR RANGE	ANGLE
G,XN	ABX	8-23	C	8-23	BF3-I		4PI

211

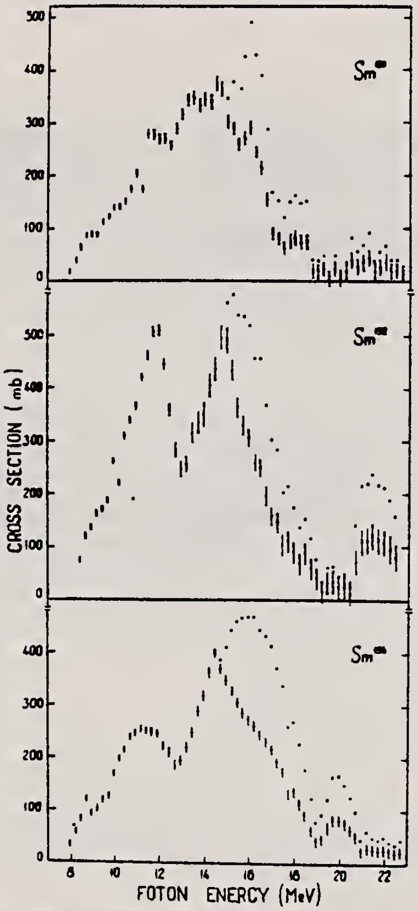

Fig. 3. The photoneutron and photoabsorption cross sections of ^{150}Sm, ^{152}Sm and ^{154}Sm. The symbols are the same as in fig. 2.

REF. O. V. Vasil'ev, G. N. Zalesnyi, S. F. Semenko, and V. A. Semenov
Yad. Fiz. 10, 460 (1969)
Sov. J. Nucl. Phys. 10, 263 (1970)

ELEM. SYM.	A	Z
Sm	152	62

METHOD

REF. NO.	
69 Va 3	egf

REACTION	RESULT	EXCITATION ENERGY	SOURCE TYPE	SOURCE RANGE	DETECTOR TYPE	DETECTOR RANGE	ANGLE
G,XN	ABX	8-22	C	8-22	BF3-I		4PI

241 + SEE 69VA2

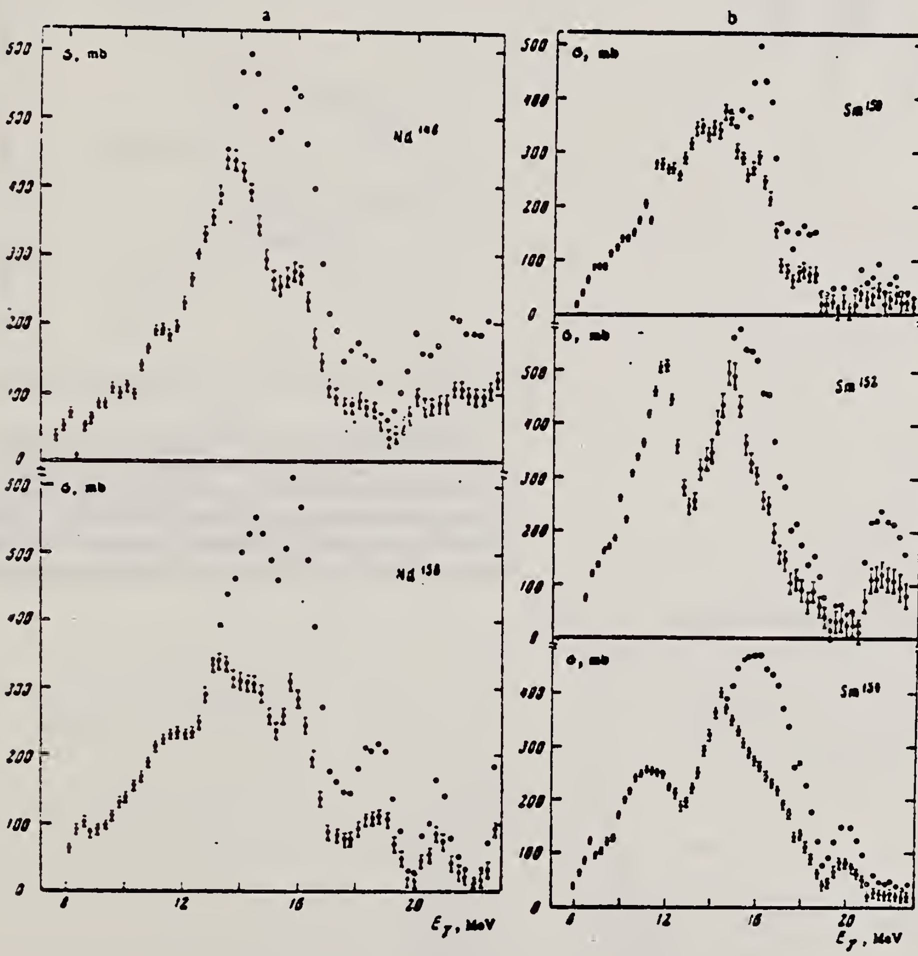

FIG. 2. Photoabsorption cross sections (black points) and photoneutron cross sections (light points): a – for Nd^{148} and Nd^{150} and b – for Sm^{150}, Sm^{152}, and Sm^{154}. The indicated errors are statistical.

[over]

Table I. Giant resonance parameters of $Nd^{148,150}$ and $Sm^{150,152,154}$

Parameters	Nucleus				
	Nd^{148}	Nd^{150}	Sm^{150}	Sm^{152}	Sm^{154}
σ_a, mb		160.0		400.0	204.0
$\hbar\omega_a$, MeV		11.25		11.55	11.00
$\hbar\Gamma_a$, MeV		3.0		2.4	3.0
σ_a^{int}, MeV-b		0.750		1.319	0.062
σ_b, mb		270.0		420.0	320.0
$\hbar\omega_b$, MeV		14.50		14.65	15.25
$\hbar\Gamma_b$, MeV		4.0		3.4	4.0
σ_b^{int}, MeV-b		1.695		2.242	2.01
$\sigma_b^{int}/\sigma_a^{int}$		2.26		1.7	2.00
σ^{int}, MeV-b	2.406	2.213	2.21[illegible]	3.079	2.478
$0.06\ NZ/A$	2.140	2.160	2.182	2.203	2.222
β_0		0.32		0.30	0.41
β_0^C		0.24		0.20	0.25
σ_d, mb	420		280		
$\hbar\omega_d$, MeV	13.65		13.6		
$\hbar\Gamma_d$, MeV	5.0		5.5		

REF.	ELEM. SYM.	A	Z
W. Bertozzi, T. Cooper, N. Ensslin, J. Heisenberg, S. Kowalski, M. Mills, W. Turchinetz, C. Williamson, S.P. Fivozinsky, J.W. Lightbody,Jr., and S. Penner Phys. Rev. Letters 28, 1711 (1972)	Sm	152	62
METHOD	REF. NO. 72 Be 3		hmg

REACTION	RESULT	EXCITATION ENERGY	SOURCE TYPE	SOURCE RANGE	DETECTOR TYPE	DETECTOR RANGE	ANGLE
E,E/	FMF	0-1	D	50-105	MAG-D		DST

.122, .367 MEV LEVELS

Ground-state rotational band.

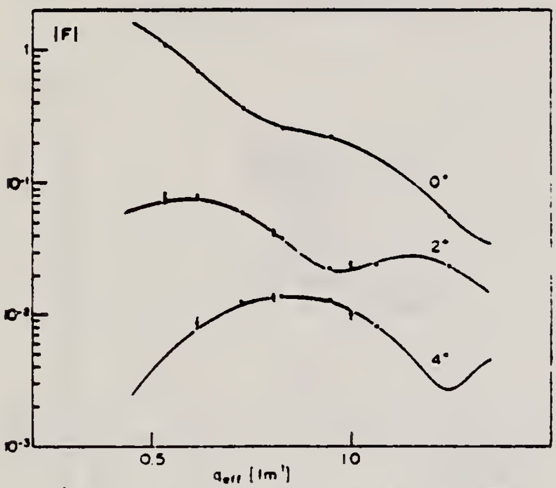

FIG. 2. Form factor F for the excitation of the ground-state rotational band; $F=(\sigma/\sigma_{Mott})^{1/2}$. For q_{eff} $=1.1$ fm^{-1} the average of two experimental points is plotted. Error bars shown represent standard deviations due to counting statistics. Where not shown, the standard deviations are smaller than the plotted points.

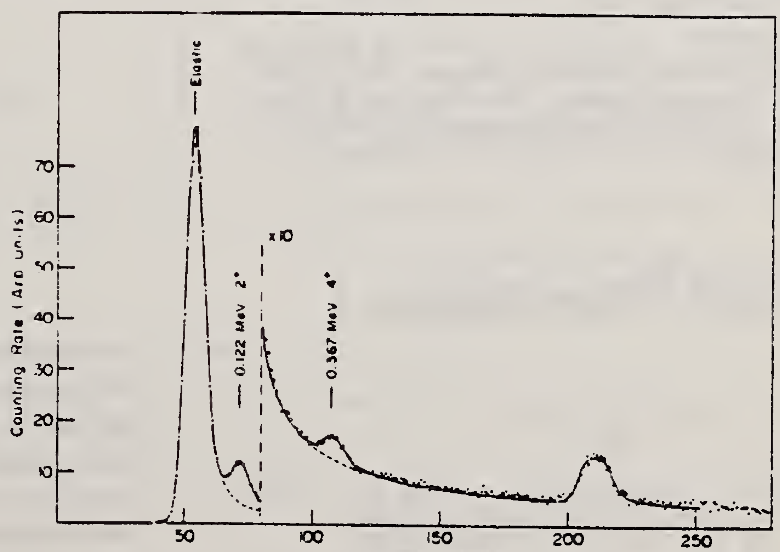

FIG. 1. Spectrum of scattered electrons from ^{152}Sm at 93.5°. Incident electron energy, 76 MeV. Besides the ground-state rotational band, the 3^- level at 1.041 MeV and the 2^+ level at 1.083 MeV are seen (channel 210).

FORM NBS-418
(REV. 7-14-64)
USCOMM-DC 26010-P64

REF.	William Bertozzi PICNS-72, 39 (1972) Sendai	ELEM. SYM.	A	Z
		Sm	152	62
METHOD		REF. NO.		
		72 Be 13		hvm

REACTION	RESULT	EXCITATION ENERGY	SOURCE TYPE	SOURCE RANGE	DETECTOR TYPE	DETECTOR RANGE	ANGLE
E,E/	FMF	0, 0	D	50-105	MAG-D		DST

0=.122,0=.367 MEV

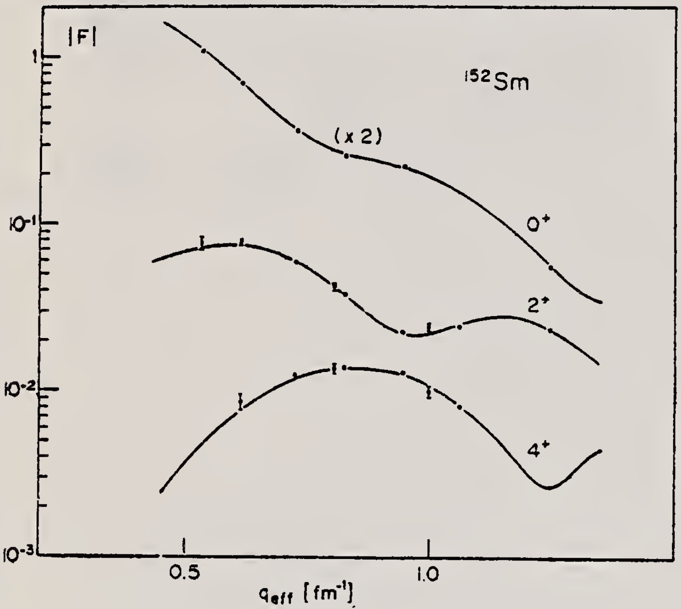

Fig. 2. Form factor F for the excitation of the ground state rotational band.

$F = \sqrt{\sigma/\sigma_{mott}}$. For $q_{eff} = 1.1\ fm^{-1}$ the average of two experimental points is plotted. Error bars shown represent standard deviations due to counting statistics. Where not shown, the standard deviations are smaller than the plotted points.

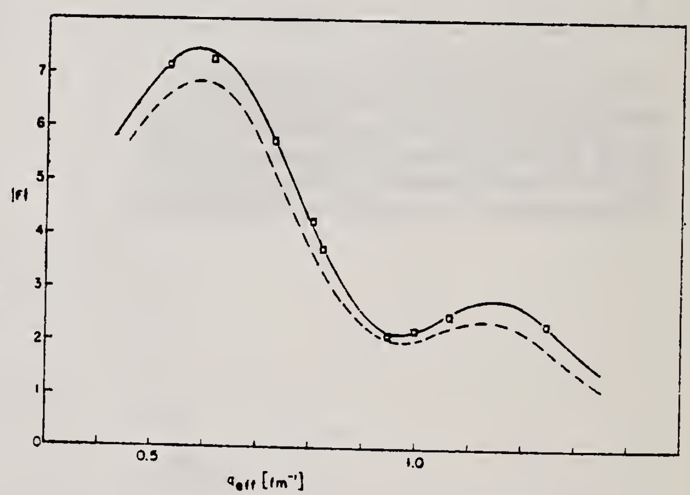

Fig. 3. Form factor for the 0-2$^+$ transition, $F = \sqrt{\sigma/\sigma_{mott}}$. The solid curve assumes $\rho(r,\theta) = \bar{\rho}[1 + \exp \frac{r-R(\theta)}{t}]^{-1}$ and the skin thickness is constant. The dashed curve assumes $\rho(r,\theta) = \bar{\rho}[1 + \exp \frac{\alpha-c}{t}]^{-1}$ with $\alpha = r[1/(1 + \Sigma\beta_L Y_{L0}^{(\theta)})]$. In this last choice the skin thickness actually varies as the radius.

REF.	Y. Torizuka, Y. Kojima, T. Saito, K. Itoh, A. Nakada, S. Mitsunobu, M. Nagao, K. Hosoyama, S. Fukuda PICNS-72, p.171 Sendai	ELEM. SYM.	A	Z
		Sm	152	62
METHOD		REF. NO.		
		72 To 6		hvm

REACTION	RESULT	EXCITATION ENERGY	SOURCE TYPE	SOURCE RANGE	DETECTOR TYPE	DETECTOR RANGE	ANGLE
E,E/	SPC	0- 31	D	150-250	MAG-D		35

LEVELS 11.5, 15.5

Fig. 8. The K=0 and K=1 form factors in ^{152}Sm calculated by assuming a deformed Fermi type charge distribution.

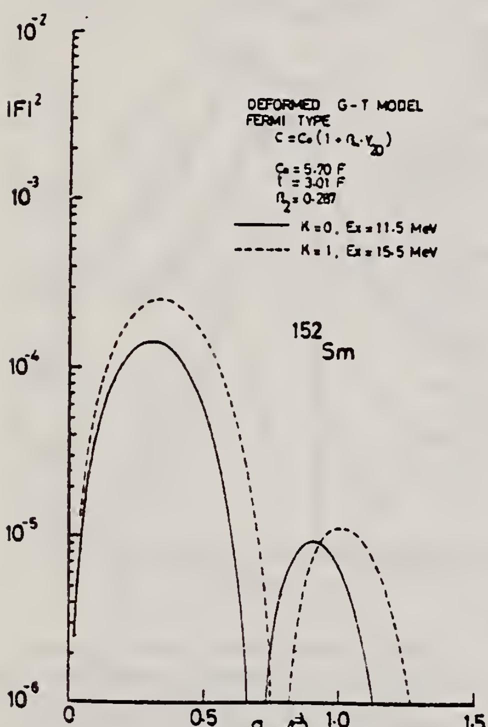

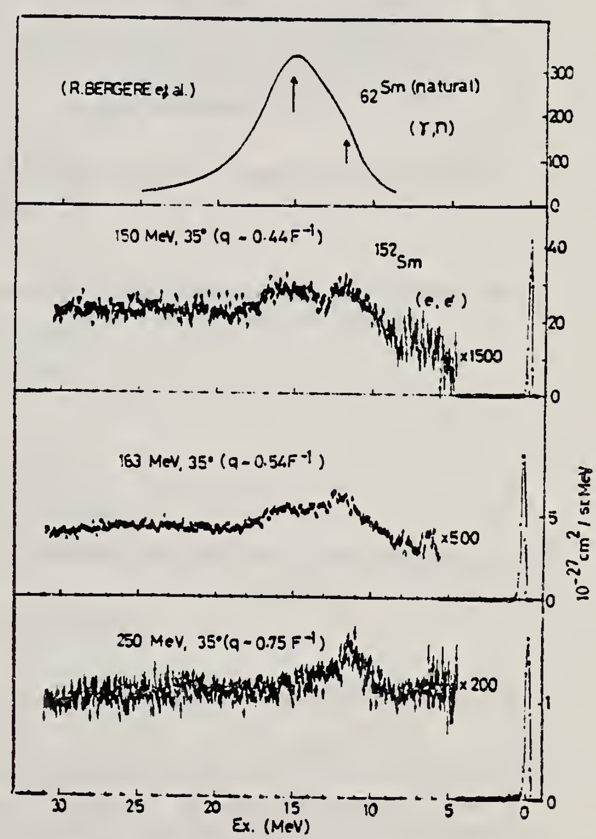

Fig. 7. The spectra of the deformed ^{152}Sm displayed as a function of the momentum transfer. The distinct peaks are seen at 11.5 and 15.5 MeV.

REF. R. Bergere, H. Beil, P. Carlos, A. Lepretre, A. Veyssiere
PICNS-73, Vol.I, p.525 Asilomar

ELEM. SYM.	A	Z
Sm	152	62

METHOD

REF. NO.	
73 Be 10	hmg

REACTION	RESULT	EXCITATION ENERGY	SOURCE TYPE	SOURCE RANGE	DETECTOR TYPE	DETECTOR RANGE	ANGLE
G,SN	ABX	8- 20	D	8- 20	BF3-I		4PI

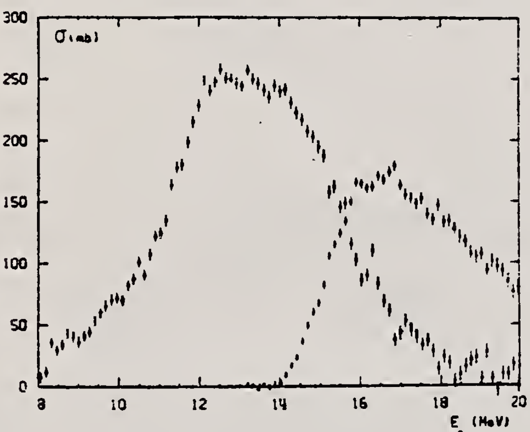

Fig. 18 Partial photoneutron cross-sections $\sigma(\gamma,n)$ and $\sigma(\gamma,2n)$ of ^{152}Sm

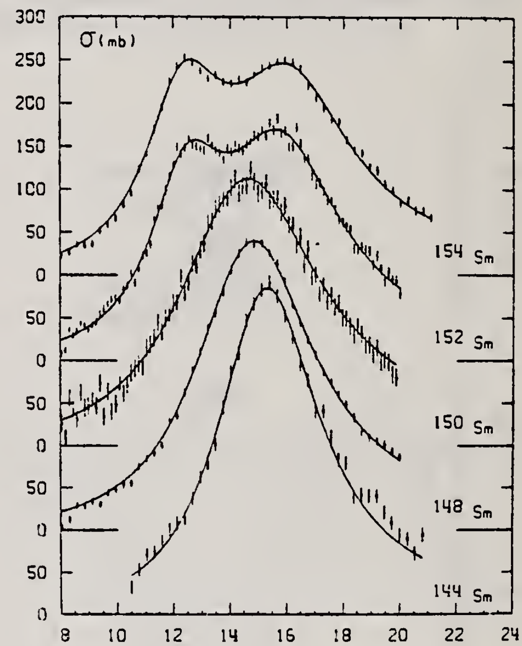

Fig. 19 Total photoneutron cross section $\sigma(\gamma,n)+\sigma(\gamma,2n)$ of Sm isotopes. The solid lines show the best 1 Lorentz line fit (^{144}Sm ^{148}Sm ^{150}Sm) or 2 Lorentz lines fit (^{152}Sm and ^{154}Sm).

Table IV

	$E_{1\,MeV}$	$\Gamma_{1\,MeV}$	$\sigma_{1\,mb}$	$E_{2\,MeV}$	$\Gamma_{2\,MeV}$	$\sigma_{2\,mb}$
^{152}Sm	12.45±0.1	3.20±0.15	183±10	15.85±0.1	5.10±0.20	226±10
^{154}Sm	12.35±0.1	3.37±0.15	192±10	16.10±0.1	5.25±0.20	204±10

REF. A.M. Goryachev, G.N. Zalesnyi, S.F. Semenko, and B.A. Tulupov
Yad. Fiz. 17, 463 (1973)
Sov. J. Nucl. Phys. 17, 236 (1973)

ELEM. SYM.	A	Z
Sm	152	62

METHOD

REF. NO.	
73 Go 6	hmg

REACTION	RESULT	EXCITATION ENERGY	SOURCE TYPE	SOURCE RANGE	DETECTOR TYPE	DETECTOR RANGE	ANGLE
G,XN	ABX	8- 20	C	8- 20	BF3-I		4PI

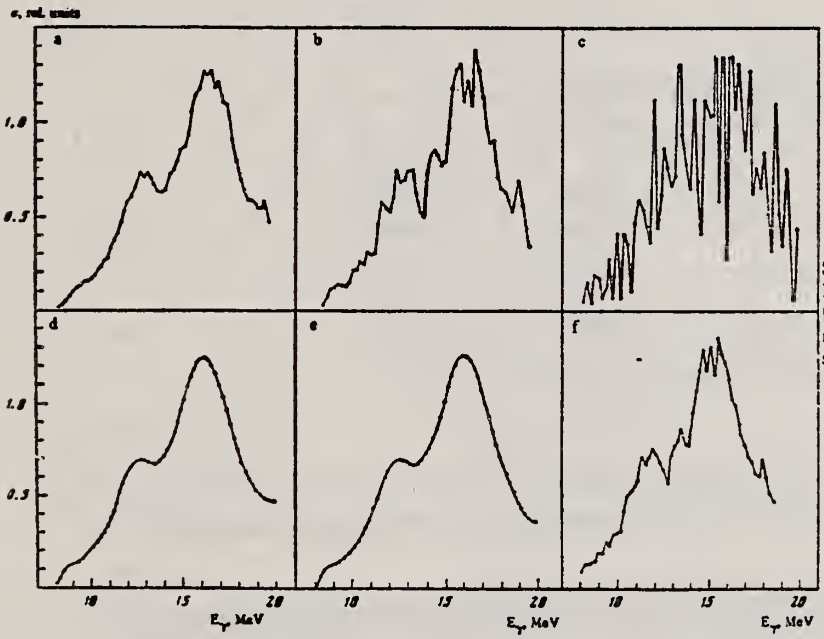

FIG. 1. Calculations of the cross section for Sm^{152} by different methods: a, b, c—the Penfold-Leiss method with 1-, 0.5-, and 0.2-MeV spacings; [16] d—the method of Tikhonov; [15] e—the method of Cook; [18] f—the cross section in c, smoothed as proposed in [17].

[15] A.N. Tikhonov, Dokl. Akad. Nauk SSSR 151, 501 (1963).

[16] A.S. Penfold and J.E. Leiss, Phys. Rev. 114, 1332 (1959).

[17] V.N. Orlin, Abstracts and Reports at the XXII Conference on Nuclear Spectroscopy and Structure, Kiev, 1972 (in Russian).

[18] B.C. Cook, Nucl. Instr. and Meth. 24, 256 (1963).

REF.

P. Carlos, H. Beil, R. Bergere, A. Lepretre, A. De Miniac, and A. Veyssiere
Nucl. Phys. A225, 171 (1974)

ELEM. SYM.	A	Z
Sm	152	62

METHOD

REF. NO.	
74 Ca 5	egf

REACTION	RESULT	EXCITATION ENERGY	SOURCE TYPE	SOURCE RANGE	DETECTOR TYPE	DETECTOR RANGE	ANGLE
G,N *	ABX	8- 20	D	8- 20	BF3-I		4PI
G,2N **	ABX	13- 20	D	13- 20	BF3-I		4PI

* 687+
** 688+

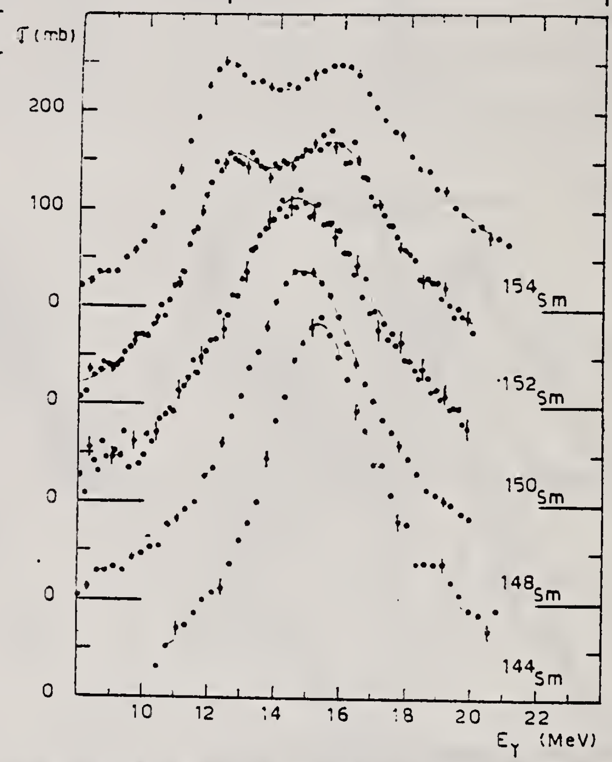

Fig. 7. Total photoneutron cross sections $\sigma_T(E)$ of the doubly even samarium isotopes. Best single Lorentz line fits are shown for ^{144}Sm, ^{148}Sm and ^{150}Sm. For ^{152}Sm and ^{154}Sm the best two Lorentz line fits are presented. Corresponding Lorentz line parameters are given in table 2.

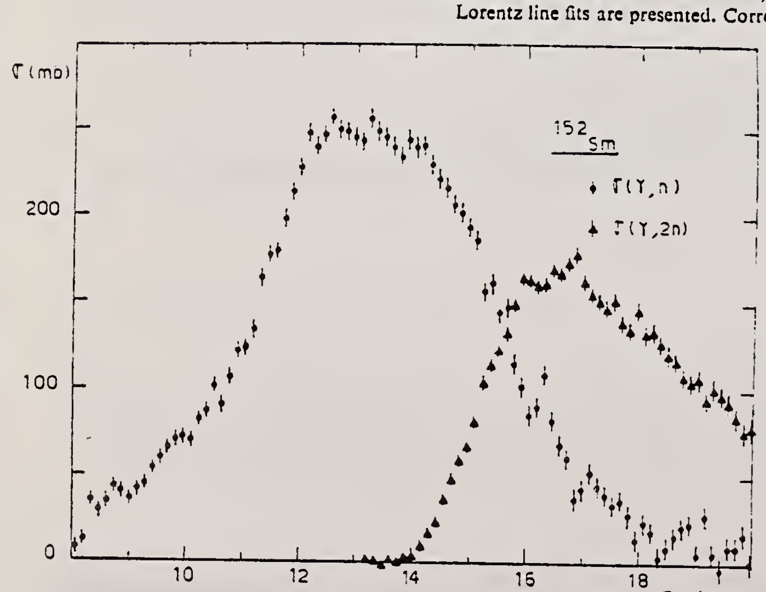

Fig. 5. Partial photoneutron cross sections $[\sigma(\gamma,n)+\sigma(\gamma,np)]$ and $\sigma(\gamma,2n)$ of ^{152}Sm.

(over)

EET 306

Table 2

Lorentz line parameters

	E_1 (MeV)	σ_1 (mb)	Γ_1 (MeV)	E_2 (MeV)	σ_2 (mb)	Γ_2 (MeV)
^{144}Sm*	15.3 ±0.1	384±20	4.37±0.15			
^{148}Sm*	14.8 ±0.1	339±12	5.1 ±0.2			
^{148}Sm**	14.1	335	4			
^{150}Sm*	14.6 ±0.1	312±20	6.0 ±0.2			
^{150}Sm**	13.6	360	5.5			
^{152}Sm*	12.45±0.10	183±10	3.2 ±0.15	15.85±0.10	226±10	5.1 ±0.[illegible]
^{152}Sm**	11.55	400	2.4	14.65	420	3.4
^{154}Sm*	12.35±0.10	192±10	3.35±0.15	16.1 ±0.1	204±10	5.25 ±0.[illegible]
^{154}Sm**	11	204	3	15.25	320	4

* Corresponding to best fits shown in fig. 7.

** Values taken from Vassilijev [23,24]) for comparison.

Table 3

Different integrated cross sections as defined in the text

	^{144}Sm	^{148}Sm	^{150}Sm	^{152}Sm	^{154}Sm
E_M (MeV)	21	20	20	20	21
σ_0 (MeV · b)	2 ±0.14	1.94±0.1	2 ±0.14	2.05±0.1	2.07±0.1
σ'_0 (MeV · b)	2.63	2.71	2.94	2.75	2.69
$\dfrac{\sigma'_0 A}{0.06\, NZ}$	1.24	1.25	1.35	1.24	1.2[illegible]
σ_{-1} (mb)	131 ±15	134 ±10	141 ±15	144 ±10	145 ±1[illegible]
σ_{-2} (mb · MeV^{-1})	8.7±0.8	9.5 ±0.7	10.3±0.9	10.6 ±0.7	10.6 ±0.7

[23] O. Vasilijev et al., Sov.J.Nucl.Phys.10, 263 (1970)

[24] O. Vasilijev et al., Sov.J.Nucl.Phys.13, 463 (1971)

REF.	ELEM. SYM.	A	Z
T. Cooper, W. Bertozzi, J. Heisenberg, S. Kowalski, W. Turchinetz, C. Williamson, L. Cardman, S. Fivozinsky, J. Lightbody, Jr., and S. Penner Phys. Rev. C13, 1083 (1976)	Sm	152	62

METHOD	REF. NO.	
	76 Co 3	hmg

REACTION	RESULT	EXCITATION ENERGY	SOURCE TYPE	SOURCE RANGE	DETECTOR TYPE	DETECTOR RANGE	ANGLE
E,E/	FMF	1, 1	D	49-106	MAG-D		DST

LEVELS .3665, .1218

TABLE II. Cross sections from ^{152}Sm data.

Energy (MeV)	Angle (deg)	q_{eff} (fm^{-1})	Elastic $\frac{d\sigma}{d\Omega}_{exp}$ (mb)	Elastic $\frac{d\sigma}{d\Omega}_{bestfit}$ (mb)	2^+ $\frac{d\sigma}{d\Omega}_{exp}$ (mb)	4^+ $\frac{d\sigma}{d\Omega}_{exp}$ (mb)
49.60	93.43	0.535	0.400×10 ±4%	0.398×10	0.802×10^{-1}±15%	...
60.53	93.43	0.615	0.111×10 ±4%	0.109×10	0.545×10^{-1}±10%	0.680×10^{-3}±25%
60.50	145.65	0.805	...	0.214×10^{-1}	0.140×10^{-2}±10%	0.961×10^{-4}±12%
67.08	93.43	0.729	0.190 ±4%	0.188	0.197×10^{-1}± 7%	0.905×10^{-3}± 6%
80.38	145.65	0.998	...	0.524×10^{-2}	0.195×10^{-3}±10%	0.300×10^{-3}±15%
89.75	93.14	0.827	0.675×10^{-1}±4%	0.762×10^{-1}	0.590×10^{-2}± 7%	0.786×10^{-3}± 5%
105.71	93.46	0.947	0.378×10^{-1}±8%	0.377×10^{-1}	0.130×10^{-2}± 7%	0.453×10^{-3}± 5%
104.95	110.79	1.062	...	0.106×10^{-1}	0.809×10^{-3}± 5%	0.933×10^{-4}± 7%
105.68	146.01	1.216	0.168×10^{-3}±4%	0.182×10^{-3}	0.119×10^{-3}± 5%	$\leq0.38\times10^{-6}$

TABLE VIII. Deformed Fermi best fit parameters.

	Units	^{152}Sm	^{154}Sm	^{232}Th	^{238}U
c_0	fm	5.8044	5.9387	6.7915	6.8054
t	fm	0.5814	0.5223	0.5713	0.6049
β_2		0.287±0.003	0.311±0.003	0.233±0.002	0.261±0.002
β_4		0.070±0.003	0.087±0.002	0.101±0.003	0.037±0.003
β_6		−0.0120	−0.180	0.0	0.0
$B(E2)$	e^2b^2	3.38 ±0.07	4.40 ±0.09	9.21 ±0.09	11.70 ±0.15
$B(E4)$	e^2b^4	0.136±0.013	0.221±0.010	1.16 ±0.05	1.20 ±0.06
rms radius	fm	5.0922	5.126	5.7723	5.842
ρ_2 Transition radius	fm	6.937	6.950	7.895	7.979
ρ_4 Transition radius	fm	7.757	7.704	8.540	8.748

REF.	A. Nakada, N. Haik, J. Alster, J. B. Bellicard, S. Cochavi, B. Frois, M. Huet, P. Leconte, P. Ludeau, M. A. Moinester, Phan Xuan Ho, and S. Turck Phys. Rev. Lett. 38, 584 (1977)	ELEM. SYM.	A	Z
		Sm	152	62
METHOD		REF. NO.		
		77 Na 2		hmg

REACTION	RESULT	EXCITATION ENERGY	SOURCE TYPE	SOURCE RANGE	DETECTOR TYPE	DETECTOR RANGE	ANGLE
E,E/	LFT	0- 1	D	252	MAG-D	-	DST
		(.122-.712)					

2+,4+,6+ STATES

Elastic and inelastic angular distributions were measured, including that for the 6^+ state at 0.712 MeV. Parameters of the charge distribution were determined, and compared with those obtained with low-energy electrons and with mass deformation parameters from α scattering. The data also compared to a Hartree-Fock calculation.

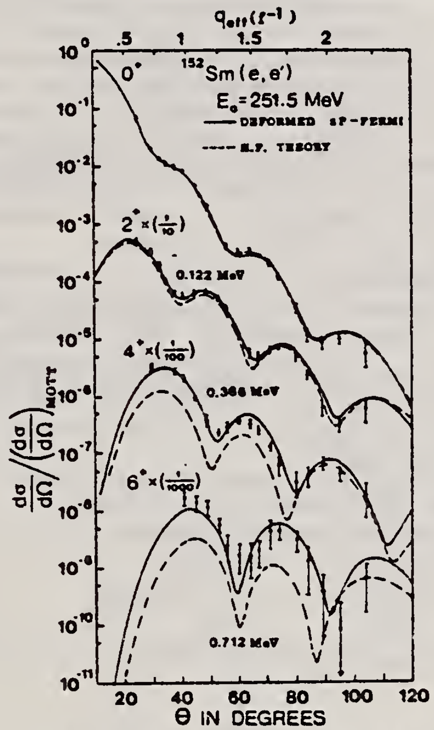

FIG. 1. Experimental values of σ/σ_{Mott} for the ground-state rotational band of ^{152}Sm, as a function of angle and $q_{eff}=q(1+\frac{4}{3}Z\alpha\langle r^2\rangle^{-1/2}E^{-1})$. The solid lines are phenomenological fits (see text) and the dashed lines are the results of the use of HF wave functions.

over

TABLE I. Charge and mass distribution parameters of Sm^{152}.

Reaction	Reference	$\langle r^2\rangle^{1/2}$	c_0	t	β_2	β_4	β_6	$B(E2)$ ($e^2 \cdot b^2$)	$B(E4)$ ($e^2 \cdot b^2$)	$B(E6)$ ($e^2 \cdot b^2$)
250 MeV (e,e')	Present work	5.0246	5.778 ±0.010	0.545 ±0.037	0.286 ±0.002	0.092 ±0.002	0.010 ±0.002	3.45 ±0.06	0.210 ±0.013	0.0114 ±0.0007
Low energy (e,e')	2,4	5.0922	5.804	0.581	0.287 ±0.003	0.070 ±0.003	−0.012[a]	3.38 ±0.07	0.136 ±0.013	
Coulomb excitation (α,α')	5				0.276 ±0.012	0.065 ±0.029		3.45 ±0.07	0.137 ±0.078	
50 MeV (α,α')	2,15				0.256	0.061	−0.006			
HF calculation	12	4.998						2.99	0.089	0.0027

[a] Fixed.

[2] D.L. Hendrie, N.K. Glendenning, B.G. Harvey, O.N. Jarvis, H.H. Duhm, J. Saudinos, and J. Mahoney, Phys. Lett. 26B, 127 (1968)

[4] W. Bertozzi, T. Cooper, N. Ensslin, J. Heisenberg, S. Kowalski, M. Mills, W. Turchinetz, C. Williamson, S.P. Fivozinsky, J.W. Lightbody, Jr., and S. Penner, Phys. Rev. Lett. 28, 1711 (1972); T. Cooper, W. Bertozzi, J. Heisenberg, S. Kowalski, W. Turchinetz, C. Williamson, L. Cardman, S. Fivozinsky, J.W. Lightbody, Jr., and S. Penner, Phys. Rev. C 13, 1083 (1976).

[5] T.K. Saylor, J.X. Saladin, I.Y. Lee, and K.A. Erb, Phys. Lett. 42B, 51 (1972); W. Bruckner, D. Husar, D. Pelte, K. Traxel, M. Samuel, and U. Smilansky, Nucl. Phys. A321, 159 (1974)

[12] D. Gogny, in Nuclear Self Consistent Fields, edited by G. Ripka and M. Porneuf (North-Holland, Amsterdam, 1976); J. Decharge, M. Girod, and D. Gogny, Phys. Lett. 55B, 361 (1975)

[15] D.L. Hendrie, Phys. Lett. 31, 478 (1973)

REF. B.S. Dolbilkin, S. Ohsawa, Y. Torizuka, T. Saito, Y. Mizuno, K. Saito
Phys. Rev. C25, 2255 (1982)

ELEM. SYM.	A	Z
Sm	152	62

METHOD

REF. NO.	
82 Do 6	egf

REACTION	RESULT	EXCITATION ENERGY	SOURCE TYPE	SOURCE RANGE	DETECTOR TYPE	DETECTOR RANGE	ANGLE
E,E/		5-33	D	150-215	MAG-D		DST

Q .38-.64 FM-1

The electron scattering cross sections from the enriched ^{148}Sm (96.5%) and ^{152}Sm (99.2%) isotopes have been measured between 5 and 33 MeV excitation energies for incident energies in the range of between 150 and 215 MeV and scattering angles of 30°, 35°, and 40°. The giant resonances at $E_x = 14.8$ ($78A^{-1/3}$), 11.6 ($61A^{-1/3}$), 15.5 ($82A^{-1/3}$), and 24 ($129A^{-1/3}$) MeV for ^{148}Sm were classified according to their momentum transfer dependence. The K splittings of the giant $E1$ ($T=1$) and $E2$ ($T=0,1$) resonances for deformed ^{152}Sm were observed in agreement with a vibrating potential model. The splittings between the $K=0^+$ and 2^+ components for the isoscalar and isovector quadrupole resonances are ~2 MeV and ~5 MeV, respectively. The fitted parameters classified as the giant monopole resonance are the same for spherical ^{148}Sm and for deformed ^{152}Sm. The difference between the isoscalar giant resonance parameters for resonance energies and width found from hadron scattering and those for electron scattering is discussed for the rare-earth region.

NUCLEAR REACTIONS ^{148,152}Sm(e,e'), enriched targets, $E_0 = 150$ to 215 MeV, $\theta = 30°, 35°, 40°$, $q = 0.38-0.64$ fm^{-1}. Measured $d^2\sigma/d\Omega\, dE_x$ up to 33 MeV in excitation energy; deduced multipolarity, excitation energy, width, sum rule exhaustion of giant resonances.

TABLE IV. Comparison between (e,e') results and theoretical results for the giant multipole resonance energy (MeV).

Type	Nucleus	Isoscalar Present work	Isoscalar Ref. 10	Isoscalar Theory Ref. 9	Isoscalar Ref. 24	Isovector Present work	Isovector Theory Ref. 10	Isovector Theory Ref. 9
GMR	^{148}Sm	15.5±0.3			15.1			
	^{152}Sm	15.7±0.3		10.7	10.5			
				18.3	15.9			
GDR	^{148}Sm					14.8	14.8	
	^{152}Sm					12.45	12.3	12.0
						15.85	16.3	15.0
GQR	^{148}Sm	11.6±0.2	10.9		11.9	24.3±0.4	26.4	
	^{152}Sm	10.6±0.2	9.9	11.0	10.5	21.0±0.9	24.1	19.5
		11.4±0.4	10.4	12.0		23.2±1.0	25.2	22.5
		12.7±0.4	11.8	13.0	13.1	26.0±0.5	28.8	25.5

(OVER)

TABLE V. Parameters of the isoscalar GQR in the Sm isotopes.

Nucleus	E_x (MeV)	Γ (MeV)	EWSR (%)	Reaction	Reference
^{144}Sm	13.0±0.3	3.9±0.2	91±25	(α,α')	25
^{144}Sm	12.4±0.4	2.6±0.4	85±15	(α,α')	6
^{144}Sm	12.1±0.2	2.4±0.2	45±15	(α,α')	8
^{144}Sm	12.5	3.4	60	(α,α')	26
^{144}Sm	11.9±0.2	2.9±0.2		(e,e')	27
^{148}Sm	12.5±0.2	4.3±0.2	104±25	(α,α')	25
^{148}Sm	11.6±0.2	3.1±0.2	100±10	(e,e')	Present work
^{150}Sm	11.8±0.2	3.3±0.2		(e,e')	27
	10.6±0.2	2.4±0.2	20±5		
^{152}Sm	11.4±0.4	2.7±0.2	45±9	(e,e')	Present work
	12.7±0.4	3.0±0.2	35±7		
^{154}Sm	12.4±0.3	4.7±0.3	102±25	(α,α')	25
^{154}Sm	12.2	4.5		(α,α')	7
^{154}Sm	11.8±0.3	3.7±0.3		(α,α')	8
^{154}Sm	10.9±0.2	4.5±0.2		(e,e')	27

TABLE VI. Comparison of the GMR parameters in the Sm isotopes obtained from various reactions.

Nucleus	E_x (MeV)	Γ (MeV)	EWSR (%)	Reaction	Reference
^{144}Sm	15.1±0.5	2.9±0.5	100±50	(α,α')	6
^{144}Sm	14.6±0.2	3.0±0.3	140±40	(α,α')	8
^{144}Sm	15.2	2.5		(α,α')	26
^{144}Sm	15.5±0.5	2.5±0.5	100±25	(p,p')	31
^{144}Sm	14.7±0.2	2.9±0.2	67±13	$(^3He,^3He')$	32
^{144}Sm	14.8±0.2	2.4±0.15	20±10	(e,e')	30
^{148}Sm	15.5±0.3	3.0±0.2	100±10	(e,e')	Present work
^{150}Sm	15.1±0.25	3.0±0.25	60±19	$(^3He,^3He')$	32
^{152}Sm	14.8±0.25	3.1±0.25	54±9	$(^3He,^3He')$	32
^{152}Sm	15.7±0.3	3.1±0.4	100±20	(e,e')	Present work
^{154}Sm	15.5±0.5	2.5±0.5	100±25	(p,p')	31
^{154}Sm	14.9±0.3	2.6±0.4	55±15	(α,α')	8

Sm
A=154

Sm
A=154

Sm
A=154

Ref. J.H. Carver, W. Turchinetz
Proc. Phys. Soc. 73, 69 (1959)

Elem. Sym.	A	Z
Sm	154	62

Method 33 MeV Synchrotron; radioactivity; NaI spectrometer; ionization chamber

Ref. No.	
59 Ca 3	EH

Reaction	E or ΔE	E_0	Γ	$\int \sigma dE$	$J\pi$	Notes
$Sm^{154}(\gamma,n)$	Bremss. $\sim$ 8-32	13.6	6.5 MeV	2.4±0.4 MeV-b		

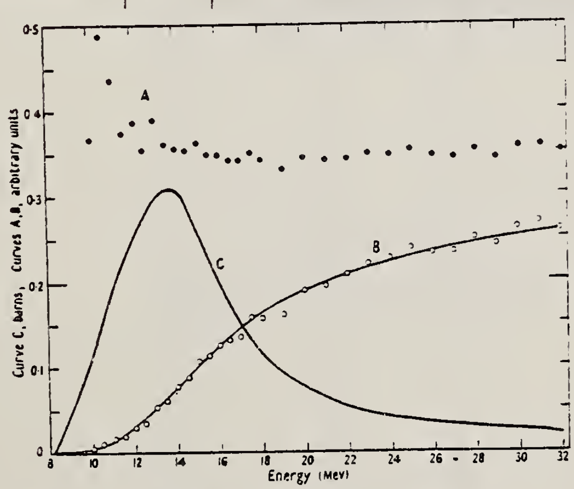

Figure 5. A, the ratio of activation curves $^{154}Sm(\gamma,n)/^{181}Ta(\gamma,n)$; B, activation curve for $^{154}Sm(\gamma,n)$; C, derived cross section: $^{154}Sm(\gamma,n)$.

Ref. K. Kotajima
Nuclear Phys. 39, 89 (1962)

Elem. Sym.	A	Z
Sm	154	62

Method
Linac; radioactivity

Ref. No. 62 Ko 3 JHH

Reaction	E or ΔE	E_0	Γ	$\int \sigma dE$	Jπ	Notes
$Sm^{154}(\gamma,p)$	Bremss. 20					Product nucleus, Pm^{153}, has $T_{1/2}$ = 5.5±0.2 min., E_β end-pt. = 1.65±0.05 MeV, E_γ's = 0.125, 0.180 MeV. $\frac{\sigma_{Sm^{154}(\gamma,p)}}{\sigma_{Sm^{154}(\gamma,n)}} = 1/950$

L. G. Moretto, R. C. Gatti, S. G. Thompson, J. T. Routti, J. H. Heisenberg, L. M. Middleman, M. R. Yearian, R. Hofstadter
Phys. Rev. 179, 1176 (1969)

ELEM. SYM.	A	Z
Sm	154	62

METHOD

REF. NO.	
69 Mo 1	hmg

REACTION	RESULT	EXCITATION ENERGY	SOURCE		DETECTOR		ANGLE
			TYPE	RANGE	TYPE	RANGE	
E,F	ABX	THR-999	D	60-999	TRK-I		DST
G,F	ABX	THR-999	C	60-999	TRK-I		DST

Tabular data given; angular distribution isotopes

999=1 GEV

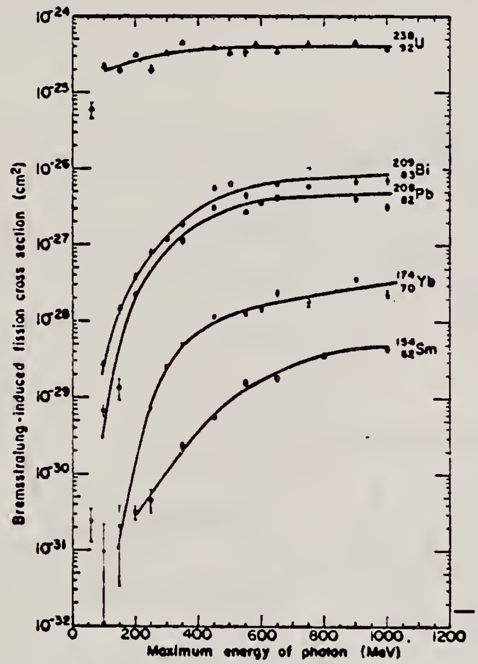

FIG. 4. Bremsstrahlung-induced fission cross section per equivalent quantum.

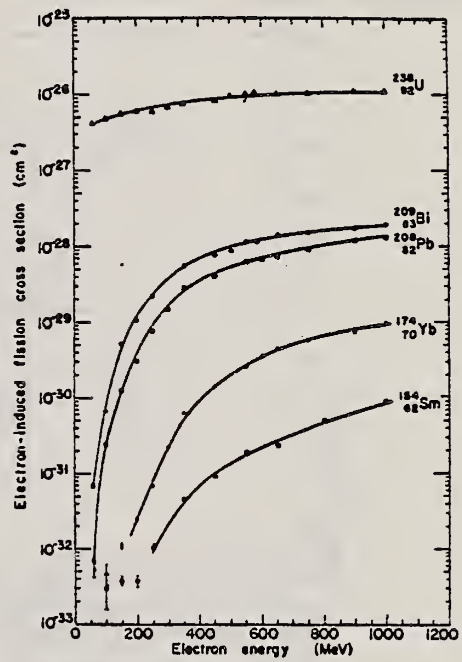

FIG. 2. Electron-induced fission cross-section data. Different symbols for the same isotope refer to different targets.

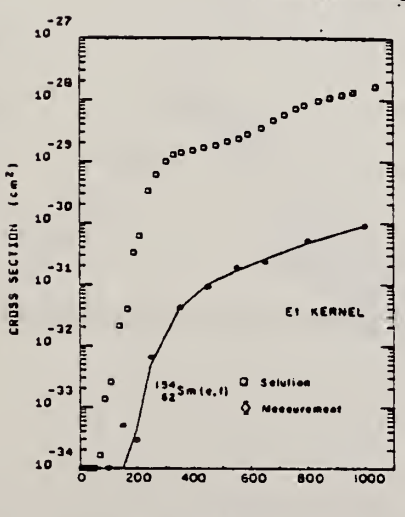

FIG. 10. Photofission cross section as a function of energy for $_{62}^{154}Sm$ (open squares) as obtained by unfolding the electron-induced fission cross-section data (diamonds) with the $E1$ kernel. The solid line is the fit to the electron-induced fission cross sections which is obtained by folding back the photofission cross section into the $E1$ kernel.

U.S. DEPARTMENT OF COMMERCE
NATIONAL BUREAU OF STANDARDS

REF.	ELEM. SYM.	A	Z
O. V. Vasilijev, G. N. Zalesny, S. F. Semenko, V. A. Semenov Phys. Letters 30B, 97 (1969)	Sm	154	62

METHOD	REF. NO.	
	69 Va 2	egf

REACTION	RESULT	EXCITATION ENERGY	SOURCE TYPE	SOURCE RANGE	DETECTOR TYPE	DETECTOR RANGE	ANGLE
G,XN	ABX	8-23	C	8-23	BF3-I		4PI

212

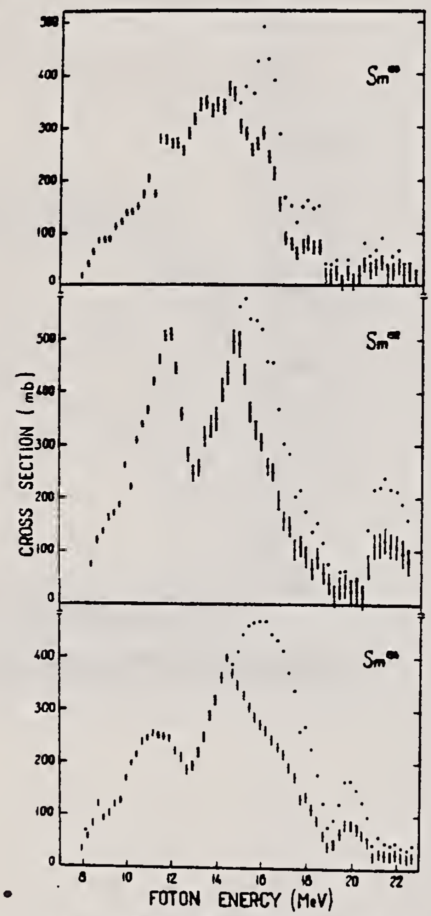

Fig. 3. The photoneutron and photoabsorption cross sections of ^{150}Sm, ^{152}Sm and ^{154}Sm. The symbols are the same as in fig. 2.

REF. O. V. Vasil'ev, G. N. Zalesnyi, S. F. Semenko, and V. A. Semenov
Yad. Fiz. 10, 460 (1969)
Sov. J. Nucl. Phys. 10, 263 (1970)

ELEM. SYM.	A	Z
Sm	154	62

METHOD

REF. NO.	
69 Va 3	egf

REACTION	RESULT	EXCITATION ENERGY	SOURCE TYPE	SOURCE RANGE	DETECTOR TYPE	DETECTOR RANGE	ANGLE
G,XN	ABX	8-22	C	8-22	BF3-I		4PI

242 SEE 69VA2

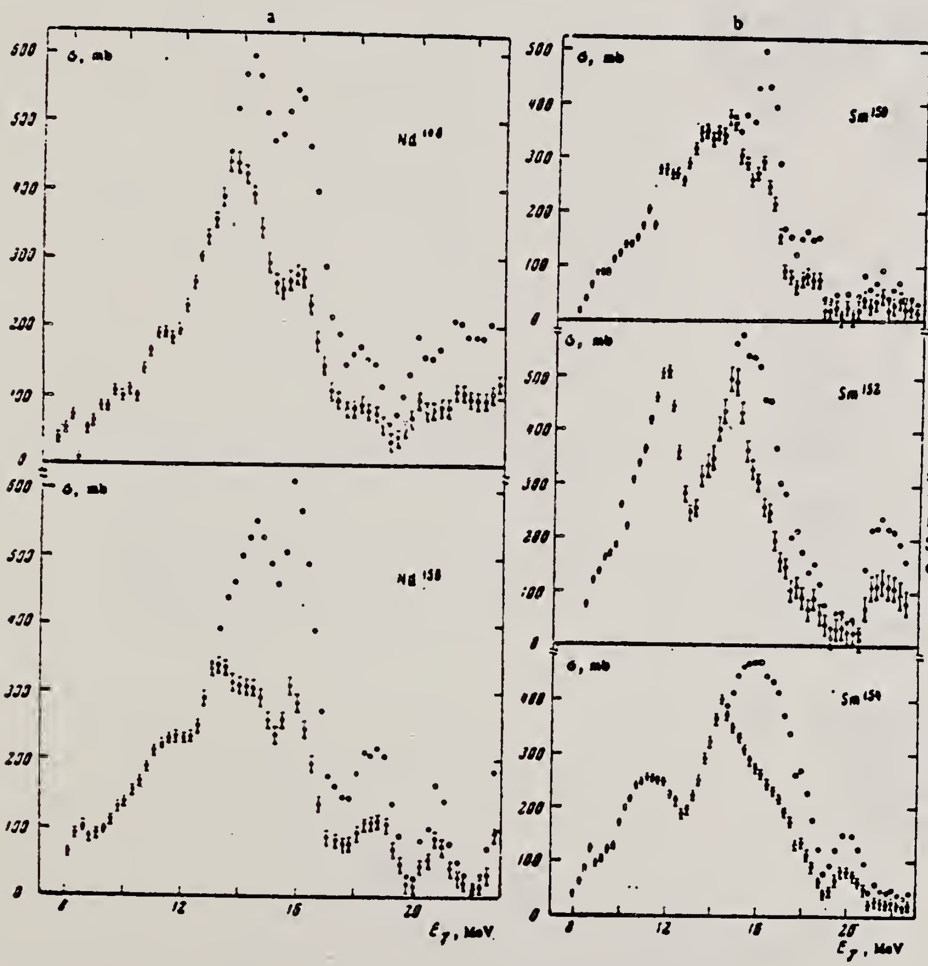

FIG. 2. Photoabsorption cross sections (black points) and photoneutron cross sections (light points): a – for Nd^{148} and Nd^{150} and b – for Sm^{150}, Sm^{152}, and Sm^{154}. The indicated errors are statistical.

[over]

Table I. Giant resonance parameters of $Nd^{148,150}$ and $Sm^{150,152,154}$

Parameters	Nucleus				
	Nd^{148}	Nd^{150}	Sm^{150}	Sm^{152}	Sm^{154}
σ_a, mb		160.0		400.0	204.0
$\hbar\omega_a$, MeV		11.25		11.55	11.00
$\hbar\Gamma_a$, MeV		3.0		2.4	3.0
σ_a^{int}, MeV-b		0.750		1.319	0.962
σ_b, mb		270.0		420.0	320.0
$\hbar\omega_b$, MeV		14.50		14.65	15.25
$\hbar\Gamma_b$, MeV		4.0		3.4	4.0
σ_b^{int}, MeV-b		1.695		2.242	2.01
$\sigma_b^{int}/\sigma_a^{int}$		2.26		1.7	2.09
σ^{int}, MeV-b	2.406	2.243	2.213	3.079	2.478
0.06 NZ/A	2.140	2.160	2.182	2.203	2.223
β_0		0.32		0.30	0.41
γ_0		0.28		0.20	0.35
σ_d, mb	420		380		
$\hbar\omega_d$, MeV	13.65		13.6		
$\hbar\Gamma_d$, MeV	5.0		5.5		

REF.	R. Bergere, H. Beil, P. Carlos, A. Lepretre, A. Veyssiere PICNS-73, Vol. I, p. 525 Asilomar	ELEM. SYM.	A	Z
		Sm	154	62
METHOD		REF. NO. 73 Be 10		hmg

REACTION	RESULT	EXCITATION ENERGY	SOURCE TYPE	SOURCE RANGE	DETECTOR TYPE	DETECTOR RANGE	ANGLE
G,SN	ABX	8- 22	D	8- 22	BF3-I		4PI

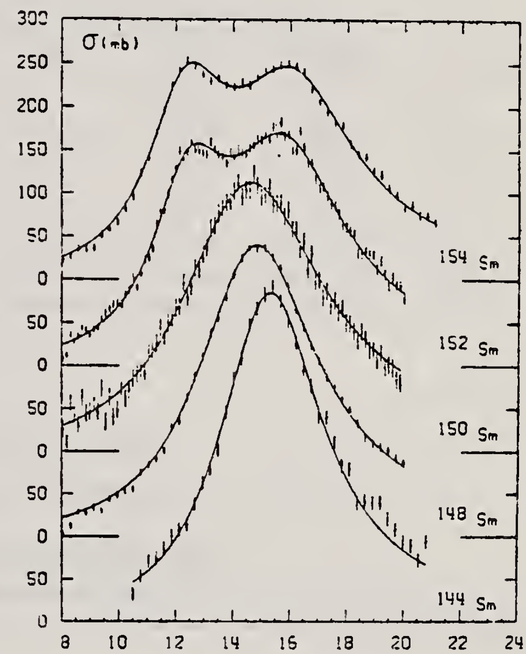

Fig. 19 Total photoneutron cross section $\sigma(\gamma,n)+\sigma(\gamma,2n)$ of Sm isotopes. The solid lines show the best 1 Lorentz line fit (^{144}Sm ^{148}Sm ^{150}Sm) or 2 Lorentz lines fit (^{152}Sm and ^{154}Sm).

Table IV

	$E_{1\,MeV}$	$\Gamma_{1\,MeV}$	$\sigma_{1\,mb}$	$E_{2\,MeV}$	$\Gamma_{2\,MeV}$	$\sigma_{2\,mb}$
^{152}Sm	12.45±0.1	3.20±0.15	183±10	15.85±0.1	5.10±0.20	226±10
^{154}Sm	12.35±0.1	3.37±0.15	192±10	16.10±0.1	5.25±0.20	204±10

REF.	ELEM. SYM.	A	Z
P. Carlos, H. Beil, R. Bergere, A. Lepretre, A. De Miniac, and A. Veyssiere Nucl. Phys. A225, 171 (1974)	Sm	154	62
METHOD	REF. NO. 74 Ca 5		egf

REACTION	RESULT	EXCITATION ENERGY	SOURCE TYPE	SOURCE RANGE	DETECTOR TYPE	DETECTOR RANGE	ANGLE
G,N *	ABX	8- 21	D	8- 21	BF3-I		4PI
G,2N **	ABX	13- 21	D	13- 21	BF3-I		4PI

* 690 +
**691+

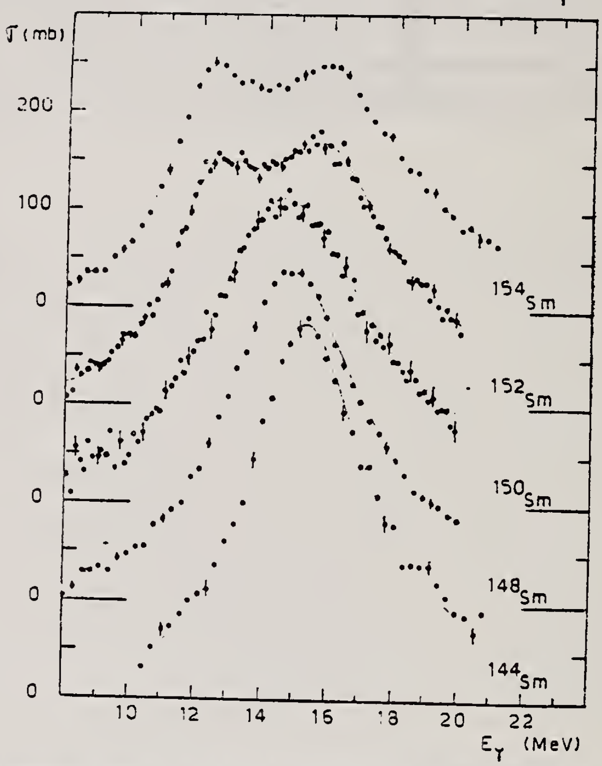

Fig. 7. Total photoneutron cross sections $\sigma_T(E)$ of the doubly even samarium isotopes. Best single Lorentz line fits are shown for ^{144}Sm, ^{148}Sm and ^{150}Sm. For ^{152}Sm and ^{154}Sm the best two Lorentz line fits are presented. Corresponding Lorentz line parameters are given in table 2.

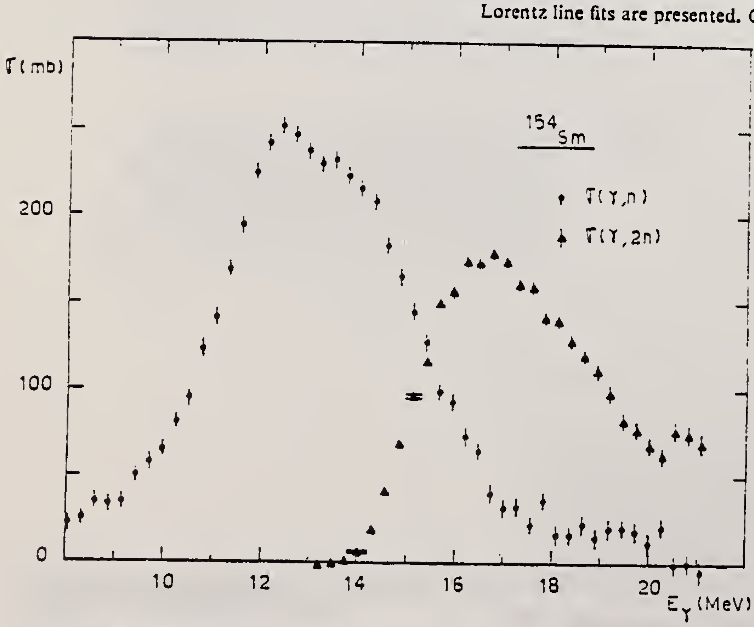

Fig. 6. Partial photoneutron cross sections $[\sigma(\gamma, n)+\sigma(\gamma, np)]$ and $\sigma(\gamma, 2n)$ of ^{154}Sm.

(over)

EET 322

Table 2
Lorentz line parameters

	E_1 (MeV)	σ_1 (mb)	Γ_1 (MeV)	E_2 (MeV)	σ_2 (mb)	Γ_2 (MeV)
^{144}Sm*	15.3 ±0.1	384±20	4.37±0.15			
^{148}Sm*	14.8 ±0.1	339±12	5.1 ±0.2			
^{148}Sm**	14.1	335	4			
^{150}Sm*	14.6 ±0.1	312±20	6.0 ±0.2			
^{150}Sm**	13.6	360	5.5			
^{152}Sm*	12.45±0.10	183±10	3.2 ±0.15	15.85±0.10	226±10	5.1 ±[illegible]
^{152}Sm**	11.55	400	2.4	14.65	420	[illegible].4
^{154}Sm*	12.35±0.10	192±10	3.35±0.15	16.1 ±0.1	204±10	5.2[illegible]±[illegible]
^{154}Sm**	11	204	3	15.25	320	4

* Corresponding to best fits shown in fig. 7.
** Values taken from Vassilijev [23,24]) for comparison.

Table 3
Different integrated cross sections as defined in the text

	^{144}Sm	^{148}Sm	^{150}Sm	^{152}Sm	^{154}Sm
E_M (MeV)	21	20	20	20	21
σ_0 (MeV · b)	2 ±0.14	1.94±0.1	2 ±0.14	2.05±0.1	2.07±0.1
σ'_0 (MeV · b)	2.63	2.71	2.94	2.75	2.69
$\dfrac{\sigma'_0 A}{0.06\,NZ}$	1.24	1.25	1.35	1.24	1.2[illegible]
σ_{-1} (mb)	131 ±15	134 ±10	141 ±15	144 ±10	145 ±10
σ_{-2} (mb · MeV^{-1})	8.7±0.8	9.5 ±0.7	10.3±0.9	10.6 ±0.7	10.6 ±0.7

[23] O. Vasilijev et al., Sov.J.Nucl.Phys. 10, 263 (1970)
[24] O. Vasilijev et al., Sov.J.Nucl.Phys. 13, 463 (1971)

REF. T. Cooper, W. Bertozzi, J. Heisenberg, S. Kowalski, W. Turchinetz, C. Williamson, L. Cardman, S. Fivozinsky, J. Lightbody, Jr., and S. Penner
Phys. Rev. C13, 1083 (1976)

ELEM. SYM.	A	Z
Sm	154	62

METHOD

REF. NO.	
76 Co 3	hmg

REACTION	RESULT	EXCITATION ENERGY	SOURCE TYPE	SOURCE RANGE	DETECTOR TYPE	DETECTOR RANGE	ANGLE
E,E/	FMF	1, 1	D	44-106	MAG-D		DST

LEVELS .082,.267

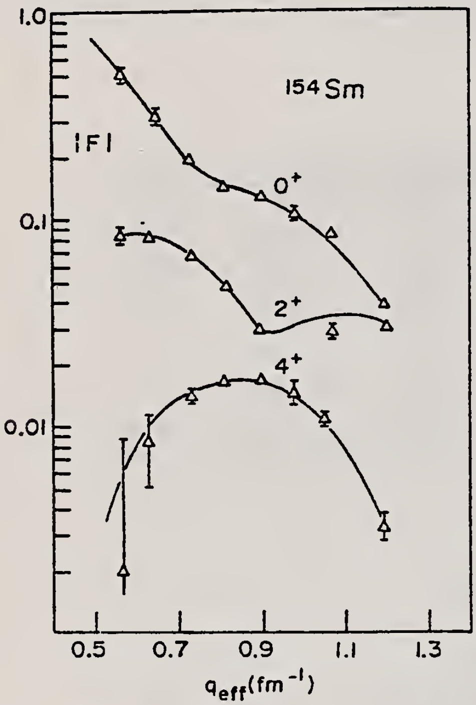

FIG. 1. Measured form factors for the elastic (0^+) and the inelastic 0.082-MeV (2^+) and 0.267-MeV (4^+) states in ^{154}Sm. The fitted curves are based on a best fit deformed Fermi charge distribution.

TABLE III. Cross sections from ^{154}Sm data.

Energy (MeV)	Angle (deg)	q_{eff} (fm^{-1})	Elastic $\frac{d\sigma}{d\Omega}_{exp}$ (mb)	Elastic $\frac{d\sigma}{d\Omega}_{bestfit}$ (mb)	2^+ $\frac{d\sigma}{d\Omega}_{exp}$ (mb)	2^+ $\frac{d\sigma}{d\Omega}_{exp}$ (mb)
44.82	110.22	0.566	0.195×10 ± 3%	0.193×10	0.520×10^{-1}	...
54.73	110.06	0.648	0.507 ± 5%	0.495	0.336×10^{-1}	0.355×10^{-3} ± 35%
65.05	110.27	0.734	0.131 ± 3%	0.131	0.159×10^{-1}	0.712×10^{-3} ± 6%
74.93	110.22	0.817	0.545×10^{-1} ± 3%	0.580×10^{-1}	0.582×10^{-2}	0.727×10^{-3} ± 5%
85.09	110.24	0.900	0.358×10^{-1} ± 4%	0.347×10^{-1}	0.178×10^{-2}	0.577×10^{-3} ± 4%
95.00	109.81	0.981	0.195×10^{-1} ± 7%	0.200×10^{-1}	...	0.351×10^{-3} ± 20%
100.33	144.97	1.195	0.425×10^{-3} ± 5%	0.411×10^{-3}	0.257×10^{-3}	0.348×10^{-5} ± 31%
105.24	110.02	1.068	0.953×10^{-2} ± 5%	0.878×10^{-2}	0.130×10^{-2}	0.139×10^{-3} ± 8%

TABLE VIII. Deformed Fermi best fit parameters.

	Units	^{152}Sm	^{154}Sm	^{232}Th	^{238}U
c_0	fm	5.8044	5.9387	6.7915	6.8054
t	fm	0.5814	0.5223	0.5713	0.6049
β_2		0.287 ± 0.003	0.311 ± 0.003	0.233 ± 0.002	0.261 ± 0.002
β_4		0.070 ± 0.003	0.087 ± 0.002	0.101 ± 0.003	0.037 ± 0.003
β_6		−0.0120	−0.180	0.0	0.0
$B(E2)$	e^2b^2	3.38 ± 0.07	4.40 ± 0.09	9.21 ± 0.09	11.70 ± 0.15
$B(E4)$	e^2b^4	0.136 ± 0.013	0.221 ± 0.010	1.16 ± 0.05	1.20 ± 0.06
rms radius	fm	5.0922	5.126	5.7723	5.842
ρ_2 Transition radius	fm	6.937	6.950	7.895	7.979
ρ_4 Transition radius	fm	7.757	7.704	8.540	8.748

REF.		ELEM. SYM.	A	Z
	F. R. Metzger Phys. Rev. C14, 543 (1976)	Sm	154	62

METHOD	REF. NO.	
	76 Me 6	hmg

REACTION	RESULT	EXCITATION ENERGY	SOURCE TYPE	SOURCE RANGE	DETECTOR TYPE	DETECTOR RANGE	ANGLE
G,G	LFT	1	C	1- 4	SCD-D		DST
		(.921)					

$$\frac{N_{\parallel} - N_{\perp}}{N_{\parallel} + N_{\perp}} = (+3.6\pm2.7)\,\%$$

TABLE I. Properties of the low-lying 1^- levels in the stable even Sm isotopes.

Isotope	$E_{exc}(1^-)$	Γ_0 (meV)	$10^3\times\frac{B(E1;1^-\to0^+)}{B(E1)_{s.p.}}$	N
^{144}Sm	3.225	220±30	3.5±0.5	82
^{148}Sm	1.465	3.1±0.4	0.5±0.1	86
^{150}Sm	1.166	5.4±0.5	1.8±0.2	88
^{152}Sm	0.963	7.3±0.6	4.2±0.4	90
^{154}Sm	0.921	7.4±1.0	4.8±0.7	92

REF.	Z. Berant, J. Tenenbaum and R. Moreh Nucl. Phys. A276, 221 (1977)	ELEM. SYM.	A	Z
		Sm	154	62

METHOD	REF. NO.	
	77 Be 6	egf

REACTION	RESULT	EXCITATION ENERGY	SOURCE TYPE	SOURCE RANGE	DETECTOR TYPE	DETECTOR RANGE	ANGLE
G,G	LFT	6	D	6	SCD-D		DST

6=6.465 MeV

Table 1

The γ-line energies E_γ of the scattered radiation from ^{154}Sm together with level energies E_x and angular distribution coefficients A

E_γ ($\pm$3 keV)	Intensity	A	Present work E_x ($\pm$ 3 keV)	Present work J^π	Refs. [2,3]) [a]) E_x	Refs. [2,3]) [a]) J^π
6383	67$\pm$1	0.105$\pm$0.011	82	2	82.05	2$^+$
5544	8$\pm$2	$-$0.14 $\pm$0.005	921	1	921.7	1$^-$
5366	45$\pm$1	0.45 $\pm$0.07	1099	0	1099.8	0$^+$
5287	8$\pm$2	0.07 $\pm$0.06	1178	2	1177.6	2$^+$
5263	7$\pm$1	0.40 $\pm$0.18	1202	(0)	1204	1$^\mp$,0$^+$
5025	5$\pm$3		1440	0, 1, 2	1440	2$^+$
4709	4$\pm$3		1756	0, 1, 2	1755.8	2, 3
4543	10$\pm$2		1922	0, 1, 2	1923	2, 3, 4
4479	< 1		1986	0, 1, 2	1987	2, 3, 4
3979	10$\pm$2					
6465	100	0.54$\pm$0.07	6465	1$^-$		

The spins J^π are obtained from the results of the present work and are based either on the values of A or on the assumption that the resonance level is deexcited by dipole transitions only.

[a]) Only those levels of refs. [2,3]) are listed which are also observed in the present work.

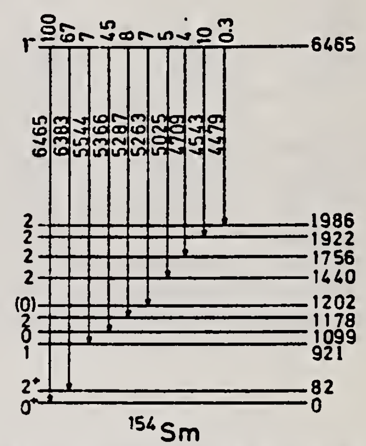

Fig. 2. Decay scheme of the 6465 keV level of ^{154}Sm showing level energies and relative intensities. The level spins are those obtained by combining the results of the present work (table 1) and those reported in refs. [2,3]).

[2]J.M. D'Auria, D. Ostrom and S.C. Guirathi, Nucl. Phys. A178, 172 (1971)

[3]S.A. Elbakr et al., Nucl. Phys. A211, 493 (1973)

Table 4

Values of Γ, Γ_0, and the energy separation δ (between the incident γ-line and the resonance level)

Scatterer	E_γ (keV)	Γ (meV)	Γ_0 (meV)	δ (eV)
^{146}Nd	7163	125$\pm$50	41$\pm$13	13.7$\pm$0.6
^{154}Sm	6465	105$\pm$50	25$\pm$13	3.6$\pm$2.0

REF G.M. Gurevich, L.E. Lazareva, V.M. Mazur, S.Yu. Merkulov, G.V. Solodukhov, V.A. Tyutin
JETP Lett. 28, 157 (1978)
Pis'ma Zh. Eksp. Teor. Fiz. 28, 168 (1978)

ELEM. SYM.	A	Z
Sm	154	62

METHOD

REF. NO.	
78 Gu 7	hg

REACTION	RESULT	EXCITATION ENERGY	SOURCE TYPE	SOURCE RANGE	DETECTOR TYPE	DETECTOR RANGE	ANGLE
G,MU-T	ABX	THR-31	C	UKN	NAI-D		4PI

The absorption method is used to measure the total photoabsorption cross section curves for deformed ^{154}Sm, ^{156}Gd, ^{168}Er, ^{174}Yb, ^{184}W, and ^{136}W nuclei in the region of the $E1$ giant resonance. The behavior of the resonance widths for nuclei in the interval $A = 153$ to 186 is discussed.

PACS numbers: 24.30.Cz, 25.20.+y, 27.70.+q

TABLE I.

Nucleus	E_1 MeV	σ_1 mb	Γ_1 MeV	E_2 MeV	σ_2 mb	Γ_2 MeV	Γ MeV	Q_0 b	β	$\sigma_{0L}/0.06\frac{ZN}{A}$
^{154}Sm	12.2	188	3.4	15.7	207	5.7	8.1 ± 0.2	6.3 ± 0.3	0.32 ± 0.02	1.28
^{156}Gd	12.3	206	3.2	15.7	220	5.5	7.7 ± 0.2	6.2 ± 0.3	0.31 ± 0.02	1.30
^{168}Er	11.9	222	3.2	15.5	275	4.5	7.4 ± 0.2	7.5 ± 0.7	0.32 ± 0.03	1.26
^{174}Yb	12.3	297	2.9	15.5	320	4.9	7.1 ± 0.2	7.0 ± 0.6	0.30 ± 0.02	1.52
^{184}W	11.9	315	2.9	14.8	321	4.7	6.8 ± 0.2	7.2 ± 0.8	0.27 ± 0.03	1.50
^{186}W	12.0	246	3.3	14.5	332	5.1	6.4 ± 0.2	6.2 ± 0.8	0.23 ± 0.03	1.48
Average error	±1.3%	±10.5%	±7.5%	±1.3%	±9.4%	±3.8%	—	—	—	—

(over)

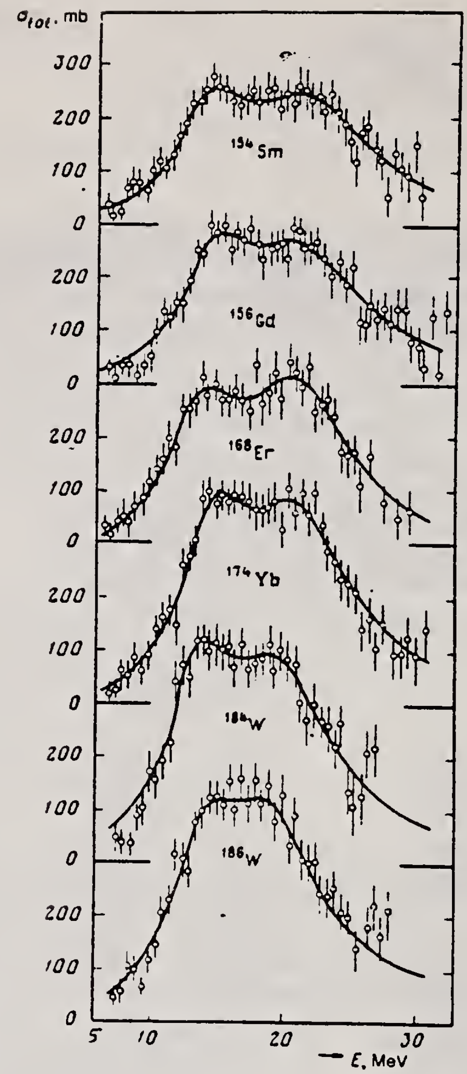

FIG. 2. Total cross sections of the photoabsorption of the nuclei ^{154}Sm, ^{156}Gd, ^{168}Er, ^{174}Yb, ^{184}W, and ^{186}W. The mean squared errors are shown.

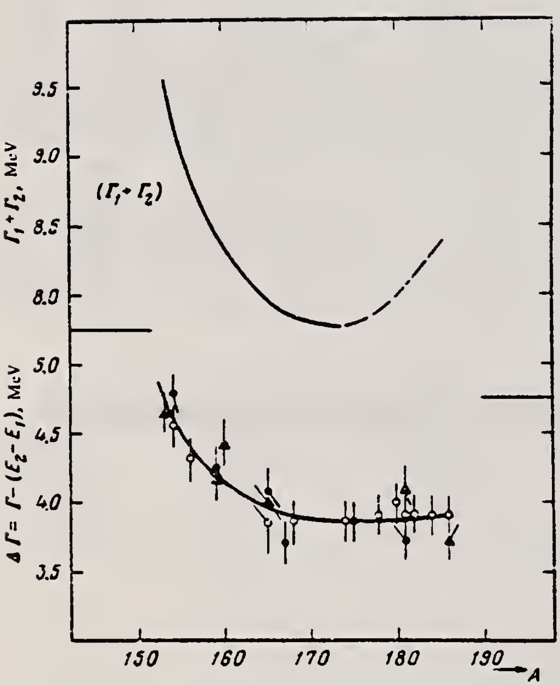

FIG. 3. Experimental values of $\Delta\Gamma = \Gamma - (E_2 - E_1)$ in the region of deformed nuclei with A = 153–186: O—present work and[11]; ●—Saclay group; ▲—Livermore group. Owing to a small systematic deviations of the absolute values, the ordinate scales for the Saclay and Livermore data are shifted 0.15 MeV upward and downward, respectively. The $(\Gamma_1 + \Gamma_2)$ curve was obtained from the $\Delta\Gamma$ curve after introduction of corrections in the interval A = 175–186.

REF.		ELEM. SYM.	A	Z
G.M. Gurevich, L.E. Lazareva, V.M. Mazur, S.Yu. Merkulov, G.V. Solodukhov, V.A. Tyutin Nucl. Phys. A351, 257 (1981)		Sm	154	62
METHOD		REF. NO.		
		81 Gu 2		hg

REACTION	RESULT	EXCITATION ENERGY	SOURCE TYPE	SOURCE RANGE	DETECTOR TYPE	DETECTOR RANGE	ANGLE
G,MU-T	ABX	THR-20	C	27	NAI-D		4PI

Abstract: The curves of the total gamma-absorption cross sections (σ_{tot}) in the E1 giant resonance energy range for the nuclei ^{154}Sm, ^{156}Gd, ^{165}Ho, ^{168}Er, ^{174}Yb, ^{178}Hf, ^{180}Hf, ^{181}Ta, ^{182}W, ^{184}W, ^{186}W and ^{197}Au have been measured using the absorption-method. Parameters of the Lorentz curves fitting the measured cross sections σ_{tot} are given. Quadrupole moments (Q_0) and nuclear deformation parameters (β) were obtained.

For deformed nuclei in the ~ 155 < A < ~ 180 region a violation of the correlation between giant resonance widths (Γ) and nuclear deformation parameters was found. Γ_1 and Γ_2, the widths of the resonances corresponding to vibrations of nucleons along and across the nuclear deformation axis, were observed to decrease with the increase of A which could be accounted for by the presence of an N = 108 subshell.

E

NUCLEAR REACTIONS ^{154}Sm, ^{156}Gd, ^{165}Ho, ^{168}Er, ^{174}Yb, ^{178,180}Hf, ^{181}Ta, ^{182,184,186}W, ^{197}Au (γ, X), E = 7-20 MeV: measured total $\sigma(E)$; deduced integrated σ, Lorentz line parameters. ^{154}Sm, ^{156}Gd, ^{165}Ho, ^{168}Er, ^{174}Yb, ^{178,180}Hf, ^{181}Ta, ^{182,184,186}W, ^{197}Au deduced β, Q_0, Γ, giant resonance evolution. Enriched, natural targets.

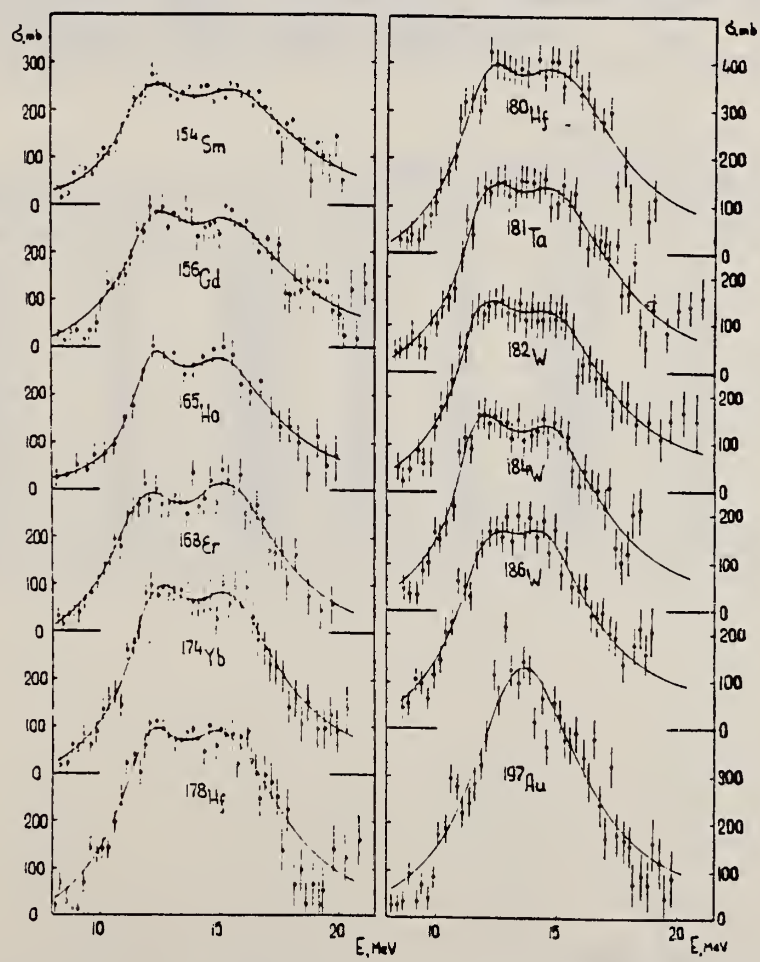

Fig. 2. Total nuclear γ-absorption cross sections (σ_{tot}) measured by the absorption method for ^{154}Sm, ^{156}Gd, ^{165}Ho, ^{168}Er, ^{174}Yb, ^{178}Hf, ^{180}Hf, ^{181}Ta, ^{182}W, ^{184}W, ^{186}W and ^{197}Au. Rms error bars are shown.

(OVER)

U.S. DEPARTMENT OF COMMERCE
NATIONAL BUREAU OF STANDARDS

Table 2

Parameters of Lorentz curves fitting the experimental data on σ_{tot}

Nucleus	E_1 (MeV)	σ_1 (mb)	Γ_1 (MeV)	E_2 (MeV)	σ_2 (mb)	Γ_2 (MeV)	$\frac{\sigma_2\Gamma_2}{\sigma_1\Gamma_1}$	Γ (MeV)
^{154}Sm	12.2	188	3.4	15.7	207	5.7	1.85	8.1
^{156}Gd	12.3	206	3.2	15.7	220	5.5	1.81	7.7
^{165}Ho	12.3	202	2.3	15.2	239	4.8	2.47	7.0
^{168}Er	11.9	222	3.2	15.5	275	4.5	1.73	7.4
^{174}Yb	12.3	297	2.9	15.5	320	4.9	1.80	7.1
^{178}Hf	12.2	291	3.1	15.5	334	4.9	1.80	7.2
^{180}Hf	12.2	286	3.2	15.3	324	5.1	1.81	7.1
^{181}Ta	12.1	272	3.0	15.0	316	5.1	1.97	6.8
^{182}W	11.9	267	3.2	14.8	303	5.6	2.01	6.8
^{184}W	11.9	315	2.9	14.8	321	4.7	1.65	6.8
^{186}W	12.0	246	3.3	14.5	332	5.1	2.07	6.4
^{197}Au	13.7	535	5.2					
Average error	1.4%	11.2%	9.3%	1.5%	9.7%	4.6%	0.22	0.2 MeV

Table 3

Ratios of nuclear ellipsoid axes (k), deformation parameters (β) and intrinsic quadrupole moments (Q_0), calculated from E_2/E_1

Nucleus	^{154}Sm	^{156}Gd	^{165}Ho	^{168}Er	^{174}Yb	^{178}Hf	^{180}Hf	^{181}Ta	^{182}W	^{184}W	^{186}W
k	1.320	1.302	1.259	1.327	1.289	1.296	1.281	1.263	1.271	1.268	1.229
β	0.326 ±0.017	0.309 ±0.016	0.266 ±0.036	0.334 ±0.032	0.296 ±0.024	0.303 ±0.032	0.288 ±0.036	0.270 ±0.026	0.278 ±0.030	0.274 ±0.032	0.235 ±0.033
Q_0	6.3 ±0.3	6.2 ±0.3	5.8 ±0.8	7.5 ±0.7	7.0 ±0.6	7.5 ±0.8	7.2 ±0.9	6.9 ±0.7	7.2 ±0.8	7.1 ±0.8	6.2 ±0.9

Table 4

Integral characteristics of E1 giant resonance

Nucleus	$\sigma_{0\,exp}$ (MeV · b)	$\sigma_{0\,exp}$/0.06NZ/A	σ_{0L} (MeV · b)	σ_{0L}/0.06NZ/A	σ_{-1} (mb)	σ_{-1L} (mb)	$\sigma_{-1L}A^{-4/3}$ (mb)	σ_{-2} (mb · MeV^{-1})	σ_{-2L} (mb · MeV^{-1})	$\sigma_{-2L}A^{-5/3}$ (μb · MeV^{-1})
^{154}Sm	1.94±0.06	0.87	2.86	1.29	117±3.5	156	0.189	9.1±0.3	14.3	3.23
^{156}Gd	2.07±0.07	0.91	2.95	1.30	143±4.6	163	0.194	10.5±0.4	14.9	3.30
^{165}Ho	1.86±0.06	0.78	2.53	1.06	155±4.4	160	0.177	10.1±0.3	12.6	2.54
^{168}Er	2.24±0.06	0.92	3.07	1.26	161±4.3	197	0.212	12.0±0.3	16.0	3.13
^{174}Yb	2.69±0.05	1.07	3.82	1.52	195±3.4	240	0.247	14.5±0.3	19.2	3.54
^{178}Hf	2.85±0.07	1.11	3.99	1.55	208±4.9	247	0.247	15.3±0.4	20.2	3.59
^{180}Hf	2.72±0.06	1.05	4.03	1.56	200±4.4	250	0.246	15.1±0.3	20.7	3.61
^{181}Ta	2.84±0.07	1.09	3.81	1.46	210±5.3	245	0.239	16.0±0.4	20.0	3.45
^{182}W	2.86±0.07	1.09	4.01	1.52	211±5.3	256	0.248	16.2±0.4	21.6	3.70
^{184}W	2.78±0.07	1.05	3.80	1.43	207±5.3	251	0.240	15.9±0.4	20.9	3.51
^{186}W	2.90±0.07	1.08	3.95	1.48	214±5.3	256	0.241	16.2±0.4	21.6	3.56
^{197}Au	3.12±0.06	1.10	4.37	1.54	229±4.2	276	0.241	18.6±0.4	23.3	3.49

EUROPIUM
Z=63

Europium is a metallic element and the least dense, softest, and most volatile of the rare earths. Europium was discovered in 1896 by E. Demarcay and has been used primarly for research purposes.

Eu

Eu

REF.	ELEM. SYM.	A	Z
R. R. Hurst and D. J. Donahue Nucl. Phys. A91, 365 (1967)	Eu		63

METHOD	REF. NO.	
Neutron capture gamma rays	67 Hu 1	EGF

REACTION	RESULT	EXCITATION ENERGY	SOURCE TYPE	SOURCE RANGE	DETECTOR TYPE	DETECTOR RANGE	ANGLE
G,N	ABX	9-11	D	9-11	BF3-I		4PI

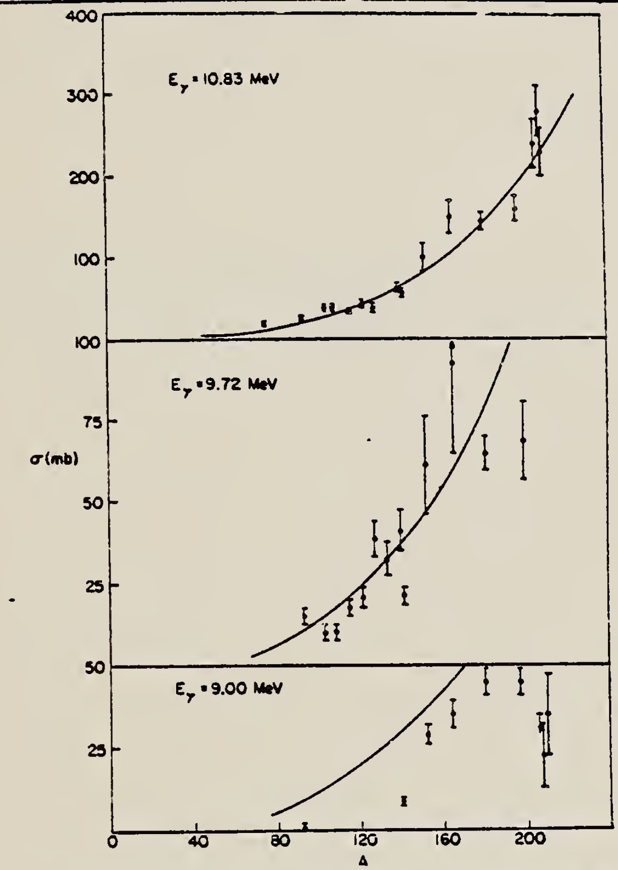

Fig. 1. Cross section (in mb) versus mass number of the target for gamma-ray energies of 9.00, 9.72 and 10.83 MeV. The solid lines are plots of eq. (1) in the text.

TABLE 1
Photoneutron cross sections (mb)

Target	7.72 MeV	9.00 MeV	9.72 MeV	10.83 MeV
^{59}Co				9.0 ± 0.8
^{75}As				20.4 ± 1.7
^{93}Nb		0.53 ± 0.10	14.6 ± 2.2	25.8 ± 2.1
^{103}Rh			10.6 ± 1.7	38.8 ± 3.1
^{107}Ag, ^{109}Ag			10.0 ± 1.5	37.6 ± 2.9
^{115}In			17.1 ± 2.6	33.3 ± 2.7
^{121}Sb, ^{123}Sb			20.7 ± 3.1	42.5 ± 3.6
^{127}I			38.7 ± 5.8	38.8 ± 3.1
^{133}Cs			31.7 ± 4.8	52.5 ± 3.8
^{139}La		8.61 ± 0.86	40.8 ± 6.5	63.0 ± 5.0
^{141}Pr			21.5 ± 3.2	58.3 ± 4.1
^{151}Eu, ^{153}Eu		28.9 ± 3.2	61.3 ± 14.7	102 ± 18
^{165}Ho		35.6 ± 4.3	92.2 ± 27.6	150 ± 20
^{181}Ta	4.14 ± 0.36	45.4 ± 3.7	65.0 ± 5.5	146 ± 12
^{197}Au		44.5 ± 3.6	68.4 ± 13.5	160 ± 15
^{206}Pb		<34.3		238 ± 29
^{208}Pb		22.6 ± 11.3		280 ± 31
^{209}Bi		36.1 ± 12.0		226 ± 27

Eu
A=151

Eu
A=151

REF.

K. N. Geller, J. Halpern, and E. G. Muirhead
Phys. Rev. 118, 1302-12 (1960)

ELEM. SYM.	A	Z
Eu	151	63

METHOD

Betatron; neutron threshold; ion chamber

REF. NO.

60 Ge 3 NVB

REACTION	RESULT	EXCITATION ENERGY	SOURCE		DETECTOR		ANGLE
			TYPE	RANGE	TYPE	RANGE	
G,N	NØX	THR	C THR		BF3-I		4 PI

THRESHØLD

TABLE I. Summary and comparison of neutron separation energies inferred from present threshold measurements with values predicted from mass data and reaction energies. All energies are expressed in the center-of-mass system in Mev.

Reaction	No. runs	Present results	Other results	Method	Reference
$Eu^{151}(\gamma,n)Eu^{150}$	1	8.04 $\pm$0.11			

REF.	ELEM. SYM.	A	Z
S. F. Semenko, O. V. Vasilijev and V. A. Semenov Phys. Letters 31B, 429 (1970)	Eu	151	63

METHOD	REF. NO.	
	70 Se 1	egf

REACTION	RESULT	EXCITATION ENERGY	SOURCE		DETECTOR		ANGLE
			TYPE	RANGE	TYPE	RANGE	
G,XN	ABX	8-24	C	8-24	BF3-I		4PI

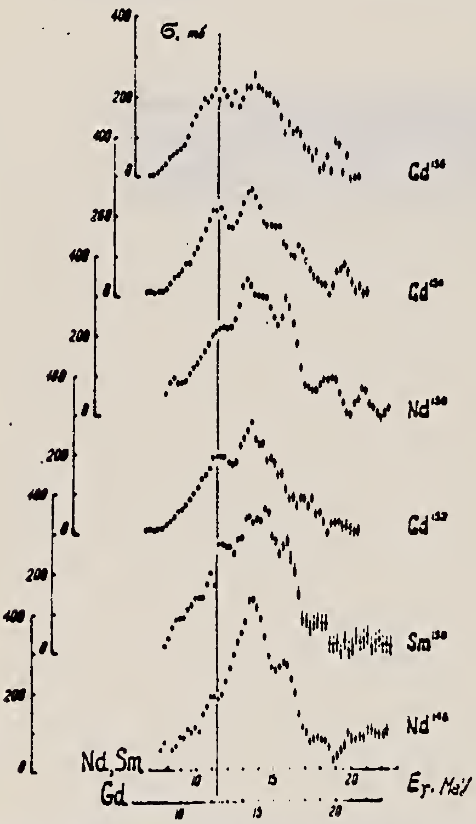

Fig. 1. The variation of the even-even nuclei giant resonance shape with the increase of Z, N in the transitional region $N = 90$. The photoabsorption curves of ^{148}Nd, ^{150}Sm, ^{152}Gd ($N = 88$) ^{150}Nd, ^{154}Gd ($N = 90$) and ^{156}Gd ($N = 92$) are presented (From the bottom). The upper energy scale is for Nd, Sm and the lower is for Gd isotopes. At the energies greater than (γ, $2n$) threshold the photoabsorption cross section was defined from the photoneutron cross section by usual correction for neutron multiplicity. Only statistical errors are plotted.
The "phase transition" effect in the giant resonance of the nuclei with $N = 88$ is emphasized by the vertical line.

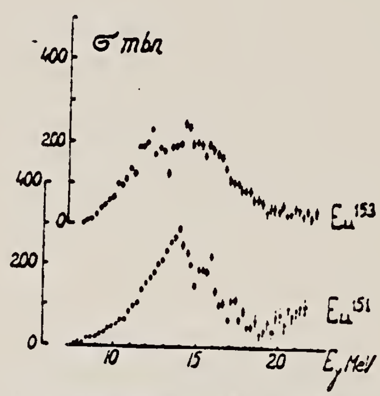

Fig. 2. The photoabsorption cross sections for ^{151}Eu and ^{153}Eu.

REF.						ELEM. SYM.	A	Z
O. V. Vasil'ev and V. A. Semenov ZhETF Pis. Red. 11, 520 (1970) JETP Letters 11, 356 (1970)						Eu	151	63
METHOD						REF. NO. 70 Va 1		egf

REACTION	RESULT	EXCITATION ENERGY	SOURCE TYPE	SOURCE RANGE	DETECTOR TYPE	DETECTOR RANGE	ANGLE
G,XN	ABX	8-22	C	8-22	BF3-I		4PI

488

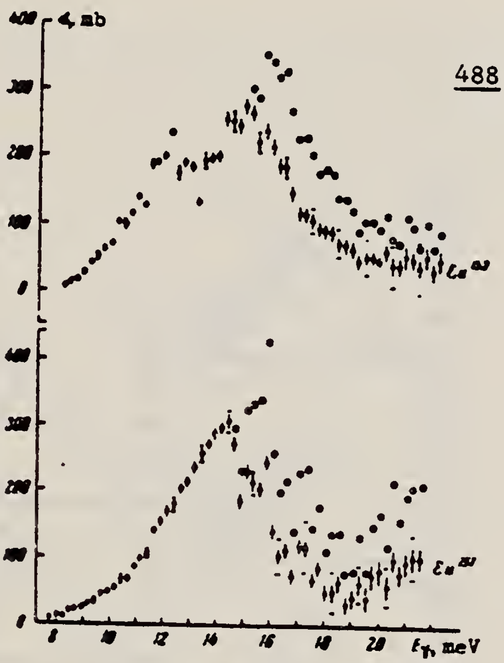

Fig. 2. Photoneutron cross sections and photoabsorption cross sections for Eu^{151} and Eu^{153}. The graphic symbols are the same as in Fig. 1.

REF.	O. V. Vasil'ev, V. A. Semenov, and S. F. Semenko Yad. Fiz. 13, 463 (1971) Sov. J. Nucl. Phys. 13, 259 (1971)	ELEM. SYM.	A	Z
		Eu	151	63
METHOD		REF. NO.		
		71 Va 2		hmg

REACTION	RESULT	EXCITATION ENERGY	SOURCE TYPE	SOURCE RANGE	DETECTOR TYPE	DETECTOR RANGE	ANGLE
G,XN	ABX	7-24	C	7-24	BF3-I		4PI
		(7.9-23.25)		(7.9-23.25)			

Table II. Parameters of giant dipole resonance

Isotope	σ_1, mb	E_1, MeV	Γ_1, MeV	$\sigma_{int\,1}$, MeV·b	σ_2, mb	E_2, MeV	Γ_2, MeV	$\sigma_{int\,2}$, MeV·b	σ_{int}	$\frac{\sigma_{int}}{0.015\,NZ/A}$	$\frac{\sigma_{int\,2}}{\sigma_{int\,1}}$	$\frac{E_2}{E_1}$	β_{eff}
Nd^{146}	332	13,8	4,1						2,12	1,00			
Sm^{148}	335	14,1	4,0						2,08	0,96			
Gd^{152}	147	12,0	3,0	0,693	259	15,0	3,2	1,29	1,99	0,90	1,87	1,25	0,28
Gd^{154}	161	11,9	2,4	0,612	250	15,0	3,5	1,39	2,00	0,89	2,27	1,26	0,29
Gd^{156}	180	11,9	2,6	0,738	243	15,2	3,6	1,37	2,11	0,94	1,86	1,27	0,31
Gd^{158}	165	11,7	2,6	0,662	249	14,9	3,8	1,49	2,16	0,94	2,25	1,28	0,32
Eu^{151}	285	14,0	4,5						2,02	0,92			
Eu^{153}	159	11,9	2,3	0,562	237	15,1	3,6	1,34	1,90	0,86	2,39	1,27	0,31

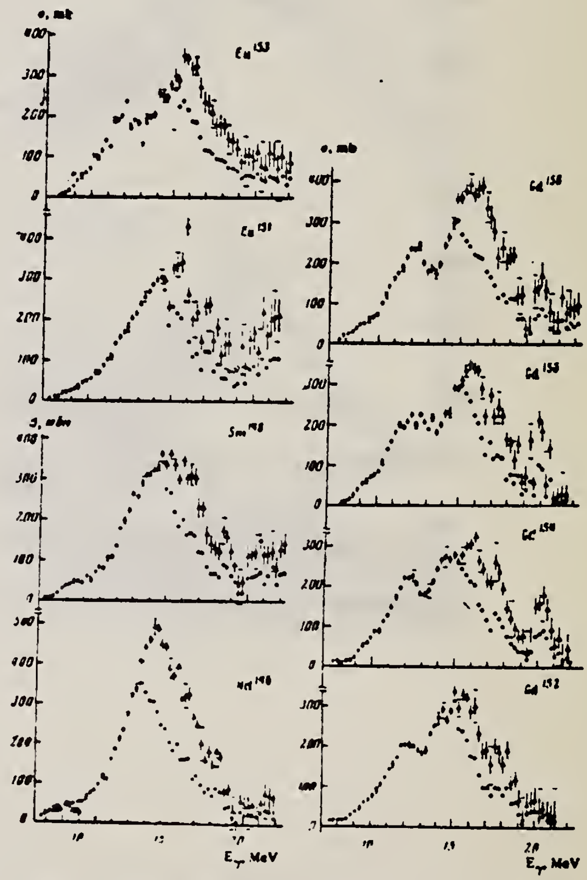

FIG. 1. Photoneutron cross sections and photoabsorption cross sections of Nd^{146}, Sm^{148}, Eu^{151}, Eu^{153}, Gd^{152}, Gd^{154}, Gd^{156} and Gd^{158} Statistical and rms experimental errors are shown (the latter horizontal bars at 9.42 MeV, 10.42 MeV etc.) At photon energies above the (γ, 2n) threshold the photoabsorption cross section errors are not shown.

Eu
A=153

Eu
A=153

REF.
K. N. Geller, J. Halpern, and E. G. Muirhead
Phys. Rev. 118, 1302-12 (1960)

ELEM. SYM.	A	Z
Eu	153	63

METHOD
Betatron; neutron threshold; ion chamber

REF. NO.
60 Ge 3 | NVB

REACTION	RESULT	EXCITATION ENERGY	SOURCE TYPE	SOURCE RANGE	DETECTOR TYPE	DETECTOR RANGE	ANGLE
G,N	NØX	THR	C THR		BF3-I		4 PI

THRESHØLD

TABLE I. Summary and comparison of neutron separation energies inferred from present threshold measurements with values predicted from mass data and reaction energies. All energies are expressed in the center-of-mass system in Mev.

Reaction	No. runs	Present results	Other results	Method	Reference
$Eu^{153}(\gamma,n)Eu^{152}$	1	8.65 ±0.13	8.66 ±0.37	mass data	p

p W. H. Johnson, Jr., and A. O. Nier, Phys. Rev. 105, 1014 (1957).

REF.	ELEM. SYM.	A	Z
U. Atzmony and S. Ofer Phys. Rev. 145, B915 (1966)	Eu	153	63

METHOD	REF. NO.	
Mössbauer effect; Gd_2O_3 source	66 At 1	JDM

REACTION	RESULT	EXCITATION ENERGY	SOURCE TYPE	SOURCE RANGE	DETECTOR TYPE	DETECTOR RANGE	ANGLE
G,G	LFT	1	D		SCD		4PI

97-keV level has either $\mu_1 = 3.21 \pm 0.22$ nm

Or $\mu_1 = (-0.52 \pm 0.22)$ nm

$T_{\frac{1}{2}} = (2.14 \pm .02) \times 10^{-10}$ sec.

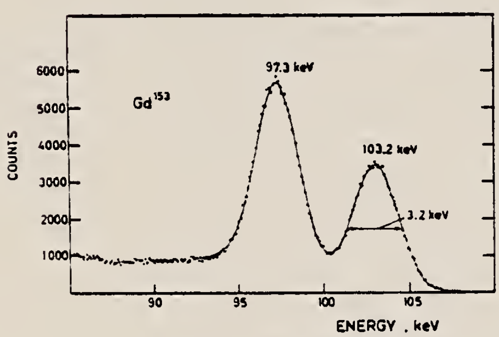

FIG. 1. γ spectrum of a Gd^{153} source taken with a Li-drifted Ge detector.

TABLE I. Summary of experimental results with [illegible] sources. Γ_m is the measured width of the absorption line at half-maximum and [illegible] is the "true" width.

Absorber	η_{97} (%)	Γ_m (mm/sec)	Γ_a (mm/sec)	f_a (%)	Θ_M (°K)	$T_{1/2}$ (10^{-10} sec)
Eu_2O_3	3.4 ±0.3	17.8±0.9	6.54±0.35	5.7 ±0.4	212±5	2.16±0.20
$EuSO_4$	2.15±0.2	15.3±1.5	6.59±0.65	0.57±0.07	129±5	2.1 ±0.2

B. L. Berman, M. A. Kelly, R. L. Bramblett, J. T. Caldwell
H. S. Davis, and S. C. Fultz
Phys. Rev. 185, 1576 (1969)

Eu	153	63

METHOD	REF. NO.	
	69 Be 8	hmg

REACTION	RESULT	EXCITATION ENERGY	SOURCE TYPE	SOURCE RANGE	DETECTOR TYPE	DETECTOR RANGE	ANGLE
G,N* 155+	ABX	8-29	D	8-29	BF3-I		4PI
G,2N** 156+	ABX	8-29	D	8-29	BF3-I		4PI
G,3N 157	ABX	8-29	D	8-29	BF3-I		4PI

* INCLUDES NP 154+
** INCLUDES 2NP

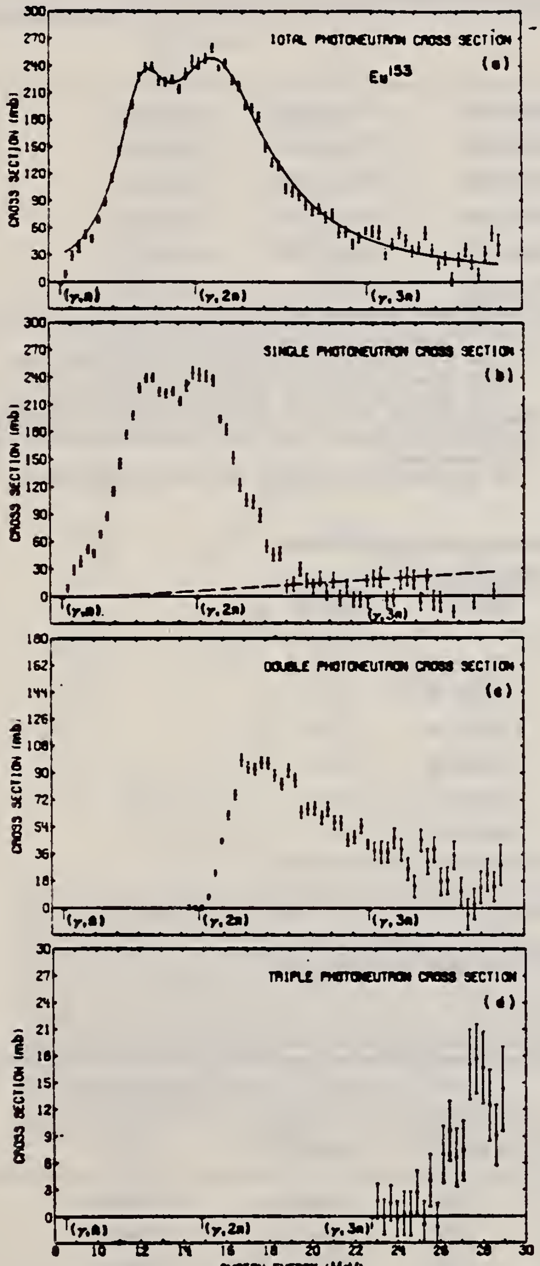

FIG. 5. Photoneutron cross sections for Eu^{153}. (a) Total photoneutron cross section $\sigma[(\gamma, n)+(\gamma, pn)+(\gamma, 2n)+(\gamma, p2n)+(\gamma, 3n)]$. The solid line is a two-component Lorentz-curve fit to the giant-resonance data (10.8–18.8 MeV). (b) Single-photoneutron cross section $\sigma[(\gamma, n)+(\gamma, pn)]$. The dashed line represents the maximum systematic error owing to the uncertainty in the normalization of the positron bremsstrahlung subtraction. (c) Double-photoneutron cross section $\sigma[(\gamma, 2n)+(\gamma, p2n)]$. (d) Triple photoneutron cross section $\sigma(\gamma, 3n)$.

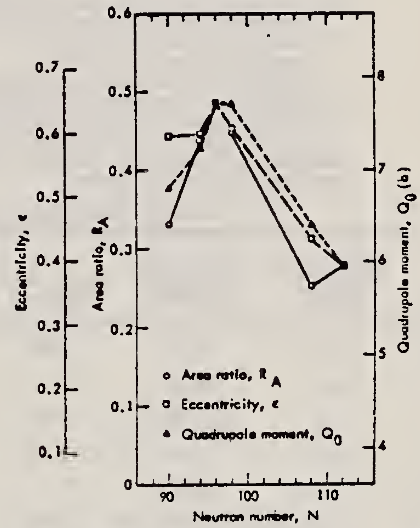

FIG. 9. The area ratio R_A, nuclear eccentricity ϵ, and intrinsic quadrupole moment Q_0 plotted versus neutron number N. The data were scaled between the value for Gd^{160} and that for W^{186}. The absolute scale for Q_0 is based on a mean radius parameter $R_0=1.26$ F. The lines merely connect the three sets of data points. The experimental uncertainties have been omitted for clarity but are given in Tables VII and VIII; their average values are 0.065 (17%) for R_A, 0.010 (1.9%) for ϵ, and 0.26b (3.7%) for Q_0.

[over]

TABLE V. Parameters of Lorentz-curve fits to the giant resonance.

Nucleus	$E_m(1)$ (MeV)	$\sigma_m(1)$ [a] (mb)	$\Gamma(1)$ (MeV)	$E_m(2)$ (MeV)	$\sigma_m(2)$ [a] (mb)	$\Gamma(2)$ (MeV)
Eu^{153}	12.33±0.06	155±9	2.75±0.26	15.79±0.10	222±6	5.83±0.30
Tb^{159} [b]	12.22±0.04	181±6	2.64±0.16	15.67±0.06	220±4	4.97±0.19
Gd^{160}	12.23±0.06	215±9	2.77±0.25	15.96±0.09	233±6	5.28±0.30
Ho^{165}	12.28±0.02	214±5	2.57±0.11	15.78±0.04	246±3	5.00±0.17
Ta^{181} [c]	12.59±0.03	171±8	1.94±0.12	15.13±0.12	265±6	4.98±0.23
W^{186}	12.59±0.03	211±14	2.29±0.14	14.88±0.08	334±8	5.18±0.14

[a] The uncertainties for σ_m given here are relative. The absolute uncertainty is 7% (10% for Tb^{159} and Ta^{181}).
[b] The data of Ref. 10 were reanalyzed to obtain the values given in this and subsequent tables (see text).
[c] The data of Ref. 11 were reanalyzed to obtain the values given in this and subsequent tables (see text).

10 R.L. Bramblett, J. T. Caldwell, R. R. Harvey, S.C. Fultz, Phys.Rev.133, B869 (1964).
11 R.L. Bramblett, J.T. Caldwell, G.F. Auchampaugh, S.C. Fultz, Phys.Rev.129, 2723 (1963)

TABLE VIII. Nuclear radius parameters.

Nucleus	Q_0 [a] (b)	Refs.	ϵ [b]	R_0 [c] (F)	Q_0 [d] (b)
Eu^{153}	6.99±0.08	e, f	0.595±0.015	1.276±0.018	6.80±0.28
Tb^{159}	7.41±0.11	e	0.598±0.009	1.274±0.013	7.23±0.26
Gd^{160}	7.55±0.17	g	0.645±0.014	1.245±0.020	7.71±0.30
Ho^{165}	7.56±0.11	e	0.604±0.006	1.246±0.011	7.71±0.26
Ta^{181}	6.89±0.21	h, i	0.433±0.010	1.306±0.025	6.43±0.26
W^{186}	5.96±0.05	g, j, k	0.390±0.006	1.259±0.011	5.96±0.21

[a] Values taken from or computed from the references listed in column 3.
[b] Values from present data (Table VII).
[c] Computed from Eq. (2) in the text.
[d] The "best" values for Q_0 deduced from the present data, computed from Eq. (2) in the text, taking R_0 to be 1.26±0.02 F.
[e] M. C. Olesen and B. Elbek, Nucl. Phys. 15, 134 (1960).
[f] R. A. Carrigan, Jr., P. D. Gupta, R. B. Sutton, M. N. Suzuki, A. C. Thompson, R. E. Coté, W. V. Prestwich, A. K. Gaigalas, and S. Raboy, Phys. Rev. Letters 20, 874 (1968).
[g] P. H. Stelson and L. Grodzins, Nucl. Data A1, 21 (1965).
[h] F. K. McGowan and P. H. Stelson, Phys. Rev. 109, 901 (1958).
[i] E. M. Bernstein and R. Graetzer, Phys. Rev. 119, 1321 (1960).
[j] R. C. Barrett, S. Bernow, S. Devons, I. Duerdoth, D. Hitlin, J. W. Kast, W. Y. Lee, E. R. Macagno, J. Rainwater, and C. S. Wu, Columbia University Program Nuclear Physics Lab. Report No. NYO-72-191, 1968, p. 74 (unpublished).
[k] R. G. Stokstad and B. Persson, Phys. Rev. 170, 1072 (1968).

TABLE IX. Integrated cross sections.

Nucleus	$E_{\gamma\,max}$ (MeV)	$\sigma_{int}[(\gamma,n)+(\gamma,pn)]$ [a] (MeV-b)	$\sigma_{int}[(\gamma,2n)+(\gamma,p2n)]$ [a] (MeV-b)	$\sigma_{int}(\gamma,3n)$ [a] (MeV-b)	$\dfrac{\sigma_{int}[(\gamma,2n)+(\gamma,p2n)]}{\sigma_{int}(\gamma,\text{total})}$ [b]	$\frac{1}{2}\pi[\sigma_m(1)\Gamma(1)+\sigma_m(2)\Gamma(2)]$ [a] (MeV-b)	$0.06\,NZ/A$ (MeV-b)
Eu^{153}	28.9	1.57	0.67	0.04	0.29±0.04	2.70±0.19	2.22
Tb^{159}	28.0	1.41	0.89	d	0.39±0.08	2.47±0.12	2.31
Gd^{160}	29.5	1.45	1.00	0.08	0.39±0.05	2.87±0.20	2.30
Ho^{165}	28.9	1.73	0.74	0.04	0.29±0.04	2.80±0.09	2.39
Ta^{181}	24.6	1.31	0.88 [e]	f	0.40 [e] ±0.08	2.59±0.15	2.61
W^{186}	28.6	1.66	1.19	0.15	0.40±0.05	3.47±0.17	2.67

[a] All measured integrated cross-section values are given for an energy region from threshold to $E_{\gamma\,max}$.
[b] The word "total" in this table refers to the total photoneutron cross section, $\sigma[(\gamma,n)+(\gamma,pn)+(\gamma,2n)+(\gamma,p2n)+(\gamma,3n)]$.
[c] The uncertainties listed here are relative; to get the absolute uncertainty, a systematic uncertainty of 7% (10% for Tb^{159} and Ta^{181}) must be folded into the values for σ_m.
[d] Not measured in Ref. 10; $\sigma_{int}[(\gamma,2n)+(\gamma,p2n)]$ contains $\frac{3}{2}\sigma_{int}(\gamma,3n)$.
[e] Because $E_{\gamma\,max}$ is so low, these values cannot be compared to the rest.
[f] Not measured in Ref. 11; the $(\gamma,3n)$ cross section below 24.6 is MeV probably negligible.

TABLE X. Integrated moments[a] of the measured photoneutron cross section and sum rules.

Nucleus	σ_{-1} (mb)	$\sigma_{-1}A^{-1/3}$ (mb)	σ_{-2} (mb-MeV^{-1})	$\dfrac{\sigma_{-2}}{0.00225\,A^{5/3}}$	$\dfrac{\sigma_{-2}K}{0.05175\,A^{5/3}}$	$\dfrac{0.05175\,A^{5/3}}{\sigma_{-2}}$ (MeV)
Eu^{153}	148	0.181	10.18	1.03	1.16±0.11	22.2±1.6
Tb^{159}	151	0.175	10.49	1.00	1.14±0.13	23.0±2.3
Gd^{160}	169	0.195	12.09	1.14	1.35±0.13	20.2±1.4
Ho^{165}	166	0.183	11.56	1.04	1.23±0.10	22.2±1.6
Ta^{181} [b]	(149)	(0.145)	(10.66)	(0.82)	(0.97±0.13)	(28.1±2.8)
W^{186}	203	0.191	14.51	1.06	1.26±0.11	21.6±1.5

[a] $\sigma_{-1}=\int_{E_{thr}}^{E_{\gamma\,max}}\sigma E^{-1}\,dE$ and $\sigma_{-2}=\int_{E_{thr}}^{E_{\gamma\,max}}\sigma E^{-2}\,dE$, where σ is the total photoneutron cross section.
[b] Because $E_{\gamma\,max}$ is so low, the values for Ta^{181} cannot be compared to the rest.

S. F. Semenko, O. V. Vasilijev and V. A. Semenov
Phys. Letters 31B, 429 (1970)

Eu	153	63

METHOD

REF. NO.	
70 Se 1	egf

REACTION	RESULT	EXCITATION ENERGY	SOURCE TYPE	SOURCE RANGE	DETECTOR TYPE	DETECTOR RANGE	ANGLE
G,XN	ABX	8-24	C	8-24	BF3-I		4PI

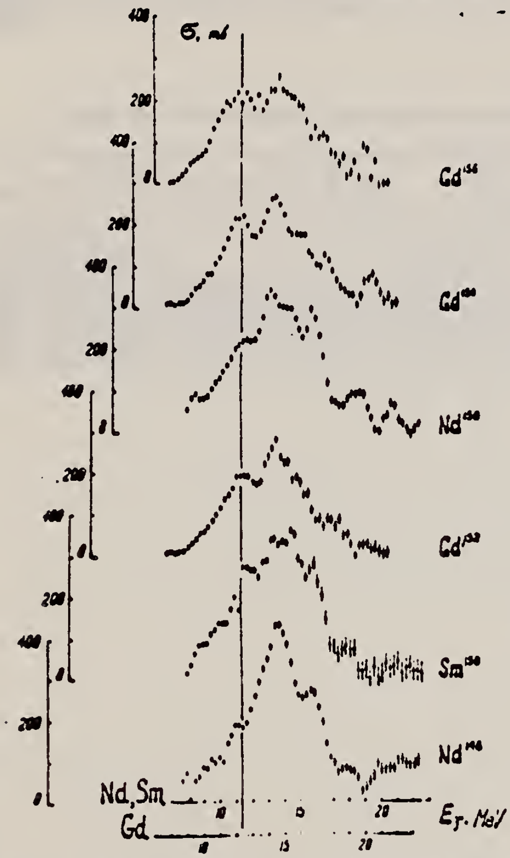

Fig. 1. The variation of the even-even nuclei giant resonance shape with the increase of Z, N in the transitional region $N = 90$. The photoabsorption curves of ^{148}Nd, ^{150}Sm, ^{152}Gd ($N = 88$) ^{150}Nd, ^{154}Gd ($N = 90$) and ^{156}Gd ($N = 92$) are presented (From the bottom). The upper energy scale is for Nd, Sm and the lower is for Gd isotopes. At the energies greater than (γ, $2n$) threshold the photoabsorption cross section was defined from the photoneutron cross section by usual correction for neutron multiplicity. Only statistical errors are plotted.
The "phase transition" effect in the giant resonance of the nuclei with $N = 88$ is emphasized by the vertical line.

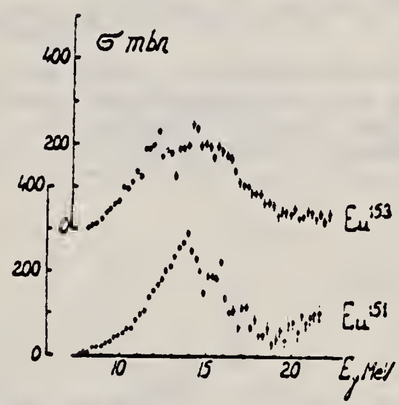

Fig. 2. The photoabsorption cross sections for ^{151}Eu and ^{153}Eu.

REF.	ELEM. SYM.	A	Z
O. V. Vasil'ev and V. A. Semenov ZhETF Pis. Red. 11, 520 (1970) JETP Letters 11, 356 (1970)	Eu	153	63
METHOD	REF. NO. 70 Va 1		egf

REACTION	RESULT	EXCITATION ENERGY	SOURCE TYPE	SOURCE RANGE	DETECTOR TYPE	DETECTOR RANGE	ANGLE
G,XN	ABX	8-22	C	8-22	BF3-I		4PI

489

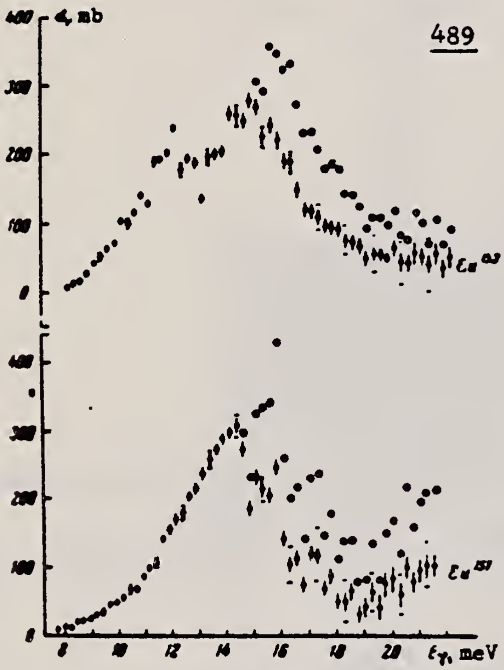

Fig. 2. Photoneutron cross sections and photoabsorption cross sections for Eu^{151} and Eu^{153}. The graphic symbols are the same as in Fig. 1.

REF. O. V. Vasil'ev, V. A. Semenov, and S. F. Semenko
Yad. Fiz. 13, 463 (1971)
Sov. J. Nucl. Phys. 13, 259 (1971)

ELEM. SYM.	A	Z
Eu	153	63

METHOD

REF. NO.	
71 Va 2	hmg

REACTION	RESULT	EXCITATION ENERGY	SOURCE TYPE	SOURCE RANGE	DETECTOR TYPE	DETECTOR RANGE	ANGLE
G,XN	ABX	8-24	C	8-24	BF3-I		4PI
		(8.5-23.25)	(8.5-23.25)				

Table II. Parameters of giant dipole resonance

Isotope	σ_1, mb	E_1, MeV	Γ_1, MeV	$\sigma_{int\,1}$, MeV·b	σ_2, mb	E_2, MeV	Γ_2, MeV	$\sigma_{int\,2}$, MeV·b	σ_{int}	$\frac{\sigma_{int}}{0.06\,NZ/A}$	$\frac{\sigma_{int\,2}}{\sigma_{int\,1}}$	$\frac{E_2}{E_1}$	β_{eff}
Nd^{146}	332	13,8	4,1						2,12	1,00			
Sm^{148}	335	14,1	4,0						2,08	0,96			
Gd^{152}	147	12,0	3,0	0,693	259	15,0	3,2	1,29	1,99	0,90	1,87	1,25	0,28
Gd^{154}	161	11,9	2,4	0,612	250	15,0	3,5	1,39	2,00	0,89	2,27	1,26	0,29
Gd^{156}	180	11,9	2,6	0,738	243	15,2	3,6	1,37	2,11	0,94	1,86	1,27	0,31
Gd^{158}	165	11,7	2,6	0,662	249	14,9	3,8	1,49	2,16	0,94	2,25	1,28	0,32
Eu^{151}	285	14,0	4,5						2,02	0,92			
Eu^{153}	150	11,9	2,3	0,562	237	15,1	3,6	1,34	1,90	0,88	2,39	1,27	0,31

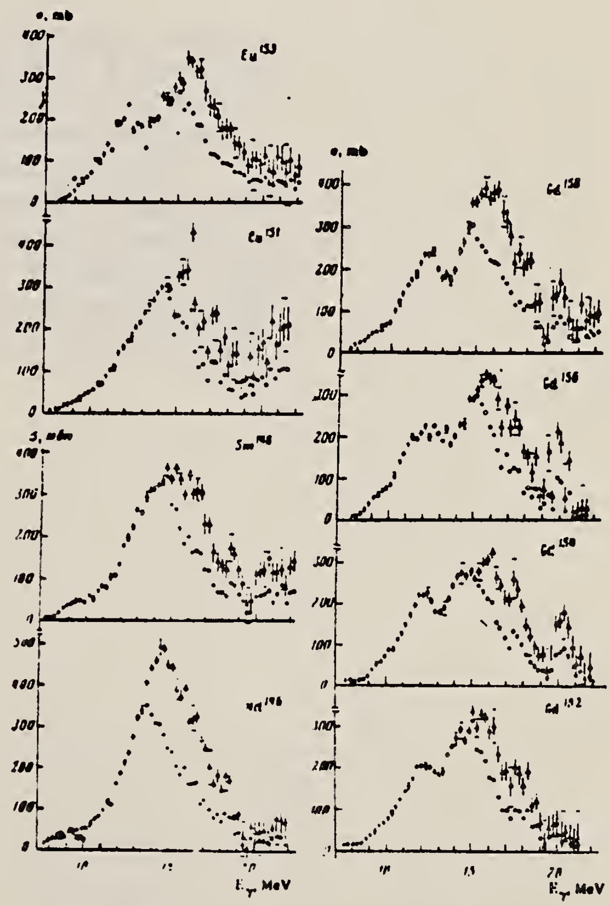

FIG. 1. Photoneutron cross sections and photoabsorption cross sections of Nd^{146}, Sm^{148}, Eu^{151}, Eu^{153}, Gd^{152}, Gd^{154}, Gd^{156} and Gd^{158} Statistical and rms experimental errors are shown (the latter horizontal bars at 9.42 MeV, 10.42 MeV etc.) At photon energies above the (γ, 2n) threshold the photoabsorption cross section errors are not shown.

GADOLINIUM
Z=64

Gadolinium was discovered by J. C. G. de Marignac and P. E. L. de Boisbaudran. In 1880 Marignac isolated a new rare earth from samarskite. In 1885 Boisbaudran isolated the element from Mosander's "didymia" — a mixture of rare earths from which the cerium and lanthanum had been extracted. With Marignac's assent, Boisbaudran named the new element gadolinia in honor of the Finnish chemist J. Gadolin. Elemental gadolinium is a metal resembling steel and is useful in nuclear reactor work because of its high thermal neutron absorption cross section of 46,000 barns.

REF.		ELEM. SYM.	A	Z
	T. Methasiri and S. A. E. Johansson Nucl. Phys. A167, 97 (1971)	Gd		64

METHOD	REF. NO.	
	71 Me 1	egf

REACTION	RESULT	EXCITATION ENERGY	SOURCE TYPE	SOURCE RANGE	DETECTOR TYPE	DETECTOR RANGE	ANGLE
G,F	ABY	THR-900	C	300-900	FRG-I		4PI

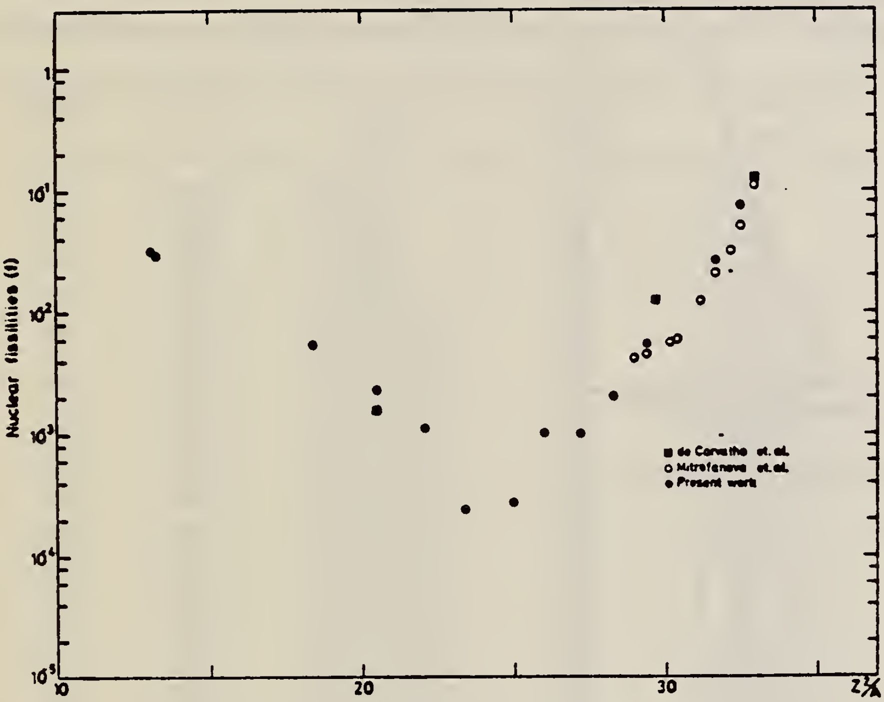

Fig. 2. Nuclear fissilities as a function of Z^2/A.

TABLE 1

The constant fission cross sections above the threshold

Element	σ_f (cm²)	Element	σ_f (cm²)
Pb	$(5.0\pm0.2)\times10^{-27}$	La	$(1.1\pm0.1)\times10^{-29}$
Au	$(1.7\pm0.1)\times10^{-27}$	Sn	$(4.3\pm1.1)\times10^{-29}$
Ta	$(3.3\pm0.2)\times10^{-28}$	Ag	$(8.4\pm2.0)\times10^{-29}$
Yb	$(1.2\pm0.2)\times10^{-28}$	Mo	$(1.7\pm0.4)\times10^{-28}$
Ho	$(5.5\pm0.3)\times10^{-29}$	Cu	$(6.6\pm1.2)\times10^{-28}$
Gd	$(5.3\pm0.8)\times10^{-29}$	Ni	$(5.8\pm0.1)\times10^{-28}$
Nd	$(1.3\pm0.2)\times10^{-29}$		

[over]

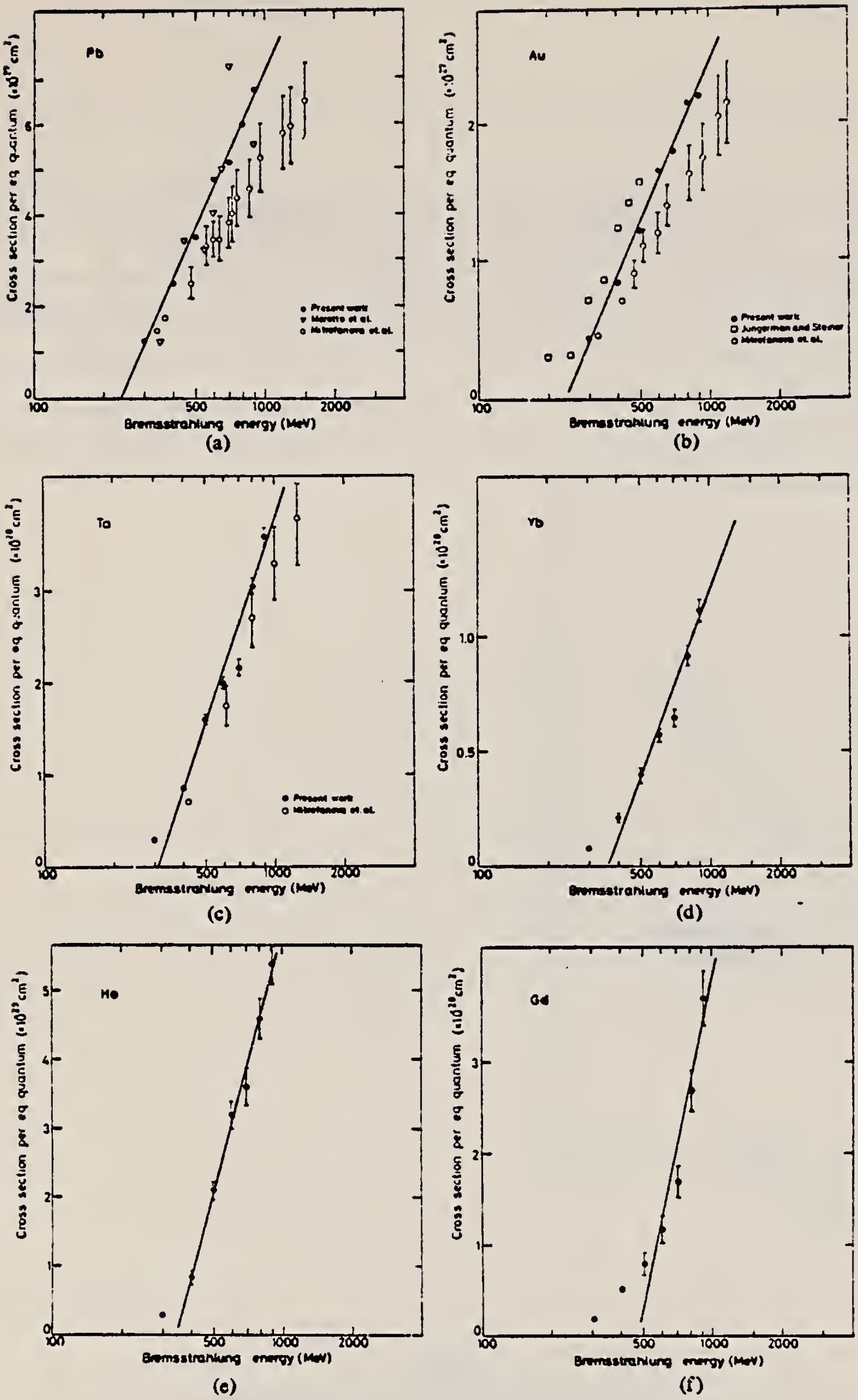

Fig. 1. Cross sections per equivalent quantum $\sigma_q(\bar{E})$ as a function of log E.

REF.	ELEM. SYM.	A	Z
V. Emma, S. Lo Nigro, C. Milone Nucl. Phys. A257, 438 (1976)	Gd		64
METHOD	REF. NO. 76 Em 2		egf

REACTION	RESULT	EXCITATION ENERGY	SOURCE TYPE	SOURCE RANGE	DETECTOR TYPE	DETECTOR RANGE	ANGLE
G,F	ABY	THR-999	C	999	TRK-I		4PI

999 = 1 GEV

TABLE 1

Measured values of σ_q at $E = 1000$ MeV and deduced values of σ_k assumed constant from E_0 to 1000 MeV

Element	Z^2/A	σ_q (mb)	E_0 (MeV)	σ_k (mb)
Bi	32.96	12.3 ± 0.6	200	7.6 ± 0.6
Pb	32.45	5.4 ± 0.4	220	3.6 ± 0.3
Tl	32.10	4.1 ± 0.3	230	2.8 ± 0.3
Au	31.68	2.0 ± 0.15	240	1.4 ± 0.2
Pt	31.18	1.1 ± 0.08	255	$(8 \pm 0.7) \times 10^{-1}$
Re	30.21	$(3.7 \pm 0.3) \times 10^{-1}$	280	$(2.9 \pm 0.3) \times 10^{-1}$
W	29.78	$(3.5 \pm 0.3) \times 10^{-1}$	290	$(2.8 \pm 0.3) \times 10^{-1}$
Ta	29.45	$(3.3 \pm 0.3) \times 10^{-1}$	300	$(2.7 \pm 0.3) \times 10^{-1}$
Hf	29.04	$(1.7 \pm 0.2) \times 10^{-1}$	310	$(1.4 \pm 0.2) \times 10^{-1}$
Yb	28.31	$(1.3 \pm 0.1) \times 10^{-1}$	330	$(1.2 \pm 0.1) \times 10^{-1}$
Tm	28.18	$(7.5 \pm 0.8) \times 10^{-2}$	335	$(6.8 \pm 0.8) \times 10^{-2}$
Ho	27.21	$(3.6 \pm 0.4) \times 10^{-2}$	355	$(3.5 \pm 0.4) \times 10^{-2}$
Dy	26.80	$(2.6 \pm 0.3) \times 10^{-2}$	360	$(2.5 \pm 0.3) \times 10^{-2}$
Tb	26.58	$(2.5 \pm 0.3) \times 10^{-2}$	370	$(2.5 \pm 0.3) \times 10^{-2}$
Gd	26.04	$(1.6 \pm 0.2) \times 10^{-2}$	380	$(1.7 \pm 0.2) \times 10^{-2}$
Sm	25.56	$(1.3 \pm 0.2) \times 10^{-2}$	390	$(1.4 \pm 0.2) \times 10^{-2}$
Nd	24.96	$(9.2 \pm 0.9) \times 10^{-3}$	405	$(1 \pm 0.1) \times 10^{-2}$
Ce	24.00	$(8 \pm 0.9) \times 10^{-3}$	420	$(9 \pm 1) \times 10^{-3}$
La	23.39	$(8.4 \pm 0.9) \times 10^{-3}$	430	$(1 \pm 0.1) \times 10^{-3}$
Sb	21.36	$(1.2 \pm 0.2) \times 10^{-2}$	460	$(1.5 \pm 0.3) \times 10^{-2}$
Te	21.19	$(8.8 \pm 1) \times 10^{-3}$	465	$(1.2 \pm 0.2) \times 10^{-2}$
Sn	21.06	$(1.3 \pm 0.2) \times 10^{-2}$	465	$(1.7 \pm 0.3) \times 10^{-2}$
Cd	20.49	$(1.7 \pm 0.3) \times 10^{-2}$	470	$(2.2 \pm 0.4) \times 10^{-2}$
Ag	20.47	$(2 \pm 0.3) \times 10^{-2}$	470	$(2.6 \pm 0.4) \times 10^{-2}$
Zn	13.76	$(2 \pm 0.4) \times 10^{-1}$	515	$(3 \pm 0.6) \times 10^{-1}$
Cu	13.44	$(2.4 \pm 0.5) \times 10^{-1}$	515	$(3.6 \pm 0.8) \times 10^{-1}$
Ni	13.35	$(2.4 \pm 0.5) \times 10^{-1}$	510	$(3.6 \pm 0.8) \times 10^{-1}$
Fe	12.10	$(3 \pm 0.6) \times 10^{-1}$	510	$(4.4 \pm 0.9) \times 10^{-1}$

[4] A.V. Mitrofanova et al. Sov. J. Nucl. Phys. 6, 512 (1968).

[7] T. Methasiri et al., Nucl. Phys. A167, 97 (1971).

[12] J.R. Nix et al., Nucl. Phys. 81, 61 (1966).

[20] N.A. Perifilov et al., JETP (Sov. Phys.) 14, 623 (1962); Proc. Symp. on the physics & chemistry of fission, Salzburg 1965, vol. 2 (IAEA) Vienna, 1965, p.283.

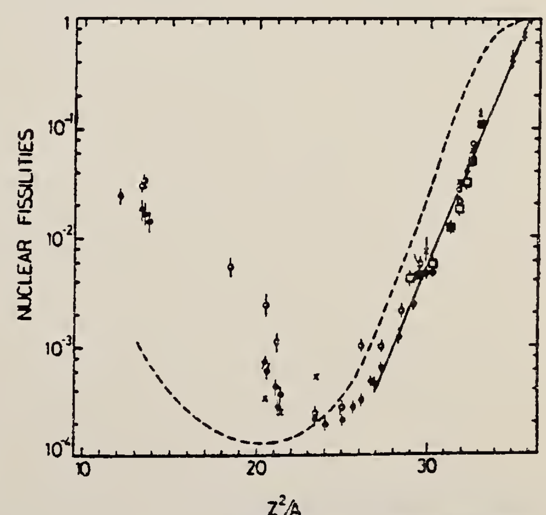

Fig. 2. Nuclear fissilities as a function of Z^2/A. Experimental points: solid circles represent our data; squares, the data from ref. [4]); open circles, the data from ref. [7]); and crosses, the data from (p,f) experiments[20]). The straight line is the best fit calculated from our data for $Z^2/A > 26$. The dashed curve is the curve VI calculated by Nix and Sassi[12]).

S. F. Semenko, O. V. Vasilijev and V. A. Semenov
Phys. Letters 31B, 429 (1970)

ELEM. SYM.	A	Z
Gd	152	64

METHOD

REF. NO.	
70 Se 1	egf

REACTION	RESULT	EXCITATION ENERGY	SOURCE TYPE	SOURCE RANGE	DETECTOR TYPE	DETECTOR RANGE	ANGLE
G,XN	ABX	8-24	C	8-24	BF3-I		4PI

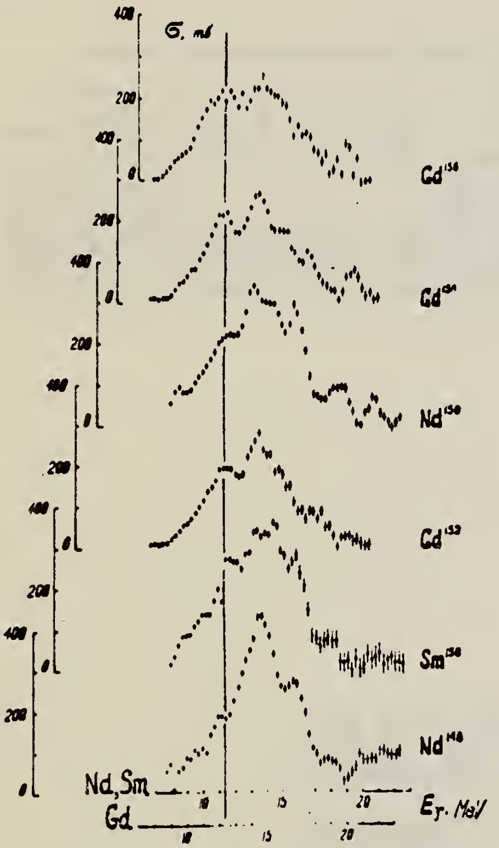

Fig. 1. The variation of the even-even nuclei giant resonance shape with the increase of Z, N in the transitional region $N = 90$. The photoabsorption curves of ^{148}Nd, ^{150}Sm, ^{152}Gd ($N = 88$) ^{150}Nd, ^{154}Gd ($N = 90$) and ^{156}Gd ($N = 92$) are presented (From the bottom). The upper energy scale is for Nd, Sm and the lower is for Gd isotopes. At the energies greater than (γ, $2n$) threshold the photoabsorption cross section was defined from the photoneutron cross section by usual correction for neutron multiplicity. Only statistical errors are plotted.
The "phase transition" effect in the giant resonance of the nuclei with $N = 88$ is emphasized by the vertical line.

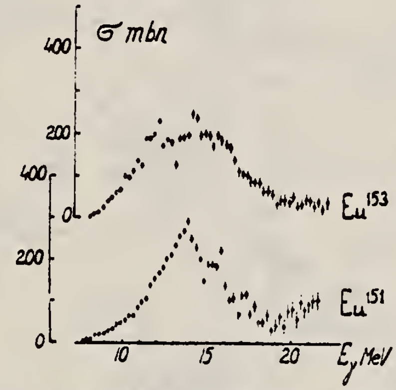

Fig. 2. The photoabsorption cross sections for ^{151}Eu and ^{153}Eu.

REF.	ELEM. SYM.	A	Z
O. V. Vasil'ev and V. A. Semenov ZhETF Pis. Red. 11, 520 (1970) JETP Letters 11, 356 (1970)	Gd	152	64

METHOD	REF. NO.	
	70 Va 1	egf

REACTION	RESULT	EXCITATION ENERGY	SOURCE TYPE	SOURCE RANGE	DETECTOR TYPE	DETECTOR RANGE	ANGLE
G,XN	ABX	8-22	C	8-22	BF3-I		4PI

490

490

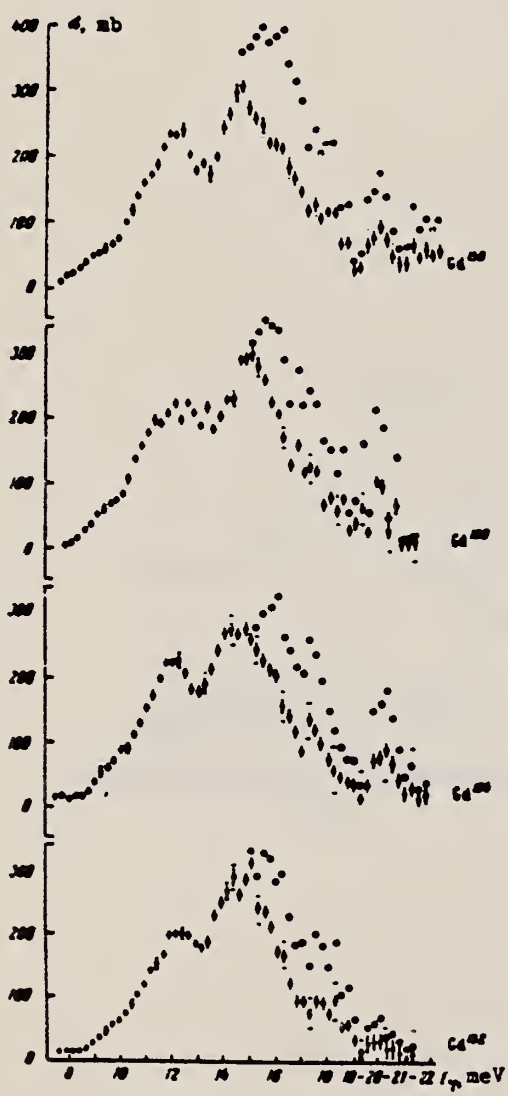

Fig. 1. Photoneutron cross sections and cross sections for the photoabsorption by the gadolinium isotopes Gd$^{152, 154, 156, 158}$ (reading upward). The statistical and mean-square errors of the photoabsorption cross sections are given. (The latter are denoted by horizontal strokes at the points 9.42 MeV, 10.42 MeV, etc.) At photon energies above the threshold of the (γ, 2n) reaction, the photoneutron cross sections, unlike the absorption cross sections, are denoted by circles.

REF.	O. V. Vasil'ev, V. A. Semenov, and S. F. Semenko Yad. Fiz. 13, 463 (1971) Sov. J. Nucl. Phys. 13, 259 (1971)	ELEM. SYM.	A	Z
		Gd	152	64
METHOD		REF. NO.		
		71 Va 2		hmg

REACTION	RESULT	EXCITATION ENERGY	SOURCE TYPE	SOURCE RANGE	DETECTOR TYPE	DETECTOR RANGE	ANGLE
G,XN	ABX	8-24	C	8-24	BF3-I		4PI
		(8.0-23.25)		(8.0-23.25)			

Table II. Parameters of giant dipole resonance

Isotope	σ_1, mb	E_1, MeV	Γ_1, MeV	$\sigma_{int\,1}$, MeV·b	σ_2, mb	E_2, MeV	Γ_2, MeV	$\sigma_{int\,2}$, MeV·b	σ_{int}	$\frac{\sigma_{int}}{0.06\,NZ/A}$	$\frac{\sigma_{int\,2}}{\sigma_{int\,1}}$	$\frac{E_2}{E_1}$	β_{eff}
Nd^{146}	332	13,8	4,1						2,12	1,00			
Sm^{148}	335	14,1	4,0						2,08	0,98			
Gd^{152}	147	12,0	3,0	0,693	259	15,0	3,2	1,29	1,99	0,90	1,87	1,25	0,28
Gd^{154}	161	11,9	2,4	0,812	250	15,0	3,5	1,39	2,00	0,89	2,27	1,26	0,29
Gd^{156}	180	11,9	2,6	0,738	243	15,2	3,6	1,37	2,11	0,94	1,86	1,27	0,31
Gd^{158}	165	11,7	2,6	0,662	249	14,9	3,8	1,49	2,16	0,94	2,25	1,28	0,32
Eu^{151}	285	14,0	4,5						2,02	0,92			
Eu^{153}	159	11,9	2,3	0,562	237	15,1	3,6	1,34	1,90	0,86	2,39	1,27	0,31

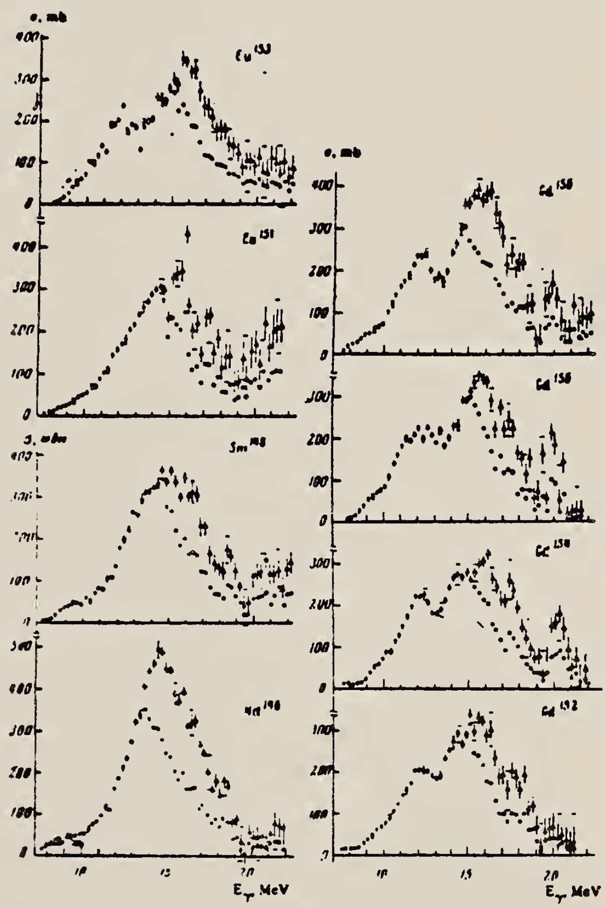

FIG. 1. Photoneutron cross sections and photoabsorption cross sections of Nd^{146}, Sm^{148}, Eu^{151}, Eu^{153}, Gd^{152}, Gd^{154}, Gd^{156} and Gd^{158} Statistical and rms experimental errors are shown (the latter horizontal bars at 9.42 MeV, 10.42 MeV etc.) At photon energies above the (γ, 2n) threshold the photoabsorption cross section errors are not shown.

Gd
A=154

Gd
A=154

S. F. Semenko, O. V. Vasilijev and V. A. Semenov
Phys. Letters 31B, 429 (1970)

Gd	154	64

METHOD	REF. NO.	
	70 Se 1	egf

REACTION	RESULT	EXCITATION ENERGY	SOURCE TYPE	SOURCE RANGE	DETECTOR TYPE	DETECTOR RANGE	ANGLE
G,XN	ABX	8-24	C	8-24	BF3-I		4PI

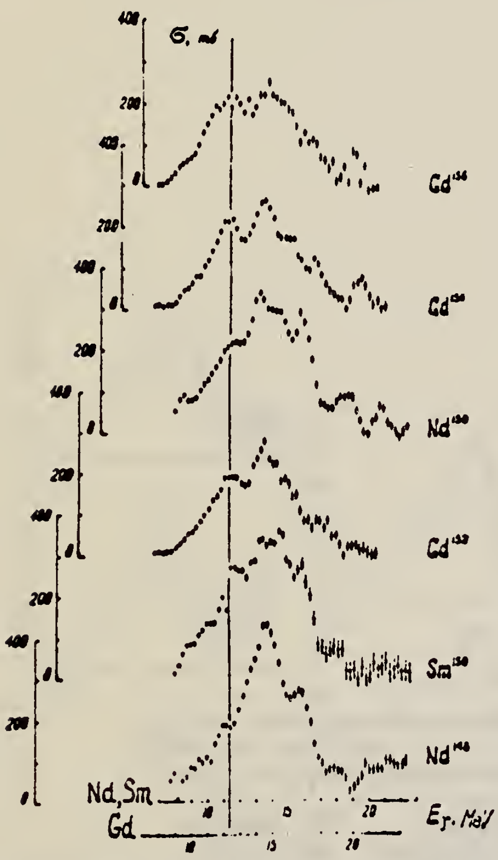

Fig. 1. The variation of the even-even nuclei giant resonance shape with the increase of Z, N in the transitional region $N = 90$. The photoabsorption curves of ^{148}Nd, ^{150}Sm, ^{152}Gd ($N = 88$) ^{150}Nd, ^{154}Gd ($N = 90$) and ^{156}Gd ($N = 92$) are presented (From the bottom). The upper energy scale is for Nd, Sm and the lower is for Gd isotopes. At the energies greater than (γ, $2n$) threshold the photoabsorption cross section was defined from the photoneutron cross section by usual correction for neutron multiplicity. Only statistical errors are plotted.
The "phase transition" effect in the giant resonance of the nuclei with $N = 88$ is emphasized by the vertical line.

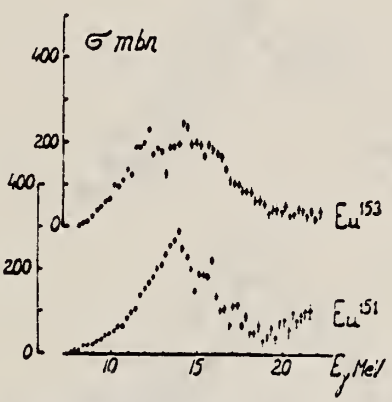

Fig. 2. The photoabsorption cross sections for ^{151}Eu and ^{153}Eu.

REF.							ELEM. SYM.	A	Z
O.V. Vasil'ev and V. A. Semenov ZhETF Pis. Red. 11, 520 (1970) JETP Letters 11, 356 (1970)							Gd	154	64
METHOD							REF. NO. 70 Va 1		egf

REACTION	RESULT	EXCITATION ENERGY	SOURCE TYPE	SOURCE RANGE	DETECTOR TYPE	DETECTOR RANGE	ANGLE
G,XN	ABX	8-22	C	8-22	BF3-I		4PI

491

491

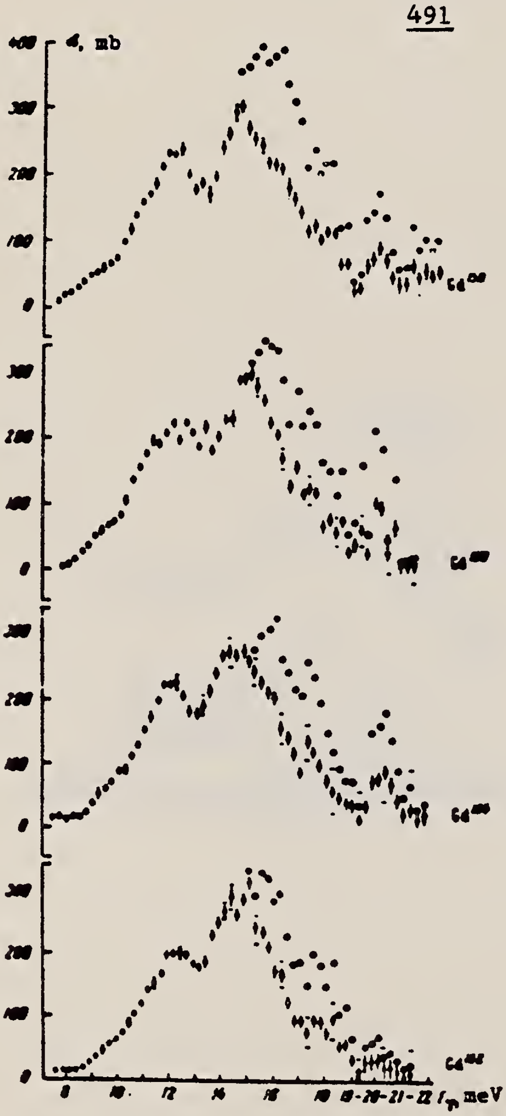

Fig. 1. Photoneutron cross sections and cross sections for the photoabsorption by the gadolinium isotopes Gd$^{152, 154, 156, 158}$ (reading upward). The statistical and mean-square errors of the photoabsorption cross sections are given. (The latter are denoted by horizontal strokes at the points 9.42 MeV, 10.42 MeV, etc.) At photon energies above the threshold of the (γ, 2n) reaction, the photoneutron cross sections, unlike the absorption cross sections, are denoted by circles.

REF.	ELEM. SYM.	A	Z
O. V. Vasil'ev, V. A. Semenov, and S. F. Semenko Yad. Fiz. 13, 463 (1971) Sov. J. Nucl. Phys. 13, 259 (1971)	Gd	154	64
METHOD	REF. NO. 71 Va 2		hmg

REACTION	RESULT	EXCITATION ENERGY	SOURCE TYPE	SOURCE RANGE	DETECTOR TYPE	DETECTOR RANGE	ANGLE
G,XN	ABX	8-24	C	8-24	BF3-I		4PI
		(8.6-23.25)		(8.6-23.25)			

Table II. Parameters of giant dipole resonance

Isotope	σ_1, mb	E_1, MeV	Γ_1, MeV	$\sigma_{int\,1}$, MeV·b	σ_2, mb	E_2, MeV	Γ_2, MeV	$\sigma_{int\,2}$, MeV·b	σ_{int}	$\frac{\sigma_{int}}{0.06\,NZ/A}$	$\frac{\sigma_{int\,2}}{\sigma_{int\,1}}$	$\frac{E_2}{E_1}$	β_{eff}
Nd^{146}	332	13,8	4,1						2,12	1,00			
Sm^{148}	335	14,1	4,0						2,08	0,96			
Gd^{152}	147	12,0	3,0	0,693	259	15,0	3,2	1,29	1,99	0,90	1,87	1,25	0,28
Gd^{154}	161	11,9	2,4	0,612	250	15,0	3,5	1,39	2,00	0,89	2,27	1,26	0,29
Gd^{156}	180	11,9	2,6	0,738	243	15,2	3,6	1,37	2,11	0,94	1,86	1,27	0,31
Gd^{158}	165	11,7	2,6	0,662	249	14,9	3,8	1,49	2,16	0,94	2,25	1,28	0,32
Eu^{151}	285	14,0	4,5						2,02	0,92			
Eu^{153}	159	11,9	2,3	0,562	237	15,1	3,6	1,34	1,90	0,86	2,39	1,27	0,31

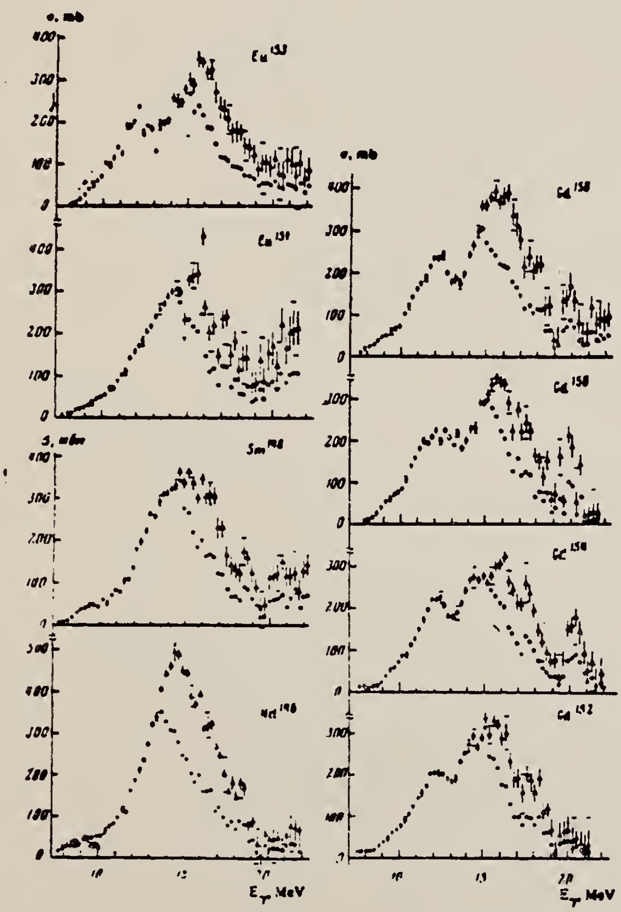

FIG. 1. Photoneutron cross sections and photoabsorption cross sections of Nd^{146}, Sm^{148}, Eu^{151}, Eu^{153}, Gd^{152}, Gd^{154}, Gd^{156} and Gd^{158} Statistical and rms experimental errors are shown (the latter horizontal bars at 9.42 MeV, 10.42 MeV etc.) At photon energies above the (γ, 2n) threshold the photoabsorption cross section errors are not shown.

Gd
A=155

Gd
A=155

Gd
A=155

Ref. B.I. Deutch, F.R. Metzger, F.J. Wilhelm
Nuclear Phys. 16, 81 (1960)

Elem. Sym.	A	Z
Gd	155	64

Method: Radioactive source; photon scattering; NaI spectrometer

Ref. No. 60 De 1 JS — NVB

Reaction	E or ΔE	E_o	Γ	$\int \sigma dE$	$J\pi$	Notes
$Gd^{155}(\gamma,\gamma)$		105 keV				Detector at 125°. Lifetime of 105 keV level: $\tau_\gamma = 6.0^{+6}_{-2})\times10^{-10}$ sec. assumes $\Gamma_o/\Gamma = 0.69$ for transition. Source (Eu^{155}) was separated and ~ 99% pure.

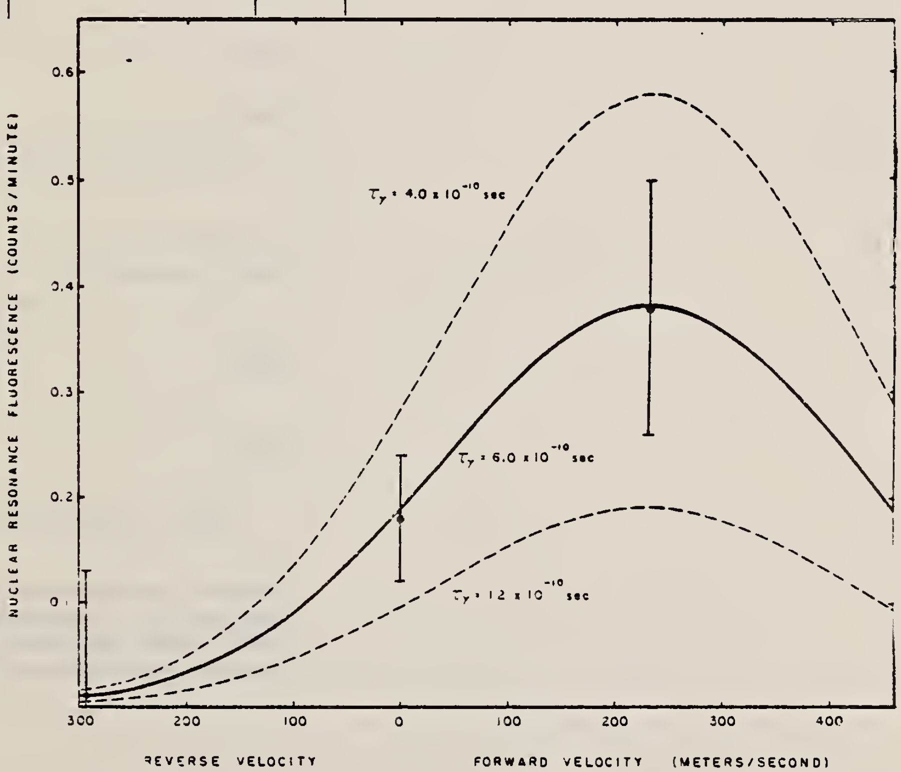

Fig. 4. The resonance scattering effect as a function of the velocity of the source. The heavy line represents the theoretical counting rate for $\tau_\gamma = 6 \times 10^{-10}$ sec for the geometry used. The dashed curves are the theoretical counting rates for the upper and lower experimental lifetime limits. The experimental points are shown for comparison purposes.

REF.	ELEM. SYM.	A	Z
A.E. Balabanov, N.N. Delyagin, and Hussein el Sayes J. Nucl. Phys. (USSR) 3, 209 (1966) Sov. J. Nucl. Phys. 3, 150 (1966)	Gd	155	64

METHOD	REF. NO.	
Mössbauer Effect	66 Ba 3	JDM

REACTION	RESULT	EXCITATION ENERGY	SOURCE TYPE	SOURCE RANGE	DETECTOR TYPE	DETECTOR RANGE	ANGLE
G,G	LFT	1	D	1	NAI-D	1	1

Γ for 86.5 keV is 0.37 ± 0.06 mm/sec.

Γ for 60.0 keV is 1.4 ± 0.4 mm/sec $\equiv$ (2.4 ± 0.7) x 10^{-9} sec.

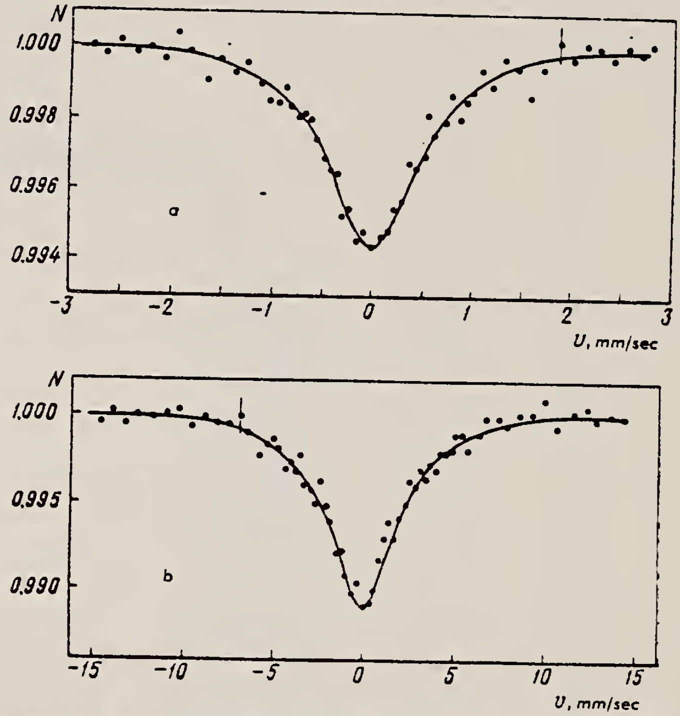

Resonance absorption spectra of γ quanta: a—86.5 keV, and b—60.0 keV, from Gd^{155} in gadolinium oxide, measured with a 190 mg/cm² absorber at 80°K. The ordinate gives the intensity of γ quanta in relative units; the abscissa is the velocity v of the source relative to the absorber.

REF.	ELEM. SYM.	A	Z
R.R. Stevens Jr., Y.K. Lee and J.C. Walker Phys. Letters 21, 401 (1966)	Gd	155	64

METHOD	REF. NO.	
Mössbauer Effect	66 St 1	JDM

REACTION	RESULT	EXCITATION ENERGY	SOURCE		DETECTOR		ANGLE
			TYPE	RANGE	TYPE	RANGE	
G,G	LFT	1	D	1	NAI-D	1	

Lower limit for τ of 1st excited state is 0.22 nanoseconds.

GD
A=156

GD
A=156

GD
A=156

S. F. Semenko, O. V. Vasilijev and V. A. Semenov
Phys. Letters 31B, 429 (1970)

ELEM. SYM.	A	Z
Gd	156	64

METHOD

REF. NO.	
70 Se 1	egf

REACTION	RESULT	EXCITATION ENERGY	SOURCE TYPE	SOURCE RANGE	DETECTOR TYPE	DETECTOR RANGE	ANGLE
G,XN	ABX	8-24	C	8-24	BF3-I		4PI

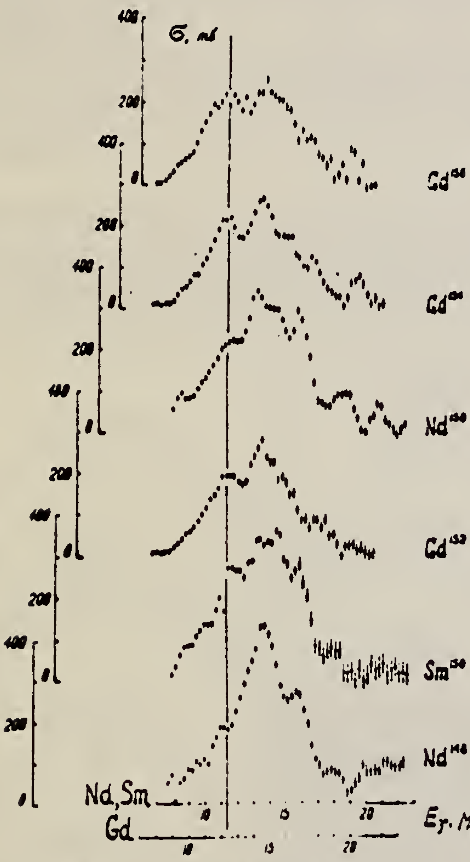

Fig. 1. The variation of the even-even nuclei giant resonance shape with the increase of Z, N in the transitional region $N = 90$. The photoabsorption curves of ^{148}Nd, ^{150}Sm, ^{152}Gd ($N = 88$) ^{150}Nd, ^{154}Gd ($N = 90$) and ^{156}Gd ($N = 92$) are presented (From the bottom). The upper energy scale is for Nd, Sm and the lower is for Gd isotopes. At the energies greater than $(\gamma, 2n)$ threshold the photoabsorption cross section was defined from the photoneutron cross section by usual correction for neutron multiplicity. Only statistical errors are plotted.
The "phase transition" effect in the giant resonance of the nuclei with $N = 88$ is emphasized by the vertical line.

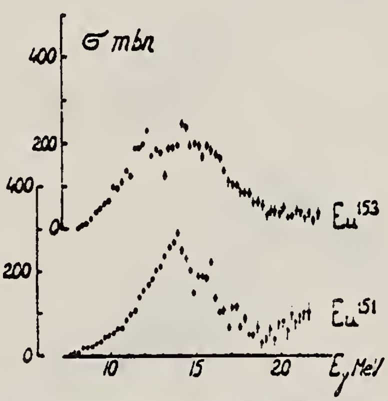

Fig. 2. The photoabsorption cross sections for ^{151}Eu and ^{153}Eu.

REF.	ELEM. SYM.	A	Z
O. V. Vasil'ev and V. A. Semenov ZhETF Pis. Red. 11, 520 (1970) JETP Letters 11, 356 (1970)	Gd	156	64
METHOD	REF. NO. 70 Va 1		egf

REACTION	RESULT	EXCITATION ENERGY	SOURCE TYPE	SOURCE RANGE	DETECTOR TYPE	DETECTOR RANGE	ANGLE
G,XN	ABX	8-22	C	8-22	BF3-I		4PI

492

492

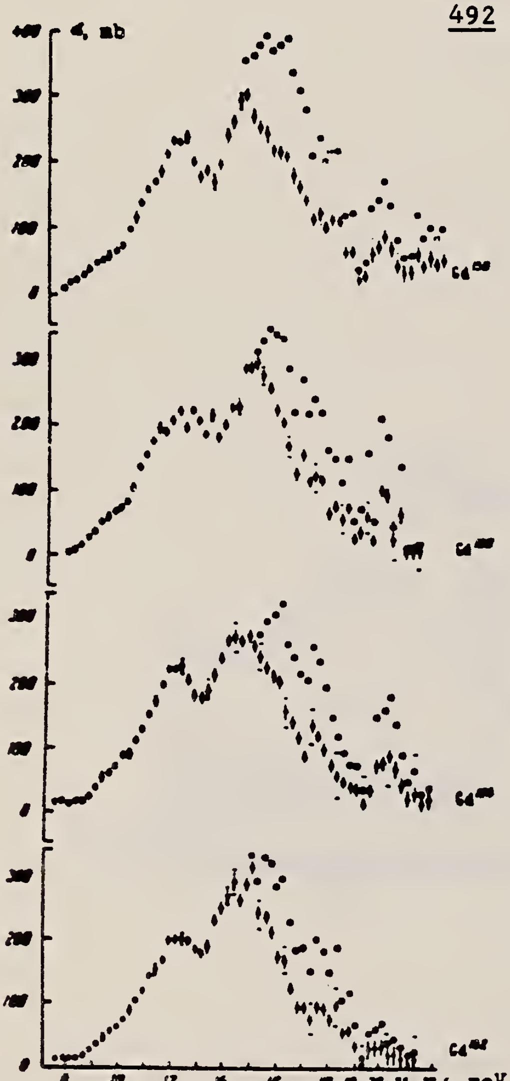

Fig. 1. Photoneutron cross sections and cross sections for the photoabsorption by the gadolinium isotopes $Gd^{152,\ 154,\ 156,\ 158}$ (reading upward). The statistical and mean-square errors of the photoabsorption cross sections are given. (The latter are denoted by horizontal strokes at the points 9.42 MeV, 10.42 MeV, etc.) At photon energies above the threshold of the (γ, 2n) reaction, the photoneutron cross sections, unlike the absorption cross sections, are denoted by circles.

G.M. Gurevich, L.E. Lazareva, V.M. Mazur, S.Yu. Merkulov,
G.V. Solodukhov, V.A. Tyutin
Nucl. Phys. A351, 257 (1981)

ELEM. SYM.	A	Z
Gd	156	64

METHOD

REF. NO.	
81 Gu 2	hg

REACTION	RESULT	EXCITATION ENERGY	SOURCE TYPE	SOURCE RANGE	DETECTOR TYPE	DETECTOR RANGE	ANGLE
G,MU-T	ABX	THR-20	C	27	NAI-D		4PI

Abstract: The curves of the total gamma-absorption cross sections (σ_{tot}) in the E1 giant resonance energy range for the nuclei ^{154}Sm, ^{156}Gd, ^{165}Ho, ^{168}Er, ^{174}Yb, ^{178}Hf, ^{180}Hf, ^{181}Ta, ^{182}W, ^{184}W, ^{186}W and ^{197}Au have been measured using the absorption method. Parameters of the Lorentz curves fitting the measured cross sections σ_{tot} are given. Quadrupole moments (Q_0) and nuclear deformation parameters (β) were obtained.

For deformed nuclei in the $\sim 155 < A < \sim 180$ region a violation of the correlation between giant resonance widths (Γ) and nuclear deformation parameters was found. Γ_1 and Γ_2, the widths of the resonances corresponding to vibrations of nucleons along and across the nuclear deformation axis, were observed to decrease with the increase of A which could be accounted for by the presence of an $N = 108$ subshell.

NUCLEAR REACTIONS ^{154}Sm, ^{156}Gd, ^{165}Ho, ^{168}Er, ^{174}Yb, ^{178,180}Hf, ^{181}Ta, ^{182,184,186}W, ^{197}Au (γ, X), $E = 7$–20 MeV; measured total $\sigma(E)$; deduced integrated σ, Lorentz line parameters. ^{154}Sm, ^{156}Gd, ^{165}Ho, ^{168}Er, ^{174}Yb, ^{178,180}Hf, ^{181}Ta, ^{182,184,186}W, ^{197}Au deduced β, Q_0, Γ, giant resonance evolution. Enriched, natural targets.

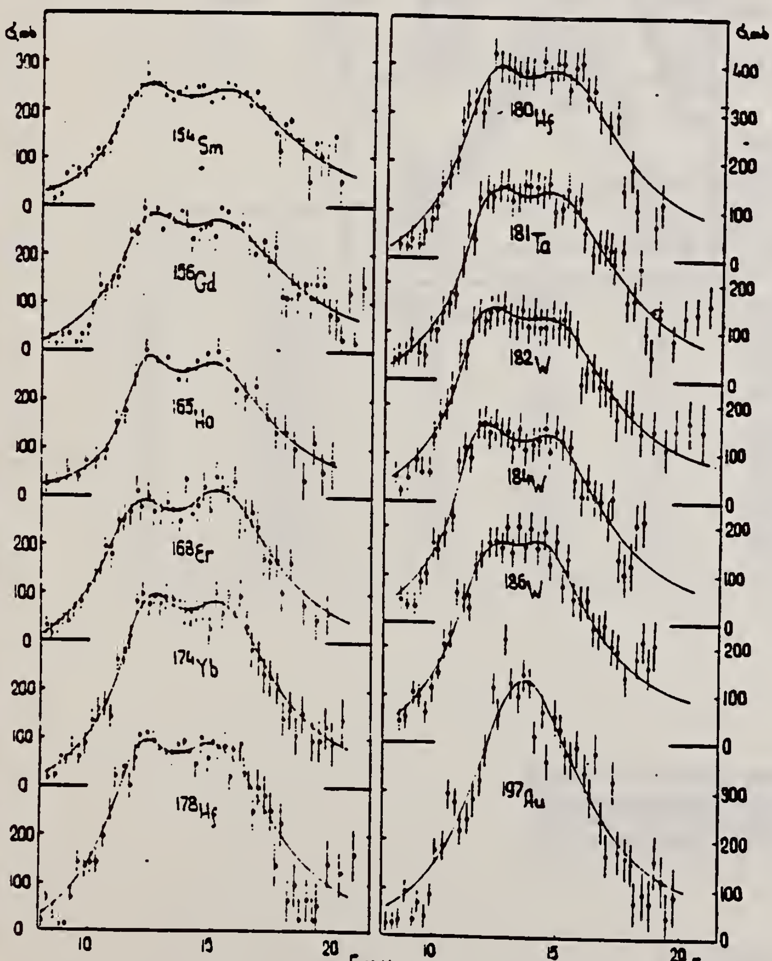

Fig. 2. Total nuclear γ-absorption cross sections (σ_{tot}) measured by the absorption method for ^{154}Sm, ^{156}Gd, ^{165}Ho, ^{168}Er, ^{174}Yb, ^{178}Hf, ^{180}Hf, ^{181}Ta, ^{182}W, ^{184}W, ^{186}W and ^{197}Au. Rms error bars are shown.

(OVER)

U.S. DEPARTMENT OF COMMERCE
NATIONAL BUREAU OF STANDARDS

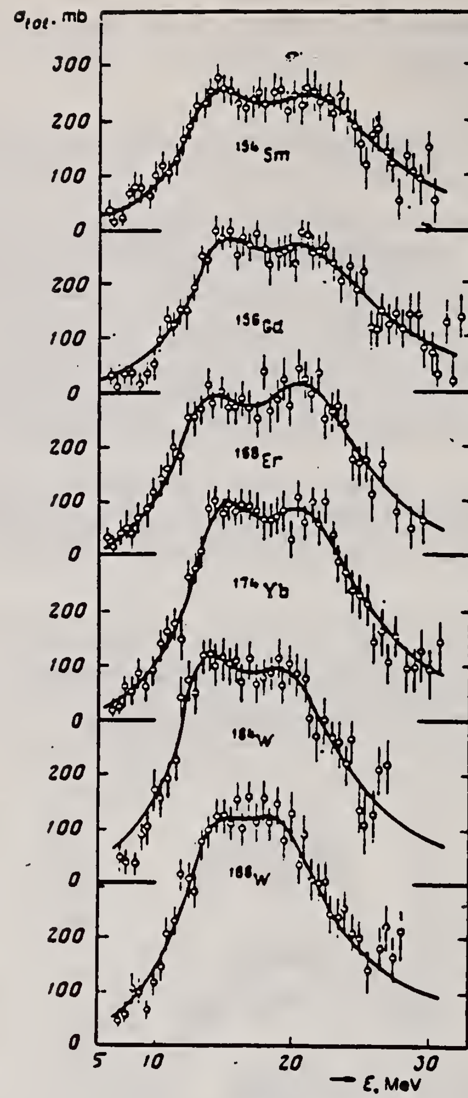

FIG. 2. Total cross sections of the photoabsorption of the nuclei ^{154}Sm, ^{156}Gd, ^{168}Er, ^{174}Yb, ^{184}W, and ^{186}W. The mean squared errors are shown.

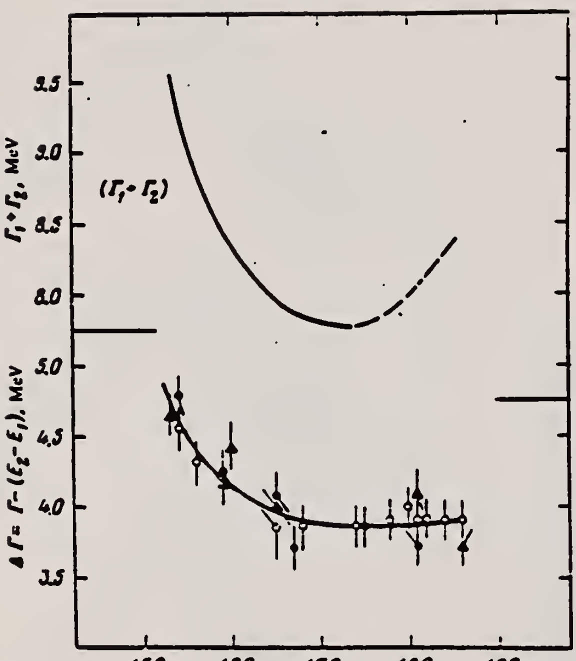

FIG. 3. Experimental values of $\Delta\Gamma = \Gamma - (E_2 - E_1)$ in the region of deformed nuclei with $A = 153$–186: ○—present work and[1]; ●—Saclay group; ▲—Livermore group. Owing to a small systematic deviations of the absolute values, the ordinate scales for the Saclay and Livermore data are shifted 0.15 MeV upward and downward, respectively. The $(\Gamma_1 + \Gamma_2)$ curve was obtained from the $\Delta\Gamma$ curve after introduction of corrections in the interval $A = 175$–186.

Table 2

Parameters of Lorentz curves fitting the experimental data on σ_{tot}

Nucleus	E_1 (MeV)	σ_1 (mb)	Γ_1 (MeV)	E_2 (MeV)	σ_2 (mb)	Γ_2 (MeV)	$\frac{\sigma_2\Gamma_2}{\sigma_1\Gamma_1}$	Γ (MeV)
^{154}Sm	12.2	188	3.4	15.7	207	5.7	1.85	8.1
^{156}Gd	12.3	206	3.2	15.7	220	5.5	1.81	7.7
^{165}Ho	12.3	202	2.3	15.2	239	4.8	2.47	7.0
^{168}Er	11.9	222	3.2	15.5	275	4.5	1.73	7.4
^{174}Yb	12.3	297	2.9	15.5	320	4.9	1.80	7.1
^{178}Hf	12.2	291	3.1	15.5	334	4.9	1.80	7.2
^{180}Hf	12.2	286	3.2	15.3	324	5.1	1.81	7.1
^{181}Ta	12.1	272	3.0	15.0	316	5.1	1.97	6.8
^{182}W	11.9	267	3.2	14.8	303	5.6	2.01	6.8
^{184}W	11.9	315	2.9	14.8	321	4.7	1.65	6.8
^{186}W	12.0	246	3.3	14.5	332	5.1	2.07	6.4
^{197}Au	13.7	535	5.2					
Average error	1.4 %	11.2 %	9.3 %	1.5 %	9.7 %	4.6 %	0.22	0.2 MeV

Table 3

Ratios of nuclear ellipsoid axes (λ), deformation parameters (β) and intrinsic quadrupole moments (Q_0), calculated from E_2/E_1

Nucleus	^{154}Sm	^{156}Gd	^{165}Ho	^{168}Er	^{174}Yb	^{178}Hf	^{180}Hf	^{181}Ta	^{182}W	^{184}W	^{186}W
λ	1.320	1.302	1.259	1.327	1.289	1.296	1.281	1.263	1.271	1.268	1.229
β	0.326 $\pm$0.017	0.309 $\pm$0.016	0.266 $\pm$0.036	0.334 $\pm$0.032	0.296 $\pm$0.024	0.303 $\pm$0.032	0.288 $\pm$0.036	0.270 $\pm$0.026	0.278 $\pm$0.030	0.274 $\pm$0.032	0.235 $\pm$0.033
Q_0	6.3 $\pm$0.3	6.2 $\pm$0.3	5.8 $\pm$0.8	7.5 $\pm$0.7	7.0 $\pm$0.6	7.5 $\pm$0.8	7.2 $\pm$0.9	6.9 $\pm$0.7	7.2 $\pm$0.8	7.1 $\pm$0.8	6.2 $\pm$0.9

Table 4

Integral characteristics of E1 giant resonance

Nucleus	$\sigma_{0,exp}$ (MeV · b)	$\frac{\sigma_{0,exp}}{0.06NZ/A}$	σ_{0L} (MeV · b)	$\frac{\sigma_{0L}}{0.06NZ/A}$	σ_{-1} (mb)	σ_{-1L} (mb)	$\sigma_{-1L}A^{-4/3}$ (mb)	σ_{-2} (mb · MeV^{-1})	σ_{-2L} (mb · MeV^{-1})	$\sigma_{-2L}A^{-5/3}$ (μb · MeV^{-1})
^{154}Sm	1.94 $\pm$ 0.06	0.87	2.86	1.29	117 $\pm$ 3.5	156	0.189	9.1 $\pm$ 0.3	14.3	3.23
^{156}Gd	2.07 $\pm$ 0.07	0.91	2.95	1.30	143 $\pm$ 4.6	163	0.194	10.5 $\pm$ 0.4	14.9	3.30
^{165}Ho	1.86 $\pm$ 0.06	0.78	2.53	1.06	155 $\pm$ 4.4	160	0.177	10.1 $\pm$ 0.3	12.6	2.54
^{168}Er	2.24 $\pm$ 0.06	0.92	3.07	1.26	161 $\pm$ 4.3	197	0.212	12.0 $\pm$ 0.3	16.0	3.13
^{174}Yb	2.69 $\pm$ 0.05	1.07	3.82	1.52	195 $\pm$ 3.4	240	0.247	14.5 $\pm$ 0.3	19.2	3.54
^{178}Hf	2.85 $\pm$ 0.07	1.11	3.99	1.55	208 $\pm$ 4.9	247	0.247	15.3 $\pm$ 0.4	20.2	3.59
^{180}Hf	2.72 $\pm$ 0.06	1.05	4.03	1.56	200 $\pm$ 4.4	250	0.246	15.1 $\pm$ 0.3	20.7	3.61
^{181}Ta	2.84 $\pm$ 0.07	1.09	3.81	1.46	210 $\pm$ 5.3	245	0.239	16.0 $\pm$ 0.4	20.0	3.45
^{182}W	2.86 $\pm$ 0.07	1.09	4.01	1.52	211 $\pm$ 5.3	256	0.248	16.2 $\pm$ 0.4	21.6	3.70
^{184}W	2.78 $\pm$ 0.07	1.05	3.80	1.43	207 $\pm$ 5.3	251	0.240	15.9 $\pm$ 0.4	20.9	3.51
^{186}W	2.90 $\pm$ 0.07	1.08	3.95	1.48	214 $\pm$ 5.3	256	0.241	16.2 $\pm$ 0.4	21.6	3.56
^{197}Au	3.12 $\pm$ 0.06	1.10	4.37	1.54	229 $\pm$ 4.2	276	0.241	18.6 $\pm$ 0.4	23.3	3.49

Gd
A=157

Gd
A=157

Gd
A=157

K. N. Geller, J. Halpern, and E. G. Muirhead
Phys. Rev. 118, 1302-12 (1960)

Gd	157	64

METHOD

Betatron; neutron threshold; ion chamber

REF. NO.	
60 Ge 3	NVB

REACTION	RESULT	EXCITATION ENERGY	SOURCE TYPE	SOURCE RANGE	DETECTOR TYPE	DETECTOR RANGE	ANGLE
G,N	NØX	THR	C THR		BF3-I		4 PI

THRESHØLD

TABLE I. Summary and comparison of neutron separation energies inferred from present threshold measurements with values predicted from mass data and reaction energies. All energies are expressed in the center-of-mass system in Mev.

Reaction	No. runs	Present results	Other results	Method	Reference
$Gd^{157}(\gamma,n)Gd^{156}$	1	6.39 ±0.11	6.32 ±0.06	mass data	q

q W. H. Johnson, Jr., and V. B. Bhanot, Phys. Rev. 107, 6 (1957).

Gd
A=158

Gd
A=158

REF.	ELEM. SYM.	A	Z
O. V. Vasil'ev and V. A. Semenov ZhETF Pis. Red. 11, 520 (1970) JETP Letters 11, 356 (1970)	Gd	158	64

METHOD	REF. NO.	
	70 Va 1	egf

REACTION	RESULT	EXCITATION ENERGY	SOURCE TYPE	SOURCE RANGE	DETECTOR TYPE	DETECTOR RANGE	ANGLE
G,XN	ABX	8-22	C	8-22	BF3-I		4PI

493

493

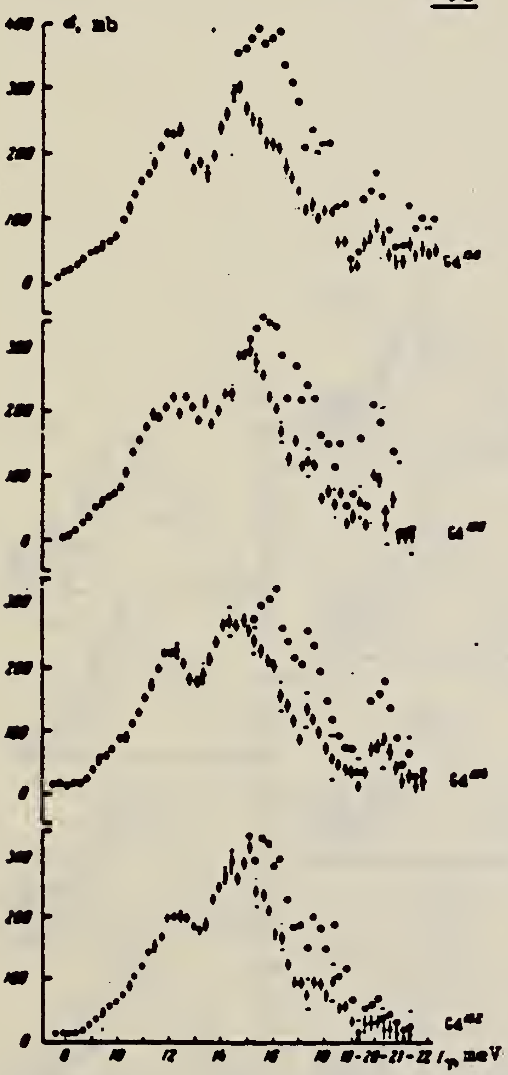

Fig. 1. Photoneutron cross sections and cross sections for the photoabsorption by the gadolinium isotopes Gd^{152}, ^{154}, ^{156}, ^{158} (reading upward). The statistical and mean-square errors of the photoabsorption cross sections are given. (The latter are denoted by horizontal strokes at the points 9.42 MeV, 10.42 MeV, etc.) At photon energies above the threshold of the (γ, 2n) reaction, the photoneutron cross sections, unlike the absorption cross sections, are denoted by circles.

REF.	O. V. Vasil'ev, V. A. Semenov, and S. F. Semenko Yad. Fiz. 13, 463 (1971) Sov. J. Nucl. Phys. 13, 259 (1971)	ELEM. SYM.	A	Z
		Gd	158	64
METHOD		REF. NO.	71 Va 2	hmg

REACTION	RESULT	EXCITATION ENERGY	SOURCE TYPE	SOURCE RANGE	DETECTOR TYPE	DETECTOR RANGE	ANGLE
G,XN	ABX	7-24	C	7-24	BF3-I		4PI
		(7.9-23.25)		(7.9-23.25)			

Table II. Parameters of giant dipole resonance

Isotope	σ_1, mb	E_1, MeV	Γ_1, MeV	$\sigma_{int\,1}$, MeV·b	σ_2, mb	E_2, MeV	Γ_2, MeV	$\sigma_{int\,2}$, MeV·b	σ_{int}	$\frac{\sigma_{int}}{0.06\,NZ/A}$	$\frac{\sigma_{int\,2}}{\sigma_{int\,1}}$	$\frac{E_2}{E_1}$	β_{eff}
Nd^{146}	332	13,8	4,1						2,12	1,00			
Sm^{148}	335	14,1	4,0						2,08	0,96			
Gd^{152}	147	12,0	3,0	0,693	259	15,0	3,2	1,29	1,99	0,90	1,87	1,25	0,28
Gd^{154}	161	11,9	2,4	0,612	250	15,0	3,5	1,39	2,00	0,89	2,27	1,26	0,29
Gd^{156}	180	11,9	2,6	0,738	243	15,2	3,6	1,37	2,11	0,94	1,86	1,27	0,31
Gd^{158}	165	11,7	2,6	0,662	249	14,9	3,8	1,49	2,16	0,94	2,25	1,28	0,32
Eu^{151}	285	14,0	4,5						2,02	0,92			
Eu^{153}	150	11,9	2,3	0,562	237	15,1	3,6	1,34	1,90	0,86	2,30	1,27	0,31

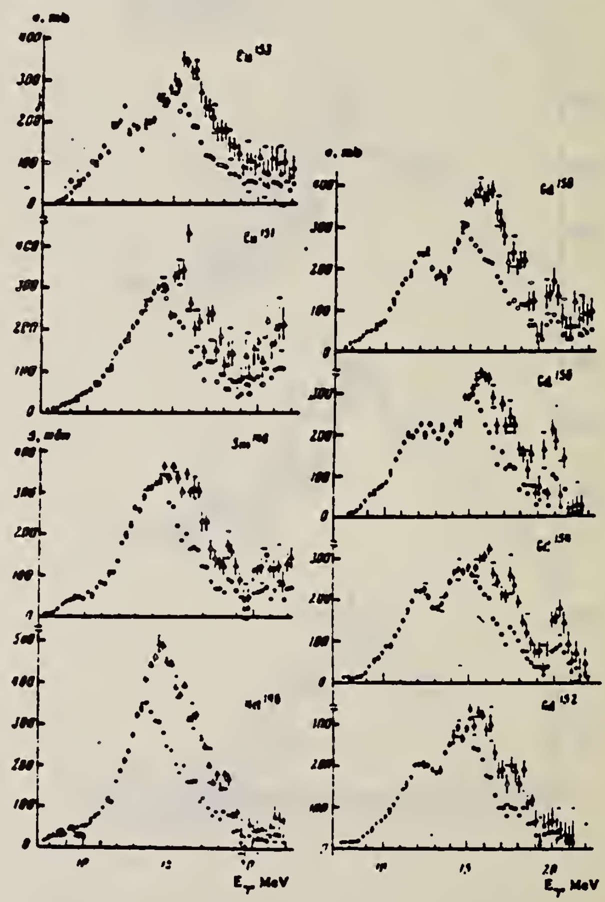

FIG. 1. Photoneutron cross sections and photoabsorption cross sections of Nd^{146}, Sm^{148}, Eu^{151}, Eu^{153}, Gd^{152}, Gd^{154}, Gd^{156} and Gd^{158} Statistical and rms experimental errors are shown (the latter horizontal bars at 9.42 MeV, 10.42 MeV etc.) At photon energies above the (γ, 2n) threshold the photoabsorption cross section errors are not shown.

Gd
A=160

Gd
A=160

Gd
A=160

Ref.	J.H. Carver, W. Turchinetz Proc. Phys. Soc. 73, 69 (1959)	Elem. Sym.	A	Z
		Gd	160	64
Method	33 MeV Synchrotron; radioactivity; NaI spectrometer; ionization chamber	Ref. No. 59 Ca 3		EH

Reaction	E or ΔE	E_0	Γ	$\int \sigma dE$	$J\pi$	Notes
$Gd^{160}(\gamma,n)$	Bremss. $\sim$ 8-32	13.5	5.3 MeV	2.2±0.4 MeV-b		

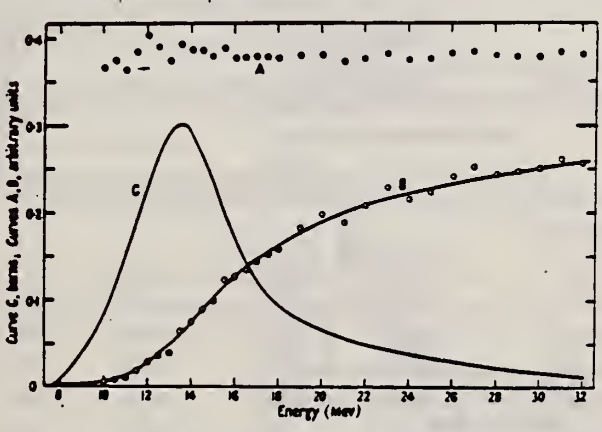

Figure 6. A, the ratio of activation curves $^{160}Gd(\gamma,n)/^{181}Ta(\gamma,n)$; B, activation curve for $^{160}Gd(\gamma,n)$; C, derived cross section: $^{160}Gd(\gamma,n)$.

REF.

B. L. Berman, M. A. Kelly, R. L. Bramblett, J. T. Caldwell
H. S. Davis, and S. C. Fultz
Phys. Rev. 185, 1576 (1969)

ELEM. SYM.	A	Z
Gd	160	64

METHOD

REF. NO.
69 Be 8 hmg

REACTION	RESULT	EXCITATION ENERGY	SOURCE TYPE	SOURCE RANGE	DETECTOR TYPE	DETECTOR RANGE	ANGLE
G,N* 159+	ABX	8-29	D	8-29	BF3-I		4PI
G,2N** 160	ABX	8-29	D	8-29	BF3-I		4PI
G,3N 161	ABX	8-29	D	8-29	BF3-I		4PI

* INCLUDES NP
** INCLUDES 2NP

159+

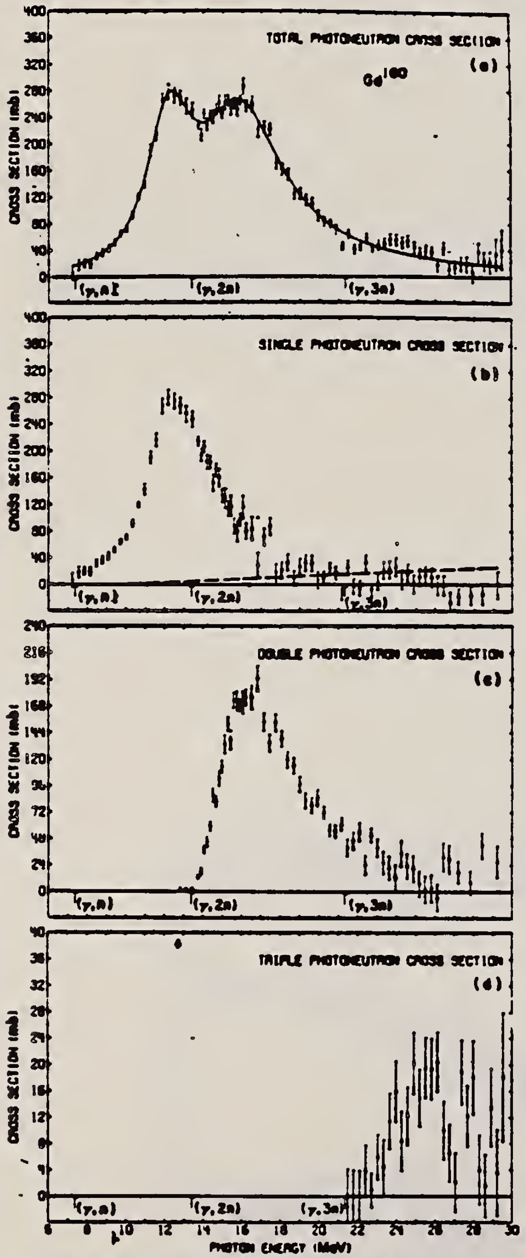

FIG. 6. Photoneutron cross sections for Gd^{160}: (a) $\sigma[(\gamma,n)+(\gamma,pn)+(\gamma,2n)+(\gamma,p2n)+(\gamma,3n)]$, (b) $\sigma[(\gamma,n)+(\gamma,pn)]$, (c) $\sigma[(\gamma,2n)+(\gamma,p2n)]$ (d) $\sigma(\gamma,3n)$.

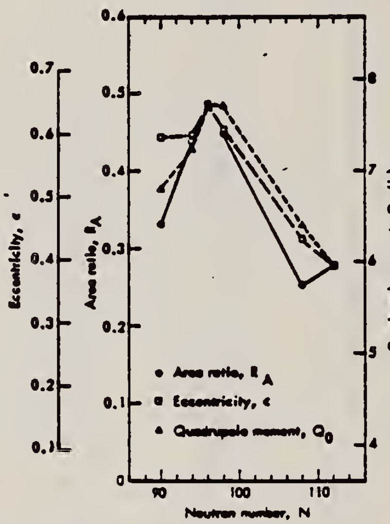

FIG. 9. The area ratio R_A, nuclear eccentricity ϵ, and intrinsic quadrupole moment Q_0 plotted versus neutron number N. The data were scaled between the value for Gd^{160} and that for W^{186}. The absolute scale for Q_0 is based on a mean radius parameter $R_0=1.26$ F. The lines merely connect the three sets of data points. The experimental uncertainties have been omitted for clarity but are given in Tables VII and VIII; their average values are 0.065 (17%) for R_A, 0.010 (1.9%) for ϵ, and 0.26b (3.7%) for Q_0.

[OVER]

TABLE V. Parameters of Lorentz-curve fits to the giant resonance.

Nucleus	$E_m(1)$ (MeV)	$\sigma_m(1)$ [a] (mb)	$\Gamma(1)$ (MeV)	$E_m(2)$ (MeV)	$\sigma_m(2)$ [a] (mb)	$\Gamma(2)$ (MeV)
Eu^{153}	12.33±0.06	155±9	2.75±0.26	15.79±0.10	222±6	5.83±0.30
Tb^{159} [b]	12.22±0.04	181±6	2.64±0.16	15.67±0.06	220±4	4.97±0.19
Gd^{160}	12.23±0.06	215±9	2.77±0.25	15.96±0.09	233±6	5.28±0.30
Ho^{165}	12.28±0.02	214±5	2.57±0.11	15.78±0.04	246±3	5.00±0.17
Ta^{181} [c]	12.59±0.03	171±8	1.94±0.12	15.13±0.12	265±6	4.98±0.23
W^{186}	12.59±0.03	211±14	2.29±0.14	14.88±0.08	334±8	5.18±0.14

[a] The uncertainties for σ_m given here are relative. The absolute uncertainty is 7% (10% for Tb^{159} and Ta^{181}).
[b] The data of Ref. 10 were reanalyzed to obtain the values given in this and subsequent tables (see text).
[c] The data of Ref. 11 were reanalyzed to obtain the values given in this and subsequent tables (see text).

[10] R.L. Bramblett, J. T. Caldwell, R. R. Harvey, S.C. Fultz, Phys.Rev.133, B869 (1964).
[11] R.L. Bramblett, J.T. Caldwell, G.F. Auchampaugh, S.C. Fultz, Phys.Rev.129, 2723 (1963)

TABLE VIII. Nuclear radius parameters.

Nucleus	Q_0 [a] (b)	Refs.	ϵ [b]	R_0 [c] (F)	Q_0 [d] (b)
Eu^{153}	6.99±0.08	e, f	0.595±0.015	1.276±0.018	6.80±0.28
Tb^{159}	7.41±0.11	e	0.598±0.009	1.274±0.013	7.23±0.26
Gd^{160}	7.55±0.17	g	0.645±0.014	1.245±0.020	7.71±0.30
Ho^{165}	7.56±0.11	e	0.604±0.006	1.246±0.011	7.71±0.26
Ta^{181}	6.89±0.21	h, i	0.433±0.010	1.306±0.025	6.43±0.26
W^{186}	5.96±0.05	g, j, k	0.390±0.006	1.259±0.011	5.96±0.21

[a] Values taken from or computed from the references listed in column 3.
[b] Values from present data (Table VII).
[c] Computed from Eq. (2) in the text.
[d] The "best" values for Q_0 deduced from the present data, computed from Eq. (2) in the text, taking R_0 to be 1.26±0.02 F.
[e] M. C. Olesen and B. Elbek, Nucl. Phys. 15, 134 (1960).
[f] R. A. Carrigan, Jr., P. D. Gupta, R. B. Sutton, M. N. Suzuki, A. C. Thompson, R. E. Coté, W. V. Prestwich, A. K. Gaigalas, and S. Raboy, Phys. Rev. Letters 20, 874 (1968).
[g] P. H. Stelson and L. Grodzins, Nucl. Data A1, 21 (1965).
[h] F. K. McGowan and P. H. Stelson, Phys. Rev. 109, 901 (1958).
[i] E. M. Bernstein and R. Graetzer, Phys. Rev. 119, 1321 (1960).
[j] R. C. Barrett, S. Bernow, S. Devons, I. Duerdoth, D. Hitlin, J. W. Kast, W. Y. Lee, E. R. Macagno, J. Rainwater, and C. S. Wu, Columbia University Pegram Nuclear Physics Lab. Report No. NYO-72-191, 1968, p. 74 (unpublished).
[k] R. G. Stokstad and B. Persson, Phys. Rev. 170, 1072 (1968).

TABLE IX. Integrated cross sections.

Nucleus	$E_{\gamma\,max}$ (MeV)	$\sigma_{int}[(\gamma,n)+(\gamma,pn)]$ [a] (MeV-b)	$\sigma_{int}[(\gamma,2n)+(\gamma,p2n)]$ [a] (MeV-b)	$\sigma_{int}(\gamma,3n)$ [a] (MeV-b)	$\dfrac{\sigma_{int}[(\gamma,2n)+(\gamma,p2n)]}{\sigma_{int}(\gamma,\text{total})}$ [b]	$\frac{1}{2}\pi[\sigma_m(1)\Gamma(1)+\sigma_m(2)\Gamma(2)]$ [c] (MeV-b)	$0.06\,NZ/A$ (MeV-b)
Eu^{153}	28.9	1.57	0.67	0.04	0.29±0.04	2.70±0.19	2.22
Tb^{159}	28.0	1.41	0.89	d	0.39±0.08	2.47±0.12	2.31
Gd^{160}	29.5	1.45	1.00	0.08	0.39±0.05	2.87±0.20	2.30
Ho^{165}	28.9	1.73	0.74	0.04	0.29±0.04	2.80±0.09	2.39
Ta^{181}	24.6	1.31	0.88 [e]	f	0.40 [e] ±0.08	2.59±0.15	2.61
W^{186}	28.6	1.66	1.19	0.15	0.40±0.05	3.47±0.17	2.67

[a] All measured integrated cross-section values are given for an energy region from threshold to $E_{\gamma\,max}$.
[b] The word "total" in this table refers to the total photoneutron cross section, $\sigma[(\gamma,n)+(\gamma,pn)+(\gamma,2n)+(\gamma,p2n)+(\gamma,3n)]$.
[c] The uncertainties listed here are relative; to get the absolute uncertainty, a systematic uncertainty of 7% (10% for Tb^{159} and Ta^{181}) must be folded into the values for σ_m.
[d] Not measured in Ref. 10; $\sigma_{int}[(\gamma,2n)+(\gamma,p2n)]$ contains $\frac{1}{2}\sigma_{int}(\gamma,3n)$.
[e] Because $E_{\gamma\,max}$ is so low, these values cannot be compared to the rest.
[f] Not measured in Ref. 11; the $(\gamma,3n)$ cross section below 24.6 is MeV probably negligible.

TABLE X. Integrated moments[a] of the measured photoneutron cross section and sum rules.

Nucleus	σ_{-1} (mb)	$\sigma_{-1}A^{-4/3}$ (mb)	σ_{-2} (mb-MeV^{-1})	$\dfrac{\sigma_{-2}}{0.00225\,A^{5/3}}$	$\dfrac{\sigma_{-2}K}{0.05175\,A^{5/3}}$	$\dfrac{0.05175\,A^{5/3}}{\sigma_{-2}}$ (MeV)
Eu^{153}	148	0.181	10.18	1.03	1.16±0.11	22.2±1.6
Tb^{159}	151	0.175	10.49	1.00	1.14±0.13	23.0±2.3
Gd^{160}	169	0.195	12.09	1.14	1.35±0.13	20.2±1.4
Ho^{165}	166	0.183	11.56	1.04	1.23±0.10	22.2±1.6
Ta^{181} [b]	(149)	(0.145)	(10.66)	(0.82)	(0.97±0.13)	(28.1±2.8)
W^{186}	203	0.191	14.51	1.06	1.26±0.11	21.6±1.5

[a] $\sigma_{-1}=\int_{E_{thr}}^{E_{\gamma\,max}}\sigma E^{-1}\,dE$ and $\sigma_{-2}=\int_{E_{thr}}^{E_{\gamma\,max}}\sigma E^{-2}\,dE$, where σ is the total photoneutron cross section.
[b] Because $E_{\gamma\,max}$ is so low, the values for Ta^{181} cannot be compared to the rest.

REF.	ELEM. SYM.	A	Z
F. Dreyer, H. Dahmen, J. Staude and H. H. Thies Nucl. Phys. A192, 433 (1972)	Gd	160	64

METHOD	REF. NO.	
	72 Dr 5	egf

REACTION	RESULT	EXCITATION ENERGY	SOURCE TYPE	SOURCE RANGE	DETECTOR TYPE	DETECTOR RANGE	ANGLE
G,N	ABX	6-33	C	6-33	ACT-I		4PI
G,XP	ABX	15-33	C	14-33	ACT-I		4PI

XP = P + NP

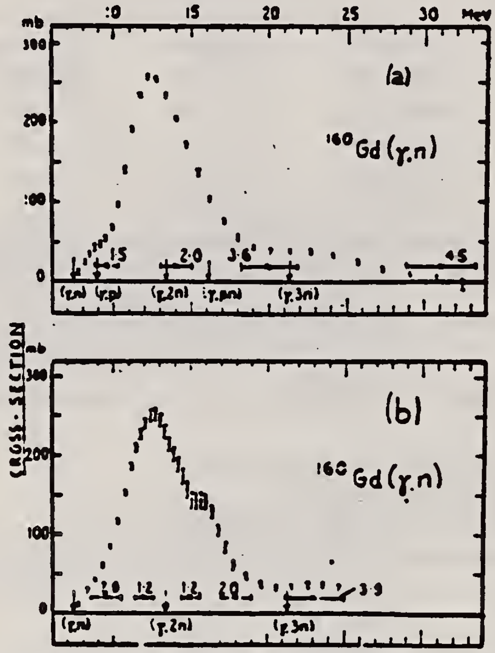

Fig. 2. Cross-section error bars represent the correlated statistical counting errors in the cross section, calculated according to the least-structure method of Cook [9]). The energy resolution, i.e. the half-width of the Cook resolution function, is indicated at representative energies by horizontal errors bars. (a) the $^{160}Gd(\gamma, n)$ cross section, present experiment (the cross section is strictly that for $[^{160}Gd(\gamma, n)+^{160}Gd(\gamma, p)]$, but the $^{160}Gd(\gamma, p)$ contribution is small as seen from fig. 3). (b) Same as (a) but here the E1 giant-resonance region is seen with increased resolution, and correspondingly increased statistical error bars.

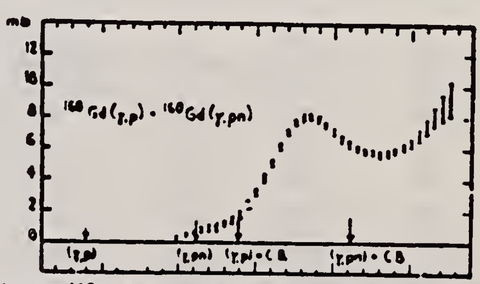

Fig. 3. The $^{160}Gd(\gamma, p)+^{160}(\gamma, pn)$ cross section, present experiment. See also caption of fig. 2.

Tb
A=159

# TERBIUM
Z=65

Carol Mosander separated terbium, in 1843, from the oxide then called yttria. He named the substance erbia, but since 1877 it has been known as terbia.

Tb
A=159

Tb
A=159

3.G. Chidley, L. Katz, S. Kowalski
Can. J. Phys. 36, 407 (1958)

ELEM. SYM.	A	Z
Tb	159	65

Betatron

REF. NO.	
58 Ch 2	NVB

REACTION	RESULT	EXCITATION ENERGY	SOURCE TYPE	SOURCE RANGE	DETECTOR TYPE	DETECTOR RANGE	ANGLE
G,N	RLY	THR	C	THR	BF3-I		4PI

See 58 Ka 1 for cross sections

THRESHØLD

TABLE I

MEASURED PHOTONEUTRON THRESHOLDS

Reaction	Measured Q value, Mev.	Other Q values, Mev.	Method	Reference
$Tb^{159}(\gamma, n)Tb^{158}$	8.16±0.05			

U.S. DEPARTMENT OF COMMERCE
NATIONAL BUREAU OF STANDARDS

.G. Fuller, B. Petree, M.S. Weiss
ys. Rev. 112, 554 (1958)

ELEM. SYM.	A	Z
Tb	159	65

Betatron; ion chamber

REF. NO.	
58 Fu 1	NVB

REACTION	RESULT	EXCITATION ENERGY	SOURCE TYPE	SOURCE RANGE	DETECTOR TYPE	DETECTOR RANGE	ANGLE
G,XN	ABY	7-40	C	7-40	BF3-I		4PI

TABLE I. Target properties and results.

Element	Form used	Weight grams	$\sigma^a(\gamma,n)^a$ barns	$\frac{\int\sigma dE^b}{NZ/A}$ Mev-b	"Γ"^{a} Mev
Sn	Sn	4.81	0.30	0.064	5.0
I	I	8.55	0.36	0.085	6.0
La	La	10.43	0.34	0.063	5.2
Ce	Ce	4.99	0.45	0.080	4.5
Sm	Sm_2O_3	2.90	0.26	0.073	8.6
Tb	Tb_4O_7	3.04	0.39	0.087	8.7
Ho	Ho_2O_3	1.87	0.41	0.079	7.5
Er	Er_2O_3	5.41	0.50	0.100	8.5
Yb	Yb_2O_3	5.57	0.50	0.090	7.0
Ta	Ta	8.41	0.49	0.077	6.0
Au	Au	3.16	0.68	0.085	4.2
Pb	Pb	8.05	0.75	0.081	3.8

[a] $\sigma^a(\gamma,n)$ is the maximum value and "Γ" the full width at $\sigma^a(\gamma,n)/2$ of the neutron production cross section corrected for multiple neutron emission. Data were not fitted with resonance lines to determine these values.
[b] Integrated neutron production cross sections corrected for multiple neutrons above $(\gamma,2n)$ threshold.

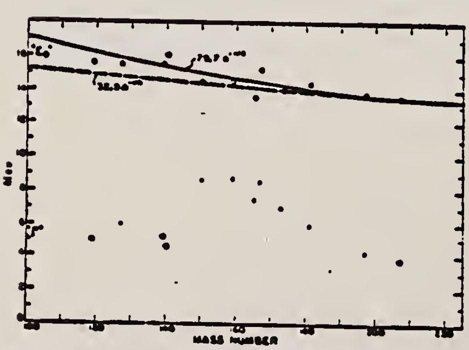

FIG. 6. Mean energy and width of giant resonances. "E_0" and "Γ" are the mean energy for photon absorption and the full width at half maximum of the giant resonance obtained from dashed histograms as in Fig. 5. No attempt was made to fit data with resonance curves to obtain these parameters.

TABLE II. Energies of resonances in deformed nuclei.[a]

Nucleus	E_m Mev	Q_0 barns	Method	E_a Mev	E_b Mev	$E_{1/2}^-$ Mev	$E_{1/2}^+$ Mev
$_{65}Tb^{159}$	14.7	6.9[b]	CE	11.9	16.2	10.8	19.5
$_{67}Ho^{165}$	14.5	7.8[b]	CE	11.5	16.0	11.0	18.5
$_{68}Er^{167}$	14.5	21[b]	SC	8.5	17.5	11.5	20.0
$_{68}Er^{166}$	14.5	7.8[b]	CE	11.6	15.9	11.5	20.0
$_{73}Ta^{181}$	14.1	12.6[c]	SC	10.5	15.9	11.3	17.3
$_{73}Ta^{181}$	14.1	6.8[b]	CE	11.9	15.2	11.3	17.3
$_{79}Au^{197}$	13.6	3.75[c]	SC	12.5	14.1	11.8	16.2

[a] CE—Coulomb excitation; SC—spectroscopic; $E_{1/2}^-$, $E_{1/2}^+$—energies at which giant resonance drops to half its maximum value.
[b] Adler, Bohr, Huus, Mottelson, and Winther, Revs. Modern Phys. 28, 432 (1956).
[c] M. L. Pool and D. N. Kundu, *Chart of Atomic Nuclei* (Longs College Book Company, Columbus, 1955).

REF.	ELEM. SYM.	A	Z
E.G. Fuller, M.S. Weiss Phys. Rev. 112, 560 (1958)	Tb	159	65

METHOD	REF. NO.	
Betatron; ion chamber	58 Fu 2	NVB

REACTION	RESULT	EXCITATION ENERGY	SOURCE TYPE	SOURCE RANGE	DETECTOR TYPE	DETECTOR RANGE	ANGLE
G,XN	ABX	8-23	C	THR-25	BF3-I		4PI

CF DANØS THEØRY

TABLE I. Resonance parameters.

	Tb^{159}	Ta^{181}	Au^{197}
B_{2n} (Mev)	15.2	14.0	14.2
E_a (Mev)	12.5	12.45	13.15
σ_a^0 (Mb)	258	308	255
Γ_a (Mev)	2.4	2.3	2.9
E_b (Mev)	16.3	15.45	13.90
σ_b^0 (Mb)	310	348	365
Γ_b (Mev)	4.0	4.4	4.0

TABLE II. Integral cross sections.

	Tb^{159}	Ta^{181}	Au^{197}
$A\int_0^{24}\sigma_n dE/0.06NZ$	1.27	1.30	1.29
$\int\sigma_b dE/\int\sigma_a dE$	2.00	2.16	1.97
$A\int_0^{\infty}(\sigma_a+\sigma_b)dE/0.06NZ$	1.27	1.35	1.22

TABLE III. Intrinsic quadrupole moments, in barns.

	Tb^{159}	Ta^{181}	Au^{197}
E_b/E_a	1.30±0.05	1.25±0.01	1.06±0.03
$Q_0(R_0=1.09\times10^{-13}$ cm)	5.6 ±0.6	5.7 ±0.3	1.6 ±0.6
Q_0 (Coulomb excitation)	6.9[a]	6.8[a]	2.6[b]

[a] Adler, Bohr, Huus, Mottelson, and Winter, Revs. Modern Phys. 28, 432 (1956).
[b] P. H. Stelson and F. K. McGowan, Phys. Rev. 99, 112 (1955).

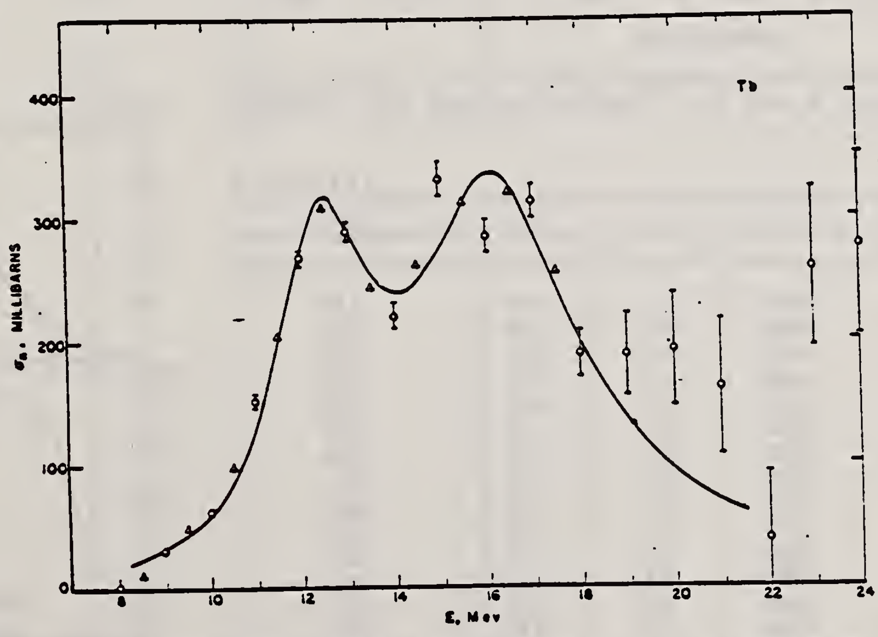

FIG. 5. Neutron cross section for terbium. Circles and triangles represent independent determinations of the cross section from the original data. Errors represent standard deviations based on the statistical uncertainties ($\sqrt{n}$) in the original activation curve data. The cross section plotted is $\sigma_n=\sigma(\gamma,n)+\sigma(\gamma,2n)+\sigma(\gamma,pn)+\cdots$. The smooth curve is calculated from the parameters given in Table I by using Eq. (5).

L. Katz, G.B. Chidley
Nuclear Reactions at Low and Medium Energies (Academy of Science, USSR: 1958) 371

ELEM. SYM.	A	Z
Tb	159	65

METHOD Betatron; neutron cross section; BF_3 counters; ion chamber monitor

REF. NO. 58 Ka 1 NVB

REACTION	RESULT	EXCITATION ENERGY	SOURCE TYPE	SOURCE RANGE	DETECTOR TYPE	DETECTOR RANGE	ANGLE
G,XN	ABX	9-22	C	9-22	BF3-I		4PI

Таблица 2

Пороги испускания фотонейтронов

Изотоп	B_n, Мэв	B_{2n}, Мэв	Изотоп	B_n, Мэв	B_{2n}, Мэв
V^{51}	11,16	20,5	La^{139}	8,81	16,1
Mn^{55}	10,14	19,2	Pr^{141}	9,46	17,6
Co^{59}	10,44	18,6	Tb^{159}	8,16	14,8
As^{75}	10,24	18,1	Ho^{165}	8,10	14,6
Y^{89}	11,82	20,7	Tm^{169}	8,00	14,7
Nb^{93}	8,86	17,1	Lu^{175}	7,77	14,2
Rh^{103}	9,46	16,8	Ta^{181}	7,65	13,8
J^{127}	9,14	16,2	Au^{197}	7,96	13,3
Cs^{133}	9,11	16,5	Bi^{209}	7,43	14,5

THRESHOLDS

не приведены, поскольку они превышают 22 *Мэв* во всех случаях, кроме золота, для которого B_{3n}=21 *Мэв*. Свойства сечений $\sigma_C(\gamma)$ сведены в табл. 3.

Таблица 3

Изотоп	$E_{макс}$, Мэв	$\sigma_n(E_\gamma)$, барн	Γ, Мэв	Σ^m, Мэв·барн	Y(22), 10^8 нейтрон/100 р·моль
V^{51}	18,4	0,062	5,2	0,33	1,62
Mn^{55}	20,2	0,060	7,0	0,39	2,01
Co^{59}	18,3	0,068	6,3	0,44	2,30
As^{75}	16,4	0,090	9,5	0,74	4,25
Y^{89}	17,1	0,172	5,2	0,93	5,33
Nb^{93}	18,0	0,156	7,5	1,17	6,80
Rh^{103}	17,5	0,160	9,4	1,40	8,28
J^{127}	15,2	0,273	6,8	1,76	11,9
Cs^{133}	16,5	0,238	7,7	1,59	10,7
La^{139}	15,5	0,325	3,8	1,55	11,2
Pr^{141}	15,0	0,320	4,9	1,93	13,1
Tb^{159}	15,6	0,274	9,8	2,49	18,1
Ho^{165}	13,5	0,305	8,9	2,52	18,7
Tm^{169}	16,4	0,250	8,4	1,91	14,9
Lu^{175}	16,0	0,225	8,4	1,90	23,0
Ta^{181}	14,5	0,380	8,5	3,15	22,0
Au^{197}	13,8	0,475	4,7	3,04	22,6
Bi^{209}	13,2	0,455	5,9	2,89	23,2

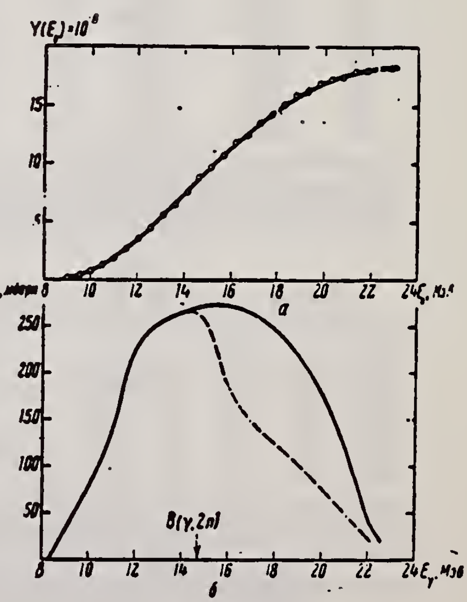

Рис. 12.
а — Выход фотонейтронов для Tb; б — $\sigma_n(E_\gamma)$ и $\sigma_C(\gamma)$ для Tb

Ref. F.R. Metzger, W.B. Todd
Nuclear Phys. 13, 177 (1959)

Elem. Sym.	A	Z
Tb	159	65

Method radioactive source; photon scattering; NaI spectrometer

Ref. No.	
59 Me 1	NVB

Reaction	E or ΔE	E_0	Γ	$\int \sigma dE$	$J\pi$	Notes
$Tb(\gamma,\gamma)$	362 kev	362 keV				Detectors at 125°, 144°. $W(\theta) = 1 + a_2 \cos^2\theta$, where $a_2 = 0.1 \pm 0.4$ Lifetime of γ transition to ground state: $\tau_\gamma = (2.0 \pm 0.3)\ 10^{-10}$ sec. Find transition to be E1 by K-conversion measurements.

K. N. Geller, J. Halpern, and E. G. Muirhead
Phys. Rev. <u>118</u>, 1302-12 (1960)

ELEM. SYM.	A	Z
Tb	159	65

METHOD

Betatron; neutron threshold; ion chamber

REF. NO.	
60 Ge 3	NVB

REACTION	RESULT	EXCITATION ENERGY	SOURCE TYPE	SOURCE RANGE	DETECTOR TYPE	DETECTOR RANGE	ANGLE
G,N	NØX	THR	C THR		BF3-I		4 PI

THRESHØLD

TABLE I. Summary and comparison of neutron separation energies inferred from present threshold measurements with values predicted from mass data and reaction energies. All energies are expressed in the center-of-mass system in Mev.

Reaction	No. runs	Present results	Other results	Method	Reference
$Tb^{159}(\gamma,n)Tb^{158}$	3	8.141±0.039	8.16 ±0.05	threshold	f

Ref. H.H. Thies, B.M. Spicer
Australian J. Phys. 13, 505 (1960)

Elem. Sym.	A	Z
Tb	159	65

Method
18 MeV electron synchrotron; BF_3 counters; ion chamber

Ref. No.	
60 Th 1	EH

Reaction	E or ΔE	E_0	Γ	$\int \sigma dE$	Jπ	Notes
$Tb^{159}(\gamma,xn)$	7-18	12.4±0.2				σ_{max} = 410 mb.
		16.0±0.2				σ_{max} = 460 mb.

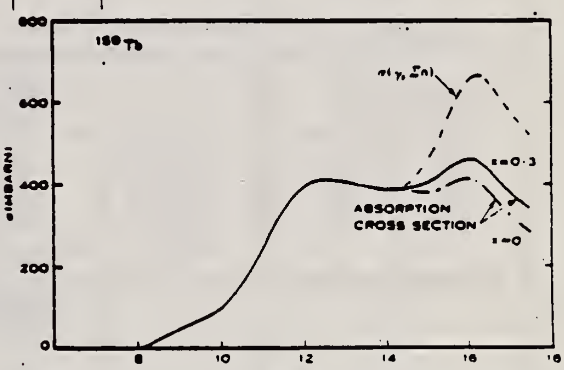

Fig. 8.—Cross section for photon absorption in ^{159}Tb, using statistical theory of nuclear reactions to correct for neutron multiplicity. The factor x is a measure of the probability that a direct photoeffect will occur.

TABLE 2
GIANT RESONANCE PARAMETERS IN DEFORMED NUCLEI

Nucleus ..	^{159}Tb		^{165}Ho	^{181}Ta	
Reference ..	Fuller and Weiss (1958)	Present Paper	Present Paper	Fuller and Weiss (1958)	Spicer et al. (1958)
$\Gamma_{G.R.}$ (MeV)	6·5	6·7 ± 0·5	7 ± 0·5	6·2 ± 0·2	6·1
E_1 (MeV)	12·5	12·4 ± 0·2	12·1 ± 0·2	12·45	12·6
$(\sigma_1)_{max.}$ (mbarn)	260	410	420	308	500
Γ_1 (MeV)	2·4	3·3	2·8	2·3	2·0
E_2 (MeV)	16·3	16·0 ± 0·2	16·2 ± 0·2	15·45	15·3
$(\sigma_2)_{max.}$ (mbarn)	310	460	510	348	450
Γ_2 (MeV)	4·0	4·5	4·7	4·4	4·0
I_2/I_1 ..	2·0	2·0	2·0	2·16	1·8
E_2/E_1 ..	1·30	1·29 ± 0·03	1·34 ± 0·03	1·25 ± 0·01	1·21 ± 0·03

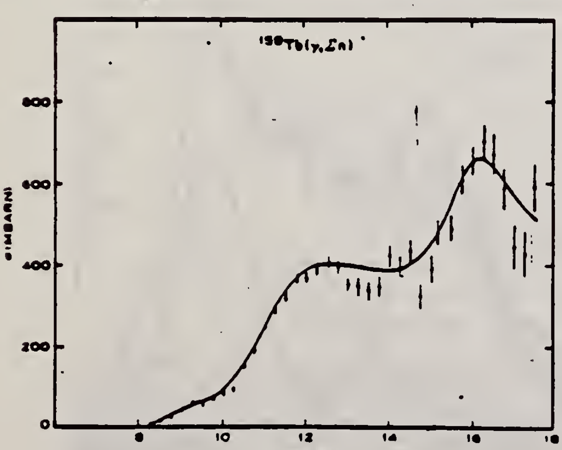

Fig. 6.—Total neutron production cross section for ^{159}Tb.

Ref. O.V.Bogdankevich, B.I.Goryachev, V.A.Zapevalov Zhur.Eksptl. i Teoret.Fiz. <u>42</u>, 1502 (1962); Soviet Phys.JETP <u>15</u>, 1044 (1962)	Elem. Sym. Tb	A 159	Z 65
Method 30 MeV Synchrotron - BF_3	Ref. No. 62Bo1		BG

Reaction	E or ΔE	E_o	Γ	$\int \sigma dE$	Jπ	Notes
(γ,n)	Threshold 21					Best fits of σ_γ by two (Fig.10) and three (Fig.11) Lorentz lines made. 2 Lorentz line approximation less likely. Data for Lorentz line fits given in Table II and Table III.

Table II

Number of line	σ_{max}, mb	E_m, MeV	Γ, MeV	σ_{int}, MeV·b	$\frac{\sigma_{int2}}{\sigma_{int1}}$	σ_{int}, MeV·b	$\frac{\sigma_{int}}{0.058NZ/A}$	ε	Q_0, b
I II	267 317	12.5 16.4	3.4 3.4	1.42 1.69	1.19	3.11	1.4	0.28	6.6±0.6

Table III

Number of line	σ_{max}, mb	E_m, MeV	Γ, MeV	σ_{int}, MeV·b	$\sigma_{int1}:\sigma_{int2}:\sigma_{int3}$	σ_{int}, MeV·b	$\frac{\sigma_{int}}{0.058NZ/A}$
I II III	278 191 305	12.25 15 17	2.5 3.2 2.0	1.09 0.96 0.96	1.09:0:96:0.96	3.01	1.35

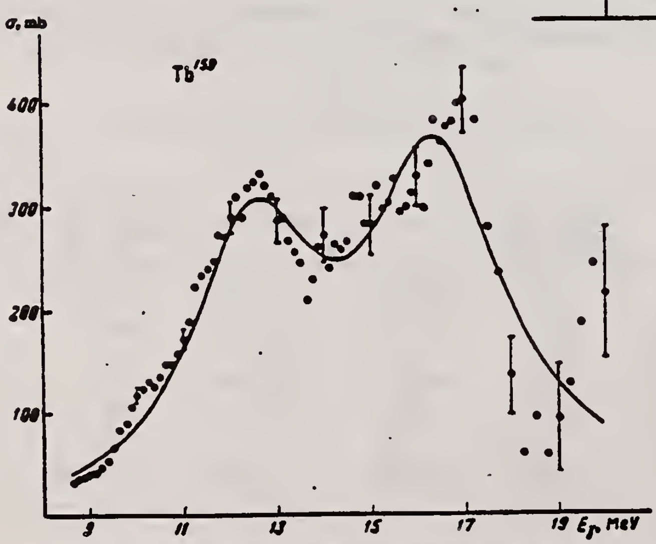

FIG. 10. Photon absorption cross section of Tb159.

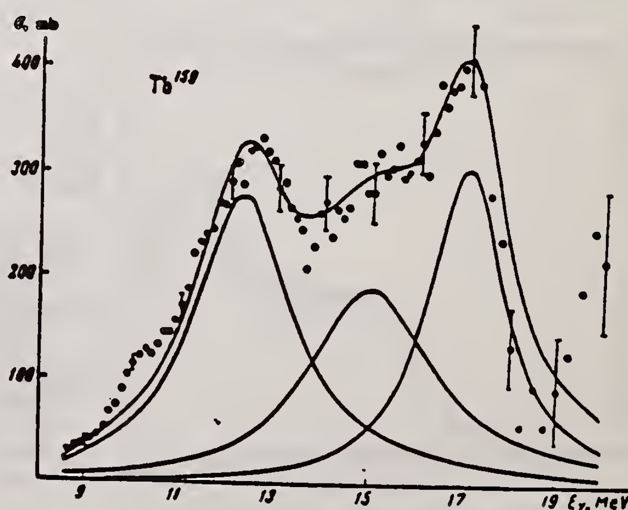

FIG. 11. Approximation of σ_γ of Tb159 by three Lorentz lines.

REF.	ELEM. SYM.	A	Z
R.L. Bramblett, J.T. Caldwell, R.R. Harvey, S.C. Fultz Phys. Rev. 133, B869-73 (1964)	Tb	159	65

METHOD	REF. NO.	
Positron annihilation; linac; ion chamber	64 Br 1	NVB

REACTION	RESULT	EXCITATION ENERGY	SOURCE TYPE	SOURCE RANGE	DETECTOR TYPE	DETECTOR RANGE	ANGLE
G,N 361	ABX	8 - 28	D	8 - 28	BF3-I		4PI
G,2N 362	ABX	14 - 28	D	8 - 28	BF3-I		4PI

Level density parameter

$a = 17\pm5\ \mathrm{MeV}^{-1}$

PØS ANNIHIL.

361 +

Quadrupole moment = 7.0±1.1 barns.

$$\int_{8}^{28} \sigma(\gamma,n+\gamma,2n)\,dE = 2.3\pm0.2\ \text{MeV-barns},$$

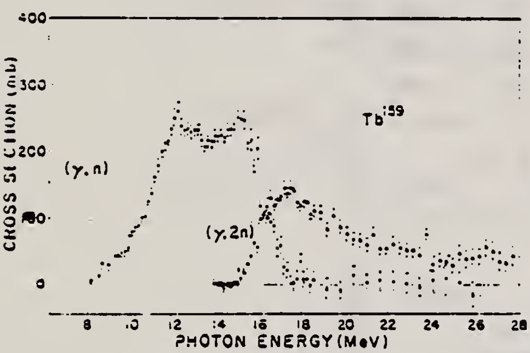

FIG. 4. The (γ,n) and $(\gamma,2n)$ cross sections of Tb^{159} up to 28 MeV. The (γ,n) cross section decreases rapidly to zero above the $(\gamma,2n)$ threshold.

TABLE III. Parameters of the Tb^{159} giant resonance.

Parameter \ Reference	This experiment	Fuller and Weiss[a]	Thies and Spicer[b]	Bogdankevich et al.[c]
E_a (MeV)	12.2 ± 0.2	12.5	12.4 ±0.2	12.5
σ_a (mb)	188 ±19	260	410	267
Γ_a (MeV)	2.67 ± 0.2	2.4	3.3	3.4
E_b (MeV)	15.6 ± 0.2	16.3	16.0 ±0.2	16.4
σ_b (mb)	233 ±23	310	460	317
Γ_b (MeV)	4.30 ± 0.4	4.0	4.5	3.4
Q_0 (b)	+7.0 ± 1.1	7.7	7.3	7.8
$\int_8^{28}\sigma_t dE$ (MeV b)	2.3 ± 0.2			

[a] See Ref. 31.
[b] See Ref. 32.
[c] See Ref. 30.

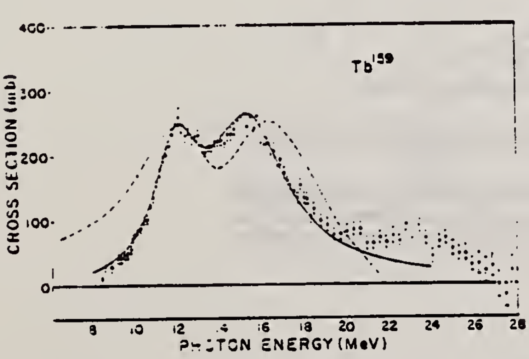

FIG. 5. The photon absorption cross section of Tb^{159} obtained by adding the (γ,n) and $(\gamma,2n)$ cross sections of Fig. 4. The electric dipole giant resonance is double peaked due to the quadrupole moment of Tb^{159}. The solid curve is the sum of two Lorentz curves with parameters given in Table III. The dashed curve is from Wilkinson (Ref. 9).

REF.	ELEM. SYM.	A	Z
M. Langevin, J. M. Loiseaux et J. M. Maison Nucl. Phys. 54, 114-124 (1964)	Tb	159	65

METHOD		REF. NO.	
Bremsstrahlung scattering	[Page 1 of 2]	64 La 1	joc

REACTION	RESULT	EXCITATION ENERGY	SOURCE TYPE	SOURCE RANGE	DETECTOR TYPE	DETECTOR RANGE	ANGLE
G,G	ABX	10-25	C		NAI-D		DST

TABLEAU 1

Le paramètre $a(E)$ de la distribution angulaire

Noyau	11.5-14. MeV			14-17.5 MeV			17.5-20 MeV			20-30 MeV	
	Exp.	Ellipsoidal	Triax.	Exp.	Ellips.	Triax.	Exp.	Ellips.	Triax.	Exp.	Ellips.
							Contribution Quadrupolaire %				
Tb	$0.5^{+0.15}_{-0.1}$	0.41	0.39	$0.54^{+0.15}_{-0.1}$	0.70	0.50	25	0.97	0.85		1
Ho	$0.27^{+0.15}_{-0.1}$	0.44	0.407	$0.43^{+0.10}_{-0.05}$	0.71	0.53	25	0.95	0.9	0.4 ± 0.1	1
Er	$0.27^{+0.15}_{-0.1}$	0.44	0.407	$0.8^{+0.15}_{-0.1}$	0.71	0.53	25	0.95	0.9		1
Ta	$0.6^{+0.15}_{-0.1}$	0.58		$0.68^{+0.15}_{-0.1}$	0.81		20	0.96			
Au		a_{exp}(11-20 MeV) = 0.9								0.7 ± 0.1	1
		a_{th} (11-20 MeV) $\approx$ 1									

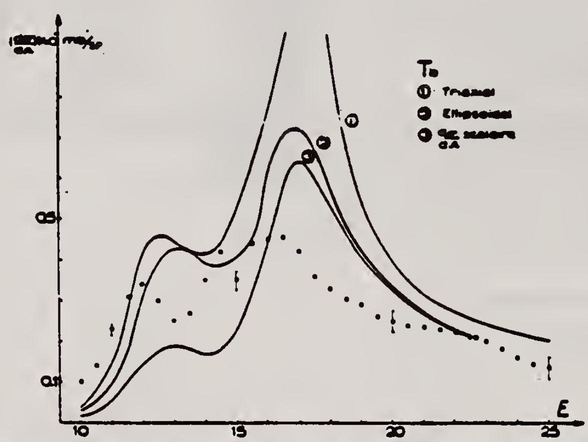

Fig. 5. Sections efficaces différentielles de diffusion obtenues pour le terbium. Les courbes tracées correspondent à l'application des relations de dispersion aux sections efficaces d'absorption de Bogdankevich *et al.* [14]) dans le cas d'une diffusion purement scalaire et d'un modèle ellipsoidal ou triaxal.

REF.	ELEM. SYM.	A	Z
M. Langevin, J. M. Loiseaux et J. M. Maison Nucl. Phys. 54, 114-124 (1964)	Tb	159	65

METHOD		REF. NO.	
Bremsstrahlung scattering	[Page 2 of 2]	64 La 1	JOC

REACTION	RESULT	EXCITATION ENERGY	SOURCE TYPE	SOURCE RANGE	DETECTOR TYPE	DETECTOR RANGE	ANGLE

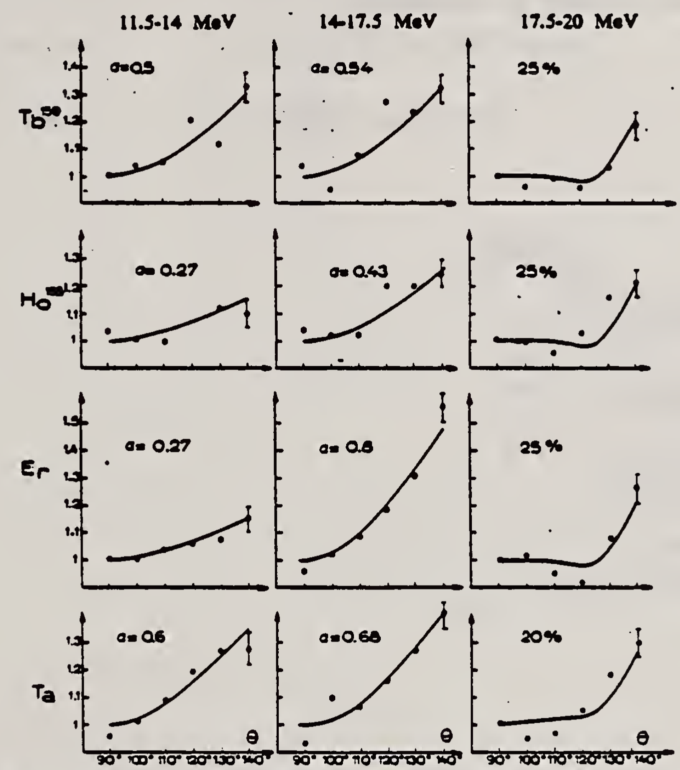

Fig. 8. Répartitions angulaires du rayonnement diffusé obtenues pour le terbium, l'holmium, l'erbium et le tantale dans les zones d'énergie 11.5-14 MeV, 14-17.5 MeV et 17.5-20 MeV.

REF.	ELEM. SYM.	A	Z
U. Atzmony, E. R. Bauminger and S. Ofer Nuclear Phys. 89, 433 (1966)	Tb	159	65

METHOD	REF. NO.	
Mössbauer Effect	66 At 2	JDM

REACTION	RESULT	EXCITATION ENERGY	SOURCE TYPE	SOURCE RANGE	DETECTOR TYPE	DETECTOR RANGE	ANGLE
G,G	LFT	1	D		SCD-D		DST

$T_{\frac{1}{2}}$ for 58 keV level $\leq (1.05\pm0.15)10^{-10}$. Magnetic moment of this level = 1.50±0.10 n.m. (and perhaps 2.10±0.15 n.m. cannot be excluded).

REF.	ELEM. SYM.	A	Z
R. S. Raghavan Phys. Rev. 143, B947 (1966)	Tb	159	65

METHOD	REF. NO.	
Centrifuge technique	66 Ra 1	JDM

REACTION	RESULT	EXCITATION ENERGY	SOURCE		DETECTOR		ANGLE
			TYPE	RANGE	TYPE	RANGE	
G,G	LFT	1	D	1	NAI-D		DST

$W = 1 + A_2 P_2(\cos\theta)$

For 363 MeV, $A_2 = +(24.3\pm3)\%$, $\tau = (2.2\pm0.15) \times 10^{-3}$ secs.

For 580 MeV, $A_2 = 0.0\pm0.06$, $\tau = (1.1\pm0.15) \times 10^{-3}$ secs.

$\delta_{363}\left(\frac{M2}{E1}\right) = -6\pm\frac{1}{2}\%$, $\delta_{580}\left(\frac{E2}{M1}\right) = \pm(3\pm1.5)\%$

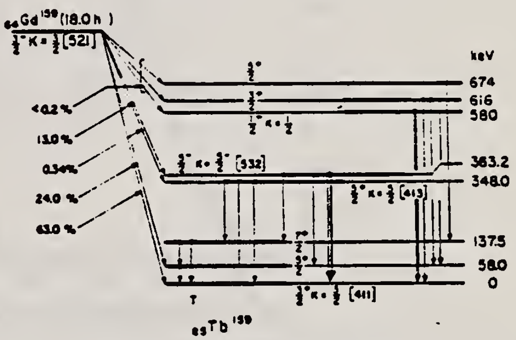

FIG. 1. Decay scheme of Gd¹⁵⁹-Tb¹⁵⁹.

947

REF.			ELEM. SYM.	A	Z
R. Bergère, H. Beil and A. Veyssière Nucl. Phys. A121, 463 (1968)			Tb	159	65
METHOD			REF. NO. 68 Be 5		egf

REACTION		RESULT	EXCITATION ENERGY	SOURCE TYPE	SOURCE RANGE	DETECTOR TYPE	DETECTOR RANGE	ANGLE
G,N	94	ABX	THR-30	D	7-30	MOD-I		4PI
G,2N	95							
G,3N	96+							

TABLE 6

Lorentz line parameters for a two line fit to the total cross section data of $^{159}_{65}$Tb

E_1(MeV)	σ_1(mb)	Γ_1(MeV)	E_2	σ_2	Γ_2
12.12	205	3.25	15.97	240	4.87

94+

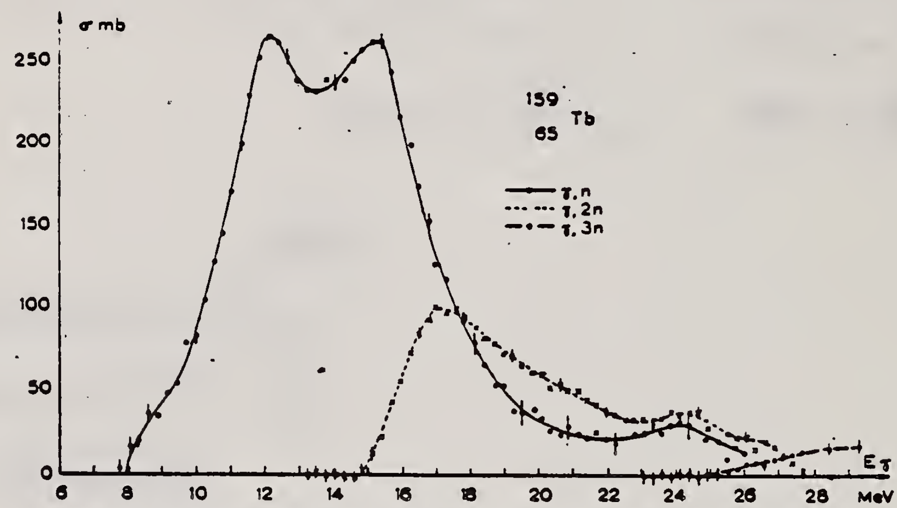

Fig. 7. Partial photonuclear cross sections $\sigma(\gamma, n)$, $\sigma(\gamma, 2n)$ and $\sigma(\gamma, 3n)$ of $^{159}_{65}$Tb.

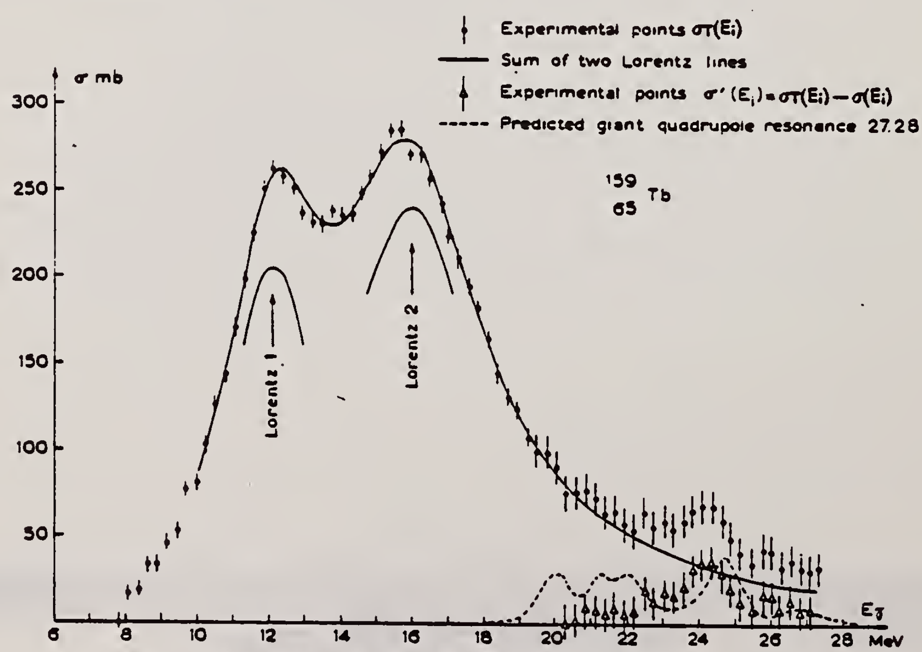

Fig. 8. Total cross section data showing a two Lorentz line fit for a $^{159}_{65}$Tb target.

REF. Y. Oka, T. Kato and A. Yamadera
Bull. Chem. Soc. Japan 41, 1606 (1968)

ELEM. SYM.	A	Z
Tb	159	65

METHOD

REF. NO.	
68 Ok 2	egf

REACTION	RESULT	EXCITATION ENERGY	SOURCE TYPE	SOURCE RANGE	DETECTOR TYPE	DETECTOR RANGE	ANGLE
G,N	ABY	THR-20	C	20	ACT-I		4PI

ISOMERIC YIELD

TABLE 1. THE PARTICULARS OF THE (γ,n) REACTION PRODUCTS AND THE DATA OBTAINED WITH 20 MeV BREMSSTRAHLUNG

Nuclide: Parent (Natural abundance, %)	Nuclide: Residual	Half-life of product (sec)	Gamma-ray determined: Energy (MeV)	Gamma-ray determined: Branching ratio (%)	Gamma-ray determined: Photopeak activity (cpm/mg)[a]	Limit of detection (μg)	Yield ($mol^{-1} \cdot R^{-1}$)
^{24}Mg(78.60)	^{23}Mg	9.9	0.511	200	2.04×10^4	0.49	8.1×10^4
^{76}Ge(7.67)	^{75m}Ge	48	0.139	100	6.37×10^3	1.6	1.1×10^4
^{78}Se(23.52)	^{77m}Se	17	0.162	100	1.82×10^4	0.55	1.2×10^4
^{92}Mo(15.86)	^{91m}Mo	65	0.650	57	2.22×10^3	4.5	2.7×10^4
^{140}Ce(88.48)	^{139m}Ce	58	0.745	100	1.06×10^4	0.95	1.3×10^4
^{142}Nd(27.13)	^{141m}Nd	64	0.760	100	3.19×10^4	3.1	1.4×10^4
^{159}Tb(100)	^{158m}Tb	11	0.111	100	2.56×10^3	3.8	2.2×10^4

a) The value corrected at the end of one-minute irradiation with the dose rate of 10^3 R/min; Counting geometry is 20% with a 3"dia.×3"NaI(Tl) detector.

REF.	ELEM. SYM.	A	Z
L.M. Dautov, Yu.A. Lysikov, U.M. Makhanov, Yu.K. Shubnyi Izv. Akad. Nauk SSSR Ser. Fiz. 36, 2544 (1972) Bull. Acad. Sci. USSR Phys. Ser. 36, 2210 (1972)	Tb	159	65

METHOD	REF. NO.	
	72 Da 14	hmg

REACTION	RESULT	EXCITATION ENERGY	SOURCE		DETECTOR		ANGLE
			TYPE	RANGE	TYPE	RANGE	
G,G	ABX	364*	D	364*	SCD-D		92

* ENERGY IN KEV

$\sigma = (5.5 \pm .7) \cdot 10^{-28}\ cm^2 \cdot sr^{-1}$, $\Gamma_{0\gamma} = (3.4 \pm .4) \cdot 10^{-6}$ eV.

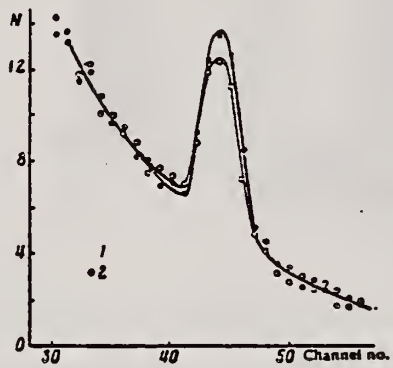

Fig. 3. The spectrum of the scattered radiation in the case ^{159}Gd ^{159}Tb at a source temperature of 1000° C. 1) Terbium scatter; 2) samarium scatter. N = = hundreds of pulses in 20 min. In nonresonance conditions (T = 20° C) the scattering from both scatterers was the same $N_{Tb}/N_{Sm} = 1.012 \pm 0.003$.

REF.

R.F. Barrett, J.R. Birkelund, B.J. Thomas, K.S. Lam, and H.H. Thies
Nucl. Phys. A210, 355 (1973)

ELEM. SYM.	A	Z
Tb	159	65

METHOD

REF. NO.	
73 Ba 20	egf

REACTION	RESULT	EXCITATION ENERGY	SOURCE TYPE	SOURCE RANGE	DETECTOR TYPE	DETECTOR RANGE	ANGLE
G,N	NOX	THR- 27	C	10- 27	BF3-I		4PI

MEAN NEUT ENERGY

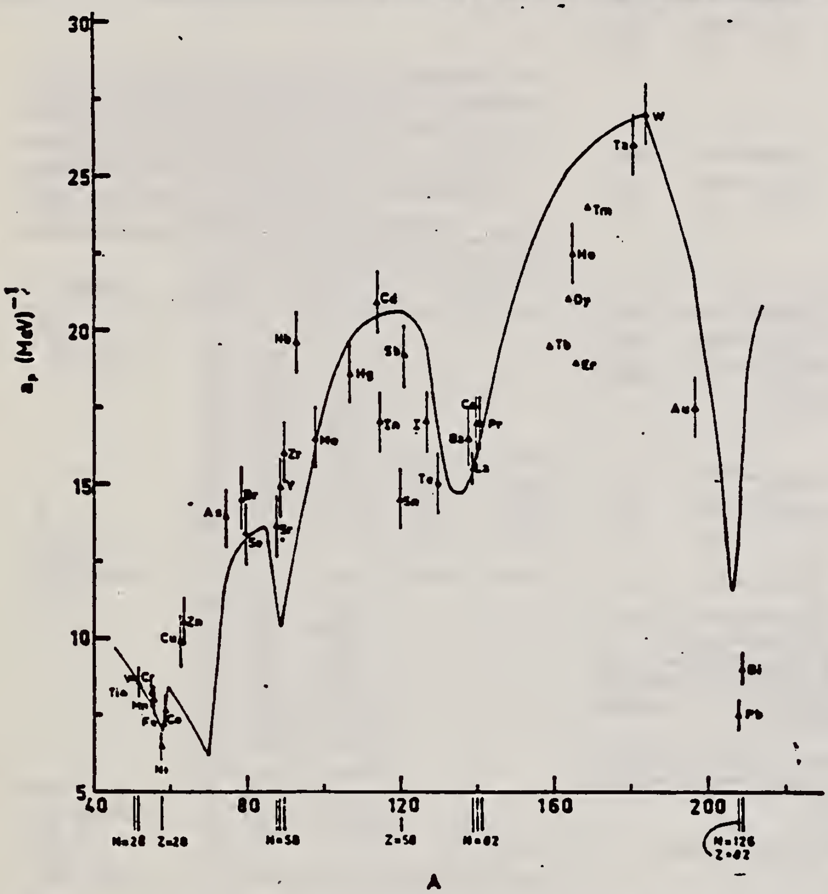

Fig. 12. Experimental values of the level density parameter a_p (Fermi gas formula plus pairing correction) versus atomic number A. The continuous curve is a least-squares fit to the data of a theoretical calculation from Newton [15]).

1
H. Baba and S. Baba, Japan Atomic Energy Research Institute report JAERI-1183 (1969).
2
H. Baba, Nucl. Phys. A159, 625 (1970).
15
T.D. Newton, Can. J. Phys. 34, 804 (1956).

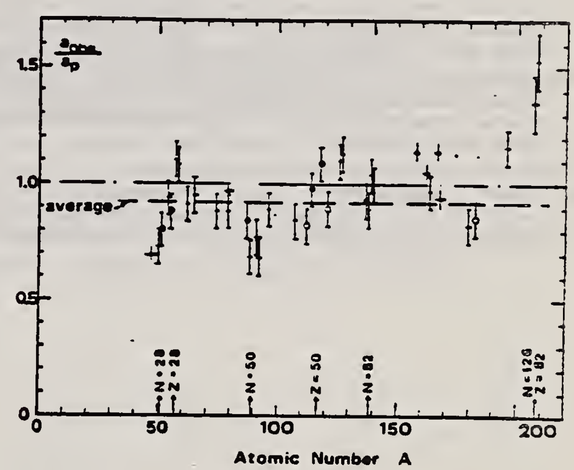

Fig. 15. Ratio a_{obs}/a_p versus atomic number A. Here a_{obs} is the level density parameter taken from the neutron resonance work of refs. [1,2]), and a_p is the level density parameter derived from the present (γ, n) work. Filled circles represent points where nuclei in the neutron resonance and in the (γ, n) experiment were the same. Open circles represent points where the respective nuclei were approximately matched. Triangles represent points which are based on measurement of neutron mean energies at two bremsstrahlung energies only.

(over)

Table 3 (continued)

Target	N (residual nucleus) [a]		Goodness of fit [b] no p.c.	Goodness of fit [b] with p.c.	$\hat{E}_n(24)$ (MeV) [c]	T (MeV) [d]	a_p (MeV^{-1}) [e]	a_{obs} (MeV^{-1}) [f]	a_{obs}/a_p
Ba	75	1%		F	1.16		16.5–^{136}Ba	15.39–^{136}Ba	0.93
	77	2%							
	78	7%							
	79	8%							
	80	11%							
	81	71%							
La	80	100%	F	F	1.25	0.72	15.5–^{138}La	13.76–^{139}La	0.89
Ce	81	89%	F	G	1.24	0.70	17.0–^{139}Ce	17.8 –^{141}Ce	1.04
	83	11%							
Pr	81	100%	G	G	1.17	0.65	17.0–^{140}Pr	17.05–^{142}Pr	1.00
Tb [g]	93	100%			1.15		19.3–^{158}Tb	21.85–^{160}Tb	1.14
Dy [g]	93	2%			1.06		20.9–$^{161.5}$Dy	21.9 –^{162}Dy	1.05
	94	19%							
	95	25%							
	96	25%							
	97	28%							
Ho	97	100%	P	G	1.06	0.56	21.4–^{164}Ho	20.66–^{166}Ho	0.97
Er [g]	95	2%			1.11		19.2–^{166}Er	21.9 –^{166}Er	1.14
	97	33%							
	98	23%							
	99	27%							
	101	15%							
Tm [g]	99	100%			1.03		24.0–^{168}Tm	22.58–^{170}Tm	0.94
Ta	107	100%		G	1.00	0.49	26.0–^{180}Ta	21.2 –^{181}Ta	0.82
W	107	26%	G	F	0.98	0.50	27.0–^{183}W	23.0 –^{183}W	0.85
	108	14%							
	109	31%							
	111	28%							
Au	117	100%		G	1.19		17.5–^{196}Au	20.24–^{198}Au	1.16
Pb ($Z = 82$)	123	24%		V.P.	1.87	1.20	7.5–^{206}Pb	10.1 –^{207}Pb	1.35
	124	23%							
	125	52%							
Bi	125	100%		F	1.65	1.03	9.0–^{208}Bi	13.8 –^{210}Bi	1.53

[a]) Neutron numbers and abundances of respective residual nuclei in (γ, n) experiments.

[b]) These give an assessment of the goodness of fit of a calculated $\hat{E}_n$ versus E_0 curve to the observed data, using the Fermi gas level density formula both without and with pairing corrections.

[c]) Bremsstrahlung photoneutron mean energies $\hat{E}_n$ for peak bremsstrahlung energy $E_0 = 24$ MeV.

[d]) Nuclear temperature from fit with constant-temperature formula.

[e]) Level density parameter a_p derived from the present (γ, n) experiment, using a Fermi gas formula plus pairing correction, and corresponding residual nucleus (the atomic weight shown is the weighted average of atomic weights of the respective isotopes present).

[f]) As column 7, but using data on n-resonance absorption from refs. [1,2]).

[g]) Measurements of $\hat{E}_n(E_0)$ for these nuclei were made only for $E_0 = 21$, 23 and 24 MeV.

REF.

H.E. Jackson, G.E. Thomas, and K.J. Wetzel
Phys. Rev. C9, 1153 (1974)

ELEM. SYM.	A	Z
Tb	159	65

METHOD

REF. NO.

74 Ja 2 hmg

REACTION	RESULT	EXCITATION ENERGY	SOURCE TYPE	SOURCE RANGE	DETECTOR TYPE	DETECTOR RANGE	ANGLE
G,G	ABX	10	D	10	SCD-D		90
		(10.83)		(10.83)			

TABLE I. Differential cross sections measured for elastic and inelastic scattering of 10.83-MeV photons. State or states populated by inelastic scattering are indicated in parentheses below the target. The errors given result from the statistical error in the measurement of the cross section relative to the calibration value, the 90° uranium inelastic cross section.

Nucleus	θ (deg)	$d\sigma/d\omega$ (elastic) (mb/sr)	$d\sigma/d\omega$ (inelastic) (mb/sr)
^{238}U			
(2^+, 45 keV)	20	1.72 ±0.17	
	30	0.97 ±0.12	
	50	0.334 ±0.039	
	60	0.23 ±0.04	
	70	0.245 ±0.024	0.136 ±0.015
	90	0.182 ±0.017	0.154 ±0.012
	120	0.189 ±0.017	0.160 ±0.013
	150	0.303 ±0.016	0.160 ±0.015
^{232}Th			
(2^+, 45 keV)	90	0.129 ±0.015	0.103 ±0.007
Pb	20	1.28 ±0.12	
	30	0.55 ±0.07	
	50	0.289 ±0.051	
	60	0.20 ±0.04	
	70	0.087 ±0.014	
	90	0.079 ±0.005	
	120	0.060 ±0.004	
	150	0.127 ±0.008	
^{209}Bi			
($\frac{1}{2}^-$, 910 keV)	90	0.101 ±0.0062	~0
^{181}Ta			
($\frac{9}{2}^+$, 136 keV)	90	0.0370 ± 0.003	0.006 56 ± 0.0015
^{159}Tb			
($\frac{5}{2}^+$, 58 keV)	90	0.0314 ± 0.003	0.0110 ± 0.0016
$\frac{7}{2}^+$, 138 keV)			0.005 11 ± 0.0011

TABLE III. Comparison of calculated and observed values of the 90° cross sections for elastic scattering and of the ratio at 90° of Raman to elastic scattering by various nuclei for 10.83-MeV photons. The parameters used in the calculations are given in Table II.

Target	$d\sigma_{elas}(90°)/d\Omega$ (mb/sr) Calc	Exp	$d\sigma^{(90°)}_{Raman}/d\sigma^{(90°)}_{elas}$ Calc	Exp
Tb	0.036	0.031 ± 0.003	0.80	0.51 ± 0.06
Ta	0.055	0.037 ± 0.003	0.28	0.18 ± 0.04
Pb	0.076	0.079 ± 0.005	0	
Bi		0.101 ± 0.006	0	~0
Th	0.128	0.129 ± 0.015	0.91	0.80 ± 0.08
U	0.157[a]	0.182 ± 0.017	1.03	0.85 ± 0.08

[a] If the Livermore parameters (Ref. 33) for ^{235}U are used then this calculated value would be 0.210 mb/sr.

33
C.D. Bowman, G.F. Auchampauch, and S.C. Fultz, Phys. Rev. 133, B676 (1964).

REF. H. E. Jackson, G. E. Thomas, K. J. Wetzel
Phys. Rev. C11, 1664 (1975)

ELEM. SYM.	A	Z
Tb	159	65

METHOD

REF. NO.	
75 Ja 1	hmg

REACTION	RESULT	EXCITATION ENERGY	SOURCE TYPE	SOURCE RANGE	DETECTOR TYPE	DETECTOR RANGE	ANGLE
G,G	ABX	11	D	11	SCD-D		DST
		(11.387)		(11.387)			

RATIO RAMAN/ELASTIC

TABLE I. Differential cross sections measured for elastic and inelastic scattering of 11.39-MeV photons. State or states populated by inelastic scattering are indicated in parentheses beside the target. The errors given result from the statistical error in the measurement of the cross section relative to the calibration value, the 90° uranium elastic cross section.

θ (deg)	$d\sigma/d\omega$ (elastic) (mb/sr)	$d\sigma/d\omega$ (inelastic) (mb/sr)
	^{238}U (2$^+$, 45 keV)	
90	0.169±0.011	0.173±0.016
150	0.355±0.041	0.236±0.24
	^{232}Th (2$^+$, 45 keV)	
150	0.331±0.035	0.210±0.022
	^{181}Ta ($\frac{9}{2}^+$, 136 keV) ($\frac{11}{2}^+$, 301 keV)	
90	0.073±0.008	0.020±0.004 0.009±0.004
150	0.145±0.015	0.017±0.004 0.017±0.004
	^{165}Ho ($\frac{9}{2}^+$, 95 keV) ($\frac{11}{2}^+$, 210 keV)	
150	0.141±0.014	0.022±0.004 0.013±0.004
	^{159}Tb ($\frac{5}{2}^+$, 58 keV) ($\frac{7}{2}^+$, 138 keV)	
90	0.062±0.006	0.024±0.003 0.013±0.003
150	0.134±0.012	0.042±0.004 0.019±0.004
	^{141}Pr	
150	0.030±0.008	...

TABLE III. Comparison of calculated and observed values of the cross sections for elastic scattering and of the ratio of Raman to elastic scattering by various nuclei for 11.387-MeV photons at 90 and 150°. The parameters used in the calculations for column 5 are given in Table II. Column 4 describes results obtained by perturbing those parameter to meet the constraint of Eq. (3) (see text).

Target	$d\sigma(\theta)d\Omega$ (mb/sr) Calc.	Exp.	$d\sigma_{\mathrm{Raman}}(\theta)/d\sigma_{\mathrm{elastic}}(\theta)$		
		$\theta=150°$			
Pr	0.025	0.030±0.008		0.0	0.0
Tb	0.094	0.134±0.012	0.53	0.57	0.46±0.04
Ho	0.170	0.141±0.014	0.28	0.28	0.25±0.04
Ta	0.160	0.145±0.015	0.23	0.22	0.23±0.04
Th	0.253	0.331±0.035	0.59	0.63	0.64±0.08
U	0.289	0.355±0.041	0.78	0.73	0.67±0.07
		$\theta=90°$			
Tb	0.062	0.062±0.006	0.76	0.82	0.60±0.07
Ta	0.109	0.074±0.008	0.32	0.30	0.38±0.07
U	0.172	0.169±0.008	1.29	1.15	1.03±0.10

REF.	ELEM. SYM.	A	Z
V. Emma, S. Lo Nigro, C. Milone Nucl. Phys. A257, 438 (1976)	Tb	159	65

METHOD	REF. NO.	
	76 Em 2	egf

REACTION	RESULT	EXCITATION ENERGY	SOURCE TYPE	SOURCE RANGE	DETECTOR TYPE	DETECTOR RANGE	ANGLE
G,F	ABY	THR-999	C	999	TRK-I		4PI

999 = 1 GEV

TABLE I

Measured values of σ_q at $E = 1000$ MeV and deduced values of σ_t assumed constant from E_0 to 1000 MeV

Element	Z^2/A	σ_q (mb)	E_0 (MeV)	σ_t (mb)
Bi	32.96	12.3 ± 0.6	200	7.6 ± 0.6
Pb	32.45	5.4 ± 0.4	220	3.6 ± 0.3
Tl	32.10	4.1 ± 0.3	230	2.8 ± 0.3
Au	31.68	2.0 ± 0.15	240	1.4 ± 0.2
Pt	31.18	1.1 ± 0.08	255	$(8 \pm 0.7) \times 10^{-1}$
Re	30.21	$(3.7 \pm 0.3) \times 10^{-1}$	280	$(2.9 \pm 0.3) \times 10^{-1}$
W	29.78	$(3.5 \pm 0.3) \times 10^{-1}$	290	$(2.8 \pm 0.3) \times 10^{-1}$
Ta	29.45	$(3.3 \pm 0.3) \times 10^{-1}$	300	$(2.7 \pm 0.3) \times 10^{-1}$
Hf	29.04	$(1.7 \pm 0.2) \times 10^{-1}$	310	$(1.4 \pm 0.2) \times 10^{-1}$
Yb	28.31	$(1.3 \pm 0.1) \times 10^{-1}$	330	$(1.2 \pm 0.1) \times 10^{-1}$
Tm	28.18	$(7.5 \pm 0.8) \times 10^{-2}$	335	$(6.8 \pm 0.8) \times 10^{-2}$
Ho	27.21	$(3.6 \pm 0.4) \times 10^{-2}$	355	$(3.5 \pm 0.4) \times 10^{-2}$
Dy	26.80	$(2.6 \pm 0.3) \times 10^{-2}$	360	$(2.5 \pm 0.3) \times 10^{-2}$
Tb	26.58	$(2.5 \pm 0.3) \times 10^{-2}$	370	$(2.5 \pm 0.3) \times 10^{-2}$
Gd	26.04	$(1.6 \pm 0.2) \times 10^{-2}$	380	$(1.7 \pm 0.2) \times 10^{-2}$
Sm	25.56	$(1.3 \pm 0.2) \times 10^{-2}$	390	$(1.4 \pm 0.2) \times 10^{-2}$
Nd	24.96	$(9.2 \pm 0.9) \times 10^{-3}$	405	$(1 \pm 0.1) \times 10^{-2}$
Ce	24.00	$(8 \pm 0.9) \times 10^{-3}$	420	$(9 \pm 1) \times 10^{-3}$
La	23.39	$(8.4 \pm 0.9) \times 10^{-3}$	430	$(1 \pm 0.1) \times 10^{-3}$
Sb	21.36	$(1.2 \pm 0.2) \times 10^{-2}$	460	$(1.5 \pm 0.3) \times 10^{-2}$
Te	21.19	$(8.8 \pm 1) \times 10^{-3}$	465	$(1.2 \pm 0.2) \times 10^{-2}$
Sn	21.06	$(1.3 \pm 0.2) \times 10^{-2}$	465	$(1.7 \pm 0.3) \times 10^{-2}$
Cd	20.49	$(1.7 \pm 0.3) \times 10^{-2}$	470	$(2.2 \pm 0.4) \times 10^{-2}$
Ag	20.47	$(2 \pm 0.3) \times 10^{-2}$	470	$(2.6 \pm 0.4) \times 10^{-2}$
Zn	13.76	$(2 \pm 0.4) \times 10^{-1}$	515	$(3 \pm 0.6) \times 10^{-1}$
Cu	13.44	$(2.4 \pm 0.5) \times 10^{-1}$	515	$(3.6 \pm 0.8) \times 10^{-1}$
Ni	13.35	$(2.4 \pm 0.5) \times 10^{-1}$	510	$(3.6 \pm 0.8) \times 10^{-1}$
Fe	12.10	$(3 \pm 0.6) \times 10^{-1}$	510	$(4.4 \pm 0.9) \times 10^{-1}$

[4] A.V. Mitrofanova et al. Sov. J. Nucl. Phys. 6, 512 (1968).

[7] T. Methasiri et al., Nucl. Phys. A167, 97 (1971).

[12] J.R. Nix et al., Nucl. Phys. 81, 61 (1966).

[20] N.A. Perifilov et al., JETP (Sov. Phys.) 14, 623 (1962); Proc. Symp. on the physics & chemistry of fission, Salzburg 1965, vol. 2 (IAEA) Vienna, 1965, p.283.

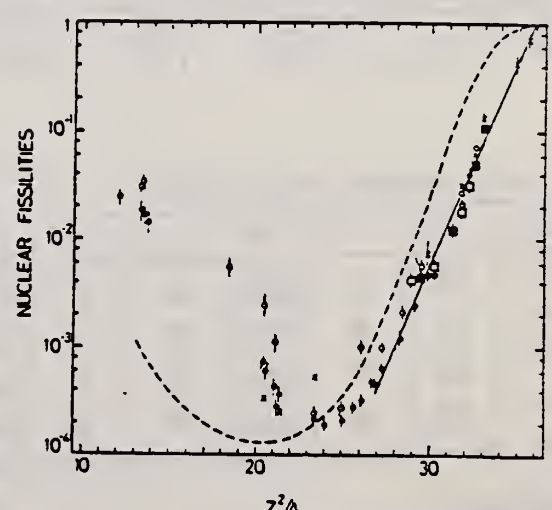

Fig. 2. Nuclear fissilities as a function of Z^2/A. Experimental points: solid circles represent our data; squares, the data from ref. [4]; open circles, the data from ref. [7]; and crosses, the data from (p,f) experiments[20]. The straight line is the best fit calculated from our data for $Z^2/A > 26$. The dashed curve is the curve VI calculated by Nix and Sassi[12].

REF.	ELEM. SYM.	A	Z
B. I. Goryachev, Yu.V. Kuznetsov, V.N. Orlin, N.A. Pzhidaeva, V. G. Shevchenko Yad. Fiz. 23, 1145 (1976) Sov. J. Nucl. Phys. 23, 609 (1976)	Tb	159	65
METHOD	REF. NO. 76 Go 4		hmg

REACTION	RESULT	EXCITATION ENERGY	SOURCE TYPE	SOURCE RANGE	DETECTOR TYPE	DETECTOR RANGE	ANGLE
G,XN	ABX	8- 23	C	UKN	BF3-I		4PI
G,2N	ABX	15- 21	C	UKN	SCI-I		4PI

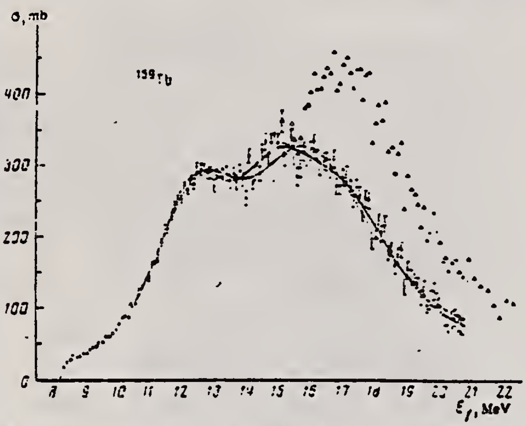

FIG. 3. Photoabsorption cross section σ_γ for ^{159}Tb (hollow and solid circles). Above the (γ, $2n$) threshold we have shown by the triangles the cross section σ_n. The thin and thick curves show respectively the fits $\bar{\sigma}_\gamma^{(2)}$ ($\sigma_1\Gamma_1:\sigma_2\Gamma_2 = 1:2$) and $\bar{\sigma}_\gamma^{(3)}$ ($\sigma_1\Gamma_1:\sigma_2\Gamma_2:\sigma_3\Gamma_3 = 1:1:1$).

TABLE 3. Static deformation β and intrinsic quadrupole moment Q_0.

Nucleus	Present work		Other photonuclear experiments		Coulomb excitation of nuclei
	β	Q_0, b	β	Q_0, b	Q_0, b
^{159}Tb	0.29	6.53±0.6	0.29 0.32 0.29	6.57 [18] 7.37 [20] 6.8 [21]	7.07 [19]
^{165}Ho	0.32	7.73±0.6	0.29 0.30 0.31	7.01 [18] 7.14 [20] 7.6 [19]	7.50 [19]
^{166}Er	0.30	7.39±0.6	0.28 0.31	6.96 [18] 7.8 [16]	
^{178}Hf	0.28	6.94±0.6			6.79 [22]

TABLE 6. Integrated cross sections.

Nucleus	σ_0, MeV-b	σ_0, 0.06 $\frac{ZN}{A}$	σ_{-1}, mb	σ_{-1}, $A^{4/3}$	σ_{-2}, MeV-b	σ_{-2}, $A^{5/3}$
^{159}Tb	3.70	1.47	210	0.263	15.9	3.41·10⁻³
^{165}Ho	3.60	1.51	218	0.241	16.1	3.2[illegible]·10⁻³
^{166}Er	3.56	1.48	216	0.237	16.1	3.21·10⁻³
^{178}Hf	3.09	1.20	196	0.196	14.8	2.03·10⁻³
Average		1.41±0.3		0.23±0.04		3.1·10⁻³±6·10⁻⁴

TABLE 1. Level-density parameters

Nucleus	a, MeV⁻¹ Present work	a, MeV⁻¹ Other studies	Nucleus	a, MeV⁻¹ Present work	a, MeV⁻¹ Other studies
^{159}Tb	—	7.7 [15]	^{166}Er	6.1±2.5	8 [16]
^{165}Ho	4.2±1.5	3.1 [15]	^{178}Hf	17.7±7.3	—

TABLE 2. Parameters of fitted curves $\bar{\sigma}_\gamma^{(2)}$

Nucleus	E_1, MeV	σ_1, mb	Γ_1, MeV	E_2, MeV	σ_2, mb	Γ_2, MeV	$\sigma_2\Gamma_2/\sigma_1\Gamma_1$	χ^2	f	E_t, MeV	E_u, MeV
^{159}Tb	12.23 12.41	192 213	2.91±0.09 3.31±0.05	15.78 15.95	295 282	5.42±0.13 5.01±0.07	2.38±0.23 2	197.3 216.8	97 98	10.4 10.4	20.8 20.6
^{165}Ho	12.31 12.67	208 225	2.74±0.11 3.26±0.06	16.23 16.40	300 293	5.67±0.17 5.02±0.09	3.11±0.27 2	176.0 200.8	97 98	10.4 10.4	20.8 20.6
^{166}Er	12.32 12.50	191 214	2.71±0.14 3.43±0.08	15.99 16.25	308 259	5.67±0.16 5.09±0.10	3.38±0.35 2	138.5 101.7	94 95	10.7 10.7	20.6 20.6
^{178}Hf	12.08 12.86	166 216	2.55±.10 3.22±0.11	15.03 15.46	281 237	6.09±0.27 5.37±0.20	4.00±1.76 2	172.1 173.7	89 90	10.8 10.8	20.0 20.0

Note. The lower values of the parameters in each column were found with the requirement $\sigma_2\Gamma_2:\sigma_1\Gamma_1 = 2:1$.

(over)

[12]A.N. Tikhonov, Dokl. Akad. Nauk SSSR 151, 501 (1963), Eng. transl. in Sov. Mathematics-Doklady.

[15]B. L. Berman et al., Phys. Rev. 185, 1576 (1969).

[16]R. Bergere et al., Nucl. Phys. A133, 417 (1969).

[18]E. G. Fuller et al., Nucl. Phys. 30, 613 (1962).

[19]H. Arenhovel et al., Phys. Rev. 157, 1109 (1967).

[20]R. Bergere et al., Nucl. Phys. A121, 463 (1968).

[21]O.V. Bogdankevich et al., Zh. Eksp.Teor.Fiz. 42, 1502 (1962); Sov. Phys. JETP 15, 1044 (1962).

[22]B.S. Dzhelepov in Struktura slozhynkh yader (Structure of Complex Nuclei), Atomizdat, 1966, p. 189.

REF.	ELEM. SYM.	A	Z
A. Suzuki and K. Shoda Nucl. Phys. A260, 172 (1976)	Tb	159	65

METHOD	REF. NO.	
	76 Su 2	egf

REACTION	RESULT	EXCITATION ENERGY	SOURCE TYPE	SOURCE RANGE	DETECTOR TYPE	DETECTOR RANGE	ANGLE
E,P	ABX	11- 18	D	15- 18	MAG-D		125

Proton yields obtained by summing protons with energies above levels given in tables.

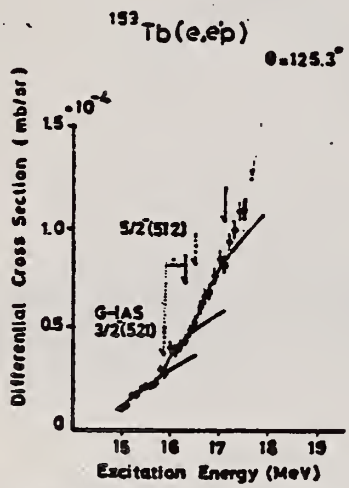

Fig. 2. Cross section of the ^{159}Tb(e, e'p) reactions. The solid curve and the dashed arrows are the cross sections and the IAR position obtained by the best fitting to the data with eq. (25). Solid arrows is the position of IAS estimated with eq. (20). G-IAS means the IAS of the ground state and the indicated figures are spin-parity and quantum numbers for the corresponding resonances.

TABLE 1

Parameters of the present experiment

Target	Atomic number	Purity (%)	Thickness (mg/cm^2)	Lowest proton energy (MeV)	Bin size (keV)	Range of measurement (MeV)
^{159}Tb	65	99.9 (natural)	14.87	4.70	100	15.0 –17.5
^{165}Ho	67	99.9 (natural)	11.64	4.70	100	15.5 –17.5
^{169}Tm	69	99 (natural)	13.40	4.70	100	15.0 –18.0
^{175}Lu	71	99.87 (enriched)	5.24	5.34	150	15.05–20.0
^{181}Ta	73	99.9 (natural)	6.73	6.16	200	16.0 –23.0

TABLE 3

Displacement energies obtained from the present data and the estimates with eqs. (20) and (21)

Target	Resonance	E^* (MeV)	E_d (exp) (MeV)	E_d a) (MeV)	$E_d(\delta = 0.3)$ b) (MeV)
^{159}Tb	1st	15.75±0.15	15.58	16.06	15.93
	2nd	16.50±0.15	15.46		
^{165}Ho	1st	16.15±0.14	15.64	16.38	16.25
^{169}Tm	1st	15.76±0.13	16.20	16.76	16.63
	2nd	16.34±0.14	16.22		
^{175}Lu	1st	16.44±0.13	16.75	17.07	16.93
	2nd	17.45±0.15	16.35		
^{181}Ta	1st	17.31±0.15	16.40	17.38	17.24

a) Estimated with eq. (20).
b) Estimated with eq. (21).

TABLE 4

Deformation parameters of IAS δ_{IAR} derived from the (e, e'p) result

Target	Resonance	IAS	Parent state	$\delta_{IAR}-\delta_p$ a)	δ_p (assumed)	δ_{IAR} a)
^{159}Tb	1st	$\frac{3}{2}^-$[521]	ground	–0.008	0.31	0.30
	2nd	$\frac{5}{2}^-$[512]	875 keV	–0.016		0.29
^{165}Ho	1st	$\frac{7}{2}^+$[633]	ground	–0.023	0.30	0.28
^{169}Tm	1st	$\frac{1}{2}^-$[521]	ground	–0.018	0.29	0.27
	2nd	$\frac{1}{2}^-$[510]	565 keV	–0.019		0.27
^{175}Lu	1st	$\frac{7}{2}^-$[514]	ground	–0.010	0.28	0.27
	2nd	$\frac{7}{2}^-$[503]	1420 keV	–0.029		0.25
^{181}Ta	1st	$\frac{7}{2}^-$[503]	670 keV	–0.046	0.26	0.21

The assumed deformation parameters for the parent states δ_p are also shown.
a) The errors are about ±0.01.

REF.	ELEM. SYM.	A	Z
T. Bar-Noy and R. Moreh Nucl. Phys. A275, 151 (1977)	Tb	159	65

METHOD	REF. NO.	
	77 Ba 7	egf

REACTION	RESULT	EXCITATION ENERGY	SOURCE TYPE	SOURCE RANGE	DETECTOR TYPE	DETECTOR RANGE	ANGLE
G,G	ABX	8- 12	D	8- 12	SCD-D		DST

Abstract: Differential cross sections for elastic and inelastic Raman scattering from the deformed heavy nuclei ^{159}Tb, ^{165}Ho and ^{237}Np were measured at five energies between 8.5 and 11.4 MeV. Angular distributions at four angles between 90° and 140° for both elastic and inelastic scattering at 9.0 and 11.4 MeV were also measured. The monoenergetic photons were obtained from thermal neutron capture in Ni and Cr. All the angular distributions and the elastic and Raman scattering at the higher energies are in good overall agreement with theoretical predictions. The theory is based on a modified simple rotator model of the giant dipole resonance in which the effect of Delbrück scattering was included. A trend of both the elastic and Raman scattering at lower energies to be stronger than expected are suggested by the data. However, the ratio between the Raman and elastic scattering seem to be in good agreement with theory throughout the whole energy range. This shows that there is no need to introduce a direct nonresonant component to the imaginary part of the elastic scattering amplitude to explain the experimental data.

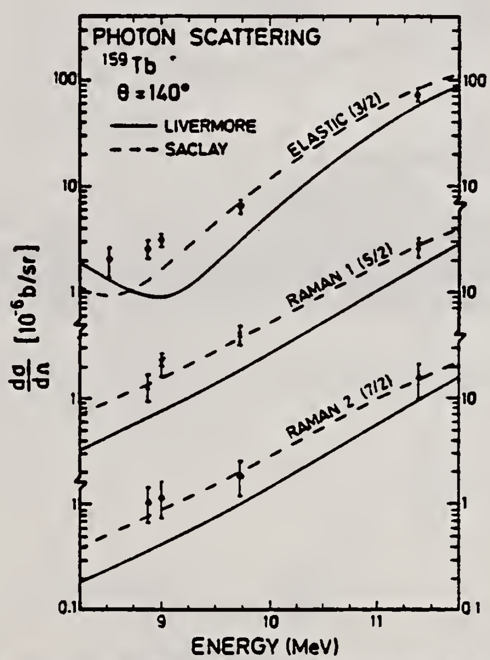

Fig. 5. Elastic and Raman inelastic differential scattering cross sections from ^{159}Tb at 140°. In the solid and dashed lines, the nuclear resonance amplitudes were obtained using parameters extracted from fits made to the Livermore and Saclay measurements respectively. (See text, table 3 and caption to fig. 3.)

over

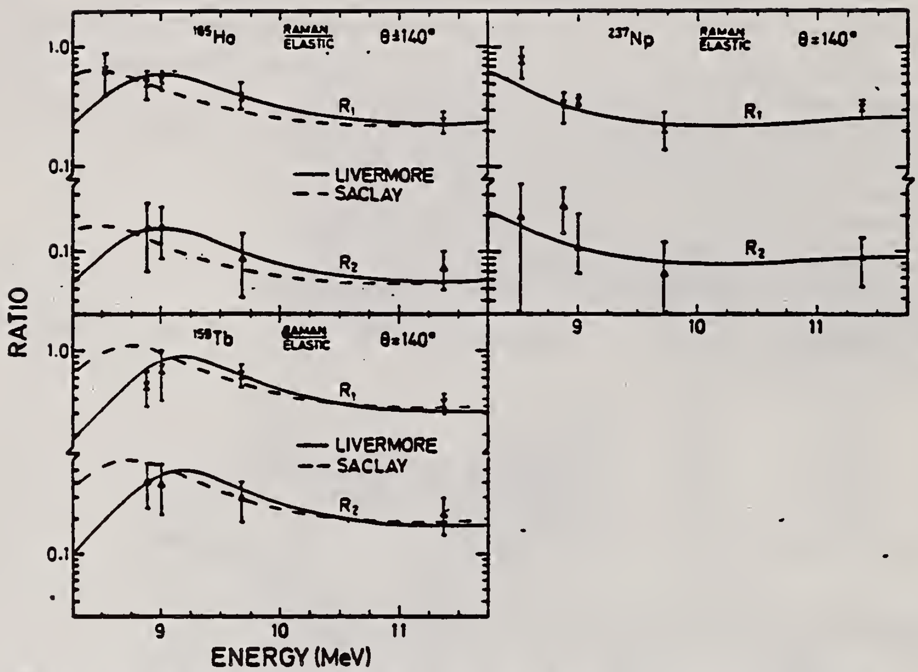

Fig. 6. Ratios of Raman/elastic scattering cross sections at 140° for ^{237}Np, ^{165}Ho and ^{159}Tb targets. Here, R_1 and R_2 refer to the first and second Raman lines. In the solid and dashed lines, the nuclear resonance amplitudes were obtained using parameters extracted from fits made to the Livermore and Saclay measurements respectively. (See text, table 3 and caption to fig. 3.)

REF.	J.J. Murphy II, H.J. Gehrhardt and D.M. Skopik Nucl. Phys. A277, 69 (1977)	ELEM. SYM.	A	Z
		Tb	159	65

METHOD	REF. NO.	
	77 Mu 3	egf

REACTION	RESULT	EXCITATION ENERGY	SOURCE TYPE	SOURCE RANGE	DETECTOR TYPE	DETECTOR RANGE	ANGLE
E,A	ABX	12-100	D	100	MAG-D		50

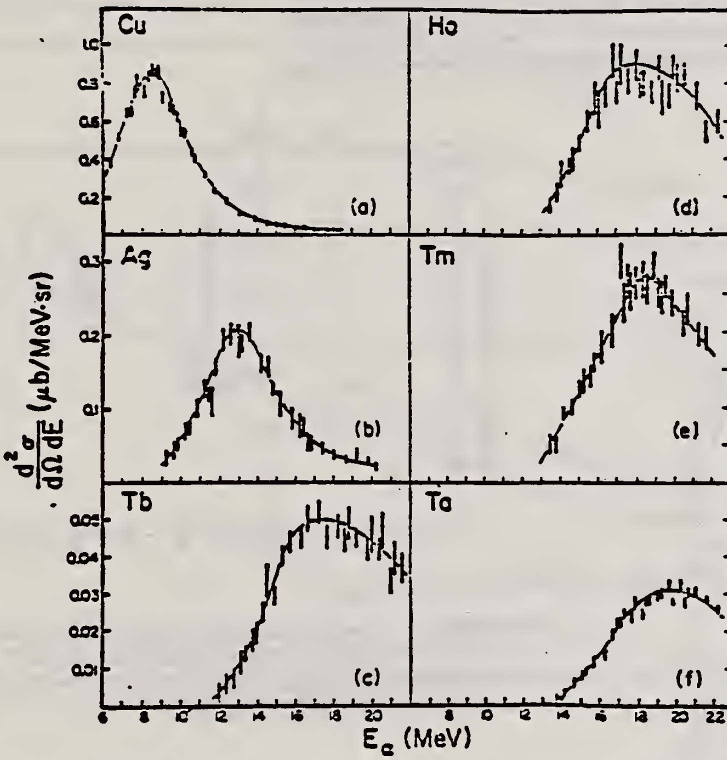

Fig. 1. The α-particle energy spectra at 50° in the lab for the six nuclei studied. Note that as Z increases, the cross section decreases and the energy of the peak increases. Errors are statistical. Curves are to guide the eye.

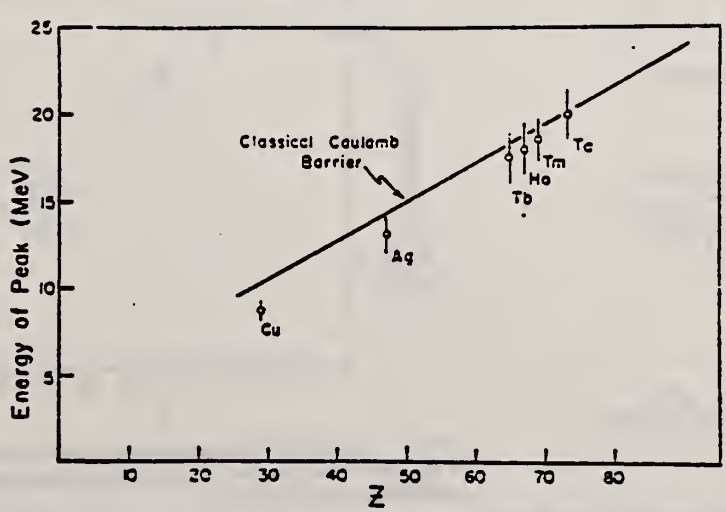

Fig. 2. Energy of the cross section peak as a function of Z. The solid line is the energy of the classical Coulomb barrier.

REF.	ELEM. SYM.	A	Z
J.J. Murphy, II, D.M. Skopik, J. Asai, and J. Uegaki Phys. Rev. C 18, 736 (1978)	Tb	159	65
METHOD	REF. NO. 78 Mu 9		hg

REACTION	RESULT	EXCITATION ENERGY	SOURCE TYPE	SOURCE RANGE	DETECTOR TYPE	DETECTOR RANGE	ANGLE
E,A	ABX	5-100	D	100	MAG-D		DST

α particles from the electrodisintegration of seven nuclei with Z between 29 and 79 have been observed. Energy spectra at 50° in the laboratory for six nuclei and angular distributions for five nuclei are reported. The cross sections exhibit a broad peak whose magnitude decreases with increasing Z; the energy of the peak increases as Z increases. Angular distributions at the highest energies measured become increasingly forward peaked suggesting a direct-reaction process.

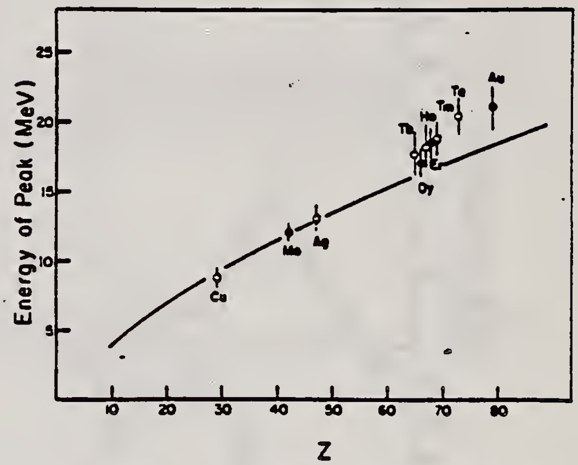

FIG. 3. Energy of the cross section peak as a function of Z. The solid line is the energy of the classical Coulomb barrier. The closed circles are the current work; the open circles are from Ref. 1.

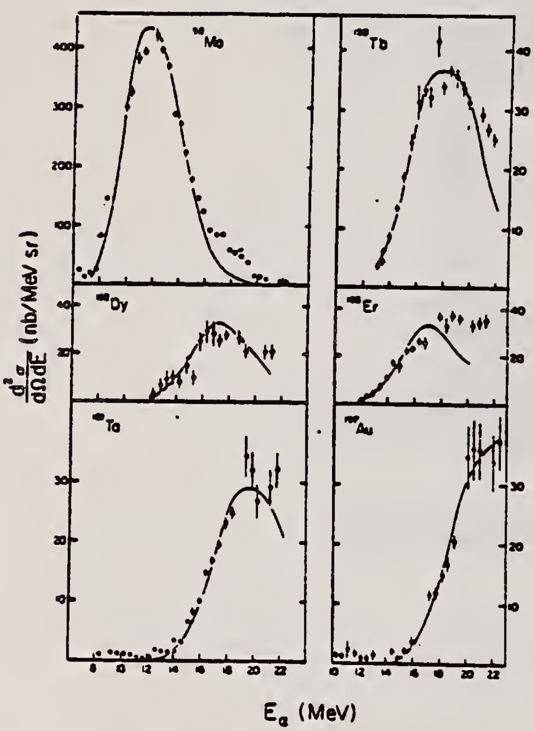

FIG. 2. The α-particle energy spectra at 50° in the laboratory for the four new nuclei studied as well as for two nuclei in which additional data have been obtained. The solid curves are the evaporation model fits described in text.

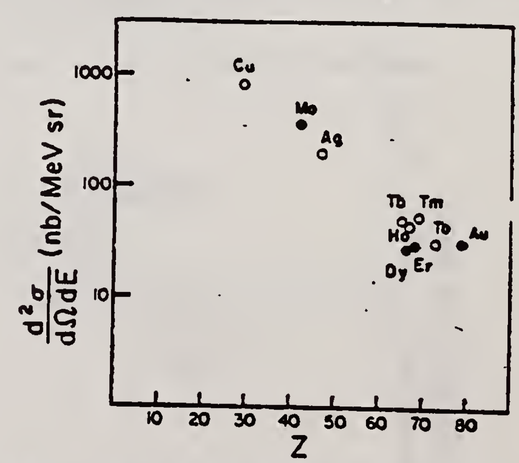

FIG. 4. Magnitude of cross section peak as a function of Z. The closed circles are the current work; the open circles are from Ref. 1.

[1] J.J. Murphy, II, H.J. Gehrhardt, and D.M. Skopik, Nucl. Phys. A277, 69 (1977).

over

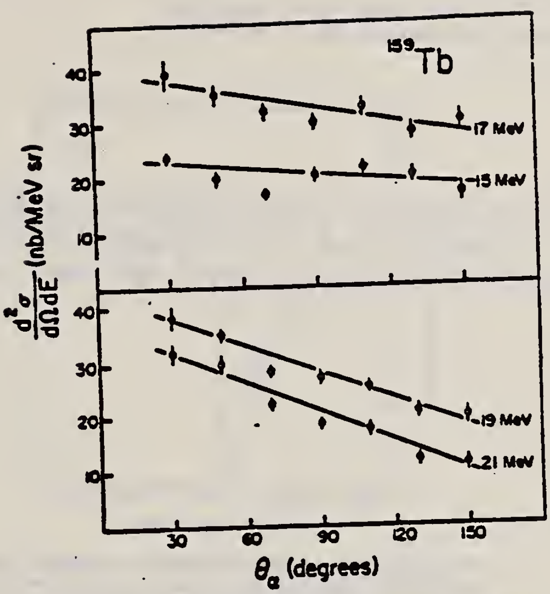

FIG. 6. Angular distributions for terbium. The comments made for Fig. 5 apply here.

REF. A. Jarund, K.R. Lindgren, B. Forkman
J. Inorg. Nucl. Chem. 43, 1725 (1981)

ELEM. SYM.	A	Z
Tb	159	65

METHOD

REF. NO.	
81 Ja 1	hg

REACTION	RESULT	EXCITATION ENERGY	SOURCE TYPE	SOURCE RANGE	DETECTOR TYPE	DETECTOR RANGE	ANGLE
G,NA24	ABY	THR-800	C	400-800	ACT-I		4PI

Abstract—The cross section for photoproduction of ^{24}Na from ^{159}Tb has been measured in the energy range 400–800 MeV. The present experimental cross section together with earlier measured ones are compared to calculations where ^{24}Na is produced in a binary fission process.

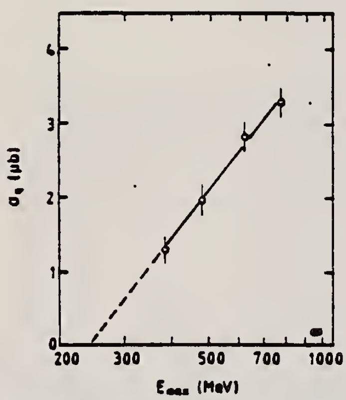

Fig. 1. Measured yields in cross section per equivalent quantum for production of ^{24}Na from ^{159}Tb as a function of maximum bremsstrahlung energy.

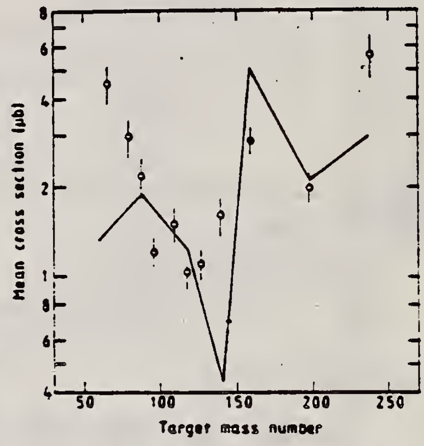

Fig. 2. Experimental mean cross sections as a function of target mass number. Open and filled circles are old and new data respectively. The curve is calculated as described in text.

DYSPROSIUM
Z=66

Lecoq de Boisbaudran separated what was called holmia into two earths; he called these holmia and dysprosia. The name dysprosium comes from the Greek *dyprositos* meaning "hard to get at".

REF.

R.G. Baker K.G. McNeill
Can. J. Phys. 39, 1158 (1961)

ELEM. SYM.		
Dy		66

METHOD Betatron; fast neutron yield, angular distribution; Si threshold detector; ion chamber

REF. NO.	
61 Ba 2	NVB

REACTION	RESULT	EXCITATION ENERGY	SOURCE		DETECTOR		ANGLE
			TYPE	RANGE	TYPE	RANGE	
G,XN	ABY	THR-22	C	22	THR-I	5-+	DST

In Table 4:

$\bar{\sigma}$ = average cross section of detector weighted with neutron spectrum

Φ = neutrons/100 roentgen/mole

$$W(\theta) = a_0 \sum_{n=1}^{\infty} [1 + A_n P_n (\cos \theta)]$$

TABLE IV

I Element	II a_0	III a_1	IV a_2	V $(\bar{\sigma}\Phi)\times10^{**}$	VI Φ_{total} (22 Mev) $\times10^7$	VII Φ_{fast}/Φ_{total}
Vanadium	245 (1±0.06)	0.01±0.08	−0.00±0.10	[illegible]	0.21	0.12
Chromium	164 (1±0.03)	0.04±0.04	−0.05±0.05	4.05	0.17	0.10
Manganese	308 (1±0.02)	0.07±0.03	−0.09±0.04	7.61	0.25	0.12
Iron	200 (1±0.03)	0.05±0.04	−0.17±0.05	4.94	0.18	0.11
Cobalt	390 (1±0.02)	0.08±0.03	−0.22±0.04	9.63	0.26	0.15
Nickel	145 (1±0.05)	0.07±0.07	−0.23±0.09	3.58	0.12	0.12
Copper	347 (1±0.02)	0.05±0.03	−0.29±0.04	8.57	0.30	0.12
Arsenic	482 (1±0.03)	0.11±0.04	−0.24±0.05	11.91	0.33	0.15
Rubidium	638 (1±0.05)	0.13±0.06	−0.14±0.08	15.76		
Strontium	409 (1±0.05)	0.10±0.06	−0.17±0.08	10.10		
Yttrium	290 (1±0.10)	0.08±0.12	−0.12±0.15	7.16		
Silver	590 (1±0.04)	0.10±0.06	−0.22±0.08	14.57	0.87	0.07
Cadmium	905 (1±0.02)	0.02±0.02	−0.26±0.03	22.35		
[illegible]	1133 (1±0.03)	0.04±0.04	−0.29±0.05	27.99	1.42	0.08
[illegible]	1048 (1±0.04)	0.10±0.06	−0.38±0.08	25.89		
Lanthanum	1595 (1±0.02)	0.02±0.03	−0.42±0.04	39.40	1.04	0.15
Cerium	1316 (1±0.05)	0.05±0.06	−0.39±0.08	32.50		
Dysprosium	1652 (1±0.08)	0.04±0.10	−0.34±0.13	40.80		
Tantalum	1558 (1±0.02)	0.04±0.03	−0.22±0.04	38.48	2.50	0.06
Tungsten	1365 (1±0.02)	−0.07±0.03	−0.24±0.04	33.71		
Mercury	1345 (1±0.02)	0.04±0.03	−0.31±0.04	33.22		
Lead	2274 (1±0.01)	0.02±0.02	−0.42±0.03	56.17	2.72	0.08
Bismuth	2162 (1±0.02)	0.05±0.03	−0.45±0.04	53.40	3.36	0.06
Thorium	3031 (1±0.04)	0.06±0.05	−0.32±0.07	74.87		
Uranium	4630 (1±0.02)	0.05±0.03	−0.17±0.04	114.36		

*$(\bar{\sigma}\Phi)$ = 2.47 × 10⁷ in millibarn-neutrons. Errors are standard errors due to counting statistics only.

U.S. DEPARTMENT OF COMMERCE
NATIONAL BUREAU OF STANDARDS

REF.	ELEM. SYM.	A	Z
R.F. Barrett, J.R. Birkelund, B.J. Thomas, K.S. Lam, and H.H. Thies Nucl. Phys. A210, 355 (1973)	Dy		66
METHOD	REF. NO. 73 Ba 20		egf

REACTION	RESULT	EXCITATION ENERGY	SOURCE TYPE	SOURCE RANGE	DETECTOR TYPE	DETECTOR RANGE	ANGLE
G,N	NOX	THR- 27	C	10- 27	BF3-I		4PI

MEAN NEUT ENERGY

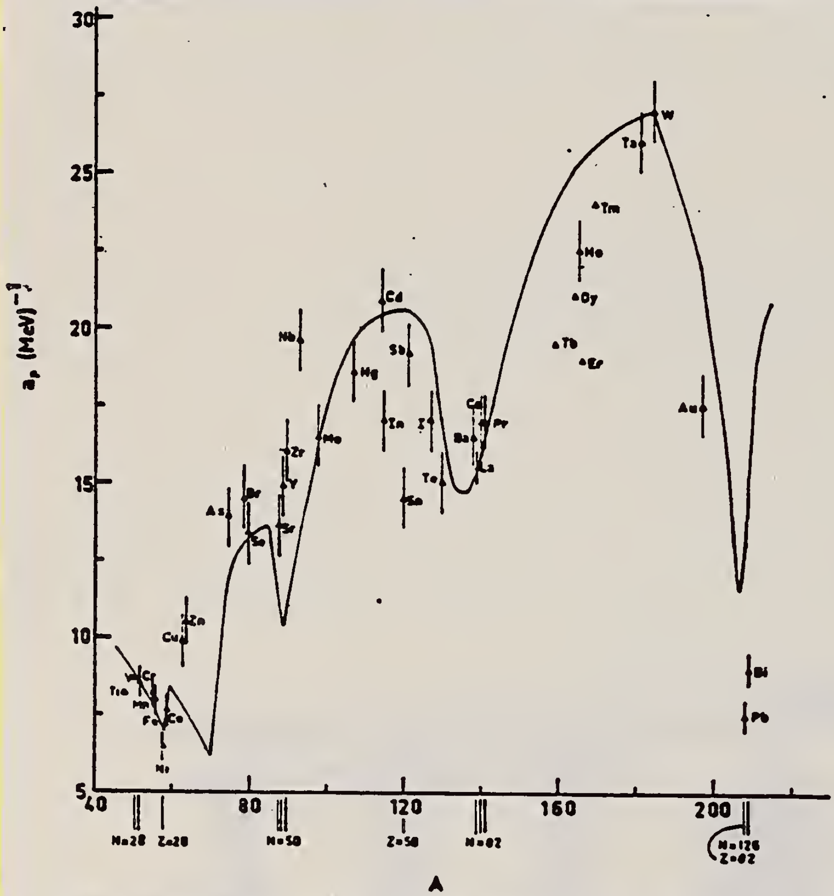

Fig. 12. Experimental values of the level density parameter a_p (Fermi gas formula plus pairing correction) versus atomic number A. The continuous curve is a least-squares fit to the data of a theoretical calculation from Newton [15]).

1
H. Baba and S. Baba, Japan Atomic Energy Research Institute report JAERI-1183 (1969).
2
H. Baba, Nucl. Phys. A159, 625 (1970).
15
T.D. Newton, Can. J. Phys. 34, 804 (1956).

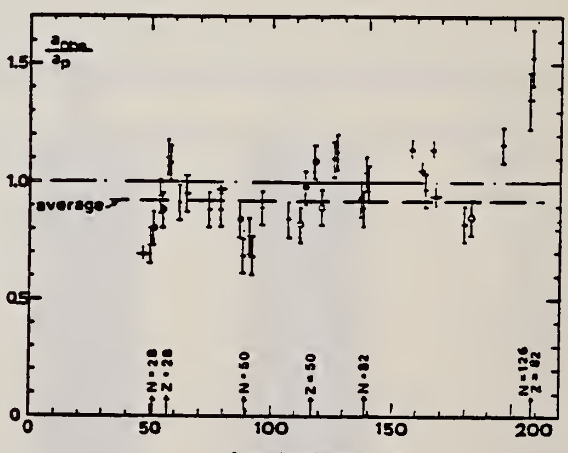

Fig. 15. Ratio a_{obs}/a_p versus atomic number A. Here a_{obs} is the level density parameter taken from the neutron resonance work of refs. [1,2]), and a_p is the level density parameter derived from the present (γ, n) work. Filled circles represent points where nuclei in the neutron resonance and in the (γ, n) experiment were the same. Open circles represent points where the respective nuclei were approximately matched. Triangles represent points which are based on measurement of neutron mean energies at two bremsstrahlung energies only.

(over)

Target	N (residual nucleus) [a]	Goodness of fit [b] no p.c.	Goodness of fit [b] with p.c.	$\hat{E}_n(24)$ (MeV) [c]	T (MeV) [d]	a_p (MeV^{-1}) [e]	a_{obs} (MeV^{-1}) [f]	a_{obs}/a_p
Ba	75 1%		F	1.16		16.5–^{136}Ba	15.39–^{136}Ba	0.93
	77 2%							
	78 7%							
	79 8%							
	80 11%							
	81 71%							
La	80 100%	F	F	1.25	0.72	15.5–^{138}La	13.76–^{139}La	0.89
Ce	81 89%	F	G	1.24	0.70	17.0–^{139}Ce	17.8 –^{141}Ce	1.04
	83 11%							
Pr	81 100%	G	G	1.17	0.65	17.0–^{140}Pr	17.05–^{142}Pr	1.00
Tb [g]	93 100%			1.15		19.3–^{158}Tb	21.85–^{160}Tb	1.14
Dy [g]	93 2%			1.06		20.9–$^{161.5}$Dy	21.9 –^{162}Dy	1.05
	94 19%							
	95 25%							
	96 25%							
	97 28%							
Ho	97 100%	P	G	1.06	0.56	21.4–^{164}Ho	20.66–^{166}Ho	0.97
Er [g]	95 2%			1.11		19.2–^{166}Er	21.9 –^{166}Er	1.14
	97 33%							
	98 23%							
	99 27%							
	101 15%							
Tm [g]	99 100%			1.03		24.0–^{168}Tm	22.58–^{170}Tm	0.94
Ta	107 100%		G	1.00	0.49	26.0–^{180}Ta	21.2 –^{181}Ta	0.82
W	107 26%	G	F	0.98	0.50	27.0–^{183}W	23.0 –^{183}W	0.85
	108 14%							
	109 31%							
	111 28%							
Au	117 100%		G	1.19		17.5–^{196}Au	20.24–^{198}Au	1.16
Pb ($Z = 82$)	123 24%		V.P.	1.87	1.20	7.5–^{206}Pb	10.1 –^{207}Pb	1.35
	124 23%							
	125 52%							
Bi	125 100%		F	1.65	1.03	9.0–^{208}Bi	13.8 –^{210}Bi	1.53

[a]) Neutron numbers and abundances of respective residual nuclei in (γ, n) experiments.

[b]) These give an assessment of the goodness of fit of a calculated $\hat{E}_n$ versus E_0 curve to the observed data, using the Fermi gas level density formula both without and with pairing corrections.

[c]) Bremsstrahlung photoneutron mean energies $\hat{E}_n$ for peak bremsstrahlung energy $E_0 = 24$ MeV.

[d]) Nuclear temperature from fit with constant-temperature formula.

[e]) Level density parameter a_p derived from the present (γ, n) experiment, using a Fermi gas formula plus pairing correction, and corresponding residual nucleus (the atomic weight shown is the weighted average of atomic weights of the respective isotopes present).

[f]) As column 7, but using data on n-resonance absorption from refs. [1,2]).

[g]) Measurements of $\hat{E}_n(E_0)$ for these nuclei were made only for $E_0 = 21$, 23 and 24 MeV.

REF.

V. Emma, S. Lo Nigro, C. Milone
Nucl. Phys. A257, 438 (1976)

ELEM. SYM.	A	Z
Dy		66

METHOD

REF. NO.	
76 Em 2	egf

REACTION	RESULT	EXCITATION ENERGY	SOURCE TYPE	SOURCE RANGE	DETECTOR TYPE	DETECTOR RANGE	ANGLE
G,F	ABY	THR-999	C	999	TRK-I		4PI

999 = 1 GEV

TABLE 1

Measured values of σ_q at $E = 1000$ MeV and deduced values of σ_k assumed constant from E_0 to 1000 MeV

Element	Z^2/A	σ_q (mb)	E_0 (MeV)	σ_k (mb)
Bi	32.96	12.3 ± 0.6	200	7.6 ± 0.6
Pb	32.45	5.4 ± 0.4	220	3.6 ± 0.3
Tl	32.10	4.1 ± 0.3	230	2.8 ± 0.3
Au	31.68	2.0 ± 0.15	240	1.4 ± 0.2
Pt	31.18	1.1 ± 0.08	255	$(8 \pm 0.7) \times 10^{-1}$
Re	30.21	$(3.7 \pm 0.3) \times 10^{-1}$	280	$(2.9 \pm 0.3) \times 10^{-1}$
W	29.78	$(3.5 \pm 0.3) \times 10^{-1}$	290	$(2.8 \pm 0.3) \times 10^{-1}$
Ta	29.45	$(3.3 \pm 0.3) \times 10^{-1}$	300	$(2.7 \pm 0.3) \times 10^{-1}$
Hf	29.04	$(1.7 \pm 0.2) \times 10^{-1}$	310	$(1.4 \pm 0.2) \times 10^{-1}$
Yb	28.31	$(1.3 \pm 0.1) \times 10^{-1}$	330	$(1.2 \pm 0.1) \times 10^{-1}$
Tm	28.18	$(7.5 \pm 0.8) \times 10^{-2}$	335	$(6.8 \pm 0.8) \times 10^{-2}$
Ho	27.21	$(3.6 \pm 0.4) \times 10^{-2}$	355	$(3.5 \pm 0.4) \times 10^{-2}$
Dy	26.80	$(2.6 \pm 0.3) \times 10^{-2}$	360	$(2.5 \pm 0.3) \times 10^{-2}$
Tb	26.58	$(2.5 \pm 0.3) \times 10^{-2}$	370	$(2.5 \pm 0.3) \times 10^{-2}$
Gd	26.04	$(1.6 \pm 0.2) \times 10^{-2}$	380	$(1.7 \pm 0.2) \times 10^{-2}$
Sm	25.56	$(1.3 \pm 0.2) \times 10^{-2}$	390	$(1.4 \pm 0.2) \times 10^{-2}$
Nd	24.96	$(9.2 \pm 0.9) \times 10^{-3}$	405	$(1 \pm 0.1) \times 10^{-2}$
Ce	24.00	$(8 \pm 0.9) \times 10^{-3}$	420	$(9 \pm 1) \times 10^{-3}$
La	23.39	$(8.4 \pm 0.9) \times 10^{-3}$	430	$(1 \pm 0.1) \times 10^{-3}$
Sb	21.36	$(1.2 \pm 0.2) \times 10^{-2}$	460	$(1.5 \pm 0.3) \times 10^{-2}$
Te	21.19	$(8.8 \pm 1) \times 10^{-3}$	465	$(1.2 \pm 0.2) \times 10^{-2}$
Sn	21.06	$(1.3 \pm 0.2) \times 10^{-2}$	465	$(1.7 \pm 0.3) \times 10^{-2}$
Cd	20.49	$(1.7 \pm 0.3) \times 10^{-2}$	470	$(2.2 \pm 0.4) \times 10^{-2}$
Ag	20.47	$(2 \pm 0.3) \times 10^{-2}$	470	$(2.6 \pm 0.4) \times 10^{-2}$
Zn	13.76	$(2 \pm 0.4) \times 10^{-1}$	515	$(3 \pm 0.6) \times 10^{-1}$
Cu	13.44	$(2.4 \pm 0.5) \times 10^{-1}$	515	$(3.6 \pm 0.8) \times 10^{-1}$
Ni	13.35	$(2.4 \pm 0.5) \times 10^{-1}$	510	$(3.6 \pm 0.8) \times 10^{-1}$
Fe	12.10	$(3 \pm 0.6) \times 10^{-1}$	510	$(4.4 \pm 0.9) \times 10^{-1}$

[4] A.V. Mitrofanova et al. Sov. J. Nucl. Phys. 6, 512 (1968).

[7] T. Methasiri et al., Nucl. Phys. A167, 97 (1971).

[12] J.R. Nix et al., Nucl. Phys. 81, 61 (1966).

[20] N.A. Perifilov et al., JETP (Sov. Phys.) 14, 623 (1962); Proc. Symp. on the physics & chemistry of fission, Salzburg 1965, vol. 2 (IAEA) Vienna, 1965, p.283.

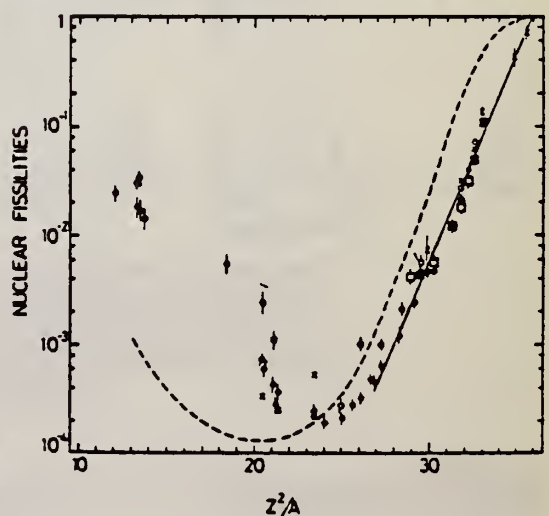

Fig. 2. Nuclear fissilities as a function of Z^2/A. Experimental points: solid circles represent our data; squares, the data from ref. [4]); open circles, the data from ref. [7]); and crosses, the data from (p,f) experiments[20]). The straight line is the best fit calculated from our data for $Z^2/A > 26$. The dashed curve is the curve VI calculated by Nix and Sassi[12]).

Dy
A=162

Dy
A=162

REF.	ELEM. SYM.	A	Z
J.J. Murphy, II, D.M. Skopik, J. Asai, and J. Uegaki Phys. Rev. C 18, 736 (1978)	Dy	162	66
METHOD	REF. NO.		
	78 Mu 9		hg

REACTION	RESULT	EXCITATION ENERGY	SOURCE TYPE	SOURCE RANGE	DETECTOR TYPE	DETECTOR RANGE	ANGLE
E,A	ABX	8-100	D	100	MAG-D		50

α particles from the electrodisintegration of seven nuclei with Z between 29 and 79 have been observed. Energy spectra at 50° in the laboratory for six nuclei and angular distribtions for five nuclei are reported. The cross sections exhibit a broad peak whose magnitude decreases with increasing Z; the energy of the peak increases as Z increases. Angular distributions at the highest energies measured become increasingly forward-peaked suggesting a direct-reaction process.

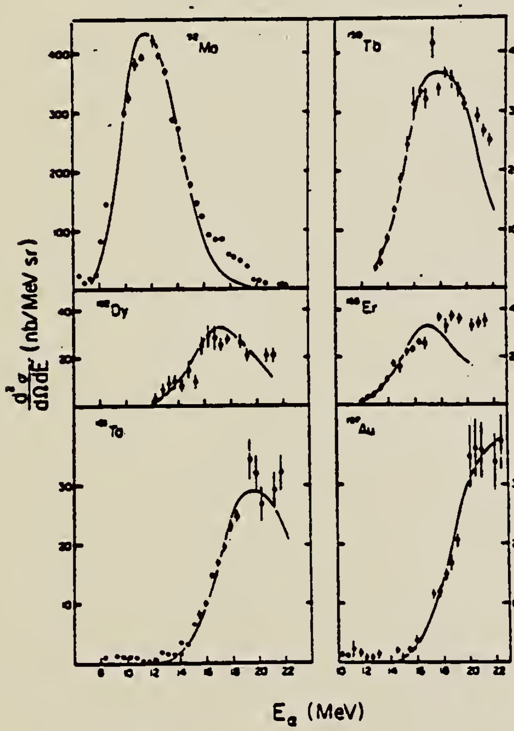

FIG. 2. The α-particle energy spectra at 50° in the laboratory for the four new nuclei studied as well as for two nuclei in which additional data have been obtained. The solid curves are the evaporation model fits described in text.

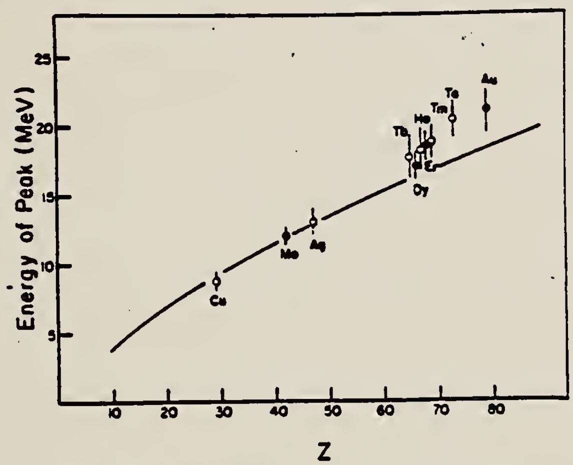

FIG. 3. Energy of the cross section peak as a function of Z. The solid line is the energy of the classical Coulomb barrier. The closed circles are the current work; the open circles are from Ref. 1.

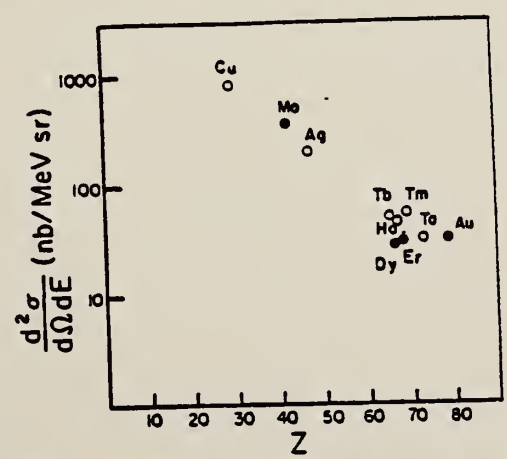

FIG. 4. Magnitude of cross section peak as a function of Z. The closed circles are the current work; the open circles are from Ref. 1.

[1] J.J. Murphy, II, H.J. Gehrhardt, and D.M. Skopik, Nucl. Phys. A277, 69 (1977)

Dy
A=163

Dy
A=163

Dy
A=163

REF.
K. N. Geller, J. Halpern, and E. G. Muirhead
Phys. Rev. 118, 1302-12 (1960)

ELEM. SYM.	A	Z
Dy	163	66

METHOD
Betatron; neutron threshold; ion chamber

REF. NO.	
60 Ge 3	NVB

REACTION	RESULT	EXCITATION ENERGY	SOURCE		DETECTOR		ANGLE
			TYPE	RANGE	TYPE	RANGE	
G,N	NØX	THR	C THR		BF3-I		4 PI

THRESHØLD

TABLE I. Summary and comparison of neutron separation energies inferred from present threshold measurements with values predicted from mass data and reaction energies. All energies are expressed in the center-of-mass system in Mev.

Reaction	No. runs	Present results	Other results	Method	Reference
$Dy^{163}(\gamma,n)Dy^{162}$	1	6.32 ±0.11	6.27 ±0.06	mass data	q

[q] W. H. Johnson, Jr., and V. B. Bhanot, Phys. Rev. 107, 6 (1957).

# HOLMIUM
Z=67

Holmium and its compounds are used for research purposes with their limited applications based primarily upon their distinctive electronic and magnetic properties. The element is of great interest to nuclear spectroscopists because there is only one naturally occuring isotope and it has one of the highest nuclear moments of the rare earth series.

J.G. Chidley, L. Katz, S. Kowalski
Can. J. Phys. 36, 407 (1958)

ELEM. SYM.	A	Z
Ho	165	67

Betatron

REF. NO.	
58 Ch 2	NVB

REACTION	RESULT	EXCITATION ENERGY	SOURCE TYPE	SOURCE RANGE	DETECTOR TYPE	DETECTOR RANGE	ANGLE
G,N	RLY	THR	C	THR	BF3-I		4PI

See 58 Ka 1 for cross sections

THRESHØLD

TABLE I

MEASURED PHOTONEUTRON THRESHOLDS

Reaction	Measured Q value, Mev.	Other Q values, Mev.	Method	Reference
$Ho^{165}(\gamma, n)Ho^{164}$	8.10±0.05			

:.G. Fuller, B. Petree, M.S. Weiss
'hys. Rev. 112, 554 (1958)

ELEM. SYM.	A	Z
Ho	165	67

Betatron; ion chamber

REF. NO.	
58 Fu 1	NVB

REACTION	RESULT	EXCITATION ENERGY	SOURCE TYPE	SOURCE RANGE	DETECTOR TYPE	DETECTOR RANGE	ANGLE
G,XN	ABX	7-40	C	7-40	BF3-I		4PI

CF DANØS THEØRY

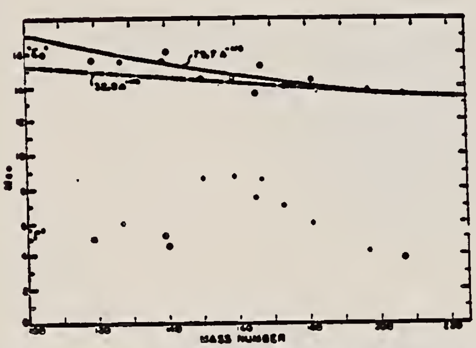

FIG. 6. Mean energy and width of giant resonances. "E_0" and "Γ" are the mean energy for photon absorption and the full width at half maximum of the giant resonance obtained from dashed histograms as in Fig. 5. No attempt was made to fit data with resonance curves to obtain these parameters.

TABLE I. Target properties and results.

Element	Form used	Weight grams	$\sigma^0(\gamma,n)$[a] barns	$\frac{S\sigma dE}{NZ/A}$[b] Mev-b	"Γ"[a] Mev
Sn	Sn	4.81	0.30	0.064	5.0
I	I	8.55	0.36	0.085	6.0
La	La	10.43	0.34	0.063	5.2
Ce	Ce	4.99	0.45	0.080	4.5
Sm	Sm_2O_3	2.90	0.26	0.073	8.6
Tb	Tb_4O_7	3.04	0.39	0.087	8.7
Ho	Ho_2O_3	1.87	0.41	0.079	7.5
Er	Er_2O_3	5.41	0.50	0.100	8.5
Yb	Yb_2O_3	5.57	0.50	0.090	7.0
Ta	Ta	8.41	0.49	0.077	6.0
Au	Au	3.16	0.68	0.085	4.2
Pb	Pb	8.05	0.75	0.081	3.8

[a] $\sigma^0(\gamma,n)$ is the maximum value and "Γ" the full width at $\sigma^0(\gamma,n)/2$ of the neutron production cross section corrected for multiple neutron emission. Data were not fitted with resonance lines to determine these values.
[b] Integrated neutron production cross sections corrected for multiple neutrons above $(\gamma,2n)$ threshold.

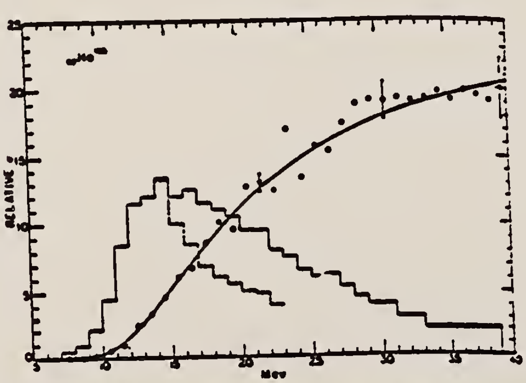

TABLE II. Energies of resonances in deformed nuclei.[a]

Nucleus	E_m Mev	Q_0 barns	Method	E_a Mev	E_b Mev	$E_{1/2}^-$ Mev	$E_{1/2}^+$ Mev
$_{65}Tb^{159}$	14.7	6.9[b]	CE	11.9	16.2	10.8	19.5
$_{67}Ho^{165}$	14.5	7.8[b]	CE	11.5	16.0	11.0	18.5
$_{68}Er^{167}$	14.5	21[b]	SC	8.5	17.5	11.5	20.0
$_{68}Er^{166}$	14.5	7.8[b]	CE	11.6	15.9	11.5	20.0
$_{73}Ta^{181}$	14.1	12.6[c]	SC	10.5	15.9	11.3	17.3
$_{73}Ta^{181}$	14.1	6.8[b]	CE	11.9	15.2	11.3	17.3
$_{79}Au^{197}$	13.6	3.75[c]	SC	12.5	14.1	11.8	16.2

[a] CE—Coulomb excitation; SC—spectroscopic; $E_{1/2}^-$, $E_{1/2}^+$—energies at which giant resonance drops to half its maximum value.
[b] Adler, Bohr, Huus, Mottelson, and Winther, Revs. Modern Phys. 28, 432 (1956).
[c] M. L. Pool and D. N. Kundu, *Chart of Atomic Nuclei* (Longs College Book Company, Columbus, 1955).

FIG. 5. Relative photoneutron production cross sections for tin, iodine, samarium, holmium, erbium, and lead. The points and smooth curves represent the integral neutron-production cross section defined by $\int_0^E \sigma_{Tn}(E)dE$, where $\sigma_{Tn}(E)=\sigma(\gamma,n)+2\sigma(\gamma,2n)+\sigma(\gamma,pn)+3\sigma(\gamma,3n)+\ldots$. The scales are normalized to give approximately the same total neutron yield at 40 Mev. The errors indicated were obtained by propagating the statistical uncertainties, $(\sqrt{n})$, in the original activation curve data through the integral cross section matrix. Solid histograms represent first differences of integral cross section curves. Dashed histograms show result of correcting for neutron multiplicity above the $(\gamma,2n)$ threshold.

REF.	ELEM. SYM.	A	Z
L. Katz, G.B. Chidley Nuclear Reactions at Low and Medium Energies (Academy of Science, USSR: 1958) 371	Ho	165	67

METHOD	REF. NO.	
Betatron; neutron cross section; BF_3 counters; ion chamber monitor	58 Ka 1	NVB

REACTION	RESULT	EXCITATION ENERGY	SOURCE TYPE	SOURCE RANGE	DETECTOR TYPE	DETECTOR RANGE	ANGLE
G,XN	ABX	9-22	C	9-22	BF3-I		4PI

Таблица 2

Порози испускания фотонейтронов

Изотоп	B_n, *Мэв*	B_{2n}, *Мэв*	Изотоп	B_n, *Мэв*	B_{2n}, *Мэв*
V^{51}	11,16	20,5	L^{139}	8,81	16,1
Mn^{55}	10,14	19,2	Pr^{141}	9,46	17,6
Co^{59}	10.44	18,6	Tb^{159}	8,16	14,8
As^{75}	10,24	18,1	Ho^{165}	8,10	14,6
Y^{89}	11,82	20,7	Tm^{169}	8,00	14,7
Nb^{93}	8,86	17,1	Lu^{175}	7,77	14,2
Rh^{103}	9,46	16,8	Ta^{181}	7,66	13,8
J^{127}	9,14	16,2	Au^{197}	7,96	13,3
Cs^{133}	9,11	16,5	Bi^{209}	7,43	14,5

THRESHOLDS

не приведены, поскольку они превышают 22 *Мэв* во всех случаях, кроме золота, для которого B_{3n}=21 *Мэв*. Свойства сечений $\sigma_C(\gamma)$ сведены в табл. 3.

Таблица 1

Изотоп	$E_{макс}$, *Мэв*	$\sigma_n(E_\gamma)$, *барн*	Γ, *Мэв*	Σ^{22}, *Мэв·барн*	Y(22), 10^8 *нейтрон/100 р·моль*
V^{51}	18,4	0,062	5,2	0,33	1,62
Mn^{55}	20,2	0.060	7,0	0,39	2.01
Co^{59}	18,3	0,068	6,3	0,44	2,30
As^{75}	16,4	0,090	9,5	0,74	4,25
Y^{89}	17,1	0,172	5,2	0,93	5,33
Nb^{93}	18,0	0,150	7,5	1,17	6,80
Rh^{1}	17.5	0,160	9,4	1,40	8,28
J^{127}	15,2	0,273	6,8	1,76	11,9
Cs^{133}	16,5	0,238	7,7	1,59	10,7
La^{139}	15,5	0,325	3,8	1,55	11,2
Pr^{141}	15,0	0,320	4,9	1,93	13,1
Tb^{159}	15,6	0,274	9,8	2,49	18,1
Ho^{165}	13,5	0,305	8,9	2,52	18,7
Tm^{169}	16,4	0,250	8,4	1,91	14,9
Lu^{175}	16,0	0,225	8,4	1,90	23,0
Ta^{181}	14,5	0,380	8,5	3,15	22,0
Au^{197}	13,8	0,475	4,7	3,04	22,6
Bi^{209}	13,2	0,455	5,9	2,89	23,2

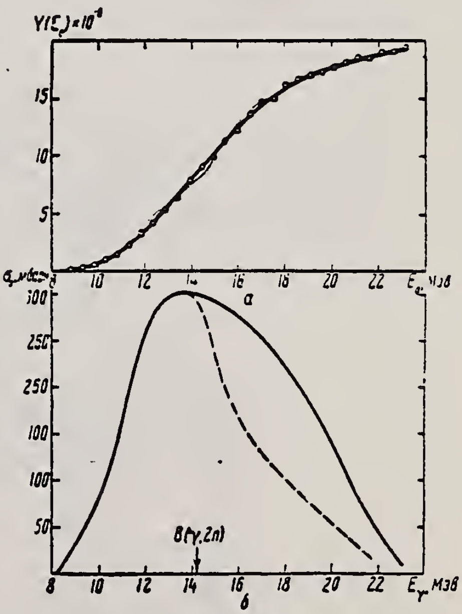

Рис. 13.

а — Выход фотонейтронов для Ho; б — $\sigma_n(E_\gamma)$ и $\sigma_C(\gamma)$ для Ho

\. .. Geller. J. Halpern, and E. G. Muirhead
Phys. Rev. 118, 1302-12 (1960)

ELEM. SYM.	A	Z
Ho	165	67

METHOD

Betatron; neutron threshold; ion chamber

REF. NO.	
60 Ge 3	NVB

REACTION	RESULT	EXCITATION ENERGY	SOURCE		DETECTOR		ANGLE
			TYPE	RANGE	TYPE	RANGE	
G,N	NØX	THR	C THR		BF3-I		4 PI

THRESHØLD

TABLE I. Summary and comparison of neutron separation energies inferred from present threshold measurements with values predicted from mass data and reaction energies. All energies are expressed in the center-of-mass system in Mev.

Reaction	No. runs	Present results	Other results	Method	Reference
$Ho^{165}(\gamma,n)Ho^{164}$	1	8.16 ±0.08	8.10 ±0.05	threshold	f

Ref. H.H. Thies, B.M. Spicer Australian J. Phys. 13, 505 (1960)	Elem. Sym. Ho	A 165	Z 67
Method 18 MeV electron synchrotron; radioactivity; BF_3 counters; ion chamber	Ref. No. 60 Th 1		EH

Reaction	E or ΔE	E_o	Γ	$\int \sigma dE$	Jπ	Notes
Ho^{165} (γ,n)	8 - 18	12.1±0.2				σ_{max} = 420 mb
		16.2±0.2				σ_{max} = 510 mb

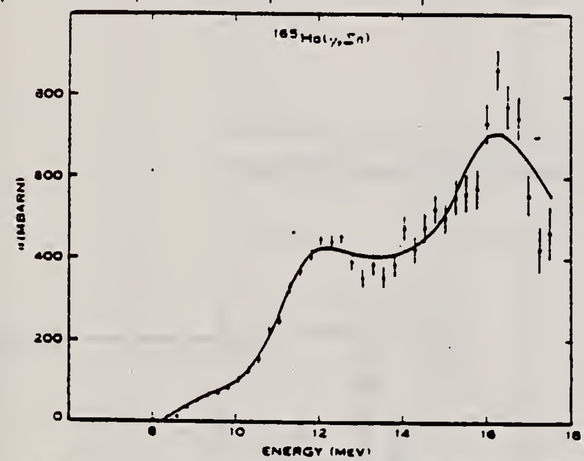

Fig. 7.—Total neutron production cross section for ^{165}Ho.

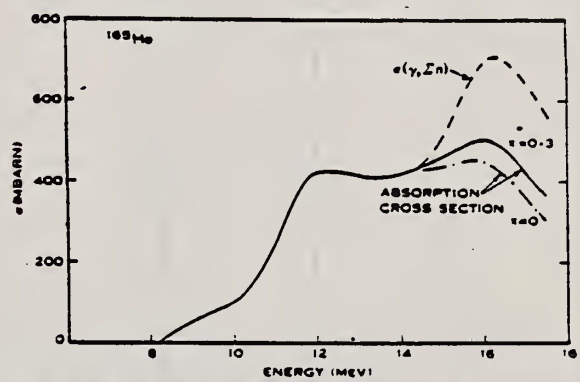

Fig. 9.—Cross section for photon absorption in ^{165}Ho. The correction for neutron multiplicity is applied using statistical theory.

Table 2

Giant Resonance Parameters in Deformed Nuclei

Nucleus ..	^{159}Tb		^{165}Ho	^{181}Ta	
Reference ..	Fuller and Weiss (1958)	Present Paper	Present Paper	Fuller and Weiss (1958)	Spicer et al. (1958)
$\Gamma_{G.R.}$ (MeV)	6·5	6·7±0·5	7±0·5	6·2±0·2	6·1
E_1 (MeV)	12·5	12·4±0·2	12·1±0·2	12·45	12·6
$(\sigma_1)_{max.}$ (mbarn)	260	410	420	308	500
Γ_1 (MeV)	2·4	3·3	2·8	2·3	2·0
E_2 (MeV)	16·3	16·0±0·2	16·2±0·2	15·45	15·3
$(\sigma_2)_{max.}$ (mbarn)	310	460	510	348	450
Γ_2 (MeV)	4·0	4·5	4·7	4·4	4·0
I_2/I_1 ..	2·0	2·0	2·0	2·16	1·8
E_2/E_1 ..	1·30	1·29±0·03	1·34±0·03	1·25±0·01	1·21±0·03

Ref.		Elem. Sym.	A	Z
	R.E. Walsh, D.J. Donahue Phys. Rev. 121, 880 (1961)	Ho	165	67

Method	Ref. No.	
Monoergic γ's from thermal n-capture; activation	61 We 1	JHH

Reaction	E or ΔE	E_0	Γ	$\int \sigma dE$	Jπ	Notes
(γ,n)	7.91-10.83					Measurement of 45-kev x-ray from K-capture in Ho^{164}. Data in Table II (millibarns), Fig. 5. $E_{\gamma\ thresh.}$ = 7.91 - 8.4 MeV.

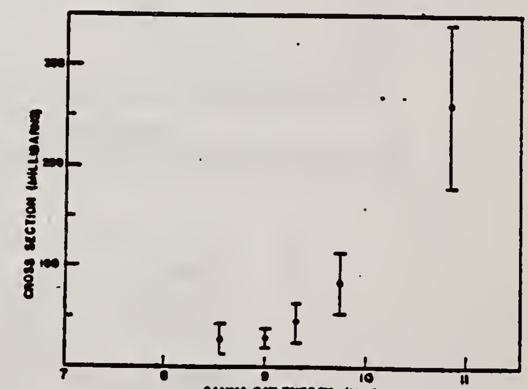

FIG. 5. Cross section vs energy, $Ho^{165}(\gamma,n)Ho^{164}$(34 min).

TABLE II. Summary of measured cross sections.

γ-ray source / Energy (Mev) / Reaction	Co 7.49	Fe 7.64	Al 7.73	Cu 7.91	Cl 8.56	Ni 8.997	Fe 9.30	Cr 9.72	Fe 10.16	N 10.83
$Ta^{181}(\gamma,n)Ta^{180m}$	0±0.05	0.5±1	4.8±1.6	14±5	32±16	44±15	···	33±33	···	120±48
$Au^{197}(\gamma,n)Au^{196}$	···	···	···	0±2	34±17	44±11	64±30	50±50	···	···
$Ho^{165}(\gamma,n)Ho^{164}$	···	···	···	0±0.1	29±15	30±18	46±21	56±51	···	260±93
$Nb^{93}(\gamma,n)Nb^{92}$	···	···	···	···	···	0.008±0.005	1.0±0.4	2.4±0.7	···	···
$Ag^{107}(\gamma,n)Ag^{106}$	···	···	···	···	···	0±0.1	···	4.4±1.5	22±16	23±7.5

Ref. E.G. Fuller, E. Hayward Nuclear Phys. 30, 613 (1962) [Erratum: Nuclear Phys. 37, 176 (1962)]	Elem. Sym. Ho	A 165	Z 67
Method 50 MeV Betatron; BF_3, NaI counters	Ref. No. 62 Fu 3		JHH

Reaction	E or ΔE	E_o	Γ	∫σdE	Jπ	Notes 515
$Ho^{165}(\gamma,xn)$	8-23.5	12.2±0.2 16.0±0.5	2.33 MeV 4.5 MeV	$\int_8^{23.5} = 3.20\pm15\%$		σ (12.2 MeV) = 318 mb σ (16 MeV) = 328 mb Correction for neutron multiplicity.
$Ho^{165}(\gamma,\gamma)$						Intrinsic nuclear quadrupole moment = 7.6±1.1 b. Analysis of scattering data indicates large tensor polarizability. NB -A re-evaluated cross section curve is given in 65 Am 1.

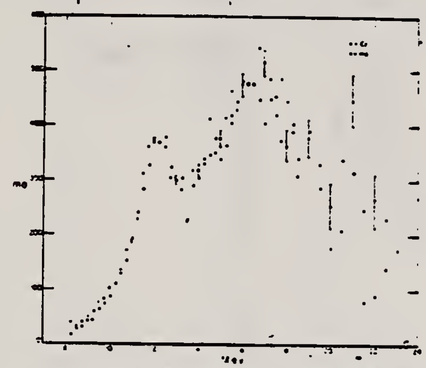

Fig. 2. Neutron producing cross sections for holmium and erbium. The uncertainties indicated result from the statistical uncertainties in the original activation curve data.

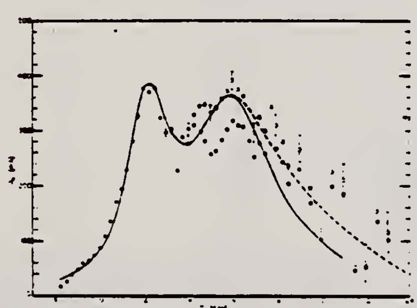

Fig. 4. The sum of the neutron producing cross sections for holmium. The errors indicated are only statistical uncertainties. The two sets of points above 13.5 MeV correspond to the multiplicity correction factors A and B given in fig. 2. The edges of the shaded region correspond to smooth curves drawn through these two sets of points. The solid curve is the sum of two Lorentz lines having the parameters σ_0 = 316 mb, E_0 = 12.2 MeV, Γ_0 = 2.33 MeV, σ_0 = 325 mb, E_0 = 16 MeV, and Γ_0 = 4.5 MeV. The dashed curve drawn above 16 MeV is a smooth curve drawn through the experimental points.

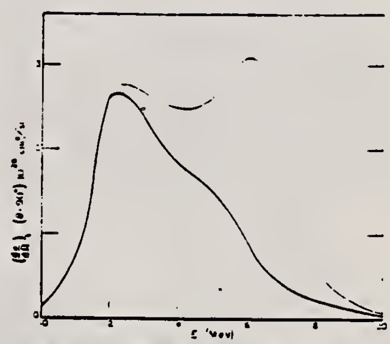

Fig. 7. The tensor scattering cross section for two and three resonance models. The absorption cross section for these resonance parameters are compared with the holmium absorption cross section in fig. 3.

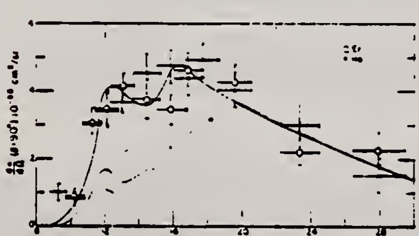

Fig. 6. The differential scattering cross sections for holmium and erbium measured at 90°. The indicated uncertainties are only statistical. The lower smooth curve was calculated using eq. (9) from a curve drawn through the data points of fig. 4. The shaded region corresponds to the limits of the scalar scattering cross section resulting from the limits of the absorption cross section given by the shaded region of fig. 4.

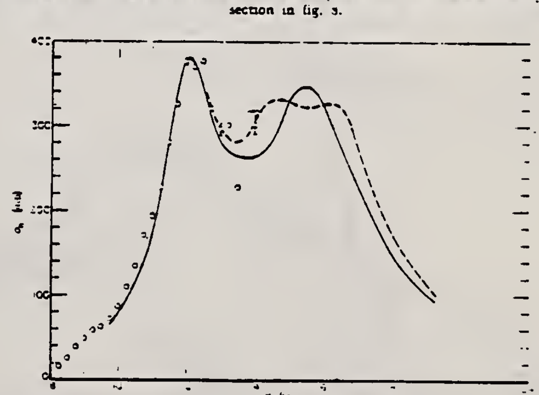

Fig. 8. Comparison of two and three resonance fits to the absorption cross section for holmium.

Davydov and Fillippov [18]) the three resonance energies correspond to a value of γ of about 20°. The values of this parameter normally assigned to nuclei in this part of the periodic table on the basis of their low lying states is only about 10°.

Ref.	Elem. Sym.	A	Z
G.C. Reinhardt, W.D. Whitehead Nuclear Phys. 30, 201 (1962)	Ho	165	67

Method	Ref. No.	
55 MeV betatron; synchrotron; $Si^{28}(n,p)Al^{28}$ activity; $Cu^{63}(\gamma,n)Cu^{62}$ monitor.	62 Re 1	EGF

Reaction	E or ΔE	E_o	Γ	$\int \sigma dE$	Jπ	Notes
$Ho^{165}(\gamma,n)$	Bremss. 55					Figure 8: Dotted curve is of form $a_o + a_1 \cos\theta + a_2 \cos^2\theta + a_2 \cos^2\theta - a_1\cos^2\theta$; solid curve is of form $a_o + a_1 \cos\theta + a_2\cos^2\theta$; errors on points are statistical errors in counting only. En ≥ 5 MeV

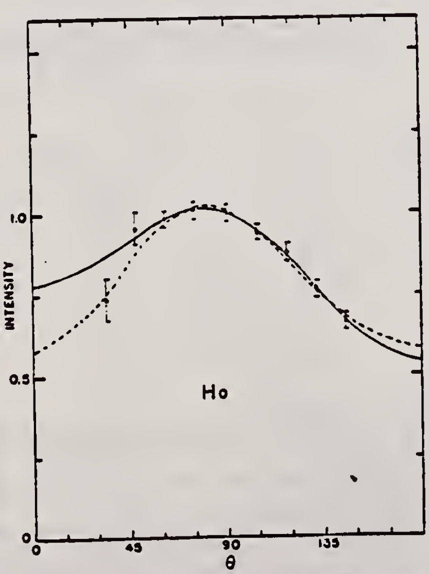

Fig. 8. Angular distribution of fast neutrons from holmium. See fig. 5.

TABLE 3

Parameters of the fit (1) for the expressions $a_0 + a_1\cos\theta + a_2\cos^2\theta$, $a + b\sin^2\theta + c\cos\theta$ and $A_0 + A_1P_1 + A_2P_2$

	Bi(1)	Bi(2)	Pr	Au	Y	Ho	[illegible]
a_0	1.00±0.02	1.00±0.02	1.00±0.02	1.00±0.02	1.00±0.03	1.00±0.02	1.00±0.01
a_1	0.15±0.03	0.18±0.04	0.17±0.04	0.14±0.03	0.17±0.06	0.12±0.03	0.14±0.03
$-a_2$	0.47±0.06	0.40±0.08	0.41±0.09	0.21±0.07	0.15±0.11	0.34±0.06	0.39±0.06
A_1*)	0.15±0.04	0.21±0.05	0.20±0.05	0.15±0.04	0.18±0.06	0.14±0.04	0.16±0.03
$-A_2$*)	0.37±0.05	0.31±0.06	0.32±0.07	0.15±0.05	0.11±0.08	0.26±0.05	0.30±0.04
a	0.53±0.06	0.60±0.05	0.59±0.09	0.79±0.07	0.85±0.11	0.66±0.06	0.61±0.06
b	0.47±0.06	0.40±0.08	0.41±0.09	0.21±0.07	0.15±0.11	0.34±0.06	0.39±0.06
c	0.15±0.03	0.18±0.04	0.17±0.04	0.14±0.03	0.17±0.06	0.12±0.03	0.14±0.03

*) Renormalized so that $A_0 = 1$

TABLE 4

Parameters of the fit (3) for the expressions $a_0 + a_1\cos\theta + a_2\cos^2\theta + a_3\cos^3\theta$, $1 + A_1P_1 + A_2P_2 + A_3P_3$

	Bi(1)	Bi(2)	Pr	Au	Y	Ho	[illegible]
a_0	1.01±0.02	1.00±0.02	1.0[illegible]±0.03	0.98±0.02	1.00±0.03	1.00±0.02	1.01±0.02
a_1	0.19±0.05	0.17±0.07	0.21±0.07	0.07±0.06	0.16±0.0[illegible]	0.12±0.05	0.17±0.05
$-a_2$	0.58±0.11	0.37±0.15	0.50±0.16	0.05±0.12	0.13±0.20	0.33±0.12	0.47±0.11
a_3	−0.17±0.15	0.05±0.24	−0.17±0.25	0.31±0.19	0.05±0.32	0.03±0.19	−0.17±0.17
A_1*)	0.11±0.15	0.23±0.18	0.15±0.20	0.27±0.13	0.20±0.22	0.15±0.14	0.09±0.13
$-A_2$*)	0.45±0.09	0.25±0.11	0.39±0.12	0.03±0.08	0.09±0.14	0.21±0.09	0.37±0.09
A_3*)	−0.06±0.09	0.02±0.11	−0.08±0.12	0.13±0.08	0.02±0.13	0.01±0.05	−0.08±0.08

*) Renormalized so that $A_0 = 1$

Ref.	Elem. Sym.	A	Z
R.L.Bramblett, J.T.Caldwell, G.F.Auchampaugh, S.C.Fuitz Phys.Rev. 129, 2723 (1963)	Ho	165	67
Method	**Ref. No.**		
positron annihilation - 4π parafin moderated neutron detector	63Br1	B G	

Reaction	E or ΔE	E_0	Γ	$\int \sigma dE$	Jπ	Notes 722+
722 (γ,n)	0 - 28			$1.47\pm0.15)_0^{28}$		(γ,2n) threshold = 14.8±0.3MeV
723+ (γ,2n)	0 - 28			$0.90\pm0.09)_0^{28}$		Intrinsic quadrupole moment = 7.40±0.90b
(γ,n) +(γ,2n) 724++(γ,np)	0 - 28	12.1 15.2	6.9	$2.37\pm0.24)_0^{28}$		Level density parameter, a= 22.0 MeV^{-1}

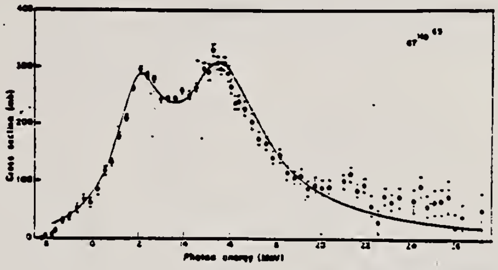

FIG. 6. The formation cross section σ(γ,n)+σ(γ,2n)+σ(γ,np) for the compound nucleus Ho165. The solid curve represents the sum of two Lorentz lines with parameters given in Table III.

TABLE III. Lorentz line parameters and intrinsic quadrupole moments for Ta and Ho.

Element	σ_a (mb)	Γ_a (MeV)	E_a (MeV)	σ_b (mb)	Γ_b (MeV)	E_b (MeV)	Q_0 (b)
Ta^{181}	198	3.00	12.75	224	5.0	15.50	6.71±0.74
Ho^{165}	200	2.65	12.10	249	4.4	15.75	7.40±0.90

FIG. 4. Cross sections for Ho from neutron yield data. Curve A consists of σ(γ,n)+2σ(γ,2n)+σ(γ,np)+3σ(γ,3n) and was obtained from single-neutron counting data. Curve B consists of 2σ(γ,2n)+6σ(γ,3n), and was obtained from double-neutron counting data.

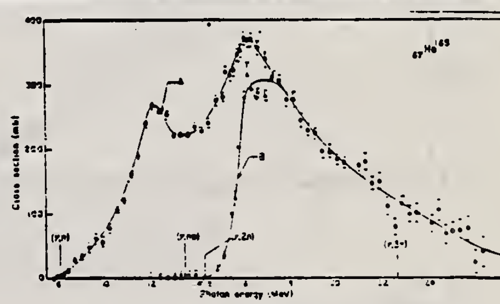

FIG. 3. Partial cross-section curves for Ho. Curve A consists of σ(γ,n)+σ(γ,np). Curve B contains σ(γ,2n)+3σ(γ,3n).

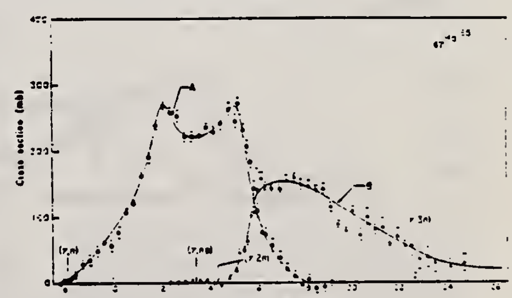

TABLE IV. Integrated cross sections, level density parameters, and σ_{-2} values.

Element	σ_{-2} (mb/MeV)	$0.00225A^{4/3}$ (mb/MeV)	a (MeV^{-1})	$\int_0^{28}\sigma dE$ (MeV·b)	$\int_0^{28}\sigma dE+W$ (MeV·b)	0.06 NZ/A (MeV·b)
Ta^{181}	10.88	13.03	15.7	2.24	2.59	2.61
Ho^{165}	10.93	11.17	22.0	2.37	2.68	2.58

REF.

M. Langevin, J.M. Loiseaux
J. de Physique **24**, 1027 (1963)

Ho	165	67

METHOD

Betatron; photon scattering

REF. NO.	
63 La 1	NVB

REACTION	RESULT	EXCITATION ENERGY	SOURCE TYPE	SOURCE RANGE	DETECTOR TYPE	DETECTOR RANGE	ANGLE
G,G	ABX	9-26	C	9-27	NAI-D		DST

In figure 4, $W(\theta) = 1 + a(\cos^2\theta)$

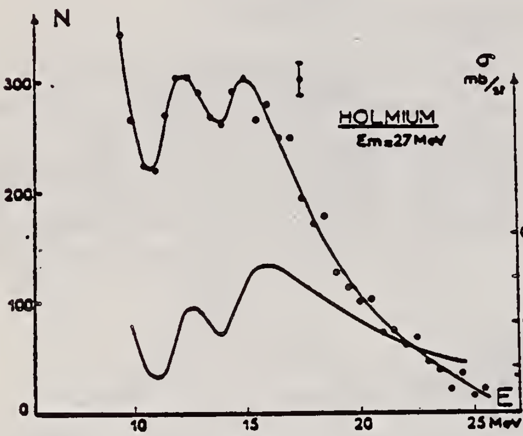

Fig. 2.

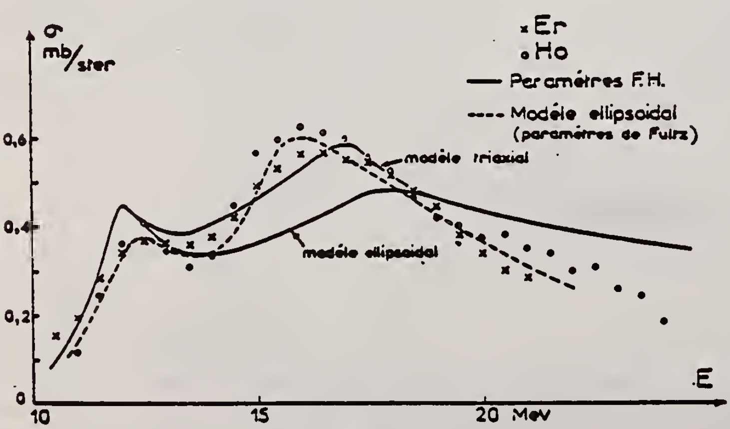

Fig. 3.

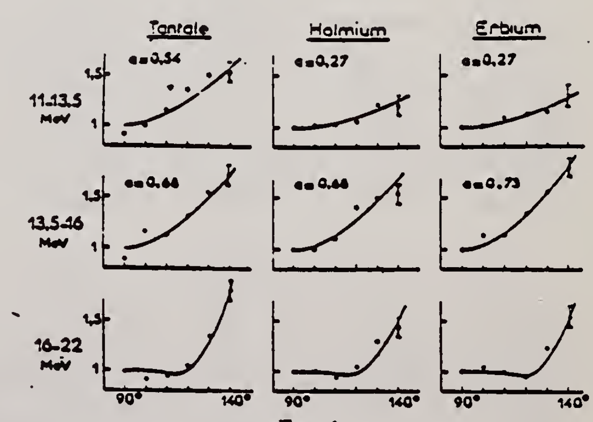

Fig. 4.

Ref.	Elem. Sym.	A	Z
P.A.Tipler, P.Axel, N.Stein, D.C.Sutton Phys.Rev. 129, 2096 (1963)	Ho	165	67
Method 25 MeV Betatron - bremsstrahlung monochrometer - NaI	Ref. No. 63Til		BG

Reaction	E or ΔE	E_o	Γ	$\int \sigma dE$	Jπ	Notes
(γ,γ')	10.92 - 19.06	12.49 16.50 see notes				Differential scattering cross section has maxima at 12.49 MeV and 16.50 MeV (135^o) Differential scattering cross section (135^o) data given in article. Raman scattering considered.

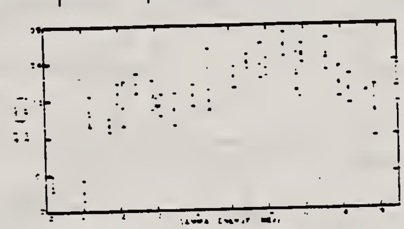

FIG. 8. Differential quasi-elastic photon scattering cross section in Ho[165]. The crosses were obtained at 135° in this experiment and correspond to a resolution of 2%. The circles are from the data of Fuller and Hayward (see reference 2) obtained at 90° with an energy resolution of 10%.

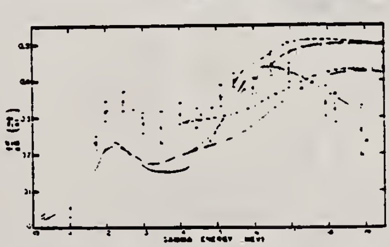

FIG. 9. Predictions for elastic scattering at 135° based on energy dependence of absorption data. All of the curves have been shifted to higher energy by 200 keV and have been reduced by 10% to facilitate comparison with the experimental points obtained in this experiment. The dash-dot curve is the scalar contribution to the scattering implied directly by the absorption data; the solid curve indicates the scalar prediction based on a two-Lorentz line fit to the absorption data below 17 MeV. The dashed curve includes the elastic part of the tensor scattering implied by the hydrodynamic model.

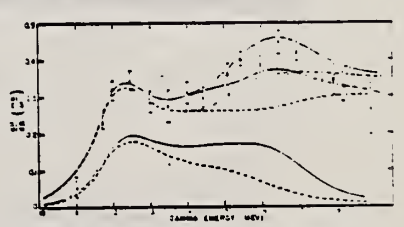

FIG. 10. Predictions for elastic plus Raman scattering at 135° based on absorption data. The upper curves include the scalar contributions obtained from the absorption data by directly applying the dispersion relations; this scalar contribution has been assumed to have a dipole angular dependence but no line fitting was used to represent the absorption data. The calculations of the tensor contributions used a two-line fit (dashed curves) or a three-line fit (solid curves). The lower curves give the tensor contributions alone while the upper curves represent the total expected scattering. All of the curves have been shifted up in energy by 100 keV and normalized by a factor of 0.62 to facilitate comparison with the experimental points.

REF.	ELEM. SYM.	A	Z
M. Langevin, J. M. Loiseaux et J. M. Maison Nucl. Phys. 54, 114-124 (1964)	Ho	165	67

METHOD		REF. NO.	
Bremsstrahlung scattering	[Page 1 of 2]	64 La 1	JOC

REACTION	RESULT	EXCITATION ENERGY	SOURCE TYPE	SOURCE RANGE	DETECTOR TYPE	DETECTOR RANGE	ANGLE
G,G	ABX	10-25	C	27	NAI-D		DST

TABLEAU 1

Le paramètre $a(E)$ de la distribution angulaire

Noyau	11.5-14. MeV Exp.	Ellipsoïdal	Triax.	14-17.5 MeV Exp.	Ellips.	Triax.	17.5-20 MeV Exp.	Ellips.	Triax.	20-30 MeV Exp.	Ellip
							Contribution Quadrupolaire %				
Tb	$0.5^{+0.15}_{-0.1}$	0.41	0.39	$0.54^{+0.15}_{-0.1}$	0.70	0.50	25	0.97	0.85		1
Ho	$0.27^{+0.15}_{-0.1}$	0.44	0.407	$0.43^{+0.10}_{-0.05}$	0.71	0.53	25	0.95	0.9	0.4 ± 0.1	1
Er	$0.27^{+0.15}_{-0.1}$	0.44	0.407	$0.8^{+0.15}_{-0.1}$	0.71	0.53	25	0.95	0.9		1
Ta	$0.6^{+0.15}_{-0.1}$	0.58		$0.68^{+0.15}_{-0.1}$	0.81		20	0.96			
Au	a_{exp}(11-20 MeV) = 0.9 a_{th} (11-20 MeV) ≈ 1									0.7 ± 0.1	1

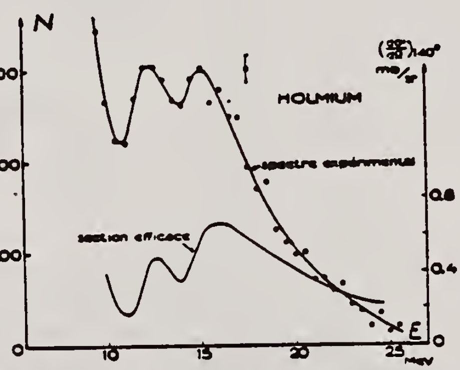

Fig. 1. Résultats expérimentaux et sections efficaces de diffusion déduites pour l'holmium, $E_m = 27$ MeV.

REF.	ELEM. SYM.	A	Z
M. Langevin, J. M. Loiseaux et J. M. Maison Nucl. Phys. 54, 114-124 (1964)	Ho	165	[illegible]

METHOD		REF. NO.	
Bremsstrahlung scattering	[Page 2 of 2]	64 La 1	JOC

REACTION	RESULT	EXCITATION ENERGY	SOURCE TYPE	SOURCE RANGE	DETECTOR TYPE	DETECTOR RANGE	ANGLE

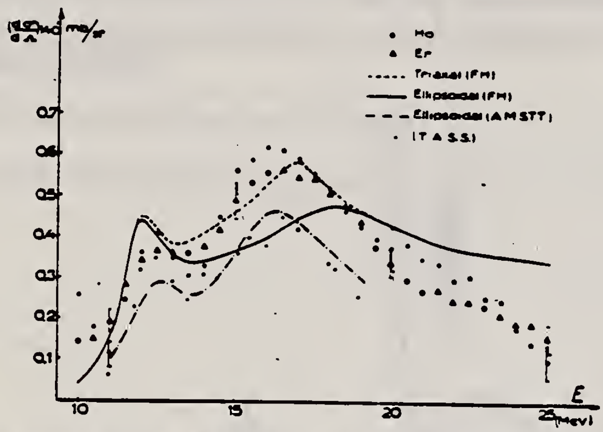

Fig. 3. Sections efficaces expérimentales differentielles de diffusion, obtenues pour l'holmium et l'erbium et comparaison avec les résultats expérimentaux de Tipler *et al.* [18]). (T.A.S.S.). Les courbes tracées correspondent à l'application des relations de dispersion aux sections efficaces d'absorption obtenues par Fuller et Hayward [4]) (F.H.) et Axel, Miller, Schuhl, Tamas et Tzara (A.M.S.T.T.) [19]).

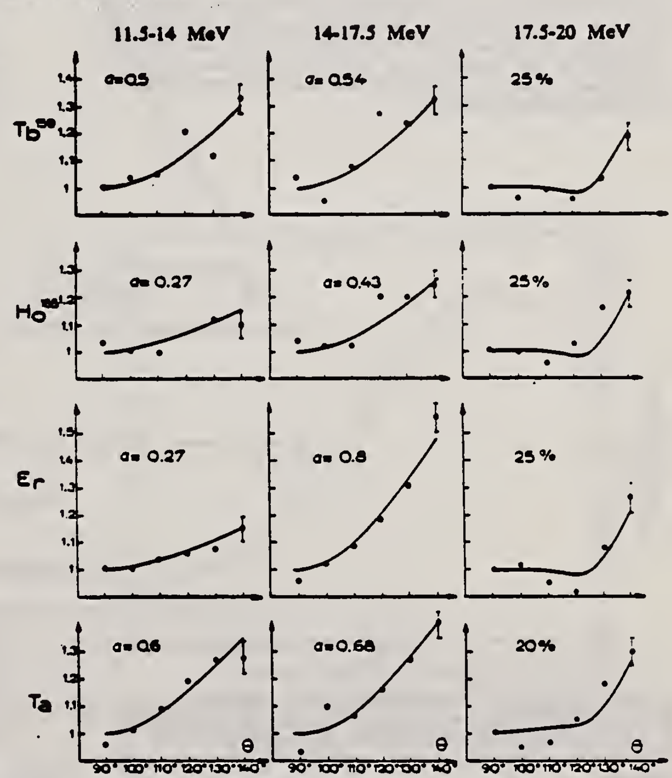

Fig. 8. Répartitions angulaires du rayonnement diffusé obtenues pour le terbium, l'holmium, l'erbium et le tantale dans les zones d'énergie 11.5-14 MeV, 14-17.5 MeV et 17.5-20 MeV.

REF.	ELEM. SYM.	A	Z
E. Ambler, E. G. Fuller, H. Marshak Phys. Rev. <u>138</u>, B117 (1965)	Ho	165	67

METHOD	REF. NO.	
Betatron; ion chamber monitor	65 Am 1	NVB

REACTION	RESULT	EXCITATION ENERGY	SOURCE		DETECTOR		ANGLE
			TYPE	RANGE	TYPE	RANGE	
$G,XN	ABY	10-20	C	10-20	BF3-I		4PI

ORIENTED TARGET

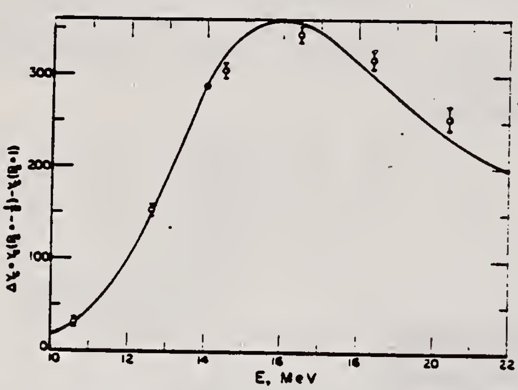

FIG. 5. Asymmetry of photoneutron yield measured at 0.29°K. The root mean square errors determined from the estimated uncertainties in the asymmetry measured at 77°K and the rms deviation of the measurements at 0.29°K are indicated in the experimental points. The abscissa represents the peak energy of the bremsstrahlung spectrum.

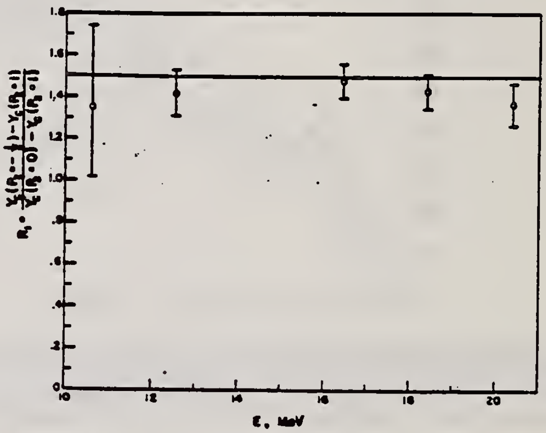

FIG. 6. Dependence of photoneutron yield asymmetry on the angle between the photon-beam direction and the nuclear alignment axis. The uncertainties indicated in the experimental points are defined in the caption for Fig. 5. The line at 1.5 is the value expected for a pure $P_2(\cos\theta)$ dependence of the alignment effect. The ordinate represents the peak energy of the bremsstrahlung spectrum.

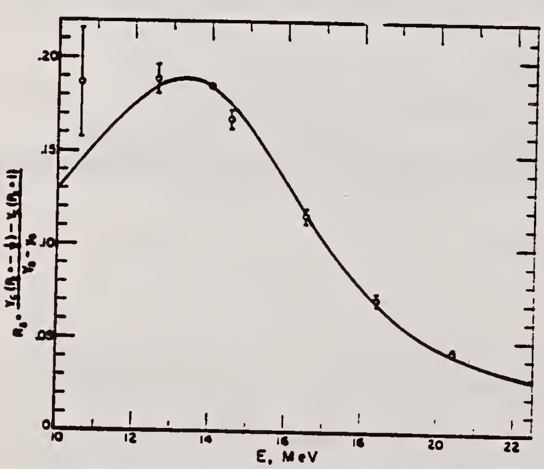

FIG. 7. Asymmetry of photoneutron yield normalized in terms of the orientation-independent yield. The uncertainties indicated in the experimental points are defined in the caption for Fig. 5. The abscissa represents the peak energy of the bremsstrahlung spectrum.

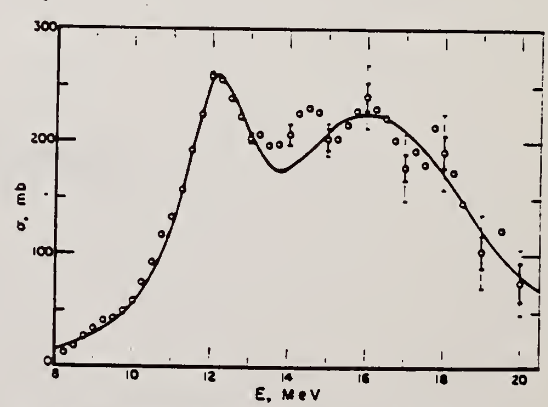

FIG. 8. Photoneutron-producing cross section for Ho^{165} as a function of photon energy. The points above 14.25 MeV have been corrected for neutron multiplicity. Horizontal bars represent typical statistical uncertainties in data points. Light extensions on the bars indicate the uncertainties in the multiplicity correction. The smooth curve is calculated from the theory of Danos and Greiner using the parameters given in Table I.

Corrected data from 62 Fu 3.

REF.
P. Axel, J. Miller, C. Schuhl, G. Tamas and C. Tzara
J. Physique et Rad. 27, 262 (1966)

ELEM. SYM.	A	Z
Ho	165	67

METHOD

[Page 1 of 2]

Monochromatic gammas from annihilation in flight of positrons.

REF. NO.	
66 Ax 1	JDM

REACTION		RESULT	EXCITATION ENERGY	SOURCE TYPE	SOURCE RANGE	DETECTOR TYPE	DETECTOR RANGE	ANGLE
G,N	719+	ABX	8-20	D	8-20	BF3-I		4PI
G,2N	720	ABX	8-20	D	8-20	BF3-I		4PI
G,G		ABX	13,16	D	13,16	NAI-D		90,135

7/9+

$$\int_{9}^{19.8} \sigma dE = 2.54 \text{ MeV-b}$$

$$\sigma_{0} = 7.4 \pm 0.4 \text{ b}$$

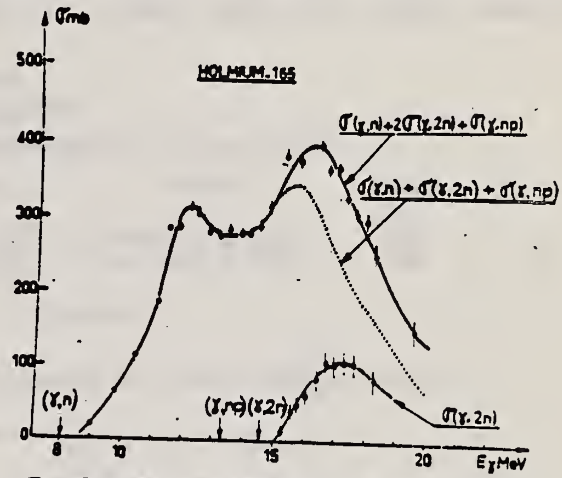

Fig. 2. — Sections efficaces de photoproduction de neutrons de ^{165}Ho mesurées dans ce travail.

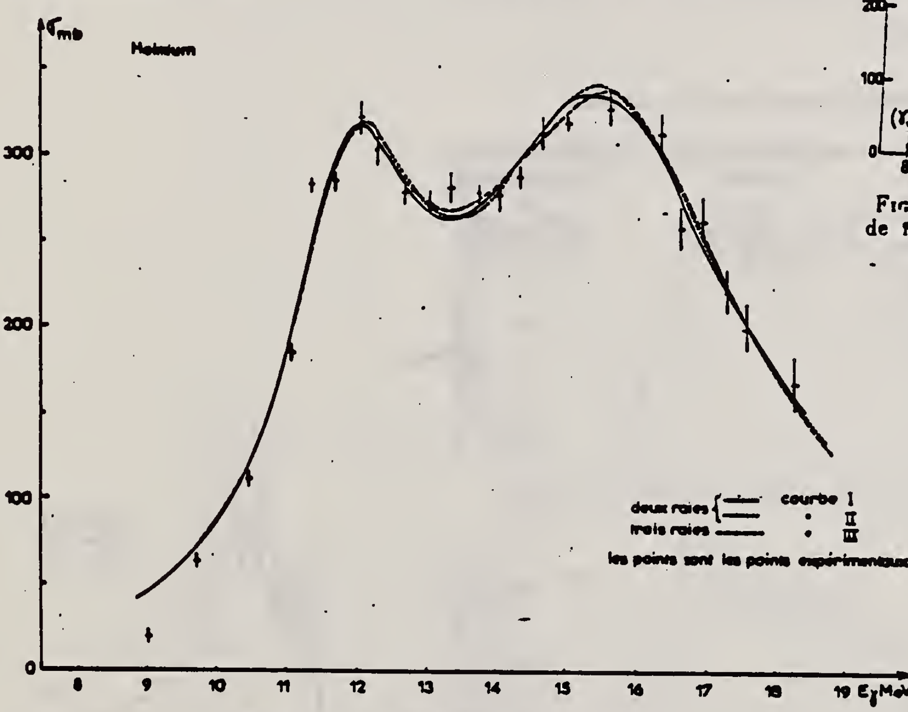

Fig. 5. — Deux ou trois raies de Lorentz.

TABLEAU 1

Décomposition en deux raies de Lorentz

1re résonance			2e résonance					Section efficace intégrée (MeV.b)			
σ_1 mb	E_1 MeV	Γ MeV	σ_2 mb	E_2 MeV	Γ MeV	E_2/E_1	$\sigma_2\,\Gamma_2/\sigma_1\,\Gamma_1$	$\frac{\Gamma}{2}\sum_i \sigma_i \Gamma_i$	$\int_0^{23} \sigma\, dE$ exp.	$0{,}06 \frac{NZ}{A} \times 1{,}4$	Q_0 b
—	—	—	—	—	—	—	—	—	—	—	—
232 ± 17	12,00 ± 0,07	2,27 ± 0,28	308 ± 16	15,55 ± 0,13	5,0 ± 0,6	1,295 ± 0,024	2,9 ± 1,1	3,24 ± 0,58	2,54	3,34	7,23 ± 0,67
240 ± 8	12,03 ± 0,015	2,43 ± 0,16	308 ± 6	15,62 ± 0,06	4,69 ± 0,20	1,297 ± 0,010	2,47 ± 0,4	3,19 ± 0,3	»	»	7,39 ± 0,4

REF.

P. Axel, J. Miller, C. Schuhl, G. Tamas and C. Tzara
J. Physique et Rad. 27, 262 (1966)

ELEM. SYM.	A	Z
Ho	165	67

METHOD

Monochromatic gammas from annihilation in flight of positrons.

REF. NO.	
66 Ax 1	JDM

ANGLE

TABLEAU 2

Décomposition en trois raies de Lorentz (courbe n° III de la figure 5)

1re résonance			2e résonance			3e résonance					
σ_1 mb	E_1 MeV	Γ_1 MeV	σ_2 mb	E_2 MeV	Γ_2 MeV	σ_3 mb	E_3 MeV	Γ_0 MeV	$\frac{\sigma_2\Gamma_2}{\sigma_1\Gamma_1}$	$\frac{\sigma_3\Gamma_3}{\sigma_1\Gamma_1}$	$\sigma_{\mathrm{int}} = \frac{\pi}{2}\Sigma_i\sigma_i\Gamma_i$
220	12,0	2,34	172	15,0	5,73	151	16,0	3,7	1,75	1,1	3,16

TABLEAU 3

Section efficace différentielle de diffusion élastique

E MeV	$\theta = 90°$	$\theta = 134°30'$	$d\sigma\,(134°30')/d\sigma\,(90°)$
12,6	0,226 ± 0,020 mb/sr	0,314 ± 0,030 mb/sr	1,46 ± 0,25
16,4	0,347 ± 0,030 mb/sr	0,430 ± 0,040 mb/sr	1,24 ± 0,20

TABLEAU 4

Calcul de $\frac{d\sigma}{d\Omega}(\theta)$ à partir des courbes d'absorption des photons

E	$\theta = 90°$	$\theta = 135°$	$d\sigma\,(135°)/d\sigma\,(90°)$ calculé	$d\sigma\,(135°)/d\sigma\,(90°)$ expérimental
12,6 MeV	0,247 mb/sr	0,307 mb/sr	1,24	1,46 ± 0,25
16,4 MeV	0,376 mb/sr	0,525 mb/sr	1,40	1,24 ± 0,20
$d\sigma\,(16{,}4)/d\sigma\,(12{,}6)$ calculé	1,52	1,71		
$d\sigma\,(16{,}4)/d\sigma\,(12{,}6)$ expérimental	1,53 ± 0,45	1,37 ± 0,27		

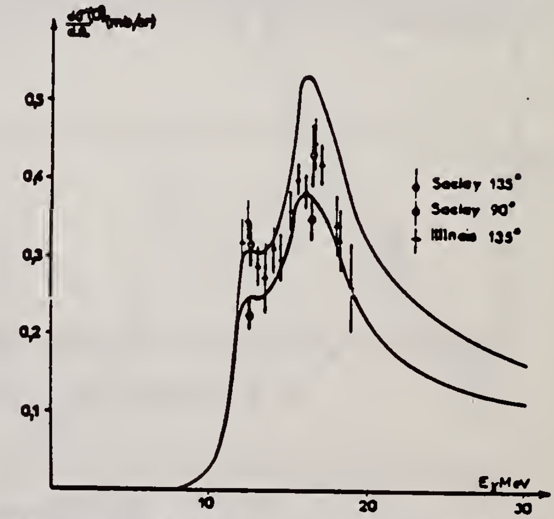

Fig. 7. — Diffusion élastique (scalaire et tensorielle) des rayonnements gamma par ^{165}Ho.

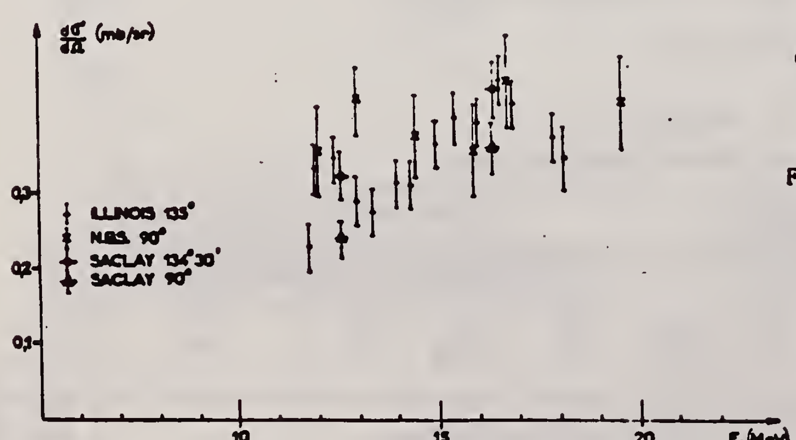

Fig. 6. — Section efficace de diffusion élastique des rayonnements gamma pour le noyau de ^{165}Ho.

REF.

P. J. Scanlon
Nuclear Phys. 88, 424 (1966)

ELEM. SYM.	A	Z
Ho	165	67

METHOD

70 MeV Synchrotron

REF. NO.	
66 Sc 1	JDM

REACTION	RESULT	EXCITATION ENERGY	SOURCE		DETECTOR		ANGLE
			TYPE	RANGE	TYPE	RANGE	
G,P	SPC	THR-70	C	70	TEL-D	6-14	90,135
G,D	RLY	THR-70	C	70	TEL-D	6-14	90,135
G,T	RLY	THR-70	C	70	TEL-D	6-14	90,135

TABLE 1

Numbers of photoparticles from ^{165}Ho with energies in the range 9.0 MeV to 13.5 for a peak photon energy of 70 MeV

Angle (deg)	Protons	Deuterons	Tritons	Deuterons/Protons	Tritons/Deuterons
90	1905	76	19	0.04	0.25
135	1017	35	11	0.03	0.3

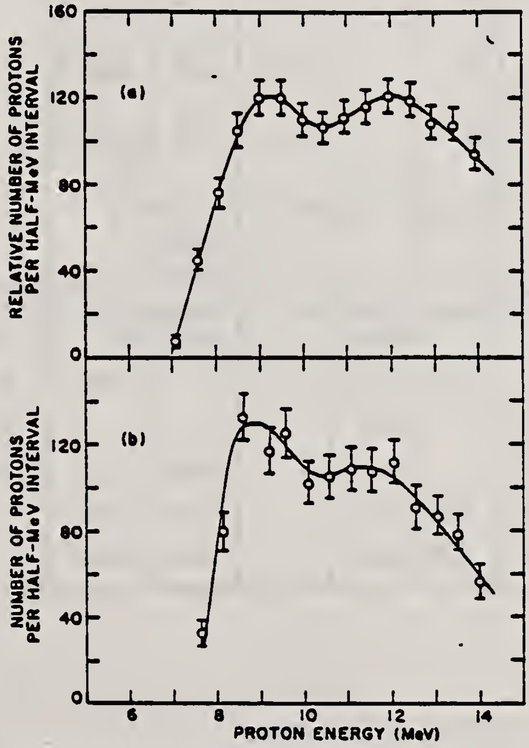

Fig. 5. Upper curve: photoproton spectrum at 90±6° to beam. Lower curve: photoproton spectrum at 135±6° to beam. The upper curve has been normalized to the same beam dose as the lower curve. Both energy scales are corrected for proton energy loss in the target.

REF.	ELEM. SYM.	A	Z
H. M. Gerstenberg and E. G. Fuller NBS Tech. Note 416, June 1967	Ho	165	67

METHOD	REF. NO.	
	67 Ge 2	HMG

REACTION	RESULT	EXCITATION ENERGY	SOURCE TYPE	SOURCE RANGE	DETECTOR TYPE	DETECTOR RANGE	ANGLE
G,N	ABY	THR-27	C	22,27	BF3-I		4PI

Table 7. Comparison of neutron yields. Yields are given in units of (neutron cm^2/MeV nucleus)x10^{-28}. The estimated uncertainties in Y and Y_c are of the order of 6% and 10%, respectively.

Element	E_o	$Y(E_o)$	UCRL	Saclay	Va.	NBS(Old)	UCRL Exp	Saclay Exp	Va. Exp	NBS(Old) Exp	Ref.
			Y_c				Y_c/Y				
Pb	27	103	86				0.83				26,30
	22	111	92	116			0.83	1.05			
Au	27	89	97				1.09				24,30,
	22	92	98	88		115	1.07	0.96		1.25	38
Ta	27	81	82	77			1.01	0.95			27,30,
	22	85	79	80		113	0.93	0.94		1.33	38
Ho	27	67	75				1.12				27,31,
	22	69	77	82		103	1.12	1.19		1.49	39
Ag	27	36									
	22	34.8									
Cu	27	14.4	13.2				0.92				28,30
	22	12.6	11.5	12.4			0.91	0.98			
Co	27	12.7	12.1				0.95				29,34
	22	10.6	9.9		13.5		0.94		1.27		
Ca	27	1.69		1.13	1.01			0.67	0.60		32,35
P	27	2.35			1.76				0.75		36
Al	27	1.92	1.62		1.38		0.84		0.72		25,37
O^{16}	27	0.54	0.42	0.48	0.42		0.78	0.89			16,32, 37
C	27	0.50	0.35	0.33	0.46		0.70	0.66			25,32, 33

Fig. 31. Absolute neutron yield as a function of atomic number. The neutron yield from calcium (Z = 20) is particularly low in comparison with the other elements because its (γ,n) threshold is high compared to the mean energy of the giant resonance.

REF.	ELEM. SYM.	A	Z
J. R. Harrington and B. M. Spicer PICNS-67 Contributions, International Conference on Nuclear Structure, Tokyo, Japan 1967 (Institute for Nuclear Study, University of Tokyo, Tanashi-shi, Tokyo, Japan) 10.16, p. 380	Ho	165	67

METHOD	REF. NO.	
	67 Ha 1	EGF

REACTION	RESULT	EXCITATION ENERGY	SOURCE TYPE	SOURCE RANGE	DETECTOR TYPE	DETECTOR RANGE	ANGLE
G,2N	RLX	14-29	C	14-29	ACT-I		4PI

YIELD TO ISOMERE

The Electric Quadrupole Giant Resonance of Ho^{165} *

J. R. Harrington and B. M. Spicer

University of Melbourne, Australia

The structure of the electric quadrupole giant resonance of Ho^{165} has been sought in the $Ho^{165}(\gamma,2n)Ho^{163m}$ cross section. The yield of Ho^{163m} was measured by counting the 308 keV γ-ray emitted in the decay of the isomeric state of Ho^{163}. The half-life of this state (0.8 sec) required that its activity be counted between betatron beam bursts. The yield of Ho^{163m} was measured at 0.5 MeV intervals between threshold and 28 MeV, and the cross section extracted by the method of Penfold and Leiss.

Bramblett et al[1)] showed that the $Ho^{165}(\gamma,n)$ cross section goes to zero at 18 MeV. Therefore, above this energy, the total γ-ray absorption cross section is manifested in the $(\gamma,2n)$ and $(\gamma,3n)$ cross sections. The statistical theory of nuclear reactions indicates that the $(\gamma,3n)$ cross section is not significant below 26 MeV. We confine attention then to the $(\gamma,2n)$ cross section, which will consist of contributions from E1 and E2 absorption. The dynamic collective theory of the E1 giant resonance predicts two Lorentz lines for Ho^{165}, and Bramblett et al[1)] show these at 12.1 and 15.75 MeV, with widths of 2.6 and 4 MeV respectively. Thus the E1 cross section above 20 MeV is smooth, and all structure in the $(\gamma,2n)$ cross section should arise from the E2 giant resonance.

The measured cross section is shown in Fig. 1a. An attempt has been made to subtract from this cross section the contribution due to E1 absorption. The result of this subtraction is shown in Fig. 1b together with the prediction of Ligensa, Greiner and Danos[2)] for the E2 cross section structure. A measure of consistency exists between theory and experiment regarding the energies of the major transitions.

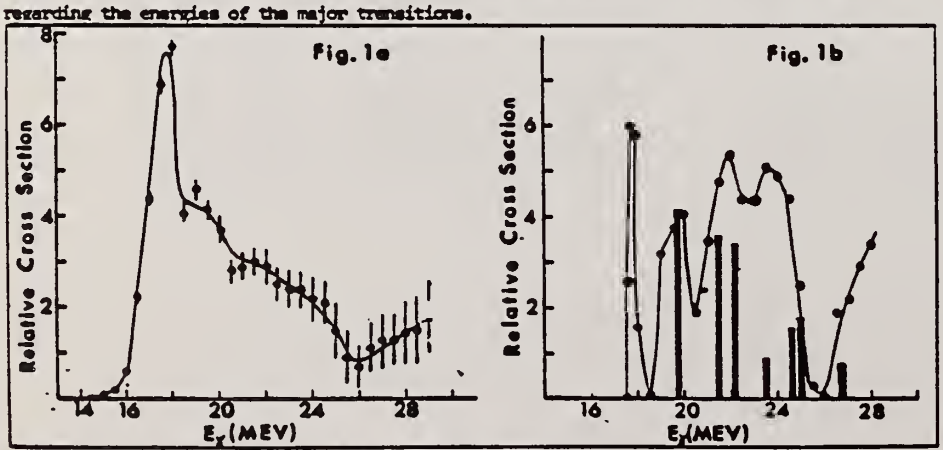

*Supported by a grant from the U.S. Army Research Office.

References: 1) R. L. Bramblett, J. T. Caldwell, G. F. Auchampaugh and S. C. Fultz: Phys.Rev. 129 (1963) 2723.

2) R. Ligensa, W. Greiner and M. Danos: Phys.Rev.Lett. 16 (1966) 364.

REF.

R. R. Hurst and D. J. Donahue
Nucl. Phys. A91, 365 (1967)

ELEM. SYM.	A	Z
Ho	165	67

METHOD

Neutron capture gamma rays

REF. NO. 67 Hu 1 EGF

REACTION	RESULT	EXCITATION ENERGY	SOURCE TYPE	SOURCE RANGE	DETECTOR TYPE	DETECTOR RANGE	ANGLE
G,N	ABX	9-11	D	9-11	BF3-I		4PI

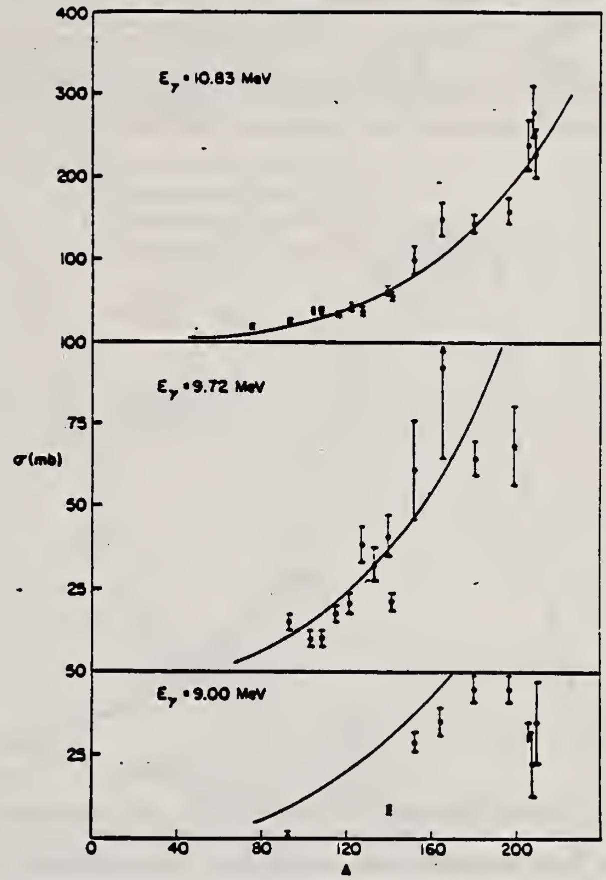

Fig. 1. Cross section (in mb) versus mass number of the target for gamma-ray energies of 9.00, 9.72 and 10.83 MeV. The solid lines are plots of eq. (1) in the text.

TABLE 1
Photoneutron cross sections (mb)

Target	7.72 MeV	9.00 MeV	9.72 MeV	10.83 MeV
^{59}Co				9.0 ± 0.8
^{75}As				20.4 ± 1.7
^{93}Nb		0.53 ± 0.10	14.6 ± 2.2	25.8 ± 2.1
^{103}Rh			10.6 ± 1.7	38.8 ± 3.1
^{107}Ag, ^{109}Ag			10.0 ± 1.5	37.6 ± 2.9
^{115}In			17.1 ± 2.6	33.3 ± 2.7
^{121}Sb, ^{123}Sb			20.7 ± 3.1	42.5 ± 3.6
^{127}I			38.7 ± 5.8	38.8 ± 3.1
^{133}Cs			31.7 ± 4.8	52.5 ± 3.8
^{139}La		8.61 ± 0.86	40.8 ± 6.5	63.0 ± 5.0
^{141}Pr			21.5 ± 3.2	58.3 ± 4.1
^{151}Eu, ^{153}Eu		28.9 ± 3.2	61.3 ± 14.7	102 ± 18
^{165}Ho		35.6 ± 4.3	92.2 ± 27.6	150 ± 20
^{181}Ta	4.14 ± 0.36	45.4 ± 3.7	65.0 ± 5.5	146 ± 12
^{197}Au		44.5 ± 3.6	68.4 ± 13.5	160 ± 15
^{206}Pb		< 34.3		238 ± 29
^{208}Pb		22.6 ± 11.3		280 ± 31
^{209}Bi		36.1 ± 12.0		226 ± 27

REF. R. Bergère, H. Beil and A. Veyssière Nucl. Phys. A121, 463 (1968)	ELEM. SYM. Ho	A 165	Z 67
METHOD [Page 1 of 2]	REF. NO. 68 Be 5		egf

REACTION		RESULT	EXCITATION ENERGY	SOURCE TYPE	SOURCE RANGE	DETECTOR TYPE	DETECTOR RANGE	ANGLE
G,N	90	ABX	THR-30	D	7-30	MOD-I		4PI
G,2N	91							
G,3N	92+							

90+

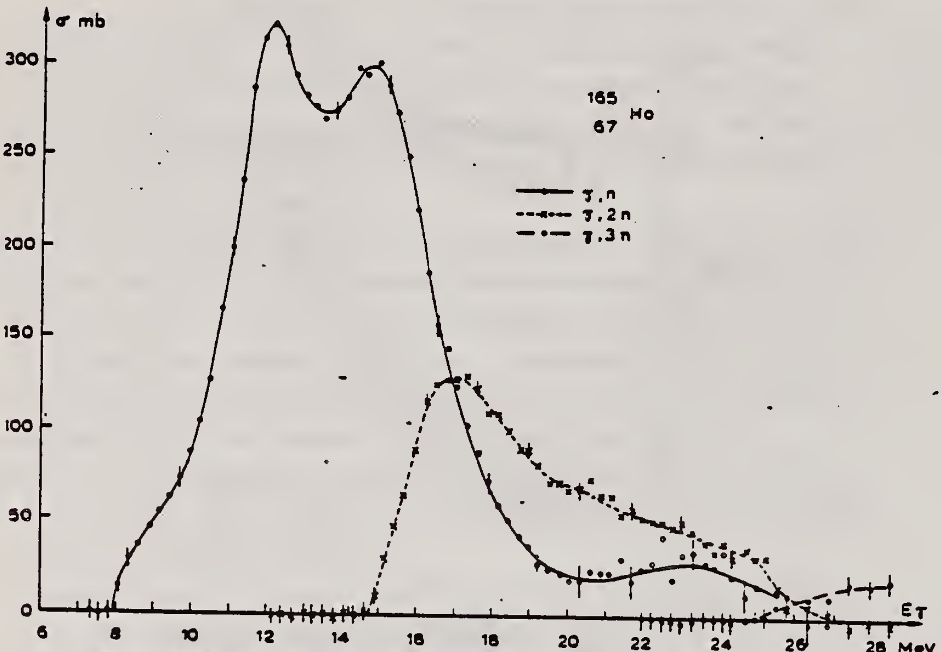

Fig. 4. Partial photonuclear cross sections $\sigma(\gamma, n)$, $\sigma(\gamma, 2n)$ and $\sigma(\gamma, 3n)$ of $^{165}_{67}$Ho.

TABLE 4

Lorentz line parameters for a two line fit to the total cross section data of $^{165}_{67}$Ho

E_1(MeV)	σ_1(mb)	Γ_1(MeV)	E_2	σ_2	Γ_2
12.07	250	2.7	15.62	285	4.8

REF.	ELEM. SYM.	A	Z
R. Bergère, H. Beil and A. Veyssière Nucl. Phys. A121, 463 (1968)	Ho	165	67

METHOD	REF. NO.	
[Page 2 of 2]	68 Be 5	egf

REACTION	RESULT	EXCITATION ENERGY	SOURCE TYPE	SOURCE RANGE	DETECTOR TYPE	DETECTOR RANGE	ANGLE

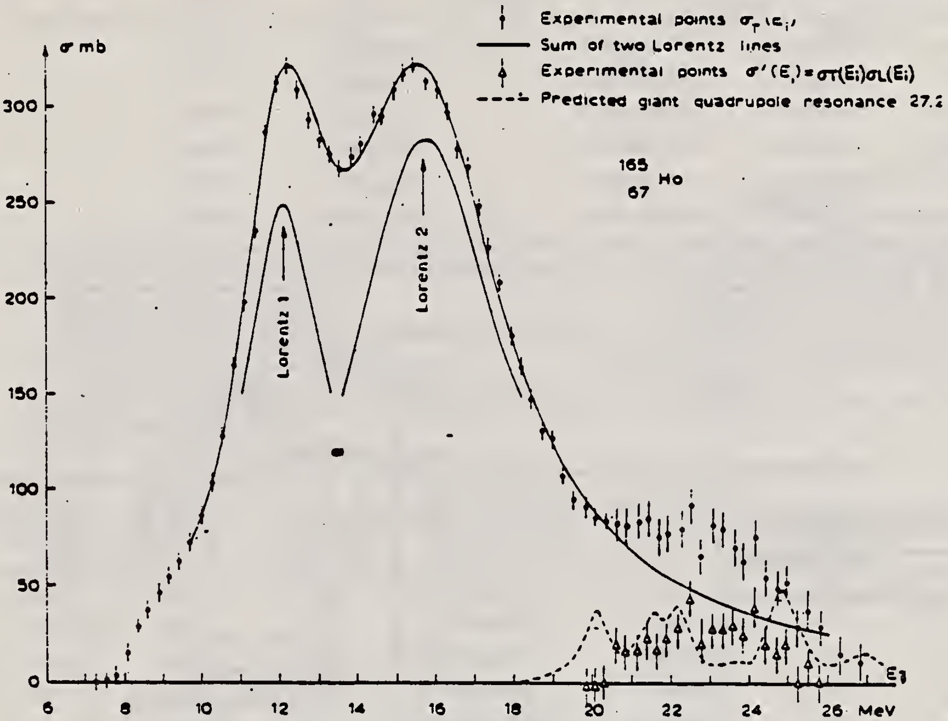

Fig. 5. Total cross section data showing a two Lorentz line fit for a $^{165}_{67}$Ho target.

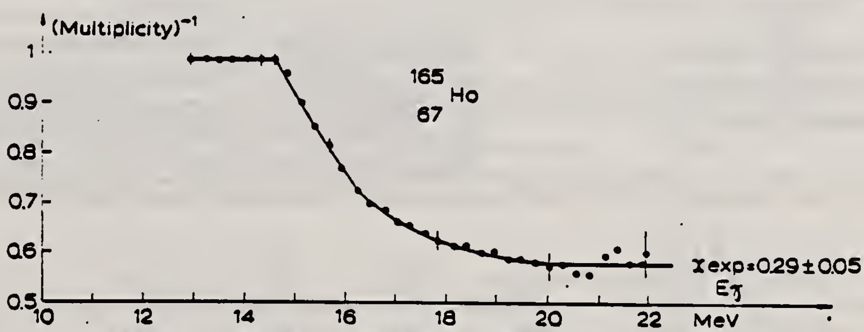

Fig. 6. Reciprocal neutron multiplicity as a function of γ-energy for $^{165}_{67}$Ho.

B. L. Berman, M. A. Kelly, R. L. Bramblett, J. T. Caldwell, H. S. Davis, and S. C. Fultz
Phys. Rev. 185, 1576 (1969)

ELEM. SYM.	A	Z
Ho	165	67

METHOD

REF. NO.	
69 Be 8	hmg

REACTION		RESULT	EXCITATION ENERGY	SOURCE TYPE	SOURCE RANGE	DETECTOR TYPE	DETECTOR RANGE	ANGLE
G,N*	163	ABX	8-29	D	8-29	BF3-I		4PI
G,2N**	164	ABX	8-29	D	8-29	BF3-I		4PI
G,3N	165+	ABX	8-29	D	8-29	BF3-I		4PI

* INCLUDES NP
** INCLUDES 2NP
162+

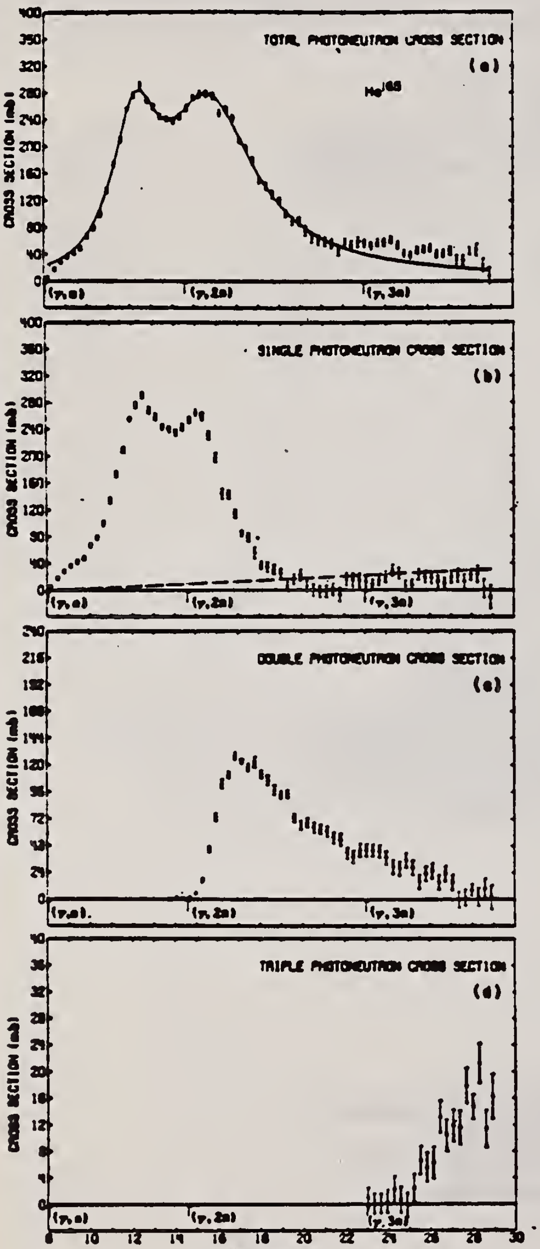

Fig. 7. Photoneutron cross sections for Ho^{165}: (a) $\sigma[(\gamma,n)+(\gamma,pn)+(\gamma,2n)+(\gamma,p2n)+(\gamma,3n)]$, (b) $\sigma[(\gamma,n)+(\gamma,pn)]$, (c) $\sigma[(\gamma,2n)+(\gamma,p2n)]$, (d) $\sigma(\gamma,3n)$.

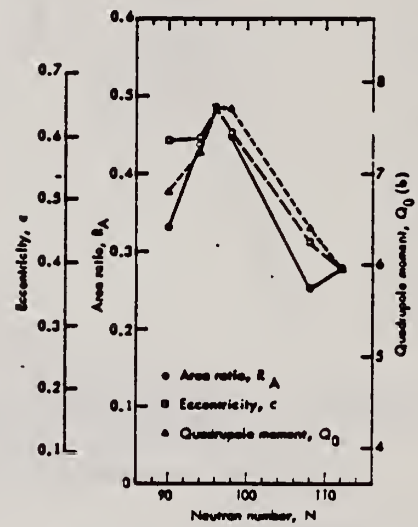

Fig. 9. The area ratio R_A, nuclear eccentricity ϵ, and intrinsic quadrupole moment Q_0 plotted versus neutron number N. The data were scaled between the value for Gd^{160} and that for W^{186}. The absolute scale for Q_0 is based on a mean radius parameter $R_0 = 1.26$ F. The lines merely connect the three sets of data points. The experimental uncertainties have been omitted for clarity but are given in Tables VII and VIII; their average values are 0.065 (17%) for R_A, 0.010 (1.9%) for ϵ, and 0.26b (3.7%) for Q_0.

[over]

Table V. Parameters of Lorentz-curve fits to the giant resonance.

Nucleus	$E_m(1)$ (MeV)	$\sigma_m(1)$ [a] (mb)	$\Gamma(1)$ (MeV)	$E_m(2)$ (MeV)	$\sigma_m(2)$ [a] (mb)	$\Gamma(2)$ (MeV)
Eu^{153}	12.33±0.06	155±9	2.75±0.26	15.79±0.10	222±6	5.83±0.30
Tb^{159} [b]	12.22±0.04	181±6	2.64±0.16	15.67±0.06	220±4	4.97±0.19
Gd^{160}	12.23±0.06	215±9	2.77±0.25	15.96±0.09	233±6	5.28±0.30
Ho^{165}	12.28±0.02	214±5	2.57±0.11	15.78±0.04	246±3	5.00±0.17
Ta^{181} [c]	12.59±0.03	171±8	1.94±0.12	15.13±0.12	265±6	4.98±0.23
W^{186}	12.59±0.03	211±14	2.29±0.14	14.88±0.08	334±8	5.18±0.14

[a] The uncertainties for σ_m given here are relative. The absolute uncertainty is 7% (10% for Tb^{159} and Ta^{181}).
[b] The data of Ref. 10 were reanalyzed to obtain the values given in this and subsequent tables (see text).
[c] The data of Ref. 11 were reanalyzed to obtain the values given in this and subsequent tables (see text).

10 R.L. Bramblett, J. T. Caldwell, R. R. Harvey, S.C. Fultz, Phys.Rev.133, B869 (1964).
11 R.L. Bramblett, J.T. Caldwell, G.F. Auchampaugh, S.C. Fultz, Phys.Rev.129, 2723 (1963)

Table VIII. Nuclear radius parameters.

Nucleus	Q_0 [a] (b)	Refs.	β [b]	R_0 [c] (F)	Q_0 [d] (b)
Eu^{153}	6.99±0.08	e, f	0.595±0.015	1.276±0.018	6.80±0.28
Tb^{159}	7.41±0.11	e	0.598±0.009	1.274±0.013	7.23±0.26
Gd^{160}	7.55±0.17	g	0.645±0.014	1.245±0.020	7.71±0.30
Ho^{165}	7.56±0.11	e	0.604±0.006	1.246±0.011	7.71±0.26
Ta^{181}	6.89±0.21	h, i	0.433±0.010	1.306±0.025	6.43±0.26
W^{186}	5.96±0.05	g, j, k	0.390±0.006	1.259±0.011	5.96±0.21

[a] Values taken from or computed from the references listed in column 3.
[b] Values from present data (Table VII).
[c] Computed from Eq. (2) in the text.
[d] The "best" values for Q_0 deduced from the present data, computed from Eq. (2) in the text, taking R_0 to be 1.26±0.02 F.
[e] M. C. Olesen and B. Elbek, Nucl. Phys. 15, 134 (1960).
[f] R. A. Carrigan, Jr., P. D. Gupta, R. B. Sutton, M. N. Suzuki, A. C. Thompson, R. E. Coté, W. V. Prestwich, A. K. Gaigalas, and S. Raboy, Phys. Rev. Letters 20, 874 (1968).
[g] P. H. Stelson and L. Grodzins, Nucl. Data A1, 21 (1965).
[h] F. K. McGowan and P. H. Stelson, Phys. Rev. 109, 901 (1958).
[i] E. M. Bernstein and R. Graetzer, Phys. Rev. 119, 1321 (1960).
[j] R. C. Barrett, S. Bernow, S. Devons, I. Duerdoth, D. Hitlin, J. W. Kast, W. Y. Lee, E. R. Macagno, J. Rainwater, and C. S. Wu, Columbia University Pegram Nuclear Physics Lab. Report No. NYO-72-191, 1968, p. 74 (unpublished).
[k] R. G. Stokstad and B. Persson, Phys. Rev. 170, 1072 (1968).

Table IX. Integrated cross sections.

Nucleus	$E_{\gamma\,max}$ (MeV)	$\sigma_{int}[(\gamma,n)+(\gamma,pn)]$ [a] (MeV-b)	$\sigma_{int}[(\gamma,2n)+(\gamma,p2n)]$ [a] (MeV-b)	$\sigma_{int}(\gamma,3n)$ [a] (MeV-b)	$\frac{\sigma_{int}[(\gamma,2n)+(\gamma,p2n)]}{\sigma_{int}(\gamma,\text{total})}$ [b]	$\frac{1}{2}\pi[\sigma_m(1)\Gamma(1)+\sigma_m(2)\Gamma(2)]$ [c] (MeV-b)	$0.06\,NZ/A$ (MeV-b)
Eu^{153}	28.9	1.57	0.67	0.04	0.29±0.04	2.70±0.19	2.22
Tb^{159}	28.0	1.41	0.89	d	0.39±0.08	2.47±0.12	2.31
Gd^{160}	29.5	1.45	1.00	0.08	0.39±0.05	2.87±0.20	2.30
Ho^{165}	28.9	1.73	0.74	0.04	0.29±0.04	2.80±0.09	2.39
Ta^{181}	24.6	1.31	0.88 [e]	f	0.40 [e] ±0.08	2.59±0.15	2.61
W^{186}	28.6	1.66	1.19	0.15	0.40±0.05	3.47±0.17	2.67

[a] All measured integrated cross-section values are given for an energy region from threshold to $E_{\gamma\,max}$.
[b] The word "total" in this table refers to the total photoneutron cross section, $\sigma[(\gamma,n)+(\gamma,pn)+(\gamma,2n)+(\gamma,p2n)+(\gamma,3n)]$.
[c] The uncertainties listed here are relative; to get the absolute uncertainty, a systematic uncertainty of 7% (10% for Tb^{159} and Ta^{181}) must be folded into the values for σ_m.
[d] Not measured in Ref. 10; $\sigma_{int}[(\gamma,2n)+(\gamma,p2n)]$ contains $\frac{1}{2}\sigma_{int}(\gamma,3n)$.
[e] Because $E_{\gamma\,max}$ is so low, these values cannot be compared to the rest.
[f] Not measured in Ref. 11; the $(\gamma,3n)$ cross section below 24.6 is MeV probably negligible.

Table X. Integrated moments[a] of the measured photoneutron cross section and sum rules.

Nucleus	σ_{-1} (mb)	$\sigma_{-1}A^{-4/3}$ (mb)	σ_{-2} (mb-MeV^{-1})	$\frac{\sigma_{-2}}{0.00225\,A^{5/3}}$	$\frac{\sigma_{-2}K}{0.05175\,A^{5/3}}$	$\frac{0.05175\,A^{5/3}}{\sigma_{-2}}$ (MeV)
Eu^{153}	148	0.181	10.18	1.03	1.16±0.11	22.2±1.6
Tb^{159}	151	0.175	10.49	1.00	1.14±0.13	23.0±2.3
Gd^{160}	169	0.195	12.09	1.14	1.35±0.13	20.2±1.4
Ho^{165}	166	0.183	11.56	1.04	1.23±0.10	22.2±1.6
Ta^{181} [b]	(149)	(0.145)	(10.66)	(0.82)	(0.97±0.13)	(28.1±2.8)
W^{186}	203	0.191	14.51	1.06	1.26±0.11	21.6±1.5

[a] $\sigma_{-1} = \int_{E_{thr}}^{E_{\gamma\,max}} \sigma E^{-1}\,dE$ and $\sigma_{-2} = \int_{E_{thr}}^{E_{\gamma\,max}} \sigma E^{-2}\,dE$, where σ is the total photoneutron cross section.
[b] Because $E_{\gamma\,max}$ is so low, the values for Ta^{181} cannot be compared to the rest.

M. A. Kelly, B. L. Berman, R. L. Bramblett and S. C. Fultz
Phys. Rev. 179, 1194 (1969)

Ho	165	67

METHOD	REF. NO.	
	69 Ke 2	hmg

REACTION	RESULT	EXCITATION ENERGY	SOURCE TYPE	SOURCE RANGE	DETECTOR TYPE	DETECTOR RANGE	ANGLE
$G,XN	ABX	10-21	D	10-21	BF3-I		4PI

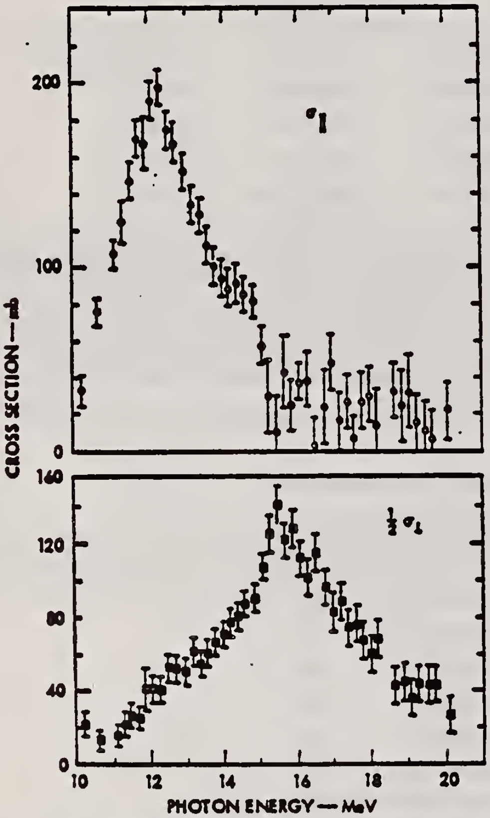

FIG. 14. The intrinsic cross sections for Ho[165]. The cross section $\sigma_{\|}$ is associated with vibrations along the nuclear symmetry axis. One-half $\sigma_\perp$ is half the cross section associated with vibrations perpendicular to the symmetry axis. The error bars represent statistical errors, and not those due to the uncertainty of f_2.

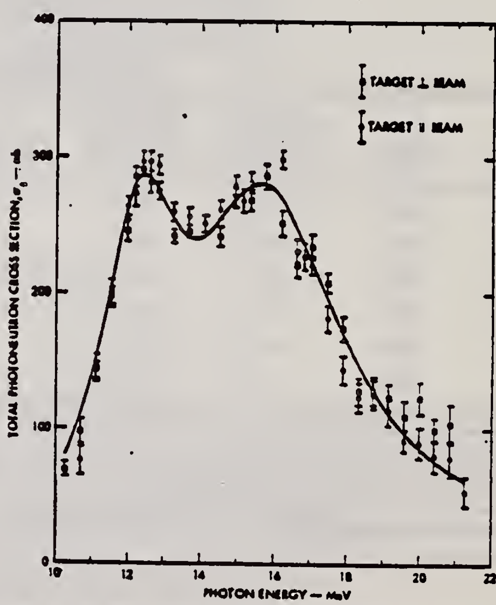

FIG. 10. The two unpolarized cross sections taken with the target oriented parallel to the photon beam and perpendicular to the beam. The target temperature during these measurements was 4.2°K; otherwise, the conditions were identical to those during the polarized runs. The solid line is a two-component Lorentz curve fit to the data, the parameters of which are given in Table III B.

[over]

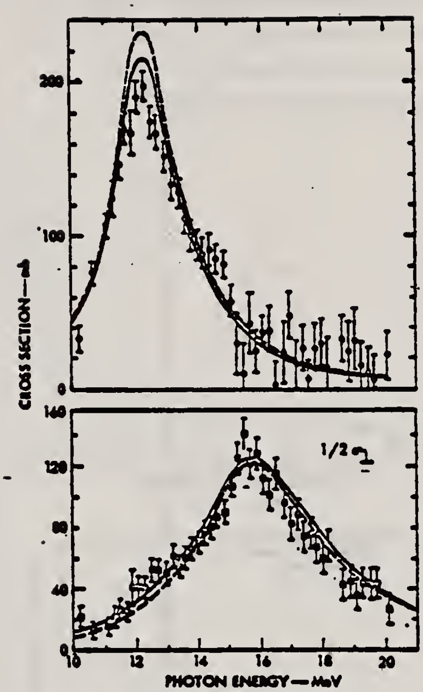

FIG. 16. The intrinsic cross sections for Ho^{165}. The cross section $\sigma_{\parallel}$ is associated with vibrations along the nuclear symmetry axis; $\sigma_{\perp}$ is that associated with vibrations perpendicular to this axis. The error bars represent statistical errors, and not those due to the uncertainty of f_2. The solid curves are those derived from the elementary collective model; the dashed ones are calculated from the dynamic collective model.

REF.		ELEM. SYM.	A	Z
T. Methasiri and S. A. E. Johansson Nucl. Phys. A167, 97 (1971)		Ho	165	67

METHOD	REF. NO.	
	71 Me 1	egf

REACTION	RESULT	EXCITATION ENERGY	SOURCE TYPE	SOURCE RANGE	DETECTOR TYPE	DETECTOR RANGE	ANGLE
G,F	ABY	THR-900	C	300-900	FRG-I		4PI

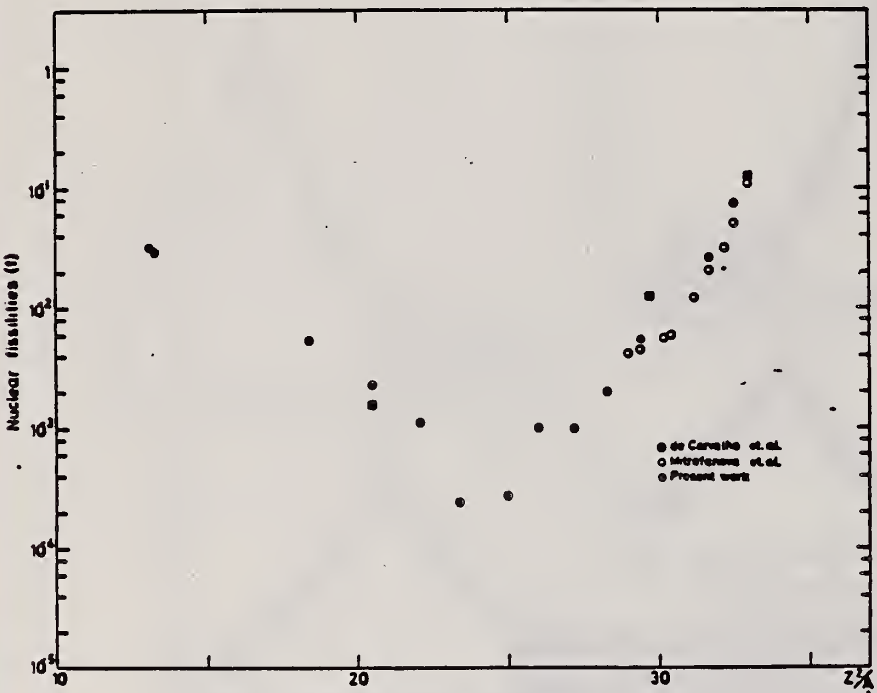

Fig. 2. Nuclear fissilities as a function of Z^2/A.

TABLE 1

The constant fission cross sections above the threshold

Element	σ_f (cm²)	Element	σ_f (cm²)
Pb	$(5.0\pm0.2)\times10^{-27}$	La	$(1.1\pm0.1)\times10^{-29}$
Au	$(1.7\pm0.1)\times10^{-27}$	Sn	$(4.3\pm1.1)\times10^{-29}$
Ta	$(3.3\pm0.2)\times10^{-28}$	Ag	$(8.4\pm2.0)\times10^{-29}$
Yb	$(1.2\pm0.2)\times10^{-28}$	Mo	$(1.7\pm0.4)\times10^{-28}$
Ho	$(5.5\pm0.3)\times10^{-29}$	Cu	$(6.6\pm1.2)\times10^{-28}$
Gd	$(5.3\pm0.8)\times10^{-29}$	Ni	$(5.8\pm0.1)\times10^{-28}$
Nd	$(1.3\pm0.2)\times10^{-29}$		

[over]

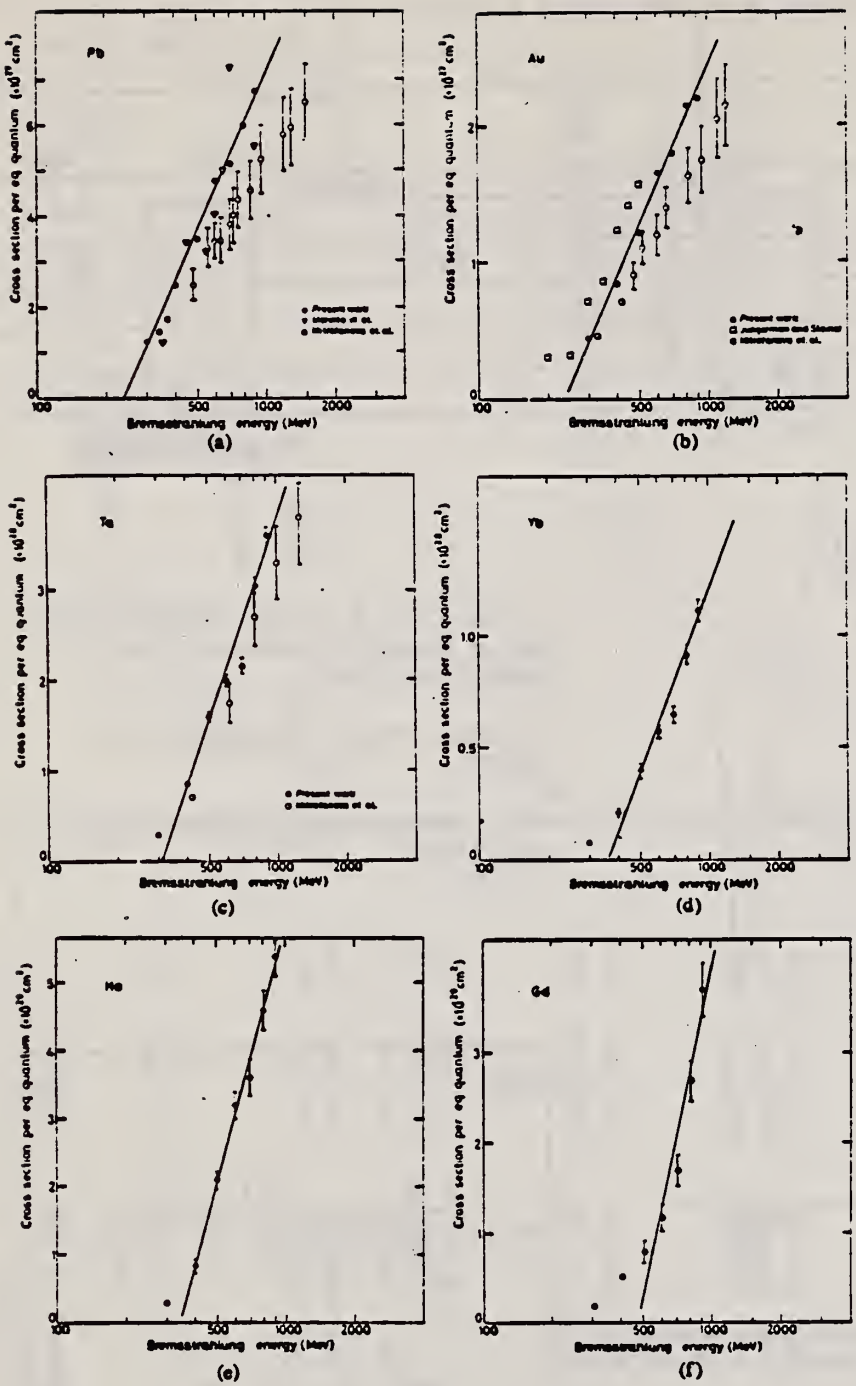

Fig. 1. Cross sections per equivalent quantum $\sigma_q(\bar{E})$ as a function of log $\bar{E}$.

REF.

R.F. Barrett, J.R. Birkelund, B.J. Thomas, K.S. Lam, and H.H. Thies
Nucl. Phys. A210, 355 (1973)

ELEM. SYM.	A	Z
Ho	165	67
REF. NO. 73 Ba 20		egf

METHOD

REACTION	RESULT	EXCITATION ENERGY	SOURCE TYPE	SOURCE RANGE	DETECTOR TYPE	DETECTOR RANGE	ANGLE
G,N	NOX	THR- 27	C	10- 27	BF3-I		4PI

MEAN NEUT ENERGY

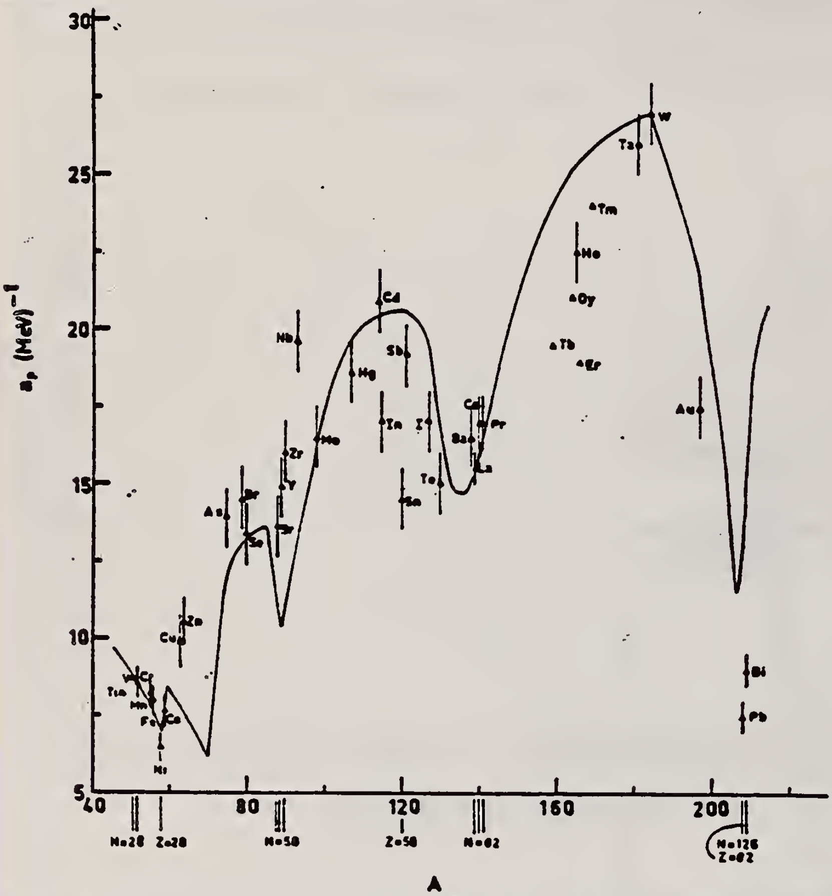

Fig. 12. Experimental values of the level density parameter a_p (Fermi gas formula plus pairing correction) versus atomic number A. The continuous curve is a least-squares fit to the data of a theoretical calculation from Newton [15].

1
H. Baba and S. Baba, Japan Atomic Energy Research Institute report JAERI-1183 (1969).
2
H. Baba, Nucl. Phys. A159, 625 (1970).
15
T.D. Newton, Can. J. Phys. 34, 804 (1956).

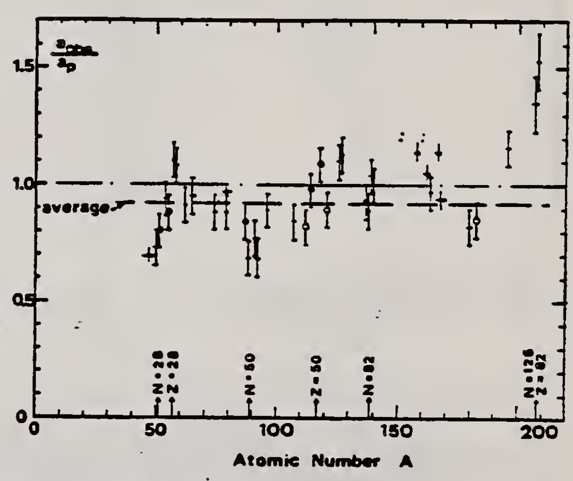

Fig. 15. Ratio a_{obs}/a_p versus atomic number A. Here a_{obs} is the level density parameter taken from the neutron resonance work of refs. [1,2]), and a_p is the level density parameter derived from the present (γ, n) work. Filled circles represent points where nuclei in the neutron resonance and in the (γ, n) experiment were the same. Open circles represent points where the respective nuclei were approximately matched. Triangles represent points which are based on measurement of neutron mean energies at two bremsstrahlung energies only.

(over)

TABLE 3 (continued)

Target	N (residual nucleus) [a]		Goodness of fit [b] no p.c.	Goodness of fit [b] with p.c.	$\hat{E}_n(24)$ (MeV) [c]	T (MeV) [d]	a_p (MeV^{-1}) [e]	a_{obs} (MeV^{-1}) [f]	a_{obs}/a_p
Ba	75	1%		F	1.16		16.5–^{136}Ba	15.39–^{136}Ba	0.93
	77	2%							
	78	7%							
	79	8%							
	80	11%							
	81	71%							
La	80	100%	F	F	1.25	0.72	15.5–^{138}La	13.76–^{139}La	0.89
Ce	81	89%	F	G	1.24	0.70	17.0–^{139}Ce	17.8 –^{141}Ce	1.04
	83	11%							
Pr	81	100%	G	G	1.17	0.65	17.0–^{140}Pr	17.05–^{142}Pr	1.00
Tb [g]	93	100%			1.15		19.3–^{158}Tb	21.85–^{160}Tb	1.14
Dy [g]	93	2%			1.06		20.9–$^{161.5}$Dy	21.9 –^{162}Dy	1.05
	94	19%							
	95	25%							
	96	25%							
	97	28%							
Ho	97	100%	P	G	1.06	0.56	21.4–^{164}Ho	20.66–^{166}Ho	0.97
Er [g]	95	2%			1.11		19.2–^{166}Er	21.9 –^{166}Er	1.14
	97	33%							
	98	23%							
	99	27%							
	101	15%							
Tm [g]	99	100%			1.03		24.0–^{169}Tm	22.58–^{170}Tm	0.94
Ta	107	100%		G	1.00	0.49	26.0–^{180}Ta	21.2 –^{181}Ta	0.82
W	107	26%	G	F	0.98	0.50	27.0–^{183}W	23.0 –^{183}W	0.85
	108	14%							
	109	31%							
	111	28%							
Au	117	100%		G	1.19		17.5–^{196}Au	20.24–^{198}Au	1.16
Pb ($Z = 82$)	123	24%		V.P.	1.87	1.20	7.5–^{206}Pb	10.1 –^{207}Pb	1.35
	124	23%							
	125	52%							
Bi	125	100%		F	1.65	1.03	9.0–^{208}Bi	13.8 –^{210}Bi	1.53

[a] Neutron numbers and abundances of respective residual nuclei in (γ, n) experiments.

[b] These give an assessment of the goodness of fit of a calculated $\hat{E}_n$ versus E_0 curve to the observed data, using the Fermi gas level density formula both without and with pairing corrections.

[c] Bremsstrahlung photoneutron mean energies $\hat{E}_n$ for peak bremsstrahlung energy $E_0 = 24$ MeV.

[d] Nuclear temperature from fit with constant-temperature formula.

[e] Level density parameter a_p derived from the present (γ, n) experiment, using a Fermi gas formula plus pairing correction, and corresponding residual nucleus (the atomic weight shown is the weighted average of atomic weights of the respective isotopes present).

[f] As column 7, but using data on n-resonance absorption from refs. [1,2]).

[g] Measurements of $\hat{E}_n(E_0)$ for these nuclei were made only for $E_0 = 21$, 23 and 24 MeV.

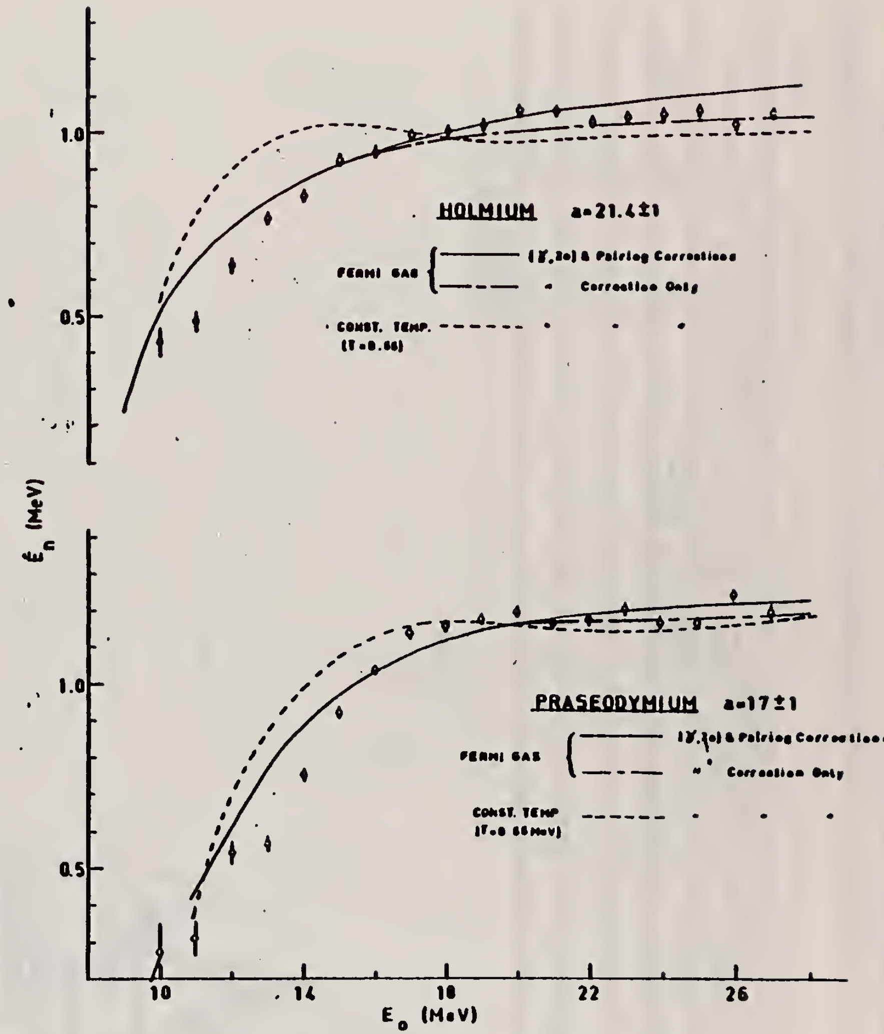

Fig. 10. Same as fig. 5, for praseodymium and holmium.

REF.	ELEM. SYM.	A	Z
D.K. Kaipov, Yu.A. Lysikov, and Yu.K. Shubnyi Izv. Akad. Nauk SSSR Ser. Fiz. 37, 1095 (1973) Bull. Acad. Sci. USSR Phys. Ser. 37, 160 (1973)	Ho	165	67
METHOD	REF. NO. 73 Ka 8		hmg

REACTION	RESULT	EXCITATION ENERGY	SOURCE TYPE	SOURCE RANGE	DETECTOR TYPE	DETECTOR RANGE	ANGLE
G,G	ABX	95*	D	95*	SCD-D		UKN

*ENERGY IN KEV

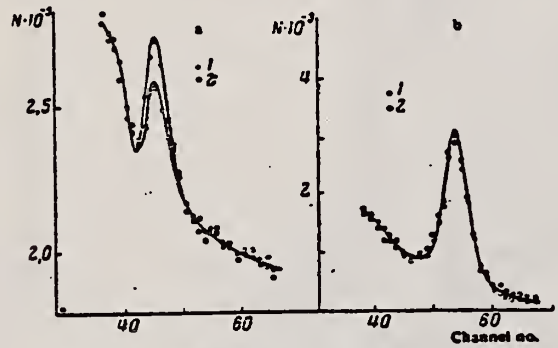

Fig. 2. Scattered radiation spectra: b) with ^{155}Eu source (E_γ = 105 keV). 1) Ho scatterer; 2) (Ta + Cd) scatterer. N is the number of pulses in an interval of 10 min. a) ^{165}Dy source. 1) Ho scatterer; 2) (Ta + Cd) scatterer. N is the number of pulses in an interval of 20 min.

The counting ratio for Ho and Ta + Cd was N_{Ta}/N_{Ho} = 1.065 ± 0.015 (this is an average for ten series of measurements). Figure 2a shows the spectrum of the scattered radiation in the region of 100 keV using the ^{165}Dy source. It is clear from this figure that the elastic peak is recorded against a background of strong Compton scattering due to the higher energy ^{165}Dy γ-rays. In this case we have found that N_{Ta}/N_{Ho} = 0.675 ± 0.118. The resonance scattering cross section was calculated by comparing the resonance scattering intensities with the Rayleigh intensity, the cross section for which can be calculated exactly. We found that $\sigma = (1.95 \pm 0.35)\cdot 10^{-25}\ \mathrm{cm}^2\cdot\mathrm{sterad}^{-1}$, which corresponds to $\Gamma_{0\gamma}$ = $= (4.85 \pm 0.82)\cdot 10^{-6}$ eV for the radiation width of the 94.69 keV level of ^{165}Ho, and $\tau_\gamma = (1.36 \pm 0.24)\cdot 10^{-10}$ sec.

REF.	ELEM. SYM.	A	Z
D. Catana, G. Baciu, M. Ionescu-Bujor, V.I.R. Niculescu, and C. Iliescu Nucl. Phys. A225, 157 (1974)	Ho	165	67
METHOD	REF. NO. 74 Ca 7		egf

REACTION	RESULT	EXCITATION ENERGY	SOURCE TYPE	SOURCE RANGE	DETECTOR TYPE	DETECTOR RANGE	ANGLE
G,XN	ABX	8- 23	C	8- 23	BF3-I		4PI

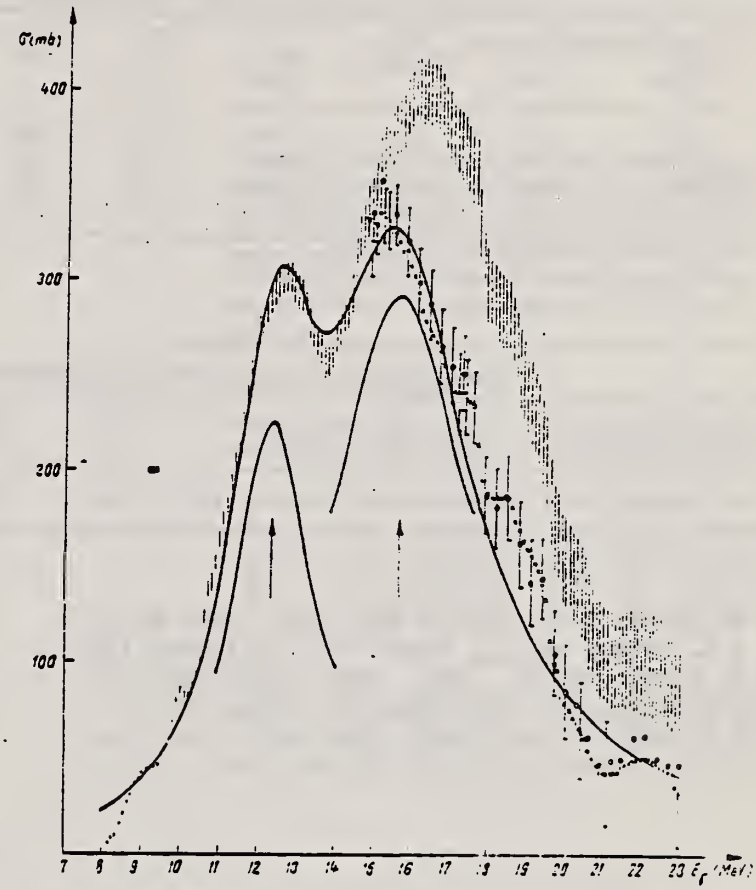

Fig. 1. Total cross section data showing a two Lorentz line fit for ^{165}Ho. The total cross secti.. has been obtained taking into account $\sigma(\gamma, 2n)$ from ref. [3]) (○) and from ref. [4]) (×).

TABLE 1

Comparison between the absolute cross section values for ^{165}Ho

E (MeV)	σ (mb)	E (MeV)	σ (mb)	E_1 (MeV)	σ_1 (mb)	E_2 (MeV)	σ_2 (mb)	Ref.
9	35.6±4	10.83	150±20					[16])
9	36 ±2	10.83	138± 6	12.4	290±11	15.3	275±11	[3])
9	48 ±5	10.83	165± 5	12.2	323±18	15.4	325±18	[4])
9	44 ±3	10.83	143± 8	12.6±0.1	301±10	15.3±0.2	330±18	present

(over)

Table 2

Comparison between the Lorentz line parameters for a two line fit of the total cross section data of ^{165}Ho

E_1	Γ_1	σ_1	E_2	Γ_2	σ_2	$\frac{\int \sigma_2 dE}{\int \sigma_1 dE}$	Ref.
12.02±0.04	2.35±0.22	236±12	15.59±0.09	4.85±0.4	308±11	2.69	[5]
12.28±0.025	2.57±0.11	214±15	15.78±0.0044	5.00±0.17	246±18	2.24	[3]
12.2	2.33	219	16	5	226	2.60	[2]
12.07	2.7	250	15.62	4.8	285	2.07	[4]
12.30	2.60	225	15.65	4.65	290	2.30	present
12.15	2.49	204	15.61	4.66	245	2.25	theory

Table 3

Integrated cross section, moments of the different measured cross sections and sum rules for ^{165}Ho

σ_σ exp. (b · MeV)	σ_{0L} (b · MeV)	$\frac{\sigma_{0L}}{0.06\, NZ/A}$	σ_{-1} exp. (mb)	σ_{-1L} (mb)	$\frac{\sigma_{-1L}}{A^{\frac{4}{3}}}$	σ_{-2} exp. (mb · MeV^{-1})	σ_{-2L} (mb · MeV^{-1})	$\frac{\sigma_{-2L}}{A^{\frac{5}{3}}}$	Ref
2.51	2.81	1.12	166	177	0.20	11.56	13.55	2.73	[3]
2.79±0.25	3.71	1.34	194±14	208	0.23	14 ±1	16.07	3.24	[4]
2.60±0.2	3.04	1.27	178±15	171	0.19	12.8±1.5	14.66	2.95	prese
	2.59	1.09		165	0.18		12.35	2.5	

Table 4

Parameters used for computation of E1 photoabsorption cross section

ε	μ_n			μ_p			κ	$\frac{\hbar^2}{2I}$	ΔE (MeV)		a	Γ (MeV)	
	$N=4$	$N=5$	$N=6$	$N=3$	$N=4$	$N=5$			n	p		$\Delta K=0$	$\Delta K=\pm 1$
0.30	0.45	0.448	0.434	0.35	0.625	0.630	0.05	0.011	0.76	1.05	1.96	1	2

2) E. Ambler et al., Phys. Rev. 138 (1965) B117
3) B.L. Berman et al., Phys. Rev. 125 (1969) 1576
4) R. Bergere et al., Nucl. Phys. A121 (1961) 463
5) P. Axel et al, J. de Phys. 27 (1966) 262
16) R.R. Hurst et al., Nucl. Phys. A91 (1967) 365

REF. H. E. Jackson, G. E. Thomas, K. J. Wetzel
Phys. Rev. C11, 1664 (1975)

ELEM. SYM.	A	Z
Ho	165	67

METHOD

REF. NO.	
75 Ja 1	hmg

REACTION	RESULT	EXCITATION ENERGY	SOURCE TYPE	SOURCE RANGE	DETECTOR TYPE	DETECTOR RANGE	ANGLE
G,G	ABX	11	D	11	SCD-D		150
		(11.387)		(11.387)			

RATIO RAMAN/ELASTIC

TABLE I. Differential cross sections measured for elastic and inelastic scattering of 11.39-MeV photons. State or states populated by inelastic scattering are indicated in parentheses beside the target. The errors given result from the statistical error in the measurement of the cross section relative to the calibration value, the 90° uranium elastic cross section.

θ (deg)	$d\sigma/d\omega$ (elastic) (mb/sr)	$d\sigma/d\omega$ (inelastic) (mb/sr)
	^{238}U (2^+, 45 keV)	
90	0.169 ± 0.011	0.173 ± 0.016
150	0.355 ± 0.041	0.236 ± 0.24
	^{232}Th (2^+, 45 keV)	
150	0.331 ± 0.035	0.210 ± 0.022
	^{181}Ta ($\frac{9}{2}^+$, 136 keV) ($\frac{11}{2}^+$, 301 keV)	
90	0.073 ± 0.008	0.020 ± 0.004 0.009 ± 0.004
150	0.145 ± 0.015	0.017 ± 0.004 0.017 ± 0.004
	^{165}Ho ($\frac{9}{2}^+$, 95 keV) ($\frac{11}{2}^+$, 210 keV)	
150	0.141 ± 0.014	0.022 ± 0.004 0.013 ± 0.004
	^{159}Tb ($\frac{5}{2}^+$, 58 keV) ($\frac{7}{2}^+$, 138 keV)	
90	0.062 ± 0.006	0.024 ± 0.003 0.013 ± 0.003
150	0.134 ± 0.012	0.042 ± 0.004 0.019 ± 0.004
	^{141}Pr	
150	0.030 ± 0.008	...

TABLE III. Comparison of calculated and observed values of the cross sections for elastic scattering and of the ratio of Raman to elastic scattering by various nuclei for 11.387-MeV photons at 90 and 150°. The parameters used in the calculations for column 5 are given in Table II. Column 4 describes results obtained by perturbing those parameter to meet the constraint of Eq. (3) (see text).

Target	$d\sigma(\theta)d\Omega$ (mb/sr) Calc.	Exp.	$d\sigma_{\mathrm{Raman}}(\theta)/d\sigma_{\mathrm{elastic}}(\theta)$		
		$\theta = 150°$			
Pr	0.025	0.030 ± 0.008		0.0	0.0
Tb	0.094	0.134 ± 0.012	0.53	0.57	0.46 ± 0.04
Ho	0.170	0.141 ± 0.014	0.28	0.28	0.25 ± 0.04
Ta	0.160	0.145 ± 0.015	0.23	0.22	0.23 ± 0.04
Th	0.253	0.331 ± 0.035	0.59	0.63	0.64 ± 0.08
U	0.289	0.355 ± 0.041	0.78	0.73	0.67 ± 0.07
		$\theta = 90°$			
Tb	0.062	0.062 ± 0.006	0.76	0.82	0.60 ± 0.07
Ta	0.109	0.074 ± 0.008	0.32	0.30	0.38 ± 0.07
U	0.172	0.169 ± 0.005	1.29	1.15	1.03 ± 0.10

REF.

V. Emma, S. Lo Nigro, C. Milone
Nucl. Phys. A257, 438 (1976)

ELEM. SYM.	A	Z
Ho	165	67

METHOD

REF. NO.	
76 Em 2	egf

REACTION	RESULT	EXCITATION ENERGY	SOURCE TYPE	SOURCE RANGE	DETECTOR TYPE	DETECTOR RANGE	ANGLE
G,F	ABY	THR-999	C	999	TRK-I		4PI

999 = 1 GEV

TABLE 1

Measured values of σ_q at $E = 1000$ MeV and deduced values of σ_k assumed constant from E_0 to 1000 MeV

Element	Z^2/A	σ_q (mb)	E_0 (MeV)	σ_k (mb)
Bi	32.96	12.3 ± 0.6	200	7.6 ± 0.6
Pb	32.45	5.4 ± 0.4	220	3.6 ± 0.3
Tl	32.10	4.1 ± 0.3	230	2.8 ± 0.3
Au	31.68	2.0 ± 0.15	240	1.4 ± 0.2
Pt	31.18	1.1 ± 0.08	255	$(8 \pm 0.7) \times 10^{-1}$
Re	30.21	$(3.7 \pm 0.3) \times 10^{-1}$	280	$(2.9 \pm 0.3) \times 10^{-1}$
W	29.78	$(3.5 \pm 0.3) \times 10^{-1}$	290	$(2.8 \pm 0.3) \times 10^{-1}$
Ta	29.45	$(3.3 \pm 0.3) \times 10^{-1}$	300	$(2.7 \pm 0.3) \times 10^{-1}$
Hf	29.04	$(1.7 \pm 0.2) \times 10^{-1}$	310	$(1.4 \pm 0.2) \times 10^{-1}$
Yb	28.31	$(1.3 \pm 0.1) \times 10^{-1}$	330	$(1.2 \pm 0.1) \times 10^{-1}$
Tm	28.18	$(7.5 \pm 0.8) \times 10^{-2}$	335	$(6.8 \pm 0.8) \times 10^{-2}$
Ho	27.21	$(3.6 \pm 0.4) \times 10^{-2}$	355	$(3.5 \pm 0.4) \times 10^{-2}$
Dy	26.80	$(2.6 \pm 0.3) \times 10^{-2}$	360	$(2.5 \pm 0.3) \times 10^{-2}$
Tb	26.58	$(2.5 \pm 0.3) \times 10^{-2}$	370	$(2.5 \pm 0.3) \times 10^{-2}$
Gd	26.04	$(1.6 \pm 0.2) \times 10^{-2}$	380	$(1.7 \pm 0.2) \times 10^{-2}$
Sm	25.56	$(1.3 \pm 0.2) \times 10^{-2}$	390	$(1.4 \pm 0.2) \times 10^{-2}$
Nd	24.96	$(9.2 \pm 0.9) \times 10^{-3}$	405	$(1 \pm 0.1) \times 10^{-2}$
Ce	24.00	$(8 \pm 0.9) \times 10^{-3}$	420	$(9 \pm 1) \times 10^{-3}$
La	23.39	$(8.4 \pm 0.9) \times 10^{-3}$	430	$(1 \pm 0.1) \times 10^{-3}$
Sb	21.36	$(1.2 \pm 0.2) \times 10^{-2}$	460	$(1.5 \pm 0.3) \times 10^{-2}$
Te	21.19	$(8.8 \pm 1) \times 10^{-3}$	465	$(1.2 \pm 0.2) \times 10^{-2}$
Sn	21.06	$(1.3 \pm 0.2) \times 10^{-2}$	465	$(1.7 \pm 0.3) \times 10^{-2}$
Cd	20.49	$(1.7 \pm 0.3) \times 10^{-2}$	470	$(2.2 \pm 0.4) \times 10^{-2}$
Ag	20.47	$(2 \pm 0.3) \times 10^{-2}$	470	$(2.6 \pm 0.4) \times 10^{-2}$
Zn	13.76	$(2 \pm 0.4) \times 10^{-1}$	515	$(3 \pm 0.6) \times 10^{-1}$
Cu	13.44	$(2.4 \pm 0.5) \times 10^{-1}$	515	$(3.6 \pm 0.8) \times 10^{-1}$
Ni	13.35	$(2.4 \pm 0.5) \times 10^{-1}$	510	$(3.6 \pm 0.8) \times 10^{-1}$
Fe	12.10	$(3 \pm 0.6) \times 10^{-1}$	510	$(4.4 \pm 0.9) \times 10^{-1}$

[4] A.V. Mitrofanova et al. Sov. J. Nucl. Phys. 6, 512 (1968).

[7] T. Methasiri et al., Nucl. Phys. A167, 97 (1971).

[12] J.R. Nix et al., Nucl. Phys. 81, 61 (1966).

[20] N.A. Perfilov et al., JETP (Sov. Phys.) 14, 623 (1962); Proc. Symp. on the physics & chemistry of fission, Salzburg 1965, vol. 2 (IAEA) Vienna, 1965, p.283.

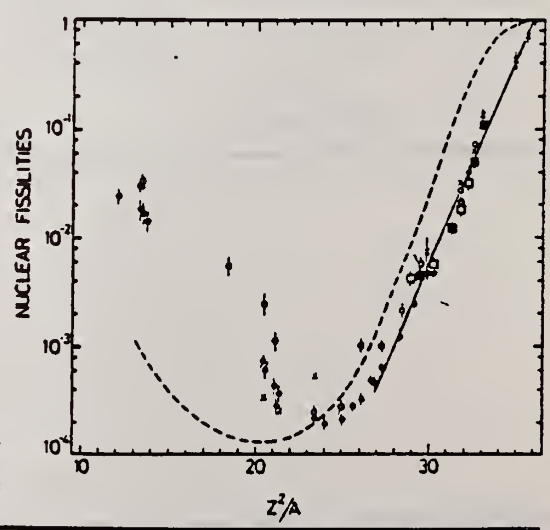

Fig. 2. Nuclear fissilities as a function of Z^2/A. Experimental points: solid circles represent our data; squares, the data from ref. [4]; open circles, the data from ref. [7]; and crosses, the data from (p, f) experiments[20]. The straight line is the best fit calculated from our data for $Z^2/A > 26$. The dashed curve is the curve VI calculated by Nix and Sassi[12].

REF.	B.I. Goryachev, Yu.V. Kuznetsov, V.N. Orlin, N.A. Pzhidaeva, V.G. Shevchenko Yad. Fiz. 23, 1145 (1976) Sov. J. Nucl. Phys. 23, 609 (1976)	ELEM. SYM.	A	Z
		Ho	165	67
METHOD		REF. NO.		
		76 Go 4		hmg

REACTION	RESULT	EXCITATION ENERGY	SOURCE TYPE	SOURCE RANGE	DETECTOR TYPE	DETECTOR RANGE	ANGLE
G,XN	ABX	8- 23	C	UKN	BF3-I		4PI
G,2N	ABX	14- 21	C	UKN	SCI-I		4PI

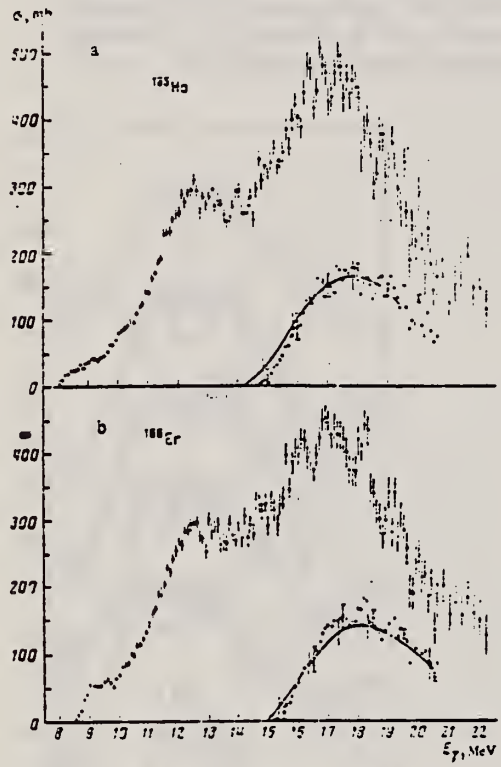

FIG. 1. Photoneutron production cross section σ_n obtained for ^{165}Ho (a) and for ^{166}Er (b). The hollow and solid circles correspond to two independent series of data. The solid curves show the $(\gamma, 2n)$ cross sections calculated from the data of a statistical experiment by the regularization method.[12] The circles near the curves give the same cross sections calculated from the formula $\sigma_n(1 - f(E, a))$.

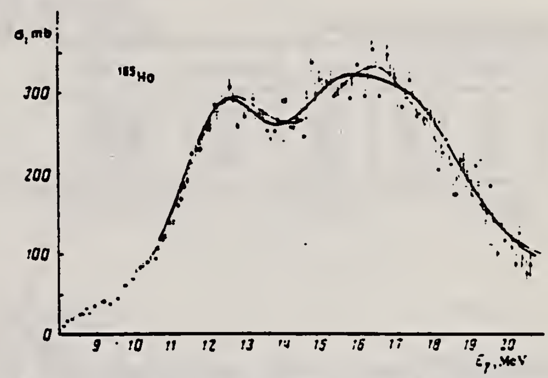

FIG. 5. Cross section σ_γ for ^{165}Ho. The thin and thick curves show respectively the approximations $\bar{\sigma}_\gamma^{(2)}$ and $\bar{\sigma}_\gamma^{(3)}$ (see the caption to Fig. 3).

TABLE 3. Static deformation β and intrinsic quadrupole moment Q_0.

Nucleus	Present work		Other photonuclear experiments		Coulomb excitation of nuclei
	β	Q_0, b	β	Q_0, b	Q_0, b
^{159}Tb	0.29	6.33±0.6	0.29 0.32 0.20	6.37 [18] 7.37 [20] 6.6 [21]	7.07 [19]
^{165}Ho	0.32	7.73±0.6	0.29 0.30 0.31	7.01 [18] 7.14 [20] 7.6 [16]	7.80 [19]
^{166}Er	0.30	7.39±0.6	0.28 0.31	6.96 [16] 7.6 [16]	
^{178}Hf	0.26	6.94±0.6			6.79 [22]

TABLE 1. Level-density parameters

Nucleus	a, MeV^{-1} Present work	a, MeV^{-1} Other studies	Nucleus	a, MeV^{-1} Present work	a, MeV^{-1} Other studies
^{159}Tb	—	7.7[15]	^{166}Er	6.1±2.5	8[16]
^{165}Ho	4.2±1.5	3.1[15]	^{178}Hf	17.7±7.3	—

(over)

TABLE 2. Parameters of fitted curves $\sigma_\gamma^{(2)}$

Nucleus	E_1, MeV	σ_1, mb	Γ_1, MeV	E_2, MeV	σ_2, mb	Γ_2, MeV	$\sigma_2\Gamma_2/\sigma_1\Gamma_1$	χ^2	f	$E_{\gamma 1}$, MeV	$E_{\gamma 2}$, MeV
^{159}Tb	12.28 12.41	192 213	2.91±0.09 3.31±0.05	15.76 15.95	295 282	3.42±0.13 3.01±0.07	2.56±0.23 2	197.3 216.8	97 98	10.4 10.4	20.6 20.6
^{165}Ho	12.31 12.47	204 223	2.74±0.11 3.26±0.06	16.23 16.46	308 293	3.67±0.17 3.02±0.09	3.11±0.27 2	176.0 200.9	97 98	10.4 10.4	20.6 20.6
^{166}Er	12.32 12.50	191 214	2.71±0.14 3.43±0.08	15.90 16.23	366 284	3.67±0.16 3.09±0.10	3.38±0.35 2	138.5 101.7	94 93	10.7 10.7	20.6 20.6
^{178}Hf	12.08 12.88	166 216	2.55±.10 3.22±0.11	13.03 13.46	281 237	6.09±0.27 3.37±0.20	4.00±1.70 2	172.1 173.7	89 90	10.6 10.6	20.0 20.0

Note. The lower values of the parameters in each column were found with the requirement $\sigma_2\Gamma_2 : \sigma_1\Gamma_1 = 2:1$.

TABLE 6. Integrated cross sections.

Nucleus	σ_0, MeV·b	$\sigma_0/0.06\frac{ZN}{A}$	σ_{-1}, mb	$\sigma_{-1}/A^{4/3}$	σ_{-2}, MeV·b	$\sigma_{-2}/A^{5/3}$
^{159}Tb	2.79	1.47	210	0.243	15.9	$3.41\cdot10^{-3}$
^{165}Ho	3.00	1.31	218	0.241	16.1	$3.25\cdot10^{-3}$
^{166}Er	2.56	1.48	216	0.237	16.1	$3.21\cdot10^{-3}$
^{178}Hf	3.08	1.20	196	0.196	14.8	$2.93\cdot10^{-3}$
Average		1.41±0.3		0.23±0.04		$3.1\cdot10^{-3}\pm6\cdot10^{-4}$

[12] A.N. Tikhonov, Dokl. Akad. Nauk SSSR 151, 501 (1963), Eng. transl. in Sov. Mathematics-Doklady.

[15] B. L. Berman et al., Phys. Rev. 185, 1576 (1969).

[16] R. Bergere et al., Nucl. Phys. A133, 417 (1969).

[18] E. G. Fuller et al., Nucl. Phys. 30, 613 (1962).

[19] H. Arenhovel et al., Phys. Rev. 157, 1109 (1967).

[20] R. Bergere et al., Nucl. Phys. A121, 463 (1968).

[21] O.V. Bogdankevich et al., Zh. Eksp.Teor.Fiz. 42, 1502 (1962); Sov. Phys. JETP 15, 1044 (1962).

[22] B.S. Dzhelepov in Struktura slozhynkh yader (Structure of Complex Nuclei), Atomizdat, 1966, p. 189.

REF.		ELEM. SYM.	A	Z
	G. M. Gurevich, L. E. Lazareva, V. M. Mazur, and G. B. Solodukhov JETP Lett. 23, 370 (1976) Pis'ma Zh. Eksp. Teor. Fiz. 23, 411 (1976)	Ho	165	67
METHOD		REF. NO.		
		76 Gu 5		hmg

REACTION	RESULT	EXCITATION ENERGY	SOURCE TYPE	SOURCE RANGE	DETECTOR TYPE	DETECTOR RANGE	ANGLE
G,MU-T	ABX	8- 21	C	35	NAI-D		4PI

We measured the total cross section for the absorption of rays in the region of $E1$ resonance for the nuclei ^{165}Ho, ^{178}Hf, ^{180}Hf, ^{181}Ta, ^{182}W, ^{197}Au, and ^{209}Bi. The singularity in the behavior of the resonance widths, observed in the region $160 < A < 185$, is apparently due to the influence of the neutron subshell $N = 108$.

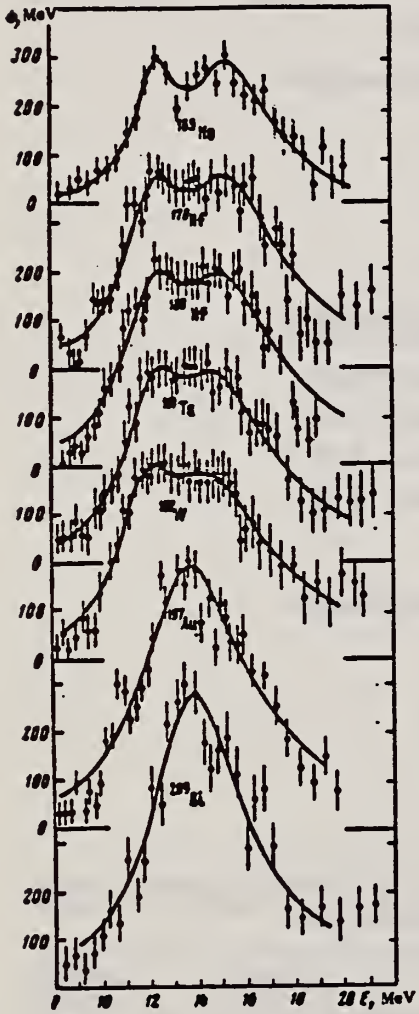

FIG. 1. Total photoabsorption cross sections for the nuclei ^{165}Ho, ^{178}Hf, ^{180}Hf, ^{181}Ta, ^{182}W, ^{197}Au, ^{209}Bi.

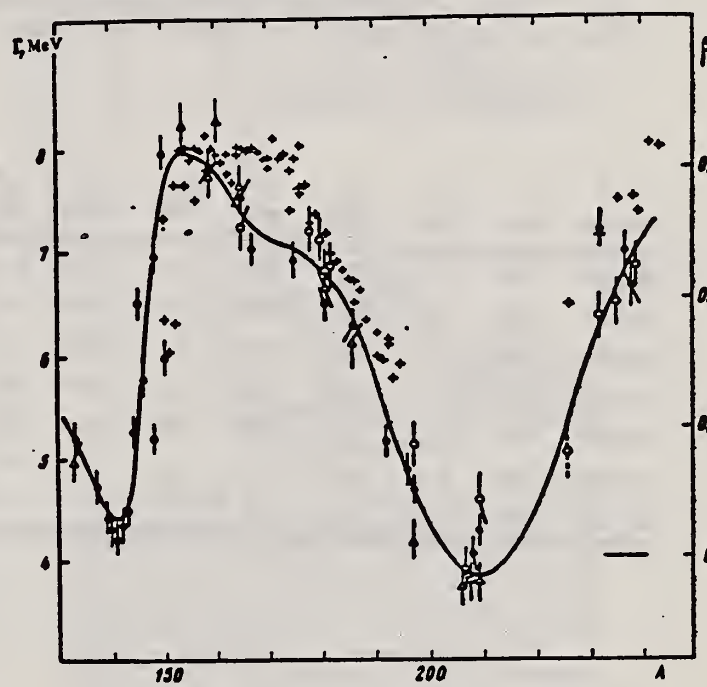

FIG. 2. Widths Γ of $E1$ giant resonance in the region of nuclei with $A > 150$ according to the data of Saclay (●), Livermore (△), and the Institute of Nuclear Research of the USSR Academy of Sciences (○). The crosses mark the deformation parameters β.

over

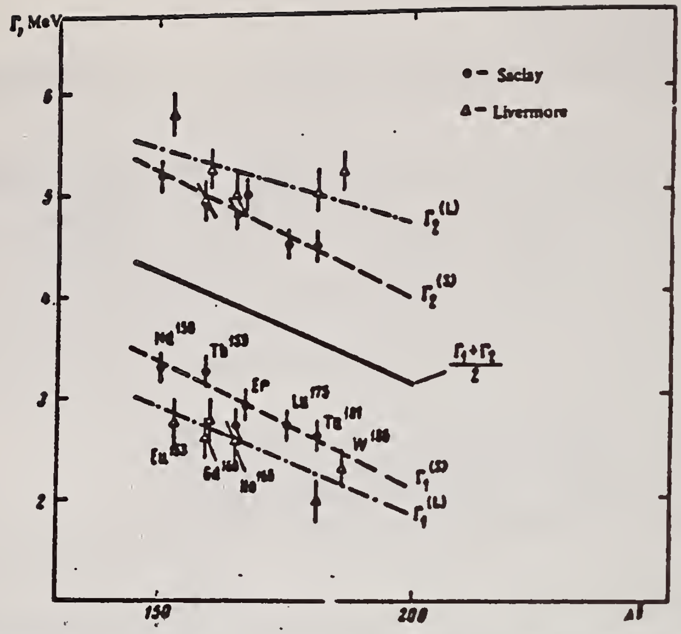

FIG. 3. Width of Lorentz lines approximating the photoabsorption cross sections, for deformed nuclei in the region $150 < A < 185$.

Nucleus	σ_1 mb	Γ_1 MeV	E_1 MeV	σ_2 mb	Γ_2 MeV	E_2 MeV	$\frac{\sigma_2\Gamma_2}{\sigma_1\Gamma_1}$	Q_0 b	β
Ho-165	235	2.0	12.2	272	4.0	15.5	2.3	6.8±0.8	0.29
Hf-178	291	3.1	12.2	334	4.9	15.5	1.8	7.5±0.8	0.28
Hf-180	286	3.2	12.2	324	5.1	15.3	1.8	7.2±0.8	0.27
Ta-181	272	3.0	12.1	316	5.1	15.0	2.0	6.8±0.8	0.26
W-182	267	3.2	11.9	303	5.6	14.8	2.0	7.2±0.8	0.26
Au-197	535	5.2	13.7	•••	•••	•••	•••	•••	•••
Bi-209	600	4.6	13.8	•••	•••	•••	•••	•••	•••

REF. G. L. Moore, F. R. Buskirk, E. B. Dally, J. N. Dyer, X. K. Maruyama, R. Pitthan
Z. Naturforsch. 31A, 668 (1976)

ELEM. SYM.	A	Z
Ho	165	67

METHOD

REF. NO.	
76 Mo 11	egf

REACTION	RESULT	EXCITATION ENERGY	SOURCE TYPE	SOURCE RANGE	DETECTOR TYPE	DETECTOR RANGE	ANGLE
E,E/	ABX	7- 40	D	75,105	MAG-D		75

E2 STRENGTH

Inelastic electron scattering confirms broadening of the isoscalar ($\Delta T=0$) E2 giant resonance in ^{165}Ho as compared to spherical nuclei. Discrepancies in magnitude between results of other experiments are reconciled. The isovector ($\Delta T=1$) E2 giant resonance is, for the first time, observed to be split into at least two parts.

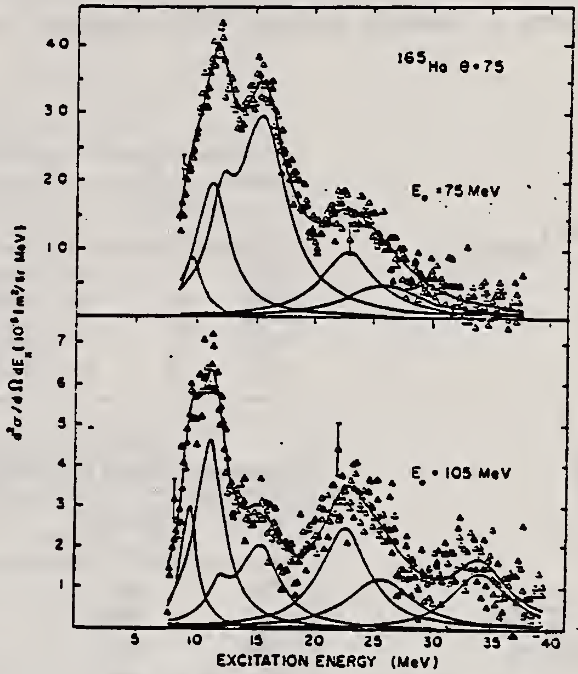

Fig. 1. Spectrum of 75 and 105 MeV electrons, scattered inelastically from ^{165}Ho at a scattering angle of 75°. The resolution is 500 keV. The background which consists of the radiation tail and the machine background has been subtracted. Note that the relative strength of the E1 and E2 resonances more than reverses, if one goes from 75 MeV to 105 MeV. Typical raw spectra; i. e., background not substracted, may be found in Ref. [4]. The form of the E1 resonance was taken from (γ, n) measurements (Ref. [9]); the height was fitted. The energy weighed sum rule exhaustion found for the E1 resonance is 108%, in excellent agreement with the values reported in Ref. [9], thus proving the reliability of the background subtraction.

Table 1. Comparison of the natural width of E2 ($\Delta T=0$) resonances in spherical and deformed nuclei. The fifth column shows that the splitting of the giant dipole resonance, i. e., the deformation of the nucleus at about 14 MeV excitation energy, is practically identical in the deformed nuclei considered.

Excitation Method	$\Gamma_{\text{spherical}}$ [MeV]	Γ_{deformed} [MeV]	$\Delta\Gamma$ [MeV]	ΔE1 [MeV] [a]	$E_x \cdot B$(E2) [%]
(e,e′)	2.8±0.2 (^{142}Nd) [b]	5.0±0.2 (^{150}Nd) [b]	2.2	3.74	88
(α,α′)	3.9±0.2 (^{144}Sm) [c]	4.7±0.3 (^{154}Sm) [c]	0.8	3.57	102
(e,e′)	2.8±0.2 (^{140}Ce) [d] 2.8±0.3 (^{208}Pb)	4.0±0.4 (^{165}Ho) [e]	1.2	3.53	75

[a] Ref. [9]; [b] Ref. [7]; [c] Ref. [8]; [d] Ref. [1,4]; [e] this work.

REF.	ELEM. SYM.	A	Z
A. Suzuki and K. Shoda Nucl. Phys. A260, 172 (1976)	Ho	165	67
METHOD	REF. NO.		
	76 Su 2		egf

REACTION	RESULT	EXCITATION ENERGY	SOURCE		DETECTOR		ANGLE
			TYPE	RANGE	TYPE	RANGE	
E,P	ABX	11- 18	D	15- 18	MAG-D		125

Proton yields obtained by summing protons with energies above levels given in tables.

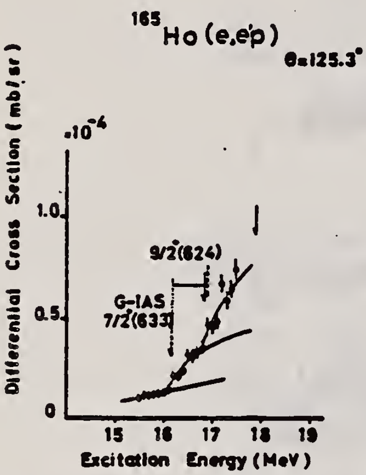

Fig. 3. Cross section of the ^{165}Ho(e, e'p) reaction. See also the caption to fig. 2.

TABLE 1

Parameters of the present experiment

Target	Atomic number	Purity (%)	Thickness (mg/cm^2)	Lowest proton energy (MeV)	Bin size (keV)	Range of measurement (MeV)
^{159}Tb	65	99.9 (natural)	14.87	4.70	100	15.0 –17.5
^{165}Ho	67	99.9 (natural)	11.64	4.70	100	15.5 –17.5
^{169}Tm	69	99 (natural)	13.40	4.70	100	15.0 –18.0
^{175}Lu	71	99.87 (enriched)	5.24	5.34	150	15.05–20.0
^{181}Ta	73	99.9 (natural)	6.73	6.16	200	16.0 –23.0

TABLE 3

Displacement energies obtained from the present data and the estimates with eqs. (20) and (21)

Target	Resonance	E^* (MeV)	E_c (exp) (MeV)	E_c [a]) (MeV)	$E_c(\delta = 0.3)$ [b]) (MeV)
^{159}Tb	1st	15.75±0.15	15.58	16.06	15.93
	2nd	16.50±0.15	15.46		
^{165}Ho	1st	16.15±0.14	15.64	16.38	16.25
^{169}Tm	1st	15.76±0.13	16.20	16.76	16.63
	2nd	16.34±0.14	16.22		
^{175}Lu	1st	16.44±0.13	16.75	17.07	16.93
	2nd	17.45±0.15	16.35		
^{181}Ta	1st	17.31±0.15	16.40	17.38	17.24

a) Estimated with eq. (20).
b) Estimated with eq. (21).

TABLE 4

Deformation parameters of IAS δ_{IAR} derived from the (e, e'p) result

Target	Resonance	IAS	Parent state	$\delta_{IAR}-\delta_p$ [a])	δ_p (assumed)	δ_{IAR} [a])
^{159}Tb	1st	$\frac{3}{2}^-$[521]	ground	−0.008	0.31	0.30
	2nd	$\frac{5}{2}^-$[512]	875 keV	−0.016		0.29
^{165}Ho	1st	$\frac{7}{2}^+$[633]	ground	−0.023	0.30	0.28
^{169}Tm	1st	$\frac{1}{2}^-$[521]	ground	−0.018	0.29	0.27
	2nd	$\frac{1}{2}^-$[510]	565 keV	−0.019		0.27
^{175}Lu	1st	$\frac{7}{2}^-$[514]	ground	−0.010	0.28	0.27
	2nd	$\frac{7}{2}^-$[503]	1420 keV	−0.029		0.25
^{181}Ta	1st	$\frac{7}{2}^-$[503]	670 keV	−0.046	0.26	0.21

The assumed deformation parameters for the parent states δ_p are also shown.
a) The errors are about ±0.01.

REF. T. Bar-Noy and R. Moreh
Nucl. Phys. A275, 151 (1977)

ELEM. SYM.	A	Z
Ho	165	67

METHOD

REF. NO.	
77 Ba 7	egf

REACTION	RESULT	EXCITATION ENERGY	SOURCE		DETECTOR		ANGLE
			TYPE	RANGE	TYPE	RANGE	
G,G	ABX	8- 12	D	8- 12	SCD-D		DST

Abstract: Differential cross sections for elastic and inelastic Raman scattering from the deformed heavy nuclei ^{159}Tb, ^{165}Ho and ^{237}Np were measured at five energies between 8.5 and 11.4 MeV. Angular distributions at four angles between 90° and 140° for both elastic and inelastic scattering at 9.0 and 11.4 MeV were also measured. The monoenergetic photons were obtained from thermal neutron capture in Ni and Cr. All the angular distributions and the elastic and Raman scattering at the higher energies are in good overall agreement with theoretical predictions. The theory is based on a modified simple rotator model of the giant dipole resonance in which the effect of Delbrück scattering was included. A trend of both the elastic and Raman scattering at lower energies to be stronger than expected are suggested by the data. However, the ratio between the Raman and elastic scattering seem to be in good agreement with theory throughout the whole energy range. This shows that there is no need to introduce a direct nonresonant component to the imaginary part of the elastic scattering amplitude to explain the experimental data.

158

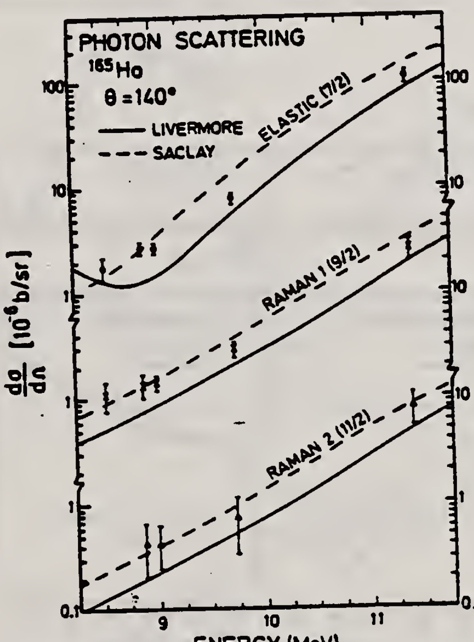

Fig. 4. Elastic and Raman inelastic differential scattering cross sections from ^{165}Ho at 140°. In the solid and dashed lines, the nuclear resonance amplitudes were obtained using parameters extracted from fits made to the Livermore and Saclay measurements respectively. (See text, table 3 and caption to fig. 3.)

over

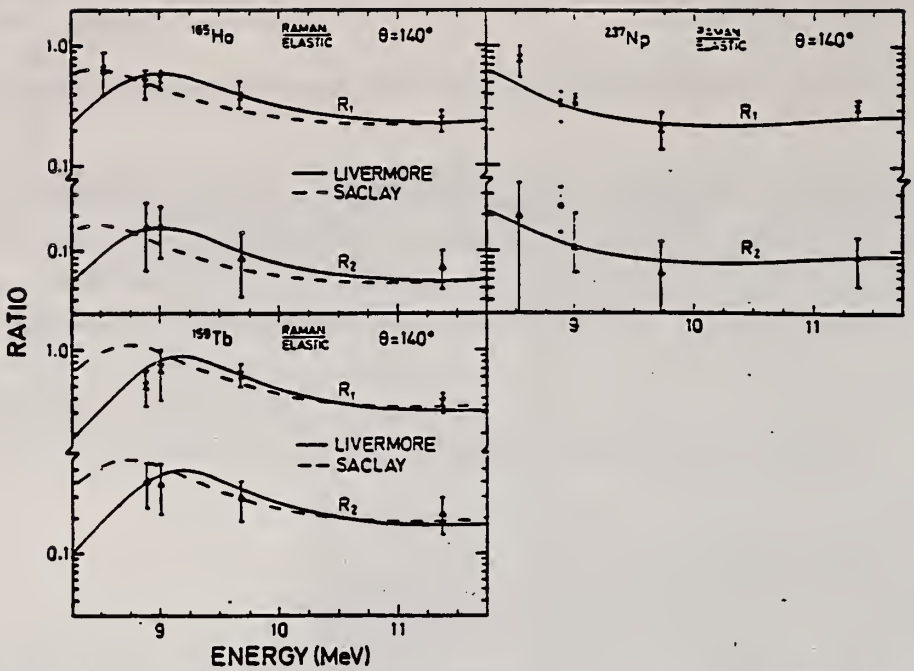

Fig. 6. Ratios of Raman/elastic scattering cross sections at 140° for ^{237}Np, ^{165}Ho and ^{159}Tb targets. Here, R_1 and R_2 refer to the first and second Raman lines. In the solid and dashed lines, the nuclear resonance amplitudes were obtained using parameters extracted from fits made to the Livermore and Saclay measurements respectively. (See text, table 3 and caption to fig. 3.)

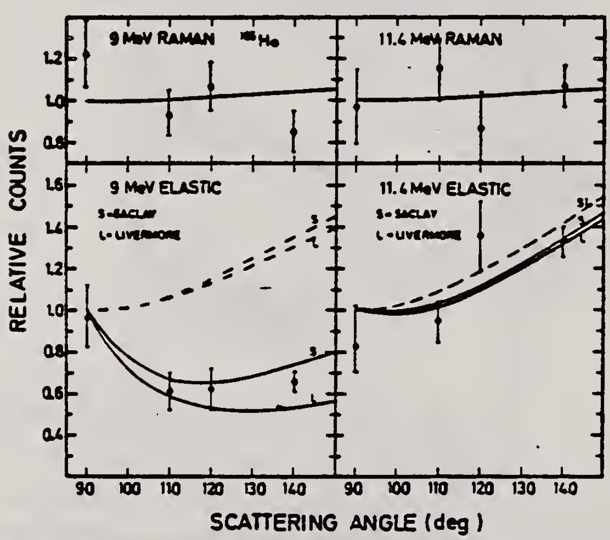

Fig. 8. Angular distributions of elastic and inelastic Raman scattered lines from ^{165}Ho. Here, S and L indicate calculated values where the nuclear resonance amplitudes were extracted from the (γ, n) data of Saclay and Livermore. See caption to fig. 7.

REF. J.J. Murphy II, H.J. Gehrhardt and D.M. Skopik
Nucl. Phys. A277, 69 (1977)

ELEM. SYM.	A	Z
Ho	165	67

METHOD

REF. NO.	
77 Mu 3	egf

REACTION	RESULT	EXCITATION ENERGY	SOURCE TYPE	SOURCE RANGE	DETECTOR TYPE	DETECTOR RANGE	ANGLE
E,A	ABX	14-100	D	100	MAG-D		50

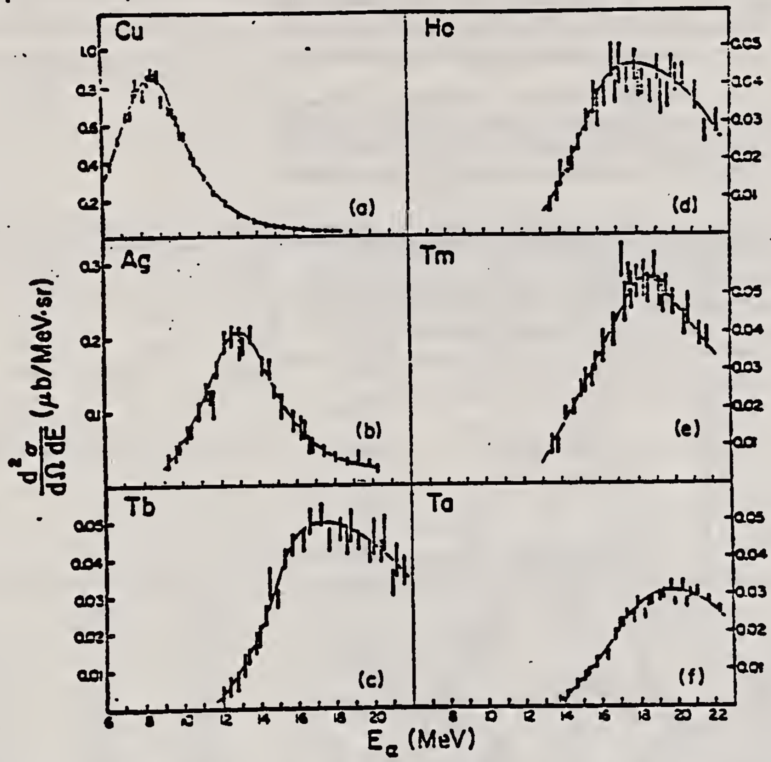

Fig. 1. The α-particle energy spectra at 50° in the lab for the six nuclei studied. Note that as Z increases, the cross section decreases and the energy of the peak increases. Errors are statistical. Curves are to guide the eye.

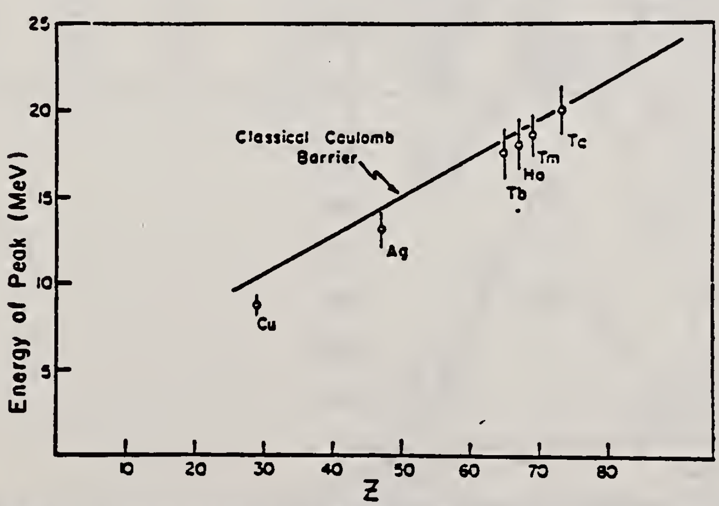

Fig. 2. Energy of the cross section peak as a function of Z. The solid line is the energy of the classical Coulomb barrier.

REF. G.M. Gurevich, L.E. Lazareva, V.M. Mazur, S.Yu. Merkulov,
G.V. Solodukhov, V.A. Tyutin
Nucl. Phys. A351, (1981)

ELEM. SYM.	A	Z
Ho	165	67

METHOD

REF. NO.	
81 Gu 2	hg

REACTION	RESULT	EXCITATION ENERGY	SOURCE TYPE	SOURCE RANGE	DETECTOR TYPE	DETECTOR RANGE	ANGLE
G,MU-T	ABX	THR-20	C	27	NAI-D		4PI

Abstract: The curves of the total gamma-absorption cross sections (σ_{tot}) in the E1 giant resonance energy range for the nuclei ^{154}Sm, ^{156}Gd, ^{165}Ho, ^{168}Er, ^{174}Yb, ^{178}Hf, ^{180}Hf, ^{181}Ta, ^{182}W, ^{184}W, ^{186}W and ^{197}Au have been measured using the absorption method. Parameters of the Lorentz curves fitting the measured cross sections σ_{tot} are given. Quadrupole moments (Q_0) and nuclear deformation parameters (β) were obtained.

For deformed nuclei in the $\sim 155 < A < \sim 180$ region a violation of the correlation between giant resonance widths (Γ) and nuclear deformation parameters was found. Γ_1 and Γ_2, the widths of the resonances corresponding to vibrations of nucleons along and across the nuclear deformation axis, were observed to decrease with the increase of A which could be accounted for by the presence of an $N = 108$ subshell.

E

NUCLEAR REACTIONS ^{154}Sm, ^{156}Gd, ^{165}Ho, ^{168}Er, ^{174}Yb, ^{178,180}Hf, ^{181}Ta, ^{182,184,186}W, ^{197}Au (γ, X), E = 7-20 MeV; measured total $\sigma(E)$; deduced integrated σ, Lorentz line parameters. ^{154}Sm, ^{156}Gd, ^{165}Ho, ^{168}Er, ^{174}Yb, ^{178,180}Hf, ^{181}Ta, ^{182,184,186}W, ^{197}Au deduced β, Q_0, Γ, giant resonance evolution. Enriched, natural targets.

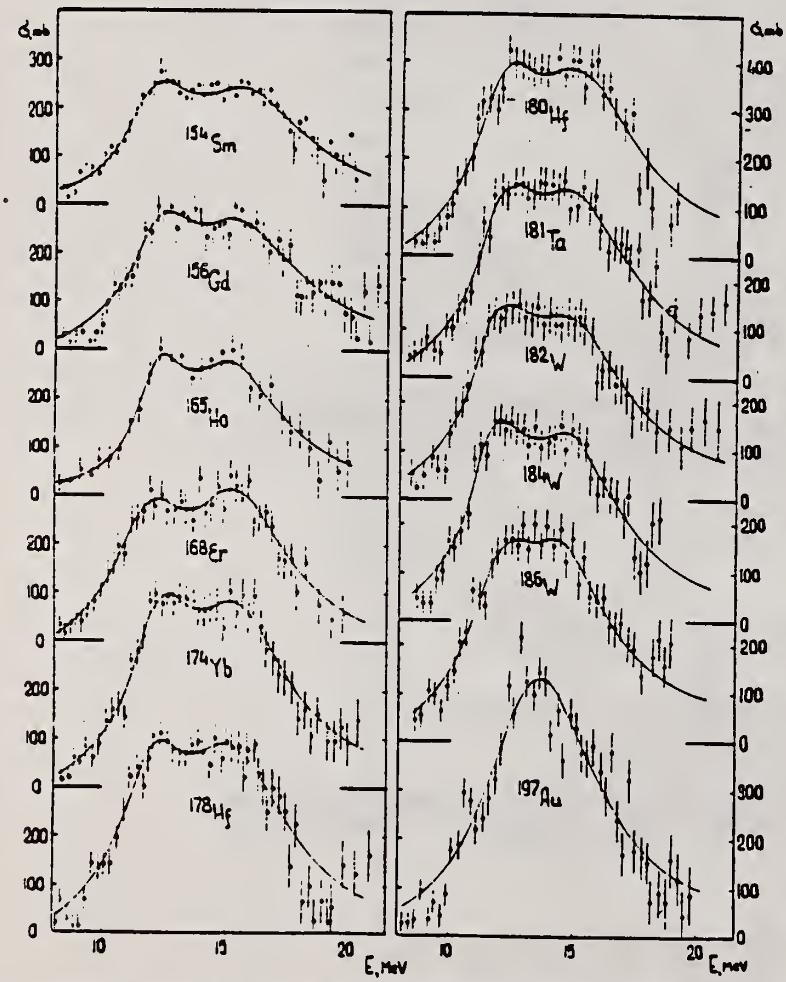

Fig. 2. Total nuclear γ-absorption cross sections (σ_{tot}) measured by the absorption method for ^{154}Sm, ^{156}Gd, ^{165}Ho, ^{168}Er, ^{174}Yb, ^{178}Hf, ^{180}Hf, ^{181}Ta, ^{182}W, ^{184}W, ^{186}W and ^{197}Au. Rms error bars are shown.

(OVER)

U.S. DEPARTMENT OF COMMERCE
NATIONAL BUREAU OF STANDARDS

Table 2

Parameters of Lorentz curves fitting the experimental data on σ_{tot}

Nucleus	E_1 (MeV)	σ_1 (mb)	Γ_1 (MeV)	E_2 (MeV)	σ_2 (mb)	Γ_2 (MeV)	$\frac{\sigma_2\Gamma_2}{\sigma_1\Gamma_1}$	Γ (MeV)
^{154}Sm	12.2	188	3.4	15.7	207	5.7	1.85	8.1
^{156}Gd	12.3	206	3.2	15.7	220	5.5	1.81	7.7
^{165}Ho	12.3	202	2.3	15.2	239	4.8	2.47	7.0
^{168}Er	11.9	222	3.2	15.5	275	4.5	1.73	7.4
^{174}Yb	12.3	297	2.9	15.5	320	4.9	1.80	7.1
^{178}Hf	12.2	291	3.1	15.5	334	4.9	1.80	7.2
^{180}Hf	12.2	286	3.2	15.3	324	5.1	1.81	7.1
^{181}Ta	12.1	272	3.0	15.0	316	5.1	1.97	6.8
^{182}W	11.9	267	3.2	14.8	303	5.6	2.01	6.8
^{184}W	11.9	315	2.9	14.8	321	4.7	1.65	6.8
^{186}W	12.0	246	3.3	14.5	332	5.1	2.07	6.4
^{197}Au	13.7	535	5.2					
Average error	1.4 %	11.2 %	9.3 %	1.5 %	9.7 %	4.6 %	0.22	0.2 MeV

Table 3

Ratios of nuclear ellipsoid axes (k), deformation parameters (β) and intrinsic quadrupole moments (Q_0), calculated from E_2/E_1

Nucleus	^{154}Sm	^{156}Gd	^{165}Ho	^{168}Er	^{174}Yb	^{178}Hf	^{180}Hf	^{181}Ta	^{182}W	^{184}W	^{186}W
k	1.320	1.302	1.259	1.327	1.289	1.296	1.281	1.263	1.271	1.268	1.229
β	0.326 ±0.017	0.309 ±0.016	0.266 ±0.036	0.334 ±0.032	0.296 ±0.024	0.303 ±0.032	0.288 ±0.036	0.270 ±0.026	0.278 ±0.030	0.274 ±0.032	0.235 ±0.033
Q_0	6.3 ±0.3	6.2 ±0.3	5.8 ±0.8	7.5 ±0.7	7.0 ±0.6	7.5 ±0.8	7.2 ±0.9	6.9 ±0.7	7.2 ±0.8	7.1 ±0.8	6.2 ±0.9

Table 4

Integral characteristics of E1 giant resonance

Nucleus	$\sigma_{0,exp}$ (MeV · b)	$\sigma_{0,exp}$/0.06NZ/A	σ_{0L} (MeV · b)	σ_{0L}/0.06NZ/A	σ_{-1} (mb)	σ_{-1L} (mb)	$\sigma_{-1L}A^{-4/3}$ (mb)	σ_{-2} (mb · MeV^{-1})	σ_{-2L} (mb · MeV^{-1})	$\sigma_{-2L}A^{-5/3}$ (μb · MeV^{-1})
^{154}Sm	1.94 ± 0.06	0.87	2.86	1.29	117 ± 3.5	156	0.189	9.1 ± 0.3	14.3	3.23
^{156}Gd	2.07 ± 0.07	0.91	2.95	1.30	143 ± 4.6	163	0.194	10.5 ± 0.4	14.9	3.30
^{165}Ho	1.86 ± 0.06	0.78	2.53	1.06	155 ± 4.4	160	0.177	10.1 ± 0.3	12.6	2.54
^{168}Er	2.24 ± 0.06	0.92	3.07	1.26	161 ± 4.3	197	0.212	12.0 ± 0.3	16.0	3.13
^{174}Yb	2.69 ± 0.05	1.07	3.82	1.52	195 ± 3.4	240	0.247	14.5 ± 0.3	19.2	3.54
^{178}Hf	2.85 ± 0.07	1.11	3.99	1.55	208 ± 4.9	247	0.247	15.3 ± 0.4	20.2	3.59
^{180}Hf	2.72 ± 0.06	1.05	4.03	1.56	200 ± 4.4	250	0.246	15.1 ± 0.3	20.7	3.61
^{181}Ta	2.84 ± 0.07	1.09	3.81	1.46	210 ± 5.3	245	0.239	16.0 ± 0.4	20.0	3.45
^{182}W	2.86 ± 0.07	1.09	4.01	1.52	211 ± 5.3	256	0.248	16.2 ± 0.4	21.6	3.70
^{184}W	2.78 ± 0.07	1.05	3.80	1.43	207 ± 5.3	251	0.240	15.9 ± 0.4	20.9	3.51
^{186}W	2.90 ± 0.07	1.08	3.95	1.48	214 ± 5.3	256	0.241	16.2 ± 0.4	21.6	3.56
^{197}Au	3.12 ± 0.06	1.10	4.37	1.54	229 ± 4.2	276	0.241	18.6 ± 0.4	23.3	3.49

REF.	ELEM. SYM.	A	Z
M. Schumacher, F. Smend, W. Mückenheim, P. Rullhusen, H.G. Börner Z. Phys. A300, 193 (1981)	Ho	165	67

METHOD	REF. NO.	
	81 Sc 6	egf

REACTION	RESULT	EXCITATION ENERGY	SOURCE TYPE	SOURCE RANGE	DETECTOR TYPE	DETECTOR RANGE	ANGLE
G,G	ABX	2-7		2-7	SCD-D		90

2.60-6.76 MEV

Elastic scattering by nuclei in the range of mass numbers between 64 and 238 has been studied with monochromatic photons in the energy range between 2 and 8 MeV. These photons were provided either by a Ti(n,γ) source installed in the tangential through channel of the Grenoble high flux reactor, or by ^{24}Na and ^{56}Co sources produced by deuteron bombardment of Al or Fe at the Göttingen cyclotron. The photoexcitation of 23 nuclear levels has been observed and the decay properties and groundstate widths of the majority of these levels have been determined. For the lead scattering target the coherent elastic differential cross section has been studied in detail. There is evidence that below the photo-neutron threshold the elastic scattering via virtual photoexcitation of the nucleus can be approximated by extrapolating the real part of the Giant Dipole Resonance amplitude along a Lorentzian curve. Coulomb corrections to Delbrück scattering seem to play a small role at 6.5 MeV.

Table 4. Properties of levels observed by photoexcitation. $(d\sigma/d\Omega)^{NRF}$: experimental differential cross section per identified isotope or element for resonance scattering through $\Theta = 90°$. I^π: spin-parity of excited level; $W(\Theta)$: angular correlation function: $g = (2I_{ex}+1)/(2I_g+1)$; Γ_0: radiative groundstate transition width. Γ: total level width. Errors in the last digits are given in parentheses

Isotope	E_γ (MeV)	$(d\sigma/d\Omega)^{NRF}$ (µb/sr)	I^π	Γ_0/Γ [e]	$W(\Theta)g\Gamma_0^2/\Gamma$ (meV)	Γ_0^f (meV)	Γ_0^g (meV)
^{238}U	2.754	13 (4)	(1)	0.77	0.145	0.084	-
^{238}U	3.254	421 (5)	1^-	0.24	0.83	1.5	0.52(15) [d]
^{209}Bi	6.555	2.1 (4)·10^2	-	-	0.74	0.74 [b]	-
^{209}Bi	7.168	1.7 (3)·10^5	$9/2^-$ [a]	1.00	710	786	820 (40) [a]
^{203}Tl	6.418	8.75(30)·10^3	1/2 [a]	0.28	30	102	82 (15) [a]
Tl	6.759	7 (3)	-	-	-	-	-
Hg	6.555	68 (17)	-	-	-	-	-
^{186}W	6.418	5.2 (3)·10^2	1^- [a]	0.32	1.75	2.4	-
^{184}W	6.555	9.8 (10)·10^2	(1)	0.52	3.44	2.9	-
^{184}W	6.759	46 (10)	(1)	0.58	0.17	0.13	-
^{181}Ta	3.010	174 (17)	-	0.72	0.42	0.59	-
^{181}Ta	6.418	62 (4)	-	0.73	0.2	0.27 [c]	-
^{181}Ta	6.759	4.8 (12)	-	-	0.018	0.018 [b]	-
^{165}Ho	6.418	10.3 (30)	-	-	0.035	0.035 [b]	-
^{165}Ho	6.759	5.6 (14)	-	-	0.021	0.021 [b]	-
Nd	2.754	2.6 (5)	-	-	-	-	-
Nd	3.254	14.0 (10)	-	-	-	-	-
Ce	6.759	13.4 (10)	-	-	-	-	-
^{121}Sb	3.452	2.20 (5)·10^3	-	0.60	2.9	4.9 [b]	-
^{100}Mo	6.418	1.53 (4)·10^4	1^- [a]	0.88	52	26	25 (8) [a]
^{94}Mo	6.555	4.4 (4)·10^3	(1)	0.33	15	21	-
Mo	6.759	6.2 (15)	-	-	-	-	-
Mo	7.168	8.2 (26)·10^2	-	-	-	-	-

[a] [11] [b] $W(\Theta)g\Gamma_0/\Gamma = 1$ assumed [c] $W(\Theta)g = 1$ assumed

[d] [28] (a small correction has been applied to the data of [28])

[e] Upper limits in case not all the transitions to lower levels were observed

[f] Present work [g] Previous work

(OVER)

Table 1. Differential cross sections for elastic scattering $(d\sigma/d\Omega)^{exp}$ of photons from ^{56}Co and ^{24}Na sources by different scattering targets, in units of μb/sr. Errors in the last digits are given in parentheses.

θ deg	Scattering targets	2.599[a] (MeV)	2.754[b] (MeV)	3.010[a] (MeV)	3.202[a] (MeV)	3.254[a] (MeV)	3.273[a] (MeV)	3.452[a] (MeV)
90	^{238}U	52.7(25)	57.5(25)[c]	56(16)	47(4)	456 (10)[c]	34(6)	49(14)
	^{209}Bi	33.1(30)	32 (2)	33(11)	32(4)	25.6(20)	29(6)	33(15)
	^{nat}Pb	31.5(23)	31.0(16)	35 (8)	27(3)	26.6(22)	25(4)	23 (8)
	^{nat}Tl	31.5(33)	-	27(12)	32(5)	24 (3)	22(7)	34(15)
	^{nat}Hg	30.0(27)	-	24(10)	28(5)	25.5(18)	26(8)	20 (8)
	^{nat}W	22.5(11)	-	17 (7)	19(3)	18.4(15)	18(5)	21 (6)
	^{181}Ta	20.0(15)	19.2 (6)	193(20)[c]	20(4)	17.3(21)	18(5)	21 (8)
	^{165}Ho	15.9(13)	-	17(10)	13(6)	15.6(20)	18(8)	-
	^{nat}Nd	11.4 (7)	14.2 (5)[d]	15 (7)	14(3)	24.2(12)[d]	13(3)	9 (6)
	^{nat}Ce	11.1 (9)	11.0 (5)	-	11(3)	9.5(13)	8(4)	-
	^{127}J	8.4(10)	8.6 (5)	-	9(2)	7 (1)	5(3)	-
	^{nat}Sb	8.0(11)	-	-	10(4)	6.8(19)	-	1,270(50)[c]
	^{nat}Sn	6.5 (7)	7.0 (5)	-	5(2)	7.6 (8)	6(3)	-
	^{nat}Cd	6.2 (5)	-	-	6(2)	6.6 (8)	7(3)	-
120	^{238}U	55.1(25)	64 (4)[c]	43(15)	55(5)	574 (10)[c]	48(5)	48(11)
	^{181}Ta	27.5(15)	25.0 (9)	227(20)[c]	22(5)	21 (2)	22(8)	-
	^{nat}Nd	17.9(30)	17.0 (9)[d]	-	-	29.8(47)[d]	-	-

[a] ^{56}Co source in Fe lattice [b] ^{24}Na source in Al lattice (part of data have been published elsewhere)
[c] Transitions to excited states observed in addition to the ground-state transition
[d] Photoexcitation of nuclear level identified from the size of the differential cross section

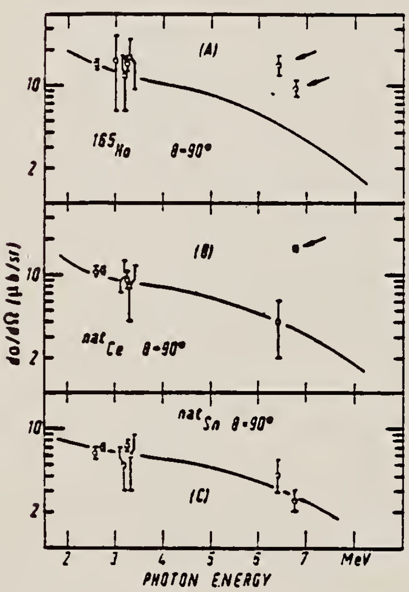

Fig. 11. Same as Fig. 9 but for (A) ^{165}Ho, (B) ^{nat}Ce and (C) ^{nat}Sn

REF. U. Zurmühl, P. Rullhusen, F. Smend, M. Schumacher, H.G. Börner
Phys. Lett. 114B, 99 (1982)

ELEM. SYM.	A	Z
Ho	165	67

METHOD

REF. NO.
82 Zu 2 egf

REACTION	RESULT	EXCITATION ENERGY	SOURCE TYPE	SOURCE RANGE	DETECTOR TYPE	DETECTOR RANGE	ANGLE
G,G	ABX	3-6	D	3-6	SCD-D		DST

SOURCE 141PR(N,G)

A procedure is presented to determine total photoabsorption cross sections σ_t by resonant scattering of γ-rays. It is shown that σ_t follows along the GDR lorentzian line down to 3.5 MeV. Indications for nonstatistical deviations from the lorentzian line are observed.

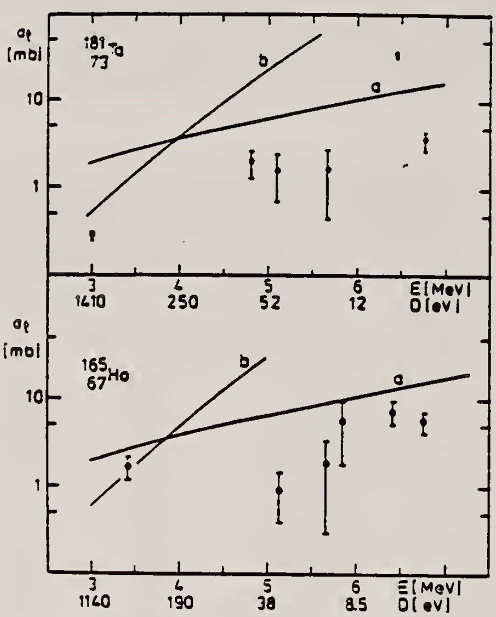

Fig. 2. Total photoabsorption cross section for ^{181}Ta and ^{165}Ho versus energy. Curve a: extrapolated lorentzian according to ref. [13]. Curve b: total photoabsorption cross section predicted by the Weisskopf model with hindrance factor 3×10^{-3}.

Ho
A=166

Ho
A=166

REF.		ELEM. SYM.	A	Z
D.K. McDaniels, P. Varghese, I. Bergqvist, D. Drake PICNS-73, Vol.II, p.951 (1973) Asilomar		Ho	166	67

METHOD	REF. NO.	
	73 Mc 6	egf

REACTION	RESULT	EXCITATION ENERGY	SOURCE TYPE	SOURCE RANGE	DETECTOR TYPE	DETECTOR RANGE	ANGLE
N,G	RLX	14- 20	D	7- 14	NAI-D		UKN

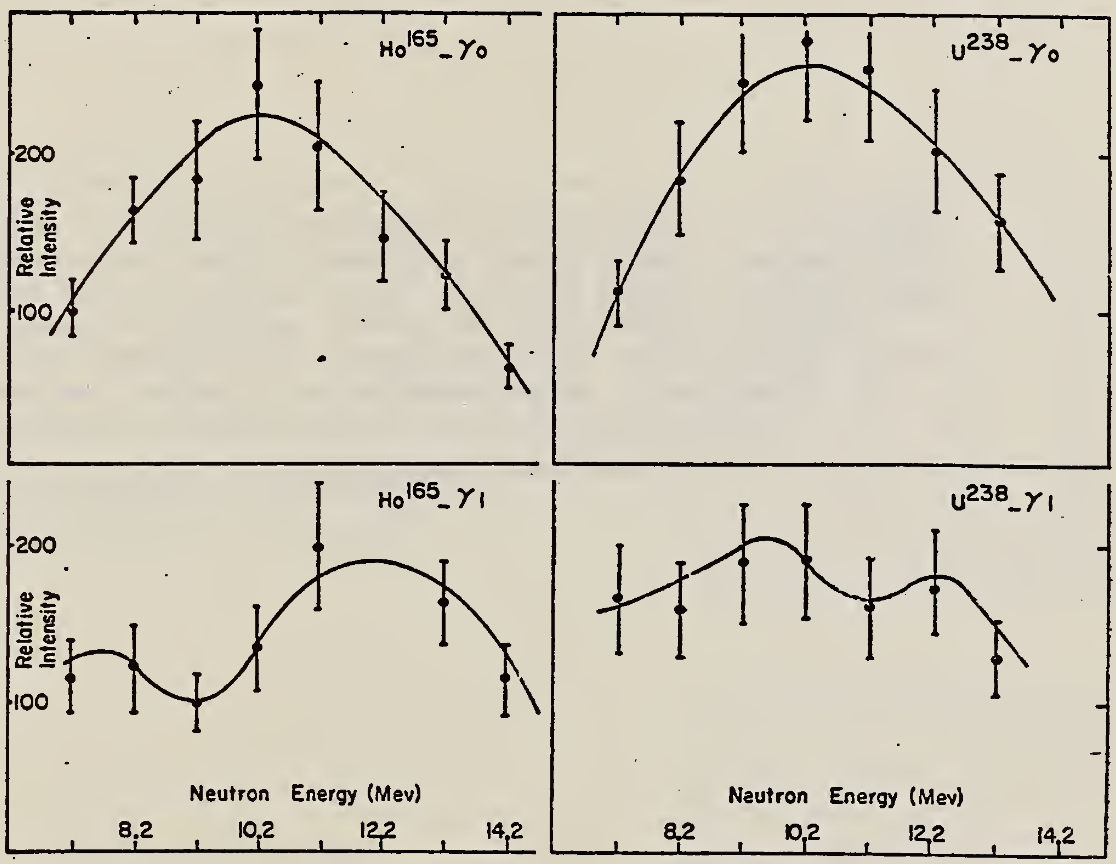

FIG. 1. The total (n,γ) cross section for ^{165}Ho and ^{238}U targets. The upper figs. show the data for transitions to the ground states of the final nucleus. The lower figs. show the data for transitions corresponding to the first peak found in the observed spectra below the one belonging to the ground state transition.

# ERBIUM
Z=68

Erbia is one of the the three fractions that C. G. Mosander discovered (1842) in Gadolin's yttria oxide. The metallic form was not produced until 1834 when Klemm and Bommer made a chemical reduction. During the late 1940's the Atomic Energy Commission developed separation methods based on the then new synthetic ion exchange resins. The element is available in high purity in up to ton quantities.

.G. Fuller, B. Petree, M.S. Weiss
'hys. Rev. 112, 554 (1958)

ELEM. SYM.	A	Z
Er		68

Betatron; ion chamber

REF. NO.	
58 Fu 1	NVB

REACTION	RESULT	EXCITATION ENERGY	SOURCE TYPE	SOURCE RANGE	DETECTOR TYPE	DETECTOR RANGE	ANGLE
G,XN	ABX	7-40	C	7-40	BF3-I		4PI

CF DANØS THEØRY

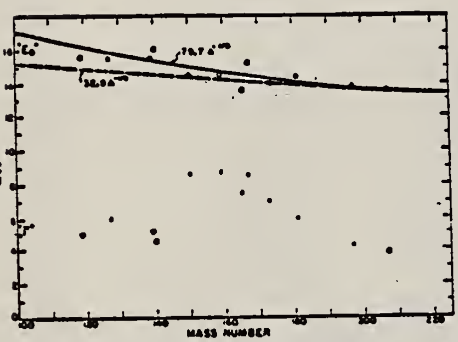

FIG. 6. Mean energy and width of giant resonances. "E_a" and "Γ" are the mean energy for photon absorption and the full width at half maximum of the giant resonance obtained from dashed histograms as in Fig. 5. No attempt was made to fit data with resonance curves to obtain these parameters.

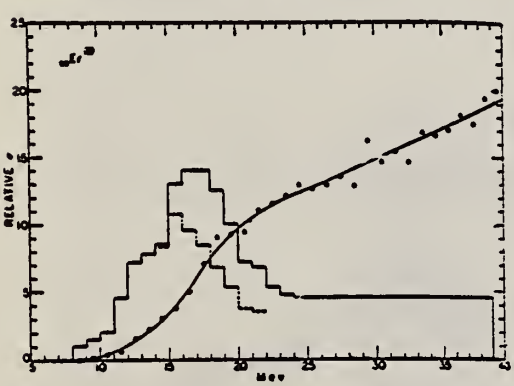

FIG. 5. Relative photoneutron production cross sections for tin, iodine, samarium, holmium, erbium, and lead. The points and smooth curves represent the integral neutron-production cross section defined by $\int_0^E \sigma_{Tn}(E)dE$, where $\sigma_{Tn}(E)=\sigma(\gamma,n)+2\sigma(\gamma,2n)+\sigma(\gamma,pn)+3\sigma(\gamma,3n)+\ldots$. The scales are normalized to give approximately the same total neutron yield at 40 Mev. The errors indicated were obtained by propagating the statistical uncertainties, $(\sqrt{n})$, in the original activation curve data through the integral cross section matrix. Solid histograms represent first differences of integral cross section curves. Dashed histograms show result of correcting for neutron multiplicity above the $(\gamma,2n)$ threshold.

TABLE I. Target properties and results.

Element	Form used	Weight grams	$\sigma^0(\gamma,n)$[a] barns	$\frac{\int\sigma dE^{b}}{NZ/A}$ Mev-b	"Γ"[a] Mev
Sn	Sn	4.81	0.30	0.064	5.0
I	I	8.55	0.36	0.085	6.0
La	La	10.43	0.34	0.063	5.2
Ce	Ce	4.99	0.45	0.080	4.5
Sm	Sm_2O_3	2.90	0.26	0.073	8.6
Tb	Tb_4O_7	3.04	0.39	0.087	8.7
Ho	Ho_2O_3	1.87	0.41	0.079	7.5
Er	Er_2O_3	5.41	0.50	0.100	8.5
Yb	Yb_2O_3	5.57	0.50	0.090	7.0
Ta	Ta	8.41	0.49	0.077	6.0
Au	Au	3.16	0.68	0.085	4.2
Pb	Pb	8.05	0.75	0.081	3.8

[a] $\sigma^0(\gamma,n)$ is the maximum value and "Γ" the full width at $\sigma^0(\gamma,n)/2$ of the neutron production cross section corrected for multiple neutron emission. Data were not fitted with resonance lines to determine these values.
[b] Integrated neutron production cross sections corrected for multiple neutrons above $(\gamma,2n)$ threshold.

TABLE II. Energies of resonances in deformed nuclei.[a]

Nucleus	E_m Mev	Q_0 barns	Method	E_a Mev	E_b Mev	$E_{1/2}^-$ Mev	$E_{1/2}^+$ Mev
$_{65}Tb^{159}$	14.7	6.9[b]	CE	11.9	16.2	10.8	19.5
$_{67}Ho^{165}$	14.5	7.8[b]	CE	11.5	16.0	11.0	18.5
$_{68}Er^{167}$	14.5	21[b]	SC	8.5	17.5	11.5	20.0
$_{68}Er^{166}$	14.5	7.8[b]	CE	11.6	15.9	11.5	20.0
$_{73}Ta^{181}$	14.1	12.6[c]	SC	10.5	15.9	11.3	17.3
$_{73}Ta^{181}$	14.1	6.8[b]	CE	11.9	15.2	11.3	17.3
$_{79}Au^{197}$	13.6	3.75[c]	SC	12.5	14.1	11.8	16.2

[a] CE—Coulomb excitation; SC—spectroscopic; $E_{1/2}^-$, $E_{1/2}^+$—energies at which giant resonance drops to half its maximum value.
[b] Adler, Bohr, Huus, Mottelson, and Winther, Revs. Modern Phys. 28, 432 (1956).
[c] M. L. Pool and D. N. Kundu, *Chart of Atomic Nuclei* (Longs College Book Company, Columbus, 1955).

Ref. E.G. Fuller, E. Hayward Nuclear Phys. 30, 613 (1962) [Erratum: Nuclear Phys. 37, 176 (1962)]	Elem. Sym. Er	A	Z 68
Method 50 MeV betatron; BF_3, NaI counters	Ref. No. 62 Fu 3		JHH

Reaction	E or ΔE	E_o	Γ	$\int \sigma dE$	Jπ	Notes
Er(γ,xn)	8-23.5	12.2±0.2 16.0±0.5	2.33 MeV 4.5 MeV	$\int_8^{23.5} = 3.20 \pm 15\%$		σ(12.2 MeV) = 318 mb. σ(16 MeV) = 328 mb. Correction for neutron multiplicity.
Er (γ,γ)						Intrinsic nuclear quadrupole moment = 7.6±1.1 b. Analysis of scattering data indicates large tensor polarizability.

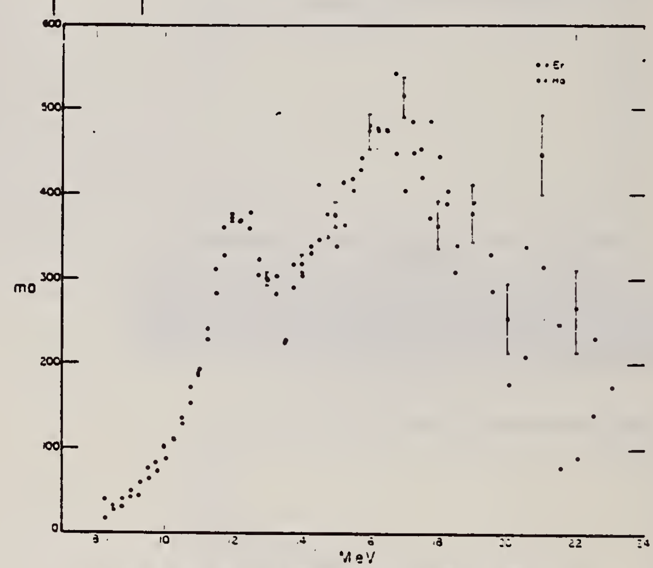

Fig. 2. Neutron production cross sections for holmium and erbium. The uncertainties indicated result from the statistical uncertainties in the original activation curve data.

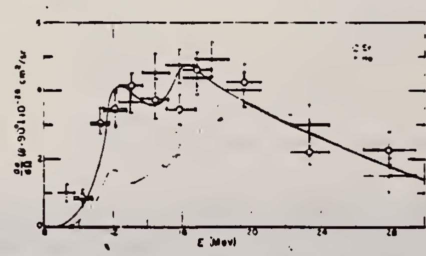

Fig. 6. The differential scattering cross sections for holmium and erbium measured at 90°. The indicated uncertainties are only statistical. The lower smooth curve was calculated using eq. (9) from a curve drawn through the data points of fig. 4. The shaded region corresponds to the limits of the scalar scattering cross section resulting from the limits of the absorption cross section given by the shaded region of fig. 4.

T. Kaminishi, C. Kojima
Jap. J. Appl. Phys. 2, 399 (1963)

Er		68

METHOD
Linac; isomer yield; activity

REF. NO.	
63 Ka 2	NVB

REACTION	RESULT	EXCITATION ENERGY	SOURCE TYPE	SOURCE RANGE	DETECTOR TYPE	DETECTOR RANGE	ANGLE
G,G/	RLY	1	C 4		ACT-I		4PI
		(0.21)					

Table II. The isomers observed

Isomer	Observed value		Referenced value[11][13]	
	Half-life	Energy (MeV)	Half-life	Energy (MeV)
Se-77m	17.5 sec	0.160	17.5 sec	0.161
Br-79m	4.80 sec	0.209	4.8 sec	0.208
Sr-87m	2.3 hr	0.390	2.8 hr	0.388
Y-89m	15.0 sec	0.920	14 sec	0.915
Rh-103m	58 min	*	57 min	0.040
Ag-107m	42 sec	0.95	44 sec	0.094
Ag-109m			40 sec	0.088
Cd-111m	47 min	0.150,0.255	49 min	0.150,0.247
In-115m	4.5 hr	0.335	4.5 hr	0.335
Sn-117m	17 day	0.160	14 day	0.159,0.161
Ba-137m	2.6 min	0.660	2.6 min	0.662
Er-167m	2.10 sec	0.209	2.5 sec	0.208
Hf-179m	18.5 sec	0.157,0.215	19 sec	0.161,0.217
W-183m	5.4 sec	0.200,0.170,0.115	5.5 sec	0.1025,0.2915 others
Ir-191m	4.90 sac	0.129, <0.07	4.9 sec	0.042-0.129
Pt-195m	4.5 day	0.065**	4.1 day	0.031-0.130
Au-197m	7.0 sec	0.10,0.27,0.40	7.2 sec	0.130,0.270,0.407
Hg-199m	43 min	0.160,0.370	42 min	0.158,0.368

* This isomer was measured with a G-M flow counter.
** This value corresponds to Pt-K X-ray energy.

Table III. Induced activation rate

Element	Beam energy (MeV)	Counting rate (×10000 cpm)	Sample form
Se	5	1300	metallic pellet
Br	4	1600	NaBr grain
Sr	6	0.3	$SrCO_3$ powder
Y	5	90	metallic grain
Rh	5	0.2*	$RhCl_3$ grain
Ag	5	180	metallic plate
Cd	6	0.5	$CdCl_2$ grain
In	6	8	metallic plate
Sn	6	0.0005	metallic plate
Ba	5	0.6	BaS powder
Er	4	4900	Er_2O_3 powder
Hf	5	1600	metallic plate
W	5	120	metallic powder
Ir	5	2100	metallic powder
Pt	5	0.3	metallic plate
Au	4	4300	metallic plate
Hg	6	0.09	metallic liquid

* The value measured with a G-M flow counter.

REF.	ELEM. SYM.	A	Z
M. Langevin, J.M. Loiseaux J. de Physique 24, 1027 (1963)	Er		68

METHOD	REF. NO.	
Betatron; photon scattering	63 La 1	NVB

REACTION	RESULT	EXCITATION ENERGY	SOURCE		DETECTOR		ANGLE
			TYPE	RANGE	TYPE	RANGE	
G,G	ABX	9-26	C	9-27	NAI-D		DST

In Figure 4, $W(\theta) = 1 + a \cos^2\theta$

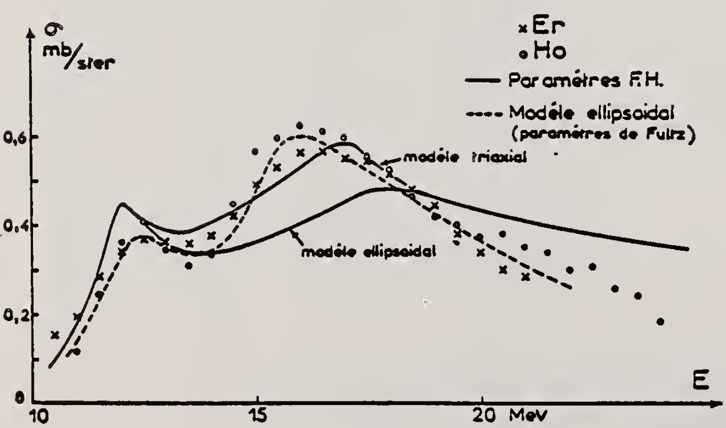

FIG. 3.

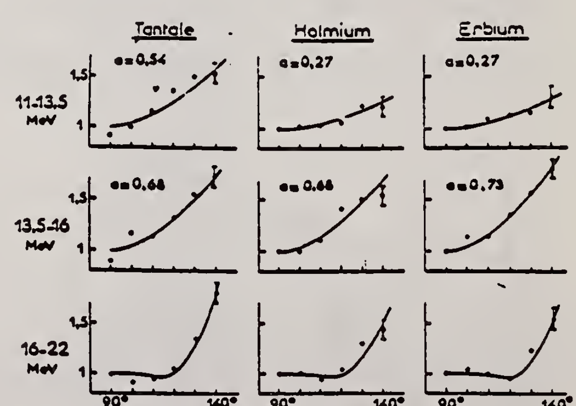

FIG. 4.

REF.
M. Langevin, J. M. Loiseaux et J. M. Maison
Nucl. Phys. 54, 114-124 (1964)

ELEM. SYM. Er | A | Z 68

METHOD
Bremsstrahlung scattering

REF. NO. 64 La 1 | JOC

REACTION	RESULT	EXCITATION ENERGY	SOURCE TYPE	SOURCE RANGE	DETECTOR TYPE	DETECTOR RANGE	ANGLE
G,G	ABX	10-25	C		NAI-D		DST

TABLEAU 1

Le paramètre $a(E)$ de la distribution angulaire

Noyau	11.5-14. MeV			14-17.5 MeV			17.5-20 MeV			20-30 MeV	
	Exp.	Ellipsoïdal	Triax.	Exp.	Ellips.	Triax.	Exp.	Ellips.	Triax.	Exp.	Ellips.
							Contribution Quadrupolaire %				
Tb	$0.5^{+0.15}_{-0.1}$	0.41	0.39	$0.54^{+0.15}_{-0.1}$	0.70	0.50	25	0.97	0.85		1
Ho	$0.27^{+0.15}_{-0.1}$	0.44	0.407	$0.43^{+0.10}_{-0.05}$	0.71	0.53	25	0.95	0.9	0.4 ± 0.1	1
Er	$0.27^{+0.15}_{-0.1}$	0.44	0.407	$0.8^{+0.15}_{-0.1}$	0.71	0.53	25	0.95	0.9		1
Ta	$0.6^{+0.15}_{-0.1}$	0.58		$0.68^{+0.15}_{-0.1}$	0.81		20	0.96			
Au		a_{exp}(11-20 MeV) = 0.9								0.7 ± 0.1	1
		a_{th} (11-20 MeV) ≈ 1									

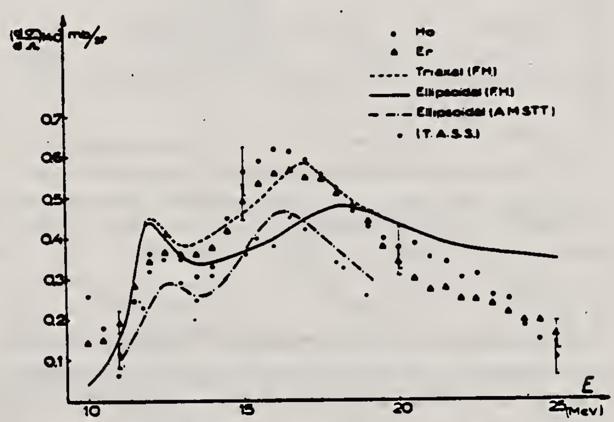

Fig. 3. Sections efficaces expérimentales differentielles de diffusion, obtenues pour l'holmium et l'erbium et comparaison avec les résultats expérimentaux de Tipler *et al.* [16]). (T.A.S.S.). Les courbes tracées correspondent à l'application des relations de dispersion aux sections efficaces d'absorption obtenues par Fuller et Hayward [8]) (F.H.) et Axel, Miller, Schuhl, Tamas et Tzara (A.M.S.T.T.)[19]).

REF.

M. Langevin, J. M. Loiseaux et J. M. Maison
Nucl. Phys. 54, 114-124 (1964)

ELEM. SYM.	A	Z
Er		68

METHOD

Bremsstrahlung scattering [Page 2 of 2]

REF. NO.	
64 La 1	JOC

REACTION	RESULT	EXCITATION ENERGY	SOURCE TYPE	SOURCE RANGE	DETECTOR TYPE	DETECTOR RANGE	ANGLE

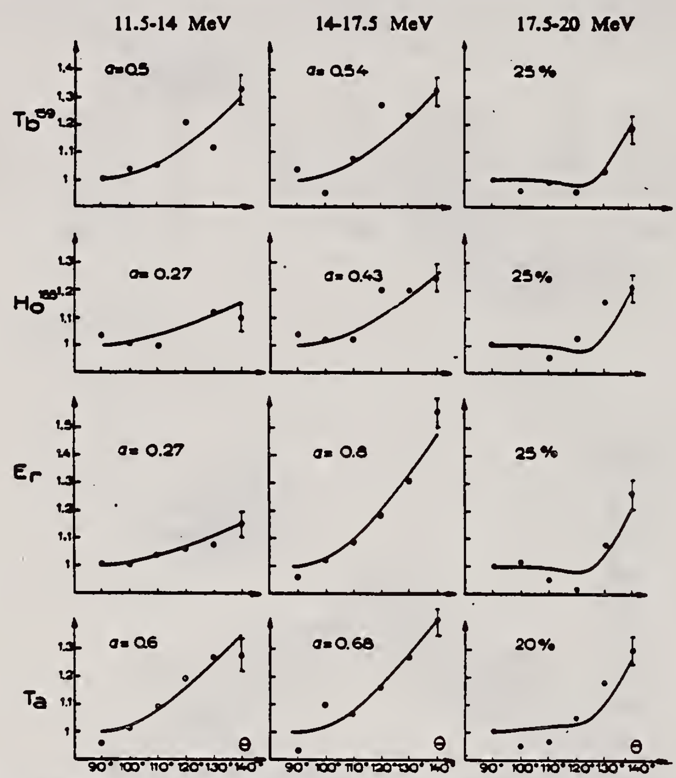

Fig. 8. Répartitions angulaires du rayonnement diffusé obtenues pour le terbium, l'holmium, l'erbium et le tantale dans les zones d'énergie 11.5-14 MeV, 14-17.5 MeV et 17.5-20 MeV.

R. Bergere, H. Beil, P. Carlos and A. Veyssiere
Nucl. Phys. A133, 417 (1969)

ELEM. SYM.	A	Z
Er		68

METHOD

REF. NO.	
69 Be 6	egf

REACTION		RESULT	EXCITATION ENERGY	SOURCE TYPE	SOURCE RANGE	DETECTOR TYPE	DETECTOR RANGE	ANGLE
G,N	481	ABX	7-21	D	7-28	MOD-I		4PI
G,2N	482	ABX	13-27	D	7-28	MOD-I		4PI
G,3N	483+	ABX	23-28	D	7-28	MOD-I		4PI

481+

x = fraction of total cross section resulting in a direct neutron
n_d = fraction of neutrons emitted by direct effect at an energy where all the evaporation neutrons go to (γ,2n) cross section
n_d = x/(2-x)

TABLEAU 3
Moments quadrupolaires intrinsèques

Cible	% isotopes	a/b ex	β_2 ex	$\beta_2[B(E_2)]$	Q_0 ex (b)	Q'_0
$_{53}$I	100 % ^{127}I	0.85	0.172		−2.3±0.4	
$_{58}$Ce	88.5 % ^{140}Ce			).104		
	11.1 % ^{142}Ce			0.118		
$_{62}$Sm	15 % ^{147}Sm	1.23	0.219		4.5±0.4	0.158
	11.2 % ^{148}Sm					
	13.8 % ^{149}Sm					
	7.5 % ^{150}Sm			0.190		3.53
	26.6 % ^{152}Sm			0.304		5.93
	22.5 % ^{154}Sm			0.351		6.58
$_{68}$Er	33.4 % ^{166}Er	1.314	0.288	0.341	6.96±0.4	7.60
	22.9 % ^{167}Er					7.80
	27.1 % ^{168}Er			0.339		7.60
	14.9 % ^{170}Er			0.329		7.45
$_{71}$Lu	97.4 % ^{175}Lu	1.282	0.262		6.95±0.3	7.20

TABLEAU 5
Valeurs de la température nucléaire et du paramètre a de densité des niveaux

	x	n_d	Θ (MeV)	$E'_\gamma - E_n$ (MeV)	a (MeV^{-1})	a' (MeV^{-1})	a'' (MeV^{-1})
I	0.05±0.005	0.03±0.03	1.30±0.20	10	6±2.5	10±3	10±2
^{140}Ce	0.21±0.05	0.12±0.03	1.05±0.20	10	9±3.5		7±3
^{142}Ce			0.8 ±0.20	6	9±4		8±3
Sm	0.18±0.04	0.10±0.03					
Er	0.20±0.05	0.11±0.03					(12±4)
Lu	0.26±0.06	0.15±0.03	0.85±0.1	9	12.5±2.5		15±3

[over]

Tableau 4

Règles de somme

Noyau cible (éléments naturels)	σ_0 (MeV · b)	σ'_0 (MeV · b)	$0.06 \frac{NZ}{A}$	$\frac{\sigma_0 A}{0.06\,NZ}$	$\frac{\sigma'_0 A}{0.06\,NZ}$	σ_{-1} (mb)	$\sigma_{-1}A^{-4/3}$	σ_{-2} (mb · MeV^{-1})	$\sigma_{-2}A^{-5/3}$
$_{53}$I	2.02 ± 0.14	2.30 ± 0.12	1.85	1.09 ± 0.07	1.24 ± 0.07	129 ± 0.10	0.20 ± 0.02	8.6 ± 0.6	2.7 ± 0.2
$_{58}$Ce	2.13 ± 0.15	2.53 ± 0.13	2.04	1.05 ± 0.07	1.24 ± 0.07	140 ± 0.12	0.19 ± 0.02	9.5 ± 0.6	2.5 ± 0.2
$_{62}$Sm	2.48 ± 0.17	2.92 ± 0.14	2.18	1.14 ± 0.07	1.34 ± 0.07	167 ± 0.14	0.21 ± 0.02	11.8 ± 0.8	2.75 ± 0.2
$_{68}$Er	2.70 ± 0.19	3.04 ± 0.16	2.42	1.12 ± 0.07	1.26 ± 0.07	186 ± 0.15	0.20 ± 0.02	13.6 ± 1	2.7 ± 0.2
$_{71}$Lu	2.65 ± 0.18	2.96 ± 0.16	2.53	1.05 ± 0.07	1.17 ± 0.07	182 ± 0.15	0.185 ± 0.02	12.9 ± 1	2.35 ± 0.2
valeur moyenne pour ces 5 corps				1.09 ± 0.07	1.25 ± 0.07		0.20 ± 0.02		2.6 ± 0.2

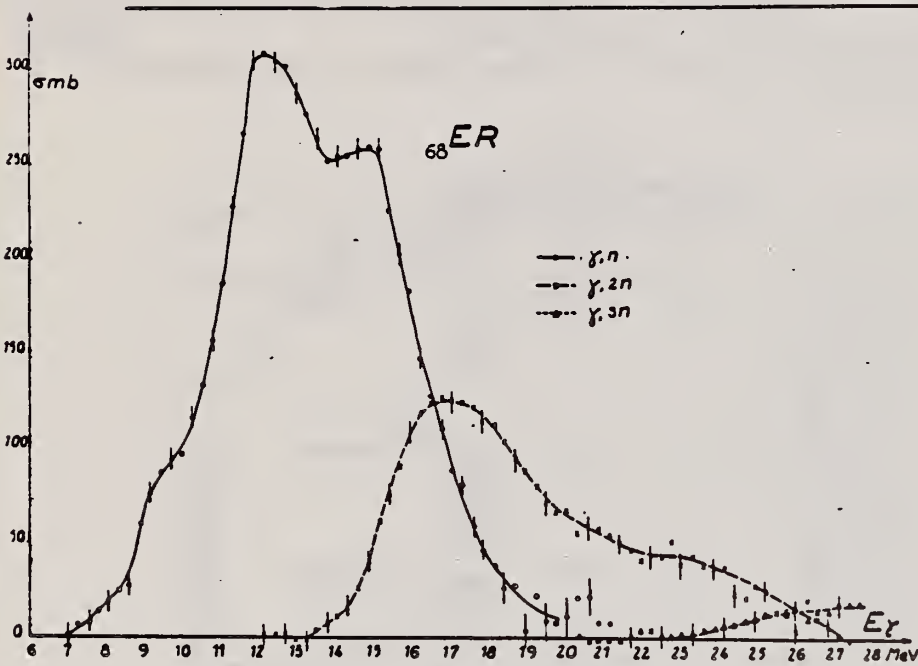

Fig. 7.

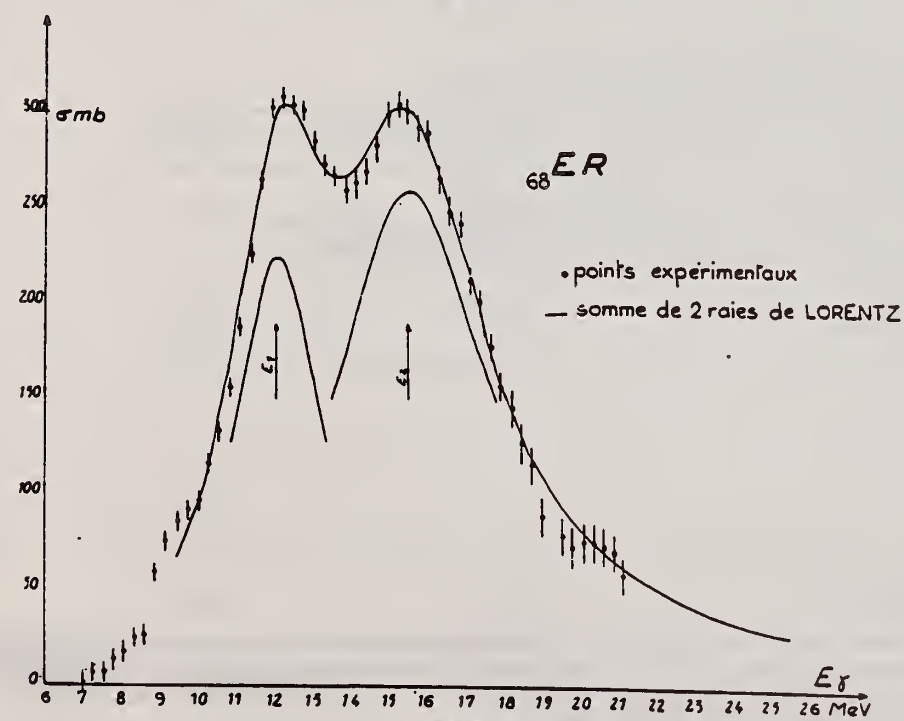

Fig. 8.

REF.	ELEM. SYM.		
R.F. Barrett, J.R. Birkelund, B.J. Thomas, K.S. Lam, and H.H. Thies Nucl. Phys. A210, 355 (1973)	Er		68
METHOD	REF. NO. 73 Ba 20		egf

REACTION	RESULT	EXCITATION ENERGY	SOURCE TYPE	SOURCE RANGE	DETECTOR TYPE	DETECTOR RANGE	ANGLE
G,N	NOX	THR- 27	C	10- 27	BF3-I		4PI

MEAN NEUT ENERGY

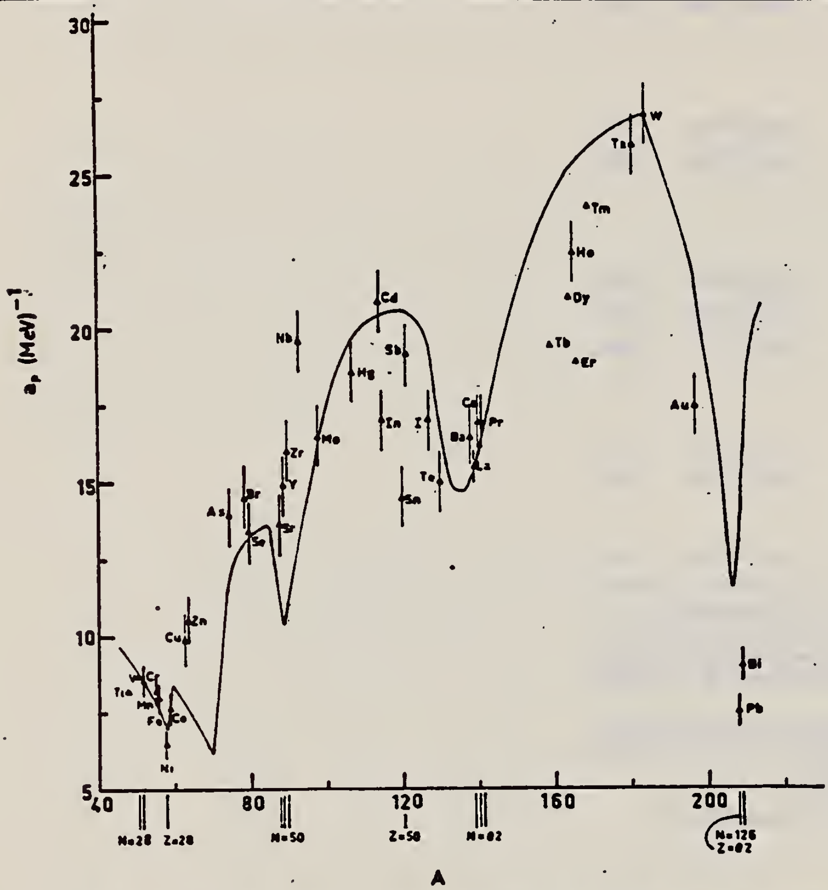

Fig. 12. Experimental values of the level density parameter a_p (Fermi gas formula plus pairing correction) versus atomic number A. The continuous curve is a least-squares fit to the data of a theoretical calculation from Newton [15]).

1
H. Baba and S. Baba, Japan Atomic Energy Research Institute report JAERI-1183 (1969).
2
H. Baba, Nucl. Phys. A159, 625 (1970).
15
T.D. Newton, Can. J. Phys. 34, 804 (1956).

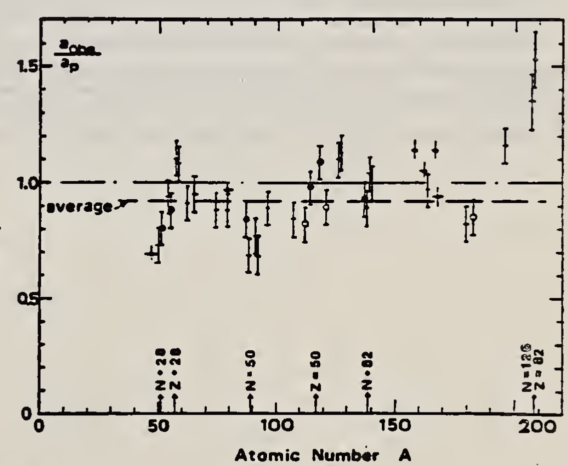

Fig. 15. Ratio a_{obs}/a_p versus atomic number A. Here a_{obs} is the level density parameter taken from the neutron resonance work of refs. [1,2]), and a_p is the level density parameter derived from the present (γ, n) work. Filled circles represent points where nuclei in the neutron resonance and in the (γ, n) experiment were the same. Open circles represent points where the respective nuclei were approximately matched. Triangles represent points which are based on measurement of neutron mean energies at two bremsstrahlung energies only.

(over)

Target	N (residual nucleus)[a]		Goodness of fit[b]) no p.c.	with p.c.	$\hat{E}_n(24)$ (MeV)[c])	T (MeV)[d])	a_p (MeV^{-1})[e])	a_{obs} (MeV^{-1})[f])	a_{obs}/a_p
Ba	75	1%		F	1.16		16.5–^{136}Ba	15.39–^{136}Ba	0.93
	77	2%							
	78	7%							
	79	8%							
	80	11%							
	81	71%							
La	80	100%	F	F	1.25	0.72	15.5–^{138}La	13.76–^{139}La	0.89
Ce	81	89%	F	G	1.24	0.70	17.0–^{139}Ce	17.8 –^{141}Ce	1.04
	83	11%							
Pr	81	100%	G	G	1.17	0.65	17.0–^{140}Pr	17.05–^{142}Pr	1.00
Tb[g])	93	100%			1.15		19.3–^{158}Tb	21.85–^{160}Tb	1.14
Dy[g])	93	2%			1.06		20.9–$^{161.5}$Dy	21.9 –^{162}Dy	1.05
	94	19%							
	95	25%							
	96	25%							
	97	28%							
Ho	97	100%	P	G	1.06	0.56	21.4–^{164}Ho	20.66–^{166}Ho	0.97
Er[g])	95	2%			1.11		19.2–^{166}Er	21.9 –^{166}Er	1.14
	97	33%							
	98	23%							
	99	27%							
	101	15%							
Tm[g])	99	100%			1.03		24.0–^{168}Tm	22.58–^{170}Tm	0.94
Ta	107	100%		G	1.00	0.49	26.0–^{180}Ta	21.2 –^{181}Ta	0.82
W	107	26%	G	F	0.98	0.50	27.0–^{183}W	23.0 –^{183}W	0.85
	108	14%							
	109	31%							
	111	28%							
Au	117	100%		G	1.19		17.5–^{196}Au	20.24–^{198}Au	1.16
Pb ($Z = 82$)	123	24%		V.P.	1.87	1.20	7.5–^{206}Pb	10.1 –^{207}Pb	1.35
	124	23%							
	125	52%							
Bi	125	100%		F	1.65	1.03	9.0–^{208}Bi	13.8 –^{210}Bi	1.53

[a]) Neutron numbers and abundances of respective residual nuclei in (γ, n) experiments.
[b]) These give an assessment of the goodness of fit of a calculated $\hat{E}_n$ versus E_0 curve to the observed data, using the Fermi gas level density formula both without and with pairing corrections.
[c]) Bremsstrahlung photoneutron mean energies $\hat{E}_n$ for peak bremsstrahlung energy $E_0 = 24$ MeV.
[d]) Nuclear temperature from fit with constant-temperature formula.
[e]) Level density parameter a_p derived from the present (γ, n) experiment, using a Fermi gas formula plus pairing correction, and corresponding residual nucleus (the atomic weight shown is the weighted average of atomic weights of the respective isotopes present).
[f]) As column 7, but using data on n-resonance absorption from refs. [1,2]).
[g]) Measurements of $\hat{E}_n(E_0)$ for these nuclei were made only for $E_0 = 21$, 23 and 24 MeV.

ER
A=166

ER
A=166

ER
A=166

REF.	F. R. Metzger and V. K. Rasmussen Phys. Rev. C8, 1099 (1973)	ELEM. SYM.	A	Z
		Er	166	68
METHOD		REF. NO.		
		73 Me 4		hmg

REACTION	RESULT	EXCITATION ENERGY	SOURCE TYPE	SOURCE RANGE	DETECTOR TYPE	DETECTOR RANGE	ANGLE
$ G,G	LFT	2	C	2	SCD-D		DST

1.66, 1.81 MEV LEVS

In addition to the previously known 1^- states of ^{166}Er at 1663 and 1830 keV, levels at 1812 ± 1 keV (^{166}Er), 1786 ± 1 keV (^{168}Er), and 1824 ± 1 keV (^{170}Er) have been excited using electron bremsstrahlung. Based on the observed angular distributions of the scattered photons, all three previously unknown levels were found to have spin 1. Linear polarization measurements using a two-slab Ge(Li) polarimeter led to negative parity assignments for the 1786- and 1824-keV levels but were inconclusive with respect to the less strongly excited 1812-keV level. Below 1.9 MeV, the 1663-, 1786-, and 1824-keV levels are the dominant $E1$ excitations in their respective isotopes, the partial widths of their ground-state transitions being Γ_0 = 32 ± 5, 46 ± 5, and 30 ± 3 meV. The $B(E1;1^- \to g.s.)/B(E1;1^- \to 2_1^+)$ ratios of 0.52 ± 0.02, 0.51 ± 0.02, and 0.53 ± 0.02 differ considerably from the ratio 1.31 ± 0.11 for the 1812-keV level and the reported ratio 0.22 for the 1830-keV 1^- state and are very close to the Alaga value of 0.50 for $K = 0^-$ levels.

TABLE II. Comparison of the experimental ratios of the counting rates in the 98 and 127° scattering geometries with the ratios expected for different values of the spins of the excited states.

Isotope	E_{level} (keV)	$N(127°)/N(98°)$ Experiment	Theory Spin 1	Theory Spin 2
^{166}Er	1663	1.39 ± 0.11	1.36	0.49
^{166}Er	1812	1.40 ± 0.17		
^{168}Er	1786	1.38 ± 0.07		
^{170}Er	1824	1.33 ± 0.09		

TABLE III. Results of the measurements using the two-slab Ge(Li) polarimeter. $N_\parallel$ and $N_\perp$ represent the counting rates in the full energy peaks with the slabs parallel and perpendicular to the scattering plane, respectively.

Isotope	E_{level} (keV)	Transition $I_i - I_f^\pi$	E_γ (keV)	$(N_\parallel - N_\perp)/(N_\parallel + N_\perp)$ (%)
^{166}Er	1662	$1^- \to 0^+$	1662	+7.4 ± 4.9
		$1^- \to 2^+$	1582	+3.7 ± 3.4
	1812	$1 \to 0^+$	1812	−5.6 ± 10.0
^{168}Er	1786	$1 \to 0^+$	1786	+16.7 ± 7.4
		$1 \to 2^+$	1706	−1.4 ± 4.3
^{170}Er	1824	$1 \to 0^+$	1824	+9.8 ± 4.8
		$1 \to 2^+$	1745	0.0 ± 3.1

TABLE IV. Widths and branching ratios of the ^{166,168,170}Er levels. The direct results of the NRF scattering experiments are listed in column 5.

Isotope	Level (keV)	Γ_0/Γ_1	$B(E1;1^- \to g.s.)/B(E1;1^- \to 2_1^+)$	Γ_0^2/Γ (meV)	Γ_0/Γ [a]	Γ_0 (meV)
^{166}Er	1663	0.60 ± 0.02 [b]	0.52 ± 0.02	12.0 ± 1.8	0.38 ± 0.01	32 ± 5
	1812	1.50 ± 0.12	1.31 ± 0.11 [c]	4.8 ± 0.6	0.60 ± 0.02	8 ± 1
	1830	≈0.33 [d]	≈0.22	...	≈0.25	2.4
^{168}Er	1786	0.59 ± 0.02	0.51 ± 0.02	17.0 ± 1.7	0.37 ± 0.01	46 ± 5
^{170}Er	1824	0.61 ± 0.02	0.53 ± 0.02	11.4 ± 1.1	0.38 ± 0.01	30 ± 3

[a] Assuming the absence of branching to levels above the 2_1^+ state.
[b] In good agreement with the value of 0.61 adopted in Ref. 18.
[c] This might be the ratio of $B(M1)$'s rather than $B(E1)$'s since the polarization experiment was not conclusive.
[d] From the decay of ^{166}Ho; see Ref. 18.

[18] Nuclear Data Sheets, 1959-1965, compiled by the Nuclear Data Group (Academic, New York, 1966).

REF.
B.I. Goryachev, Yu.V. Kuznetsov, V.N. Orlin, N.A. Pozhidaeva, and V.G. Shevchenko
ZhETF Pis. Red. 19, 65 (1974)
JETP Lett. 19, 41 (1974)

ELEM. SYM.	A	Z
Er	166	68

METHOD

REF. NO. 74 Go 4 hmg

REACTION	RESULT	EXCITATION ENERGY	SOURCE TYPE	SOURCE RANGE	DETECTOR TYPE	DETECTOR RANGE	ANGLE
G,XN	ABX	8- 21	C	8- 21	BF3-I		4PI

$\sigma(\gamma,2n)$ measured but not given.

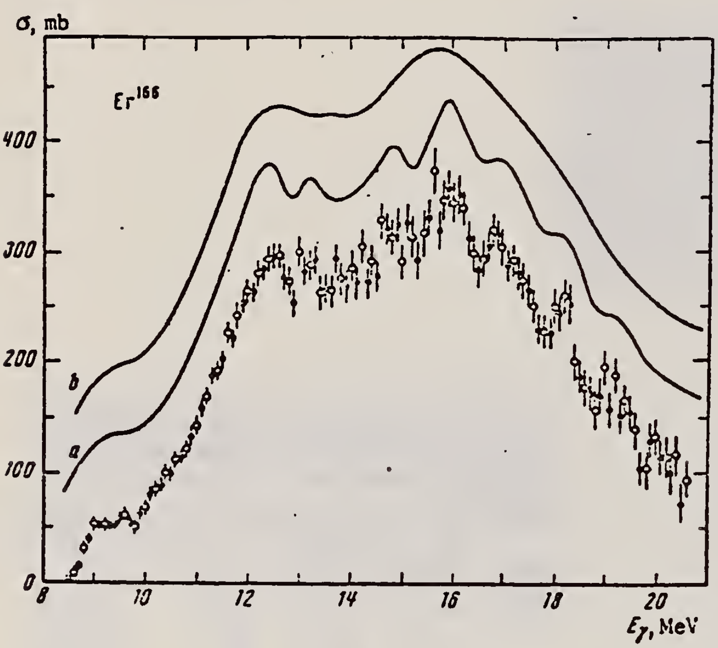

Fig. 1. Cross section σ_γ of Er^{166}; the light and dark circles correspond to two independent series of experimental data. Curves a and b were obtained by the regularization method (see the text) and are shown shifted relative to the ordinate axis.

Note: (γ,sn) cross section determined from $\sigma(\gamma,xn)$ and statistical theory which gives $\sigma(\gamma,2n)$ consistent with measurements.

See Refs. 6&7 for Regularization Method (Least Structure).

[6] A.N. Tikhonov, Dokl.Akad.Nauk SSSR 151, 501 (1963).

[7] B.S. Cook, Nucl.Instr. and Meth. 24, 256 (1963).

Nucleus	σ_{int}, MeV-b	β	Q_0, b
Er^{166}	3.05 ± 0.3	0.33	7.76
Hf^{178}	3.16 ± 0.3	0.26	6.72

The table lists the values of the integral cross sections σ_{int} calculated from σ_γ and the deformation parameters β, as well as the values Q_0 of the intrinsic quadrupole moments of the nuclei, corresponding to the obtained values of β.

REF.	ELEM. SYM.	A	Z
T. Cooper, W. Bertozzi, J. Heisenberg, S. Kowalski W. Turchinetz, C. Williamson, L. Cardman, S. Fivozinsky, J. Lightbody, Jr., and S. Penner Phys. Rev. C13, 1083 (1976)	Er	166	68

METHOD	REF. NO.	
	76 Co 3	hmg

REACTION	RESULT	EXCITATION ENERGY	SOURCE TYPE	SOURCE RANGE	DETECTOR TYPE	DETECTOR RANGE	ANGLE
E,E/	FMF	1, 1	D	34-111	MAG-D		DST

LEVELS .081,.265

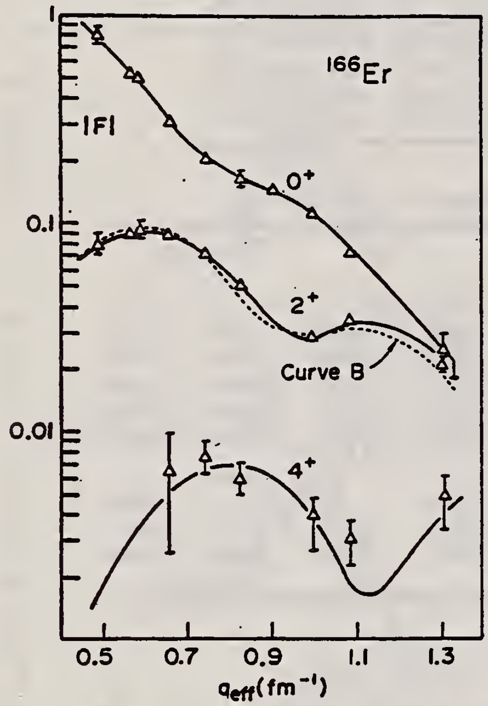

FIG. 5. Measured form factors for the elastic (0$^+$) and the inelastic 0.081-MeV (2$^+$) and 0.265-MeV (4$^+$) states in ^{166}Er. The solid line represents the quoted best fit. Curve B gives the result for the 2$^+$ state using a deformed Fermi distribution.

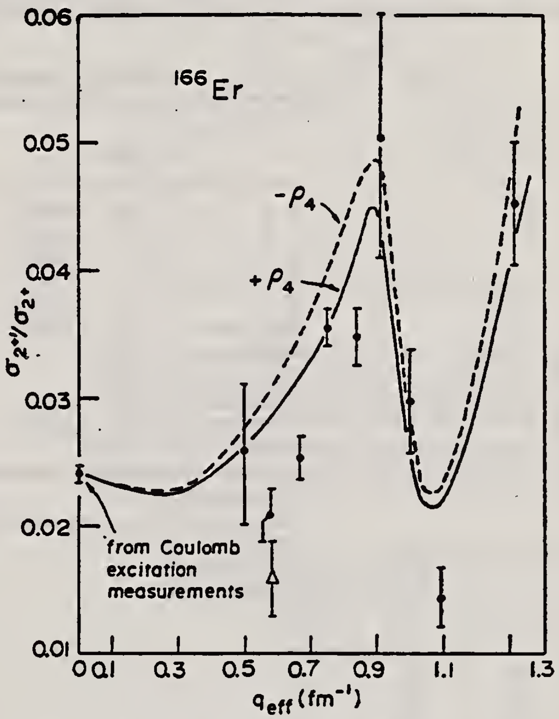

FIG. 9. Ratio of the cross sections observed for exciting the 0.786-MeV (2$^{+\prime}$) γ-vibrational level to that for exciting the 0.081-MeV (2$^+$) state. The best fit curves differ only in the sign of the of the ρ_4 component of the charge distribution, since the sign is not determined by form factor fits to the ground state rotational band data.

(over)

TABLE IV. Cross sections of ^{166}Er.

Energy (MeV)	Angle (deg)	q_{eff} (fm^{-1})	Elastic $\frac{d\sigma}{d\Omega}_{exp}$ (mb)	Elastic $\frac{d\sigma}{d\Omega}_{bestfit}$ (mb)	2^+ $\frac{d\sigma}{d\Omega}_{exp}$ (mb)	4^+ $\frac{d\sigma}{d\Omega}_{exp}$ (mb)	$2^+\gamma$ vibrational $\frac{d\sigma}{d\Omega}_{exp}$ (mb)
34.65	109.95	0.495	$0.948\times10 \pm 4\%$	0.933×10	$0.964\times10^{-1}\pm 6\%$	...	$0.258\times10^{-2}\pm 22\%$
39.64	127.81	0.588	$0.146\times10 \pm 5\%$	0.142×10	$0.433\times10^{-1}\pm 4\%$	...	$0.681\times10^{-3}\pm 18\%$
44.51	109.95	0.577	$0.241\times10 \pm 5\%$	0.237×10	$0.761\times10^{-1}\pm 3\%$	...	$0.163\times10^{-2}\pm 10\%$
54.88	109.95	0.663	$0.588 \pm 4\%$	0.566	$0.484\times10^{-1}\pm 3\%$	$0.231\times10^{-3}\pm 49\%$	$0.121\times10^{-2}\pm 2\%$
64.82	110.16	0.746	$0.170 \pm 3\%$	0.177	$0.214\times10^{-1}\pm 2\%$	$0.246\times10^{-3}\pm 17\%$	$0.735\times10^{-3}\pm 3\%$
75.99	110.13	0.831	$0.886\times10^{-1}\pm 7\%$	0.850×10^{-1}	$0.754\times10^{-2}\pm 3\%$	$0.106\times10^{-3}\pm 15\%$	$0.275\times10^{-3}\pm 6\%$
84.17	110.01	0.906	$0.521\times10^{-1}\pm 5\%$	0.512×10^{-1}	$0.240\times10^{-2}\pm 7\%$	$0.513\times10^{-4}\pm 57\%$	$0.124\times10^{-3}\pm 18\%$
95.23	110.03	0.999	$0.235\times10^{-1}\pm 3\%$	0.239×10^{-1}	$0.151\times10^{-2}\pm 4\%$	$0.303\times10^{-4}\pm 30\%$	$0.444\times10^{-4}\pm 13\%$
95.00	127.81	1.092	$0.497\times10^{-2}\pm 3\%$	0.485×10^{-2}	$0.937\times10^{-3}\pm 4\%$	$0.859\times10^{-5}\pm 39\%$	$0.139\times10^{-4}\pm 2\%$
110.20	147.24	1.315	$0.165\times10^{-3}\pm 10\%$	0.172×10^{-3}	$0.977\times10^{-4}\pm 15\%$	$0.483\times10^{-5}\pm 13\%$	$0.423\times10^{-5}\pm 11\%$

TABLE IX. Transition charge parameters of ^{166}Er and ^{176}Yb.

		^{166}Er			^{176}Yb		
	Units	ρ_0	ρ_2	ρ_4	ρ_0	ρ_2	ρ_4
c	fm	6.1610	5.8632	5.8556	6.3306	6.0151	5.1866
t	fm	0.4872	0.5598	0.7271	0.4868	0.5188	0.9093
β_2		0.3266	0.3503	0.3325	0.3100	0.3346	0.3874
β_4		0.0	0.0	0.0199	−0.054	−0.054	−0.0875
β_6		−0.0180	−0.0180	−0.0180 [a]	−0.006	−0.006	−0.006 [a]
rms radius	fm	5.2380 [b]			5.3150 [c]		
$B(E2)$	e^2b^2		5.670 [d]			5.350 [e]	
$B(E4)$	e^2b^2			0.0919			0.0092
χ^2/freedom		0.42	2.62	2.68	1.18	1.23	3.14
Transition radius	fm	5.2380	6.9088	8.4777	5.3150	6.8689	6.6962

[a] Reference 3.
[b] Interpolated value from nearest neighbors.
[c] Reference 23.
[d] Reference 25.
[e] Reference 24.

[3] D.L. Hendrie, Phys. Lett. 36, 571 (1973); ibid. et al. Phys. Lett. 26B, 127 (1968).

[23] A. Thompson (private commun.) Eidgenoessische TH Zuerich, 1974 (unpublished).

[24] R.O. Sayer et al., Phys. Rev. C1, 1525 (1970).

[25] P.H. Stelson, Nucl. Data A1, 21 (1965).

REF.	B.I. Goryachev, Yu.V. Kuznetsov, V.N. Orlin, N.A. Pzhidaeva, V.G. Shevchenko Yad. Fiz. 23, 1145 (1976) Sov. J. Nucl. Phys. 23, 609 (1976)	ELEM. SYM.	A	Z
		Er	166	68
METHOD		REF. NO.		
		76 Go 4		hmg

REACTION	RESULT	EXCITATION ENERGY	SOURCE TYPE	SOURCE RANGE	DETECTOR TYPE	DETECTOR RANGE	ANGLE
G,XN	ABX	8- 23	C	UKN	BF3-I		4PI
G,2N	ABX	15- 21	C	UKN	SCI-I		4PI

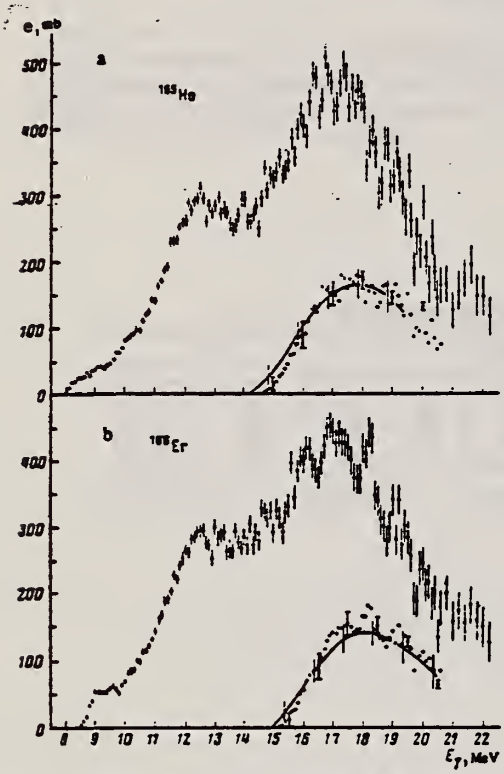

FIG. 1. Photoneutron production cross section σ_n obtained for ^{165}Ho (a) and for ^{166}Er (b). The hollow and solid circles correspond to two independent series of data. The solid curves show the $(\gamma, 2n)$ cross sections calculated from the data of a statistical experiment by the regularization method.[12] The circles near the curves give the same cross sections calculated from the formula $\sigma_n(1-f(E,a))$.

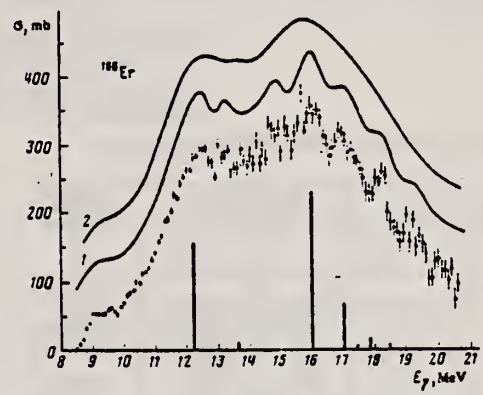

FIG. 6. Cross section σ_γ for ^{166}Er: The hollow and solid circles correspond to two independent series of experimental data. Curves 1 and 2 were obtained by the regularization method and are shown shifted along the ordinate axis. The heavy vertical bars show the dipole transition spectrum calculated by means of a version of the dynamic collective model based on a rotational-vibrational model of surface oscillations.

TABLE 4. Parameters of curve fitted to the cross section σ_γ in ^{166}Er.

Number of resonance	E_k, MeV	σ_k, mb	Γ_k, MeV	$\sigma_k\Gamma_k/\sigma_1\Gamma_1$
1	12.26	210	2.63	1.00
2	13.44	34	0.94±0.27	0.06±0.02
3	14.77	161	2.25±0.15	0.65±0.05
4	15.93	112	0.93±0.08	0.19±0.01
5	16.98	89	1.08±0.12	0.17±0.01
6	17.7	114	4.67±0.44	0.95±0.01
7	16.2	62	0.55±0.16	0.06±0.02

$\chi^2=79.3$, $f=75$, $E_1=10.7$ MeV, $E_2=20.1$ MeV

TABLE 1. Level-density parameters

Nucleus	a, MeV^{-1} Present work	a, MeV^{-1} Other studies	Nucleus	a, MeV^{-1} Present work	a, MeV^{-1} Other studies
^{159}Tb	—	7.7[15]	^{166}Er	6.1±2.5	8[16]
^{165}Ho	4.2±1.5	3.1[15]	^{178}Hf	17.7±7.3	—

(over)

TABLE 2. Parameters of fitted curves $\sigma_\gamma^{(2)}$

Nucleus	E_1, MeV	σ_1, mb	Γ_1, MeV	E_2, MeV	σ_2, mb	Γ_2, MeV	$\sigma_2\Gamma_2/\sigma_1\Gamma_1$	χ^2	f	E_{i}, MeV	E_{f}, MeV
^{159}Tb	12.28 12.41	192 213	2.91±0.09 3.31±0.05	15.76 15.95	295 282	5.42±0.13 5.01±0.07	2.56±0.23 2	197.3 216.8	97 98	10.4 10.4	20.6 20.6
^{165}Ho	12.31 12.47	204 225	2.74±0.11 3.26±0.06	16.23 16.46	306 293	5.67±0.17 5.02±0.09	3.11±0.27 2	176.0 200.8	97 98	10.4 10.4	20.6 20.6
^{166}Er	12.32 12.50	191 214	2.71±0.14 3.43±0.08	15.99 16.25	308 289	5.67±0.16 5.09±0.10	3.38±0.35 2	123.5 161.7	94 95	10.7 10.7	20.6 20.6
^{178}Hf	12.68 12.88	166 216	2.55±0.10 3.22±0.11	15.05 15.46	281 237	6.09±0.27 5.57±0.20	4.00±1.76 2	172.1 175.7	89 90	10.6 10.6	20.0 20.0

Note. The lower values of the parameters in each column were found with the requirement $\sigma_2\Gamma_2 : \sigma_1\Gamma_1 = 2:1$.

TABLE 3. Static deformation β and intrinsic quadrupole moment Q_0.

Nucleus	Present work		Other photonuclear experiments		Coulomb excitation of nuclei
	β	Q_0, b	β	Q_0, b	Q_0, b
^{159}Tb	0.29	6.53±0.6	0.29 0.32 0.29	6.37 [19] 7.37 [20] 6.6 [21]	7.07 [19]
^{165}Ho	0.32	7.73±0.6	0.29 0.30 0.31	7.01 [19] 7.14 [20] 7.6 [19]	7.80 [19]
^{166}Er	0.30	7.39±0.6	0.28 0.31	6.96 [16] 7.6 [19]	
^{178}Hf	0.26	6.94±0.6			6.79 [22]

TABLE 6. Integrated cross sections.

Nucleus	σ_0, MeV-b	$\sigma_0/0.06\frac{ZN}{A}$	σ_{-1}, mb	$\sigma_{-1}/A^{4/3}$	σ_{-2}, MeV-b	$\sigma_{-2}/A^{5/3}$
^{159}Tb	3.70	1.47	210	0.243	15.9	$3.41\cdot10^{-3}$
^{165}Ho	3.60	1.31	218	0.241	16.1	$3.25\cdot10^{-3}$
^{166}Er	3.56	1.48	216	0.237	16.1	$3.21\cdot10^{-3}$
^{178}Hf	3.08	1.20	196	0.196	14.8	$2.63\cdot10^{-3}$
Average		1.41±0.3		0.23±0.04		$3.1\cdot10^{-3}\pm6\cdot10^{-4}$

[12] A.N. Tikhonov, Dokl. Akad. Nauk SSSR 151, 501 (1963), Eng. transl. in Sov. Mathematics-Doklady.

[15] B. L. Berman et al., Phys. Rev. 185, 1576 (1969).

[16] R. Bergere et al., Nucl. Phys. A133, 417 (1969).

[18] E. G. Fuller et al., Nucl. Phys. 30, 613 (1962).

[19] H. Arenhovel et al., Phys. Rev. 157, 1109 (1967).

[20] R. Bergere et al., Nucl. Phys. A121, 463 (1968).

[21] O.V. Bogdankevich et al., Zh. Eksp.Teor.Fiz. 42, 1502 (1962); Sov. Phys. JETP 15, 1044 (1962).

[22] B.S. Dzhelepov in Struktura slozhynkh yader (Structure of Complex Nuclei), Atomizdat, 1966, p. 189.

REF.	F. R. Metzger Phys. Rev. C13, 626 (1976)	ELEM. SYM.	A	Z
		Er	166	68
METHOD		REF. NO. 76 Me 4		hmg

REACTION	RESULT	EXCITATION ENERGY	SOURCE TYPE	SOURCE RANGE	DETECTOR TYPE	DETECTOR RANGE	ANGLE
G,G	LFT	1- 4	C	2- 4	SCD-D		DST
		(1.66 - 3.19)					

13 STATES, 1.66-3.19

Some 40 states in ^{166,168,170}Er, most of them previously unknown, have been excited using bremsstrahlung with $\leq$4.2 MeV endpoint energy. For all but three of these levels, the angular distribution of the resonantly scattered radiation favors the assignment of spin 1. For some of the strongly excited levels, linear polarization measurements have been performed. They indicate that these levels have positive parity. The branching ratios further characterize them as $K = 1$ excitations.

TABLE II. Properties of levels excited in ^{166}Er with photons of $\leq$3.3 MeV energy.

E_{level} (MeV)	I^{π}	Γ_0^2/Γ (meV)	(Γ_0/Γ) [a]	Γ_0 (meV)
1.663 [b]	1^-	12.0±0.8	0.39±0.01	32±5
1.812 [b]	1^{+} [c]	4.8±0.6	0.60±0.02	8±1
1.830 [b]	1^-		~0.25	2.4
2.201	$1^{(+)}$	5.4±0.9	0.36±0.03	15±3
2.464	(1)	3.9±0.8	0.63±0.08	6±2
2.524	(1)	8.3±1.7	0.71±0.10	12±3
2.601	(1)	15.4±1.6	0.62±0.10	25±5
2.679	(1)	9.1±1.9	0.56±0.08 [d]	16±5
2.768	(1)	5.8±1.1	0.46±0.09	13±4
2.782	(2)	2.2±0.5	0.7 ±0.2	3±1
2.811	1	18.6±2.3	0.32±0.04	58±11
3.141	1	35.0±4.0	0.72±0.05	49±7
3.193	1	23.8±2.7	0.71±0.05	33±5

[a] This is really $\Gamma_0/(\Gamma_0+\Gamma_1)$ since, in addition to the ground state transitions, only the cascade γ rays to the first 2^+ state at 80.6 keV could be observed in the presence of the nonresonant background, which increased rapidly with decreasing γ energy.

[b] See Ref. 1.

[c] See Ref. 9.

[d] (Combining our value $\Gamma_0/\Gamma = 0.60\pm0.15$ with the ratio 0.55 ± 0.09 reported in Ref. 11.)

[1] F.R. Metzger et al., Phys. Rev. C8, 1099 (1973).

[9] F. R. Metzger et al., Bull. Am. Phys. Soc. 18, 1386 (1973).

[11] S. B. Burson et al., Phys. Rev. 158, 1161 (1967).

REF.	ELEM. SYM.	A	Z
J.J. Murphy, II, D.M. Skopik, J. Asai, and J. Uegaki Phys. Rev. C 18, 736 (1978)	Er	166	68

METHOD	REF. NO.	
	78 Mu 9	hg

REACTION	RESULT	EXCITATION ENERGY	SOURCE TYPE	SOURCE RANGE	DETECTOR TYPE	DETECTOR RANGE	ANGLE
E,A	ABX	7-100	D	100	MAG-D		DST

α particles from the electrodisintegration of seven nuclei with Z between 29 and 79 have been observed. Energy spectra at 50° in the laboratory for six nuclei and angular distribtions for five nuclei are reported. The cross sections exhibit a broad peak whose magnitude decreases with increasing Z; the energy of the peak increases as Z increases. Angular distributions at the highest energies measured become increasingly forward peaked suggesting a direct-reaction process.

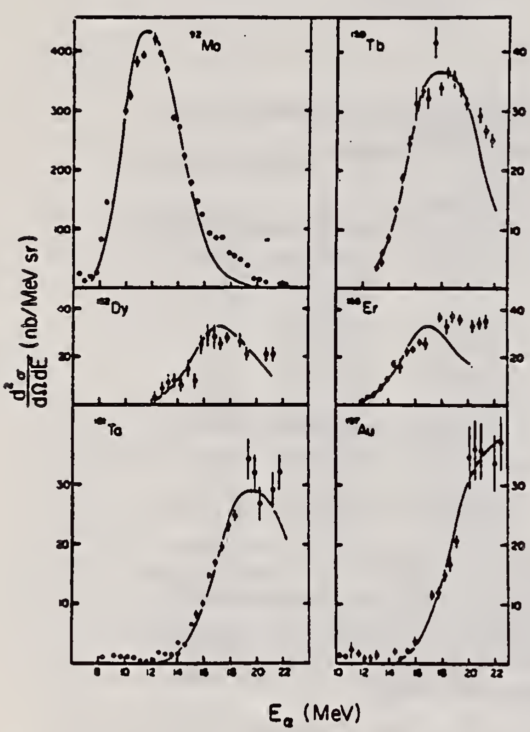

FIG. 2. The α-particle energy spectra at 50° in the laboratory for the four new nuclei studied as well as for two nuclei in which additional data have been obtained. The solid curves are the evaporation model fits described in text.

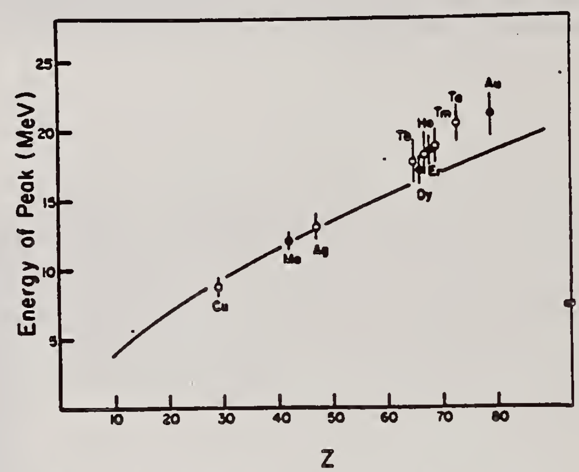

FIG. 3. Energy of the cross section peak as a function of Z. The solid line is the energy of the classical Coulomb barrier. The closed circles are the current work; the open circles are from Ref. 1.

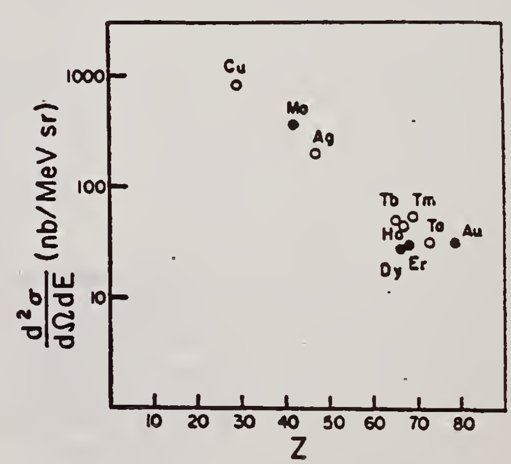

FIG. 4. Magnitude of cross section peak as a function of Z. The closed circles are the current work; the open circles are from Ref. 1.

[1] J.J. Murphy, II, H.J. Gehrhardt, and D.M. Skopik, Nucl. Phys. A277, 69 (1977).

over

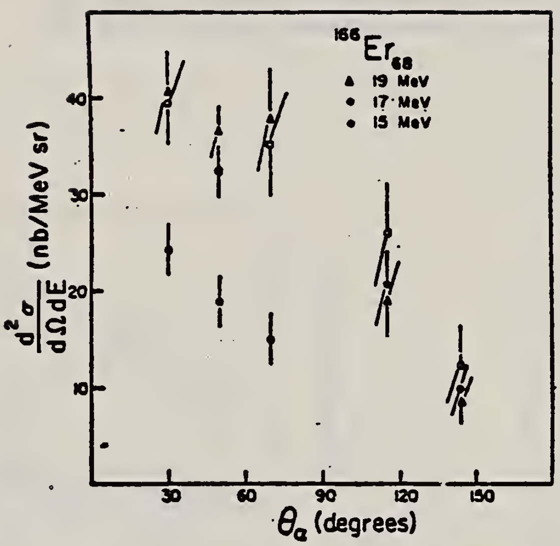

FIG. 7. Angular distributions for erbium. The comments made for Fig. 5 apply here.

REF.	A.M. Nathan, R. Moreh Phys. Lett. 91B, 38 (1980)	ELEM. SYM.	A	Z
		ER	166	68
METHOD		REF. NO.	80 Na 1	hg

REACTION	RESULT	EXCITATION ENERGY	SOURCE TYPE	SOURCE RANGE	DETECTOR TYPE	DETECTOR RANGE	ANGLE
G,G/	SPC	16	D	14-17	MAG-D		DST
		(16.4)		(14.4-16.6)			

BRAN RATIO, VIBR ELAS

Quasi-monochromatic photons in the range E_γ = 14.4–16.6 MeV have been used to study inelastic scattering to the 2^+, γ-vibrational band head in ^{166}Er. The results for transitions to this branch are drastically smaller (by a factor ≈ 3–5) than the predictions of the dynamic collective model (DCM).

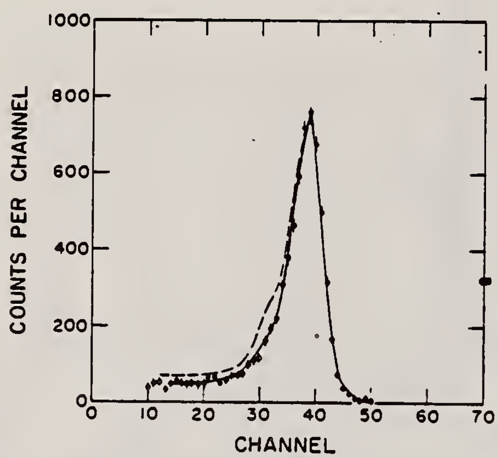

Fig. 1. Spectra at 109° of 16.4 MeV tagged photons scattered from ^{166,168}Er measured with a 24 × 30 cm^2 NaI detector. This spectrum was obtained by merging separate spectra of energies 16.2, 16.4 and 16.6 MeV. The solid line is the shape of the detector response to elastically scattered photons, which was obtained with a ^{209}Bi target. The dashed line shows the calculated spectrum obtained by adding a 10% inelastic branch (to the 785 keV level) to the pure elastic peak.

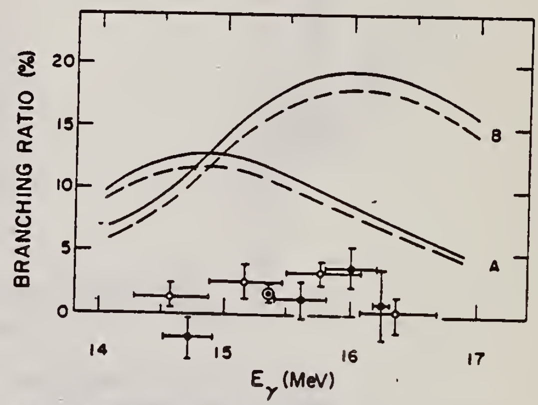

Fig. 2. Measured and calculated branching ratios of the vibrational inelastic to the elastic plus rotational inelastic cross sections. The closed (open) circles are data taken at 90° (109°). The double circle represents the measured average branching ratio over all energies. The solid (dashed) lines, A and B, are the results obtained at 90° (109°) using the parameters given in table 1 and the DCM code of Arenhövel [12].

Er
A=167

Er
A=167

Er
A=167

K. N. Geller, J. Halpern, and E. G. Muirhead
Phys. Rev. 118, 1302-12 (1960)

ELEM. SYM.	A	Z
Er	167	68

METHOD

Betatron; neutron threshold; ion chamber

REF. NO.	
60 Ge 3	NVB

REACTION	RESULT	EXCITATION ENERGY	SOURCE TYPE	SOURCE RANGE	DETECTOR TYPE	DETECTOR RANGE	ANGLE
G,N	NØX	THR	C THR		BF3-I		4 PI

THRESHØLD

TABLE I. Summary and comparison of neutron separation energies inferred from present threshold measurements with values predicted from mass data and reaction energies. All energies are expressed in the center-of-mass system in Mev.

Reaction	No. runs	Present results	Other results	Method	Reference
$Er^{167}(\gamma,n)Er^{166}$	1	6.64 ±0.08(6.56)	6.45 ±0.06	mass data	q

[q] W. H. Johnson, Jr., and V. B. Bhanot, Phys. Rev. 107, 6 (1957).

TABLE II. Comparison of measured threshold energies with neutron binding energies predicted by mass data for transitions with $\Delta I \geq 7/2$. All energies in Mev.

Reaction	ΔI[a]	Observed threshold	Mass data Q value	$E_{th}-Q$	Excited state energy
$Cr^{52}(\gamma,n)Cr^{51}$	7/2	12.18±0.14	12.053±0.004[b]	0.13±0.14	...
$Y^{89}(\gamma,n)Y^{88}$	7/2	11.59±0.08	11.53 ±0.40[c]	0.06±0.41	0.387[d]
$In^{115}(\gamma,n)In^{114}$	7/2	9.22±0.03	9.35 ±0.43[c]	−0.13±0.43	0.191[a]
$Ce^{142}(\gamma,n)Ce^{141}$	(7/2)[e]	7.24±0.07	6.97 ±0.07[f]	0.27±0.10	...
$Nd^{145}(\gamma,n)Nd^{144}$	7/2	6.38±0.16	5.97 ±0.19[f]	0.41±0.25	0.690[a]
$Sm^{149}(\gamma,n)Sm^{148}$	7/2	6.45±0.16	5.87 ±0.28[f]	0.58±0.33	0.562[a]
$Er^{167}(\gamma,n)Er^{166}$	7/2	6.65±0.08	6.45 ±0.06[g]	0.20±0.10	0.081[a]
$Hf^{177}(\gamma,n)Hf^{176}$	7/2	6.69±0.03	6.28 ±0.06[g]	0.64±0.07	0.088[a]
$Hf^{179}(\gamma,n)Hf^{178}$	9/2	6.31±0.07	6.17 ±0.06[g]	0.14±0.09	0.093[a]
$Hf^{180}(\gamma,n)Hf^{179}$	9/2	7.85±0.11	7.32 ±0.06[g]	0.53±0.13	0.375[a]

[a] D. Strominger, J. M. Hollander, and G. T. Seaborg, Revs. Modern Phys. 30, 585 (1958).
[b] C. F. Giese and J. L. Benson, Phys. Rev. 110, 712 (1958).
[c] Henry E. Duckworth, *Mass Spectroscopy* (Cambridge University Press, New York, 1958), p. 177.
[d] S. Dzelepov and L. K. Peker, Atomic Energy of Canada Limited Report Tr. AECL-457 (unpublished).
[e] The discrepancy in the case of Ce^{142} predicts a ground-state spin for Ce^{142} of 0, since the spin of Ce^{141} is known to be 7/2.
[f] W. H. Johnson, Jr., and A. O. Nier, Phys. Rev. 105, 1014 (1957).
[g] W. H. Johnson, Jr., and V. B. Bhanot, Phys. Rev. 107, 6 (1957).

ER
A=168

ER
A=168

REF.	ELEM. SYM.	A	Z
F. R. Metzger and V. K. Rasmussen Phys. Rev. C8, 1099 (1973)	Er	168	68

METHOD	REF. NO.	
	73 Me 4	hmg

REACTION	RESULT	EXCITATION ENERGY	SOURCE TYPE	SOURCE RANGE	DETECTOR TYPE	DETECTOR RANGE	ANGLE
$ G,G	LFT	2	C	2	SCD-D		DST

1.786 MEV LEVEL

In addition to the previously known 1⁻ states of ^{166}Er at 1663 and 1830 keV, levels at 1812 ± 1 keV (^{166}Er), 1786 ± 1 keV (^{168}Er), and 1824 ± 1 keV (^{170}Er) have been excited using electron bremsstrahlung. Based on the observed angular distributions of the scattered photons, all three previously unknown levels were found to have spin 1. Linear polarization measurements using a two-slab Ge(Li) polarimeter led to negative parity assignments for the 1786- and 1824-keV levels but were inconclusive with respect to the less strongly excited 1812-keV level. Below 1.9 MeV, the 1663-, 1786-, and 1824-keV levels are the dominant $E1$ excitations in their respective isotopes, the partial widths of their ground-state transitions being Γ_0 = 32 ± 5, 46 ± 5, and 30 ± 3 meV. The $B(E1;1^- \to \text{g.s.})/B(E1;1^- \to 2_1^+)$ ratios of 0.52 ± 0.02, 0.51 ± 0.02, and 0.53 ± 0.02 differ considerably from the ratio 1.31 ± 0.11 for the 1812-keV level and the reported ratio 0.22 for the 1830-keV 1⁻ state and are very close to the Alaga value of 0.50 for $K = 0^-$ levels

TABLE III. Results of the measurements using the two-slab Ge(Li) polarimeter. $N_\parallel$ and $N_\perp$ represent the counting rates in the full energy peaks with the slabs parallel and perpendicular to the scattering plane, respectively.

Isotope	E_{level} (keV)	Transition $I_i - I_f^\pi$	E_γ (keV)	$(N_\parallel - N_\perp)/(N_\parallel + N_\perp)$ (%)
^{166}Er	1662	$1^- - 0^+$	1662	+7.4 ± 4.9
		$1^- - 2^+$	1582	+3.7 ± 3.4
	1812	$1 - 0^+$	1812	−5.6 ± 10.0
^{168}Er	1786	$1 - 0^+$	1786	+16.7 ± 7.4
		$1 - 2^+$	1706	−1.4 ± 4.3
^{170}Er	1824	$1 - 0^+$	1824	+9.8 ± 4.8
		$1 - 2^+$	1745	0.0 ± 3.1

TABLE II. Comparison of the experimental ratios of the counting rates in the 98 and 127° scattering geometries with the ratios expected for different values of the spins of the excited states.

Isotope	E_{level} (keV)	$N(127°)/N(98°)$ Experiment	Theory Spin 1	Theory Spin 2
^{166}Er	1663	1.39 ± 0.11	1.36	0.49
^{166}Er	1812	1.40 ± 0.17		
^{168}Er	1786	1.38 ± 0.07		
^{170}Er	1824	1.33 ± 0.09		

TABLE IV. Widths and branching ratios of the ^{166,168,170}Er levels. The direct results of the NRF scattering experiments are listed in column 5.

Isotope	Level (keV)	Γ_0/Γ_1	$B(E1;1^- \to \text{g.s.})/B(E1;1^- \to 2_1^+)$	Γ_0^2/Γ (meV)	Γ_0/Γ [a]	Γ_0 (meV)
^{166}Er	1663	0.60 ± 0.02 [b]	0.52 ± 0.02	12.0 ± 1.8	0.38 ± 0.01	32 ± 5
	1812	1.50 ± 0.12	1.31 ± 0.11 [c]	4.8 ± 0.6	0.60 ± 0.02	8 ± 1
	1830	≈0.33 [d]	≈0.22	···	≈0.25	2.4
^{168}Er	1786	0.59 ± 0.02	0.51 ± 0.02	17.0 ± 1.7	0.37 ± 0.01	46 ± 5
^{170}Er	1824	0.61 ± 0.02	0.53 ± 0.02	11.4 ± 1.1	0.38 ± 0.01	30 ± 3

[a] Assuming the absence of branching to levels above the 2_1^+ state.
[b] In good agreement with the value of 0.61 adopted in Ref. 18.
[c] This might be the ratio of $B(M1)$'s rather than $B(E1)$'s since the polarization experiment was not conclusive.
[d] From the decay of ^{166}Ho; see Ref. 18.

FORM NBS-418 (REV. 7-14-64) USCOMM-NBS-DC

[18] Nuclear Data Sheets, 1959-1965, compiled by the Nuclear Data Group (Academic, New York, 1966).

REF.	F. R. Metzger Phys. Rev. C13, 626 (1976)	ELEM. SYM.	A	Z
		Er	168	68

METHOD	REF. NO.	
	76 Me 4	hmg

REACTION	RESULT	EXCITATION ENERGY	SOURCE TYPE	SOURCE RANGE	DETECTOR TYPE	DETECTOR RANGE	ANGLE
G,G	LFT	1- 4	C	1- 4	SCD-D		DST
		(1.786-3.481)					

20 STATES, 1.79-3.48

Some 40 states in ^{166,168,170}Er, most of them previously unknown, have been excited using bremsstrahlung with $\leq$4.2 MeV endpoint energy. For all but three of these levels, the angular distribution of the resonantly scattered radiation favors the assignment of spin 1. For some of the strongly excited levels, linear polarization measurements have been performed. They indicate that these levels have positive parity. The branching ratios further characterize them as $K = 1$ excitations.

TABLE III. Properties of levels excited in ^{168}Er with photons of $\leq$3.5 MeV energy.

E_{level} (MeV)	I^{π}	Γ_0^2/Γ (meV)	(Γ_0/Γ) [a]	Γ_0 (meV)
1.786 [b]	1^-	17.0±1.7	0.37±0.01	46±5
1.935	(1)	1.5±0.4	~1	~1.5
(2.136)	(1, 2)	2.1±0.6 [c]	0.62±0.15	3.4±1.3
2.363	(1)	3.1±0.5	0.8±0.1	4±1
2.417	(1)	3.3±0.9	0.36±0.07	9±3
2.495	(1)	6.5±0.8	0.66±0.06	10±2
2.676	(1)	10.4±1.1	0.76±0.05	14±2
2.728	(1)	7.6±1.0	0.50±0.05	15±3
2.792	1	12.0±1.2	0.9±0.1	13±2
2.798	1	13.7±1.4	0.9±0.1	15±3
2.828	(1)	4.3±0.9	0.62±0.10	7±2
2.849	(1)	5.1±1.5	0.70±0.12	7±3
2.856	(1)	3.3±1.1	0.35±0.07	10±4
2.946	(1)	4.6±1.2	0.39±0.05	12±4
3.358	1	30.7±4.0	0.61±0.04	50±8
3.391	$1^{(+)}$	78±7	0.69±0.03	113±12
3.410	(1)	16.6±2.2	0.54±0.05	31±6
3.458	1	37±5	0.63±0.06	59±10
3.469	(1)	23±6	?	
3.481	(1)	17±5	0.42±0.07	41±14

[a] This is really $\Gamma_0/(\Gamma_0+\Gamma_1)$ since, in addition to the ground state transition, only the cascade transitions to the first 2^+ state at 79.8 keV could be observed.
[b] See Ref. 1.
[c] (Assuming spin 1.)

[1] F. R. Metzger et al., Phys. Rev. C8, 1099 (1973).

REF. G.M. Gurevich, L.E. Lazareva, V.M. Mazur, S.Yu. Merkulov, G.V. Solodukhov, V.A. Tyutin
JETP Lett. 28, 157 (1978)
Pis'ma Zh. Eksp. Teor. Fiz. 28, 168 (1978)

ELEM. SYM.	A	Z
Er	168	68

METHOD

REF. NO.	
78 Gu 7	hg

REACTION	RESULT	EXCITATION ENERGY	SOURCE TYPE	SOURCE RANGE	DETECTOR TYPE	DETECTOR RANGE	ANGLE
G,MU-T	ABX	THR-30	C	UKN	NAI-D		4PI

The absorption method is used to measure the total photoabsorption cross section curves for deformed ^{154}Sm, ^{156}Gd, ^{168}Er, ^{174}Yb, ^{184}W, and ^{186}W nuclei in the region of the $E1$ giant resonance. The behavior of the resonance widths for nuclei in the interval $A = 153$ to 186 is discussed.

PACS numbers: 24.30.Cz, 25.20.+y, 27.70.+q

TABLE I.

Nucleus	E_1 MeV	σ_1 mb	Γ_1 MeV	E_2 MeV	σ_2 mb	Γ_2 MeV	Γ MeV	Q_0 b	β -	$\sigma_0 L/0.06\frac{ZN}{A}$
^{154}Sm	12.2	188	3.4	15.7	207	5.7	8.1 ± 0.2	6.3 ± 0.3	0.32 ± 0.02	1.28
^{156}Gd	12.3	206	3.2	15.7	220	5.5	7.7 ± 0.2	6.2 ± 0.3	0.31 ± 0.02	1.30
^{168}Er	11.9	222	3.2	15.5	275	4.5	7.4 ± 0.2	7.5 ± 0.7	0.32 ± 0.03	1.26
^{174}Yb	12.3	297	2.9	15.5	320	4.9	7.1 ± 0.2	7.0 ± 0.6	0.30 ± 0.02	1.52
^{184}W	11.9	315	2.9	14.8	321	4.7	6.8 ± 0.2	7.2 ± 0.8	0.27 ± 0.03	1.50
^{186}W	12.0	246	3.3	14.5	332	5.1	6.4 ± 0.2	6.2 ± 0.8	0.23 ± 0.03	1.48
Average error	±1.3%	±10.5%	±7.5%	±1.3%	±9.4%	±3.8%	—	—	—	—

(over)

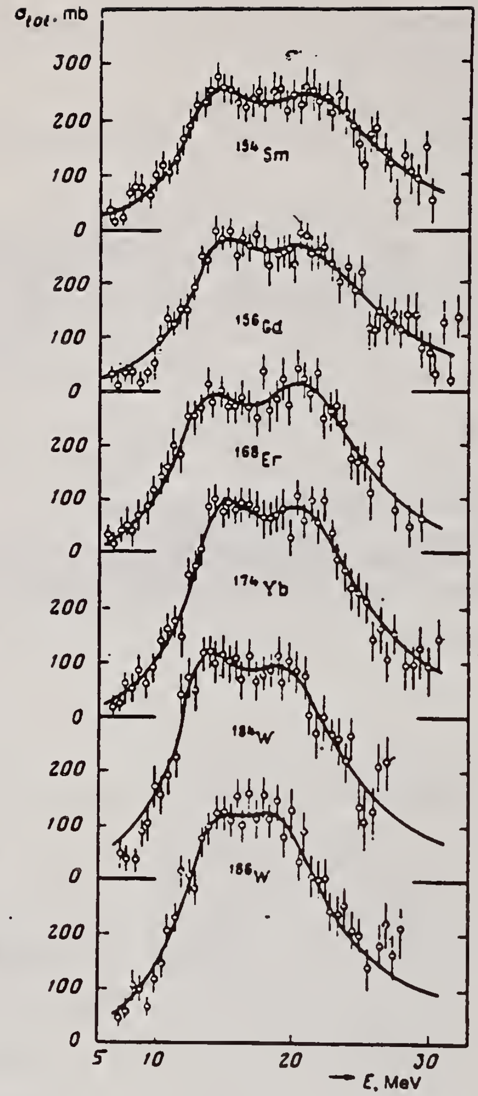

FIG. 2. Total cross sections of the photoabsorption of the nuclei ^{154}Sm, ^{156}Gd, ^{168}Er, ^{174}Yb, ^{184}W, and ^{186}W. The mean squared errors are shown.

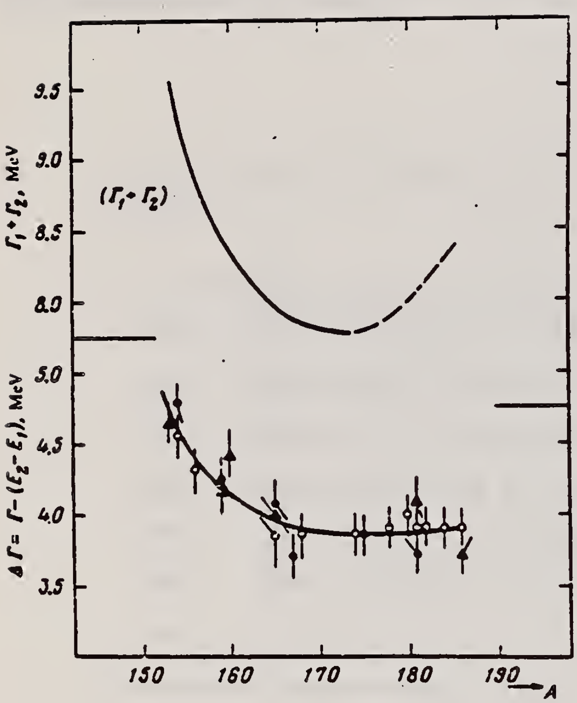

FIG. 3. Experimental values of $\Delta\Gamma = \Gamma - (E_2 - E_1)$ in the region of deformed nuclei with A = 153–186: ○—present work and[11]; ●—Saclay group; ▲—Livermore group. Owing to a small systematic deviations of the absolute values, the ordinate scales for the Saclay and Livermore data are shifted 0.15 MeV upward and downward, respectively. The $(\Gamma_1 + \Gamma_2)$ curve was obtained from the $\Delta\Gamma$ curve after introduction of corrections in the interval A = 175–186.

REF. G.M. Gurevich, L.E. Lazareva, V.M. Mazur, S.Yu. Merkulov, G.V. Solodukhov, V.A. Tyutin
Nucl. Phys. A351, 257 (1981)

ELEM. SYM.	A	Z
Er	168	68

METHOD

REF. NO.	
81 Gu. 2	hg

REACTION	RESULT	EXCITATION ENERGY	SOURCE		DETECTOR		ANGLE
			TYPE	RANGE	TYPE	RANGE	
G,MU-T	ABX	THR-20	C	27	NAI-D		4PI

Abstract: The curves of the total gamma-absorption cross sections (σ_{tot}) in the E1 giant resonance energy range for the nuclei ^{154}Sm, ^{156}Gd, ^{165}Ho, ^{168}Er, ^{174}Yb, ^{178}Hf, ^{180}Hf, ^{181}Ta, ^{182}W, ^{184}W, ^{186}W and ^{197}Au have been measured using the absorption method. Parameters of the Lorentz curves fitting the measured cross sections σ_{tot} are given. Quadrupole moments (Q_0) and nuclear deformation parameters (β) were obtained.

For deformed nuclei in the $\sim 155 < A < \sim 180$ region a violation of the correlation between giant resonance widths (Γ) and nuclear deformation parameters was found. Γ_1 and Γ_2, the widths of the resonances corresponding to vibrations of nucleons along and across the nuclear deformation axis, were observed to decrease with the increase of A which could be accounted for by the presence of an $N = 108$ subshell.

NUCLEAR REACTIONS ^{154}Sm, ^{156}Gd, ^{165}Ho, ^{168}Er, ^{174}Yb, ^{178,180}Hf, ^{181}Ta, ^{182,184,186}W, ^{197}Au (γ, X), E = 7-20 MeV; measured total $\sigma(E)$; deduced integrated σ, Lorentz line parameters. ^{154}Sm, ^{156}Gd, ^{165}Ho, ^{168}Er, ^{174}Yb, ^{178,180}Hf, ^{181}Ta, ^{182,184,186}W, ^{197}Au deduced β, Q_0, Γ, giant resonance evolution. Enriched, natural targets.

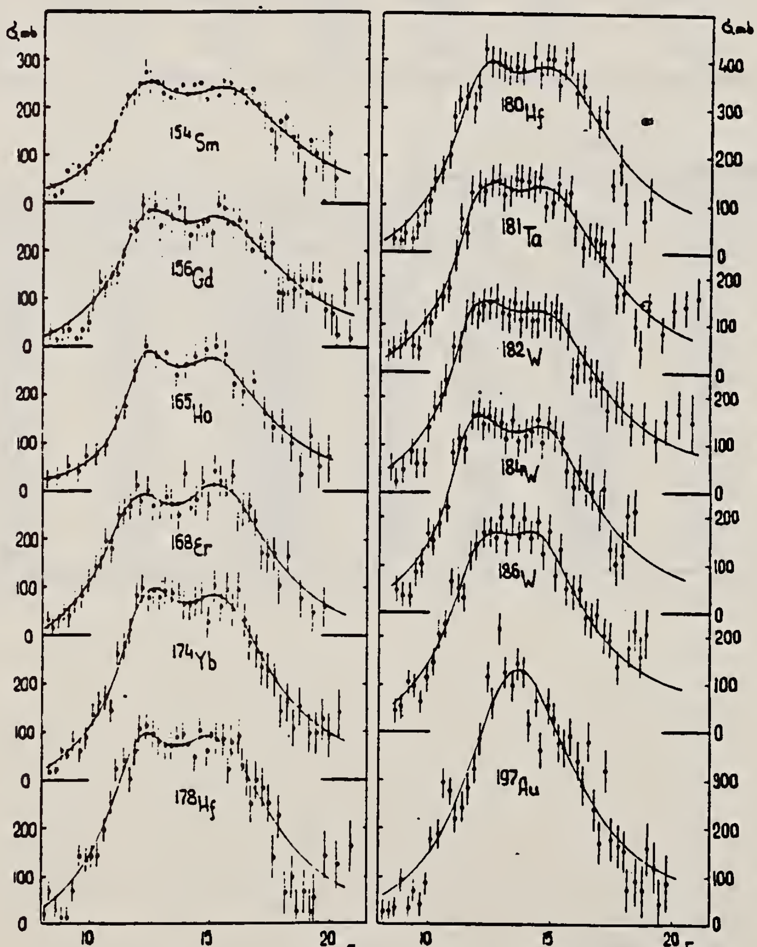

Fig. 2. Total nuclear γ-absorption cross sections (σ_{tot}) measured by the absorption method for ^{154}Sm, ^{156}Gd, ^{165}Ho, ^{168}Er, ^{174}Yb, ^{178}Hf, ^{180}Hf, ^{181}Ta, ^{182}W, ^{184}W, ^{186}W and ^{197}Au. Rms error bars are shown.

(OVER)

U.S. DEPARTMENT OF COMMERCE
NATIONAL BUREAU OF STANDARDS

TABLE 2

Parameters of Lorentz curves fitting the experimental data on σ_{tot}

Nucleus	E_1 (MeV)	σ_1 (mb)	Γ_1 (MeV)	E_2 (MeV)	σ_2 (mb)	Γ_2 (MeV)	$\frac{\sigma_2\Gamma_2}{\sigma_1\Gamma_1}$	Γ (MeV)
^{154}Sm	12.2	188	3.4	15.7	207	5.7	1.85	8.1
^{156}Gd	12.3	206	3.2	15.7	220	5.5	1.81	7.7
^{165}Ho	12.3	202	2.3	15.2	239	4.8	2.47	7.0
^{168}Er	11.9	222	3.2	15.5	275	4.5	1.73	7.4
^{174}Yb	12.3	297	2.9	15.5	320	4.9	1.80	7.1
^{178}Hf	12.2	291	3.1	15.5	334	4.9	1.80	7.2
^{180}Hf	12.2	286	3.2	15.3	324	5.1	1.81	7.1
^{181}Ta	12.1	272	3.0	15.0	316	5.1	1.97	6.8
^{182}W	11.9	267	3.2	14.8	303	5.6	2.01	6.8
^{184}W	11.9	315	2.9	14.8	321	4.7	1.65	6.8
^{186}W	12.0	246	3.3	14.5	332	5.1	2.07	6.4
^{197}Au	13.7	535	5.2					
Average error	1.4 %	11.2 %	9.3 %	1.5 %	9.7 %	4.6 %	0.22	0.2 MeV

TABLE 3

Ratios of nuclear ellipsoid axes (k), deformation parameters (β) and intrinsic quadrupole moments (Q_0), calculated from E_2/E_1

Nucleus	^{154}Sm	^{156}Gd	^{165}Ho	^{168}Er	^{174}Yb	^{178}Hf	^{180}Hf	^{181}Ta	^{182}W	^{184}W	^{186}W
k	1.320	1.302	1.259	1.327	1.289	1.296	1.281	1.263	1.271	1.268	1.229
β	0.326 ±0.017	0.309 ±0.016	0.266 ±0.036	0.334 ±0.032	0.296 ±0.024	0.303 ±0.032	0.288 ±0.036	0.270 ±0.026	0.278 ±0.030	0.274 ±0.032	0.235 ±0.033
Q_0	6.3 ±0.3	6.2 ±0.3	5.8 ±0.8	7.5 ±0.7	7.0 ±0.6	7.5 ±0.8	7.2 ±0.9	6.9 ±0.7	7.2 ±0.8	7.1 ±0.8	6.2 ±0.9

TABLE 4

Integral characteristics of E1 giant resonance

Nucleus	$\sigma_{0\,exp}$ (MeV · b)	$\frac{\sigma_{0\,exp}}{0.06NZ/A}$	σ_{0L} (MeV · b)	$\frac{\sigma_{0L}}{0.06NZ/A}$	σ_{-1} (mb)	σ_{-1L} (mb)	$\sigma_{-1L}A^{-4/3}$ (mb)	σ_{-2} (mb · MeV^{-1})	σ_{-2L} (mb · MeV^{-1})	$\sigma_{-2L}A^{-5/3}$ (μb · MeV^{-1})
^{154}Sm	1.94 ± 0.06	0.87	2.86	1.29	117 ± 3.5	156	0.189	9.1 ± 0.3	14.3	3.23
^{156}Gd	2.07 ± 0.07	0.91	2.95	1.30	143 ± 4.6	163	0.194	10.5 ± 0.4	14.9	3.30
^{165}Ho	1.86 ± 0.06	0.78	2.53	1.06	155 ± 4.4	160	0.177	10.1 ± 0.3	12.6	2.54
^{168}Er	2.24 ± 0.06	0.92	3.07	1.26	161 ± 4.3	197	0.212	12.0 ± 0.3	16.0	3.13
^{174}Yb	2.69 ± 0.05	1.07	3.82	1.52	195 ± 3.4	240	0.247	14.5 ± 0.3	19.2	3.54
^{178}Hf	2.85 ± 0.07	1.11	3.99	1.55	208 ± 4.9	247	0.247	15.3 ± 0.4	20.2	3.59
^{180}Hf	2.72 ± 0.06	1.05	4.03	1.56	200 ± 4.4	250	0.246	15.1 ± 0.3	20.7	3.61
^{181}Ta	2.84 ± 0.07	1.09	3.81	1.46	210 ± 5.3	245	0.239	16.0 ± 0.4	20.0	3.45
^{182}W	2.86 ± 0.07	1.09	4.01	1.52	211 ± 5.3	256	0.248	16.2 ± 0.4	21.6	3.70
^{184}W	2.78 ± 0.07	1.05	3.80	1.43	207 ± 5.3	251	0.240	15.9 ± 0.4	20.9	3.51
^{186}W	2.90 ± 0.07	1.08	3.95	1.48	214 ± 5.3	256	0.241	16.2 ± 0.4	21.6	3.56
^{197}Au	3.12 ± 0.06	1.10	4.37	1.54	229 ± 4.2	276	0.241	18.6 ± 0.4	23.3	3.49

Er

A=170

Er

A=170

Er

A=170

Ref. K. Miyano, T. Kuroyanagi
Nuclear Phys. 49, 315 (1963)

Elem. Sym.	A	Z
Er	170	68

Method
Linac; radioactivity

Ref. No.	
63 Mi 3	JHH

Reaction	E or ΔE	E_o	Γ	$\int \sigma dE$	Jπ	Notes
$Er^{170}(\gamma,p)$	Bremss. 21					Mostly identification of Ho^{169} and study of decay scheme No cross section data.

REF.	ELEM. SYM.	A	Z
F. R. Metzger and V. K. Rasmussen Phys. Rev. C8, 1099 (1973)	Er	170	68

METHOD	REF. NO.	
	73 Me 4	hmg

REACTION	RESULT	EXCITATION ENERGY	SOURCE TYPE	SOURCE RANGE	DETECTOR TYPE	DETECTOR RANGE	ANGLE
$ G,G	LFT	2	C	2	SCD-D		DST

1.824 MEV LEVEL

In addition to the previously known 1^- states of ^{166}Er at 1663 and 1830 keV, levels at 1812 ± 1 keV (^{166}Er), 1786 ± 1 keV (^{168}Er), and 1824 ± 1 keV (^{170}Er) have been excited using electron bremsstrahlung. Based on the observed angular distributions of the scattered photons, all three previously unknown levels were found to have spin 1. Linear polarization measurements using a two-slab Ge(Li) polarimeter led to negative parity assignments for the 1786- and 1824-keV levels but were inconclusive with respect to the less strongly excited 1812-keV level. Below 1.9 MeV, the 1663-, 1786-, and 1824-keV levels are the dominant $E1$ excitations in their respective isotopes, the partial widths of their ground-state transitions being Γ_0 = 32 ± 5, 46 ± 5, and 30 ± 3 meV. The $B(E1;1^- \to \text{g.s.})/B(E1;1^- \to 2_1^+)$ ratios of 0.52 ± 0.02, 0.51 ± 0.02, and 0.53 ± 0.02 differ considerably from the ratio 1.31 ± 0.11 for the 1812-keV level and the reported ratio 0.22 for the 1830-keV 1^- state and are very close to the Alaga value of 0.50 for $K=0^-$ levels.

TABLE III. Results of the measurements using the two-slab Ge(Li) polarimeter. $N_\parallel$ and $N_\perp$ represent the counting rates in the full energy peaks with the slabs parallel and perpendicular to the scattering plane, respectively.

Isotope	E_{level} (keV)	Transition $I_i \to I_f^\pi$	E_γ (keV)	$(N_\parallel - N_\perp)/(N_\parallel + N_\perp)$ (%)
^{166}Er	1662	$1^- \to 0^+$	1662	+7.4 ± 4.9
		$1^- \to 2^+$	1582	+3.7 ± 3.4
	1812	$1 \to 0^+$	1812	−5.6 ± 10.0
^{168}Er	1786	$1 \to 0^+$	1786	+16.7 ± 7.4
		$1 \to 2^+$	1706	−1.4 ± 4.3
^{170}Er	1824	$1 \to 0^+$	1824	+9.8 ± 4.8
		$1 \to 2^+$	1745	0.0 ± 3.1

TABLE II. Comparison of the experimental ratios of the counting rates in the 98 and 127° scattering geometries with the ratios expected for different values of the spins of the excited states.

Isotope	E_{level} (keV)	$N(127°)/N(98°)$ Experiment	Theory Spin 1	Theory Spin 2
^{166}Er	1663	1.39 ± 0.11	1.36	0.49
^{166}Er	1812	1.40 ± 0.17		
^{168}Er	1786	1.38 ± 0.07		
^{170}Er	1824	1.33 ± 0.09		

TABLE IV. Widths and branching ratios of the ^{166,168,170}Er levels. The direct results of the NRF scattering experiments are listed in column 5.

Isotope	Level (keV)	Γ_0/Γ_1	$B(E1;1^- \to \text{g.s.})/B(E1;1^- \to 2_1^+)$	Γ_0^2/Γ (meV)	Γ_0/Γ [a]	Γ_0 (meV)
^{166}Er	1663	0.60 ± 0.02 [b]	0.52 ± 0.02	12.0 ± 1.8	0.38 ± 0.01	32 ± 5
	1812	1.50 ± 0.12	1.31 ± 0.11 [c]	4.8 ± 0.8	0.60 ± 0.02	8 ± 1
	1830	≈0.33 [d]	≈0.22	···	≈0.25	2.4
^{168}Er	1786	0.59 ± 0.02	0.51 ± 0.02	17.0 ± 1.7	0.37 ± 0.01	46 ± 5
^{170}Er	1824	0.61 ± 0.02	0.53 ± 0.02	11.4 ± 1.1	0.38 ± 0.01	30 ± 3

[a] Assuming the absence of branching to levels above the 2_1^+ state.
[b] In good agreement with the value of 0.61 adopted in Ref. 18.
[c] This might be the ratio of $B(M1)$'s rather than $B(E1)$'s since the polarization experiment was not conclusive.
[d] From the decay of ^{166}Ho; see Ref. 18.

[18] Nuclear Data Sheets, 1959-1965, compiled by the Nuclear Data Group (Academic, New York, 1966).

REF.	F. R. Metzger Phys. Rev. C13, 626 (1976)	ELEM. SYM.	A	Z
		Er	170	68

METHOD	REF. NO.	
	76 Me 4	hmg

REACTION	RESULT	EXCITATION ENERGY	SOURCE TYPE	SOURCE RANGE	DETECTOR TYPE	DETECTOR RANGE	ANGLE
G,G	LFT	1- 4	C	1- 4	SCD-D		DST
		(1.824-3.406)					

10 STATES, 1.82-3.41

Some 40 states in ^{166,168,170}Er, most of them previously unknown, have been excited using bremsstrahlung with ≤4.2 MeV endpoint energy. For all but three of these levels, the angular distribution of the resonantly scattered radiation favors the assignment of spin 1. For some of the strongly excited levels, linear polarization measurements have been performed. They indicate that these levels have positive parity. The branching ratios further characterize them as $K = 1$ excitations.

TABLE IV. Properties of levels excited in ^{170}Er with photons of ≤4.2 MeV energy.

E_{level} (MeV)	I^{π}	Γ_0^2/Γ (meV)	(Γ_0/Γ) [a]	Γ_0 (meV)
1.824 [b]	1^-	11.4±1.1	0.38±0.01	30±3
2.039	$(1^+, 2^+)$ [c]	1.2±0.3 [d]	0.52 [c]	2.3±0.7 [d]
2.133	(1)	3.7±0.5	0.72±0.05	5±1
2.701	(1)	11.5±2.2	0.67±0.06	17±4
2.751	(1)	3±1	~1	3±1
2.789	1^+	24.4±2.5	0.67±0.02	37±4
2.930	(1)	3.3±1.0	0.50±0.15	7±3
2.938	(1)	5.3±1.2	0.60±0.10	9±3
3.064	(1)	14.1±3.9	0.33±0.09	43±7
3.406	$1^{(+)}$	100±12	0.69±0.02	145±18

[a] This is really $\Gamma_0/(\Gamma_0+\Gamma_1)$ since, in addition to the ground state transitions, only the cascade γ rays to the first 2^+ state at 79.3 keV could be observed.
[b] See Ref. 1.
[c] See Ref. 5.
[d] (Assuming spin 1.)

[1] F. R. Metzger et al., Phys. Rev. C8, 1099 (1973).
[5] K. Kawade et al., J. Phys. Soc. Japan 36, 1221 (1974).

# THULIUM
Z=69

Thulium is a very rare metallic element belonging to the rare earth group and was discovered in 1879 by P. T. Cleve while examining crude erbium oxide. The name comes from the Latin word *Thule* meaning the remote part of the northernmost inhabitable world. In 1911, C. James obtained a pure compound of the substance by the fractional crystallization of its impure bromate; this separation involved more than 15,000 operations.

TM
A=169

TM
A=169

B.G. Chidley, L. Katz, S. Kowalski
Can. J. Phys. 36, 407 (1958)

ELEM. SYM.	A	Z
Tm	169	69

Betatron

REF. NO.	
58 Ch 2	NVB

REACTION	RESULT	EXCITATION ENERGY	SOURCE TYPE	SOURCE RANGE	DETECTOR TYPE	DETECTOR RANGE	ANGLE
G,N	RLY	THR	C	THR	BF3-I		4PI

See 58 Kà 1 for cross sections

THRESHØLD

TABLE I

MEASURED PHOTONEUTRON THRESHOLDS

Reaction	Measured Q value, Mev.	Other Q values, Mev.	Method	Reference
$Tm^{169}(\gamma, n)Tm^{168}$	8.00±0.05			

	ELEM. SYM.	A	Z
L. Katz, G.B. Chidley Nuclear Reactions at Low and Medium Energies (Academy of Science, USSR: 1958) 371	Tm	169	69
METHOD: Betatron; neutron cross section; BF_3 counters; ion chamber monitor	REF. NO. 58 Ka 1		NVB

REACTION	RESULT	EXCITATION ENERGY	SOURCE TYPE	SOURCE RANGE	DETECTOR TYPE	DETECTOR RANGE	ANGLE
G,XN	ABX	8-22	C	8-22	BF3-I		4PI

Таблица 2

Пороги испускания фотонейтронов

Изотоп	B_n, Мэв	B_{2n}, Мэв	Изотоп	B_n, Мэв	B_{2n}, Мэв
V^{51}	11,16	20,5	L^{139}	8,81	16,1
Mn^{55}	10,14	19,2	Pr^{141}	9,46	17,6
Co^{59}	10,44	18,6	Tb^{159}	8,16	14,8
As^{75}	10,24	18,1	Ho^{165}	8,10	14,6
Y^{89}	11,82	20,7	Tm^{169}	[illegible]	14,7
Nb^{93}	8,86	17,1	Lu^{175}	[illegible]	14,2
Rh^{103}	9,46	16,8	Ta^{181}	7,66	13,8
J^{127}	9,14	16,2	Au^{197}	7,96	13,3
Cs^{133}	9,11	16,5	Bi^{209}	7,43	14,5

THRESHOLDS

не приведены, поскольку они превышают 22 *Мэв* во всех случаях, кроме золота, для которого B_{3n}=21 *Мэв*. Свойства сечений $\sigma_C(\gamma)$ сведены в табл. 3.

Таблица 1

Изотоп	$E_{макс}$, Мэв	$\sigma_n(E_\gamma)$, барн	Γ, Мэв	Σ^{30}, Мэв·барн	Y(22), 10^8 нейтрон/100 р·моль
V^{51}	18,4	0,062	5,2	0,33	1,62
Mn^{55}	20,2	0.060	7,0	0,39	2,01
Co^{59}	18,3	0,068	6,3	0,44	2,30
As^{75}	16,4	0,090	9,5	0,74	4,25
Y^{89}	17,1	0,172	5,2	0.93	5,33
Nb^{93}	18,0	0,150	7,5	1,17	6,80
Rh^{103}	17,5	0,160	9,4	1,40	8,28
J^{127}	15,2	0,273	6,8	1,76	11,9
Cs^{133}	16,5	0,238	7,7	1,59	10,7
La^{139}	15,5	0,325	3,8	1,55	11,2
Pr^{141}	15,0	0,320	4,9	1,93	13,1
Tb^{159}	15,6	0,274	9,8	2,49	18,1
Ho^{165}	13,5	0,305	8,9	2,52	18,7
Tm^{169}	16,4	0,250	8,4	1,91	14,9
Lu^{175}	16,0	0,225	8,4	1,90	23,0
Ta^{181}	14,5	0,380	8,5	3,15	22,0
Au^{197}	13,8	0,475	4,7	3,04	22,6
Bi^{209}	13,2	0,455	5,9	2,89	23,2

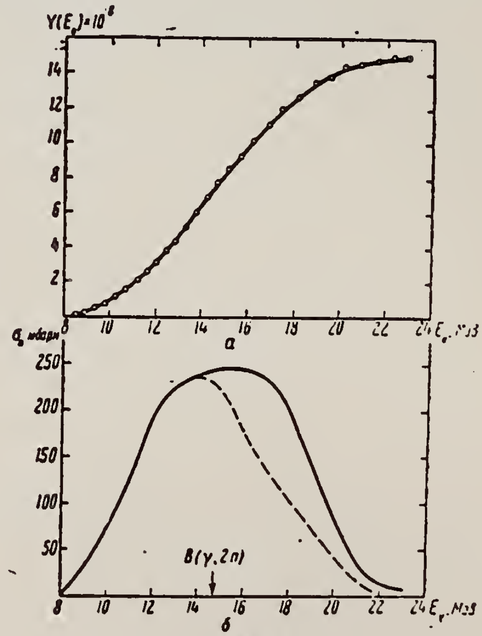

Рис. 14.

a — Выход фотонейтронов для Tm; б — $\sigma_n(E_\gamma)$ и $\sigma_C(\gamma)$ для Tm

REF. K. N. Geller, J. Halpern, and E. G. Muirhead
Phys. Rev. 118, 1302-12 (1960)

ELEM. SYM.	A	Z
Tm	169	69

METHOD

Betatron; neutron threshold; ion chamber

REF. NO.	
60 Ge 3	NVB

REACTION	RESULT	EXCITATION ENERGY	SOURCE TYPE	SOURCE RANGE	DETECTOR TYPE	DETECTOR RANGE	ANGLE
G,N	NØX	THR	C THR		BF3-I		4 PI

THRESHØLD

TABLE I. Summary and comparison of neutron separation energies inferred from present threshold measurements with values predicted from mass data and reaction energies. All energies are expressed in the center-of-mass system in Mev.

Reaction	No. runs	Present results	Other results	Method	Reference
$Tm^{169}(\gamma,n)Tm^{168}$	2	8.11 ±0.05	8.00 ±0.05	threshold	f

REF.

R.F. Barrett, J.R. Birkelund, B.J. Thomas, K.S. Lam, and H.H. Thies
Nucl. Phys. A210, 355 (1973)

ELEM. SYM.	A	Z
Tm	169	69

METHOD

REF. NO.	
73 Ba 20	egf

REACTION	RESULT	EXCITATION ENERGY	SOURCE TYPE	SOURCE RANGE	DETECTOR TYPE	DETECTOR RANGE	ANGLE
G,N	NOX	THR- 27	C	10- 27	BF3-I		4PI

MEAN NEUT ENERGY

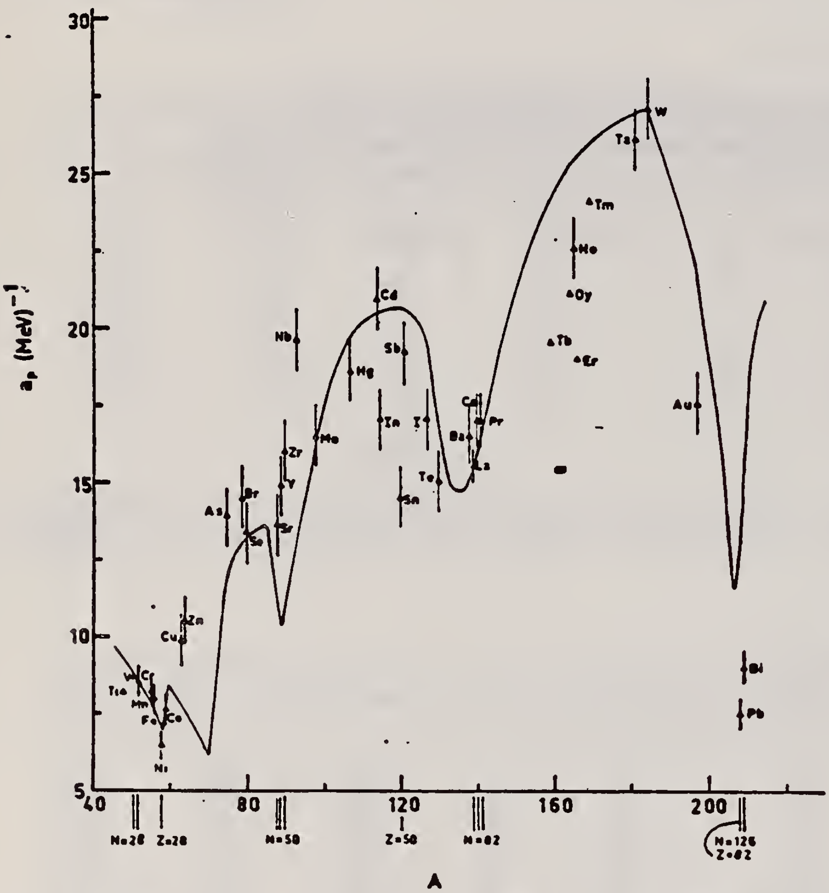

Fig. 12. Experimental values of the level density parameter a_p (Fermi gas formula plus pairing correction) versus atomic number A. The continuous curve is a least-squares fit to the data of a theoretical calculation from Newton [15]).

1
H. Baba and S. Baba, Japan Atomic Energy Research Institute report JAERI-1183 (1969).
2
H. Baba, Nucl. Phys. A159, 625 (1970).
15
T.D. Newton, Can. J. Phys. 34, 804 (1956).

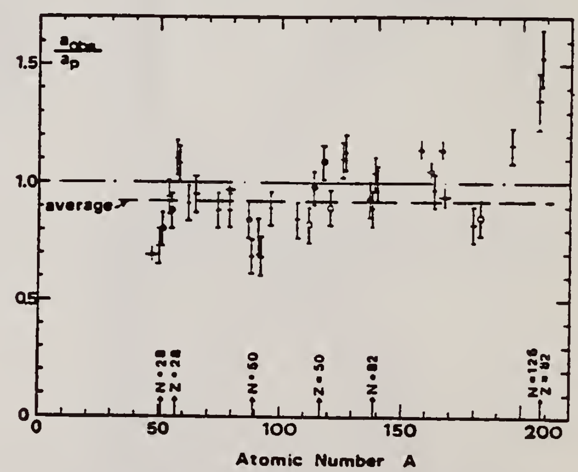

Fig. 15. Ratio a_{obs}/a_p versus atomic number A. Here a_{obs} is the level density parameter taken from the neutron resonance work of refs. [1,2]), and a_p is the level density parameter derived from the present (γ, n) work. Filled circles represent points where nuclei in the neutron resonance and in the (γ, n) experiment were the same. Open circles represent points where the respective nuclei were approximately matched. Triangles represent points which are based on measurement of neutron mean energies at two bremsstrahlung energies only.

(over)

Table 3 (continued)

Target	N (residual nucleus) [a]	Goodness of fit [b] no p.c.	Goodness of fit [b] with p.c.	$\hat{E}_n(24)$ (MeV) [c]	T (MeV) [d]	a_p (MeV^{-1}) [e]	a_{obs} (MeV^{-1}) [f]	a_{obs}/a_p
Ba	75 1%		F	1.16		16.5–^{136}Ba	15.39–^{136}Ba	0.93
	77 2%							
	78 7%							
	79 8%							
	80 11%							
	81 71%							
La	80 100%	F	F	1.25	0.72	15.5–^{138}La	13.76–^{139}La	0.89
Ce	81 89%	F	G	1.24	0.70	17.0–^{139}Ce	17.8 –^{141}Ce	1.04
	83 11%							
Pr	81 100%	G	G	1.17	0.65	17.0–^{140}Pr	17.05–^{142}Pr	1.00
Tb [g]	93 100%			1.15		19.3–^{158}Tb	21.85–^{160}Tb	1.14
Dy [g]	93 2%			1.06		20.9–$^{161.5}$Dy	21.9 –^{162}Dy	1.05
	94 19%							
	95 25%							
	96 25%							
	97 28%							
Ho	97 100%	P	G	1.06	0.56	21.4–^{164}Ho	20.66–^{166}Ho	0.97
Er [g]	95 2%			1.11		19.2–^{166}Er	21.9 –^{166}Er	1.14
	97 33%							
	98 23%							
	99 27%							
	101 15%							
Tm [g]	99 100%			1.03		24.0–^{168}Tm	22.58–^{170}Tm	0.94
Ta	107 100%		G	1.00	0.49	26.0–^{180}Ta	21.2 –^{181}Ta	0.82
W	107 26%	G	F	0.98	0.50	27.0–^{183}W	23.0 –^{183}W	0.85
	108 14%							
	109 31%							
	111 28%							
Au	117 100%		G	1.19		17.5–^{196}Au	20.24–^{198}Au	1.16
Pb ($Z = 82$)	123 24%		V.P.	1.87	1.20	7.5–^{206}Pb	10.1 –^{207}Pb	1.35
	124 23%							
	125 52%							
Bi	125 100%		F	1.65	1.03	9.0–^{208}Bi	13.8 –^{210}Bi	1.53

[a]) Neutron numbers and abundances of respective residual nuclei in (γ, n) experiments.

[b]) These give an assessment of the goodness of fit of a calculated $\hat{E}_n$ versus E_0 curve to the observed data, using the Fermi gas level density formula both without and with pairing corrections.

[c]) Bremsstrahlung photoneutron mean energies $\hat{E}_n$ for peak bremsstrahlung energy $E_0 = 24$ MeV.

[d]) Nuclear temperature from fit with constant-temperature formula.

[e]) Level density parameter a_p derived from the present (γ, n) experiment, using a Fermi gas formula plus pairing correction, and corresponding residual nucleus (the atomic weight shown is the weighted average of atomic weights of the respective isotopes present).

[f]) As column 7, but using data on n-resonance absorption from refs. [1,2]).

[g]) Measurements of $\hat{E}_n(E_0)$ for these nuclei were made only for $E_0 = 21$, 23 and 24 MeV.

REF.		ELEM. SYM.	A	Z
	A. Suzuki, K. Shoda, M. Sugawara, T. Saito, H. Miyase, S. Oikawa, and J. Uegaki PICNS-73, Vol.I, p.195 Asilomar	Tm	169	69
METHOD		REF. NO. 73 Su 10		hmg

REACTION	RESULT	EXCITATION ENERGY	SOURCE TYPE	SOURCE RANGE	DETECTOR TYPE	DETECTOR RANGE	ANGLE
E,P	RLY	5- 20	D	15- 20	MAG-D		125

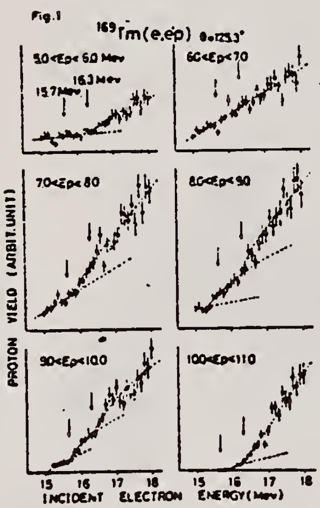

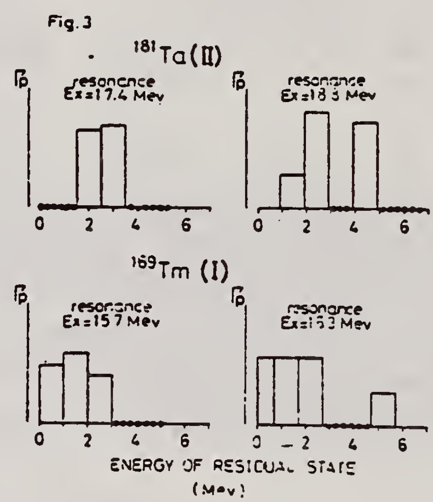

REF.	ELEM. SYM.	A	Z
V. Emma, S. Lo Nigro, C. Milone Nucl. Phys. A257, 438 (1976)	Tm	169	69

METHOD	REF. NO.	
	76 Em 2	egf

REACTION	RESULT	EXCITATION ENERGY	SOURCE TYPE	SOURCE RANGE	DETECTOR TYPE	DETECTOR RANGE	ANGLE
G,F	ABY	THR-999	C	999	TRK-I		4PI

999 = 1 GEV

TABLE I

Measured values of σ_q at $E = 1000$ MeV and deduced values of σ_k assumed constant from E_0 to 1000 MeV

Element	Z^2/A	σ_q (mb)	E_0 (MeV)	σ_k (mb)
Bi	32.96	12.3 ± 0.6	200	7.6 ± 0.6
Pb	32.45	5.4 ± 0.4	220	3.6 ± 0.3
Tl	32.10	4.1 ± 0.3	230	2.8 ± 0.3
Au	31.68	2.0 ± 0.15	240	1.4 ± 0.2
Pt	31.18	1.1 ± 0.08	255	$(8 \pm 0.7) \times 10^{-1}$
Re	30.21	$(3.7 \pm 0.3) \times 10^{-1}$	280	$(2.9 \pm 0.3) \times 10^{-1}$
W	29.78	$(3.5 \pm 0.3) \times 10^{-1}$	290	$(2.8 \pm 0.3) \times 10^{-1}$
Ta	29.45	$(3.3 \pm 0.3) \times 10^{-1}$	300	$(2.7 \pm 0.3) \times 10^{-1}$
Hf	29.04	$(1.7 \pm 0.2) \times 10^{-1}$	310	$(1.4 \pm 0.2) \times 10^{-1}$
Yb	28.31	$(1.3 \pm 0.1) \times 10^{-1}$	330	$(1.2 \pm 0.1) \times 10^{-1}$
Tm	28.18	$(7.5 \pm 0.8) \times 10^{-2}$	335	$(6.8 \pm 0.8) \times 10^{-2}$
Ho	27.21	$(3.6 \pm 0.4) \times 10^{-2}$	355	$(3.5 \pm 0.4) \times 10^{-2}$
Dy	26.80	$(2.6 \pm 0.3) \times 10^{-2}$	360	$(2.5 \pm 0.3) \times 10^{-2}$
Tb	26.58	$(2.5 \pm 0.3) \times 10^{-2}$	370	$(2.5 \pm 0.3) \times 10^{-2}$
Gd	26.04	$(1.6 \pm 0.2) \times 10^{-2}$	380	$(1.7 \pm 0.2) \times 10^{-2}$
Sm	25.56	$(1.3 \pm 0.2) \times 10^{-2}$	390	$(1.4 \pm 0.2) \times 10^{-2}$
Nd	24.96	$(9.2 \pm 0.9) \times 10^{-3}$	405	$(1 \pm 0.1) \times 10^{-2}$
Ce	24.00	$(8 \pm 0.9) \times 10^{-3}$	420	$(9 \pm 1) \times 10^{-3}$
La	23.39	$(8.4 \pm 0.9) \times 10^{-3}$	430	$(1 \pm 0.1) \times 10^{-3}$
Sb	21.36	$(1.2 \pm 0.2) \times 10^{-2}$	460	$(1.5 \pm 0.3) \times 10^{-2}$
Te	21.19	$(8.8 \pm 1) \times 10^{-3}$	465	$(1.2 \pm 0.2) \times 10^{-2}$
Sn	21.06	$(1.3 \pm 0.2) \times 10^{-2}$	465	$(1.7 \pm 0.3) \times 10^{-2}$
Cd	20.49	$(1.7 \pm 0.3) \times 10^{-2}$	470	$(2.2 \pm 0.4) \times 10^{-2}$
Ag	20.47	$(2 \pm 0.3) \times 10^{-2}$	470	$(2.6 \pm 0.4) \times 10^{-2}$
Zn	13.76	$(2 \pm 0.4) \times 10^{-1}$	515	$(3 \pm 0.6) \times 10^{-1}$
Cu	13.44	$(2.4 \pm 0.5) \times 10^{-1}$	515	$(3.6 \pm 0.8) \times 10^{-1}$
Ni	13.35	$(2.4 \pm 0.5) \times 10^{-1}$	510	$(3.6 \pm 0.8) \times 10^{-1}$
Fe	12.10	$(3 \pm 0.6) \times 10^{-1}$	510	$(4.4 \pm 0.9) \times 10^{-1}$

[4] A.V. Mitrofanova et al. Sov. J. Nucl. Phys. 6, 512 (1968).

[7] T. Methasiri et al., Nucl. Phys. A167, 97 (1971).

[12] J.R. Nix et al., Nucl. Phys. 81, 61 (1966).

[20] N.A. Perifilov et al., JETP (Sov. Phys.) 14, 623 (1962); Proc. Symp. on the physics & chemistry of fission, Salzburg 1965, vol. 2 (IAEA) Vienna, 1965, p.283.

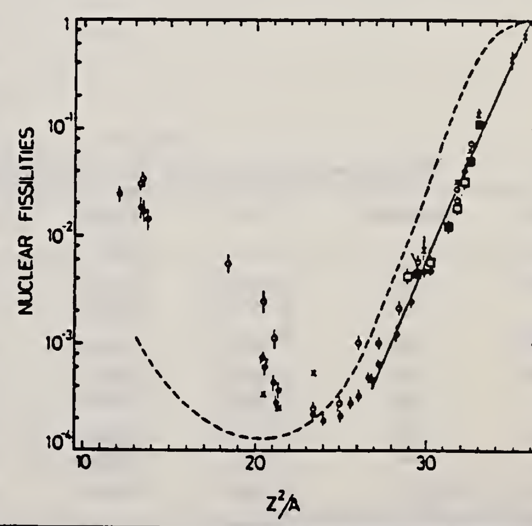

Fig. 2. Nuclear fissilities as a function of Z^2/A. Experimental points: solid circles represent our data; squares, the data from ref. [4]; open circles, the data from ref. [7]; and crosses, the data from (p,f) experiments[20]. The straight line is the best fit calculated from our data for $Z^2/A > 26$. The dashed curve is the curve VI calculated by Nix and Sassi[12].

REF.	A. Suzuki and K. Shoda Nucl. Phys. A260, 172 (1976)	ELEM. SYM.	A	Z
		Tm	169	69
METHOD		REF. NO.		
		76 Su 2		egf

REACTION	RESULT	EXCITATION ENERGY	SOURCE		DETECTOR		ANGLE
			TYPE	RANGE	TYPE	RANGE	
E,P	ABX	10- 18	D	15- 18	MAG-D		125

Proton yields obtained by summing protons with energies above levels given in tables.

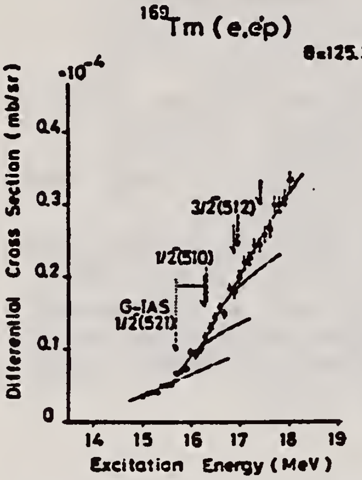

Fig. 4. Cross section of the ^{169}Tm(e, e'p) reaction. See also the caption to fig. 2.

TABLE 1

Parameters of the present experiment

Target	Atomic number	Purity (%)	Thickness (mg/cm²)	Lowest proton energy (MeV)	Bin size (keV)	Range of measurement (MeV)
^{159}Tb	65	99.9 (natural)	14.87	4.70	100	15.0 -17.5
^{165}Ho	67	99.9 (natural)	11.64	4.70	100	15.5 -17.5
^{169}Tm	69	99 (natural)	13.40	4.70	100	15.0 -18.0
^{175}Lu	71	99.87 (enriched)	5.24	5.34	150	15.05-20.0
^{181}Ta	73	99.9 (natural)	6.73	6.16	200	16.0 -23.0

TABLE 3

Displacement energies obtained from the present data and the estimates with eqs. (20) and (21)

Target	Resonance	E^* (MeV)	E_c (exp) (MeV)	E_c[a]) (MeV)	$E_c(\delta = 0.3)$[b]) (MeV)
^{159}Tb	1st 2nd	15.75±0.15 16.50±0.15	15.58 15.46	16.06	15.93
^{165}Ho	1st	16.15±0.14	15.64	16.38	16.25
^{169}Tm	1st 2nd	15.76±0.13 16.34±0.14	16.20 16.22	16.76	16.63
^{175}Lu	1st 2nd	16.44±0.13 17.45±0.15	16.75 16.35	17.07	16.93
^{181}Ta	1st	17.31±0.15	16.40	17.38	17.24

[a]) Estimated with eq. (20).
[b]) Estimated with eq. (21).

TABLE 4

Deformation parameters of IAS δ_{IAR} derived from the (e, e'p) result

Target	Resonance	IAS	Parent state	$\delta_{IAR}-\delta_p$[a])	δ_p (assumed)	δ_{IAR}[a])
^{159}Tb	1st	$\frac{3}{2}^-$[521]	ground	−0.008	0.31	0.30
	2nd	$\frac{5}{2}^-$[512]	875 keV	−0.016		0.29
^{165}Ho	1st	$\frac{7}{2}^+$[633]	ground	−0.023	0.30	0.28
^{169}Tm	1st	$\frac{1}{2}^-$[521]	ground	−0.018	0.29	0.27
	2nd	$\frac{1}{2}^-$[510]	565 keV	−0.019		0.27
^{175}Lu	1st	$\frac{7}{2}^-$[514]	ground	−0.010	0.28	0.27
	2nd	$\frac{7}{2}^-$[503]	1420 keV	−0.029		0.25
^{181}Ta	1st	$\frac{7}{2}^-$[503]	670 keV	−0.046	0.26	0.21

The assumed deformation parameters for the parent states δ_p are also shown.
[a]) The errors are about ±0.01.

REF.	J.J. Murphy II, H.J. Gehrhardt and D.M. Skopik Nucl. Phys. A277, 69 (1977)	ELEM. SYM.	A	Z
		Tm	169	69
METHOD		REF. NO.		
		77 Mu 3		egf

REACTION	RESULT	EXCITATION ENERGY	SOURCE TYPE	SOURCE RANGE	DETECTOR TYPE	DETECTOR RANGE	ANGLE
E,A	ABX	13-100	D	100	MAG-D		DST

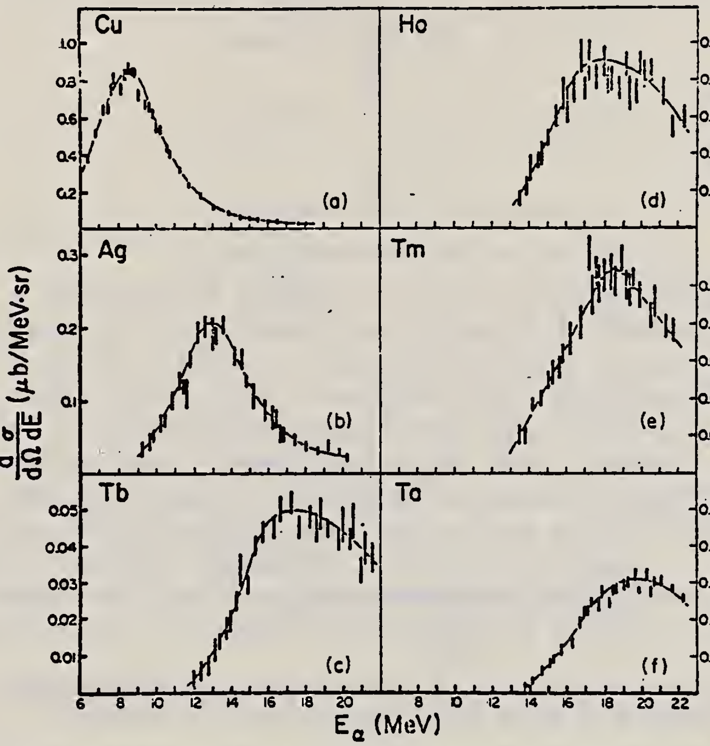

Fig. 1. The α-particle energy spectra at 50° in the lab for the six nuclei studied. Note that as Z increases, the cross section decreases and the energy of the peak increases. Errors are statistical. Curves are to guide the eye.

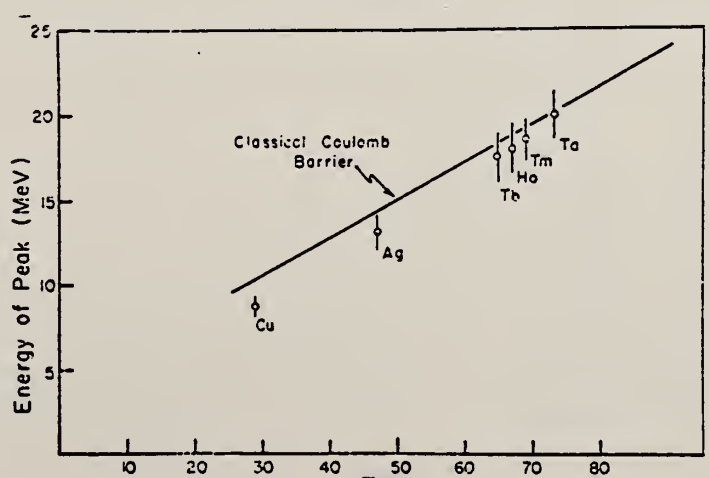

(over)

Fig. 2. Energy of the cross section peak as a function of Z. The solid line is the energy of the classical Coulomb barrier.

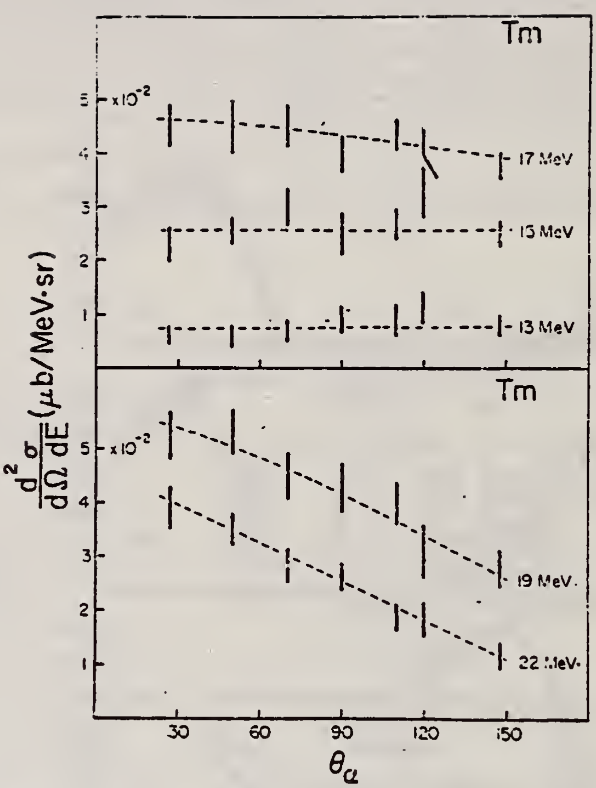

Fig. 5. Angular distributions for thulium ($Z = 69$). The forward peaking at high energies is taken as evidence of α-clusters in this nucleus. Errors are statistical. Curves are to guide the eye.

YTTERBIUM
Z=70

Ytterbium is a fascinating element of the Periodic Table primarily because of its valence variation in different environments. In the divalent state the element has a completed 4f level but in the trivalent state this level is incomplete with thirteen electrons. This dual valence gives rise to interesting and variable chemical and alloying properties. The application of modest pressure (16,0000 atm) changes the electrical conductivity from metallic to semiconducting. Higher pressures increase the semiconducting properties until at a pressure of 40,000 atm, ytterbium reverses to its metallic conducting state.

YB

:.G. Fuller, B. Petree, M.S. Weiss
?hys. Rev. 112, 554 (1958)

ELEM. SYM.	A	Z
Yb		70

Betatron; ion chamber

REF. NO.	
58 Fu 1	NVB

REACTION	RESULT	EXCITATION ENERGY	SOURCE TYPE	SOURCE RANGE	DETECTOR TYPE	DETECTOR RANGE	ANGLE
G,XN	ABY	7-40	C	7-40	BF3-I		4PI

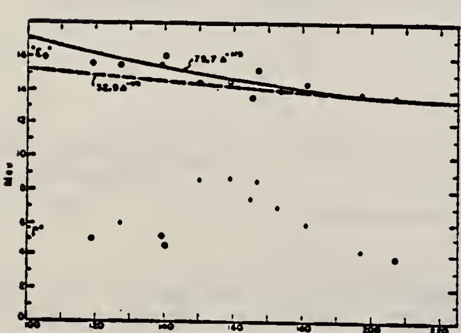

FIG. 6. Mean energy and width of giant resonances. "E_0" and "Γ" are the mean energy for photon absorption and the full width at half maximum of the giant resonance obtained from dashed histograms as in Fig. 5. No attempt was made to fit data with resonance curves to obtain these parameters.

TABLE I. Target properties and results.

Element	Form used	Weight grams	$\sigma^0(\gamma,n)$[a] barns	$\frac{\int\sigma dE}{NZ/A}$[b] Mev-b	"Γ"[a] Mev
Sn	Sn	4.81	0.30	0.064	5.0
I	I	8.55	0.36	0.085	6.0
La	La	10.43	0.34	0.063	5.2
Ce	Ce	4.99	0.45	0.080	4.5
Sm	Sm_2O_3	2.90	0.26	0.073	8.6
Tb	Tb_4O_7	3.04	0.39	0.087	8.7
Ho	Ho_2O_3	1.87	0.41	0.079	7.5
Er	Er_2O_3	5.41	0.50	0.100	8.5
Yb	Yb_2O_3	5.57	0.50	0.090	7.0
Ta	Ta	8.41	0.49	0.077	6.0
Au	Au	3.16	0.68	0.085	4.2
Pb	Pb	8.05	0.75	0.081	3.8

[a] $\sigma^0(\gamma,n)$ is the maximum value and "Γ" the full width at $\sigma^0(\gamma,n)/2$ of the neutron production cross section corrected for multiple neutron emission. Data were not fitted with resonance lines to determine these values.
[b] Integrated neutron production cross sections corrected for multiple neutrons above $(\gamma,2n)$ threshold.

REF. T. Methasiri and S. A. E. Johansson
Nucl. Phys. A167, 97 (1971)

ELEM. SYM.	A	Z
Yb		70

METHOD

REF. NO.	
71 Me 1	egf

REACTION	RESULT	EXCITATION ENERGY	SOURCE		DETECTOR		ANGLE
			TYPE	RANGE	TYPE	RANGE	
G,F	ABY	THR-900	C	300-900	FRG-I		4PI

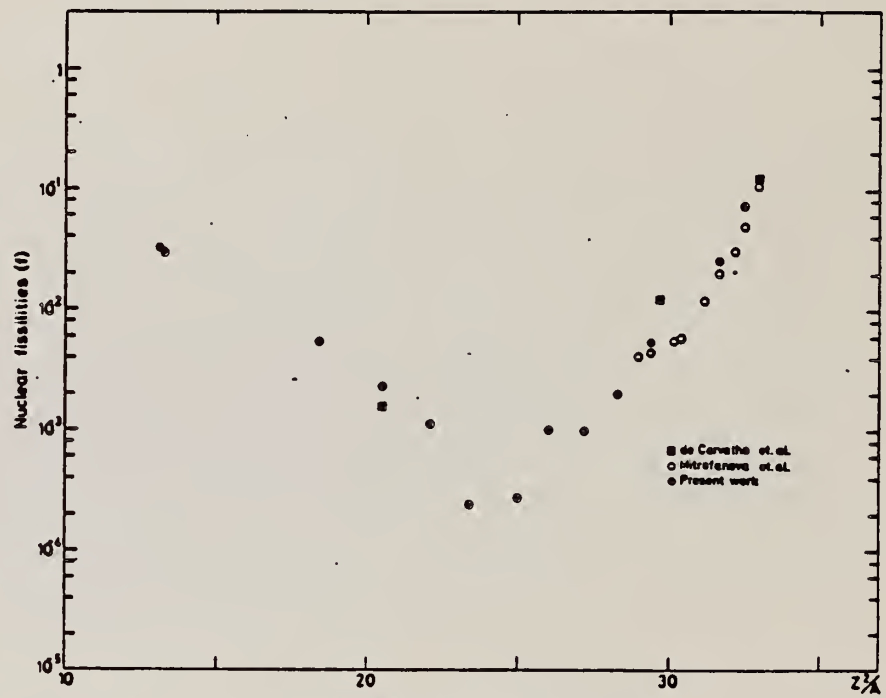

Fig. 2. Nuclear fissilities as a function of Z^2/A.

TABLE 1

The constant fission cross sections above the threshold

Element	σ_f (cm²)	Element	σ_f (cm²)
Pb	$(5.0\pm0.2)\times10^{-27}$	La	$(1.1\pm0.1)\times10^{-29}$
Au	$(1.7\pm0.1)\times10^{-27}$	Sn	$(4.3\pm1.1)\times10^{-29}$
Ta	$(3.3\pm0.2)\times10^{-28}$	Ag	$(8.4\pm2.0)\times10^{-29}$
Yb	$(1.2\pm0.2)\times10^{-28}$	Mo	$(1.7\pm0.4)\times10^{-28}$
Ho	$(5.5\pm0.3)\times10^{-29}$	Cu	$(6.6\pm1.2)\times10^{-28}$
Gd	$(5.3\pm0.8)\times10^{-29}$	Ni	$(5.8\pm0.1)\times10^{-28}$
Nd	$(1.3\pm0.2)\times10^{-29}$		

[over]

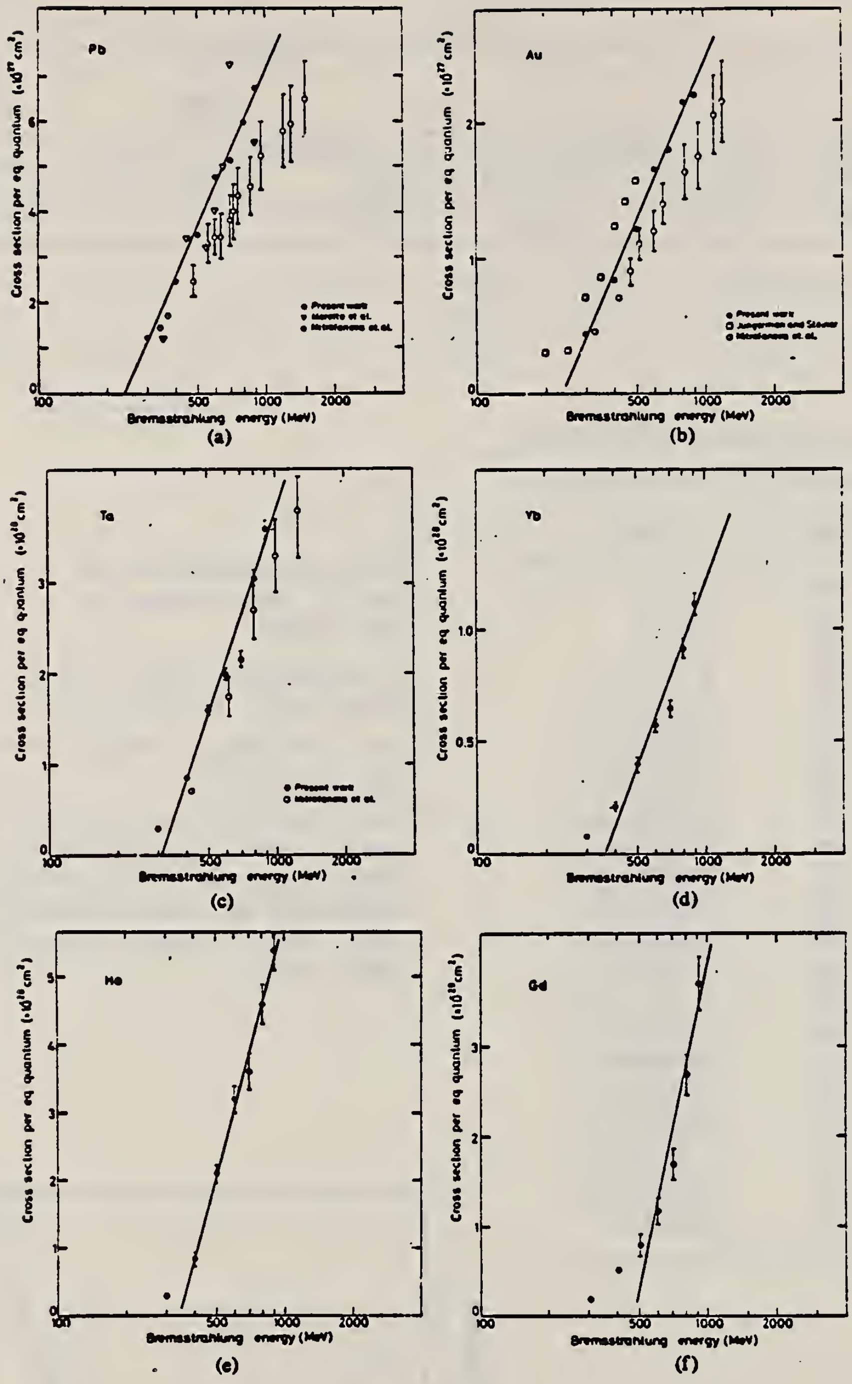

Fig. 1. Cross sections per equivalent quantum $\sigma_q(E)$ as a function of log E.

REF.	ELEM. SYM.	A	Z
V. Emma, S. Lo Nigro, C. Milone Nucl. Phys. A257, 438 (1976)	Yb		70
METHOD	REF. NO. 76 Em 2		egf

REACTION	RESULT	EXCITATION ENERGY	SOURCE TYPE	SOURCE RANGE	DETECTOR TYPE	DETECTOR RANGE	ANGLE
G,F	ABY	THR-999	C	999	TRK-I		4PI

999 = 1 GEV

TABLE I

Measured values of σ_q at $E = 1000$ MeV and deduced values of σ_k assumed constant from E_0 to 1000 MeV

Element	Z^2/A	σ_q (mb)	E_0 (MeV)	σ_k (mb)
Bi	32.96	12.3 ± 0.6	200	7.6 ± 0.6
Pb	32.45	5.4 ± 0.4	220	3.6 ± 0.3
Tl	32.10	4.1 ± 0.3	230	2.8 ± 0.3
Au	31.68	2.0 ± 0.15	240	1.4 ± 0.2
Pt	31.18	1.1 ± 0.08	255	$(8\ \ \pm0.7)\times10^{-1}$
Re	30.21	$(3.7\pm0.3)\times10^{-1}$	280	$(2.9\pm0.3)\times10^{-1}$
W	29.78	$(3.5\pm0.3)\times10^{-1}$	290	$(2.8\pm0.3)\times10^{-1}$
Ta	29.45	$(3.3\pm0.3)\times10^{-1}$	300	$(2.7\pm0.3)\times10^{-1}$
Hf	29.04	$(1.7\pm0.2)\times10^{-1}$	310	$(1.4\pm0.2)\times10^{-1}$
Yb	28.31	$(1.3\pm0.1)\times10^{-1}$	330	$(1.2\pm0.1)\times10^{-1}$
Tm	28.18	$(7.5\pm0.8)\times10^{-2}$	335	$(6.8\pm0.8)\times10^{-2}$
Ho	27.21	$(3.6\pm0.4)\times10^{-2}$	355	$(3.5\pm0.4)\times10^{-2}$
Dy	26.80	$(2.6\pm0.3)\times10^{-2}$	360	$(2.5\pm0.3)\times10^{-2}$
Tb	26.58	$(2.5\pm0.3)\times10^{-2}$	370	$(2.5\pm0.3)\times10^{-2}$
Gd	26.04	$(1.6\pm0.2)\times10^{-2}$	380	$(1.7\pm0.2)\times10^{-2}$
Sm	25.56	$(1.3\pm0.2)\times10^{-2}$	390	$(1.4\pm0.2)\times10^{-2}$
Nd	24.96	$(9.2\pm0.9)\times10^{-3}$	405	$(1\ \ \pm0.1)\times10^{-2}$
Ce	24.00	$(8\ \ \pm0.9)\times10^{-3}$	420	$(9\ \ \pm1\ \ )\times10^{-3}$
La	23.39	$(8.4\pm0.9)\times10^{-3}$	430	$(1\ \ \pm0.1)\times10^{-3}$
Sb	21.36	$(1.2\pm0.2)\times10^{-2}$	460	$(1.5\pm0.3)\times10^{-2}$
Te	21.19	$(8.8\pm1\ \ )\times10^{-3}$	465	$(1.2\pm0.2)\times10^{-2}$
Sn	21.06	$(1.3\pm0.2)\times10^{-2}$	465	$(1.7\pm0.3)\times10^{-2}$
Cd	20.49	$(1.7\pm0.3)\times10^{-2}$	470	$(2.2\pm0.4)\times10^{-2}$
Ag	20.47	$(2\ \ \pm0.3)\times10^{-2}$	470	$(2.6\pm0.4)\times10^{-2}$
Zn	13.76	$(2\ \ \pm0.4)\times10^{-1}$	515	$(3\ \ \pm0.6)\times10^{-1}$
Cu	13.44	$(2.4\pm0.5)\times10^{-1}$	515	$(3.6\pm0.8)\times10^{-1}$
Ni	13.35	$(2.4\pm0.5)\times10^{-1}$	510	$(3.6\pm0.8)\times10^{-1}$
Fe	12.10	$(3\ \ \pm0.6)\times10^{-1}$	510	$(4.4\pm0.9)\times10^{-1}$

[4] A.V. Mitrofanova et al. Sov. J. Nucl. Phys. 6, 512 (1968).

[7] T. Methasiri et al., Nucl. Phys. A167, 97 (1971).

[12] J.R. Nix et al., Nucl. Phys. 81, 61 (1966).

[20] N.A. Perifilov et al., JETP (Sov. Phys.) 14, 623 (1962); Proc. Symp. on the physics & chemistry of fission, Salzburg 1965, vol. 2 (IAEA) Vienna, 1965, p.283.

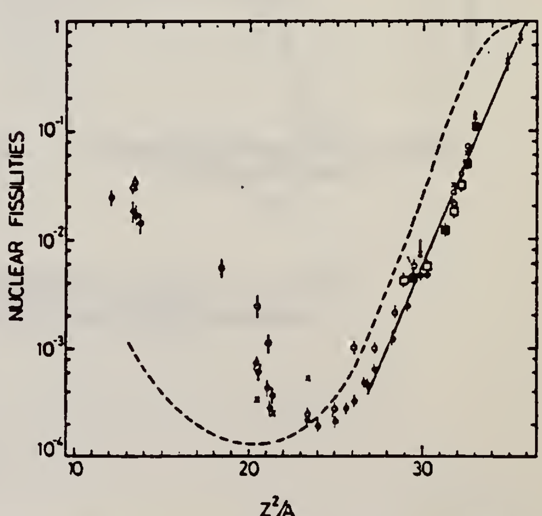

Fig. 2. Nuclear fissilities as a function of Z^2/A. Experimental points: solid circles represent our data; squares, the data from ref. [4]); open circles, the data from ref. [7]); and crosses, the data from (p,f) experiments[20]). The straight line is the best fit calculated from our data for $Z^2/A > 26$. The dashed curve is the curve VI calculated by Nix and Sassi[12]).

Y_B
A=173

Y_B
A=173

Y_B
A=173

REF.

K. N. Geller, J. Halpern, and E. G. Muirhead
Phys. Rev. 118, 1302-12 (1960)

Yb	173	70

METHOD

Betatron; neutron threshold; ion chamber

REF. NO.	
60 Ge 3	NVB

REACTION	RESULT	EXCITATION ENERGY	SOURCE TYPE	SOURCE RANGE	DETECTOR TYPE	DETECTOR RANGE	ANGLE
G,N	NØX	THR	C THR		BF3-I		4 PI

THRESHØLD

TABLE I. Summary and comparison of neutron separation energies inferred from present threshold measurements with values predicted from mass data and reaction energies. All energies are expressed in the center-of-mass system in Mev.

Reaction	No. runs	Present results	Other results	Method	Reference
$Yb^{173}(\gamma,n)Yb^{172}$	1	6.50 ±0.08	6.35 ±0.06	mass data	q

q W. H. Johnson, Jr., and A. O. Nier, Phys. Rev. 105, 1014 (1957).

YB
A=174

YB
A=174

YB
A=174

REF.	ELEM. SYM.	A	Z
L. G. Moretto, R. C. Gatti, S. G. Thompson, J. T. Routti, J. H. Heisenberg, L. M. Middleman, M. R. Yearian, R. Hofstadter Phys. Rev. 179, 1176 (1969)	Yb	174	70
METHOD	REF. NO. 69 Mo 1		hmg

REACTION	RESULT	EXCITATION ENERGY	SOURCE TYPE	SOURCE RANGE	DETECTOR TYPE	DETECTOR RANGE	ANGLE
E,F	ABX	THR-999	D	60-999	TRK-I		DST
G,F	ABX	THR-999	C	60-999	TRK-I		DST

Tabular data given; angular distribution isotopes

999= 1 GEV

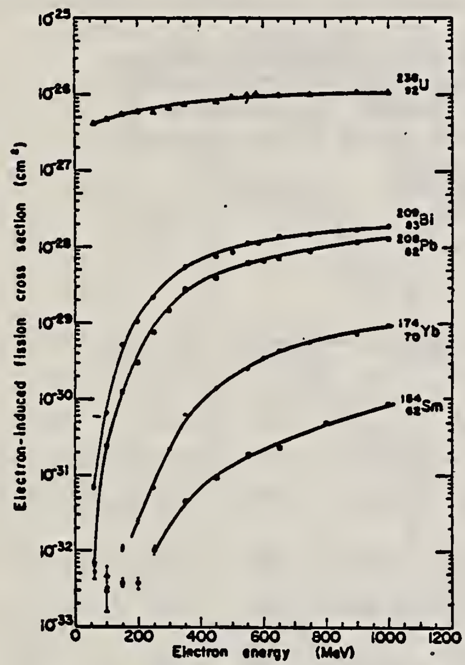

FIG. 2. Electron-induced fission cross-section data. Different symbols for the same isotope refer to different targets.

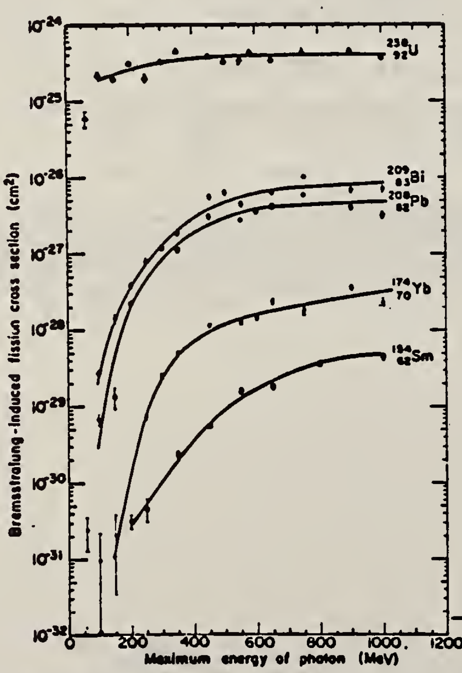

FIG. 4. Bremsstrahlung-induced fission cross section per equivalent quantum.

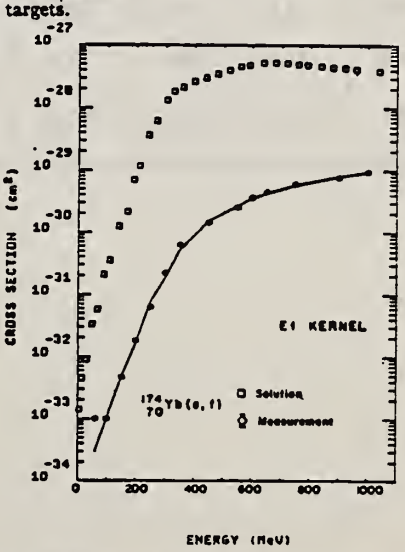

FIG. 9. Photofission cross section as a function of energy for $_{70}^{174}$Yb (open squares) as obtained by unfolding the electron-induced fission cross-section data (diamonds) with the $E1$ kernel. The solid line is the fit to the electron-induced fission cross sections which is obtained by folding back the photofission cross section into the $E1$ kernel.

REF.	ELEM. SYM.	A	Z
G.M. Gurevich, L.E. Lazareva, V.M. Mazur, S.Yu. Merkulov, G.V. Solodukhov, V.A. Tyutin JETP Lett. 28, 157 (1978) Pis'ma Zh. Eksp. Teor. Fiz. 28, 168 (1978)	Yb	174	70

METHOD	REF. NO.	
	78 Gu 7	hg

REACTION	RESULT	EXCITATION ENERGY	SOURCE TYPE	SOURCE RANGE	DETECTOR TYPE	DETECTOR RANGE	ANGLE
G,MU-T	ABX	THR-31	C	UKN	NAI-D		4PI

The absorption method is used to measure the total photoabsorption cross section curves for deformed ^{154}Sm, ^{156}Gd, ^{168}Er, ^{174}Yb, ^{184}W, and ^{186}W nuclei in the region of the $E1$ giant resonance. The behavior of the resonance widths for nuclei in the interval $A = 153$ to 186 is discussed.

PACS numbers: 24.30.Cz, 25.20.+y, 27.70.+q

TABLE I.

Nucleus	E_1 MeV	σ_1 mb	Γ_1 MeV	E_2 MeV	σ_2 mb	Γ_2 MeV	Γ MeV	Q_0 b	β	$\sigma_0 L/0.06\frac{ZN}{A}$
^{154}Sm	12.2	188	3.4	15.7	207	5.7	8.1 ± 0.2	6.3 ± 0.3	0.32 ± 0.02	1.28
^{156}Gd	12.3	206	3.2	15.7	220	5.5	7.7 ± 0.2	6.2 ± 0.3	0.31 ± 0.02	1.30
^{168}Er	11.9	222	3.2	15.5	275	4.5	7.4 ± 0.2	7.5 ± 0.7	0.32 ± 0.03	1.26
^{174}Yb	12.3	297	2.9	15.5	320	4.9	7.1 ± 0.2	7.0 ± 0.6	0.30 ± 0.02	1.52
^{184}W	11.9	315	2.9	14.8	321	4.7	6.8 ± 0.2	7.2 ± 0.8	0.27 ± 0.03	1.50
^{186}W	12.0	246	3.3	14.5	332	5.1	6.4 ± 0.2	6.2 ± 0.8	0.23 ± 0.03	1.48
Average error	±1.3%	±10.5%	±7.5%	±1.3%	±9.4%	±3.8%	—	—	—	—

(over)

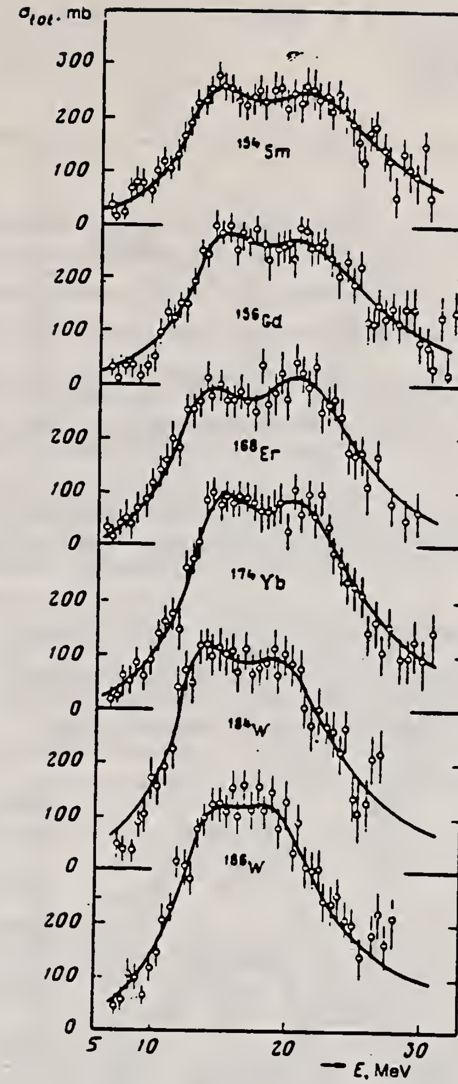

FIG. 2. Total cross sections of the photoabsorption of the nuclei ^{154}Sm, ^{156}Gd, ^{168}Er, ^{174}Yb, ^{184}W, and ^{186}W. The mean squared errors are shown.

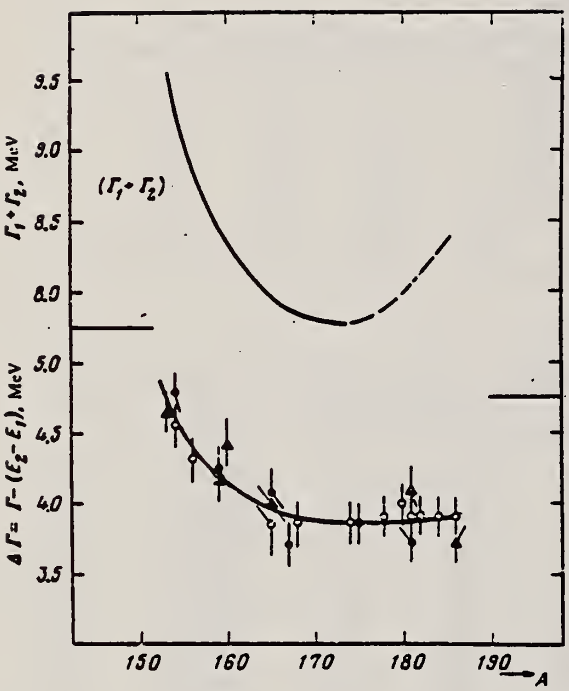

FIG. 3. Experimental values of $\Delta\Gamma = \Gamma - (E_2 - E_1)$ in the region of deformed nuclei with A = 153–186: ○—present work and[11]; ●—Saclay group; ▲—Livermore group. Owing to a small systematic deviations of the absolute values, the ordinate scales for the Saclay and Livermore data are shifted 0.15 MeV upward and downward, respectively. The $(\Gamma_1 + \Gamma_2)$ curve was obtained from the $\Delta\Gamma$ curve after introduction of corrections in the interval A = 175–186.

REF.	ELEM. SYM.	A	Z
G.M. Gurevich, L.E. Lazareva, V.M. Mazur, S.Yu. Merkulov, G.V. Solodukhov, V.A. Tyutin Nucl. Phys. A351, 257 (1981)	Yb	174	70

METHOD	REF. NO.	
	81 Gu 2	hg

REACTION	RESULT	EXCITATION ENERGY	SOURCE TYPE	SOURCE RANGE	DETECTOR TYPE	DETECTOR RANGE	ANGLE
G,MU-T	ABX	THR-20	C	27	NAI-D		4PI

Abstract: The curves of the total gamma-absorption cross sections (σ_{tot}) in the E1 giant resonance energy range for the nuclei ^{154}Sm, ^{156}Gd, ^{165}Ho, ^{168}Er, ^{174}Yb, ^{178}Hf, ^{180}Hf, ^{181}Ta, ^{182}W, ^{184}W, ^{186}W and ^{197}Au have been measured using the absorption method. Parameters of the Lorentz curves fitting the measured cross sections σ_{tot} are given. Quadrupole moments (Q_0) and nuclear deformation parameters (β) were obtained.

For deformed nuclei in the $\sim 155 < A < \sim 180$ region a violation of the correlation between giant resonance widths (Γ) and nuclear deformation parameters was found. Γ_1 and Γ_2, the widths of the resonances corresponding to vibrations of nucleons along and across the nuclear deformation axis, were observed to decrease with the increase of A which could be accounted for by the presence of an $N = 108$ subshell.

E

NUCLEAR REACTIONS ^{154}Sm, ^{156}Gd, ^{165}Ho, ^{168}Er, ^{174}Yb, ^{178,180}Hf, ^{181}Ta, ^{182,184,186}W, ^{197}Au (γ, X), E = 7–20 MeV; measured total $\sigma(E)$; deduced integrated σ, Lorentz line parameters. ^{154}Sm, ^{156}Gd, ^{165}Ho, ^{168}Er, ^{174}Yb, ^{178,180}Hf, ^{181}Ta, ^{182,184,186}W, ^{197}Au deduced β, Q_0, Γ, giant resonance evolution. Enriched, natural targets.

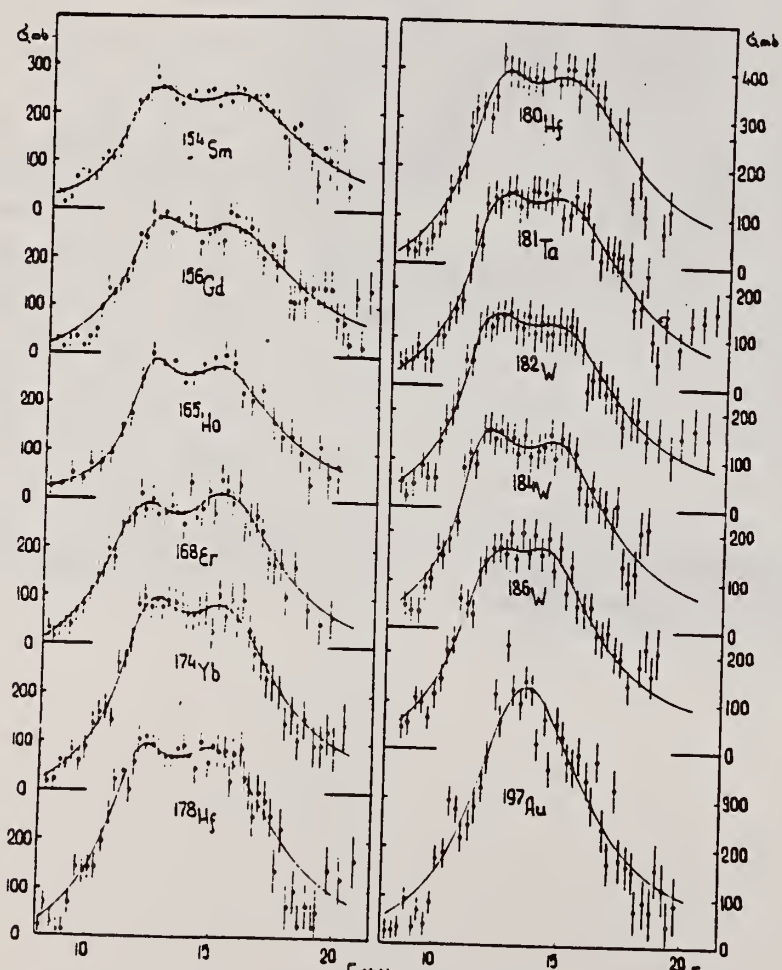

Fig. 2. Total nuclear γ-absorption cross sections (σ_{tot}) measured by the absorption method for ^{154}Sm, ^{156}Gd, ^{165}Ho, ^{168}Er, ^{174}Yb, ^{178}Hf, ^{180}Hf, ^{181}Ta, ^{182}W, ^{184}W, ^{186}W and ^{197}Au. Rms error bars are shown.

(OVER)

U.S. DEPARTMENT OF COMMERCE
NATIONAL BUREAU OF STANDARDS

TABLE 2

Parameters of Lorentz curves fitting the experimental data on σ_{tot}

Nucleus	E_1 (MeV)	σ_1 (mb)	Γ_1 (MeV)	E_2 (MeV)	σ_2 (mb)	Γ_2 (MeV)	$\frac{\sigma_2\Gamma_2}{\sigma_1\Gamma_1}$	Γ (MeV)
^{154}Sm	12.2	188	3.4	15.7	207	5.7	1.85	8.1
^{156}Gd	12.3	206	3.2	15.7	220	5.5	1.81	7.7
^{165}Ho	12.3	202	2.3	15.2	239	4.8	2.47	7.0
^{168}Er	11.9	222	3.2	15.5	275	4.5	1.73	7.4
^{174}Yb	12.3	297	2.9	15.5	320	4.9	1.80	7.1
^{178}Hf	12.2	291	3.1	15.5	334	4.9	1.80	7.2
^{180}Hf	12.2	286	3.2	15.3	324	5.1	1.81	7.1
^{181}Ta	12.1	272	3.0	15.0	316	5.1	1.97	6.8
^{182}W	11.9	267	3.2	14.8	303	5.6	2.01	6.8
^{184}W	11.9	315	2.9	14.8	321	4.7	1.65	6.8
^{186}W	12.0	246	3.3	14.5	332	5.1	2.07	6.4
^{197}Au	13.7	535	5.2					
Average error	1.4 %	11.2 %	9.3 %	1.5 %	9.7 %	4.6 %	0.22	0.2 MeV

TABLE 3

Ratios of nuclear ellipsoid axes (k), deformation parameters (β) and intrinsic quadrupole moments (Q_0), calculated from E_2/E_1

Nucleus	^{154}Sm	^{156}Gd	^{165}Ho	^{168}Er	^{174}Yb	^{178}Hf	^{180}Hf	^{181}Ta	^{182}W	^{184}W	^{186}W
k	1.320	1.302	1.259	1.327	1.289	1.296	1.281	1.263	1.271	1.268	1.229
β	0.326 ±0.017	0.309 ±0.016	0.266 ±0.036	0.334 ±0.032	0.296 ±0.024	0.303 ±0.032	0.288 ±0.036	0.270 ±0.026	0.278 ±0.030	0.274 ±0.032	0.235 ±0.033
Q_0	6.3 ±0.3	6.2 ±0.3	5.8 ±0.8	7.5 ±0.7	7.0 ±0.6	7.5 ±0.8	7.2 ±0.9	6.9 ±0.7	7.2 ±0.8	7.1 ±0.8	6.2 ±0.9

TABLE 4

Integral characteristics of E1 giant resonance

Nucleus	$\sigma_{0\,exp}$ (MeV · b)	$\frac{\sigma_{0\,exp}}{0.06NZ/A}$	σ_{0L} (MeV · b)	$\frac{\sigma_{0L}}{0.06NZ/A}$	σ_{-1} (mb)	σ_{-1L} (mb)	$\sigma_{-1L}A^{-4/3}$ (mb)	σ_{-2} (mb · MeV^{-1})	σ_{-2L} (mb · MeV^{-1})	$\sigma_{-2L}A^{-5/3}$ (μb · MeV^{-1})
^{154}Sm	1.94 ± 0.06	0.87	2.86	1.29	117 ± 3.5	156	0.189	9.1 ± 0.3	14.3	3.23
^{156}Gd	2.07 ± 0.07	0.91	2.95	1.30	143 ± 4.6	163	0.194	10.5 ± 0.4	14.9	3.30
^{165}Ho	1.86 ± 0.06	0.78	2.53	1.06	155 ± 4.4	160	0.177	10.1 ± 0.3	12.6	2.54
^{168}Er	2.24 ± 0.06	0.92	3.07	1.26	161 ± 4.3	197	0.212	12.0 ± 0.3	16.0	3.13
^{174}Yb	2.69 ± 0.05	1.07	3.82	1.52	195 ± 3.4	240	0.247	14.5 ± 0.3	19.2	3.54
^{178}Hf	2.85 ± 0.07	1.11	3.99	1.55	208 ± 4.9	247	0.247	15.3 ± 0.4	20.2	3.59
^{180}Hf	2.72 ± 0.06	1.05	4.03	1.56	200 ± 4.4	250	0.246	15.1 ± 0.3	20.7	3.61
^{181}Ta	2.84 ± 0.07	1.09	3.81	1.46	210 ± 5.3	245	0.239	16.0 ± 0.4	20.0	3.45
^{182}W	2.86 ± 0.07	1.09	4.01	1.52	211 ± 5.3	256	0.248	16.2 ± 0.4	21.6	3.70
^{184}W	2.78 ± 0.07	1.05	3.80	1.43	207 ± 5.3	251	0.240	15.9 ± 0.4	20.9	3.54
^{186}W	2.90 ± 0.07	1.08	3.95	1.48	214 ± 5.3	256	0.241	16.2 ± 0.4	21.6	3.56
^{197}Au	3.12 ± 0.06	1.10	4.37	1.54	229 ± 4.2	276	0.241	18.6 ± 0.4	23.3	3.49

Y_B
A=176

Y_B
A=176

Y_B
A=176

REF.	T. Cooper, W. Bertozzi, J. Heisenberg, S. Kowalski, W. Turchinetz, C. Williamson, L. Cardman, S. Fivozinsky, J. Lightbody, Jr., and S. Penner Phys. Rev. C13, 1083 (1976)	ELEM. SYM.	A	Z
		Yb	176	70
METHOD		REF. NO.		
		76 Co 3		hmg

REACTION	RESULT	EXCITATION ENERGY	SOURCE TYPE	SOURCE RANGE	DETECTOR TYPE	DETECTOR RANGE	ANGLE
E,E/	FMF	1, 1	D	34-111	MAG-D		DST

LEVELS .082,.267

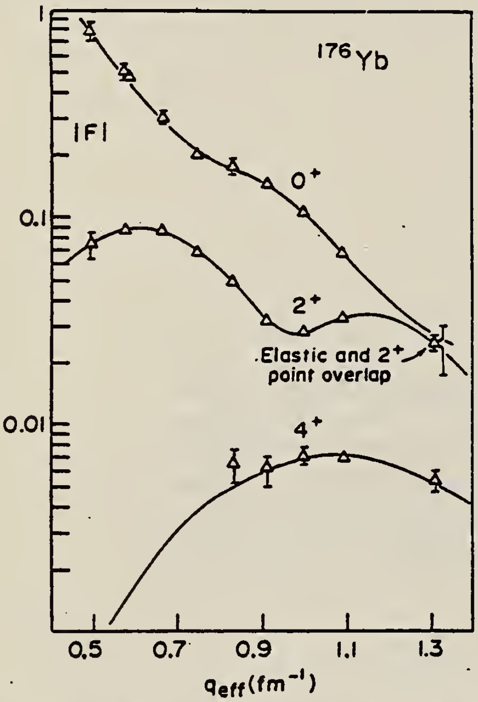

FIG. 6. Measured form factors for the elastic (0$^+$) and the inelastic 0.081-MeV (2$^+$) and 0.267-MeV (4$^+$) states in ^{176}Yb. The fitted curves are based on a best fit deformed Fermi charge distribution.

TABLE IX. Transition charge parameters of ^{166}Er and ^{176}Yb.

	Units	^{166}Er ρ_0	^{166}Er ρ_2	^{166}Er ρ_4	^{176}Yb ρ_0	^{176}Yb ρ_2	^{176}Yb ρ_4
c	fm	6.1610	5.8632	5.8556	6.3306	6.0151	5.1866
t	fm	0.4872	0.5593	0.7271	0.4868	0.5188	0.9093
β_2		0.3266	0.3503	0.3325	0.3100	0.3346	0.3874
β_4		0.0	0.0	0.0199	−0.054	−0.054	−0.0875
β_6		−0.0180	−0.0180	−0.0180 [a]	−0.006	−0.006	−0.006 [a]
rms radius	fm	5.2380 [b]			5.3150 [c]		
$B(E2)$	e^2b^2		5.670 [d]			5.350 [e]	
$B(E4)$	e^2b^2			0.0919			0.0092
χ^2/freedom		0.42	2.62	2.68	1.18	1.23	3.14
Transition radius	fm	5.2380	6.9088	8.4777	5.3150	6.8689	6.6962

[a] Reference 3.
[b] Interpolated value from nearest neighbors.
[c] Reference 23.
[d] Reference 25.
[e] Reference 24.

TABLE V. Cross sections of ^{176}Yb.

Energy (MeV)	Angle (deg)	q_{eff} (fm^{-1})	Elastic $\frac{d\sigma}{d\Omega}_{exp}$ (mb)	Elastic $\frac{d\sigma}{d\Omega}_{bestfit}$ (mb)	2$^+$ $\frac{d\sigma}{d\Omega}_{exp}$ (mb)	4$^+$ $\frac{d\sigma}{d\Omega}_{exp}$ (mb)
34.72	109.95	0.498	0.995×10 ±5%	0.964×10	0.379×10^{-1}± 8%	...
39.62	127.81	0.591	0.146×10 ±3%	0.145×10	0.463×10^{-1}± 4%	...
44.53	109.95	0.580	0.245×10 ±5%	0.239×10	0.707×10^{-1}± 4%	...
54.90	109.95	0.666	0.591 ±5%	0.569	0.456×10^{-1}± 3%	...
64.77	110.16	0.749	0.176 ±4%	0.191	0.205×10^{-1}± 2%	-0.322×10^{-4}± 130%
74.97	110.13	0.834	0.108 ±7%	0.967×10^{-1}	0.795×10^{-2}± 3%	0.140×10^{-3}± 20%
85.09	110.03	0.917	0.561×10^{-1}±4%	0.537×10^{-1}	0.248×10^{-2}± 4%	0.929×10^{-4}± 19%
95.30	110.03	1.002	0.244×10^{-1}±4%	0.246×10^{-1}	0.154×10^{-2}± 5%	0.103×10^{-3}± 10%
95.00	127.81	1.096	0.444×10^{-2}±4%	0.453×10^{-2}	0.100×10^{-2}± 3%	0.416×10^{-4}± 9%
110.21	147.24	1.319	0.170×10^{-3}±9%	0.246×10^{-3}	0.139×10^{-3}±12%	0.596×10^{-5}± 25%

[3] D.L. Hendrie, Phys. Lett. 36, 571 (1973); ibid. et al. Phys. Lett. 26B, 127 (1968).

[23] A. Thompson (priv. commun.) Eidgenoessische TH Zuerich, 1974 (unpublished).

[24] R.O. Sayer et al., Phys. Rev. C1, 1525 (1970).

[25] P.H. Stelson, Nucl. Data A1, 21 (1965).

# LUTETIUM
Z=71

Lutetium was discovered independently by C. A. von Welsbach and G. Urbain in 1907-08. Urbain called the new oxide *lutecia* — an old Roman name for his native city, Paris. Of all the rare earth metals, lutetium is the hardest and the most dense.

Lu

REF.	ELEM. SYM.	A	Z
R. Bergere, H. Beil, P. Carlos and A. Veyssiere Nucl. Phys. A133, 417 (1969)	Lu		71

METHOD	REF. NO.	
	69 Be 6	egf

REACTION		RESULT	EXCITATION ENERGY	SOURCE TYPE	SOURCE RANGE	DETECTOR TYPE	DETECTOR RANGE	ANGLE
G,N	484	ABX	7-24	D	7-28	MOD-I		4PI
G,2N	485	ABX	14-28	D	7-28	MOD-I		4PI
G,3N	486t	ABX	24-28	D	7-28	MOD-I		4PI

612

x = fraction of total cross section resulting in a direct neutron

n_d = fraction of neutrons emitted by direct effect at an energy where all the evaporation neutrons go to (γ,2n) cross section

$n_d = x/(2-x)$

Tableau 3

Moments quadrupolaires intrinsèques

Cible	% isotopes	a/b ex	β_2 ex	$\beta_2[B(E_2)]$	Q_0 ex (b)	Q'_0
$_{53}$I	100 % ^{127}I	0.85	0.172		-2.3 ± 0.4	
$_{58}$Ce	88.5 % ^{140}Ce			0.104		
	11.1 % ^{142}Ce			0.118		
$_{62}$Sm	15 % ^{147}Sm					0.158
	11.2 % ^{148}Sm					
	13.8 % ^{149}Sm	1.23	0.219		4.5 ± 0.4	
	7.5 % ^{150}Sm			0.190		3.53
	26.6 % ^{152}Sm			0.304		5.93
	22.5 % ^{154}Sm			0.351		6.58
$_{68}$Er	33.4 % ^{166}Er			0.341		7.60
	22.9 % ^{167}Er	1.314	0.288		6.96 ± 0.4	7.80
	27.1 % ^{168}Er			0.339		7.60
	14.9 % ^{170}Er			0.329		7.45
$_{71}$Lu	97.4 % ^{175}Lu	1.282	0.262		6.95 ± 0.3	7.20

Tableau 5

Valeurs de la température nucléaire et du paramètre a de densité des niveaux

	x	n_d	Θ (MeV)	$E'_\gamma - E_n$ (MeV)	a (MeV^{-1})	a' (MeV^{-1})	a'' (MeV^{-1})
I	0.05 ± 0.005	0.03 ± 0.03	1.30 ± 0.20	10	6 ± 2.5	10 ± 3	10 ± 2
^{140}Ce	0.21 ± 0.05	0.12 ± 0.03	1.05 ± 0.20	10	9 ± 3.5		7 ± 3
^{142}Ce			0.8 ± 0.20	6	9 ± 4		8 ± 3
Sm	0.18 ± 0.04	0.10 ± 0.03					
Er	0.20 ± 0.05	0.11 ± 0.03					(12 ± 4)
Lu	0.26 ± 0.06	0.15 ± 0.03	0.85 ± 0.1	9	12.5 ± 2.5		15 ± 3

over

TABLEAU 4

Règles de somme

Noyau cible (éléments naturels)	σ_0 (MeV · b)	σ'_0 (MeV · b)	$0.06 \frac{NZ}{A}$	$\frac{\sigma_0 A}{0.06\, NZ}$	$\frac{\sigma'_0 A}{0.06\, NZ}$	σ_{-1} (mb)	$\sigma_{-1} A^{-1/3}$	σ_{-2} (mb · MeV^{-1})	$\sigma_{-2} A^{-4/3}$
$_{53}$I	2.02 ± 0.14	2.30 ± 0.12	1.85	1.09 ± 0.07	1.24 ± 0.07	129 ± 0.10	0.20 ± 0.02	8.6 ± 0.6	2.7 ± 0.2
$_{58}$Ce	2.13 ± 0.15	2.53 ± 0.13	2.04	1.05 ± 0.07	1.24 ± 0.07	140 ± 0.12	0.19 ± 0.02	9.5 ± 0.6	2.5 ± 0.2
$_{62}$Sm	2.48 ± 0.17	2.92 ± 0.14	2.18	1.14 ± 0.07	1.34 ± 0.07	167 ± 0.14	0.21 ± 0.02	11.8 ± 0.8	2.75 ± 0.2
$_{68}$Er	2.70 ± 0.19	3.04 ± 0.16	2.42	1.12 ± 0.07	1.26 ± 0.07	186 ± 0.15	0.20 ± 0.02	13.6 ± 1	2.7 ± 0.2
$_{71}$Lu	2.65 ± 0.18	2.96 ± 0.16	2.53	1.05 ± 0.07	1.17 ± 0.07	182 ± 0.15	0.185 ± 0.02	12.9 ± 1	2.35 ± 0.2
valeur moyenne pour ces 5 corps				1.09 ± 0.07	1.25 ± 0.07		0.20 ± 0.02		2.6 ± 0.2

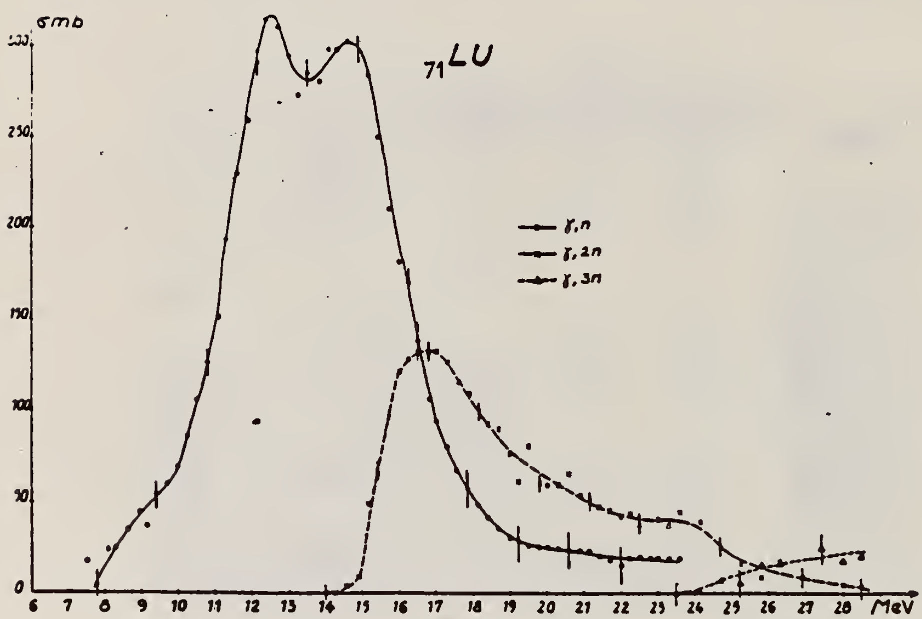

Fig. 9.

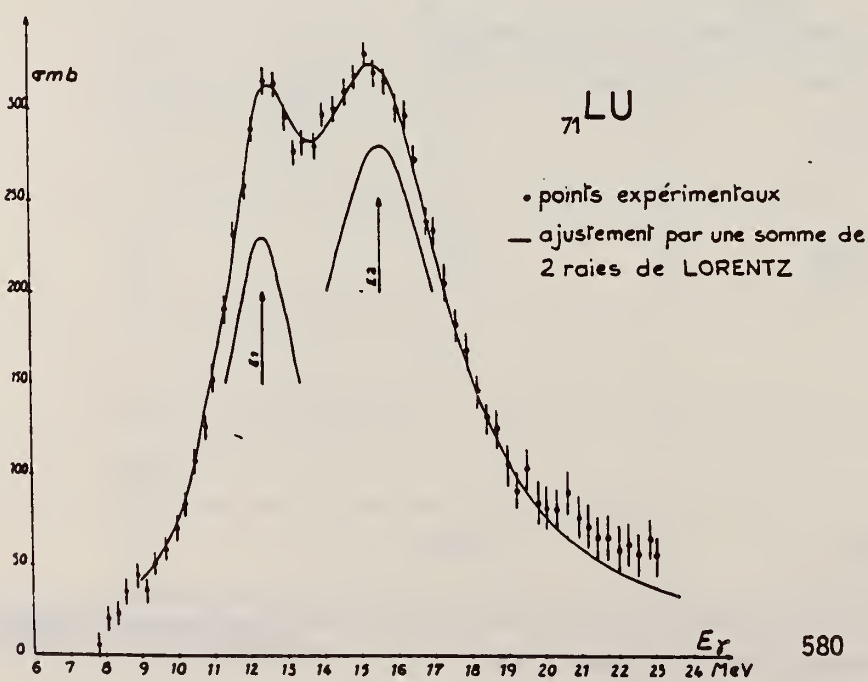

Fig. 10.

Lu
A=175

Lu
A=175

Lu
A=175

REF.	ELEM. SYM.	A	Z
L. Katz, G.B. Chidley Nuclear Reactions at Low and Medium Energies (Academy of Science, USSR: 1958) 371	Lu	175	71

METHOD	REF. NO.	
Betatron; neutron cross section; BF_3 counters; ion chamber monitor	58 Ka 1	NVB

REACTION	RESULT	EXCITATION ENERGY	SOURCE		DETECTOR		ANGLE
			TYPE	RANGE	TYPE	RANGE	
G,XN	ABX	8-22	C	8-22	BF3-I		4PI

Таблица 2

Пороги испускания фотонейтронов

Изотоп	B_n, *Мэв*	B_{2n}, *Мэв*	Изотоп	B_n, *Мэв*	B_{2n}, *Мэв*
V^{51}	11,16	20,5	L^{139}	8,81	16,1
Mn^{55}	10,14	19,2	Pr^{141}	9,46	17,6
Co^{59}	10,44	18,6	Tb^{159}	8,16	14,8
As^{75}	10,24	18,1	Ho^{165}	8,10	14,6
Y^{89}	11,82	20,7	Tm^{169}	8,00	14,7
Nb^{93}	8,86	17,1	Lu^{175}	7,77	14,2
Rh^{103}	9,46	16,8	Ta^{181}	7,66	13,8
J^{127}	9,14	16,2	Au^{197}	7,96	13,3
Cs^{133}	9,11	16,5	Bi^{209}	7,43	14,5

THRESHOLDS

не приведены, поскольку они превышают 2. *Мэв* во всех случаях, кроме золота, для которого $B_{3n}=21$ *Мэв*. Свойства сечений $\sigma_0(\gamma)$ сведены в табл. 3.

Таблица 1

Изотоп	$E_{макс}$, *Мэв*	$\sigma_n(E_\gamma)$, *барн*	Γ, *Мэв*	Σ^{22}, *Мэв·барн*	Y(22), 10^8 *нейтрон/100 р·моль*
V^{51}	18,4	0,062	5,2	0,33	1,62
Mn^{55}	20,2	0,060	7,0	0,39	2,01
Co^{59}	18,3	0,068	6,3	0,44	2,30
As^{75}	16,4	0,090	9,5	0,74	4,25
Y^{89}	17,1	0,172	5,2	0,93	5,33
Nb^{93}	18,0	0,156	7,5	1,17	6,80
Rh^{103}	17,5	0,160	9,4	1,40	8,28
J^{127}	15,2	0,273	6,8	1,76	11,9
Cs^{133}	16,5	0,238	7,7	1,59	10,7
La^{139}	15,5	0,325	3,8	1,55	11,2
Pr^{141}	15,0	0,320	4,9	1,93	13,1
Tb^{159}	15,6	0,274	9,8	2,49	18,1
Ho^{165}	13,5	0,305	8,9	2,52	18,7
Tm^{169}	16,4	0,250	8,4	1,91	14,9
Lu^{175}	16,0	0,225	8,4	1,90	23,0
Ta^{181}	14,5	0,380	8,5	3,15	22,0
Au^{197}	13,8	0,475	4,7	3,04	22,6
Bi^{209}	13,2	0,455	5,9	2,89	23,2

Ref. H.J. King, L. Katz
Can. J. Phys. 36, 415 (1958)

Elem. Sym.	A	Z
Lu	175	71

Method 24 MeV betatron; neutron yield; BF_3 counters; Victoreen dosimeter

Ref. No.	
58 Ki 1	EH

Reaction	E or ΔE	E_o	Γ	$\int \sigma dE$	Jπ	Notes
$Lu^{175}(\gamma,n)$	Bremss. 8-23	16	8.4 MeV	$\int^{23} = 1.9$MeV-mb		$\sigma = 225$ mb; $E_{th} = 7.77 \pm 0.05$ MeV Neutron yield at 20 MeV is 1.93×10^9 n/mole/100 r.

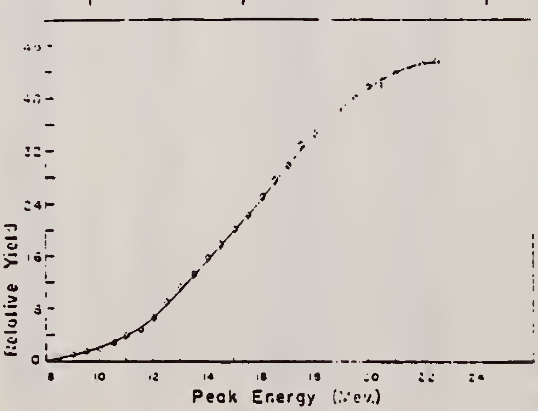

Fig. 2.

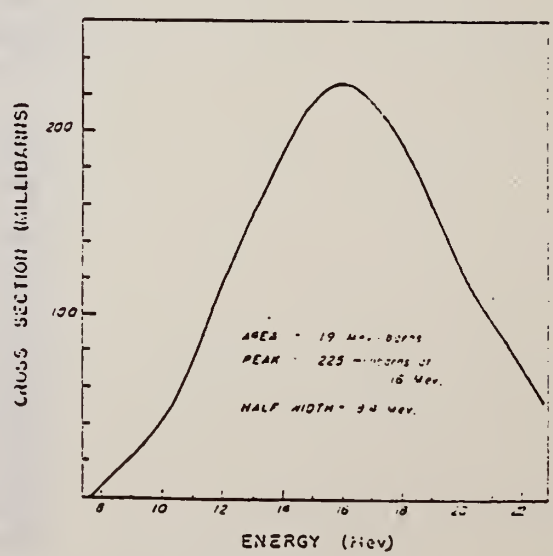

Fig. 3. $_{71}Lu^{175}$ cross section.

REF.	ELEM. SYM.	A	Z
K. N. Geller, J. Halpern, and E. G. Muirhead Phys. Rev. 118, 1302-12 (1960)	Lu	175	71

METHOD	REF. NO.	
Betatron; neutron threshold; ion chamber	60 Ge 3	NVB

REACTION	RESULT	EXCITATION ENERGY	SOURCE TYPE	SOURCE RANGE	DETECTOR TYPE	DETECTOR RANGE	ANGLE
G,N	NØX	THR	C THR		BF3-I		4 PI

THRESHØLD

TABLE I. Summary and comparison of neutron separation energies inferred from present threshold measurements with values predicted from mass data and reaction energies. All energies are expressed in the center-of-mass system in Mev.

Reaction	No. runs	Present results	Other results	Method	Reference
$Lu^{175}(\gamma,n)Lu^{174}$	1	7.88 ±0.08			

Ref.						Elem. Sym.	A	Z
B.I. Deutch Nuclear Phys. 30, 191 (1962)						Lu	175	71

Method	Ref. No.	
Hf^{175} source on centrifuge rotor; nuclear resonance flourscence; NaI	62 De 2	JHH

Reaction	E or ΔE	E_o	Γ	$\int \sigma dE$	Jπ	Notes
$Lu^{175}(\gamma,\gamma)$	345 keV		$\frac{\Gamma_o}{\hbar}$ = 5.16±0.26 X10^{10}sec		$5/2^+$ E 2 M1	Mean lifetime $\tau_\gamma = (4.71 \pm 0.10)10^{-10}$sec $\omega(\theta) = 1+(-0.20\pm0.28)P_2(\cos\theta)$

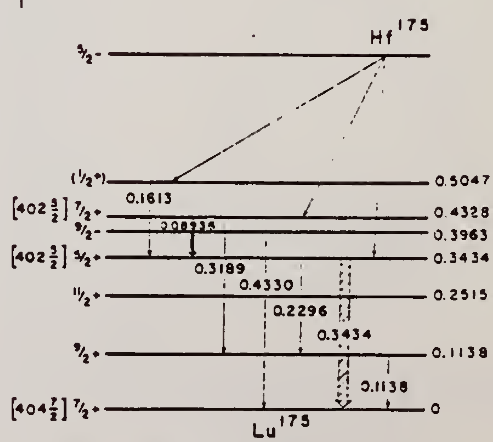

Fig. 1. The decay scheme of Hf^{175}. Energies are given in MeV

REF.		ELEM. SYM.	A	Z
	A. Suzuki and K. Shoda Nucl. Phys. A260, 172 (1976)	Lu	175	71
METHOD		REF. NO. 76 Su 2		egf

REACTION	RESULT	EXCITATION ENERGY	SOURCE TYPE	SOURCE RANGE	DETECTOR TYPE	DETECTOR RANGE	ANGLE
E,P	ABX	11- 20	D	15- 20	MAG-D		125

Proton yields obtained by summing protons with energies above levels given in tables.

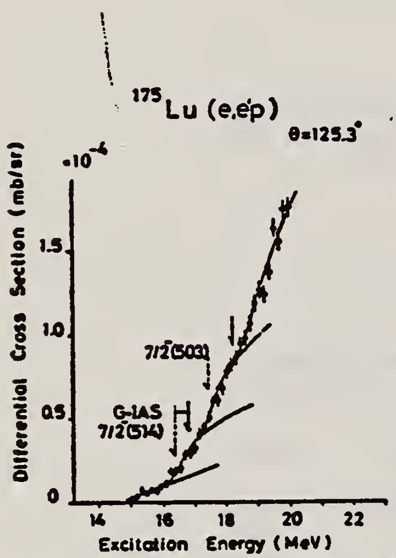

Fig. 5. Cross section of the ^{175}Lu(e, e'p) reaction. See also the caption to fig. 2.

TABLE 1

Parameters of the present experiment

Target	Atomic number	Purity (%)	Thickness (mg/cm²)	Lowest proton energy (MeV)	Bin size (keV)	Range of measurement (MeV)
^{159}Tb	65	99.9 (natural)	14.87	4.70	100	15.0 –17.5
^{165}Ho	67	99.9 (natural)	11.64	4.70	100	15.5 –17.5
^{169}Tm	69	99 (natural)	13.40	4.70	100	15.0 –18.0
^{175}Lu	71	99.87 (enriched)	5.24	5.34	150	15.05–20.0
^{181}Ta	73	99.9 (natural)	6.73	6.16	200	16.0 –23.0

TABLE 3

Displacement energies obtained from the present data and the estimates with eqs. (20) and (21)

Target	Resonance	E^* (MeV)	E_d (exp) (MeV)	E_d [a]) (MeV)	$E_d(\delta = 0.3)$ [b]) (MeV)
^{159}Tb	1st 2nd	15.75±0.15 16.50±0.15	15.58 15.46	16.06	15.93
^{165}Ho	1st	16.15±0.14	15.64	16.38	16.25
^{169}Tm	1st 2nd	15.76±0.13 16.34±0.14	16.20 16.22	16.76	16.63
^{175}Lu	1st 2nd	16.44±0.13 17.45±0.15	16.75 16.35	17.07	16.93
^{181}Ta	1st	17.31±0.15	16.40	17.38	17.24

[a]) Estimated with eq. (20).
[b]) Estimated with eq. (21).

TABLE 4

Deformation parameters of IAS δ_{IAR} derived from the (e, e'p) result

Target	Resonance	IAS	Parent state	$\delta_{IAR}-\delta_p$ [a])	δ_p (assumed)	δ_{IAR} [a])
^{159}Tb	1st	$\frac{3}{2}^-$[521]	ground	—0.008	0.31	0.30
	2nd	$\frac{5}{2}^-$[512]	875 keV	—0.016		0.29
^{165}Ho	1st	$\frac{7}{2}^+$[633]	ground	—0.023	0.30	0.28
^{169}Tm	1st	$\frac{1}{2}^-$[521]	ground	—0.018	0.29	0.27
	2nd	$\frac{1}{2}^-$[510]	565 keV	—0.019		0.27
^{175}Lu	1st	$\frac{7}{2}^-$[514]	ground	—0.010	0.28	0.27
	2nd	$\frac{7}{2}^-$[503]	1420 keV	—0.029		0.25
^{181}Ta	1st	$\frac{7}{2}^-$[503]	670 keV	—0.046	0.26	0.21

The assumed deformation parameters for the parent states δ_p are also shown.
[a]) The errors are about ±0.01.

REF.	T. Bar-Noy and R. Moreh Nucl. Phys. A288, 192 (1977)	ELEM. SYM. Lu	A 175	Z 71
METHOD		REF. NO. 77 Ba 9		egf

REACTION	RESULT	EXCITATION ENERGY	SOURCE TYPE	SOURCE RANGE	DETECTOR TYPE	DETECTOR RANGE	ANGLE
G,G	ABX	8- 12	D	8- 12	SCD-D		140

Abstract: Differential cross sections for elastic and inelastic Raman scattering from ^{175}Lu and ^{181}Ta were measured. Five photon energies between 8.5 and 11.4 MeV were used and were obtained from the (n, γ) reaction on Ni and Cr using thermal neutrons. The results are compared with calculations using a modified simple rotator model (SRM) of the giant dipole resonance (GDR) in which the effect of Delbrück scattering was incorporated. In general, fair agreement between theory and experiment is obtained. A new set of GDR parameters is extracted, based on photon scattering data and, as expected, yield better agreement between experimental and predicted cross sections.

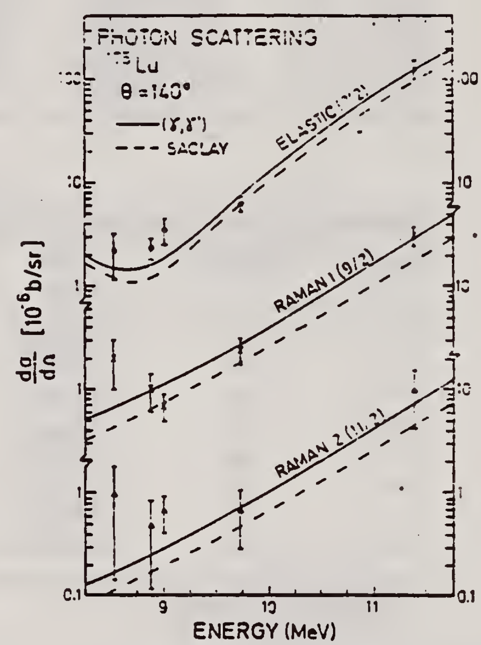

Fig. 4. Elastic and Raman inelastic differential cross sections for ^{175}Lu at 140°. The dashed line is calculated using GDR parameters extracted from the photoneutron data of the Saclay group. The solid line is calculated using GDR parameters extracted from the present photon scattering data (table 2). The elastic curves include contributions from Thomson, Delbrück, and nuclear resonance scattering.

over

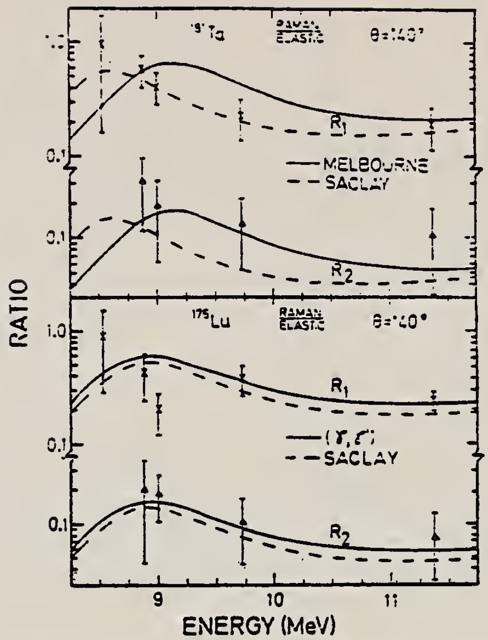

Fig. 5. Ratios of Raman/elastic scattering cross sections at 140° for ^{175}Lu and ^{181}Ta. R_1 and R_2 refer to the first and second Raman lines (fig. 1). The GDR parameters used in calculating the nuclear resonance amplitudes are explained in the captions to figs. 3 and 4.

Table 1

Differential cross sections (in μb/sr) of elastic and Raman inelastic scattering at $\theta = 140°$

E (MeV)	^{175}Lu			^{181}Ta		
	elastic $I_0 = \frac{7}{2}^+$	Raman 1 $\frac{9}{2}^+$, 114	Raman 2 $\frac{11}{2}^+$, 251	elastic $I_0 = \frac{7}{2}^+$	Raman 1 $\frac{9}{2}^+$, 136	Raman 2 $\frac{11}{2}^+$, 301
8.53	2.2±1.0	2.0±1.0	0.9±0.7	1.8±0.7	1.7±0.7	
8.88	2.3±0.6	1.0±0.5	0.5±0.3	1.8±0.4	1.0±0.3	0.5±0.3
9.00	3.5±1.0	0.7±0.2	0.7±0.2	2.5±0.3	1.0±0.3	0.5±0.3
9.72	6.2±1.1	2.4±0.7	0.7±0.4	7.6±1.0	1.7±0.7	1.0±0.6
11.39	120 ±20	31 ±7	10 ±5	107 ±15	21 ±8	11 ±8
11.39 [a]				131 ±14	17 ±4	17 ±4

[a] Experimental results of ref. [3] (calculated for 140° from measured values at 150°).

[3] H.E. Jackson, G.E. Thomas and K.J. Wetzel, Phys. Rev. C11, 1664 (1975)

Lu
A=176

Lu
A=176

Lu
A=176

REF. Yoshihisa Watanabe, Takeshi Mukoyama
Nucl. Sci. Eng. 80, 92 (1982)

ELEM. SYM.	A	Z
Lu	176	71

METHOD

REF. NO.	
82 Wa 4	egf

REACTION	RESULT	EXCITATION ENERGY	SOURCE TYPE	SOURCE RANGE	DETECTOR TYPE	DETECTOR RANGE	ANGLE
G,G/	ABY	1	C	1.3*	ACT-I		4PI

1=1.08 MEV, *CO-60

A photoexcitation process by gamma rays from a ^{60}Co source has been studied for the nuclei of ^{87}Sr, ^{111}Cd, ^{115}In, and ^{176}Lu. The induced isomeric activity was measured with a Ge(Li) detector. The flux of photons scattered into the target has been estimated with the Monte Carlo method using the single-scattering approximation. From the observed induced activities and the calculated photon flux, the integral cross sections for isomer production by photoexcitation were obtained and compared with other experimental data.

TABLE II

Integral Cross Sections for the Isomer Production by Photoexcitation ($\times 10^{-25}$ cm$^2\cdot$eV)

	^{87}Sr	^{111}Cd	^{115}In	^{176}Lu	Photon Source	Reference
Chertok and Booth		0.6 ± 0.2	0.71 ± 0.23		Bremsstrahlung	5
Booth and Brownson	$0.85^{+0.4}_{-0.3}$		1.15 ± 0.4		Bremsstrahlung	6
Boivin et al.		$0.8^{+0.4}_{-0.05}$	3^{+4}_{-2}		Bremsstrahlung	7
Lakosi et al.		1.02 ± 0.26	1.05 ± 0.27		^{60}Co	11
Yoshihara	3.0 ± 0.8[a]	1.5 ± 0.3	2.3 ± 0.4	69 ± 12[a] 140 ± 30[a]	^{60}Co	3
Veres	0.5 to 0.62	0.8 to 1.5	0.9 to 5		^{60}Co	23
Present work	4.2 ± 0.6[b] 5.6 ± 0.8[c]	1.1 ± 0.2	3.5 ± 0.2	39 ± 27[b] 48 ± 34[c]	^{60}Co	

[a]Obtained as the relative value to ^{115}In.
[b]Provided that the partial level width $g\Gamma_0 = 1 \times 10^{-3}$ eV.
[c]Provided that the partial level width $g\Gamma_0 = 1 \times 10^{-4}$ eV.

DEFINITIONS OF ABBREVIATIONS AND SYMBOLS

Note: In this list definitions are given for various photoneutron reactions in which the following symbols are used: N, NL, nN, SN and XN. Corresponding definitions apply for reactions involving other nuclear particles where the symbols N (neutron) is replaced by, e.g. P, D, T, HE, A etc. Where unknown reactions result in the production of a specific radionuclide, the chemical symbol and mass number is listed as the reaction product, e.g. a G,NA22 reaction in ^{59}Co.

A	alpha particle
ANAL	analysis
ABI	absolute integrated cross-section data
ABX	absolute cross-section data
ABY	absolute yield data. Often means cross-section per equivalent quantum is listed.
ACT	measurement of induced radioactivity of the target
ASM	asymmetric, asymmetry
AVG	average
BBL	bubble chamber
BEL B(EL)	reduced electric radiative transition probability
BF3	BF_3 neutron counter with moderator e.g., Halpern detector, long counter
BML	reduced magnetic radiative transition probability, B(ML)
BREAKS	levels located by "breaks" in the yield curve
BRKUP	breakup
BRMS	bremsstrahlung
BTW	between
C	continuous. Used to describe a photon source or a detector response function. Contrast with D = discrete.
CCH	cloud chamber
CF	compared with
CHRGD	charged
CMPT	Compton
COIN COINC	coincidence, coincide
COH	coherent
CK	Cerenkov
D	deuteron or discrete. When discrete, it is used to describe a photon source or a detector response function. Contrast with C = continuous.
DLTE	energy loss
DLTQ	momentum transfer
DST	distribution
DT BAL	detailed balance
E	electron
E/	inelastically scattered electron
E+	positron
EDST	energy distribution or spectrum
E/N	used only to indicate a coincidence experiment as in (E,E/N).

	N stands for any outgoing particle measured in coincidence with an inelastically scattered electron. Distinguish from eg., (E,N) which is used to represent an electron induced reaction when only the outgoing particle N is detected.
EMU	emulsions (photographic plates)
EXCIT	excited
F	fission
FMF	form factor
FM-1	inverse femtometers
FRAG	fragment
G	photon
G/	inelastically scattered photon
G-WIDTH	gamma-ray transition width
HAD	hadrons, hadron production
HE He3	^{3}He particle
INT	interaction, integral, intensity
INC	includes
ION	ionization chamber
ISOB	isobaric
ISM	isomer
J	multiplicity of particle defined by following symbol e.g. (G,PJN) with remark J = 2,3,5,7
JPI J-PI	spin and parity of a nuclear state
K	second multiplicity index, e.g. (G,JPKN) with both J & K positive integers greater than 1
KE	kinetic energy
L	may be an integer or zero that always follows a reaction product symbol. This is used to indicate transitions to specific states in the residual nuclide. When the letter is used as in (G,NL) the cross section given is that for the sum of transitions to two or more specific final states.
LFT	excited state lifetime
LIM	limit
LV,LVS	level, levels
LQD	liquid
MAG	magnetic spectrometer
MEAS	measurement(s)
MGC	magnetic Compton spectrometer
MGP	magnetic pair spectrometer
MOD	moderated neutron detector not employing a BF_3 counter, e.g. rhodium foil, Szilard-Chalmers reaction, ^{3}He, ^{6}Li reactions, GD loaded liquid scintillator, etc.
MSP	mass spectrometer
MULT	multiple, multipole, multiplicity
MU-T	used only in combination with G to indicate a total photon absorption cross section measurement, i.e. (G,MU-T)
N	neutron (see also XN and SN). The notation (G,N) is used to indicate a reaction in which only a single neutron is emitted, i.e. the reaction that can, in many cases, be measured by observing the radioactive decay of the residual nuclide.

nN	where n is any integer. (G,nN) indicates the sum over all reaction cross sections in which n neutrons are emitted.
NAI	NaI(Tl) spectrometer
NEUT	neutron(s)
NOX	no cross-section data
P	proton (see also XP)
PART	particle(s)
PHOT	photon(s)
PI	pion, usually written as PI+, PI-, PI0 to indicate charge
POL	polarized or polarization
Q-SQUAR	momentum transfer squared (q^2)
RCL	recoil
REL	relative
RLI	relative integrated cross-section data
RLX	relative cross-section data
RSP	reaction spectrometer
RLY	relative yield data
SCTD	scattered
SCD	semiconductor (solid state) detector
SCI	scintillator detector other than NaI, e.g., CsI, KI, organic (liquid or solid), stilbene, He
SEP	separation
SEP ISOTP	separated isotope used
SIG	SIGMA (cross section)
SN	sum of neutron producing reactions, $\sigma(\gamma,SN)=\sigma(\gamma,N) + \sigma(\gamma,NP) + \sigma(\gamma,2N) + \sigma(\gamma,3N)$ + etc.
SPC	photon or particle energy spectrum
SPK	spark chamber
SPL	spallation
STAT	statistical
SYM	symetric, symmetry
T	triton
TEL	counter telescope
THR	threshold for reaction or threshold detector, e.g., $^{29}Si(n,p)^{29}Al$.
TOF	time-of-flight detector
TRK	tracks of particles or fragments observed in solid materials (glass, mylar, etc.)
TRNS	transition
UKN UNK	unknown
VIB	vibrational
VIR PHOT	virtual photon(s)
XN	all neutrons, total neutron yield, $\sigma(\gamma,XN) = \sigma(\gamma,N) + 2\sigma(\gamma,2N) + 3\sigma(\gamma,3N) + \sigma(\gamma,NP)$ + etc.
XP	all protons, total proton yield $\sigma(\gamma,XP) = \sigma(\gamma,P) + \sigma(\gamma,NP) + 2\sigma(\gamma,2P)$ + etc.
XX XXX	reaction products defined in REMARKS
YLD	yield

4PI	a 4π geometry was used or a method like radioactivity or a total absorption measurement
999	energy defined in REMARKS
$	indicates the measurement involved beams or targets that were either polarized or aligned, or that the polarization of the reaction products was determined. The polarized particle is indicated in REMARKS.
* or @	symbols used to indicate that the units associated with the numerals on one or both sides of the symbol in a specific column are not MeV. The units are defined in REMARKS.

NBS-114A (REV. 2-8C)

U.S. DEPT. OF COMM. BIBLIOGRAPHIC DATA SHEET (See instructions)	1. PUBLICATION OR REPORT NO.	2. Performing Organ. Report No.	3. Publication Date

4. TITLE AND SUBTITLE

Photonuclear Data-Abstract Sheets
1955-1982

5. AUTHOR(S)

E.G. Fuller and Henry Gerstenberg

6. PERFORMING ORGANIZATION (If joint or other than NBS, see instructions)

NATIONAL BUREAU OF STANDARDS
DEPARTMENT OF COMMERCE
WASHINGTON, D.C. 20234

7. Contract/Grant No.

8. Type of Report & Period Covered

9. SPONSORING ORGANIZATION NAME AND COMPLETE ADDRESS (Street, City, State, ZIP)

10. SUPPLEMENTARY NOTES

☐ Document describes a computer program; SF-185, FIPS Software Summary, is attached.

11. ABSTRACT (A 200-word or less factual summary of most significant information. If document includes a significant bibliography or literature survey, mention it here)

These abstract sheets cover most classes of experimental photonuclear data leading to information of the electromagnetic matrix element between the ground and excited states of a given nucleus. This fifteen volume work contains nearly 7200 abstract sheets and covers 89 chemical elements from hydrogen through americium. It represents a twenty-seven year history of the study of electromagnetic interactions. The sheets are ordered by target element, target isotope, and by an assigned bibliographic reference code. Information is given on the type of measurement, excitation energies studied, source type and energies, detector type, and angular ranges covered in the measurement. For a given reference, the relevant figures and tables are mounted on a separate sheet for each nuclide studied.

12. KEY WORDS (Six to twelve entries; alphabetical order; capitalize only proper names; and separate key words by semicolons)

data-abstract sheets, elements, experimental, isotopes, nuclear physics, photonuclear reactions

13. AVAILABILITY

☐ Unlimited
☒ For Official Distribution. Do Not Release to NTIS
☐ Order From Superintendent of Documents, U.S. Government Printing Office, Washington, D.C. 20402.
☐ Order From National Technical Information Service (NTIS), Springfield, VA. 22161

14. NO. OF PRINTED PAGES

15. Price